THE UNIVERSITY OF QUEENSLAND

AUSTRALIA

The Effect of Microwave Heating on Ore Sorting

Vladimir Rizmanoski

Dipl. Eng. Chemical Engineering

A thesis submitted for the degree of Doctor of Philosophy at

The University of Queensland in January 2012

Sustainable Minerals Institute

Julius Kruttschnitt Mineral Research Centre

Abstract

Today the Mining industry is being challenged to develop methodologies and technology to process the lower grade and mineralogically complex ore types using ore sorting. The potential of microwave driven selective heating as an excitation tool to underpin sorting is possibly not well known in the mining and mineral industries due to very few applications and lack of awareness of the potential users. This thesis investigates the conditions under which this process is technically effective and can be utilised. A detailed investigation was conducted to understand the reasons for selective heating of specific mineral phases and how infrared sensing can be used as an identification technique to discriminate certain particles from others. This thesis also quantifies the impact of other important factors on the sorting process including; particle shape and size, mineral composition and most importantly the textures of the mineral bearing particles which have a tendency to heat quickly when exposed to microwave energy.

An extensive assembly of analytical techniques such as optical microscopy, high-resolution X-ray computed tomography and XL Scanning Electron Microscopy (used by the Mineral Liberation Analyser) were utilised to obtain a mineralogical characterisation of the tested ores. The choice of microwave applicators enabled heating to be carried out in multimode and single mode types of cavity. By engineering synthetic samples a more comprehensive investigation was carried out which enabled some focusing questions from the thesis hypothesis to be addressed. The synthetic samples were used to experimentally validate an adopted theoretical approach of investigating the influence of mineral texture upon selective heating.

The supplied ore from the Bingham Canyon Mine, USA (operated by Rio Tinto's Kennecott Utah Copper Corporation) was experimentally tested in two steps of investigations. The first step involved the approach of an "ideal", theoretical sorter for which rock particles had to be destroyed (necessary to perform assaying analysis). The temperature threshold for economically

justifiable sorting was determined from a temperature difference and assayed metal content of heated particles. In the second step, samples were analysed by heating them in two applicators and the temperature threshold was determined as a function of mineral texture which caused selective heating as in contrast to assayed metal content.

The results showed from the exposure of synthetic particles (with designed textures of microwave more responsive minerals) that it is advantageous to use both multimode and single mode cavities for better understanding of microwave heating of the ore. It was also shown that the texture of microwave responsive minerals has a significant effect on the formation of the temperature profiles which are used to evaluate selectivity and potential for the separation as opposed to only mineral composition of the ore particles. It was demonstrated that the types of ores studied in this work, will respond to microwave selective heating to the extent that infrared detection can be applied to perform selection between cold and hot particles defined by a set threshold.

Declaration by Author

This thesis is composed of my original work, and contains no material previously published or written by another person except where due reference has been made in the text. I have clearly stated the contribution by others to jointly-authored works that I have included in my thesis.

I have clearly stated the contribution of others to my thesis as a whole, including statistical assistance, survey design, data analysis, significant technical procedures, professional editorial advice, and any other original research work used or reported in my thesis. The content of my thesis is the result of work I have carried out since the commencement of my research higher degree candidature and does not include a substantial part of work that has been submitted to qualify for the award of any other degree or diploma in any university or other tertiary institution. I have clearly stated which parts of my thesis, if any, have been submitted to qualify for another award.

I acknowledge that an electronic copy of my thesis must be lodged with the University Library and, subject to the General Award Rules of The University of Queensland, immediately made available for research and study in accordance with the *Copyright Act 1968*.

I acknowledge that copyright of all material contained in my thesis resides with the copyright holder(s) of that material. Where appropriate I have obtained copyright permission from the copyright holder to reproduce material in this thesis.

Publications During Candidature

Rizmanoski, V 2011, 'The effect of microwave pretreatment on impact breakage of copper ore', Minerals Engineering, vol. 24, no. 14, pp. 1609-18

Publications Included in This Thesis

No publications included.

Contributions by Others to the Thesis

Dr. Nenad Djordjevic provided guidance with respect to the detailed characterization of the ore, initial microwave apparatus set-up, experimental design and data analysis. He also regularly reviewed technical outcomes of the thesis and provided advices. Dr. Rob Morrison provided guidance regarding experiments and statistical data analysis for the first step of experimental investigations. Professor Sam Kingman provided advices, guidance with respect to the testing of dielectric properties of synthetic ore particles and initial structure for the chapters.

Review and comments on the initial draft of the thesis were performed by Dr. Nenad Djordjevic, Professor Sam Kingman and Dr. Rob Morrison.

Richard Hartner performed optical analysis on prepared ore particles and Geoffrey Genn performed measurement of dielectric properties on selected minerals. Their contributions are referenced in this thesis.

Funding for this research program was provided by The University of Queensland through the Julius Kruttschnitt Mineral Research Centre (JKMRC) and Rio Tinto's Technological Resources Pty. Limited.

Statement of Parts of the Thesis Submitted to Qualify for the Award of Another Degree

None.

Acknowledgements

This magnificent journey would not be possible without the guidance, support and generous contribution of many. With a great respect I would like to thank those who made this thesis possible. My special thanks to Dr. Nenad Djordjevic, Dr. Rob Morrison and Professor Sam Kingman, for their direction, support and encouragement through my research. Professor Benjamin Adair is also thanked for his excellent support and generous discussions during internal meetings.

I would like to thank my fellow researchers for higher degree Vladimir Jokovic and Geoffrey Genn along with Dr. John Tucker for the hours of valuable discussions on the complex nature of the microwave technology, and from The University of Nottingham to Dr. Georgios Dimitrakis and Dr. Chris Dodds for the many useful brain-storming meetings.

I would also like to acknowledge the special contribution from Leslie King of National Instruments, Mark Stringer from Festo, Graham Sheridan and Michelle Cardy for helping me to make my paper ideas become alive.

I also would like to acknowledge all past and present students, JKMRC and JKTech personnel for their assistance during my study; you have made this a great time in my life. The University of Queensland and Rio Tinto's Technological Resources Pty. Limited are also gratefully acknowledged for the generous scholarship.

To my great friend Andree Phillips thank you for your unlimited support and absolute confidence in my ability.

I would like to thank to all my beloved family, without your love and support I would not have made it this far.

Keywords

mining engineering, microwave energy, particle sorting technology, process control, simulation, thermal characterisation, multimode cavity, waveguide applicator, materials engineering, chemical engineering design, particle technology

Australian and New Zealand Standard Research Classifications (ANZSRC)

ANZSRC code 090407 Process Control and Simulation, 40%

ANZSRC code 091405 Mining Engineering, 40%

ANZSRC code 091299 Materials Engineering not elsewhere classified, 20%

Fields of Research (FoR) Classification

FoR code: 0914 Resources Engineering and Extractive Metallurgy, 40%

FoR code: 0912 Materials Engineering, 20%

FoR code: 0904 Chemical Engineering, 40%

Contents

Figures

Tables

"Life is and will ever remain an equation incapable of solution, but it contains certain known factors."

Nikola Tesla (1856-1943)
"A Machine to End War" (Liberty, February, 1935)

Chapter 1 - Introduction

Over the centuries, ore sorting as a method of mineral recovery has always been present. However, due to its unique benefits greater focus is being applied by the mineral industry to develop methodologies and technologies to process lower grade and mineralogically complex ore types. The origin of ore recovery started with hand selection. At the present time, new developments in reliable sensor technologies have brought upgrades in ore sorting to be implemented in the mineral industry in both small and big steps.

1.1 Overview

The general aim of sorting can be defined in two ways. The first aim is concentration to produce one or more finished products, or pre-concentration to upgrade and produce a smaller bulk for further processing. The second aim is scavenging or salvaging to make an acceptable feed from a low or marginal grade deposit. Either as a concentration, or salvage objective, sorting has numerous advantages because it gives a great deal of flexibility. Some of these opportunities come from: overall reduction of plant capital costs, reduction in operating costs as well as ore transportation cost, achieving higher overall economic metallurgical recovery, increasing the life time of a mine by increasing reserves to include in situ and stockpiled previously below the cut-off grade material, and reducing environmental impact (by generating less fines as the waste or rejection of wastes containing harmful components). In addition, a unique method for recovery of particular mineral or

elimination of one mineral from another is presented when sorting is utilised as a major concentration technique.

To achieve the best recovery-grade ratio, the liberation of the valuable components is the very important factor. It does not mean that the particles must be liberated completely before being introduced to the sorting machine but the economic liberation is needed to determine the reasonable amount of valuable components in the waste portion. The research in this thesis addresses the problem of processing ore which has potential for selective heating to find the natural best recovery-grade ratio which can be later incorporated in economic studies.

The potential of microwave selective heating used for sorting is not well known in the mining and mineral industry due to very few applications and a lack of awareness of potential uses. This thesis investigates the conditions under which this process is technically effective and can be adapted for industrial use. A detailed investigation was conducted to understand the reasons for selective heating and how infrared sensing can be used as an identification technique to discriminate particles. It also examined important factors such as particle shape and size, mineral composition and most importantly textures of the minerals which have a tendency to heat quickly when exposed to microwave energy.

An extensive group of analytical techniques such as: optical microscopy, high-resolution X-ray computed tomography, and XL Scanning Electron Microscopy used by Mineral Liberation Analyser were utilised to obtain mineralogical characterisation of the tested ore. The choice of microwave applicators enabled heating to be carried out in multimode and single mode types of electromagnetic field. By engineering synthetic samples, a more comprehensive investigation was enabled to address some focusing questions from thesis hypothesis. They were used to experimentally validate an adopted theoretical approach of investigating influence of mineral texture upon selective heating.

The supplied ore from the Bingham Canyon Mine was experimentally tested in two steps. The first involved an approach of “ideal “ theoretical sorter for which rock

particles had to be destroyed, necessary to perform assaying analysis, and in the second step samples were analysed by heating them in two applicators.

1.2 Research Hypothesis and Objectives

The published literature about sorting has several common topics. It covers the material that needs to be sorted, a method for presentation or feeding, a method for particle examination followed by a method for comprehending obtained information, and finally a method for separating ore from waste. A comprehensive review of the published literature shows that no detailed study has been conducted to unveil the potential for mineral recovery of microwave treated copper bearing minerals, assisted with infrared detection. Therefore, the focusing questions of this thesis are as follows:

- Is it possible to develop a method of characterising ores for microwave infrared sorting?
- Do the composition and texture of minerals have a dominant effect on the potential to apply microwave infrared sorting?
- Is it possible to identify an intrinsic non responsiveness of the ore to the heating by applying different approaches for microwave heating?

Therefore, the main hypothesis which will be tested within this thesis is stated as follows:

"*The texture in addition to composition of minerals within ore particles, especially microwave absorbing minerals, has a significant effect on the creation of the temperature profiles which are used to evaluate selectivity and potential for the mineral sorting.*"

The research had the following objectives:

- Detailed chemical and mineralogical characterization of selected two different types of ore.
- Evaluation of the interaction of applied microwave energy with synthetic samples under controlled conditions to study selective heating in a controlled manner.

- Evaluation of the interaction of applied microwave energy with real ore particles under controlled conditions in order to determine temperature thresholds for sorting.
- Define the correlation connection between the mineralogical characterisation of any ore and the observed selective heating to determine the best natural grade/recovery ratio for any particular sample.

1.3 Thesis Outline

Chapter 2: Literature Review

This chapter aims to provide the reader with sufficient background to the study of mineral sorting. The literature review emphasises the sorting process using available sensors within the electromagnetic spectrum, indicating its advances and limitations. Some new sorting machines, which have been developed based on new detector technologies, are introduced and a summary of the operational processes is presented. Additionally the review provides an insight into previous experimental studies of microwave heating of minerals and studies for the implementation of microwave energy in the mineral industry.

Chapter 3: Experimental Methodology

This chapter discusses in general terms, the nature of volumetric microwave heating, materials interactions with microwaves, complex permittivity of minerals followed by physical properties of minerals. The favourable cases for microwave sorting are defined and explained. Furthermore, this chapter describes the experimental approach adopted to investigate the hypothesis of this thesis. Descriptions of the procedures for detailed experimental investigations, including procedure and techniques used for the mineralogical characterization of ores are given.

Chapter 4: Study of Synthetic Samples and Particle Characterisation by Image Analysis

This chapter presents the results of detailed study of synthetic samples which were used to experimentally validate the adopted theoretical approach of investigating the influence of mineral texture upon selective heating. A procedure to create synthetic samples is provided, followed by their bulk dielectric properties measurement.

Detailed descriptions of how these synthetic samples were tested in two different applicators are given and results commented. In addition, this chapter provides results from particle characterisation by image analysis on two ore types which were chosen for further experimental investigations to address the thesis hypothesis.

Chapter 5: Study of the "LRO" Ore Type

This chapter presents the results of experimental investigation for the first supplied ore type which was tested in two steps. The first step involved a detailed mineralogical characterization of ore, reproducibility study and discussion for the potential of microwave sorting, using temperature separation curves with pre-concentration objective. The second step discussed separability using different responses of textural properties of rock particles from heating results after exposing them in two different applicators. Some particles were tested in great detail to further substantiate behaviour of selective heating; these results are also presented and discussed.

Chapter 6: Study of the "QZ Ohio" Ore Type

This chapter presents the results of experimental investigation for the second supplied ore type. As in the previous chapter, ore was tested in two steps with a scavenging or salvaging objective. Recovery of economically valuable metals was also investigated with controlled flotation testing which was performed on three groups made of cold, medium and hot ore particles after applying microwave energy. The separability using different responses of textural properties of rock particles from heating results after exposing them in two different applicators was used as well. It was implemented to find the best natural recovery-grade ratio which can be later provided and incorporated in economic studies.

Chapter 7: Conclusions and Recommendations for Future Work

This chapter presents a summary of the work, the main findings and conclusions drawn. The practical implications of the results on microwave assisted infrared sorting of copper bearing minerals are addressed. The chapter also presents the scope for some future work.

Chapter 2 - Literature Review
Current Trends in Mineral Sorting and Use of Microwave Radiation in Mineral Processing

2.1 Current Trends and Improvements in Mineral Sorting

In mineral processing there is always a need for concentration and separation. The sorting of an ore as a method of mineral concentration was probably practiced in the very first mining operation. Cohen (2000) and Kelly and Spottiswood (1995) defined these processes in a very similar way and they are all based upon utilizing differences in the physical properties of mixed solids. Physical separation methods normally produce concentrates of unaltered minerals that have retained their natural characteristics and crystal structures. It is possible to define them as follows:

1. Radiation sorting,
2. Gravity separation,
3. Magnetic separation,
4. Electrostatic separation,
5. Separation based on surface phenomena.

In recent years radiation sorting, compared to traditional pre-concentration processes, has developed most rapidly following the development of sensor technology. Radiation sorting depends, on differential responses to externally applied radiations Cohen (2000). Some processes utilize differential radiation emissions, with or without externally applied stimulus. Many types of radiation can be used for solid–solid separation, including visible, ultraviolet, and infrared light; X-rays, gamma-rays, and electron beams; ultrasound; and a range of radio frequencies. The method of separation relies on differential effects of transmission, absorption, reflection,

modulation, or emission. In the words of Kleine (2010), “sensor-based sorting is the only mineral processing technique where the separating force is separated from the property on which basis is sorted.”

In the past three decades a significant amount of work has been undertaken for the experimental studies of microwave heating minerals and studies for the utilisation of microwave energy in the mineral industry. One of these studies started in Julius Kruttschnitt Mineral Research Centre at The University of Queensland in Australia to use microwave heating in conjunction with infrared sensors as a radiation sorting technology to detect particles which have copper bearing minerals. In order to evaluate this experimental approach one of the objectives was to investigate the influence of texture and composition of minerals, especially microwave absorbing minerals, and their effect on selective heating and potential for the mineral sorting.

Table 2-1 shows an overview of available sensors within the electromagnetic spectrum which are used to detect material properties and groups of minerals for which they can be applied. Salter and Wyat (1991) in their overview commented that various combinations of discrimination techniques have been used in some sorting machines. According to Commodas Ultrasort (a part of TiTech) sensors and technologies marked with an asterisk are still under development and valuation. There is an apparent need to close these gaps and to validate these sensors on different ore types and make them more versatile. At this time, research is also focused on developing suitable methods to establish the sortability of ores. Information collected from these new methods for ore sorting will be more universal and economical than testing samples through sorting machines.

With a very low ore grade a lot of mining operations are performed on low profit margins or being forced to be shut down in the near future as commented by Schodde (2010). Sensor based sorting provides alternative mineral recovery once the mining operations reach less profitable or more complex parts of the ore body.

Table 2-1 Available Sensors within the Electro Magnetic Spectrum which are used to detect material properties, sourced from Bergmann (2009).

Radiation	Wavelength [m]	Sensor/ Technology	Material Property	Mineral Application
Gamma Rays	10^{-10}-10^{-12}	RM (Radiometric)	Natural Gamma Radiation	Uranium, Precious Metals
X-Rays	10^{-9} - 10^{-10}	XRT (X-ray transmission)	Atomic Density	Base/Precious Metals Coal,
		XRF	Visible Fluorescence under X-rays	Diamonds Diamonds
Ultraviolet (UV)	10^{-7} - 10^{-9}	COL (CCD Colour Camera)	Reflection, Brightness, Transparency	Base/Precious Metals Ind. Minerals, Diamonds
Visible (VIS)	10^{-5} - 10^{-7}	PM (Photometric)	Monochromatic Reflection/ Absorption	Ind. Minerals, Diamonds
Near Infrared (NIR)	10^{-4} - 10^{-5}	NIR (Near Infrared Spectrometry) *	Reflection, Absorption	Base metals Industrial Minerals
Infrared (IR)	10^{-1} - 10^{-4}	IR (Infrared cam)*	Heat conductivity, heat dissipation	Base Metals Industrial Minerals
Microwave	10^{1} - 10^{-1}	MW-IR (heating in conjunction with IR)*	Sulphides & Metals heat faster than other minerals	Base/Precious Metals
Radio waves	10^{3} - 10^{1}			
Alternating current (AC)	10^{4} - 10^{3}	EM (Electro-Magnetic sensor)	Conductivity	Base Metals

The sensor based sorting technology ensures that only the valuable mineral fraction is retained for further processing and waste or barren material discarded. At the present time information which needs to be processed in real time can be processed very quickly due to the fast computer processors which are becoming more and more powerful. Sorters use a number of intelligent detection criteria to identify ore and mineral characteristics. Time to execute these sophisticated detection algorithms, achieve a process of separation and deploy ejection systems can be measured in

milliseconds. These short times are required to achieve large throughputs which are necessary for mining operations. Some of these sensors have been already tested in various studies.

2.1.1 Radiometric

Radiometric sorting of South African gold ores using uranium as a tracer has become practical and economical due to the introduction of microprocessors into the sorting machines. In the sorter the particles are presented individually to the X-ray counting system and mass determination system. Implementation of radiometric sorting for South African gold ores was proposed by The Canadian Department of Mines because they already had two commercial units installed at Bicroft Uranium and at Beaverlodge in Canada. They also had two units of this type fully operational in the uranium mine at Mary Kathleen in Queensland, Australia. Typical performance figures are given by Böhme (1983) in Table 2-2:

Table 2-2 Performance figures manufactured by Gunson's Sorters

Throughput per machine up to	48 ton/h
Average particle mass	70-95 g
Mass rejection	61-67%
Uranium recovery	91-94%
Gold recovery	92-96%
Reject grades	0.04 kg U_3O_8/ton

This installation covered the screen fractions -65+25 mm and therefore "shape corrections" had to be applied. Screen fractions above +65mm were considered to be implemented in operation while fractions below 25mm were investigated to see whether they will be below economic limit for sorting.

The disadvantage of this type of sorting is that it is volumetric sorting. It needs to determine mass of each particle and compute the grade of each particle from its radioactivity and mass. It is also not suitable for copper ore because of lack of radioactive elements.

2.1.2 Dual energy X-ray transmission

The X-ray transmission scanning method is used to inspect baggage content, at airports security points. Similar technology is implemented in mining as dual energy

X-ray transmission (DE-XRT) sorting. This technology and its combination with others are studied in more detail by Gaft et al. (2005).

Ketelholdt and Bergman (2010) gave technical insight of the sorter pilot plant at Mintek, Randburg South Africa. They stated that DE-XRT is particularly suitable for dry coarse coal in the size range -120 mm +12 mm.

The data is collected as digital imagery from an X-ray sensor system which works like a line-scan camera. The X-rays penetrate the material and are collected by the sensor system consisting of two channels, each capturing the image of the material in different X-ray energy levels. Within the imagery different shades of grey are used to correspond to the modulation of the amplitude within the sensor which detects the x-ray attenuation through the particle. Atomic density of the material and its thickness influence x-ray attenuation. In data images different colour pixels are matched to corresponding atomic densities. This method can be accomplished almost regardless of the thickness of the material (Ketelhodt, L. & Bergmann 2010).

Two tons of screen fractions -40+20 mm from the Witbank coalfields were tested to remove shale using a Commodas PRO Secondary XRT belt 1200 sorter, which can handle screen fractions -60mm +10mm at 40 to 50 t/h. A 55 kW compressor with an operating pressure of 8 bars was used to operate ejecting system. Combined results from three different size fractions showed that shale can be removed in 20.4% as waste from mass feed.

The same system was used in Wedel, Germany. A half of tonne of lignite sample collected from various collieries in Texas, USA was tested to remove pyritic sulphides and associated mercury to produce clean power station lignite. Although the experimental results show that DE-XRT sorting can effectively remove and reduce pyritic sulphur in lignite, the optimal cut-off settings need to be determined to maximize the pyrite removal.

Similar technology was used by Kuliman (2006) and this work presents results on the efficiency of sorting using a variety of coal samples. Zinc and led ores also showed promising results and this detection is described by de Jong (2005).

2.1.3 Near infrared

Reflectance spectroscopy is used to detect mineral like talc, which is a problem for the flotation process. Continuous measurement of these properties are now possible with new near-infrared (NIR) systems mounted over-the-conveyor belt. Goetz *et al.* (2009) tested this system and developed predictive models for concentrations of swelling clays, kaolinite, muscovite and biotite. This is achieved with conveyor samples of copper ore using "QS-8000" over the conveyor system. The results were precise enough to be used for real-time, process decision making.

The system "QS-8000" is capturing high quality reflectance spectra of materials moving on a belt. It is composed of: illumination, spectrometer and a switch gear box which includes an I/O card, power supplies, communications and thermal control. Its head illuminates an 18 cm diameter spot on the conveyor material. Problems with dust they resolved with build in air knife over the illumination head window.

Measurements were made on 45 copper ore samples. The study showed that these minerals can be quantified, in particular swelling clays to ±0.5% using an on-line system that views ore moving down a conveyor. Now the metallurgical process, chemical and energy usage can be optimised by providing real-time analysis of mineral concentration and chemical properties, parameters associated with processes such as agglomeration and flotation may be determined continuously.

RWTH Aachen University was involved in research project sponsored by Anglo American in 2008 to test near infrared spectroscopy (NIRS) and establish sorting potential for Skorpion mine. For this mine located in Namibia which has an annual production of 150 000 t/a of super high grade pure zinc there is economic potential to upgrade current sub economic material including the marginal dump (over 2 000 000 tonnes), average grade of 2.5 per cent Zn by implementing near infrared spectroscopy. This opportunity came from zinc bearing minerals such as sauconite, hemimorphite, smithsonite, and hydrozincite, which display diagnostic responses in the near-infrared

spectrum. Ore bearing minerals can be identified through three major absorption features in the NIR. The reflectance comes from OH and H_2O molecular bonds. Non zinc bearing clay minerals, calcite and impure quartz does not exhibit these characteristics which can be used to distinguish from economic minerals (Robben et al. 2010).

In comparison with DE-XRT, near infrared spectroscopy is a surface measurement technology. Test work was conducted with PolySort (sorting system) build by TiTech which needed to be trained with pre classified samples. Statistical means were calculated for chosen groups and integrated in sorting algorithm.

The samples were scanned perpendicular to the conveyer belt in a line. The wavelengths in the NIR were used to decide which rock type group the material belonged too. For this test work the group which represents the gangue waste material was removed by compressed air activating air valves. The classification result was improved by using a filter enhanced the scan point around the neighbour of the particle. The software was configured to suppress ejection in a neighbourhood if ore material was detected, to receive a high recovery. The PolySort was successful in identifying 77 precent of the right rock types. With this identification rate it was able to recover 85 precent zinc ore of the 46.4 precent for the marginal dump material and a mass pull of 71.1 per cent for the pit samples (Robben et al. 2010).

The results presented a link between zinc grades and spectral response in the wave length region from 2210 to 2345 μm. The research project demonstrated that use of near infrared spectroscopy for sorting zinc ore in Skorpion mine can work with further technology improvements.

The Commonwealth Scientific and Industrial Research Organisation (CSIRO) was developing sensor technology for ore sorting and mineral characterisation using laser reflectance. Mid-infrared reflectance measurements using a DPSS Optical Parametric Oscillator (OPO) for on-line determination of mineralogy for ore sorting and characterisation was described by Death, Pollard and Rogers (2005). The visible spectrum (VIS) frequently does not provide sufficient contrast to reliably differentiate

ore from gangue. The monitoring of only discrete spectral bands can help improve contrast between ore and gangue. This can be done by either filtering reflected light or using a particularly bright source such as a laser. Two or more carefully selected discrete spectra can be monitored to determine the surface mineralogy of a particle. Talc was used as an example because the visible reflectance spectra of mineral talc are broad and vary considerably with the mineral source. This complicates development of a generic sorting technique for talc using colour only. However, the near infrared spectra of talc show much more structure, with the OH absorption bands around 1390μm of talc distinct from the associated gangue. This can be used to increase sorting efficiency and shows yet another sensor application in mid-infrared spectrum.

2.1.4 Optical-Photometric

Very successful photometric systems were developed from early 1970s for South African gold mines. Keys, Gordon and Peveret (1974) gave an overview of high-throughput, multi-stream photometric sorting machine.

The Photometric Sorter which separates rocks into two categories according to light-reflectance properties was tested on Witwatersrand ore (which is normally referred to as reef). The “accept” category in the case of the Doornfontein machine, includes those rocks having higher reflectance properties, distinguishing them from surrounding darker matrix which is recognised by the machine as reef. In the reject we also have either quartzite ranging from light green through olive green to nearly black or tuff. In this ore deposit gold is associated and occurs mainly with a lighter phase which is accepted by this ore sorting machine (Keys, Gordon & Peveret 1974).

Sorting machine Model 13 was designed to handle rocks in size fractions -80+30mm at rates of 45 to 65 tonnes per hour depending on particle size. Particles were fed continuously to a conveyor belt with random distribution in such manner that there was evident space between particles. The conveyor belt was introduced to scanning zone where information for each particle concerning its size, light-reflectance pattern, and location on the belt was obtained. After the scanning zone an instant decision to accept or reject particle was made and air blast was applied by solenoid-operated valves to accepted rocks to separate them from the rest of the stream. For the same

model they listed operating requirements. Most of the requirements were regarding compressed air, electricity, air and water. It was determined that the amount of compressed air required is a function of the size of the rock being sorted. For a typical case to blast one tonne of material it would require $35m^3$ of air. For example to accept 28 precent with a feed rate of 20t/h the air requirement would be approximately 500m3/h, but it was also commented that requirements should be doubled to compensate for short term fluctuations in feed rate or percentage accepted. Electrical requirements for the sorting system were around 15kW including vibrating feeders. This did not include any other electrical consumption. Clean water was listed as requirement to feed the wetting sprays over the secondary feeder which consumed 15l/s. (Keys, Gordon & Peveret 1974)

For the maintenance they pointed that half of the cost went to white sorter belts which needed to be replaced. The blast manifold was another item subject to wear. Its costs were reduced by removing sine sand which acted as a scouring agent and use of replaceable blast slot inserts fabricated from polyethylene. Laser tubes, mirror drum and circuit boards also needed to be replaced.

The reef picking operation managed to accomplish 31 precent of the run-of-mine material was being sent to the storage dump. Therefore the mill feed was upgraded from 10 g/t to some 14 g/t it also reduced tonnage by 53,000 t per month at 1.7 g/t of gold contained some 5 per cent of the gold in the run-of-mine material (Keys, Gordon & Peveret 1974).

The opto-electronic ore sorting was implemented by Tanzanite One Mining Ltd to concentrate coloured gemstones. The summary of this optical sorting was given by Ketelhodt and Jacobs (2006). System met the production requirement for which it was developed, 80% purity with a 98% recovery rate was being accomplished.

Crushing and screening process reduces material to -30mm size fraction before it is sent to dense media separation. Sinks are collected and screened on a triple deck Sweco washing screen, so that the feed for the sorting machines is in a size range ratio

of not more than 3:1. The washing of the feed material is very important as it removes all the dirt and dust off the particle and reviles their colour for optical sensors.

Sorting then is performed by two MikroSort ConcSort BSX-063 machines using 0.6 metre wide pan feeders. The first machine is used for larger size particles (-30 mm +12 mm) with a processing rate of 240kg/h. The second machine is used to simultaneously sort two different sizes. The first track is used for size of -12 mm +5 mm with a rate of 210kg/h and then the second track is used for size -5 mm +2 mm with a rate of 150kg/h. The finer material was treated with hot air blow onto the feeder to reduce lumping of the feed material. It was discovered that the lumping of feeder material reduces the sorting efficiency in this size range. Larger material (+5 mm) was fed and provided to the sorter in a drip-dried condition, as the moisture on the stones enhanced the natural colours of the ore (Ketelhodt, L & Jacobs 2006).

The total power requirement for the sorting plant is approximately 60 kW, the belt speed of both sorters are set at 2,75 m/s and compressor station is set between 4.5 and 7.4 bar.

In sorting it is good practice to test existing systems for their performance which is usually done with tracers. This work was described by Kleine and Wotruba (2010) and carried out in the mine Tirisano in the Republic of South Africa. The optical sorting plant had two sections: the screen and the containerised optical sorter. Test work was done after two months of full reliable operation, which provided good work flow and enabled for test to be performed under real production conditions. The target of this test work is to analyse the effectiveness of an optical sorter under real production conditions. The sorting algorithm was adapted to achieve the highest possible recovery.

To assess the efficiency of selecting diamonds, two sets of tracers were used during the test work. The main interest was to investigate possible losses within the smaller size ranges as discovered with the first test work. For the coarser particle size (- 25 + 8 mm), a set of 30 quartz particle tracers in the size range - 9 + 7 mm were used. The finer particle size used a set of 50 quartz and glass particle tracers in the size range -4

+ 2mm. The increased amount of tracers in the smaller size fraction, were chosen to achieve better representativeness of results as greater losses were expected. All tracers were marked to avoid mistakes in identifying them in the process of sorting. (Kleine & Wotruba 2010)

A test procedure was done with same settings of the sorter as for normal operations. Results showed that the tracers with size range - 9 + 7 mm were fully recovered through all throughputs while tracers with smaller size range - 4 + 2 mm had decline in recovery reaching 80%. The feed rates were from 5 t/h to 22 t/h, with 22 t/h being the maximum possible rate for the installed system. At 24 t/h dedusting system was not powerful enough to keep the detection area free of dust.

The work with tracers confirmed that optical sorting on the base of transparency can adequately be used to recover diamonds. This opened possibility to detect low or non-luminescent diamonds from XRF sorting tailings as well. After this evaluation the following feed rates were chosen:

- The coarse fraction -25+8 mm feed rates was 20t/h providing a recovery of 99 precent.
- The finer fraction -8+2 mm feed rates was 17t/h providing a recovery of 88 precent.

This sorting process has been applied to sort alluvial recovery tailings in South Africa and with a future implementation on recovery tailings of a primary deposit in Lesotho (Kleine & Wotruba 2010).

The disadvantage of this type of sorting is that it usually needs cleaning of the material to remove dirt and dust off the particles in order to revile their colour for the sensors. In addition there is not strong relation between copper grade and the colour of the minerals associated with copper mineralisation.

2.1.5 Beat Frequency and Induction Balance

At the beginning of 1980s, work of Nash and Schwaneke (1978) (cited in Sivamohan (1991)) used technique known as “beat frequency” or “induction balance” to sort copper bearing ore.

A laboratory unit used this induction balance technique which was developed by The Bureau of Mines, USA. The unit was tested on upper Michigan ore size (-2.5 to +1.3cm) and particles of sorted portions contained native copper or 80 precent copper. The sorting process rejected 80 precent of the original feed. The same process for coarse fragments (-10 to +5 cm) resulted in higher copper recoveries, with about 60 precent of the ore being rejected. The characteristic of the beat frequency technique is that it is using a high frequency alternating current to energise a detector. When an ore fragment with a conducting material passes through the detector it reacts with the electrical field which changes the frequency. Variation in frequency is used to identify highly conductive rock fragments. The International Sorting Systems Corp (ISSC) tested this approach with beat frequency technique by developing a sorter. The system was tested with a goal to separate out the native copper bearing ore fragments. Copper was recovered in 61 precent of the feed, which had 13 precent of conglomeritic type of native copper from Michigan ore. Successful results were found only with sizes between -100 mm to +12 mm ore fragments. In 1970 the ISSC installed a 100t/h sorting plant in Michigan to sort the material with a native copper content (Sivamohan & Forssberg 1991).

2.1.6 Thermal Identification of Rocks by Microwave Heating

Microwave heating is directly connected to the dielectric properties of materials which can give information about their heating capabilities. This interaction is accompanied with amplitude and phase shifts in the electromagnetic field which can be measured. Information gathered from microwave attenuation then can be used to affiliate certain characteristics of rocks and make a decision regarding their sortability.

Another approach is microwave heating accompanied with infrared imaging of rocks during or immediately after microwave exposure. In infrared spectra heat flux became visible on the surface. This is a great advantage because heat flux is carrying information from the composition and overall volume of the particle which is then reflected on the surface. Temperature difference from the surface of rock particles is then used to calculate a threshold for sorting.

During the 1980s Slater, Nordin and Downing (1989) used microwaves to sort rocks on the principle of microwave attenuation for discriminating rocks. Their work is described and reviewed by Sivamohan (1991) who commented the following points:

- Microwave sorting process for discriminating diamond containing kimberlite from gabbro was developed. It was upgraded from a laboratory to a full scale prototype plant of 100t/h.
- The full scale model used already existing radiometric sorters 'Model 17' by replacing the scintillation counter sensing system by the microwave attenuation system.
- The transmitter used a frequency of 10.525 GHz and low power of 100mW.
- The rock particle separation system which used compressed air in the 'Model 17' was replaced with pulsed water ejectors.

2.2 Summary

For all sorters it is possible to identify five processes which are necessary for them to operate and these are: preparation, presentation, inspection, data analysis and separation. Their consecutive flow is described in Figure 2-1 presenting material flow in a full line and data flow in broken line.

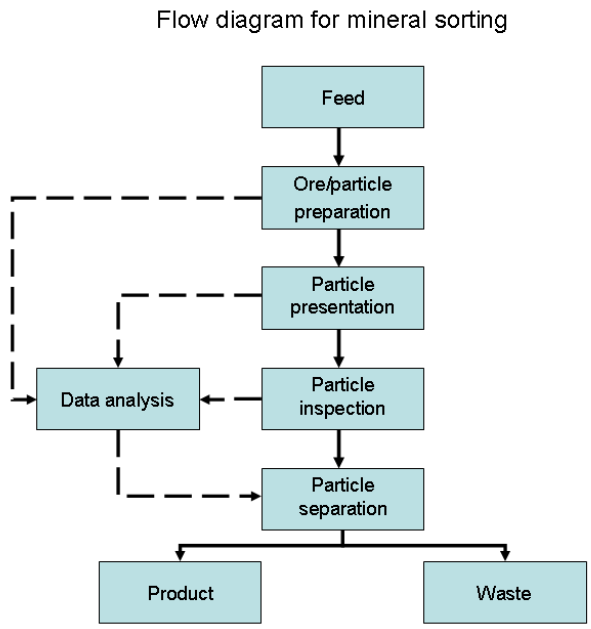

Figure 2-1 Operational processes in ore sorting based upon Cohen (2000) and Salter and Wyatt (1991)

Data analysis is the most important process because it is established on sorting algorithms which have to be robust enough to include all factors which influence sorting quality during a full scale sorting operations. The work and observations of Cheesman (2006) classifies these factors into two major groups.

The first group is environmental and geological and involves:

1. **Mineral characteristics:**
    a. Breakage characteristics
    b. Friability
    c. Weathering and oxidation
2. **Ore body (Dump) characteristics**
    a. Interlocked and contact pieces
    b. Variation in feed composition (geological) and grade
        i. Rock types not classified by algorithm
        ii. Variation in percentage to be rejected
    c. Variation in fines content in feed
    d. Presence of foreign objects (tramp) in feed

The second group refers to factors which came from design, equipment and plant operation:

1. **Feed preparation:**

a. Foreign object, tramp removal
b. Crushing:
    i. Liberation
    ii. Size distribution
c. Screening:
    i. Slimes and fine mud management
    ii. Screening efficiency

2. Mechanical setup:

a. Wear
b. Valves
c. Dust management
d. Algorithm robustness
    i. Extremes in temperature
    ii. Feed variations
    iii. Double sided sorting
e. Feed presentation and ejection:
    i. Rock condition: moisture, coatings and slimes
    ii. Breaking monolayer
    iii. Bouncing, spinning
    iv. Light quality

From data obtained from full scale operational sorters it is feasible to set some guidelines for the processes in sensor based mineral sorting. For the process of ore/particle preparation it is possible to say that suitable liberation is required and that rejecting 30% of mass feed will be economically justifiable for most sorting operations Cohen (2000). Screening into a narrow feed size range which is 3:1 top to bottom will be acceptable for most of the sorting algorithms. It is also possible to say that the most common throughputs for sizes -120 mm + 60 mm are 85-100 t/h while for sizes -60 mm +30 mm on average treats 30-40 t/h. In the case of Tirisano mine in the Republic of South Africa work of Kleine and Wotruba (2010) feed rates were from 5 t/h to 22 t/h, for size rates -9 + 7 mm.

The process of particle presentation usually involves vibrating belt feeders specifically designed conveyor belts (with channels or material properties) in conjunction with chutes or stabiliser wheels to provide closely positioned streams of

particles in one layer. Typical speeds for conveyor belts are from 2 to 6 m/s. An alternative to conveyor belts are systems which are designed to inspect and sort particles along a predefined falling trajectory. These systems are good for inspecting multiple sides of rock particles.

Data analysis is directly connected to the process of inspection of the particles. It includes data feedback from particle preparation, particle presentation and incorporates all information from factors which influence sorting quality. The process of inspection is the most significant process for successful sorting and it is performed in real time. Performance of algorithms and inspection processes can be improved by testing systems with tracers or developing new sortability methods to set specific thresholds. Most identifiable problems come from signal to noise ratio, poor resolution or inadequate surface details identification.

From the 1970s mechanical and hydraulic systems had been used for the separation process but none of them had better performance than water and air jets, ejecting particles from conveyor belts or from their predefined falling trajectories. For higher throughputs compressed air is technically a much better option. The ejector valves can respond in milliseconds and the time blast can be easily adjusted to correspond to chosen size fractions. Usual compressed air consumptions are between 5 to 35 m^3 per tonne of feed, but capacity requirements should be double, to compensate for short term fluctuations in feed rate or percentage accepted.

Giving guidelines for economic aspects is very challenging because for every ore type potentially there should be a discriminative technique which can be used for sorting with more or less success. Costs of actual testing, or testing under pilot plant conditions can be significantly reduced if suitable methods to establish the sortability of ores could be applied. So, there is a need for methodologies which can be used for testing lots of different ore types without major investments. These methods can give us insights into which ore types will have best response to specific sorting technology. The bottom line is, whether the pre concentration can produce enough profit after all long and short term costs are calculated. These costs can include installation costs, operating costs, spares and maintenance costs, labour and operator costs.

2.3 Experimental Studies of Microwave Heating Minerals and Studies for the Utilisation of Microwave Energy in Mineral Industry

The interest in to the microwave heating of natural minerals started with research for the application of microwave energy in mineral industry. Early work in this field was focused on heating rates of selected groups of minerals exposing them to set power levels and set exposures times. This was a very basic and fast approach which could group minerals in three essential groups. These groups are: minerals which heats very rapidly, minerals which have good response to microwave heating and minerals which appear transparent or heat very slowly. This was also an indirect way of measuring dielectric properties.

A descriptive study in this manner was performed by Chen *et al*. (1984) where he had exposed 40 minerals to microwave radiation at 2.45 GHz and various powers and gave descriptions of observed changes. This work located carbonates jarosite-type compounds, silicates, some sulphates, fergusonite, monazite, (low Fe) sphalerite, and stibnite in the group which did not heat well after exposing them to 5 min and 150 W of microwave power. The second group was mostly made of oxides and uranium minerals. Most of them did not go under changes and some of them like cassiterite, hematite and magnetite had very good heating response. The third group had sulphides, sulphosalts and arsenides which heated very rapidly and some of them fused during heating. For some of those minerals the heating response is given in Table 2-3.

Table 2-3 Heating responses of various minerals after 3-5 min exposure time, sourced from (Chen et al. 1984)

Mineral	*Power (W)*	*Heating Response*
Arsenopyrite	80	Heats with some sparking
Bornite	20	Heats readily
Chalcopyrite	15	Heats readily with emission of sulphur fumes
Galena	30	Heats readily with much arcing
Pyrite	30	Heats readily with emission of sulphur fumes
Pyrrhotite	50	Heats readily with arcing at high temperatures
Sphalerite	>100	Does not heat

Research was continued by Walkiewicz *et al.* (1988). He expanded testing on more than one hundred compounds and nineteen minerals using a 2.45 GHz a commercial microwave oven and 1kW of microwave power.

Both of these studies are important because results obtained showed that minerals of value will absorb microwaves whereas common host rock minerals are poor heaters. This valuable information guides us to microwave assisted sorting. It can be argued, at this point, that during crushing and sieving to a chosen size we can expect two sets of populations of particles. First population has three groups which all include minerals of value whether they are fully liberated, partially liberated, or still interlocked within host rock minerals. Second population will be rocks which are entirely composed gangue minerals.

Table 2-4 Effect of microwave heating on the temperature of natural minerals, sourced from (Walkiewicz, Kazonich & McGill 1988)

Mineral	***Chemical Composition***	***Temperature(^oC)***	***Time (min)***
Albite	$NaAlSi_3O_8$	69	7
Arizonite	Fe_2O_3*3TuO_2	290	10
Chalcocite	Cu_2S	746	7
Chalcopyrite	$CuFeS_2$	920	1
Chromite	$FeCr_2O_4$	155	7
Cinnabar	HgS	144	8.5
Galena	PbS	956	7
Hematite	Fe_2O_3	182	7
Magnetite	Fe_3O_4	1258	2.75
Marble	$CaCO_3$	74	4.25
Molybdenite	MoS_2	192	7
Orpiment	As_2S_3	92	4.5
Orthoclase	$KAlSi_3O_8$	67	7
Pyrite	FeS_2	1019	6.75
Pyrrhotite	$Fe_{1-x}S$	686	1.75
Quartz	SiO_2	79	7
Sphalerite	ZnS	88	7
Tetrahedrite	$(Cu,Fe)_{12}Sb_4S_{13}$	151	7
Zircon	$ZrSO_4$	52	7

If microwave energy is applied to both populations of rock particles the temperature difference between them can be expected. This temperature difference can be quickly measured in infrared spectra from the surfaces of rock particles and used as a sensor based discriminative technique. It needs to be noted that for these studies minerals of value were associated with minerals which contain commercial metals such as copper,

molybdenum etc. This association cannot be used for the gemstones such as diamond, which can have a very low microwave loss, as seen in work of Slater, Nordin and Downing (1989).

Patent by Djordjevic (2007) explored this detection method in more details. Considering that the host rock minerals have natural variations which can cause variation in temperature difference more detailed studies of dielectric properties which influence heating are required. This necessity to predict heating behaviour led to a second approach which was more difficult and involved measuring complex permittivity.

In the past two decades interest in developing new approaches to reduce energy necessary for mineral liberation grew along with demand for industrial minerals and energy. Grinding mills and crushers are designed to use large amounts of energy in order to liberate minerals from the gangue which can be processed further for concentration. Demand for the energy becomes even more evident for processing of low grade ore which can require finer grinding to free valuable minerals. To improve efficiency of crushing and grinding it is possible to either make optimisation and improvements in existing technology or use new technology to treat ore where energy transfer is more efficient.

Thermally assisted liberation caused by microwave volumetric and selective heating has been used to investigate reductions in ore strength. This can potentially reduce energy needs for comminution and liberation by initiating fracture along minerals, which have tendency to heat very rapidly when placed in strong electromagnetic fields, and gangue minerals. The potential of this technology lies in efficiency of energy transfer and selectivity of microwave heating. Ore treated in this manner would have reduced strength and therefore be more economic by decreasing costs for crushing and milling.

The economic aspects of considerations for the commercial microwave processing of ores were presented by Bradshaw *et al.* (2007). It is concluded that there is a critical power density (~ 10^9 W/m^3 for absorbing phase) below which microwaves will not

efficiently fracture an ore and that very high power densities combined with short residence times will be economic. For the pilot plant scale-ups it was concluded that using pulsing systems with detailed mineralogical investigation and expertise in mineral processing will give the most promising results.

A very detailed study was done by Kingman *et al* (2000) on four different types of ore: Norwegian ilmenite ore, a refractory gold ore from Papua New Guinea, a sulphide ore from Portugal and an open pit carbonatite ore from South Africa. Microwave treated ore was tested to examine improvements in grinding. Tests were done using multimode oven with constant power and different time exposures. Changes in Bond Work Index (the energy input required to reduce the size of feed material from infinite size to a set size) were presented as a function of different time exposures. Best results were achieved with ilmenite and carbonatite ores which had several good absorbers surrounded with gangue material which did not heat very rapidly. A mineralogical investigation identified these minerals to be coarse grains of magnetite (excellent heater) and ilmenite (good heater) in a plagioclase (poor heater) as matrix. The refractory gold ore which contained finely disseminated pyrite grains in K-feldspar and quartz gangue did not show significant changes in the Bond Work Index. The study also concluded that small particles which are finely disseminated in discrete elements respond poorly to microwave treatment resulting with small reductions in required grinding energy. It was suggested that for effective microwave treatment, ores should have a consistent mineralogy and a good absorber of microwave radiation in a transparent gangue matrix.

This work was continued by Vorster (2001) who used a similar approach on the massive copper and copper-zinc ore form Neves Corvo, Portugal and Mambula ore from South Africa. Samples of the ore approximately similar mass (0.5 kg) were treated with microwave energy at 2.6 kW and 2.45 GHz for different time durations. The samples were then grinded to approximately $P_{80\%}$ passing the 53 μm sieve. The experimental results showed up to 70% reduction in the Bond Work Index for the samples treated for 90 seconds. The Mambula ore which had good heaters but a different matrix composition only showed a reduction in work index of 26% after 90s exposure at same power levels.

A study which involved both types of microwave cavities multimode and single mode was carried out by Cumbane (2003) on Palabora ore from South Africa and Zinkgruvan ore from Sweden. The study was complemented with measurements of dielectric properties for sulphides, oxides and silicates. These minerals were present in tested ore as well. The results showed that for Palabora ore exposed in a single mode cavity were higher electric fields were achieved, liberation of copper sulphides on coarse size was much better than for Zinkgruvan ore where sphalerite and galena finely dispersed in feldspar did not undergo to same effect.

Palabora copper ore was also tested by Sahyoun (2004) in two different cavities. First was Panasonic II 2600 multimode microwave oven where three different power levels and time exposures were used. To enhance development of micro fractures all microwave treated samples were quenched in water and then dried overnight at a temperature of 65 ^{o}C. The second cavity was single mode, a rectangular industrial cavity excited at 2.45 GHz by a Sairem 15 kW microwave generator. This time exposure time was constant for 0.5 seconds and four different power levels were used to create the base line for testing. Tested sample in the first instance was purified of dolerite in order to see how sensitive the Palabora ore is to microwave treatment. In second sets of tests dolerite was present which represented a more realistic material in the plant. For the first oven the decrease in the comparative Bond Work Index from 1306 kWh/t to 5.6 kWh/t was noted, with a slight increase for the longest time exposure. For the second oven the largest increase was for the first exposure time for the two different powers applied. It was reported that dolerite was not affected by microwave treatment.

A low grade copper ore from Palabora was again subjected to microwave treatment where ore strength was tested using laboratory rod mill by Scott (2006). Although his study was based on energy inputs that do not make the process cost effective he also reported ore weakening after microwave treatment.

A study by Kobusheshe (2010) involved experimental work to demonstrate the occurrence of microwave induced fracture in ores containing hydrated minerals and

examine the mechanisms under which it occurs. He also highlighted limitations of the microwave system used which was single mode cavity. Reflected power fluctuated and could not be easily maintained, because it was dependent on the packing density of the batch sample and the dielectric properties of the ore, all of which varied from one batch sample to another. The results presented that significant micro and macro fractures were observed in ores segments where good heaters of microwave energy were located, such as metal oxides and sulphides. It also appeared that damage was located in certain mineral phases where dehydration ore was undergoing.

The influence of modulated microwave energy on copper ore breakage was investigated by the Author of this thesis. The work was published as a study relevant to the thesis but not forming part of it. This approach to power delivery was applied to ascertain whether the strength of porphyry copper ore, which originate from Rio Tinto's Bingham Canyon mine operated by Rio Tinto's Kennecott Utah Copper Corporation (marked by the mine as Low Recovery Ore - LRO), can be reduced with lower average modulated power levels then using continuous power. Changes in resistance to breakage of the treated and untreated ore were quantified by comparative drop weight tests. Mineralogical investigation for the ore was carried out with the Mineral Liberation Analyser (MLA) for the surface identification of minerals and X-ray tomography for volumetric analysis. The comparative drop weight tests showed that material treated for 5 s at 5 kW of modulated power was weaker than untreated material. However, this degree of breakage which was achieved could be achieved with substantially less mechanical energy. It is very possible that using higher microwave power, better liberation results then using conventional methods can be achieved.

In recent year's work of Weert and Kondos (2007) and Weert *et al*. (2009) was focused in testing various sulphides ores in order to identify what kind of conditions would be beneficial for potential microwave/infrared sorting measuring their temperatures. Research work was supported by Barrick Gold Corp. Test work was conducted on five different ores, with the main focus to identify temperature thresholds for three groups: cold, medium and hot. The first two were tested using a

domestic microwave oven with 1.1 kW and afterwards assayed for molybdenum and sulphur.

The ore type from Malmbjerg deposit located in Eastern Greenland was tested one rock at the time placing them in the middle of the microwave oven turntable. Temperatures were tested immediately after microwave exposure for 60s. Rocks which temperature reached up to 75^{o}C were considered to be cold, medium group was between 75 ^{o}C and 135 ^{o}C and all rocks with temperatures above 135 ^{o}C were characterised as hot. The assaying results showed that the hot group indeed had a sixfold increase in the content of molybdenum. Sulphur presented a similar trend.

For the second ore type which came from Spinifex Ridge in the East Pilbara region of W. Australia the testing procedure was changed. The rocks were much smaller, so three rocks were placed at the centre of the microwave oven. Rocks were heated for 30s and maximum temperatures were from 29.2 ^{o}C to 180 ^{o}C. The assaying results showed lower molybdenum grades comparing to previous ore type with increased distribution in the hot group. This indicated that cut-off grade rocks can be transformed in much higher grade by sorting.

For the next three ore types new type BP-110 of microwave oven was used (manufactured by Microwave Research and Applications). The cavity floor of the microwave oven was mapped using a 25-point grid which was used to place rocks in predefined positions in the volume of the multimode cavity. Rocks for two ore types were heated up for 30s.

The ore from Mineral Park, Arizona, USA had two samples called “fresh ore” and “leached ore”. After testing both samples they were divided in three groups with two thresholds 50 ^{o}C and 100 ^{o}C. Rocks from each of these groups were crushed, riffled and assayed. Final results revealed that there is minor segregation of molybdenum and copper in all three groups. Molybdenum appears more evenly divided in Mineral Park ore, making upgrading by MW/IR sorting less promising.

A Canadian sample from Mount Polley was tested in the same manner as the ore from the USA with the only difference being that the rock particles were smaller in size. Assaying was performed for copper, silver, gold, iron, molybdenum and sulphur. For this sample, microwave infrared sorting responded most likely to chalcopyrite because iron content did not follow the sulphur content to suggest pyrite. Gold and silver distributions in three groups followed the copper contents. Maximum temperatures for this ore sample were from 30 ^{o}C to 150 ^{o}C.

The last ore type tested came from Mexico and was provided by Castle Gold from Canada. Sorting testing was performed on 100 rock fragments and microwave exposure time was changed to 20s. For this sample, copper and gold contents were concentrated up to 5 and 6 times which made group "hot" very economic for further processing.

Work of Weert and his colleagues is important because it identifies the necessity to establish suitable methods to test the sortability of ores using microwave/infrared detection. On the other hand this work lacked consistency in testing. Samples were tested under different conditions and there were no clear comments regarding influences of mineral textures, chosen time for the exposure or microwave power applied.

2.4 Summary

All these studies are very important because they support the concept of selective heating and provide good starting positions which can be used for study of the microwave assisted infrared sorting. The following conclusions can be made from reviewed literature.

The investigation of mineralogical composition and textures can help to design and optimise a process for discrimination. Applied powers for microwave sorting can be significantly lower considering that some particles had an excellent response to heating even with non-economic power levels for microwave liberation. Breakage is most effective when high microwave power is applied for a short time which causes differential stress between mineral phases. For the same load lower power and longer

time will also produce localised heating which can be used to identify particles which have possible content for sorting. The design of the cavity is important because all microwave systems have existing feedback between load and microwave generator which needs to be tuned in order to deliver maximum energy transfer. The way in which the material is presented to the electric field also plays an important role. This refers to whether the particles are exposed to electric field in packed layers, in one layer with spacing between them or presented individually without the influence of other particles and their overall bulk properties. There is an upper limit to the particle size, related to the penetration depth and exposure time required for heating. Systems can be redesigned to obtain more information during particle presentation to detectors and microwave exposure. For microwave heating and sorting there is a strong need for standardisation and determination of dielectric properties of minerals.

Chapter 3- Theory of Microwave Heating and Experimental Methodology

3.1 Introduction

The main aim of this chapter is to provide an overview of the nature of volumetric microwave heating, materials interactions with microwaves, complex permittivity of minerals, followed by physical properties of minerals. An insight into these topics will provide a theoretical approach to closer define favourable cases for microwave sorting. In detail the microwave processing systems will be discussed including a design of a travelling wave applicator, specifically designed for this study. Furthermore, this chapter describes the experimental approach adopted to investigate the hypothesis of this thesis. Descriptions will be presented for the procedures for detailed experimental investigations, including procedure and techniques used for the mineralogical characterization of ores.

3.2 Electrical Volumetric Heating

Conventional heating is processed through heat transfer that can be defined as the transfer of energy across a system boundary caused solely by a temperature difference, most commonly comprised of conduction, convection and radiation or their combinations (Thomas 1999). A simple example would be a heating object enclosed in the oven and surrounded by heating elements. For this case, energy is transferred with gradual heat flow from a heating source to a heating object. Physical properties of material such as specific heating capacity, thermal conductivity, density and initial temperature will govern the heating rate. During the process of heating, on

the surface of the heating objects, corners and edges will have higher temperatures then inside of the object as they are longer exposed to a heat flux.

The electrical volumetric heating provides some advantages over conventional heating, like: quick start up and stopping, reduction in processing times, material selective heating and rapid heating rates. These advantages come from interaction of electromagnetic energy with dielectric materials. Meredith (1998) comments that by electrical means, volumetric heating is possible where in all the infinitesimal elements constituting the volume of a load are each heated individually, ideally at substantially the same rate. The heat energy injected into the material is transferred through the surface electromagnetically, and does not flow as a heat flux, as in conventional heating.

According to the authors Metaxas & Meredith (1983), Feher (2009) and Schubert & Regier (2005) heating by electromagnetic energy occurs at molecular or atomic level and is due to a combination of: electronic polarisation, atomic polarisation, dipolar polarisation and interfacial polarisation. Any dielectric material can be heated to some extent by electrical volumetric heating provided that it is neither a perfect electrical conductor nor a perfect insulator (Meredith 1998). The dielectric materials can be characterised through physical properties such as conductivity and dielectric constant (which will be introduced later in more detail).

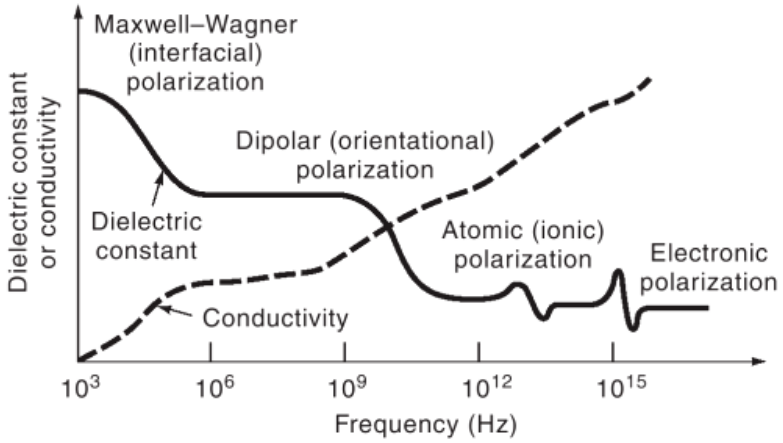

Figure 3-1 Dielectric dispersion for various types of polarisation, after (Dyer 2001)

Figure 3-1 illustrates the dispersion of a dielectric constant and conductivity that may be observed in materials in the frequency range 10^3 Hz to 10^{15} Hz. For some materials at certain frequencies a particular type of electronic polarisation may become more

dominant than others, which will be mostly defined by physical properties of that material.

It can be considered that conversion of microwave energy into heat, a process that involves interaction between microwave fields and the conductivity or dielectric properties of the material. Considering that electromagnetic field has electric and magnetic component same analogy can be applied to magnetic component. The complex permittivity is a measure of the ability of a dielectric to absorb and to store electrical potential energy. The real component or the real permittivity (ε') characterize the penetration of microwaves into the material, and the loss factor (ε'') indicate the material's ability to store the energy.

"Since, with most dielectric measuring techniques, it is difficult to separate the losses due to conduction from those due to polarisation, all form of losses can be grouped together, thus defining an effective loss factor ε''_{eff} given by:

$$\varepsilon''_{eff}(\omega) = \varepsilon''_{d}(\omega) + \varepsilon''_{e}(\omega) + \varepsilon''_{a}(\omega) + \varepsilon''_{MW}(\omega) + \sigma/\varepsilon_{o}\,\omega \quad (3\text{-}1)$$

where the subscripts d, e, a and MW refer to dipolar, electronic, atomic and Maxwell-Wagner respectively." As remarked by authors Metaxas & Meredith (1983).

For the ore particles it is also important mentioning depolarisation factors. They can be taken into consideration both from the macroscopic level (caused by the different shapes of the ore particles) and the microscopic level (the geometries of the various mineral phases present). The electric field within a dielectric particle will be lower than the applied field by depolarisation, caused by the generation of polarisation charges at any boundary between different dielectric media whose surface is perpendicular to the applied field. The net field inside the sample is thus reduced, while the field outside the sample remains the same.

In the general case the ratio of the electric field inside the workload to that in the surroundings lays in the range 1 and 1/ε'; generally and in practice it is a variable function of position within the workload. For the special case of sphere embedded in

otherwise uniform electric field (in air), the internal (E_2) and external (E_1) fields are related by: $E_2 = \frac{3}{2+\varepsilon'} E_1$ (3-2)

as interpreted by Meredith (1998) and sourced from Stratton (1941).

When depolarisation factors are large, the electric field inside the sample could be reduced to zero. The sample is then completely shielded from effects of the microwaves. To avoid this, surface charges must be reduced. This could be accomplished by placing the tested sample parallel to the electric field. A lot of mathematical approximations can be found in literature for depolarisation factors of regular shapes however, yet for material such as ore particles where are large variability of textures and shapes of particles it would be beneficial to obtain these approximations empirically. The best empirical approach to identify and approximate these depolarisation factors is out of the scope of this experimental research.

The microwave radiation is the term associated with any electromagnetic radiation in the microwave frequency range of 300 MHz–300 GHz. International convention dictates that microwave ovens (and other industrial, scientific and medical microwave applications) operate at specific frequencies. The most preferred frequency for microwave ovens is 2.45 GHz which came as a compromise for the heating of water-containing foodstuffs; there has to be significant dielectric loss but at the same time the electric field has to penetrate the sample. At this frequency the electric field swings the orientation of water molecules 10^9 times every second, creating an intense heat that can escalate very quickly (depending on the volume of the load) (Lew et al. 2002).

3.2.1 Calculation of Power

Energy [J] is usually defined as a capacity to do work and it can be stored in many ways. However, power [J/s=W] is the time rate of dissipation of energy. As Meredith (1998) has remarked: “In principle, with volumetric heating the average temperature of the workload continues to rise as long as power is applied, irrespective of the temperatures of oven walls or the air inside the oven”.

In the work of Metaxas & Meredith (1983) the following calculation for the average power which refers to the power density inside the material can be found:

$$P_{av} = \frac{1}{2}\omega\varepsilon^{"}\varepsilon_0 \int_V \left(E^* \cdot E\right) dV \qquad (3\text{-}3)$$

In special cases, where the electric field can be assumed constant, attains the more familiar form, using $E^* \cdot E = E^2$

$$P_{av} = \omega\varepsilon^{"}\varepsilon_0 E_{rms}^2 V \qquad (3\text{-}4)$$

Substituting ε_0=8.854 10^{-12} [F/m] yields with $\omega = 2\pi f$

$$P_{av} = 0.556 \cdot 10^{-10}\varepsilon^{"} f E_{rms}^2 V \qquad (3\text{-}5)$$

where:

P = Power [W]

f = Applied Frequency [Hz]

E_{rms} = Electrical field strength inside the mineral [V/m]

E^*, E= Conjugate electrical field strength, electrical field strength [V/m]

ε_0 = 8.854×10^{-12} Permittivity of free space [F/m]

$\varepsilon_{eff}^{"}$ = Effective loss factor [F/m]

V=Volume [m^3].

For a material which exhibits magnetic losses the power density equation takes the form:

$$P_{av} = \omega\varepsilon_{eff}^{"}\varepsilon_0 E_{rms}^2 V + \omega\mu_{eff}^{"}\mu_0 H_{rms}^2 V \qquad (3\text{-}6)$$

where:

H_{rms} = Electrical field strength inside the mineral [V/m]

μ_0 = Permeability of free space [Tm/A]

$\mu_{eff}^{"}$ = Effective magnetic loss factor [Tm/A].

For this study it is considered that the content of ferromagnetic minerals is much lower compared to all others rock forming minerals. For the minerals which exhibit small ferromagnetic properties, the effect was also minimised where possible, by experimental design to expose rock particles to electric field component of the electromagnetic waves and minimise the influence of the magnetic component. The average power which refers to the power density inside the material comes from both

electric and magnetic losses. To which extent the ratio between magnetic and electric component are driving the average power density within the mineral phases is beyond the research of this thesis work.

3.2.2 Calculation of Temperature Rise for Microwave Heating of Materials

If the energy balance for the load is placed the following energy distribution can be seen:

[Energy transferred from the electromagnetic field] = [Energy absorbed in the material] + [Energy lost in surrounding medium from the material] + [Energy lost by radiation from the material]

From energy balance it can be seen that heating and cooling are occurring simultaneously which leads to transient thermal calculations to determine heating rates. Transient thermal calculations are mathematically very complex and usually numerical modelling is applied. However, it is still possible to calculate approximate heating rates if some assumptions are made. To calculate energy lost by radiation energy calculation from Stefan-Boltzmann Law can be applied which states: "The radiation energy per unit time from a blackbody is proportional to the fourth power of the absolute temperature" (Thomas 1999). It can be expressed as

$q = \varepsilon \sigma T^4 A$ (3-7)

where:

q = heat transfer per unit time [W]

σ = 5.6703 10^{-8} [W/m^{2}K4] - The Stefan-Boltzmann Constant

T = absolute temperature in Kelvin [K]

A = area of the emitting body [m^2]

ε = emissivity of the object (ε = 1 for a black body).

A very simplified form can be given as a conduction equation:

$$\rho C_p \frac{\partial T}{\partial t} = \lambda \nabla^2 T + Q \qquad (3\text{-}8)$$

where, C_p =specific heat is given in [J/kgK] and λ= thermal conductivity [W/mK].

This simplistic form has to be extended with terms for convection in order to get an accurate numerical solution. For the given system where material is placed on the

surface which does not conduct heat well and it is surrounded with stagnant air, it can be stated that the energy lost is minimised and most of the energy is absorbed by the material.

The power required to raise the temperature of material from T_0 [^{o}C] to T [^{o}C] with a mass of m [kg] in defined time frame t is given by equation:

$$P = \frac{Q_h}{t} = \frac{mc_p(T - T_0)}{t} \qquad (3\text{-}9)$$

Substituting P, using Equation 3-4, in Equation 3-9 derives the form of Equation 3-10:

$$\frac{(T - T_0)}{t} = \frac{0.556 \cdot 10^{-10} \varepsilon'' f E_{rms}^2}{\rho C_p} \left[\frac{^0C}{s} \right] \qquad (3\text{-}10)$$

Where:

ρ = is the density of the material in [kg/m^3]

C_p =specific heat is given in [J/kg^{o}C].

ε'' = Loss Factor [F/m]

A similar approach is used by Metaxas & Meredith (1983). From Equation 3-10 it can be observed that the temperature rate is dependent upon frequency "f" and ($\varepsilon'' E_{rms}^2$) which is usually a function of the temperature, due to the variation of the loss factor with temperature. Density and specific heat also have a large influence particularly when heterogeneous materials like real rock particles are involved.

3.3 Materials Interaction with Microwaves

Generally the materials can be grouped according their interaction with microwaves in three groups:

- *Conductors*: materials have loosely bound electrons (one or two) in the outer (valence) shell that can move easily under the influence of a voltage to form current. Conductors include elemental metals such as copper, gold, silver or aluminium. They are used to conduct microwaves through coaxial cables or waveguides.
- *Insulators:* behave almost transparent to microwaves. Insulators include glass, plastic, rubber, silicon dioxide, silicon nitride and very commonly used Teflon®.
- *Absorbers:* are lossy materials or dielectrics which absorb microwaves.

This grouping is done after Chen et al. (1984) and Church et al. (1988). For this study in very broad definition it is considered that most common forming rock minerals belong to the insulators group which behaves "almost" transparent to microwaves, while minerals of interest belong to absorbers group.

3.3.1 The Penetration Depth of Microwave Energy into Materials

It is useful to define penetration depth, taking into account that materials are grouped according to whether the microwaves penetrate the material or not.

The penetration depth is defined as the distance from the surface of the material at which the power drops to e^{-1}, (e ≈ 2.718, Euler's number) from its value at the surface. It is given as:

$$D_P = \frac{1}{2\alpha} \qquad [\text{m}] \qquad (3\text{-}11)$$

Where α is the attenuation factor which is a real part of propagation factor for the electric field (von Hippel 1954). It can also be expressed as:

$$D_P = \frac{c}{2\pi f \sqrt{2\varepsilon' \left[1 + \sqrt{\left(\frac{\varepsilon''}{\varepsilon'} \right)^2} - 1 \right]}} \qquad (3\text{-}12)$$

With c being the speed of light in free space (c = 3 x 10^8 m/s). The penetration depth of microwaves into a material is therefore inversely proportional to the frequency. Shorter-wave electromagnetic waves have less penetration than longer waves. Also, electromagnetic waves do not penetrate deeply into moist materials where both the dielectric constants and loss factors are moderately high. This does not mean that there is no heating beyond penetration depth. It means that more than 60% of heat will be dissipated in the layer of material between surface and penetration depth (Meredith 1998).

Penetration depth is an important concept which is often used to consider whether an electromagnetic field at a certain frequency can provide relatively good penetration into the material. For quick assessment it can be used with frequency bands presented in Table 3-1.

Table 3-1 Typical frequencies used and their approximate band designations, after Pozar (1997)

Typical frequencies and their usage		Approximate band designations	
AM broadcast band	535-1605 kHz	L-band	1-2 GHz
Short wave radio	3-30 MHz	S-band	2-4 GHz
FM broadcast band	88-108 MHz	C-band	4-8 GHz
VHF TV (2-4)	54-72 MHz	X-band	8-12 GHz
VHF TV (5-6)	76-88 MHz	Ku-band	12-18 GHz
UHF TV (7-13)	174-216 MHz	K-band	18-26 GHz
UHF TV (14-831	470-890 MHz	Ka-band	26-40 GHz
Microwave ovens	0.915 and 2.45 GHz	U-band	40-60 GHz

For low loss dielectrics $\left(\varepsilon^{''}/\varepsilon'\right) << 1$ and the penetration depth approximates, with an error up to 10%, to:

$$D_P = \frac{\lambda_0^{'}\left(\varepsilon'\right)^{1/2}}{2\pi\varepsilon^{''}} \qquad (3\text{-}13)$$

Harrison's (1997) work compared the depth of penetration for the two commonly used frequencies for microwave heating at 915 MHz and 2.45 GHz. The measurement of dielectric properties was undertaken for selected minerals using an open ended coaxial line sensor and compared with available literature results. Values were calculated using Equation 3-13. The depth of penetration in common rock forming minerals is large when compared to the depth of penetration in ore minerals. For example at 2.45 GHz the depth of penetration for quartz and feldspar is measured in meters, whereas the depth of penetration for chalcopyrite and pyrite is measured in millimetres and centimetres, as seen in Table 3-2.

Table 3-2 Variation of penetration depth for various minerals at two microwave frequencies after Harrison (1997)

Mineral	Depth of Penetration at 915 MHz (From Literature) [m]	Depth of Penetration at 915 MHz (Measured) [m]	Depth of Penetration at 2.45 GHz (From Literature) [m]	Depth of Penetration at 2.45 GHz (Measured) [m]
Quartz	-	3.97	3.27	5.86
Feldspar	2.28	-	1.06	-
Hematite	0.15	0.29	0.07	0.21
Ilmenite	0.06	0.63	0.01	0.31
Chalcopyrite	0.06	0.70	0.05	0.33
Pyrites	0.09	0.21	-	0.11
Magnetite	0.32	0.26	-	0.06
Galena	0.10	0.92	0.09	0.84

Considering that 60% of heat is dissipated in the layer between surface and penetration depth and taking into account large differences in compared values it can be seen why for this study, common rock forming minerals are considered to be "almost" transparent to microwaves.

3.3.2 Influence of Particle Size on Heating Rate during Microwave Heating

Earlier studies of Jelinek et al. (1949), Walkiewicz et al. (1988) and Salsman et al. (1996) have determined that particle size has an effect on the heating rate of a material and how it reacts with microwaves. When testing bulk properties of materials porosity of material changes with particle size. This influences bulk density of material which impacts heating rate as seen in Equation 3-10.

The earliest work performed on the dielectric heating of granular materials was undertaken by Jelinek et al. (1949). They tested granular alumina and sand. The heating rate of granular alumina increased linearly with an increase in particle size. The heating rates of sand were also found to increase with an increase in particle size. This was in agreement with electromagnetic theory which suggests that larger particles are heated more rapidly than smaller particle size. Opposite results were reported by Walkiewicz et al. (1988). They reported on the effect of particle size on heating properties of graphite. It was found that finer size graphite heats better with microwave radiation than the larger sizes.

Salsman et al. (1996) theoretically modelled and experimentally demonstrated the heating rate of sulphide ores to be directly proportional to the mass and volume of high loss material. A peak tensile stress in the host rock, caused by heat stress between mineral phases, increased with increasing particle sizes. It was also shown that the heating rate was directly proportional to the grain size of the sulphide ores. Following this study Kingman et al. (2000), also reported the effect of mineralogy and grain size on microwave assisted grinding. According to these results, ores which contained minerals in small particles which were finely disseminated in discrete elements responded poorly to microwave treatment in terms of reductions in required grinding energy.

In literature opposing results can be sourced. The cause for opposing results can be found in the absence of standardised sample preparation and testing. In some studies different frequencies were used as well as different temperature measuring techniques. Experimental results and research by Harrison (1997) corrected for this when various minerals and their relationship with sizes were studied. To standardise the results, 50g representative samples of a mineral were exposed in the same glass container and placed in the same position in the 650W microwave oven at 2.45 GHz. The minerals have been sieved, where possible, into five different particle size ranges. The results indicate the effect of particle size on the heating rates of minerals could be divided into 3 behavioural patterns:

- Group A - An increase in particle size causes a decrease in heating rates
- Group B - No discernible change in heating rate
- Group C - An increase in particle size causes an increase in heating rates

Figure 3-2 to Figure 3-4 present some of the minerals which are good representatives of their groups.

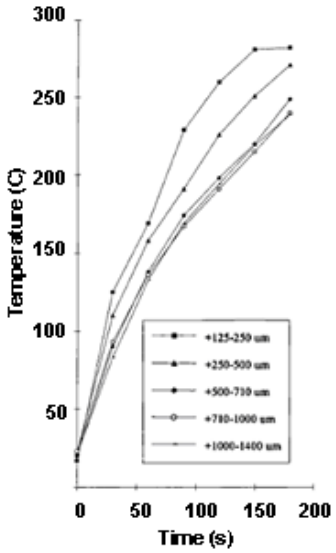

Figure 3-2 Heating rates for 50g of representative samples of *Pyrrhotite* and their five different particle sizes, after Harrison (1997). Belongs to *Group A*.

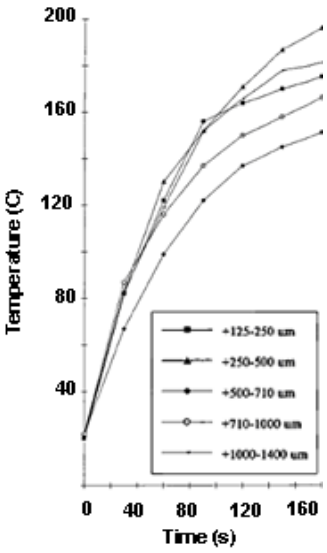

Figure 3-3 Heating rates for 50g of representative samples of *Chalcopyrite* and their five different particle sizes, after Harrison (1997). Belongs to *Group B*.

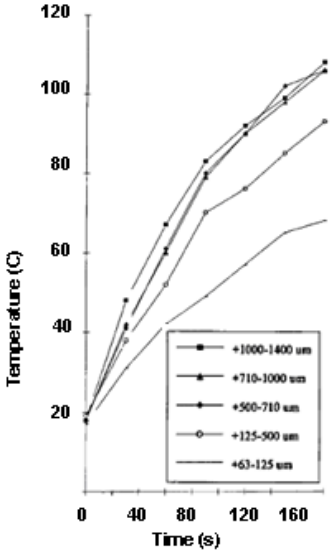

Figure 3-4 Heating rates for 50g of representative samples of *Cassiterite* and their five different particle sizes, after Harrison (1997). Belongs to *Group C*.

Table 3-3 shows results of the heating rates with particle size variation for some selected rock forming minerals. It is also commented whether the heating effect decreases while particle size increases. While some minerals show no difference like

chalcopyrite, pyrites or calcite some minerals have a slight tendency toward "group A" like quartz or feldspar.

Table 3-3 Results of Heating Rate with Particle Size Variation, after Harrison (1997).

Mineral Type	As Particle Size Increases, Does The Heating Effect Decrease?	Class of Particle Size Effect
Calcite	No difference	B
Sphalerite	No, the reverse	C
Mica	Yes, very slightly	A
Quartz	Yes, very slightly	A
Feldspar	Yes, very slightly	A
Fluorspar	Yes, very slightly	A
Batytes	Yes, very slightly	A
Wolframite	No, the reverse	C
Dolomite	No difference	B
Gypsum	No, the reverse	C
Bauxite	No difference	B
Cassiterite	No, the reverse	C
Hematite	Yes	A
Ilmenite	No difference	B
Chalcopyrite	No difference	B
Pyrites	No difference	B
Pyrrhotite	Yes	A
Chalcocite	Yes	A
Magnetite	Yes	A
Bornite	Yes	A
Galena	Yes	A

It is important to emphasize that this separation in groups was carried out for pure minerals and not a combination of minerals. Heating rates of combined minerals with different textures and structures, which can be found in real rock particles, may result with completely different results. This will be explained in more details later on.

In literature some authors have found that hematite is a good absorber of microwave energy like Chen et al. (1984) and Walkiewicz et al. (1988) while others like Wright et al. (1989) reported the opposite. Harrison (1997) reported slight temperature change when exposed to microwaves. Although, they all used a similar approach by testing for heating rate in a domestic microwave oven these observed differences to microwave heating may be related to preparation of the samples or to purity of the mineral.

3.4 Complex Permittivity of Minerals

Permittivity is a physical property relating the ability of a material to propagate an electromagnetic field. The permittivity is a measure of how an electric field affects, and is affected by, a dielectric medium. In the frequency domain, the complex permittivity $\varepsilon = \varepsilon' - i\varepsilon''$ of a material can be expressed through real part and complex part defined with imaginary unit (i). The real part ε' is defined as the dielectric constant and represents stored energy when the material is exposed to an electric field. It has to be noted that it is conveniently termed dielectric constant but it is not considering that it is frequency and temperature dependant. Only for the free space dielectric constant can be taken as a constant which is ε_o=8.854 x 10^{-12} [F/m]. The dielectric loss factor ε'', which is the imaginary part, influences energy absorption and attenuation. More detailed definitions can be found in works of Metaxas (1983), Schubert and Regier (2005), and Feher (2009).

The complex permittivity of minerals varies over a wide range even within a homogeneous material; there is variation at different temperatures and frequencies. The problem becomes less complicated if the measurements are set to certain frequencies which are usually 915 MHz and 2.45 GHz set for industrial applications. These industrial frequencies can have slightly varied values due to different countries and regions.

There are two techniques which were used over the years to measure complex permittivity of minerals. The resonant cavity perturbation method is a reliable and simple technique to determine the complex permittivity of dielectric materials in the GHz range, and it has been widely used. The second technique is coaxial line method or open-ended coaxial line technique (Czichos, Saito & Smith 2006).

The open-ended coaxial line technique was used in experimental work to study heating effects by Harrison (1997) and the work was undertaken at The National Physical Laboratory at Teddington in Middlesex, UK. Measurements were performed over the frequency range of 0.1-6 GHz. Table 3-4 shows the variation of dielectric constant and loss factor for minerals is presented. The values are given for the room

temperature and there was no information about extrapolation to a solid density considering that the powder samples were tested.

From Harrison's work it can be seen that quartz, which is common as gangue mineral, has much lower values for dielectric properties compared to chalcopyrite and pyrites. The value for the loss factor is much lower which to a great extent influences the conversion of electromagnetic energy into thermal energy. This shows that the heating rate for quartz will be much slower than for chalcopyrite or pyrites which is in agreement with the observed heating rates from various research studies.

Table 3-4 Values are given for the two industrial frequencies at 2.45GHz and 915MIHz data obtained from (Harrison 1997)

Minerals	Dielectric constant (ε') at 915MHz	Loss factor at (ε'') 915MHz	Loss tangent at 915MHz	Dielectric constant (ε') at 2.45GHz	Loss factor (ε'') at 2.45GHz	Loss tangent at 2.45GHz
Quartz	2.32	0.04	0.017	2.26	0.01	0.018
Ilmenite	4	0.33	0.083	3.75	0.24	0.088
Chalcopyrite	5	0.33	0.066	4.75	0.26	0.069
Hematite	5.2	0.8	0.154	4.9	0.4	0.163
Galena	7	0.3	0.043	6.75	0.12	0.044
Pyrites	9	1.5	0.167	8.25	1	0.182
Magnetite	13.5	1.5	0.111	14.5	2.5	0.103

The resonant cavity perturbation method was used by Cumbane (2003) which allowed him to investigate behaviour of dielectric properties with temperature change at set frequency of 2.216 GHz which was one of three resonant frequencies. Results are given in Table 3-5. All minerals were softly compressed powders and from most abundant groups of minerals. From silicates he used quartz and orthoclase (member of feldspar group) which were taken as common gangue minerals. From the metal oxides he used hematite, magnetite, ilmenite and cassiterite. And the last group used was sulphides with pyrite, chalcopyrite, galena, sphalerite, and chalcocite. Results revealed that gangue minerals had minimal alterations in their dielectric properties with temperature change. The largest alterations were reported for sulphides followed by oxides.

Recent studies and measurements by Geoffrey Genn (2012) obtained data from cavity perturbation measurements using the 'C1' cavity at the University of Nottingham. The Landau-Lifshitz-Looyenga mixture equation (Landau & Lifshitz 1960) was used to

calculate the dielectric properties of the solid phase from powder data. When powder samples are prepared, measured dielectric properties are actually for the mixture of air and mineral under testing. Air influence can be reduced by compacting the sample as much as possible. With lightly compacted powders it is recommended to extrapolate data up to the solid phase. More details can be found in work of Arai, Binner & Cross (1995).

Table 3-5 Cumbane (2003) measurements not extrapolated to solid density at the room temp.

Minerals	Dielectric constant (ε') at 2.21GHz	Loss factor (ε'') at 2.21GHz	Loss tangent at 2.21GHz
Sulphides			
Pyrite	7.55	0.85	0.113
Chalcopyrite	7.95	0.38	0.048
Galena	6.65	0.15	0.023
Sphalerite	3.5	0.12	0.034
Chalcocite	8.6	0.55	0.064
Oxides			
Cassiterite	5.216	0.25	0.048
Hematite	4.399	0.18	0.041
Ilmenite	9.201	0.78	0.085
Magnetite	4.463	0.15	0.034
Wolframite	4.924	0.11	0.022
Silicates			
Quartz	2.65	0.03	0.011
Orthoclase	1.86	0.01	0.005

Table 3-6 Genn measurements extrapolated to solid density at the room temperature

Minerals	Dielectric constant (ε') at 912MHz	Loss factor at (ε'') 912MHz	Loss tangent at 912MHz	Dielectric constant (ε') at 2.468GHz	Loss factor (ε'') at 2.468GHz	Loss tangent at 2.468GHz
Pyrite	27.58±4.14	6.69±0.67	0.243	25.75±3.86	4.70±0.47	0.183
Chalcopyrite	21.76±3.26	1.71±0.17	0.079	22.36±3.35	1.65±0.16	0.074
Garnet	11.00±1.65	0.01±0.05	0.001	11.64±1.75	0.02±0.01	0.002
Mica	6.18±0.93	0.07±0.01	0.011	6.32±0.95	0.07±0.01	0.011
Molybdenite	13.68±2.05	1.34±0.13	0.098	12.71±1.91	1.46±0.15	0.115
Quartz	4.45±0.67	0.01±0.05	0.002	4.64±0.70	0.02±0.01	0.004

The ratio of the real and imaginary parts of permittivity represents another important parameter, the tangent of loss angle (tan $\delta = \varepsilon'' / \varepsilon'$). Considering that imaginary and real parts can have different trends with frequency and temperature change, this is a good approach to combine them in to one parameter. Tangent of loss angle then can be compared for chosen groups of minerals at specific values, for example one of the industrial frequencies and the room temperature.

Table 3-7 shows the ratios for loss tangent between very absorbing minerals and Quartz at 2.45 GHz or very closely to 2.45 GHz and the room temperature. It can be observed that chosen minerals will have a tendency to heat five to ten times faster than quartz. This effect becomes even more evident when values are extrapolated to solid density.

Table 3-7 Compared ratios for loss tangent between very absorbing minerals and Quartz as very common gangue mineral in three different studies.

Study by	Loss tangent ratio Pyrite / Quartz	Loss tangent ratio Chalcopyrite / Quartz	Loss tangent ratio Magnetite / Quartz
Harrison (1997)	10.11	3.83	5.72
Cumbane (2003)	10.27	4.36	3.09
Genn (2009)	45.75	18.5	-

The study by Harrison (1997) which measured dielectric properties with frequency change and another study by Cumbane (2003) followed by a study of Genn (2012) which investigated dielectric properties with temperature change clearly place complex permittivity as one of guiding factors in the volumetric heating and determines heating rates. The higher the ratio for loss tangent between the mineral of interest and the gangue minerals, the higher selective heating will be and good conditions for selective heating.

3.5 Physical Properties of Minerals

3.5.1 Thermal conductivity of rocks and minerals

From Equation 3-14 it can be seen that the energy which is lost through conduction can be expressed as:

$$Q = \lambda \nabla^2 T \qquad (3\text{-}14)$$

In this case temperature diffusion is defined in all directions. Conduction takes place when a temperature gradient exists in a solid medium. Conductive heat flow occurs in the direction of decreasing temperature because higher temperature equates to higher molecular energy or more molecular movement. Thermal conductivity for many rocks is, to a good approximation, isotropic, particularly for volcanic and plutonic rocks. In contrast to this, thermal conductivity of many sedimentary and metamorphic rocks is

strongly anisotropic, and lateral heat flow will be significant. Therefore information on anisotropy is often needed, requiring laboratory measurements in different directions (Clauser & Huenges 1995). Temperature measurements are usually performed along one direction. Under steady state conditions and when the heat transfer is dependent only on the temperature gradient, thermal conductivity is defined as: The quantity of heat (q) transmitted through a unit thickness (L) in a direction normal to a surface of unit area (A) due to a unit of temperature gradient (ΔT). The form of Equation 3-14 becomes the following:

$$q_i = \lambda_i \cdot \frac{\partial T}{\partial x_i} \qquad (3\text{-}15)$$

which becomes even more simplified for the case of conduction through a one layer of block,

$$q = \frac{\lambda \cdot A \cdot \Delta T}{L} \qquad (3\text{-}16)$$

where,

L= thickness of the block [m]

A= surface area defined for heat conduction [m^2].

Thermal conductivity is a function of mineral orientation, porosity, moisture content and density. The work of Schon (1995) defines these factors in more details. Figure 3-5 shows thermal conductivity for selected rocks. It can be seen how different these ranges can be with a sandstone and quartzite extending to the highest values of thermal conductivity within the selected group of minerals.

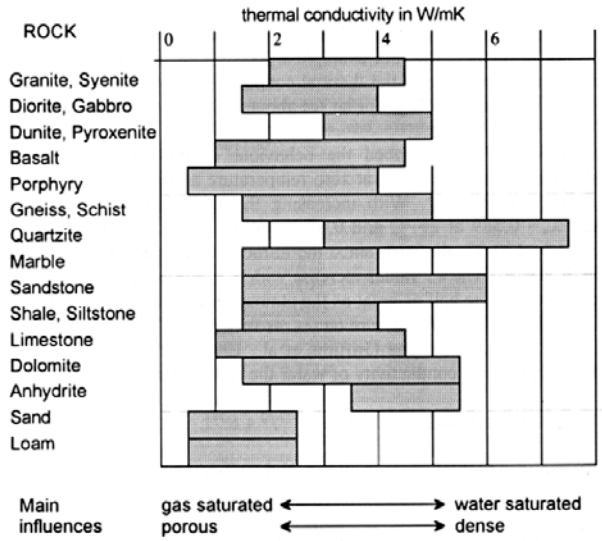

Figure 3-5 The thermal conductivity for various types of rocks with main influences. Sourced from (Schon 1995)

Because silicates constitute by far the largest fraction of the earth's crust and mantle, it is suitable to have understanding in values for thermal conduction in metamorphic rocks, subdivided according to quartz content followed secondly by the largest fraction of plutonic rocks, subdivided according to feldspar content.

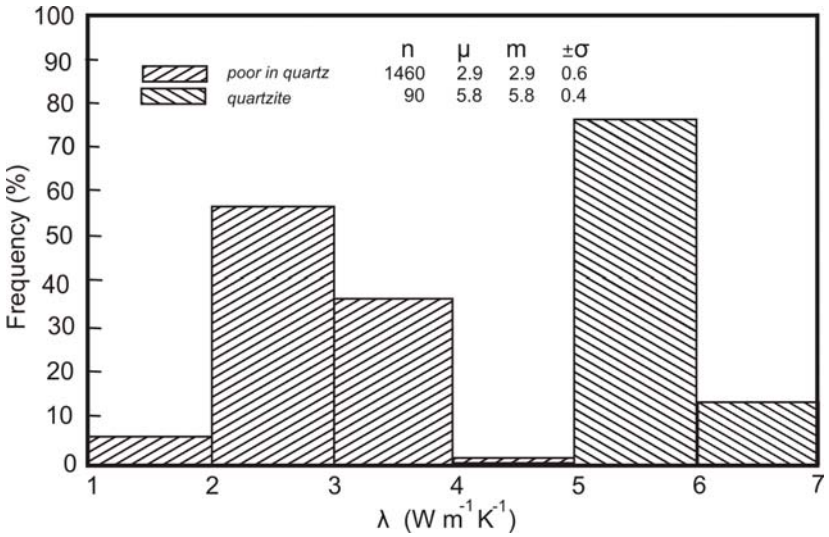

Figure 3-6 Thermal conductivity of metamorphic rocks, subdivided according to quartz content. Sourced from (Clauser & Huenges 1995).

In Figure 3-6 thermal conductivity of metamorphic rocks is given.

- Histogram for high quartz content is made up of data from quartzite.
- Histogram for low quartz content are from quartz-mica schist, gneisses, marble, serpentinite, talc, serpentinized peridotite, homfels, eclogite, albitite, leptite, schist, slate, phyllite, amphibolite, mylonite and greenstone (Clauser & Huenges 1995).

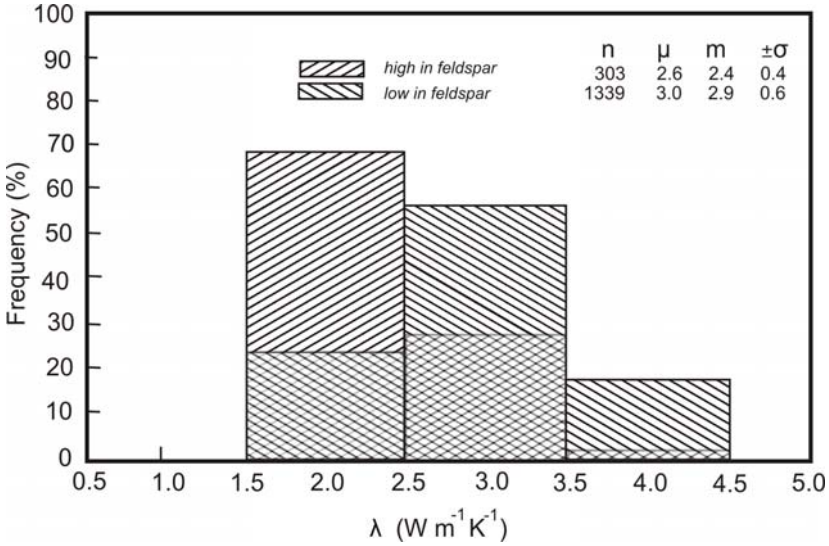

Figure 3-7 Thermal conductivity of plutonic rocks, subdivided according to feldspar content. Sourced from (Clauser & Huenges 1995).

In Figure 3-6 thermal conductivity of plutonic rocks can be seen.

- Histogram for high feldspar content is composed of data from: syenite (including alkali and nepheline syenite), granosyenite, syenite porphyry, and anorthosite.
- Histogram for lower feldspar content are from granite (including alkali granite, plagiogranite, granodiorite, tonalite, quartz monzonite), quartz- and quartz-feldspar-porphyry, diorite (including monzonite), gabbro (including quartz and olivine gabbro), porphyrite dykes (lamporphyre, diabase, quartz dolerite), and ultramafic rocks (pyroxenite, peridotite, lherzolite, hypersthenite, bronzitite, dunite, olivinite, homblendite, cumberlandite) (Clauser & Huenges 1995).

For a more precise calculation thermal conductivity is required on elevated temperatures, while in literature usually data at room temperatures can be found. Early research of Birch and Clark (1940) confirmed that thermal conductivity is decreasing with increasing temperatures. Sass et al. (1992) suggested empirical relations between thermal conductivity and temperature which involved value measured at room temperature. This relation was derived from experimental measured data from previous study done by Birch and Clark (1940).

$$\lambda(T) = \frac{\lambda(0)}{1.007 + T \cdot \left(0.0036 - \frac{0.0072}{\lambda(0)} \right)} \qquad (3\text{-}17)$$

Where

$$\lambda(0) = \lambda(25) \cdot \left[1.007 + 25 \cdot \left(0.0037 - \frac{0.0074}{\lambda(25)} \right) \right] \qquad (3\text{-}18)$$

Clauser (1995) also commented that Sass's equation yields useful estimates of the temperature dependence of thermal conductivity for crystalline rocks, independent of mineralogy for the temperature range of 0-250^{o}C.

Table 3-8 Thermal conductivity for some selected minerals. Directions of anisotropy in table are specified in two ways: (1) by the mineral's optical axes a-, b-, or c- (100, 010, 001), (2) by the thermal conductivity components normal or parallel to the direction of maximum thermal conductivity

Mineral	Sourced from Clauser & Huenges (1995)		Sourced from Horai & Baldridge (1972)
	Measurement temperature [◦C], State	Thermal conductivity [W/mK]	Thermal conductivity [W/mK] Ambient conditions
Andradite	-	-	3.09
Anhydrite	25-35, a:	50.36±0.27	4.76
Apatite	35, a:	1.27±0.02	1.38±0.01
Biotite	33,‖	3.14	2.02±0.32
	32,⊥	0.52±0.01	
Calcite	30,⊥	3.16	3.59
	30,‖	3.63	
Chalcopyrite	-	-	8.20
Chlorite	30, a:	3.06±1.18	5.15±0.77
Chromite	35, a:	2.19±0.15	2.52
Epidote	31,‖	3.10	2.83±0.21
	32,⊥	2.93	
	31,‖	2.50±0.02	
Galena	35, a:	2.76±0.18	2.28
Grossularite	?	5.32	5.48±0.21
Gypsum	?	1.30	-
Hematite	30, a:	12.42±1.74	11.28
Magnesite	25-100,⊥	7.32±0.57	5.84
	25-100,‖	7.86 ±0.17	
	34-35, a:	8.18 ±1.20	
Magnetite	22-33, a:	4.61±0.42	5.10
Muscovite	30,‖	3.89	2.28±0.07
	32-45,⊥	0.62±0.11	
Pyrite	35, a:	23.15±2.00	19.21
α Quartz	30,⊥	6.15	7.69
	30,‖	10.17	
Serpentine	32,⊥	2.41± 0.10	3.53±1.28
	?,‖	2.76 ±0.03	
	30-34, a:	2.61 ±0.38	
Sphalerite	-	-	12.72
Spinel	35-70, a:	12.14±1.23	9.48
Talc	29-34, ‖	10.69 ±1.35	6.10±0.90
	30, ⊥	1.76	
	30, a:	2.97	

In Table 3-8 thermal conductivity for some selected minerals can be found. The values are sourced from two studies. The values from Horai & Baldridge (1972) are for powders so the information about anisotropy of tested minerals was lost. The

study of Clauser & Huenges (1995) took anisotropy into consideration and provided information about the state of measurement along with temperatures.

3.5.2 Specific Heat Capacity of Minerals

Knowledge of the specific heat capacity is very important if we want to calculate the heating rate of rock particles. Specific heat capacity [J/kg K] is defined as the amount of heat required to raise the temperature of the unit mass [1 kg] of a substance by a unit temperature increase [1 K] (Thomas 1999). Values are generally determined with experiment, which involves in most cases calorimeter. In engineering calculations, when a system exchanges a certain amount of heat within the process, we use average specific heat, which stands for ratio between heat, which was exchanged, and finite temperature difference. It can be defined by Equation 3-19.

$$c_p = \left(\frac{\partial H_h}{\partial T} \right)_p = \frac{\partial Q_h}{\partial T} \qquad (3\text{-}19)$$

Specific heat capacity is related to the thermal conductivity λ and the thermal diffusivity κ by the Equation 3-20:

$$\kappa = \frac{\lambda}{c_p \rho} \qquad (3\text{-}20)$$

where ρ is density. It is also temperature dependent. A detailed study of specific heat capacities and their temperature dependence, on more than 150 various minerals, was done by Waples & Waples (2004). They defined heat capacity with approximation to be uniform in all directions or isotropic. In this respect, it contrasts strongly with thermal conductivity, which may be highly anisotropic.

It is important to establish a standard reference temperature in order to compare heat capacities of the various minerals. Table 3-9 shows measured specific heat capacities along their values for 20°C as the reference temperature. In their study all minerals were included to create a histogram showing distribution of measured specific heat capacities which can be seen in Figure 3-8.

It can be seen from this work that the great majority of the specific heat capacities of minerals at 20°C are between about 600 and 900 J/kg/K, with a strong preference for values at 800 J/kg/K as seen in Figure 3-8. The mean value for all the inorganic minerals in their database is 660 J/kg/K, with a standard deviation of 235 J/kg/K.

Table 3-9 Measured Specific Heat Capacities for Chosen Various Classes of Minerals, and the Temperatures at Which the Measurements Were Made. Sourced from (Waples & Waples 2004)

Mineral	Density (g/cm3)	Measurement temperature (◦C)	Cp (J/kg/K) at measurement temperature	Cp (J/kg/K) at 20^{o}C
Adularia	2.59	20	685	685
Anatase	3.84	25	820	811
Andradite	3.86	0	750	785
Anhydrite	2.9	20	585	585
Apatite	3.225	20	700	700
Arcanite	2.66	20	715	715
Biotite	3	20	770	770
Bromyrite	6.477	20	180	180
Brucite	2.38	35	1300	1260
Calcite	2.745	20	815	815
Cassiterite	6.95	20	375	375
Chalcocite	5.65	20	510	510
Chalcopyrite	4.2	20	534	534
Chlorite	2.8	20	600	600
Chromite	4.9	20	690	690
Dolomite	2.84	20	870	870
Epidote	3.4	20	780	780
Epsomite	1.677	32	1510	1472
Galena	7.55	20	210	210
Grossularite	3.594	127	713	593
Gypsum	2.32	20	1070	1070
Hematite	5.15	20	620	620
Kaolinite	2.65	0	930	974
Kieserite	2.571	9	1000	1025
Lime	3.45	20	750	750
Magnesite	2.975	20	880	880
Magnetite	5.175	20	586	586
Microcline	2.58	20	700	700
Molybdenite	4.65	20	574	574
Muscovite	2.85	20	760	760
Nepheline	2.6	20	800	800
Oligoclase	2.64	20	837	837
Olivine	3.4	0	550	576
Orthoclase	2.6	20	628	628
Pyrite	5.05	20	510	510
Quartz	2.648	20	740	740
Serpentine	2.55	20	650	650
Sphalerite	4	0	450	471
Spinel	3.6	20	820	820
Talc	2.8	20	750	750
Thenardite	2.664	25	971	960
Vermiculite	2.78	20	770	770
Wollastonite	2.845	0	695	728

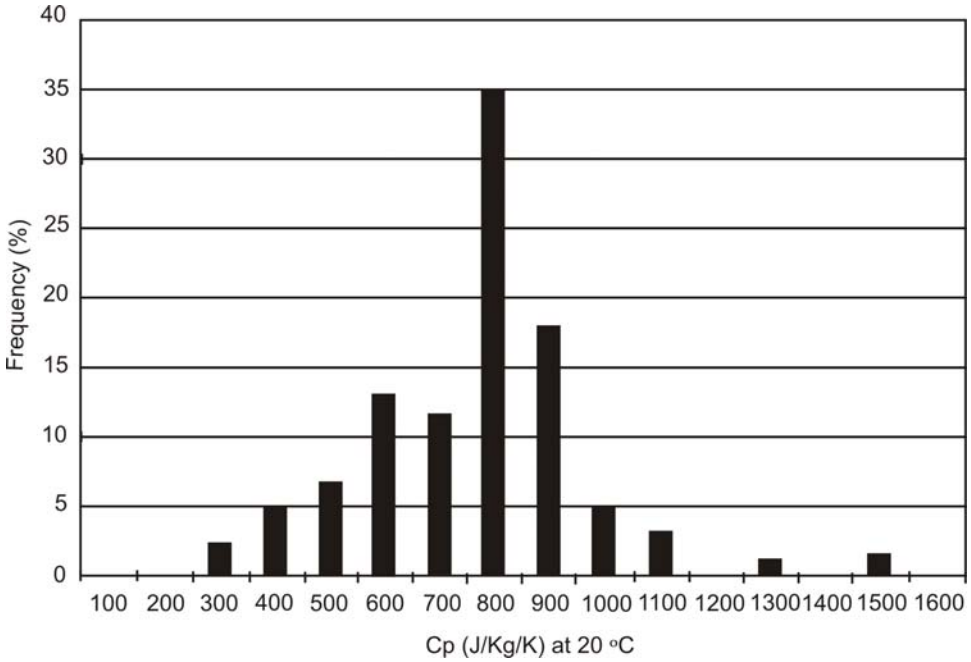

Figure 3-8 Histogram showing distribution of measured specific heat capacities of minerals corrected to 20°C. Values on x-axis refer to maximum value in group. After (Waples & Waples 2004)

Waples and Waples (2004) commented more about generic values for some groups. The lowest values generally occur in compounds that contain one or more heavy-metal atoms (especially sulphides, silver halides, tungstates, and some oxides and carbonates), whereas the highest values are for minerals such as epsomite, brucite, and gypsum, which are either hydroxides or contain significant amounts of water of crystallization. This is why the span from 180 J/kg/K for bromyrite (AgBr) to a very high value of 1485 J/kg/K for epsomite can be seen. Most importantly they observed that various types of silicates have specific heat capacities which cluster near the middle of the range.

Many measurements on different temperatures using a calorimeter confirmed temperature dependence of specific heat capacity. It increases as the temperature increases. This effect has to be included when heating rates are calculated; otherwise it can produce values which can be very different when compared with experimental results. A good equation was developed by Waples & Waples (2004) as third-order polynomial equation with correlation coefficient $r^2 = 0.93$ for non-porous rocks.

$$C_{pnT} = 8.95 \cdot 10^{-10} T^3 - 2.13 \cdot 10^{-6} T^2 + 0.00172 \cdot T + 0716 \qquad (3\text{-}21)$$

Specific heat capacity in Equation 3-21 is given as normalised value, where C_{pnT} =[J/kgK] and T=[K]. Normalization was carried out by dividing all reported specific heat capacities in their study by value for the same rock at 200^{o}C. It can be adapted to calculate the specific heat capacity of any mineral or nonporous rock in any units at any temperature T_2 if the value on temperature T_1 was measured. It is obtained in two steps:

1. First, Equation 3-21 is applied at both temperatures to obtain normalised values
2. These normalised values are then applied in Equation 3-22 to calculate value of specific heat capacity at temperature T_2.

$$C_{pT2} = \frac{C_{pnT2} \cdot C_{pT1}}{C_{pnT1}} \qquad \text{[J/kgK]} \qquad (3\text{-}22)$$

3.6 Defining Favourable Cases for Microwave Sorting

Eventually in microwave assisted infrared sorting everything comes to a measurement of surface temperature. The temperature profiles on rock particles are based on the relationship between minerals and temperature, that is, on the thermal state of minerals and the changes that take place in minerals depending on temperature.

Temperature is one of the parameters which affect almost all physical and chemical properties of minerals; it defines kinetics of material systems and the state equilibrium. The thermodynamic states of minerals during and after heating are determined by two closely connected processes:

- The mechanism of heat transfer considered as a transient thermal state
- The thermo kinetic processes which determine the variations of the physical and chemical properties of the minerals investigated.

These two thermal processes will determine all the aspects of the heating temperature profiles from the time volumetric heating starts, until the system reaches the state equilibrium

In a well defined material system which constitutes the object of heating and microwave apparatus, heating rates and temperatures profiles will also depend on the

way in which thermal energy is fed to the system. This can be continuous or pulsed microwave exposure.

A system of rock particles can be raised to the desired temperature by heating. The desired level of energy needed to produce temperature profiles which can be used to create discrimination criteria will be determined by particle size, mineral composition and texture of the rock particles. The process by which heat is transferred depends on a difference of temperature existing between parts which have higher heating rates and ones with much slower heating rates. This creates temperature gradient; heat will spontaneously pass from the warmer to the colder parts of the body. Thermal energy will propagate in rock particles by conduction and from the surface by convection and radiation.

During thermal conduction heat is transferred gradually from one molecule to the next within a body, without any apparent displacement of substance. Warmer molecules in minerals carrying out faster motions hit against contiguous colder molecules passing them some of their kinetic energy, therefore making colder molecules become warmer and warmer molecules colder. For rock particles heat transferred to another body will be a function of contact surface between rock particle and the body. The contact surface is dependent upon particle's shape and form. For more angular shapes contact surface can be very small, while for flaky shapes can be larger.

By thermal convection, heat is transferred in a surrounding fluid (in this case air). The amount of heat transferred depends on the flow regime around rock particles. If the equipment for microwave exposure is designed to realise designed throughputs and at the same time prevent forced heat convection we can approximate that the heat loss will be insignificant to affect overall temperature difference which we can measure very fast with non-contact measuring techniques. For more details about the influence of coefficient of heat transfer see Appendix B**.**

By thermal radiation, heat is transferred as radiant energy, in the form of electromagnetic waves which are partly or wholly changed into heat on meeting a body in their path. It usually belongs to electromagnetic waves with higher frequency like infrared and near infrared. This is energy which can be measured quickly, in real

time by infrared camera, and used to calculate temperature differences of rock particles. The temperature difference calculated from before and after volumetric heating can then be compared with set temperature threshold.

One, two or even all three mechanisms may operate in any heat transfer, depending on the nature and state of minerals subjected to a temperature change by volumetric heating. In microwave assisted infrared sorting, heat transfer by conduction is predominant. In conventional heating the body is usually surrounded with a heating source (object of heating placed in the oven) and it gets hot progressively from the outside towards the inside. This means that the temperature varies more quickly in points nearer to the surfaces than in points placed deeper inside the body.

In volumetric heating of rock particle heat is generated within the body with different heating rates. Although the whole volume of rock particle is exposed to microwave energy, different heating rates originate from heterogeneity of mineral types. Minerals with higher values of dielectric loss tangents will have the largest heating rates consequently making them as the main sources of heating. This defines selective heating which means that the body will be heated from the inside towards the outside, and it significantly influence the type and the intensity of the temperature profiles that can be measured on the surface. Depending on particle's size, certain time will be necessary for the heat transfer to take place within the whole mass of the particle's body. Figure 3-9 shows this effect of selective heating for the ore particle which was exposed to 1 kW of microwave power for 5 seconds. The heating of the particle and the cooling effect was recorded with an IR camera with 25 frames per second.

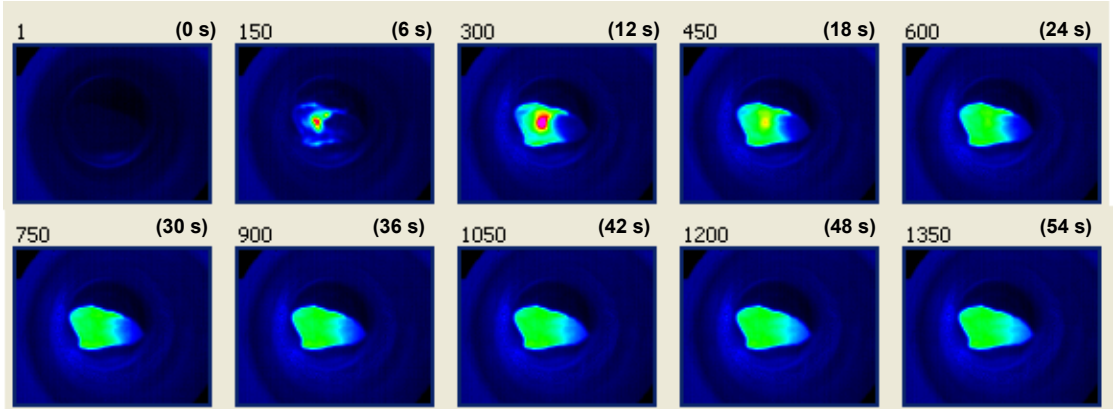

Figure 3-9 Selective heating followed by equilibrium state caused by cooling. Frames are extracted in time intervals of 6 s.

In a range of measured temperatures, the surfaces of equal temperature form isothermal surface. The temperature variation between them can be either larger or smaller depending of temperature gradient. This temperature gradient can be defined between two incremental isothermal surfaces. The limit of the ratio between the temperatures difference ΔT and the distance Δn between two surfaces, when Δn tends towards zero, as defined in Equation 3-23:

$$Tgrad = \lim_{\Delta n \to 0} \left[\frac{\Delta T}{\Delta n} \right] \qquad (3\text{-}23)$$

Figure 3-10 shows formation of isothermal surfaces during heating on the visible surface of rock particle, governed by the temperature gradient from inside the volume of the particle. Isothermal surfaces with different temperatures are correlated to a corresponding specific colour. Colour palette covers temperature span between 25 and 50 ^{o}C.

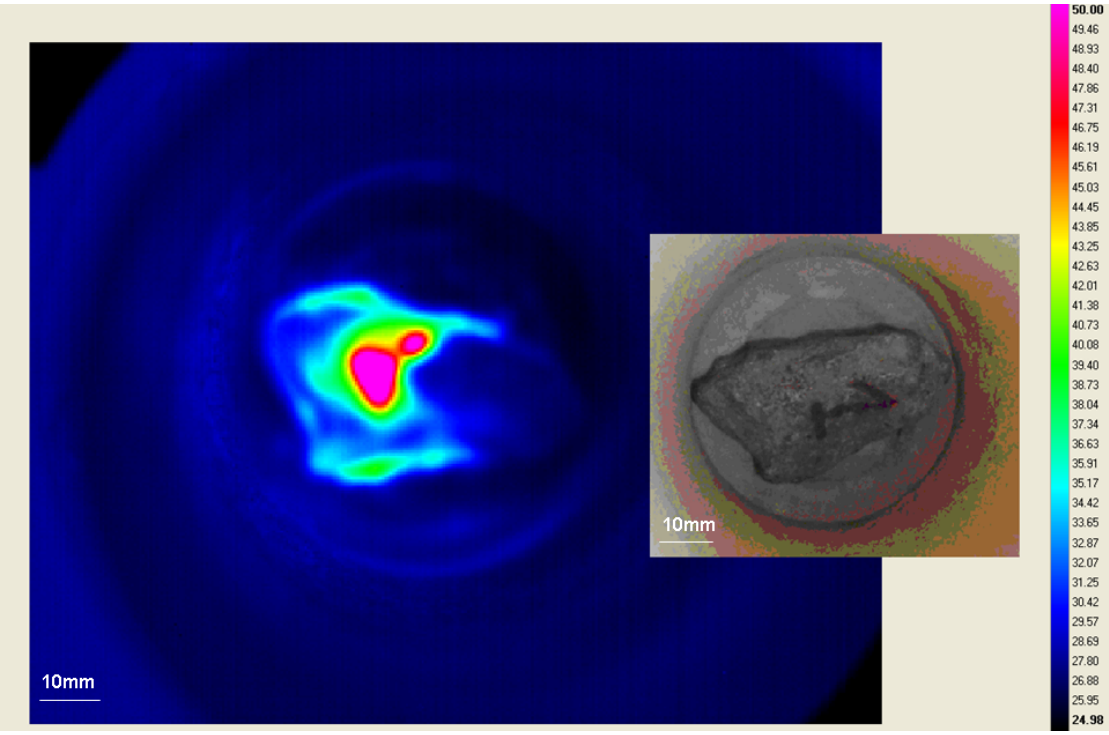

Figure 3-10 Forming of isothermal surfaces during heating on the visible surface of rock particle

The temperature profile can be defined as temperature distribution in all points of the system in a certain time frame. Whether the temperature profile is independent of time or changes within it, heat is transferred in a steady or unsteady manner. In the steady mode, heat remains constant at any point of the system. Heat entering the body comes out wholly through the surface of the whole body. In the unsteady mode, heat is accumulated in the system.

The temperature profile can be indirectly studied measuring maximum or mean temperatures on the surface of rock particles with time.

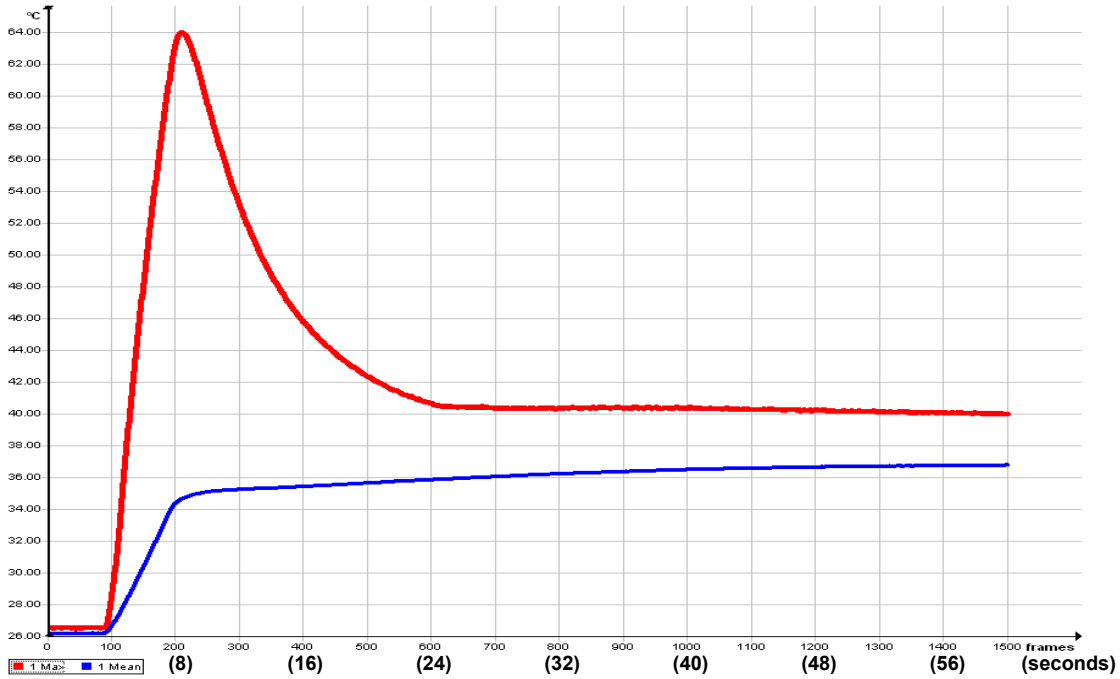

Figure 3-11 Maximum temperature (in red) and mean temperature (in blue) for the rock particle heated for 5 seconds and showed in Figure 3-9 and Figure 3-10.

To study temperature profile of particle shown in Figure 3-9 and Figure 3-10 maximum temperature was calculated from the pixel with the highest temperature on the visible rock surface, while mean temperature was calculated as average value of all temperatures of pixels which compose visible rock surface. Figure 3-11 clearly shows the section of positive heat accumulation which is defined with a very steep increase for maximum temperature and an increase of mean temperature. After this section when maximum temperature reaches its absolute maximum it starts to decrease rapidly defining heat loss. Mean temperature continues to increase only slightly, this is caused by reduced temperature gradients, which confirms that heat is coming from the inside of the volume towards the outside. The following section exhibits almost constant values for both temperatures with the tendency to merge after a long enough time reaching a state of equilibrium.

These heating profiles will depend upon multiple mineral properties which can influence each other; a quick overview can be seen in Figure 3-12.

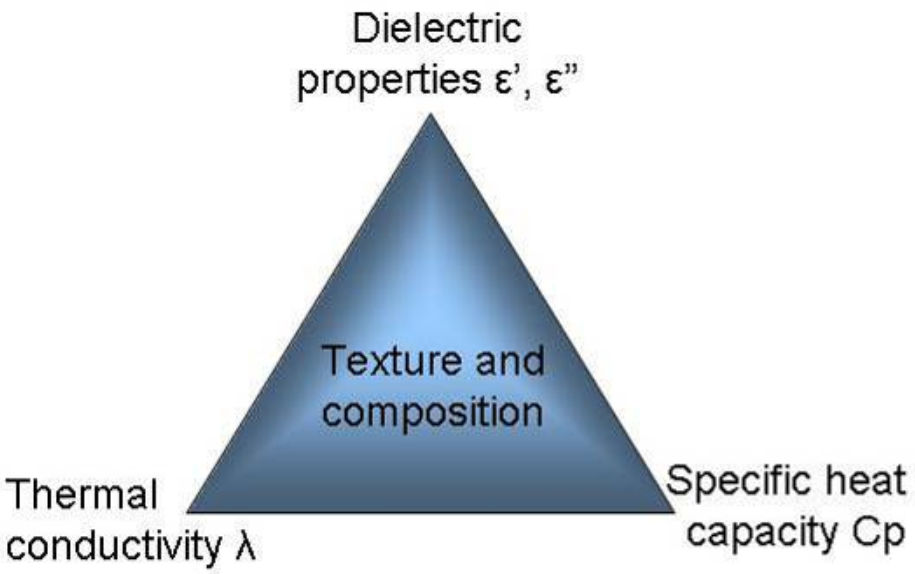

Figure 3-12 Properties of minerals which have to be taken into consideration for microwave sorting

In order to achieve microwave assisted infrared sorting it can be seen that mineral properties such as thermal conductivity, specific heat capacity and dielectric properties have to be balanced in the right way by texture and composition. The easiest way to define favourable cases is to define rock particles as two-component systems consisting of matrix or common rock forming minerals and minerals of our interest. A favourable case is defined when a mineral of interest responds very well to microwave heating in poorly responsive matrix, creating good conditions for selective heating. Parkhomenko (1967) commented that: "In addition to the rocks which lack any orderly arrangement of mineral grains, there are many rocks in which the grains exhibit some preferred orientation. This orientation of grains constitutes the texture of a rock". It is assumed that most common grain inclusions can be described through four following textures which can be seen in Figure 3-13.

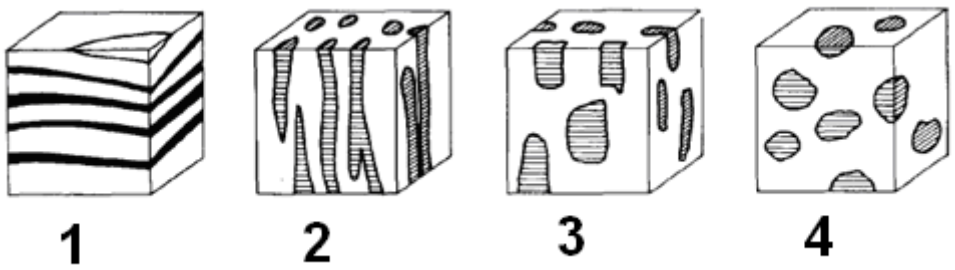

Figure 3-13 Most common grain inclusions can be described through four following textures

1. Banded texture. The rock is assumed to consist of a matrix and parallel or nearly parallel, closely sized platy inclusions composed of pure mineral of our interest.
2. Rod-like texture. The rock is assumed to consist of a matrix and oriented closely sized rod-like inclusions composed of a mineral of our interest. These inclusions can also be connected to resemble more vein-like texture.
3. A rock texture consisting of a matrix and a variety of closely sized inclusions having shapes that can be described as flaky, more or less elongated or platy, composed of a mineral of our interest.
4. Granular texture. The rock is assumed to consist of a matrix and randomly oriented closely sized blocky inclusions, convex or concave grains, composed of pure mineral of our interest.

Position and size of this grain inclusion is important. Temperature profiles will be different, if these inclusions are dispersed throughout the volume or located closely to each other in the one part of the volume, previous studies like Harrison's (1997) have correlated heating rates with minerals sizes. The slowest heating rate is expected when grains are deeply embedded in the middle of the rock matrix. Closer to the matrix surface larger temperature gradients will be able to be measured. These temperature gradients are at the same time influenced by thermal conductivity of the matrix or effective thermal conductivity. If the matrix is composed of two well represented minerals, then simplified mixing rules to obtain effective thermal conductivity can be applied.

If more generic values from previous studies are used to provide an overview it can be seen that all ore types, which have copper bearing sulphides (or sulphides) and a matrix made of quartzite, will be excellent candidates for microwave assisted infrared sorting. It is important that for the best discrimination results, minerals of economic interest are in the relatively transparent matrix with at least five to ten times lower values of dielectric properties which will then influence even greater differences in heating rates.

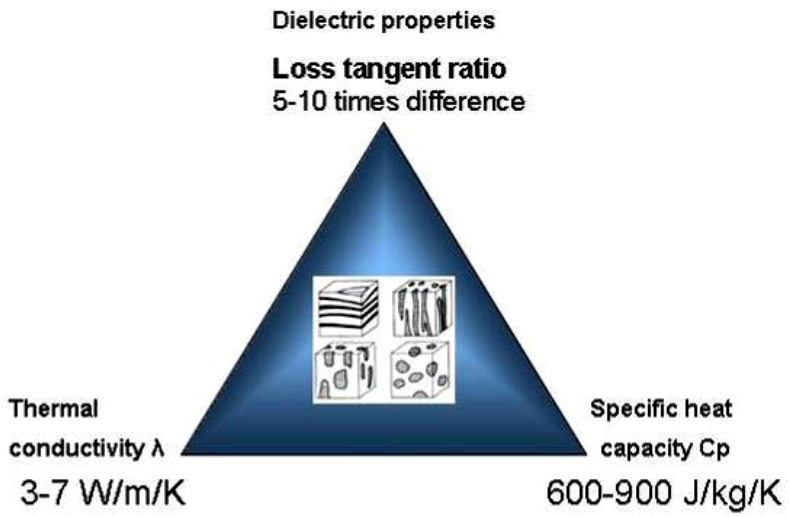

Figure 3-14 Generic values which can be used as a good guidance

Figure 3-14 shows more generic values which can be used as a good guidance for deciding favourable cases. Although, the boundaries have been located it has to be noted that for in situ rock fragments all these factors can be enhanced or compensated by texture and composition of the mineral phases involved.

3.7 Multimode Domestic Microwave Oven

There is a growing interest in the use of microwave domestic ovens in scientific research, which is due to a number of advantages associated with its exploitation. More importantly it is cost effective and simplistic in exposing materials to microwave energy. The microwave multimode oven is finding an extensive use for processing materials and it has been applied to a range of diverse areas such as: the testing of organic, inorganic and mineral powders, ceramics, drying materials, treatment of coal, preparing catalysts, and polymer materials. Some of these studies were focused on using domestic ovens because of future implementation of tested materials in food processing, for which microwave domestic ovens were optimised and designed. Other studies were focused purely by testing feasibility of processing materials by microwave energy. In both cases they were used because the investigation of the interaction between the material and multimode distribution of strength of electric field can be utilised.

The analytical solutions predicting field patterns just by analytical modal analysis can become potentially challenging when used in three dimensions. For this reason

modern finite element method (FEM) or finite difference time domain method (FDTD) are used to solve problems in three dimensions. In order to visualise electromagnetic field and multiple modes a simple model of domestic oven is defined. The microwave oven is a metallic box connected to a 500 W, 2.45 GHz microwave source via a rectangular waveguide operating in the TE_{10} mode. Figure 3-15 shows a 3-D visual solution of electromagnetic field pattern for vertical cross section of a multi-mode applicator with a spherical object placed as load on the rotating tray. This solution is achieved using High Frequency Structural Simulator (HFSS-Part of ANSYS simulation software). The geometry and material properties were sourced from model documentation for microwave oven tutorial for Multiphysics-COMSOL (COMSOL Multiphysics (formerly FEMLAB) is a finite element analysis, solver and simulation software). In the model, microwaves are supplied from the generator via waveguide into the cavity. The waves undergo multiple reflections from the walls. The reflected waves interfere with incoming waves and, in doing so; establish a distribution of electrical field strengths within the internal volume that correspond too many different stable modes of propagation. These multimodes include the volume of load as well. This is why it is defined as a multi- mode applicator.

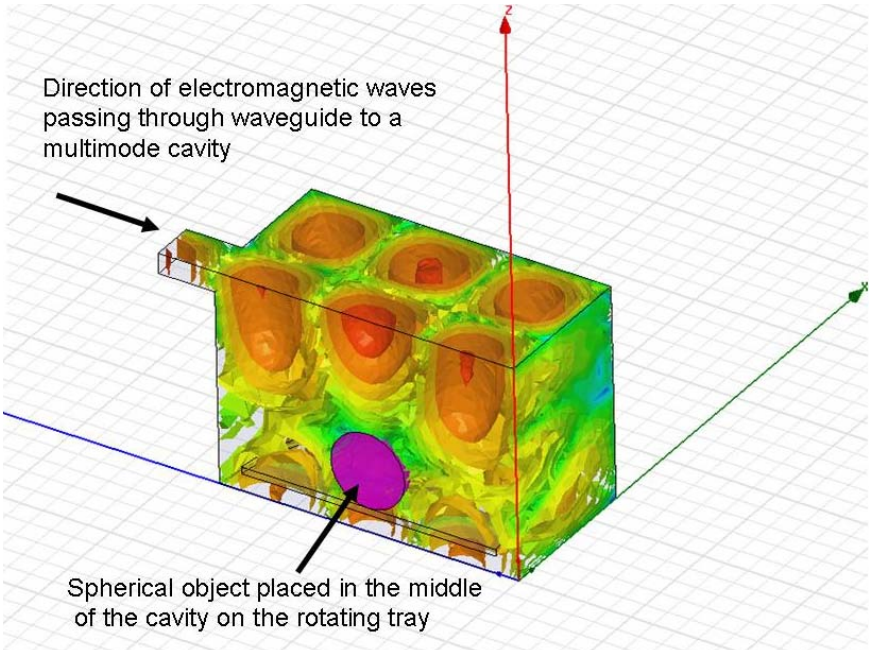

Figure 3-15 Multiple modes spread out through all volume of the applicator cavity solution achieved through HFSS

For multimode applicators including domestic microwave ovens dielectric properties of a load are important although size and location of the load will have an important

influence as well. In agreement with electromagnetic theory and volumetric heating better power transfers are achievable if the loads have larger volumes. This is supported by the fact that the electric field strength within the load will become the most dominant factor determining heating rate as seen in Equation 3-10. If the volume of the load is larger it means that it can accommodate more modes, particularly if the spatial distance between modes is very small. It can be stated that the average field strength will be higher and will eventually increase the heating rate of the load.

The spatial distribution of field strength is unknown because it is a direct function of reflection of electromagnetic waves from the walls of the cavity as well as from the load. The reflection of microwaves depends on multiple factors. For example: shape and dimensions of cavity, moving parts in the cavity, position of the waveguide entry, volume and asymmetry of the load. This is why in some studies, where interaction of known field strength with material is required, domestic microwave ovens are not a good solution.

Necessity to compare performance of microwave ovens exists and this is why since 1990 most microwave oven manufacturers have adopted a single standard for measuring the power output for microwave ovens. Standard IEC (2010) involves a borosilicate glass dish filled with 1 kg of water at 10 ^{o}C. The dish is placed at the centre of the base of the oven and the time required to heat the water to 20 ^{o}C is determined. Since the amount of heat required to raise the temperature of the water by 10 ^{o}C is known, the average power [W] delivered by the oven to the load can be calculated (Schubert & Regier 2005).

Some of the results from the previous studies, performed for the food industry, are taken into consideration as guidance in using domestic microwave oven to test ore particles. In the work of James et al. (1994) five different types of microwave ovens were studied to investigate reduction in power output with reduction of the load's volume. Standard IEC procedure was followed and the water load from 1.0 kg to 0.25 kg was reduced. For the similar size cavity with the glass turntable in the centre reduction in power output was 11.1%.

Another study of Burfoot et al. (1990) involved 102 individual ovens from 70 different models to look at variability between and within models and the effect of oven features on reheating performance. Repeatability within the ovens was tested by using mashed potato as a very homogenous load and every test was repeated five times with each oven. Reheating in 63 of the 102 ovens was easily repeatable with standard deviations of approximately 2 ^{o}C or less. Nine ovens produced standard deviations greater than 4 ^{o}C, and in four of these, standard deviations were greater than 6 ^{o}C.

It has to be emphasised that work of James et al. (1994) compared oven types and did not try to map the field distribution within an oven by moving a water load around it and recording the rate of rise of temperature. Results of that experiment apply only to water and it can be expected that once different material is placed in the cavity the field distribution will be changed completely. As guidance, it can be stated that it is better for heterogeneous material such as ore particles, to be heated in batches than as individual particles. This will increase the volume of the load. Effect can be enhanced by spreading the particles around on the turn table which will allow them to have greater chance of passing through multiple modes. From the study of Burfoot et al. (1990) it can be concluded that the majority of microwave ovens are capable for repeatable testing with standard deviations of approximately 2 ^{o}C or less on homogenous material like mashed potatoes, but for the heterogeneous material like ore particles separate repeatability study is needed.

3.8 Modes, Fields Patterns and Energy distribution in Multimode cavity

Mehdizadeh (2009) provided very simple way to a phenomenological explanation of multimode cavity operation through modes designation. He has designated letters to the modes. In Figure 3-16 (A) the resonant frequencies of modes A–P for an empty cavity are shown. In this designation, a mode designated by a letter could be an indexed mode of rectangular cavity, or a specific resonant mode of a cavity with more complex shape. The microwave source has a fixed centre frequency (for a domestic microwave oven that is 2.45 GHz) and a finite bandwidth of Δf_s (usually 40–100 MHz) which include modes D and E of the empty cavity.

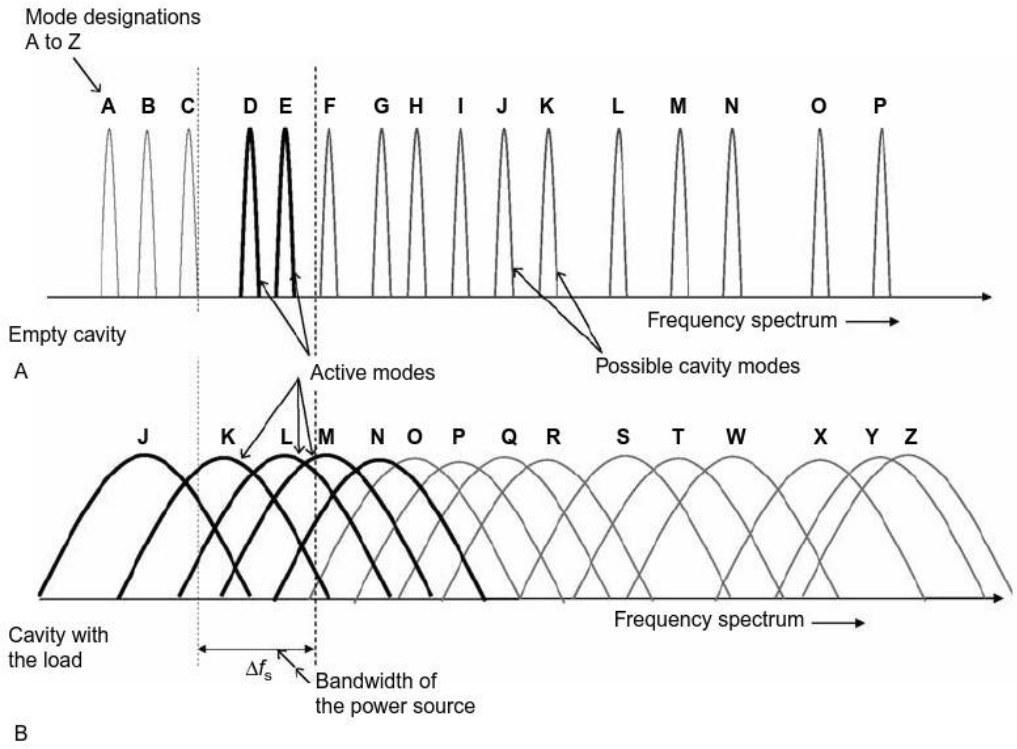

Figure 3-16 A phenomenological explanation of multimode cavity operation through modes designation after Mehdizadeh (2009).

As a result, it means that modes D and E are now operating, or active modes. Since there is no dielectric load, some of the power from the microwave source is dissipated on the walls of the cavity in the form of surface currents, and the rest is reflected. In Figure 3-16 (B) a lossy dielectric load is inserted into the cavity. A reduction of the Q factor (Q factor is more defined in Chapter 4 section 4.4) for each mode due to the increase in cavity loss is causing modes to be widened in the frequency band. The original modes D and E are no longer within the bandwidth of the microwave source. The introduction of the dielectric load has pushed those modes down in frequency. Instead of modes D and E, modes J, K, L, and M are either fully or partially within the bandwidth of the source, and have become active. This example demonstrates that modes K and L are strongly coupled, while modes J and M are weakly coupled, which means that their fields are not as strong. This is the reason for the robustness of microwave heating with multimode cavities. Even if the load changes, there is an abundance of other modes, few of which are always within the bandwidth of the source. With the existence of strongly coupled modes field patterns will appear. Another explanation can be given through optical beam model.

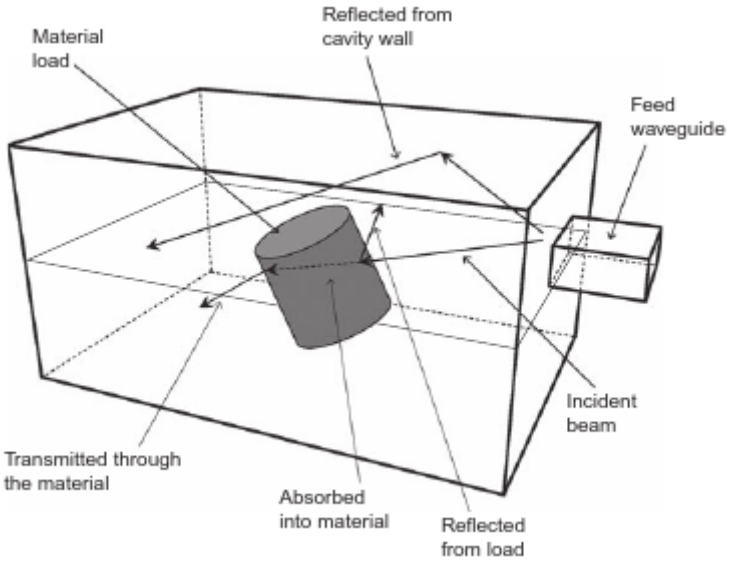

Figure 3-17 Schematic of an optical beam model for the operation of a multimode cavity after Mehdizadeh (2009)

Earlier study of James et al. (1994) indicated that it was easier to couple energy transfer into larger volumes of homogenous material. If the optical beam model is used to explain interactions of microwaves with the placed load in the cavity as showed in Figure 3-17 it can be seen that the incident beam has multiple reflections from the cavity walls including the reflection from the surface of the placed load. Some of that incident wave will be absorbed into homogenous material and some transmitted. How much energy will be absorbed depends of material properties, shape, and volume and penetration depth. By placing load's volume into the cavity remaining volume of the cavity is reduced and left to accommodate creation of multimodes. The possible shapes of these modes will be influenced by the remaining cavity space and modified boundary conditions from the surface of the load. To achieve more uniform heating rotation of the load is performed. This introduction of mechanical movement improves heating by stirring the fields caused by continuous modification of the boundary conditions for incident beam. If the volume of the load from Figure 3-17 is divided into smaller volumes and distributed in more than one place in the cavity it can be stated that potential for modification of the boundary conditions for incident beam will be even greater as shown in Figure 3-18. Riegert performed experimental and modelling work to visualise field patterns created in multimode cavity without a dielectric load (sourced from Mehdizadeh (2009)).

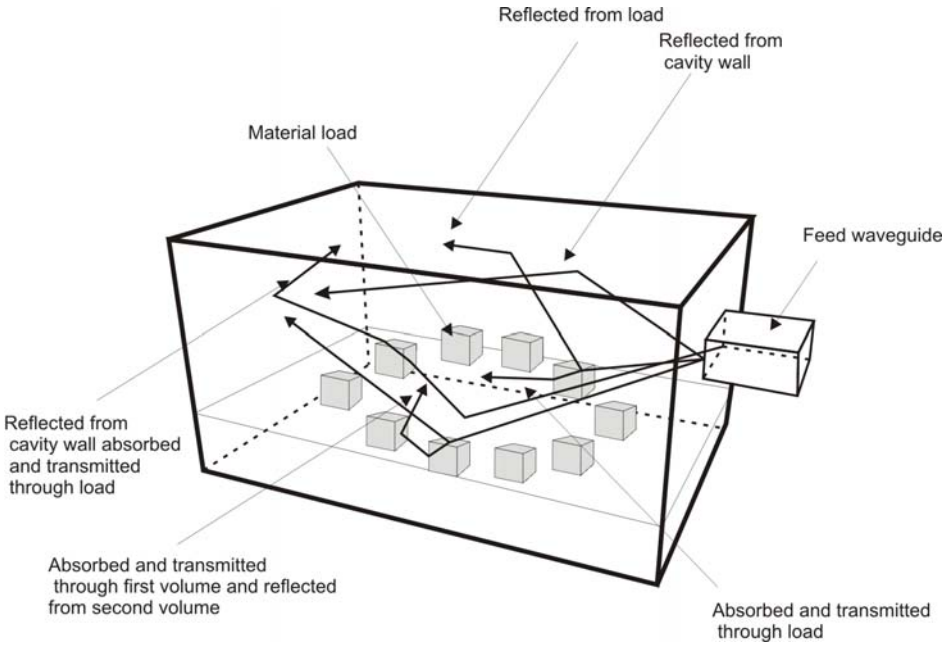

Figure 3-18 Modification of the boundary conditions for incident beam by distributing volume in smaller fragments

Figure 3-19 shows an example of the capability of FEM methods to predict the heating behaviour of the microwave multimode cavities. A resistive sheet composed of a carbon-loaded polymer, which had a sheet resistivity of 400Ω/sq was placed 5 cm above the bottom of a rectangular multimode cavity with the dimensions of 35 cm width, 30 cm length, and 25 cm height. This location is usually used to position glass rotating tray in domestic microwave ovens. The cavity was fed with a 2.45 GHz microwaves and a low power of 100 W. A layer of thermal fax paper was placed above the resistive sheet, and the structure was sandwiched between two thin layers of glass to ensure intimate contact between the resistive sheet and the thermal paper. As the resistive sheet was heated, the pattern of electric field nodes was shown as dark areas in Figure 3-19 A). The experimental setting with all its features was solved in 3-D with the COMSOL package. The results of the modelling (white spots with higher E field intensity), as shown in Figure 3-19 B), correspond extremely well with the location of the electric field nodes (dark hot spots) on the thermal fax paper.

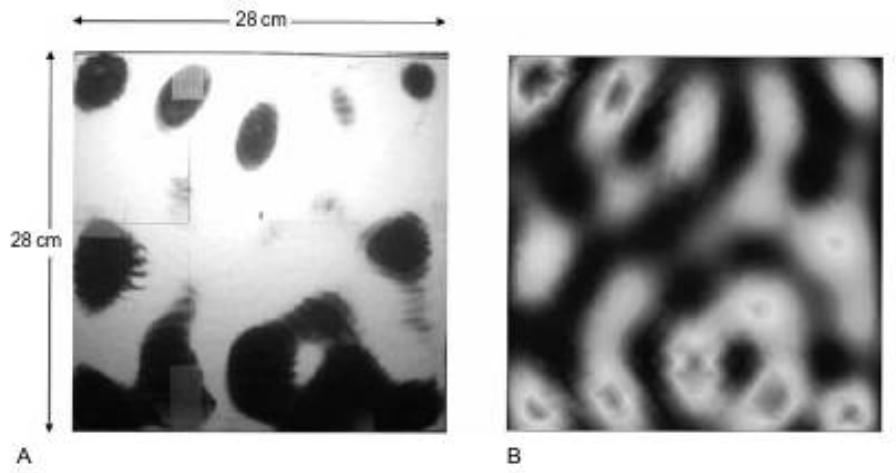

Figure 3-19 Sourced from Mehdizadeh (2009), experimental and modelling work of Riegert

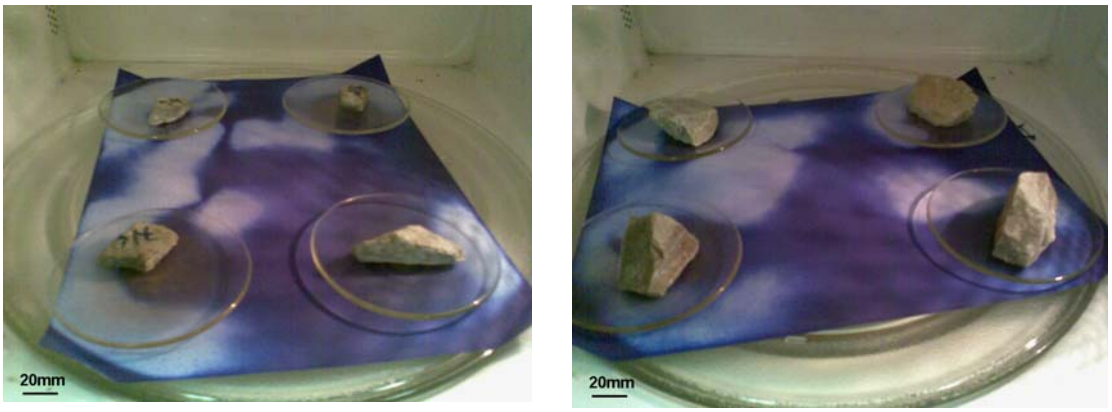

a) Pattern of field nodes created on the thermal paper for the 31.5x22.4mm particle size. Tested ore type: QZ Ohio.

b) Pattern of field nodes created on the thermal paper for the 45x37.5mm particle size. Tested ore type: QZ Ohio.

Figure 3-20 Pattern of field nodes created after 12 s of exposure time to 1.2 kW of applied power

Model "Sharp" 380-J was used for experimental studies in this thesis. This model has a glass rotating tray and the position of the wave guide is on the right side of the cavity. A quick experiment was derived to visualise field patterns in this domestic oven using one of the supplied ore as dielectric load. Two different rock sizes were used as shown in Figure 3-20.

Thermal paper with chemical which has microwave active composition (manufactured by Atlanta Chemical Engineering L.L.C.) was placed on the glass rotating tray. Rock particles were symmetrically arranged and placed on concave glass dishes to minimise contact between thermal paper and surface of the particles. The particles were then heated up for 12 s using 1.2 kW of applied power. Throughout exposures glass tray

rotated load for full 360 degrees. As expected, the thermal paper showed the existence of multiple field nodes in the plane which corresponds to the surface of the rotating glass tray. The field patterns and the energy distribution were different because the load was different.

Consequently it can be stated that it is better if material such as ore particles is heated in batches. This will increase the volume of the load. The effect can be enhanced by spreading the particles around on the turn table which will allow them to have even greater chance of passing through multiple modes. During the exposures there will always be modes which are strongly coupled with the load. Additionally this means that the particle made of a less responsive mineral will a have higher possibility for a better energy transfer within the same batch of material.

3.9 Different Applicators Made From WR340 Waveguide

Even simple waveguides can be used as applicators. Simulation software HFSS was used to investigate electromagnetic field in the WR 340 waveguide equipped with a vertical opening for the load insertion and a choice for three different endings. All three endings were chosen to demonstrate different behaviours of electric field. At the same time this would define the type of applicator. The geometry of the models was cut in the half to provide better presentation of the modelling results.

3.9.1 Theoretical Applicator with the Perfectly Matched Layer (PML)

A perfectly matched layer (PML) is an artificial absorbing layer for wave equations, commonly used to shorten computational regions in numerical methods to simulate problems with open boundaries. The main characteristic of a PML (which distinguishes it from an ordinary absorbing material) is that it is designed so that wave is incident upon the PML from a non-PML medium do not reflect at the interface. This property allows the PML to strongly absorb outgoing waves from the interior of a computational region without reflecting them back into the interior. It is used in the FDTD and FEM methods. As it can be seen from Figure 3-21 by changing the phase component of the wave, amplitude component will move from the generator toward PML with its constant value. This means that the E-field will be very uniform within

the waveguide. This type of E-field uniformity is experimentally very challenging to achieve due to reflections from inserted load, especially if the properties of the load are not constant.

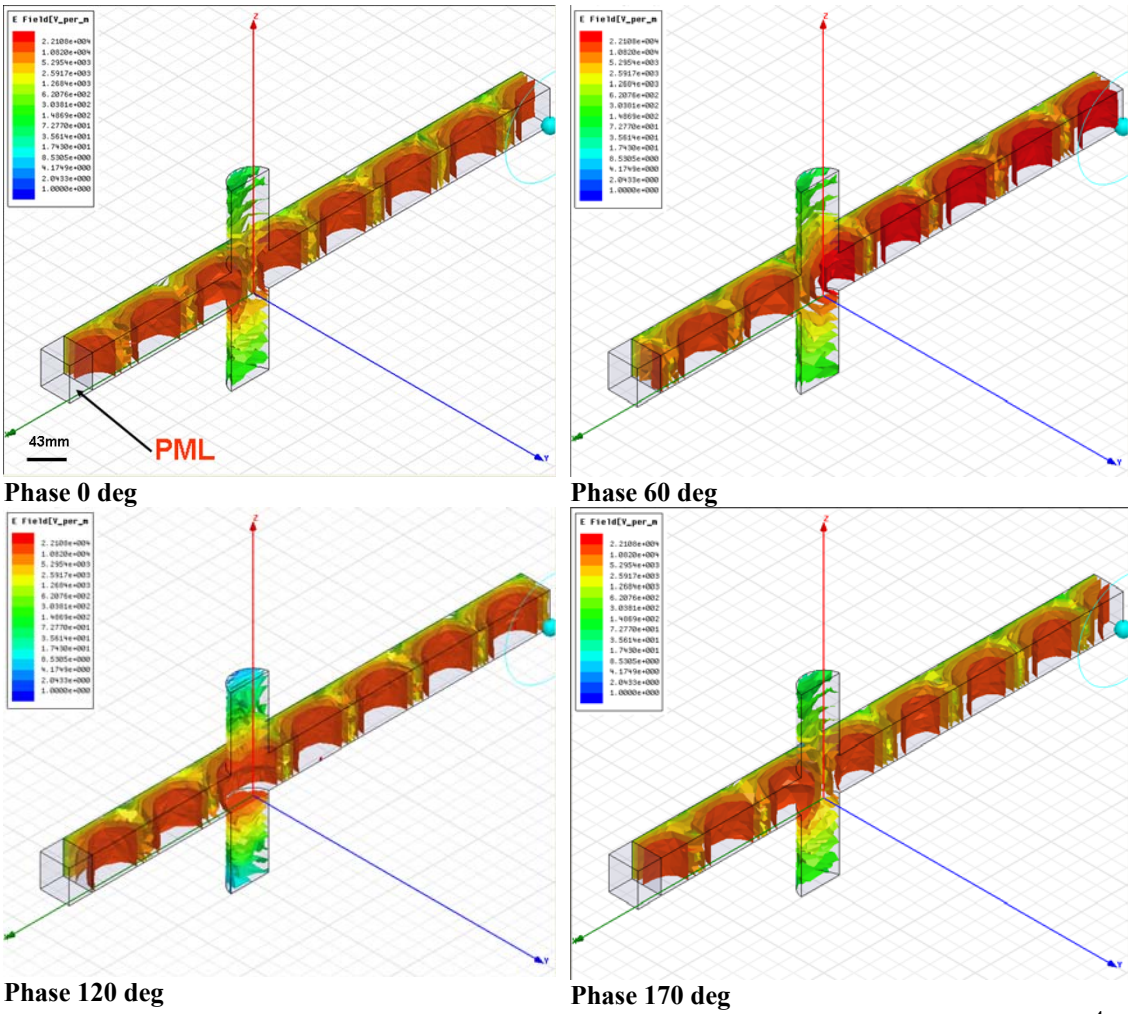

Phase 0 deg **Phase 60 deg**

Phase 120 deg **Phase 170 deg**

Figure 3-21 Theoretical Applicator with the Perfectly Matched Layer. E-Field scale: *max* 2.2*10^4 V/m *min* 1.0 V/m

3.9.2 Applicator with the Standing Wave Pattern

Waveguide with a short circuit at the end establish a standing wave within the waveguide configuration. Fixed position short circuits can be found with waveguide applicators designed for a specific process or material where the position of the short has been optimized for maximum power coupling.

A movable short circuit is preferred so that the short position can be optimized for each case, typically for locating high electric fields where the load can be heated. Figure 3-22 indicates that by changing the phase component, intensity of the

amplitude component will change. If the load is inserted through vertical opening in the middle of the waveguide (for the given model) it will be exposed to a maximum of E- field only by moving sort circuit in z-direction to match the phase component of the standing wave.

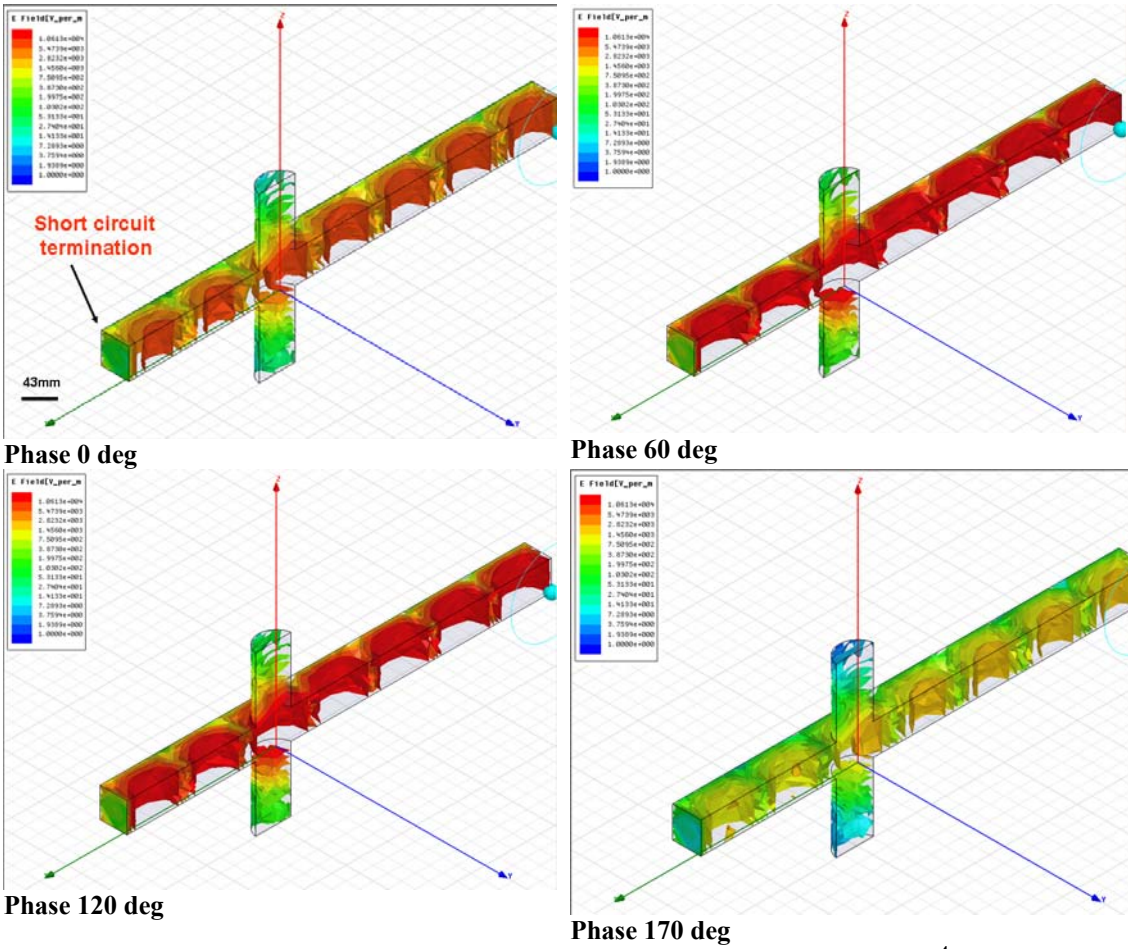

Phase 0 deg **Phase 60 deg**

Phase 120 deg **Phase 170 deg**

Figure 3-22 Applicator with the Standing Wave Pattern. E-Field scale: *max* 1.0*10^4 V/m *min* 1.0 V/m

3.9.3 Travelling Wave Applicator - Experimental Setting with the Dummy Load

By Metaxas (1983) applicators in which power is mostly absorbed by the workload with the residue being dissipated in an absorbing terminating load are described as travelling wave applicators. A wide variety of waveguide terminations are available for a variety of applications. For the industrial microwave heating systems most commonly are used dummy loads for the maximum absorption and short circuits for maximum reflection of minimum absorption. Dummy loads can be grouped into two main categories, dry loads and wet loads. The dry loads are preferred for applications where standing waves must be minimized such as with travelling wave applicators.

By definition, wet loads are designed to absorb microwave power directly into a high loss fluid medium, such as water. Wet loads are quite adequate and often used in isolator configurations.

Figure 3-23 shows propagation of microwaves through rectangular waveguide which is terminated with a dummy load for a maximum absorption. This experimental setting is used to expose thin dielectric continuous material which passes in y-direction in the middle of the rectangular waveguide where E-field is the strongest. The microwave power enters the waveguide section and exits toward a load at the other end of the section. The E-field intensity profile in the cross-section of the waveguide (in the x – y plane) has a sine function shape for single mode.

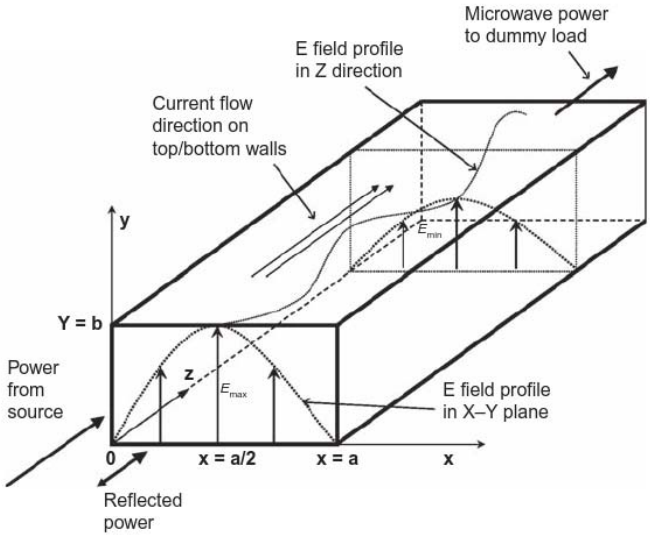

Figure 3-23 Propagation of microwaves through travelling wave applicators. After Mehdizadeh (2009)

As Mehdizadeh (2009) explains: "If the load and source are impedance matched, which means there are no standing waves, the E-field would be uniform in the longitudinal z-direction. In cases where there is a mismatch, a standing-wave pattern will be formed where the maximum E-field varies along the z-direction, and the ratio of maximum to minimum field will depend on the mismatch level".

A new model was created (see Figure 3-24) to describe experimental setting with isolator configuration. The experimental setting was equipped with a dummy load made of quartz tube with a constant flow of distilled water used to absorb microwave energy. This configuration shows that the standing wave will be created. It also shows

that the highest intensity of the E-field is around the tube with the water when the phase component of the whole system is matched. In Figure 3-24 as expected, a very high concentration of E-field can be seen around a dummy load (for the phase component of 60 deg). This model did not include any load between source of the microwaves and the dummy load.

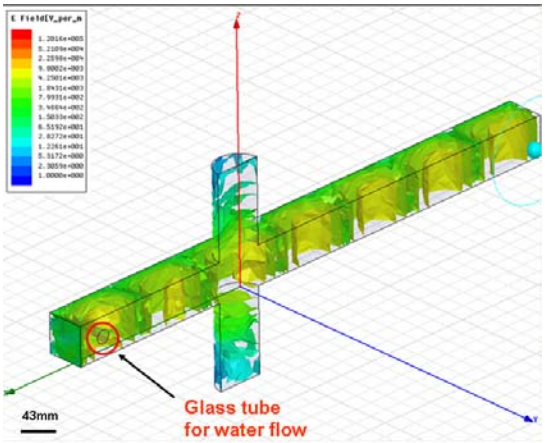

Phase 0 deg

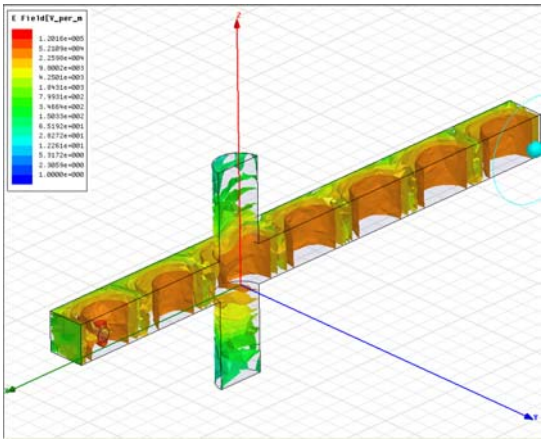

Phase 60 deg

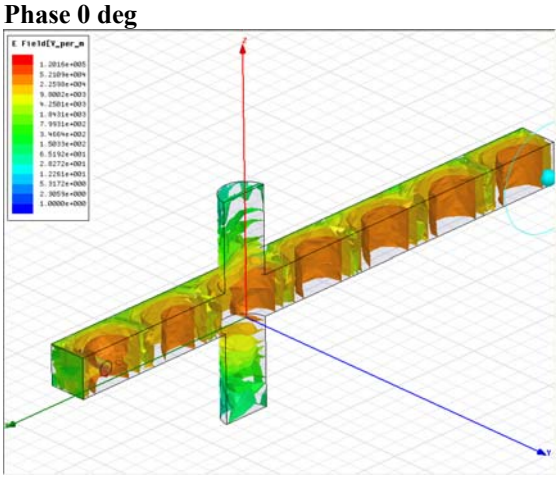

Phase 120 deg

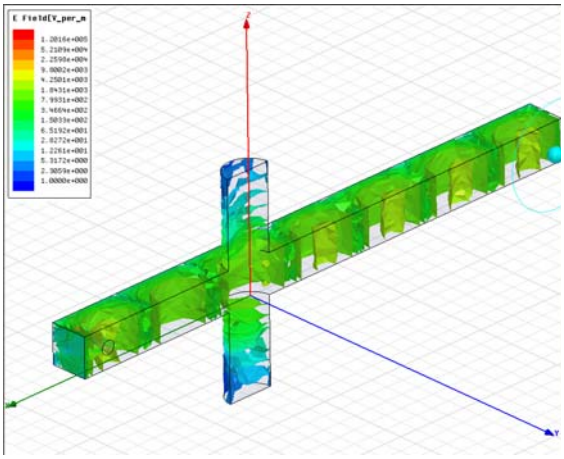

Phase 170 deg

Figure 3-24 Experimental Setting with the Dummy Load. E-Field scale: *max* 1.2*10^5 V/m *min* 1.0 V/m

3.9.4 E field and Volumetric Loss Display

The next step to investigate was to model E-field changes when heterogeneous load is inserted into a previously described model of the experimental setting with isolator configuration and shown in Figure 3-24.

The heterogeneous load was created as a two-component and geometrically simplified rock particle. Matrix of the rock particle was in the shape of cylinder and made of quartz (as common gangue mineral and almost no responsive to microwave heating),

while second component was chalcopyrite in the shape of cubic grains (as common copper bearing mineral and very responsive to microwave heating).

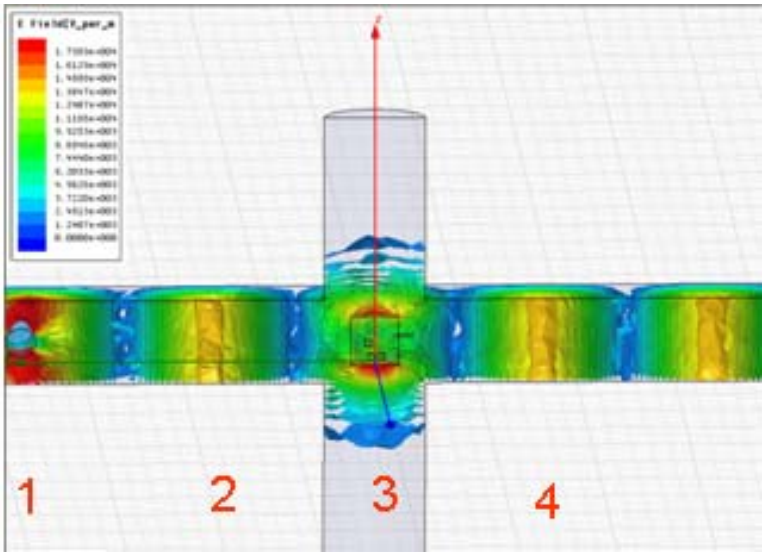

Figure 3-25 E field in the applicator and load

Figure 3-25 shows E-field in the travelling wave applicator loaded with simplified rock particle made of quartz and chalcopyrite.

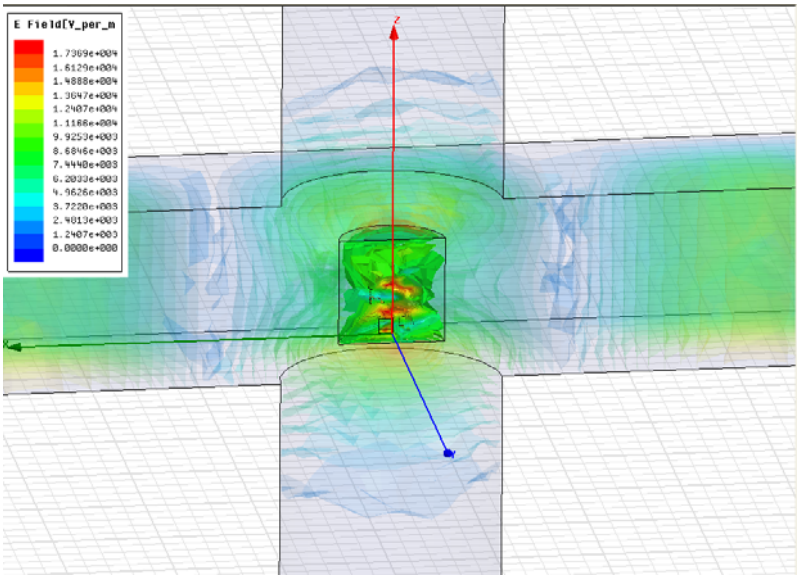

Figure 3-26 E field in the matrix made of quartz

The highest intensities for the E-field can be found in labelled positions number one and three. The position number one shows very strong intensity induced by water load while position number three shows interaction of one of the nods with a rock particle. It can be seen that the shape of the node has changed from sine function shape by interacting with the load.

Higher values of the E-field can be found on the top and the bottom, or on the edges of the quartz cylinder. Figure 3-26 shows an E-field inside the volume of the load.

Intensity of the field is gradually decreasing from the periphery of the quartz cylinder toward the centre due to the partial absorption of the quartz material, only to start rising in the centre where grains of chalcopyrite (as more absorbing material) are located.

With known electrical field strength inside the mineral it was possible to calculate volumetric loss which could be also calculated by applying Equation 3-5. From the Figure 3-27 it can be seen that the volumetric loss is the highest on the edges of the cube grains, which is in agreement with volumetric heating and this chosen geometry for the grains. It can also be seen that the volumetric loss is not the same for every grain due to their different locations within the matrix material.

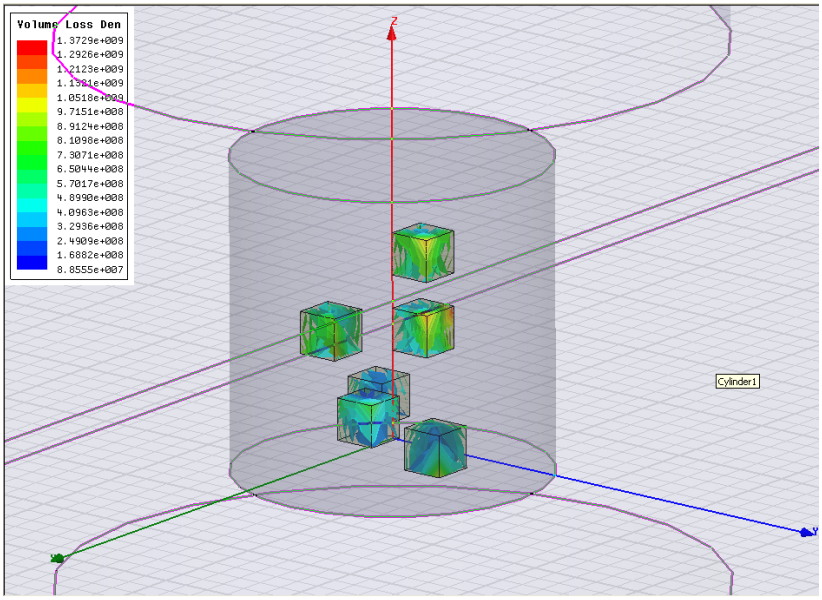

Figure 3-27 Volumetric loss for chalcopyrite cubic grains embedded in quartz matrix

3.9.5 Thermal Paper Pattern

To test the prediction of FEM modelling using HFSS software a synthetic sample of plaster was casted with embedded chalcopyrite grains (Figure 3-28 shows X-ray radiogram of the sample). Before testing the sample was dried for a day in the convective oven at 70 ^{o}C to remove any remaining water content. Plaster was chosen because it would provide similar conditions from the modelling regarding microwave energy absorption, which was a highly responsive mineral such as chalcopyrite

surrounded with less responsive matrix. It also enabled to cast a matrix in cylindrical shape which was used in the model.

The goal was to achieve validation of the anticipated microwave energy pattern, which is necessary for obtaining the desired uniform heat release within the irradiated material. This validation represented a predicted distribution of the microwave energy in the processing cavity for the specific application. A simple test with thermal paper offered precisely that - simple visual proof of microwave energy patterns.

Thermal paper was made by painting cardboard with chemical which has microwave active composition (MWAC manufactured by Atlanta Chemical Engineering L.L.C.).

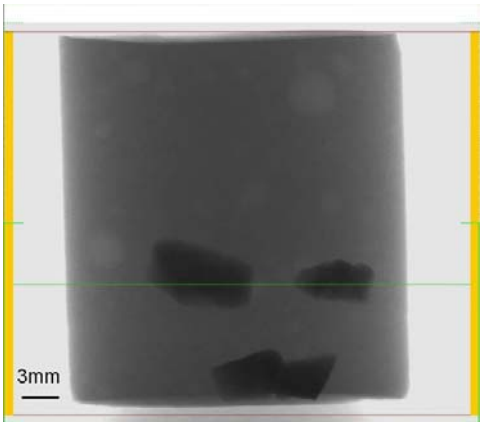

Figure 3-28 Synthetic plaster sample with chalcopyrite grains size -4.75+3.35

Figure 3-29 TWA applicator with dummy water load

Figure 3-29 shows experimental apparatus used with numbers indicating the locations of the nodes predicted by modelling. On the left side there is a dummy load with plastic tubes providing the constant water flow through quartz cylinder. This section continues on the right with a vertical opening long enough to prevent any wave propagation and wide enough to insert testing samples into the applicator.

Three stripes of prepared thermal paper were used. Two were cut to match the width of the WR 340 waveguide and obtain full coverage of the bottom surface in the waveguide. The third one was narrower and positioned from the beginning of the dummy load, under the quartz tube and passing through vertical opening.

Patterns were obtained in two exposures. The first for the empty applicator and the second for the applicator loaded with plaster sample. Exposure time in both cases was 10s using 0.6 kW applied power. In Figure 3-30 patterns from both exposures can be seen. First on the top is from the loaded applicator and the second, covering the longer section is from the empty applicator. By comparing results from modelling (see Figure 3-25) first four nods can be easily identified on the thermal paper. The first node is distorted from its sinusoidal shape and it looks more like a stripe due to the influence of quartz tube with water. The second node is detected and it has retained its sinusoidal shape. The mark of the third shows that it has been twisted out of its normal shape which can be explained by a sudden change in the geometry of the applicator which has changed its boundary conditions by the vertical opening. At the end node four can be identified followed by node five with similar intensity.

Figure 3-30 Thermal paper patterns from both exposures

Figure 3-31 shows in more detail the pattern from second exposure with synthetic plaster sample placed on the same spot as it was during microwave heating.

Figure 3-31 Thermal paper pattern

To avoid contact between plaster sample and thermal paper, small paper ring was placed between them with a height of 5 mm during exposure. It can be seen that intensity of the E-field created at the place of the load was much higher compared to the neighbouring node.

3.9.6 Summary

The information of E-field and material interactions is important to the design of the microwave applicator, because the dielectric properties of the tested material will become a part of the applicator's functioning. This is a unique feature which has to be taken with a great importance. The modelling software can help to a large extent in predicting field patterns and assessing different heating scenarios (good results achieved with homogenous material such as some types of food), but for a treatment of heterogeneous materials such as rock fragments, best results can be achieved combining them with experimental testing.

3.10 Travelling Wave Applicator

Processing equipment needs to be designed precisely around an application and requires proper planning for optimised operation. Furthermore there is an experimental requirement to design an applicator which can test particles continuously from the same batch tested in a domestic microwave oven. To do so it was decided that a travelling wave applicator designed as a state machine will be the best option to conduct the experiment and collect the necessary data. The state machines are used in applications where distinguishable states exist. Each state can lead to one or multiple states, and can also end the process flow. State Machine architecture can be used to implement complex decision-making algorithms represented by state diagrams or flow charts (Lab View 2011).

Domestic microwave ovens are also designed as a state machine. Figure 3-32 describes a very simple state machine which is applied in most domestic microwave ovens to perform operation of heating. It can be seen that initial state starts with the input from a user by setting the time for operation. For this state machine constant power is assumed to simplify a number of states. Once operation is enabled it can be interrupted by opening the door (for example to stir the content or change the load position) or by timed operation. When the time set by timer is timed out, cooking is complete and the idle state is taken.

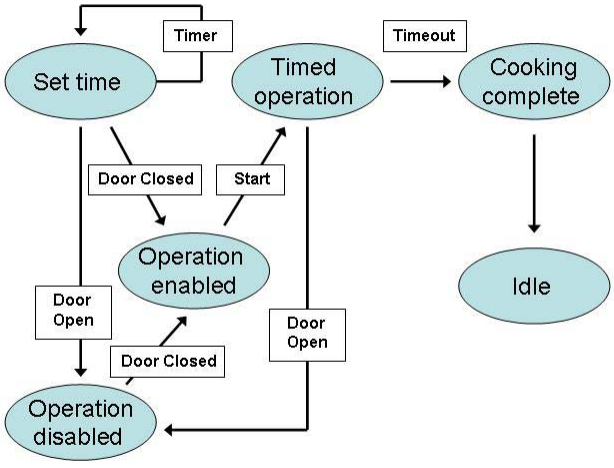

Figure 3-32 Flowchart for the state machine used in most of domestic microwave ovens

It should be mentioned that the state machines are used in applications where different states exist. To initiate change from one state to another user input needs to be given or in-state calculation to determine which state will be next. It is good to have "initialize" state, followed by a default state where many different actions can be performed. Each state can end the process flow, and can also lead to one or multiple states. The actions performed can depend on previous and current inputs as well as states. Shutdown or idle state can then be used to perform clean up actions which place the state machine ready for the next employment.

A travelling wave applicator for which schematic can be seen in Figure 3-33 and applicator itself in Figure 3-34 was constructed from a standard rectangular WR340 waveguide components arranged in such a way that the target load passes through in the point between water load at one end, and a microwave source from the other end. The components used to build applicator came from different manufactures (Sairem, Festo, Ocean Controls...). Author of this thesis used these components to assemble applicator and build universal controlling platform by Lab View (refer to Appendix A for more details). As microwaves pass along the waveguide they are absorbed by the load according to the dielectric properties and size of the load. A water load is attached to the end of the waveguide to absorb any microwave energy that is not absorbed by the load. It is also there to establish constant power delivery through waveguide which is delivered when steady state is reached. A steady state is reached by using an automatic tuner, which matches the impedance of the overall system with the impedance of the microwave generator.

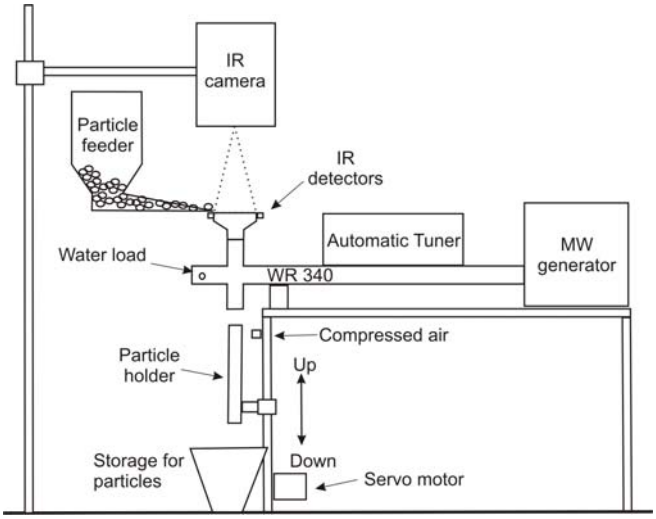

Figure 3-33 Schematics of design for the travelling wave applicator

Figure 3-34 Travelling wave applicator designed and constructed to perform experiment

The travelling wave applicator based system was automated to collect data and to reduce any possible errors which could be caused by repetitive tasks exposing large amounts of particles while testing. Automation was designed using a state machine whose main purpose was to provide the same conditions for microwave exposure to every particle during testing. Figure 3-35 shows states which were used in this experiment to have continuous flow of particles through the travelling wave applicator.

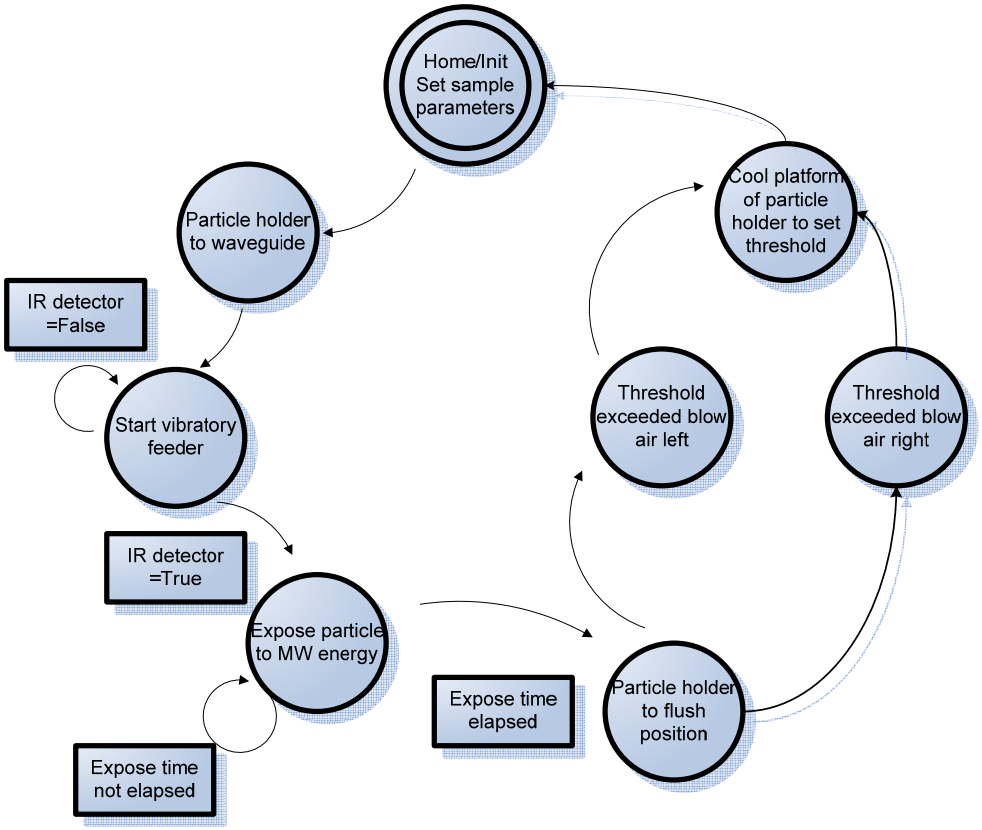

Figure 3-35 State Machine used in the experiment

- "Home or initial state" was used to set parameters for sample testing. These parameters involve: the amount of power used, time of exposure, two thresholds in temperatures and region of interest for temperature calculation. The first temperature threshold is for sorting particles into cold and hot groups according to their reached temperatures during exposures. The second temperature threshold is to cool the background i.e. particle holder made of Teflon® used to remove particles from an applicator. It was usually set to match the room temperature during testing. Region of interest is a surface from which mean and maximum temperatures are calculated using infrared camera.
- "Particle holder to waveguide" state prepared the applicator to accept incoming particles for testing. A batch of numbered particles is fed into the waveguide by two serial connected feeders. The speed of vibrations on the feeder closer to the cavity is higher to provide better separation of closely positioned particles. At the same time the infrared detector is enabled and ready to create a signal for a passing object which interrupts or completely breaks the infrared beam.
- "Start vibratory feeder" state was enabled by the particle holder being inside the applicator. The state machine stays in this state if the Boolean signal is "False". This means that the particle has not still passed through the guiding funnel with infrared detector, and into the particle holder. Once the particle passes interrupting the beam, condition to move to another state is met.
- "Expose particle to microwave energy" is state for which timing was defined in an "Initial state" at the beginning. This is the most important state in the experiment because in this state rock particles are interacting with electromagnetic energy and simultaneously data is collected, processed and stored in real time. Interaction of the particles with microwaves can be described by negative feedback which is conditioned by the type of applicator and automatic tuner used to control the system. A feedback system, in general engineering terms, is a system whose output is fed back to the input. Depending on the output, input is adjusted to reach a steady-state. When feedback acts in response to an event/external influence, it can influence the

input by negative feedback which can be seen in Figure 3-36. Negative feedback is also known as a self-correcting feedback, which tends to reduce the input signal that caused the disturbance in the system. Calculated temperatures from a region of interest are compared with these set thresholds and an input for a new state is created.

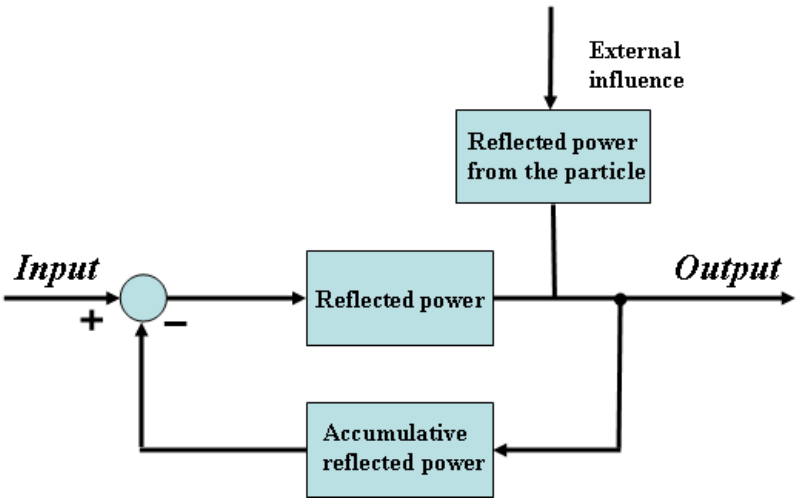

Figure 3-36 Negative feedback applied to travelling wave applicator

- When the exposed time has elapsed the particle holder is assuming a new position where particles can be flushed by compressed air to a bin reserved for cold or hot group. Inputs from the previous state whether the surface temperature of the particle has reached values higher or below set threshold will perform actual physical separation into the cold or hot group.
- After flushing the particle, a new average temperature of background is calculated and compared with room temperature. If there is any residual heat, the particle holder is cooled down by forced convection using compressed air. If there is no residual heat the state machine will loop until all particles from one batch testing are exposed to microwaves. Looping can be stopped by user command at any time. This will place the state machine in a home state.

All of these states will produce repeatable testing for very complex material like rock particles. It will minimise the possibility for error and allow real time data collection during heating. Detailed descriptions of hardware and software used to build and control this travelling wave applicator as a state machine can be found in Appendix A.

3.11 Experimental Methodology

The overall aim of developed experimental methodology was to investigate possibility of sorting ore with microwave pre-treatment followed by the infrared measurement of temperature. Two different copper ore types were supplied from Bingham Canyon Mine operated by Rio Tinto's Kennecott Utah Copper Corporation. The sorting criterion was based upon temperature threshold determined by mineral content which needs to be recovered from the concentrated material. The remaining material was considered to be the waste, with mineral contents below economic value for the recovery. Selected ore types were tested in two closely related experimental steps. Both steps of experimental investigations involved testing on representative sample groups. Figure 3-37 illustrates test work procedure.

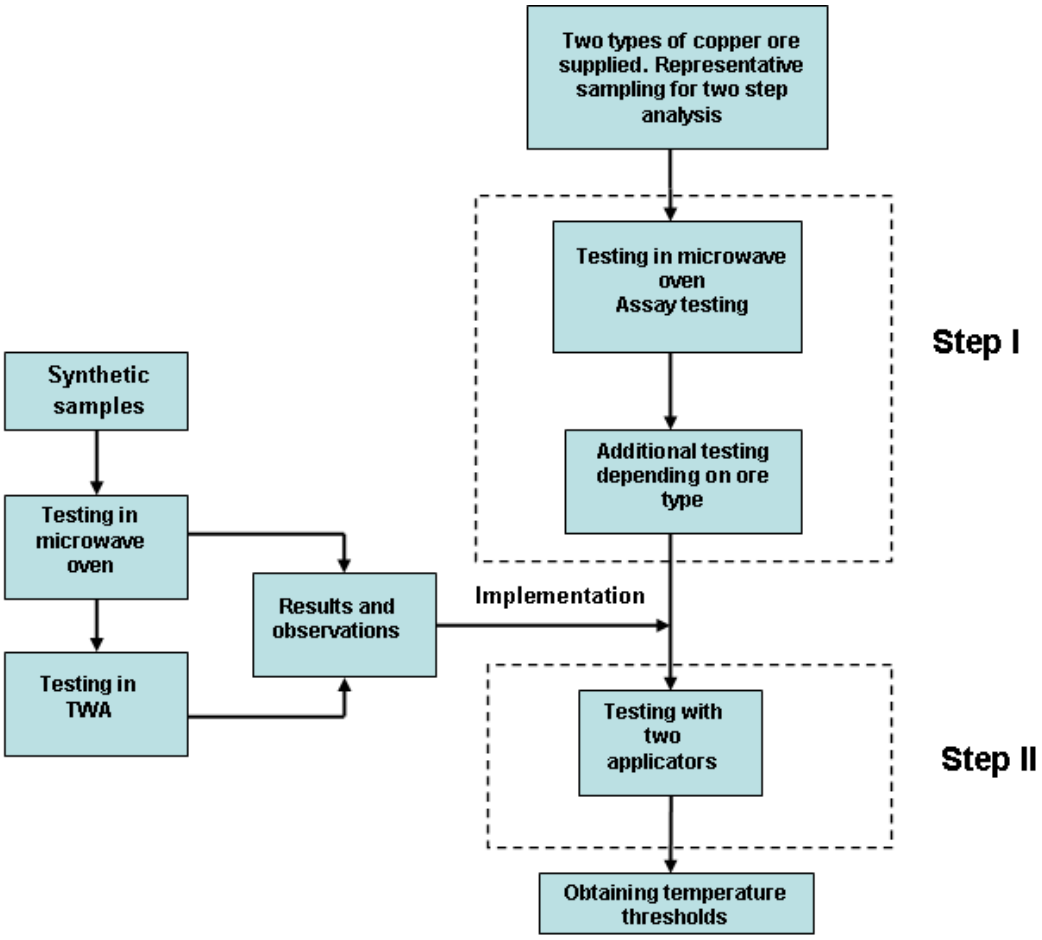

Figure 3-37 Diagram of test work procedure adopted to address the hypothesis

For the better understanding of interactions between microwave radiation and mineralogy of real ore particles synthetic samples were created. Because dielectric

properties of the tested materials become a part of the applicator's functioning the interactions of E-field and material was studied in two microwave applicators which had two different E-field distributions. The first was multimode domestic oven and the second travelling wave applicator. Results and observations from synthetic ore particles were then implemented in the second step of experimental investigation.

- The first step involved testing ore for reproducibility and separability using multi-mode excitation in a domestic microwave oven. The particle classification was done through assaying for copper, iron and molybdenum. After microwave exposure the obtained data from assaying was used along with measured temperature difference to create separation curves. The separation curves were created by plotting sorted measured temperature increase versus cumulative mass and assayed metals mass. This step also involved additional testing such as testing on a larger population and flotation testing which were performed for a chosen ore type.

- The second step involved testing representative groups of particles in two microwave applicators. Temperature increases were then compared from both applicators, correlation with particle texture and composition was investigated.

Three measuring techniques were used to complete an investigation about ore types and their interaction with microwave energy. They were:

- High-resolution X-ray computed tomography
- Mineral Liberation Analyser
- Automated Mineral Identification by Optical Microscopy

Their implementations in these experimental studies are illustrated in following sections.

3.11.1 High-resolution X-ray computed tomography (HRXCT)

After extensive usage for medical research, high-resolution X-ray computed tomography (HRXCT) gave very promising results used by the mineral industry to study texture and structure of different ore types. Information which is obtained is of great importance for geological and metallurgical studies, especially for ones which

involve optimisation of metallurgical processes and liberation of specific mineral phases.

As Kyle *et al.* (2008) describes, "The HRXCT produces two-dimensional images ("slices") that reveal the interior of an object as if it had been sliced open along the image plane for viewing. By acquiring a contiguous set of slices, a volumetric map of a sample can be obtained, allowing three-dimensional inspection and measurement of features of interest. HRXCT images reflect differences in X-ray attenuation that arise principally from differences in density and atomic number within the object".

Information is most commonly saved in a form of digital radiograms which are used to build a volumetric map of a sample. Mathematical algorithms are used to merge all two dimensional information in correct order and form new three dimensional information. Physics and mathematics of computed tomography are summarised by Smith (1990) who described three novel reconstruction methods and later Stock (1999) who not only provided algorithms he also provided some guidance on how it can be potentially used to study: inorganic matrix composites, transport in porous media, calcified tissue and fatigue crack closure.

To perform HRXCT, a Micro-CT SkyScan 1172 was used which can supply X-ray energy from an X-ray tube with adjustable power. For most rock particles the current applied was between 50 to 100 μA and the voltage delivered between 70 and 100 kV adjusting them to maximise power. Another parameter used, was "exposure time" which was between 1.7 s to 5 s. Exposure time was determined by the operator combining them with voltage and current parameters to obtain the best results for scanning and reconstruction.

Figure 3-38 shows the interior of SkyScan 1172 micro tomograph with a platform to hold sample for scanning in the middle. Platform can rotate 360 degrees in very fine steps for precise scanning.

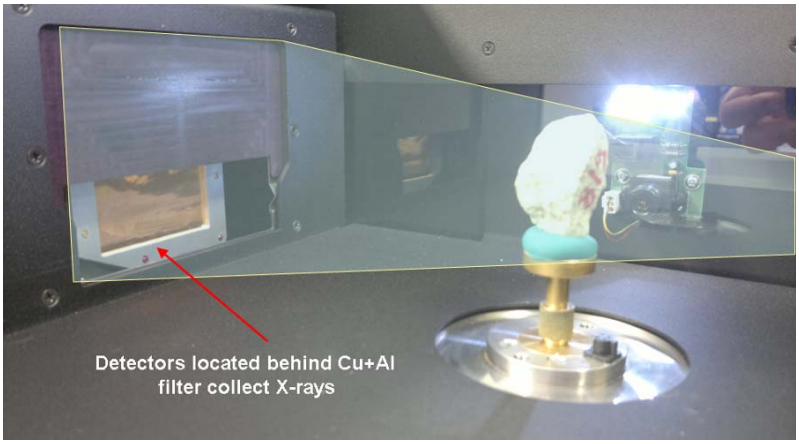

Figure 3-38 Rock particle is exposed to energy of X-rays

Detectors which collect attenuated X-rays after they pass through rock particles are located behind filters as seen in the image Figure 3-38. For all rock particles scanning an aluminium-copper filter was used to improve image quality by hardening the X-ray beam after passing through the rock particles. This effect is caused by a polychromatic beam. Work of Ketcham and Carlson (2001) describes that "lower-energy X-rays are attenuated more readily than higher-energy X-rays, a polychromatic beam passing through an object preferentially loses the lower energy parts of its spectrum. The end result is a beam that, though diminished in overall intensity, has a higher average energy than the incident beam."

By the same authors, beam hardening is also associated with ring artefacts. In reconstructed data full or partial circles centred on the rotational axis are present. They are caused by shifts in output from individual detectors or sets of detectors, which cause the corresponding ray or rays in each view to have anomalous values; the position of a ring corresponds to the area of greatest overlap of these rays during reconstruction.

Micro-CT SkyScan 1172 was designed for medical research and belongs to a group of medical CT systems which usually use a limited dose of relatively low energy. For these systems it is common to have energy of X-rays lower than 125 keV (Ketcham & Carlson 2001).

Scanned images reflect changes in density so phases of materials with higher density will clearly be distinguishable from the phases with lower density. In HXCT linear

attenuation coefficients are used to identify and group selected phases according their densities. In researches of Tsuchiyama et al. (2000) and Denison et al. (1997) we can find linear attenuation coefficients for most common minerals along with their corresponding densities calculated for three different X-ray energies. Tsuchiyama used 100 keV and Denison used 70 and 80 keV.

Both studies reported values for linear attenuation coefficients between 0.4 and 1.0 cm^{-1} for most common rock forming minerals, including quartz. In both studies exceptions were magnetite and almandine, and others were fayalite, ilmenite and siderite.

In the study of Grasberg porphyry Cu-Au ores (in Papua, Indonesia), Kyle et al. (2008) used HXCT to distinguish gold, metallic sulphides and oxide minerals from a typical rock forming matrix e.g. quartz. He calculated linear attenuation coefficients for common porphyry–skarn metallic minerals multiplying the mass attenuation coefficient by mass density. This data can be used to predict the ability to differentiate minerals with HRXCT. The values shown here are based on end-member compositions and densities and were calculated using the XCOM Photon Cross-Sections Database (NIST 2010). In Figure 3-39 we can see that for X-ray energy up to 100 keV, linear attenuation coefficient for quartz is below 1 cm^{-1} which corresponds with earlier findings. Above quartz there is group of metallic minerals with much higher linear attenuation coefficients. This means that it becomes easy to distinguish between rock forming minerals and minerals of interest which are metallic oxide and sulphide minerals.

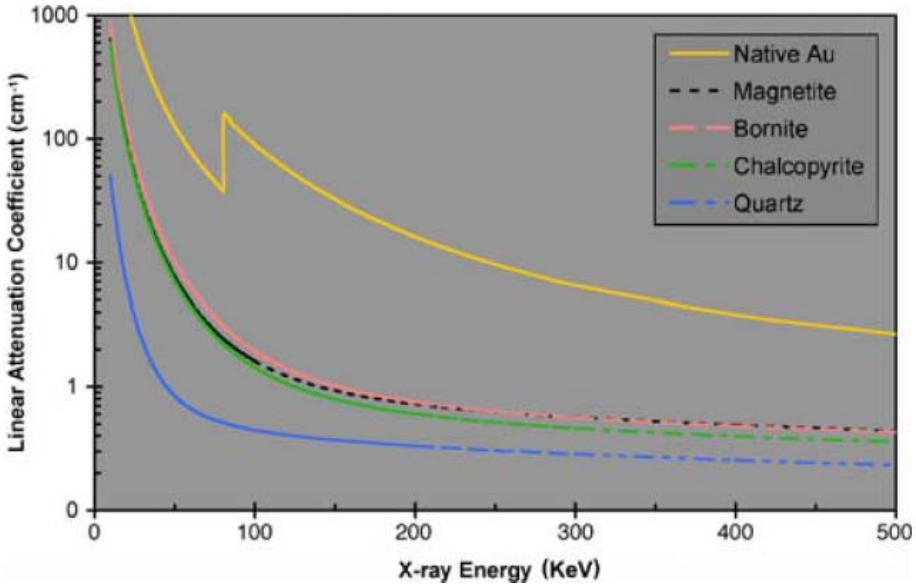

Figure 3-39 Linear attenuation coefficients as a function of X-ray energy for dominant Grasberg Cu–Au porphyry metallic minerals compared to quartz as a typical rock-forming mineral. After Kyle et al. (2008)

Figure 3-40 shows that attenuation coefficient spectra for many metallic oxide and sulphide minerals common to porphyry–skarn ore systems are similar. Because of their similar mass densities (4.2 to 5.2 g/cm3), these minerals are more difficult to differentiate. From these studies it can be seen that Micro-CT SkyScan 1172 can be used to investigate texture and structure of mineral phases with higher density in the matrix of most common rock forming minerals.

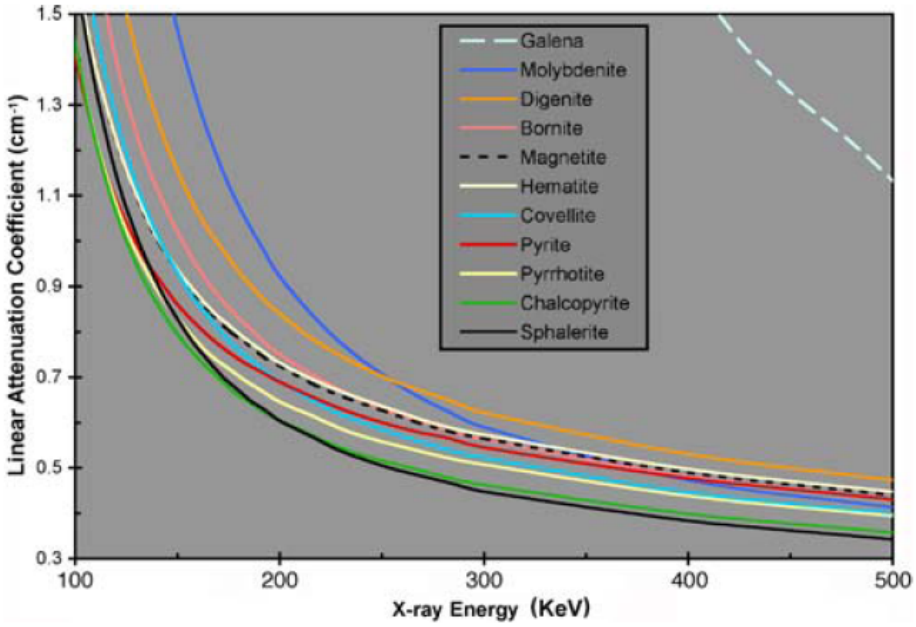

Figure 3-40 Linear attenuation coefficients as a function of X-ray energy for common porphyry–skarn sulphide and oxide minerals. After Kyle et al. (2008)

For this study high-resolution X-ray computed tomography is used to obtain information about texture and structure of minerals with higher densities, which are associated with minerals that have a tendency to heat more. This information is then used to explain certain behaviour of particles during microwave exposures and also used to describe and predict heating patterns which we can observe during and after heating.

During this study tomography was applied in the following manners;

- Some particles were fully scanned with a very fine rotating step in order to produce better reconstructed results, so that the volumetric content of particles can be investigated in more detail.
- For some particles digital radiograms were taken in larger rotating steps to illustrate the position of minerals of interest from different angles.
- Most samples were scanned in situ, while samples which were also tested by optical microscopy were scanned in epoxy resin.

Figure 3-41 shows half of a rock particle in epoxy resin on the sample holder previously prepared for MLA or optical microscopy testing. The resin appears to be transparent and does not show up in reconstructed data if the right sets of settings are chosen.

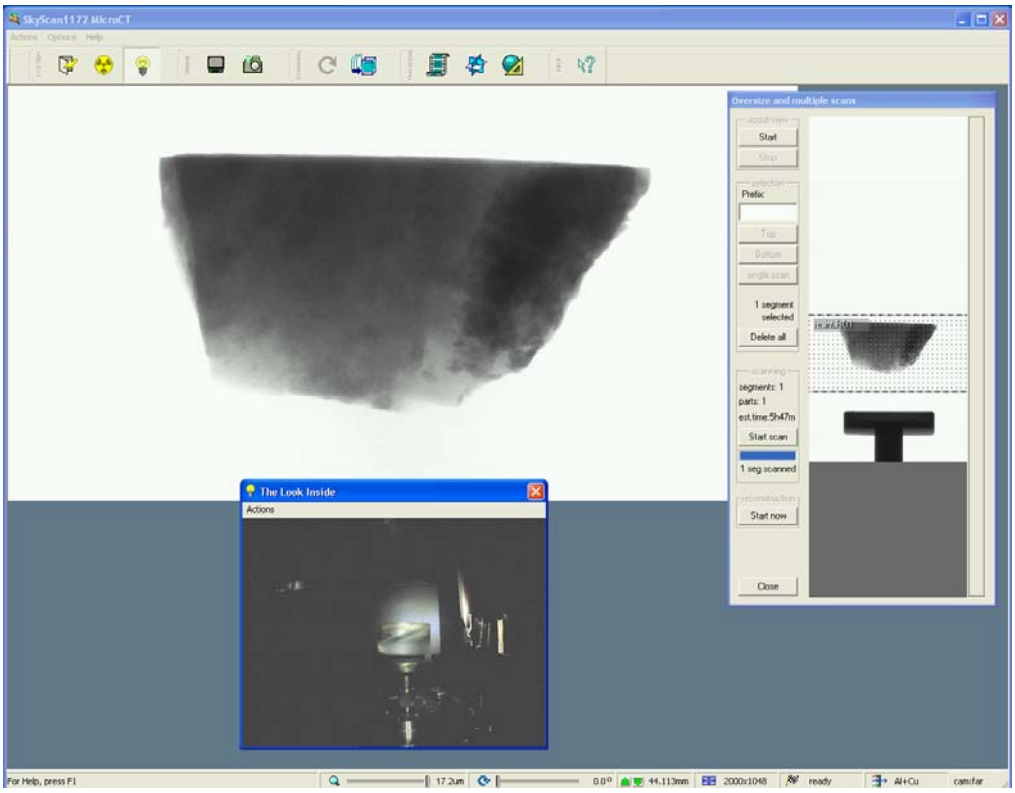

Figure 3-41 Half of rock particle in epoxy resin. Small image at the bottom displays cylindrical shape of epoxy resin which cannot be seen in digital radiogram

3.11.2 Mineral Liberation Analyser

Mineral Liberation Analyser (MLA) belongs to automated mineralogy systems which have found applications in many mineral processing investigations. Developed by JKMRC of the University of Queensland it is designed to collect and analyse hundreds of thousands of measurement points, collect data for processing and provide statistically reliable information.

> "Mineral Liberation Analyser at JKMRC comprises a standard Philips Analytical XL Scanning Electron Microscope (SEM) combined with a mineral liberation analysis software package and special sample preparation technique. The software package offers automated multiple sample measurement, batch and interactive data processing, and user-controlled presentation of mineral liberation data." (Gu et al. 1998)

To realise the fully developed study of in situ rock particles MLA is used along HRXCT to identify groups of minerals. Considering that high-resolution X-ray computed tomography is used to provide information about the quantity of mineral

phases and their distribution within the volume of rock particles, it is complemented with two dimensional MLA analyses to identify those groups of minerals.

To obtain information about mineral liberation for processing plants, usually representative sample is collected in the form of fine particles. Sample is set in an epoxy resin in a round mould to form a hardened block, and a cross section of which is polished, is coated with carbon before presented to the MLA system. For this study similar procedure was followed with a difference, where rock particles were cut in half and then placed in resin with chosen plane for analysis. For some particles, which were analysed in situ, plain was created during polishing procedure. Focus of this sample preparation was to create large surfaces to identify as much minerals as possible in one plain. Information collected from surface analysis is considered to be statistically reliable to divide minerals in two groups. First is common rock forming minerals and second is metal rich microwave absorbing minerals.

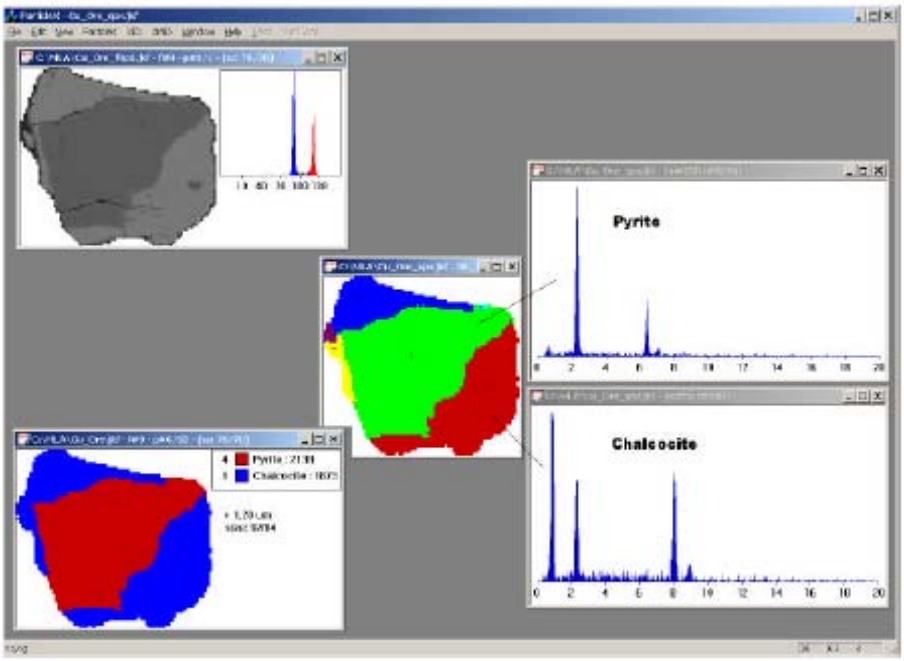

Figure 3-42 MLA area x-ray analysis of a composite particle; after segmentation, 5 grains are delineated and one x-ray spectrum is collected to provide their mineral identity. Sourced from (Gu, Ying 2003)

Figure 3-42 shows analysis of composite particle. Back-scattered electron (BSE) signals from SEM are used to create sample images where background is usually very black due to epoxy resin material and all other phases are presented with different

degrees of brightness according to the average atomic number of the mineral phase present. More details can be found in work of Gu (1998).

There are four basic steps involved in MLA data processing and presentation; they are illustrated by Gu (2003).

- Particle extraction: identification of each likely particle by discrimination against the background
- Particle de-agglomeration: identification of the particles that are two or more separate particles that are touching each other. Avery specialized procedure has been developed for particle de-agglomeration both automatically and interactively
- Mineral grain segmentation: identification of mineral phases within each particle and creation of coloured mineral maps. The MLA system uses a sophisticated morphological method for automatic segmentation.
- Data extraction: creation of a standard database containing quantitative description of each particle section and mineral grains within.

Following these steps MLA analysis is able to provide necessary information to identify minerals which individual behaviour or group characteristic can studied.

3.11.3 Automated Mineral Identification by Optical Microscopy

Automated mineral identification by optical microscopy for this study was used along high-resolution X-ray computed tomography and scanning by mineral liberation analyser to identify minerals. The MLA provides very detail identification of minerals phases because by analysing hundreds of thousands of measurement points for which this procedure takes a lot of time. Optical microscope images are produced ordinarily and much faster to create two dimensional large mineral maps. Modern optical analysis and some advances were summarised by Berry et al. (2008) and multispectral imaging of ore minerals in optical microscopy by Pirard (2004).

Identification of minerals was focused primly to recognize two sulphides; chalcopyrite and pyrite. These two minerals belong to the group of minerals of our interest. Chalcopyrite and pyrite have high density comparing to common rock forming minerals and belong to group which heats readily when exposed to

microwave energy. They also belong to non-opaque minerals which can be much easier identified from others. Technique for recognition used multiple rules and object-oriented classification using three transmitted light image layers.

Figure 3-43 shows a Leica DM 6000© microscope with a high precision stage suitable for direct tiling of image frames and good registration of multiple image layers which was used to perform automated optical mineral identification.

Figure 3-43 Leica DM6000© microscope

Currently, up to four images are recorded by this type of microscope: transmitted light plane polarised, transmitted light crossed polars, reflected light and transmitted light crossed polars with a tint plate. All image analysis was carried out using *e*Cognition® Developer Version 8.

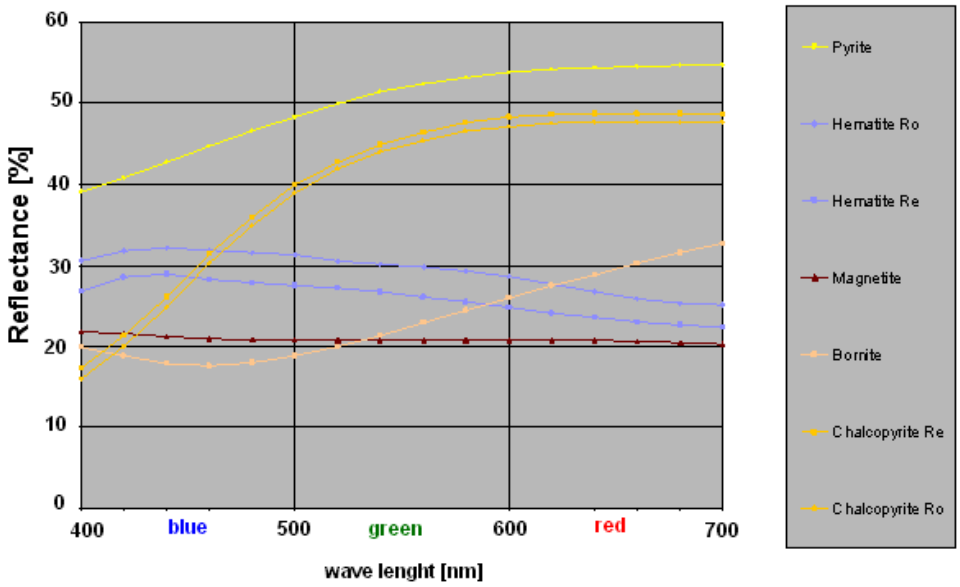

Figure 3-44 Reflectance for the opaque minerals which was used for identification of Pyrite and Chalcopyrite Hartner (2011)

Study of Hartner (2011) explains this procedure in more detail. Figure 3-44 shows Reflectance for the opaque minerals which was used for identification of pyrite and chalcopyrite and used by Hartner. The four images were read directly in 12 greyscale bands. Objects based on homogeneity across all bands were produced by segmentation algorithm. These objects were then classified using a complex set of rules (Process Tree) that are based on image brightness in all 12 bands. Opaque and non-opaque minerals were classified in the same sample. Similar approach was used in previous study by Berry et al. (2008).

Figure 3-45 shows two sulphides; chalcopyrite and pyrite which were detected using reflectance and segmentation. Chalcopyrite is in turquoise blue and pyrite in yellow colour. These same minerals can be identified in the right side of X-ray radiogram (see Figure 3-46) by presenting their distribution within the volume of the tested particle.

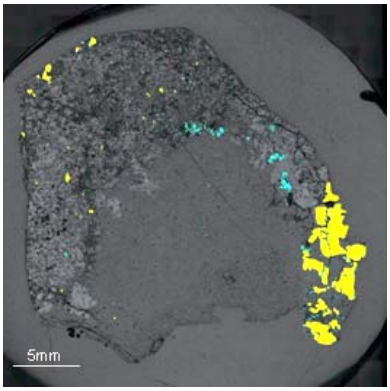

Figure 3-45 Minerals identified after applying algorithm

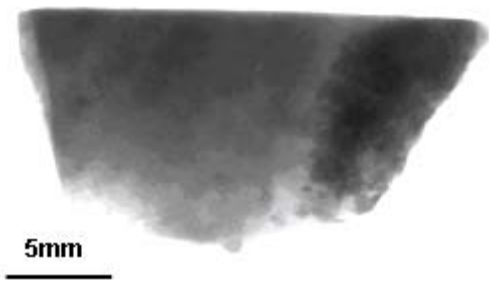

Figure 3-46 X-ray radiogram for particle No. 3 Set No. 7

3.12 Summary

In this chapter, an overview of microwave heating in theory and experimental methodology were presented. It should be noted that not all types of ore are good candidates for microwave assisted infrared sorting. From literature available studies were reviewed to obtain dielectric and physical properties of minerals in order to place boundaries which can be used as first step of assessment whether the chosen ore type has potential for microwave assisted infrared sorting.

Microwave processing systems were discussed considering that the tested ore will become a part of the applicator's functioning. Information presented was focused on two types of applicators: domestic microwave oven as multimode cavity and travelling wave applicator as single mode waveguide. Each of them is capable of producing specific type of E-field which can be used to treat ore particles.

Finally, experimental methodology was presented with three measuring techniques which were used to complete an investigation about ore types and their interaction with microwave energy.

Chapter 4-Study of Synthetic Samples

4.1 Introduction

The previous chapter provided an insight into basic physical properties of minerals, which have to be taken into account prior to exposing rock particles to electromagnetic energy and observing their thermal patterns with IR detector. This chapter will present the results of a detailed study of synthetic samples which were used to experimentally validate adopted theoretical approach of investigating influence of mineral texture upon selective heating. Procedure how to create synthetic samples (with predefined shape and form) will be provided, followed by measurement of their bulk dielectric properties. Testing procedure in two different applicators will be provided and results commented. In addition, this chapter also provides results from particle characterisation by image analysis on two ore types which were chosen for further experimental investigations.

4.2 Experimental objective

This study was conducted to investigate the behaviour of synthetic samples, which were created as simplified ore particles, and their interaction with microwaves, using two different applicators. For this laboratory testing, the first applicator was a domestic microwave oven used as a multimode cavity. The second was a travelling wave applicator, which was specially designed to test each particle individually, as a single mode waveguide. The objective was to compare surface temperatures after exposing synthetic samples in groups and individually (using the best case scenario

for the absorption of microwave energy) and observe differences between mineral containing and barren particles.

4.3 Creating Poly (methyl methacrylate) PMMA and quartz mixture samples with embedded pyrite grains

Synthetic samples had to be made from two phases. The first was a microwave absorbing phase, usually a mineral of interest, and the second phase was a matrix a much less absorbing phase. For the design of synthetic samples it was necessary to know the electromagnetic and thermal properties of materials and ideally properties should be within the boundaries recommended in Chapter 3, section 3.6:

1. **Electro-magnetic properties**
   - Dielectric constant : between 1 and 10
   - Dielectric loss factor : between 0.01 and 0.0001
2. **Thermal properties**
   - Thermal conductivity: between 3 and 7 [W/mK]
   - Specific heat capacity: between 600 and 900 [J/kgC]

Table 4-1 shows the electro-magnetic and thermal material properties of the materials chosen to manufacture synthetic samples. The values were obtained from literature or measured.

From an earlier study by Harrison (1997) which investigated the influence of grain size on the heating rates of minerals, pyrite was described as a mineral for which there were no increasing heating rate with increased grain size. Pyrite is a very common sulphide mineral and it occurs in a wide variety of geological conditions. It is also associated with sulphides of copper and other minerals. As a sulphide mineral it is also ascribed to a group that has a good response to microwave heating, according to most studies which we can find in literature.

For all the above reasons it was decided that pyrite is a good mineral to use as a heating source, or mineral of interest in synthetic samples. Using the same amounts of pyrite different textures can be created which will not be affected so much by grain size. For those textures different temperature profiles can be seen and investigated.

Table 4-1 Material properties obtained from literature or their measured values

Property	**Density [g/cm^3]**		**Specific heat capacity [J/kgC]**		**Thermal conductivity[W/mK]**		**Dielectric loss factor ε''**		**Dielectric constant ε'**	
PMMA	1.2 at 20 °C	1.15 at 23 °C	1. 1466 no temperature specification 2. 1398 at 34.25 °C	X	1. 0.167-0.25 no temperature specification 2. 0.185 at 47 °C 3. 0.192 at	X	<0.1 at 2.45 GHz and 23°C	0.016±0.0025 at 2.45 GHz and 23°C	<3.0 at 2.45 GHz and 23°C	2.321±0.0157 at 2.45 GHz and 23°C
Source	(Assael et al. 2005)	measured	1. (MIT) 2. (Assael et al. 2005)	measured	1. (MIT) 2. (Blaine & Cassel) 3. (Assael, Antoniadis &	measured	(Yussuf et al. 2007)	measured	(Yussuf et al. 2007)	measured
Quartz sand	2.648	2.54	1. 740.50 at 24.85 °C	X	1. 7.69 at room °C	X	0.01 at 2.45 GHz and room temp. ***powder***	0.013±0.0024 at 2.45 GHz and 23°C	2.26 at 2.45 GHz and room temp. ***powder***	2.756±0.013 at 2.45 GHz and 23°C
Source	(Waples & Waples 2004)	measured	1. (Knacke et al.1991)	measured	1. Horai & Baldridge (1972)	measured	(Harrison 1997)	measured	(Harrison 1997)	measured
Pyrite	5.05	4.845	1. 517.08	X	1. 19.21 at room°C	X	1.00 at 2.45 GHz and room temp. ***powder***	8.957±4.736 at 2.45 GHz and 23°C	8.25 at 2.45 GHz and room temp. ***powder***	21.52±4.759 at 2.45 GHz and 23°C
Source	(Waples & Waples 2004)	measured	1. (Knacke et al.1991)	measured	1. Horai & Baldridge (1972)	measured	(Harrison 1997)	measured	(Harrison 1997)	measured

To create a relatively transparent matrix for microwave heating, quartz was chosen as the base mineral. Quartz belongs to silicates and it is one of the most represented minerals in the earth's crust. It was decided that dried quartz sand could be pulverised and then used to create a desirable matrix.

The next step would be to add the right amount of adhesive compound to hold the material together, in this case poly (methyl methacrylate) (PMMA). This adhesive compound is a transparent thermoplastic, often used as a light or shatter-resistant alternative to glass. It is sometimes called acrylic glass. By chemical terms, it is the synthetic polymer of methyl methacrylate. PMMA was chosen because it can easily bind together pulverised quartz sand with pyrite grains and provide mechanical properties to synthetic samples which can match real rock particles. It also allows the creation of different textures, embedding grains of minerals before hardening. Figure 4-1 shows the materials used and prepared for dielectric probe measurement.

The simple mass ratio rule was applied in designing synthetic samples. From Table 4-1 it can be seen that PMMA has excellent properties in relation to microwave heating. Bearing in mind that it is used as an adhesive which binds together pulverised sand, it's very low value of dielectric loss factor is within the desired range. The specific heat capacity is higher than for common gangue minerals and the thermal conductivity is lower. The effect of these two properties can be corrected by searching for the minimum possible ratio of quartz sand and adhesive. This had to be empirically determined.

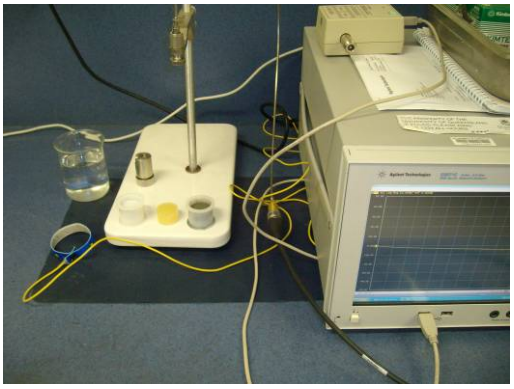

Figure 4-1 Pulverised sand, (on the left) PMMA cylinder and pyrite (on the right). The sand and pyrite were pressed into the tablets and prepared for dielectric probe measurement

Figure 4-2 PMMA material used to create synthetic particle samples

Initial experiments were carried out to determine the minimum ratio of PMMA and pulverised quartz sand. Eleven sets of adhesive and quartz sand were prepared having mass portions with ranges from five precent to fifteen precent of PMMA adhesive. It was determined that the minimum mass portion, which can be used without compromising mechanical properties of synthetic samples, and creating mineral texture was ten precent.

Poly (methyl methacrylate) with commercial name LECOSET™ 100 (Acrylic), a mix 1 part liquid with 2 parts powder, was used and it can be seen in Figure 4-2. The time for air curing was 10 to 12 minutes. The chemical reaction between a powder component and a liquid component of PMMA is exothermal. Because of the nature of the chemical reaction all components were cooled down below 20 ^{o}C, especially liquid monomer in order to slow down the reaction.

The shape of the cube mould was created out of Teflon®, which was chosen to reduce the possibility of the matrix sticking to the walls, and its resistance to chemically react with PMMA. Figure 4-3 shows the mould with its front side, which can be taken out to easily remove the sample after the setting time.

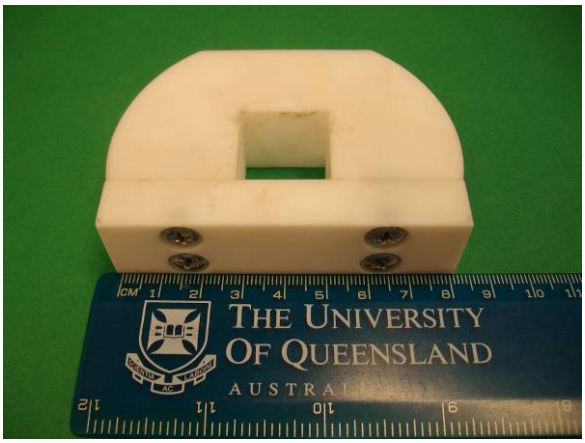

Figure 4-3 Teflon mould with cubical shape in the middle used to create synthetic samples

A cooled water bath was prepared before mixing all components. It was used to cool down glass and plastic containers used during mixing. After measuring the quartz powder the whole content was placed in a glass container in the water bath. The right amount of liquid LECOSET™ monomer was added using a syringe to the powder component starting the chemical reaction in the disposable plastic container. A glass laboratory stick was used to rapidly mix the liquid and powder components. After five

seconds of rapid mixing viscous PMMA was poured from the disposable plastic container on the surface of the quartz powder. To increase the contact surface PMMA was poured in circular motions. Mixing was continued in the glass container first with a glass stick and then with fingers using protective gloves. Process mixing was stopped when the adhesive had been well distributed within the whole mass of the quartz sand.

For the synthetic particles, without mineral grains, the freshly made matrix material was placed directly into the mould applying compression from the top. For the synthetic particles, with mineral grains, the matrix was placed in layers into the mould. This approach allowed placing the mineral grains with tweezers in the desirable position within the volume of the matrix. Figure 4-4 shows all synthetic samples created. To flatten the top and bottom of the cubes, a polishing rotating disc was used to remove all roughness from the surface.

Figure 4-4 Cubes made of Quartz sand, PMMA and pyrite grains

After the preparation of the synthetic particles they were labelled. To assure that the order of the tracers or particles, with designed structure of minerals is random, three numbers from one to eleven were chosen. This was done using Matlabs' random function, which generated numbers three, five and nine. Those numbers were then dedicated to the tracers. It was also decided that the increasing sequence of numbers should be followed with increasing grain sizes used in synthetic samples. Position three was given to the cube with the smallest grain size, while position nine was given to the cube with the largest grain size.

Using the described procedure, synthetic particles as simplified ore particles, with the constant shape and form, were created with an average measured mass of 16.91±0.59g. For the synthetic particles with created texture or tracers more details can be found in Table 4-2.

Table 4-2 Mass of tracers and mass of pyrite used with the grain sizes

Sample label	Mass of particle, g	Mass of pyrite grains, g	Mass % of pyrite	Grain size, mm
Cube No. 3	17.8	3.59	20.2	-4.75+3.35
Cube No. 5	17.3	3.56	20.6	-6.70+4.75
Cube No. 9	17.53	3.51	20.0	-9.50+6.70

4.4 Tomography of the cubes (Synthetic particles)

For the assessment of synthetic particles, X-ray Cone Beam Tomography was used to present created texture and point to possible localised heating areas. Digital x-ray radiograms allow us to visualise and measure proximity of embedded minerals to the surface of the minerals. The distance of heating minerals will be reflected on the heating patterns on the surface of the synthetic particles which will be possible to measure using an infrared cameras previously explained in Chapter 3, section 3.6.

4.4.1 Empty Cube containing matrix material only

Figure 4-5 and Figure 4-6 show x-ray radiograms of a synthetic cube created entirely of pulverised quartz sand and PMMA used as adhesive. There are no additional minerals and the created texture is very uniform in all directions.

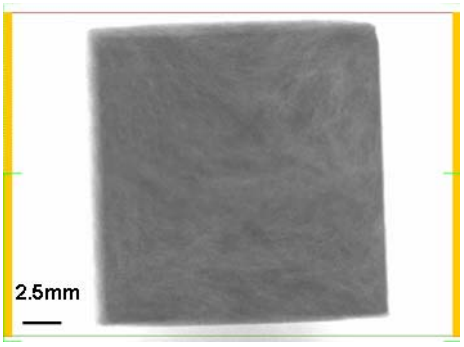

Figure 4-5 Empty cube, matrix only. Position of cube: 0 degree according the position of X-ray source

This particular cube was later labelled as “Cube No. 7” and it was used in other testing along with the cubes which had microwave absorbing mineral.

For all others cubes and including this one, made in the same manner it can be stated that they present barren rock particles. They represent particles made of common rock forming minerals which have low dielectric properties and have a tendency to heat less when exposed to applied microwave energy.

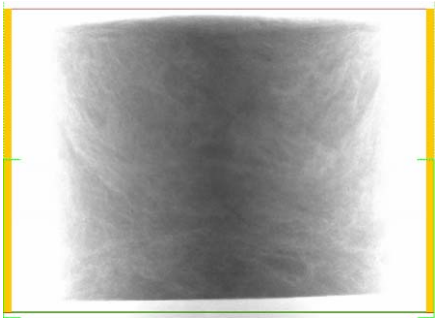

Figure 4-6 Empty cube, matrix only. Position of cube: 45 degree according the position of X-ray source

4.4.2 Cube No. 3

Figure 4-7 to Figure 4-9 we show x-ray radiograms of the particle labelled "Cube No. 3" containing eight grains of pyrite with one in every corner of the cube. This particular texture has a symmetrical structure of the mineral grains which will respond very quickly to microwave heating. This is mostly due to the proximity of the mineral grains to the surface of the cubes. Every grain will become a source of heating, which will start to form four points with consecutive radial isothermal surfaces on the surface of the cube. Heat will spread radially from the source because created temperature gradient will pass through the matrix, with homogenous properties.

Because of the symmetrical structure it should be easy to see a very prompt response to microwave heating from any of the six surfaces on the cube which will fall in front of the infrared detector.

Figure 4-10 shows the reconstruction of the one horizontal plane, indicated in a green horizontal line in Figure 4-7. This plane displays the locations of the first four pyrite grains i.e. heating sources. The density change within the synthetic sample was studied using a red profile line which was placed across from one side to another passing through mineral grains three and four. After removing air as the base line (it is now under the horizontal dotted line in Figure 4-11) a considerable leap in density can be seen when passing through pyrite. Following the rest of the profile it can be stated

that these grains are embedded in homogenous material and that there will not be a preferential direction for the heat to follow.

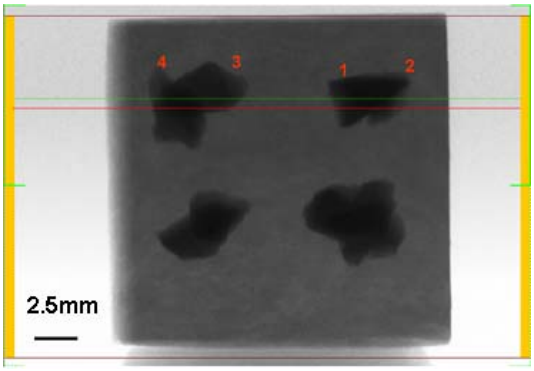

Figure 4-7 Position of Cube 3: 0 degree according the position of X-ray source

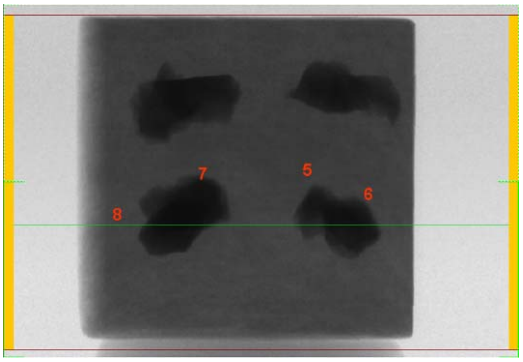

Figure 4-8 Position of Cube 3: 90 degree according the position of X-ray source

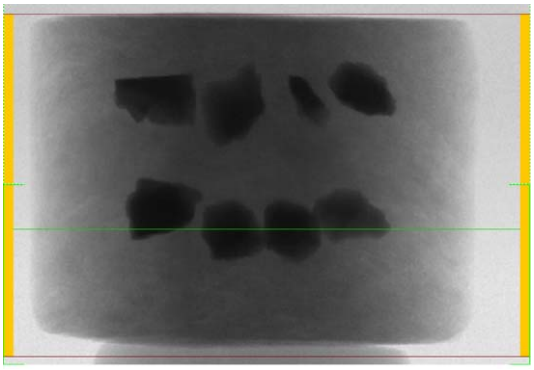

Figure 4-9 Position of Cube 3: 115 degree according the position of X-ray source

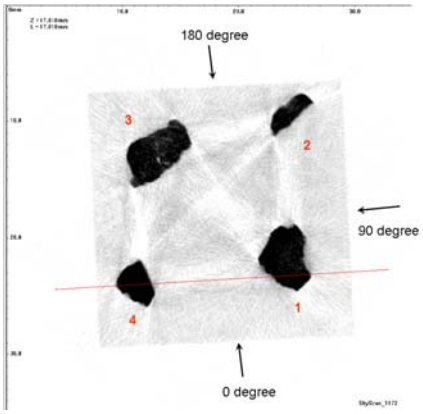

Figure 4-10 Horizontal plane of the Cube 3 reconstructed and indicated in green colour

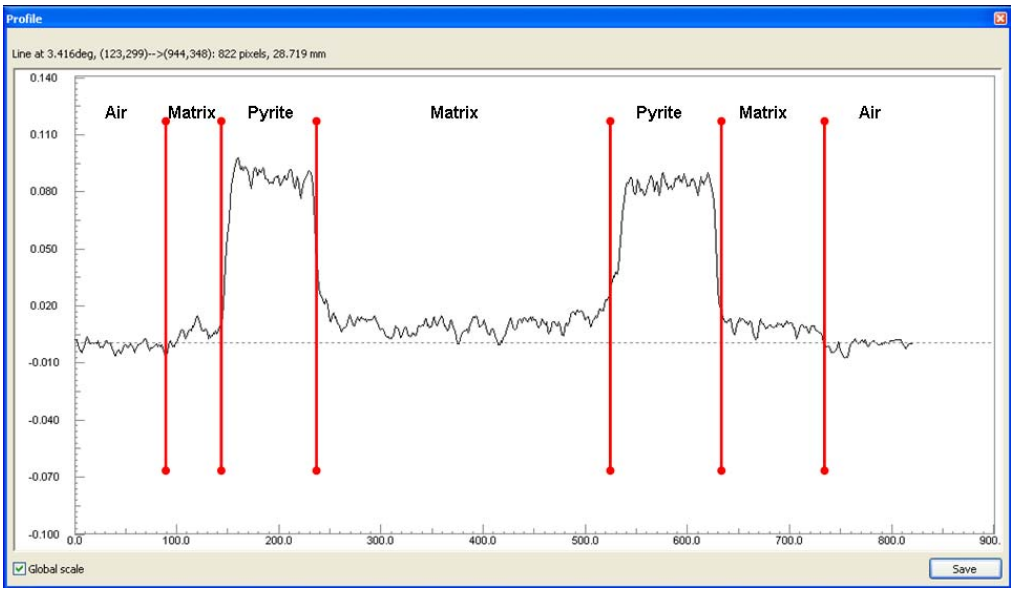

Figure 4-11 X-ray attenuation coefficient change indicating density change in reconstructed horizontal plane indicated in red colour in Figure 4-10

Figure 4-12 shows the designed structure from multiple views in reconstructed X, Y and Z planes for the "Cube No. 3".

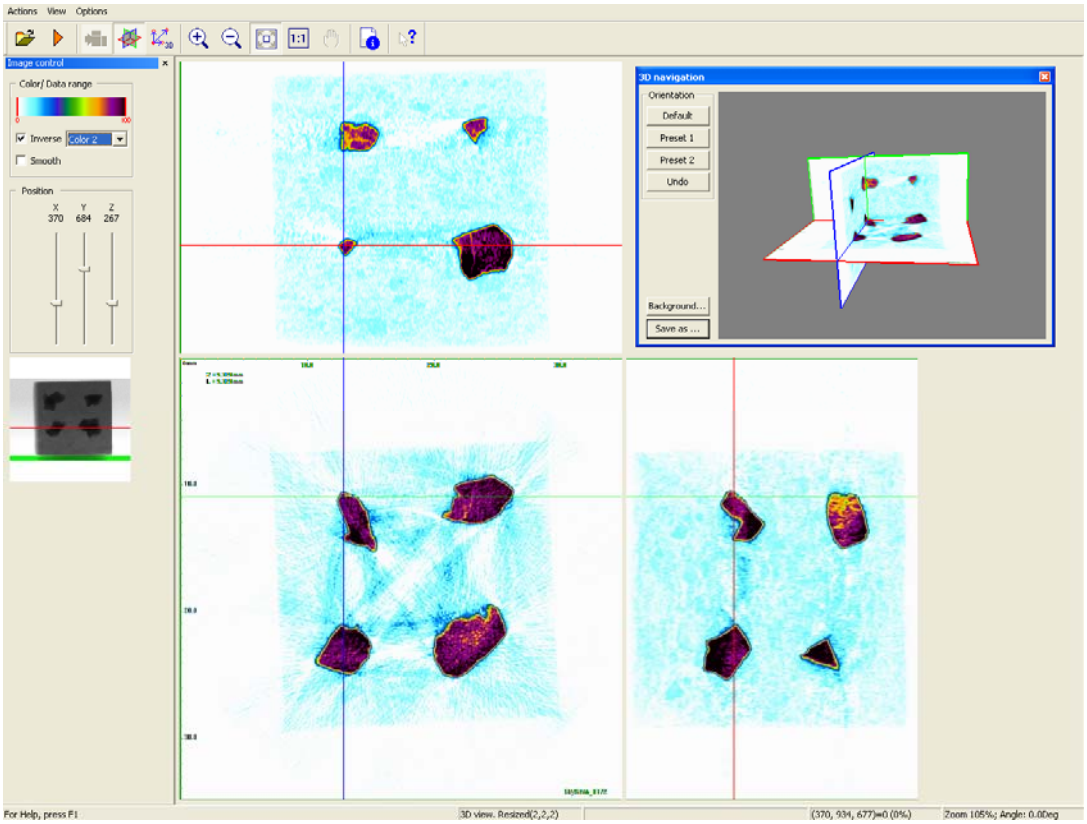

Figure 4-12 Reconstructed x, y and z planes locating positions of the four embedded pyrite minerals in the cube. In the top right image x-plane is in the blue colour, y-plane in green and z-plane in red colour

4.4.3 Cube No. 5

The "Cube No. 5" and its structure with three grains of pyrite can be seen in x-ray radiograms in Figure 4-13, Figure 4-14 and Figure 4-15. It should be noticed that larger grain size were used. For this particular texture a semi symmetrical structure was chosen. Three grains were arranged in triangular shape along the one of the larger diagonals connecting opposing corners of the cube. This structure will have three sides of the cube which will be directly affected by the grain proximity to the surface. On those surfaces it will be easy to identify points with the highest localised heating. The remaining three surfaces will have heating patterns which are produced by the collective effect of all three grains, working as one heating source. Figure 4-16 shows one of the horizontal planes reconstructed with two of the three grains. The proximity of those grains to the surface can also be seen. Figure 4-17 shows the density change from the reconstructed plane. It can be seen that the density change is very similar to "Cube No. 3". This is predominantly because mineral grains come from the same larger mineral crystal of pyrite as in "Cube No. 3" and the matrix was prepared according to the same procedure.

Figure 4-18 shows a designed structure from multiple views in reconstructed X, Y and Z planes.

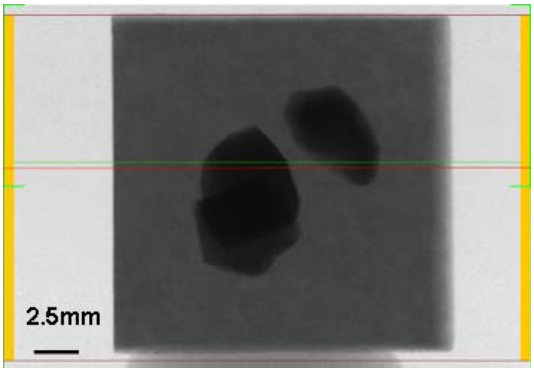

Figure 4-13 Position of Cube 5: 0 degree according the position of X-ray source

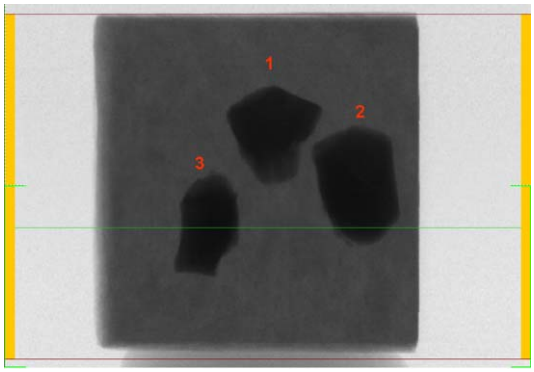

Figure 4-14 Position of Cube 5: 90 degree according the position of X-ray source

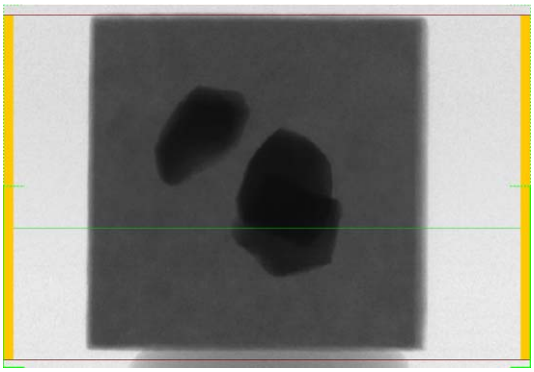

Figure 4-15 Position of Cube 5: 180 degree according the position of X-ray source

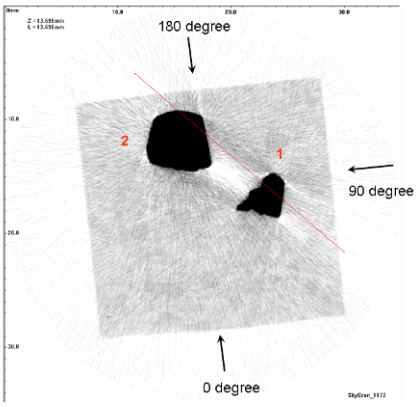

Figure 4-16 Figure 4-13 First two grains of pyrite and their positions in common plane for the Cube 5.

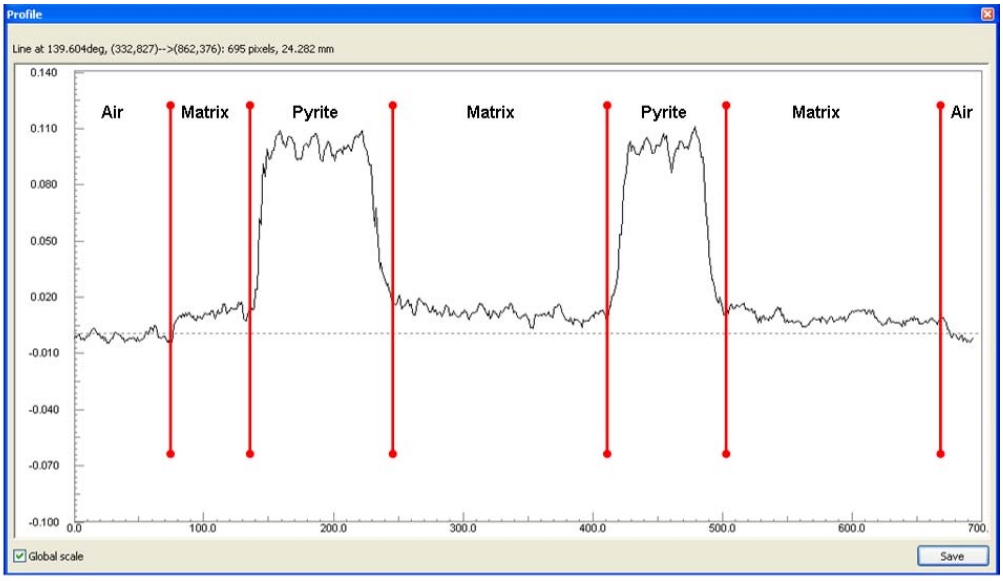

Figure 4-17 X-ray attenuation coefficient change indicating density change in reconstructed horizontal plane indicated in red colour in Figure 4-16

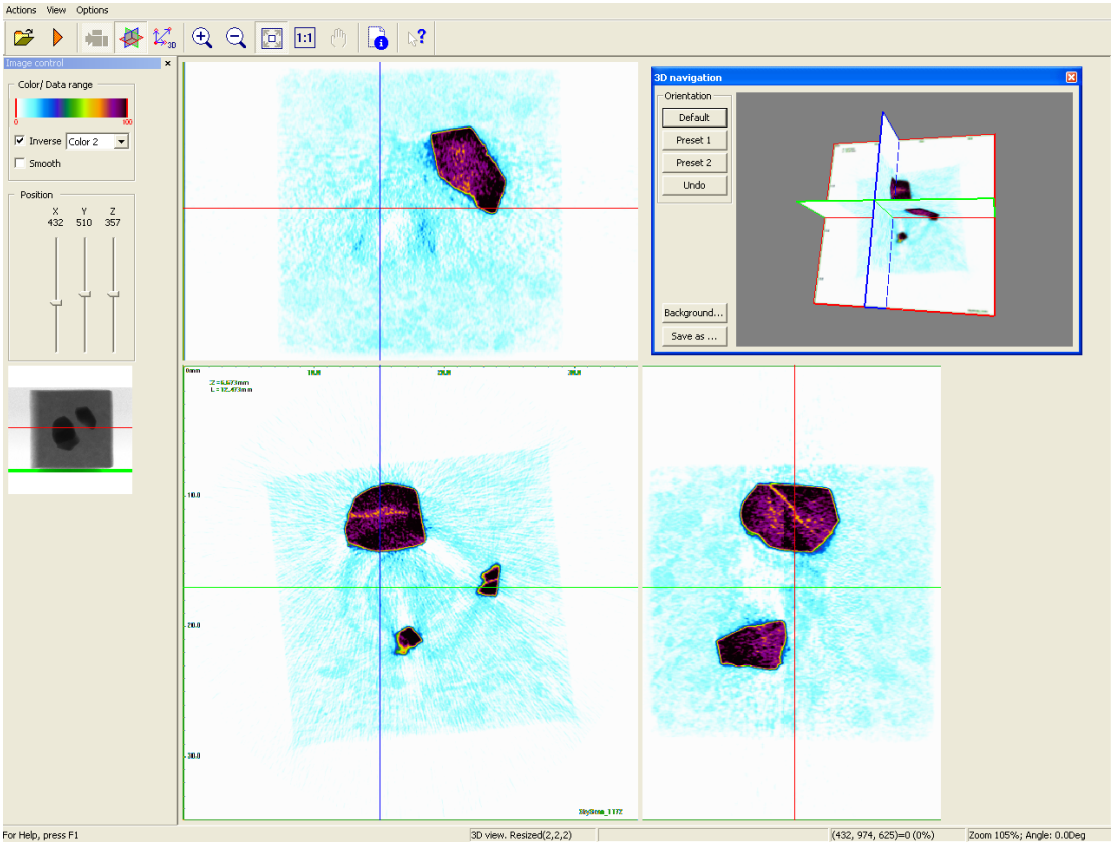

Figure 4-18 Reconstructed x, y and z planes locating positions of the three embedded pyrite minerals in the cube. In the top right image x-plane is in the blue colour, y-plane in green and z-plane in red colour

4.4.4 Cube No. 9

The "Cube No. 9" had a very simple structure as presented in x-ray radiograms from Figure 4-19 to Figure 4-21. The whole mineral grain, which acts as a heating source, was deeply embedded in the middle of the matrix.

This was the most symmetrical structure which will result in very similar isothermal surfaces. Whichever of the six sides of the cube is presented to the infrared thermal camera, the highest temperature will be in the middle of the surface. Considering that the heat is coming from the one source it will spread radially towards the surface of the cube. Homogenous bulk properties of the matrix will cause the temperature gradient to be equal in all directions without any specific directional preferences. This will create isothermal surfaces which will have concentric spherical shapes. The heat front will reach the centre of the cube sides first while the corners of the cube will be reached last, taking into consideration that they are the furthers from the heating source.

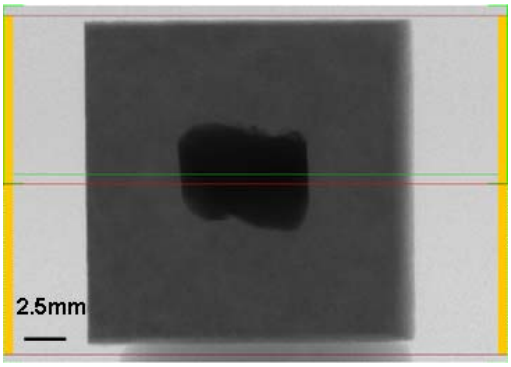

Figure 4-19 Position of cube Cube 9 : 0 degree according the position of X-ray source

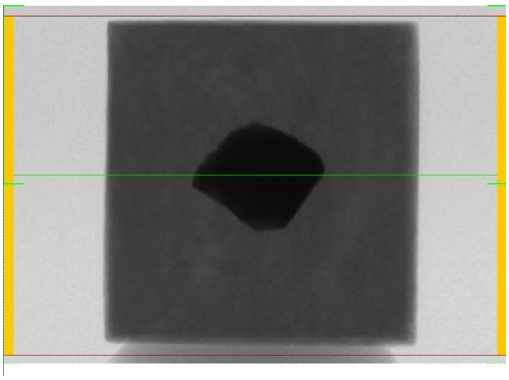

Figure 4-20 Position of cube Cube 9 : 90 degree according the position of X-ray source

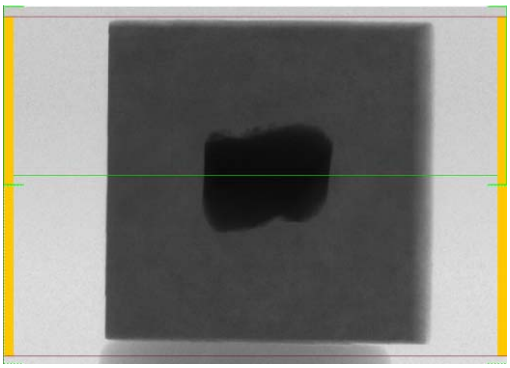

Figure 4-21 Position of cube Cube 9 : 180 degree according the position of X-ray source

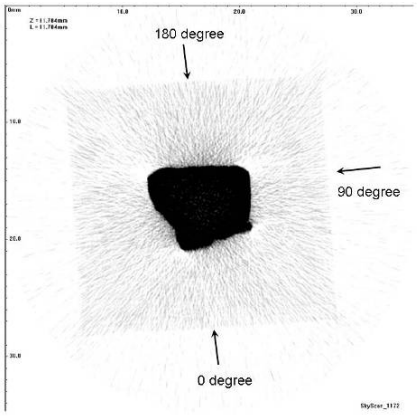

Figure 4-22 Horizontal plane reconstructed and indicated in green colour in Figure 4-19.

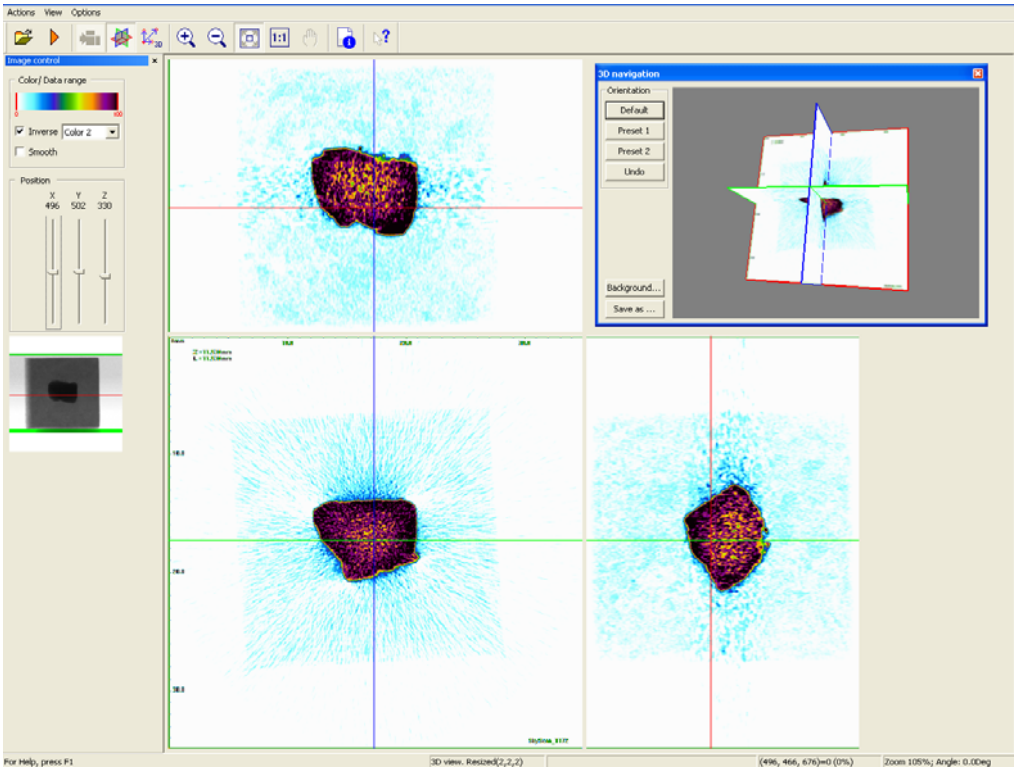

Figure 4-23 Reconstructed x, y and z planes locating position of the one embedded pyrite mineral in the cube. In the top right image x-plane is in the blue colour, y-plane in green and z-plane in red colour

Figure 4-22 shows one of the planes reconstructed to locate the mineral grain, while Figure 4-23 shows the designed structure from multiple views in reconstructed X, Y and Z planes.

4.5 Measuring Bulk Dielectric Properties of Synthetic Particles Using Resonant Cavity Technique

The experimental objective was to measure bulk dielectric properties of synthetic particles as they would be used in actual testing. For this reason three randomly chosen (random choice determined by Matlab function) synthetic particles without pyrite texture and three used as tracers were measured.

The Resonant Cavity Method uses a resonant cavity for the sample holder, and a network analyser to measure the resonant frequency and the Q of the cavity when it's both empty and has the sample in it. From this, permittivity can be calculated (Czichos et al. 2006).

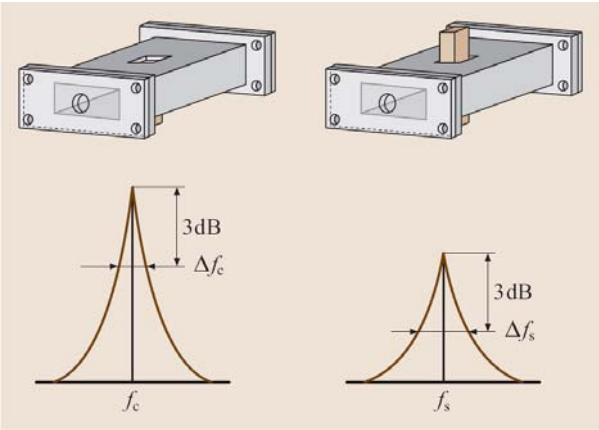

Figure 4-24 Scattering parameter S21 measured for an empty cavity and for cavity with a specimen inserted after Czichos et al. (2006)

The cavity is connected to a network analyser by using suitable adapters and cables. The resonance is indicated by a sharp increase in the magnitude of the S21 parameter, with a peak value at the resonant frequency. The resonant cavity method is a two port measurement therefore, the S21 parameter presents forward transmission (insertion) gain with the output port terminated in a matched load. When the dielectric specimen is inserted into the empty cavity the resonant frequency decreases from f_c to f_s while the bandwidth Δf at half power (3 dB), below the S21 peak, increases from Δf_c to Δf_s as it is shown in Figure 3-21. A shift in resonant frequency is related to the specimen dielectric constant, while the larger bandwidth corresponds to a smaller quality factor

Q, due to dielectric loss. Then the dielectric constant can be calculated by using Equation 4-1 and dielectric loss factor using Equation 4-2.

$$\varepsilon_r' = 1 + \frac{V_c(f_c - f_s)}{2V_s f_s} \qquad (4\text{-}1)$$

$$\varepsilon_r'' = \frac{V_c}{4V_s} \cdot \left(\frac{1}{Q_s} - \frac{1}{Q_c} \right) \qquad (4\text{-}2)$$

Where :

fc = Resonant Frequency of Empty Cavity

fs = Resonant Frequency of Filled Cavity

Qc = Q of Empty Cavity

Qs = Q of Filled Cavity

Vc = Volume of Empty Cavity

Vs = Volume of Sample.

Resonant cavities are usually made from closed sections of waveguide or high-permittivity dielectric material. Electric and magnetic energy is stored in the cavity and the only losses are due to finite conductivity of cavity walls and dielectric losses of material filling the cavity (Pozar 1997). The quality factor or "Q" is used to estimate different power loss mechanisms within the resonant cavities. By Metaxas & Meredith (1983) it can be estimated as:

$$Q = 2\pi \frac{\text{energy stored}}{\text{energy lost per cycle}} \qquad (4\text{-}3)$$

although it can be decomposed into three parts as seen in Equation 4-4.

$$\frac{1}{Q} = \frac{1}{Q_c} + \frac{1}{Q_d} + \frac{1}{Q_{ext}} \qquad (4\text{-}4)$$

The first is Q_c, resulting from the power loss in the walls which have finite conductivity; the second is Q_d, resulting from the power loss in the lossy dielectric material filling the cavity:

$$Q_d \approx \frac{1}{\tan\delta} \cdot \frac{V_c}{4V_s} \qquad (4\text{-}5)$$

and Q_{ext}, resulting from power loss through unclosed surfaces (holes) of the cavity geometry (Pozar 1997). If the Q_c and Q_{ext} are minimised through the choice of material and design of the resonant cavity then quality factor becomes a function of

the lossy dielectric material filling the cavity, as seen in Equation 4-5. For this reason in resonant cavities Q-factor can be used to calculate dielectric properties of materials at resonant frequencies.

4.5.1 Validation of the Cavity with the Material of Known Dielectric Properties and Testing Synthetic Particles

The ASTM 2520 standard covers resonant cavity technique in more details and this standard was used as a guide for measuring dielectric properties of synthetic cubes. It provides three measurement techniques. Test method "A" is for specimens precisely formed to the inside dimension of a waveguide. Test method "B" is for specimens of specified geometry that occupy a very small portion of the space inside a resonant cavity. Finally, test method "C" uses a resonant cavity with fewer restrictions on specimen size, geometry and placement, and this method was used as guidance.

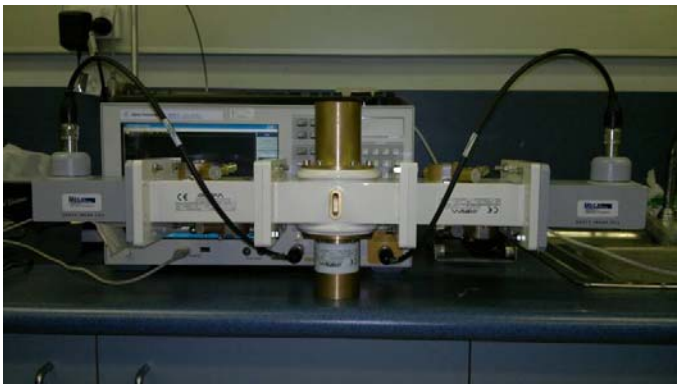

Figure 4-25 The resonant cavity from outside

Figure 4-25 shows the apparatus used, which in reality is a short section of WR340 waveguide with an opening in the middle to insert the testing sample and two metallic plates used to convert waveguide into the resonant cavity. The metallic plate on each end had an iris hole to feed energy in and out of the cavity as it can be seen in red circle in Figure 4-26.

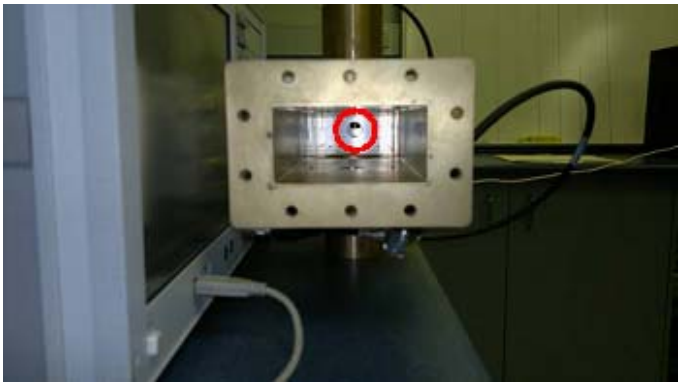

Figure 4-26 Cavity from inside, with iris hole in red circle

Considering that the synthetic particles were comprised from high and low loss materials, a less sensitive cavity (operating in TE_{101} mode with dimensions x=a=4.3cm, z=b=8.6cm and y=69cm) was used for which Q-factor was still above 2000 as recommended by ASTM 2520 standard.

Measurements and calculations were obtained through Agilent software "85071E option 300" (from the same manufacturer of the network analyser used in the measurement) which had all necessary calculations from the ASTM 2520 standard. To evaluate the cavity, initial testing and calibration were performed on a material of known properties from literature and measured by a different measuring technique. The PMMA previously casted into cylindrical shape with dimensions: 30 mm in diameter and 15 mm in height (see Figure 4-1) was placed on the thin piece of paper on the bottom of the cavity in the middle of the resonant cavity. Table 4-3 shows mean values from four measurements which are in good agreement with other sourced values.

Table 4-3 Measured values for PMMA used to test performance of the cavity

Property	**PMMA**	***Source***
Dielectric constant ε'	1. 2.321±0.0157 at 2.45 GHz and 23°C 2. 2.0458±0.021 at 21 °C and 2.475 GHz	1. measured by dielectric probe kit 2. resonant cavity
	< 3.0 at 2.45 GHz and 23°C	(Yussuf et al. 2007)
Dielectric loss factor ε''	1. 0.016±0.0025 at 2.45 GHz and 23°C 2. 0.0136±0.003 at 21 °C and 2.475 GHz	1. measured by dielectric probe kit 2. resonant cavity
	< 0.1 at 2.45 GHz and 23°C	(Yussuf et al. 2007)

The chosen synthetic particles were tested in two positions in regards to the length of the resonant cavity. The first was parallel and the second was under angle of 45 degrees as shown in Figure 4-27.

Because of depolarisation effect these two positions were investigated. Measurements were repeated three times and depolarisation effect was examined on macroscopic level caused by the different positions (not by different shapes) of the synthetic ore particles.

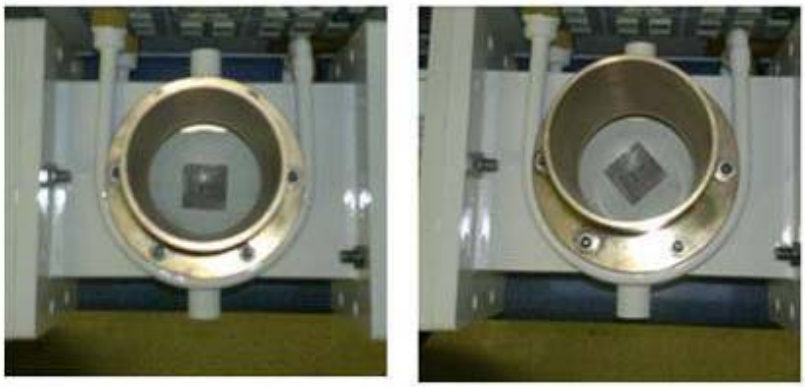

Figure 4-27 Two positions chosen to perform measurements

The aim of rotating the particles was to investigate whether the difference between two types of created particles was equally distinguishable. Table 4-4 and Table 4-5 show the results from the measurements and they can be commented by observing loss tangent (defined in Chapter 3) which can be used as a parameter to describe responsiveness of the material to electromagnetic field.

Table 4-4 Measurement was performed on 21 ^{o}C at 2.475 GHz for parallel position in regards to the length of the resonant cavity

Numbers up				
Num. of sample	Sample name	Dielectrics constant	Dielectric loss	Loss tangent
1	Cube 7	2.571± 0.0017	0.0114±0.00050	0.0044
2	Cube 4	2.601± 0.0040	0.0135±0.00040	0.0052
3	Cube 11	2.627± 0.0031	0.0115±0.00040	0.0044
4	***Cube 3***	2.779± 0.0087	0.0243±0.00026	0.0088
5	***Cube 5***	2.631± 0.0105	0.0222±0.00060	0.0084
6	***Cube 9***	2.693± 0.0042	0.0191±0.00072	0.0071

Table 4-5 Measurement was performed on 21 ^{o}C at 2.475 GHz rotated for 45 degrees as seen in Figure 4-27

Rotated for the 45 deg				
Num. of sample	Sample name	Dielectrics constant	Dielectric loss	Loss tangent
1	Cube 7	2.630± 0.0794	0.0122±0.00062	0.0046
2	Cube 4	2.575± 0.0036	0.0132±0.00035	0.0051
3	Cube 11	2.533± 0.0061	0.0105±0.00036	0.0041
4	***Cube 3***	2.631± 0.0044	0.0198±0.00052	0.0075
5	***Cube 5***	2.572± 0.0069	0.0202±0.00053	0.0078
6	***Cube 9***	2.681± 0.0026	0.0196±0.00030	0.0073

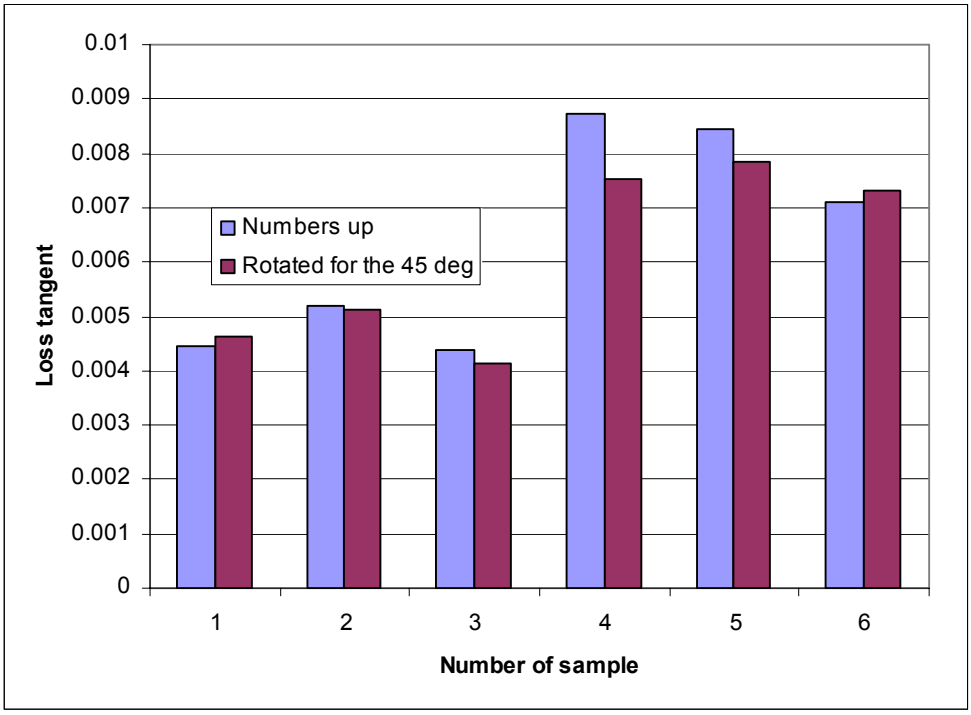

Figure 4-28 Loss tangent for synthetic regular shape samples with mineral texture and used as tracers were higher compared with a non pyrite bearing particles

It can be seen that the group of particles used as tracers had much greater values of loss tangent when compared with a non pyrite bearing particles. This trend can also be seen when the measurements were repeated with rotated positions of the samples (as seen in Figure 4-28).

4.5.2 Conclusions

This method, as any other, has its limitations, however, it met the objectives and it has been proven effective in the characterization of many ceramic and organic material systems for which ASTM 2520 standard is frequently used. The following conclusions can be made:

- The resonant cavity used, proved to be suitable to measure bulk properties of synthetic rock particles.
- The difference in bulk dielectric properties between synthetic particles characterised as tracers and particles without pyrite mineral was easily measured along with the presence of depolarisation effect.

4.6 Test Procedure:

4.6.1 Exposing Synthetic Particles to Multimode Electromagnetic Field in Domestic Microwave Oven

Figure 4-29 shows a domestic microwave oven used for this experiment manufactured by SHARP. It is a "Carousel" Model 380-J capable of delivering 1200 Watts of microwave power to the load. The interior of the oven along with internal cavity dimensions is shown in Figure 4-30. The turning mechanism is in the middle of the oven and the waveguide port is on the right side.

Figure 4-29 Domestic microwave oven used in this experiment

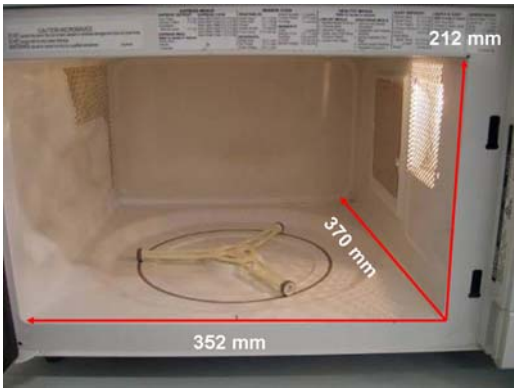

Figure 4-30 Interior of domestic oven. Turning mechanism is in the middle of the oven and the waveguide port is on the right side.

The glass microwave tray, which can be seen in Figure 4-31, was separated into eleven sections for eleven synthetic particles. Those same particles were then distributed along the edges of rotating tray in order to cover the larger area of the tray. This was done to ensure that particles have a greater chance of passing through the multiple modes if the spatial distance between the modes is larger than the chosen particle size. During repeatable exposures, particles were positioned in numbered order clockwise. This is represented with a red arrow in Figure 4-31. Once allocated on the edge of the tray they did not have any preferred position.

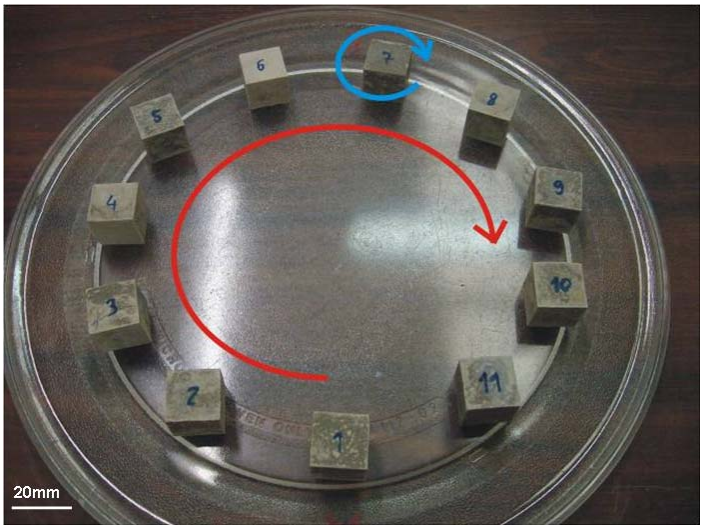

Figure 4-31 Fixed position in red and free position in blue

In industrial conditions the real rock particles (when they take their most stable position) can be measured for their temperature profiles on the conveyor belt from the top surface, while the temperature profiles from the bottom stay hidden. To complete the temperature profile it would be beneficial to have information from both the top and bottom surfaces. This is why synthetic particles were tested first with their labels or numbers up and then a second time with their numbers rotated down. With this arrangement, exposure to the microwave energy was repeated four times. Two times with the numbers "up" and two times with the numbers "down".

Before the microwave exposure, an infrared captured image of the synthetic particles was taken using an infrared camera manufactured by CEDIP (see Figure 4-32). This camera is capable of detecting electromagnetic waves with the wave length between 2-5μm or in infrared spectrum. A tray with synthetic particles was then placed in the oven and exposed to the 1200 W of applied microwave power. Time for the exposure was 12 seconds. This time was chosen because the glass tray makes a full rotation within the oven. During this time all particles rotated with the tray and assumed their starting positions after exposure.

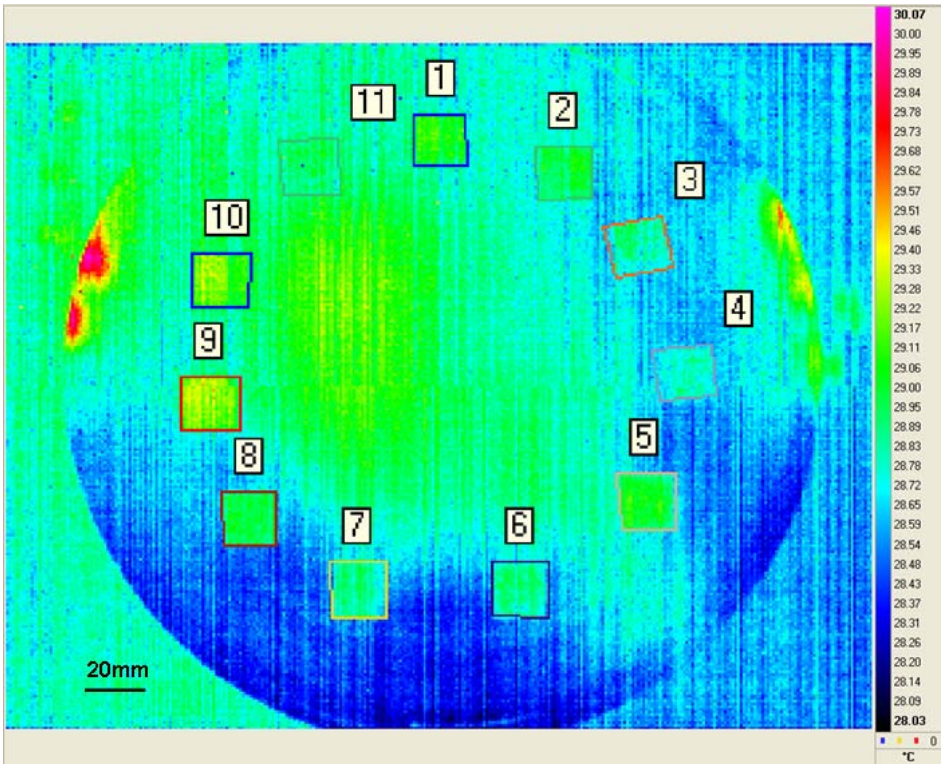

Figure 4-32 Temperatures before exposure

An infrared camera was positioned very closely to the microwave oven on the distance from which the images of the tray with the particles could be easily captured.

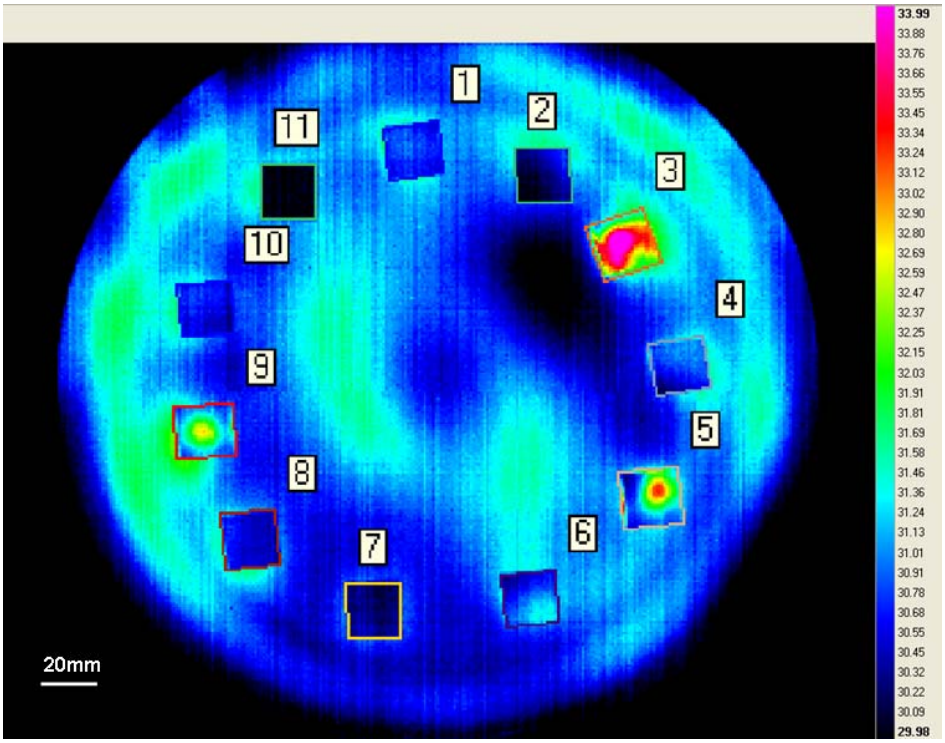

Figure 4-33 Temperatures after exposure

Figure 4-33 shows the thermal infrared image taken five seconds after the exposure. This time was necessary to take the tray from the oven and position it in front of the infrared camera for image capturing. After every exposure synthetic particles were

cooled down to room temperature. Forced convection was used by placing them on the mesh surface which had an air fan below. All data was collected and then analysed with provided software for the infrared camera.

4.6.2 Exposing Synthetic Particles to Electromagnetic Field in the Travelling Wave Applicator

For this experimental set-up a travelling wave applicator was used. All synthetic particles were placed in a numbered sequence on the vibratory feeder which can be seen in Figure 4-34 on the right side. Particles were fed one by one into the applicator. The generator was set for 1200 W with an exposure time of 12 seconds. All these settings were adjusted using a graphic user interface prior to initialising the testing sequence. The infrared camera was positioned perpendicular to the travelling wave applicator to reduce reading temperatures errors from the surfaces of synthetic particles (see Figure 4-34).

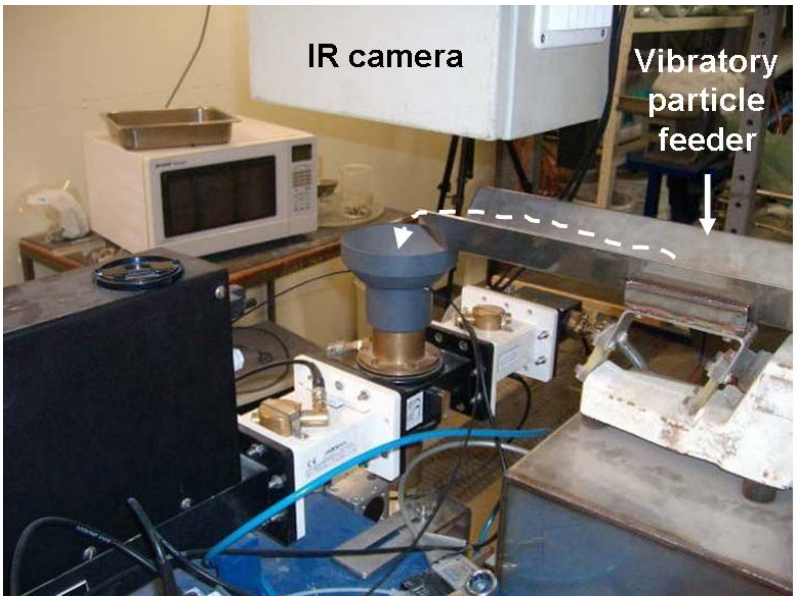

Figure 4-34 Feeding and inspection part of the travelling wave applicator

For repeatable testing it was important to guide particles to the narrow particle holder which was done using a guiding funnel. Figure 4-35 shows the guiding funnel placed over the particle holder.

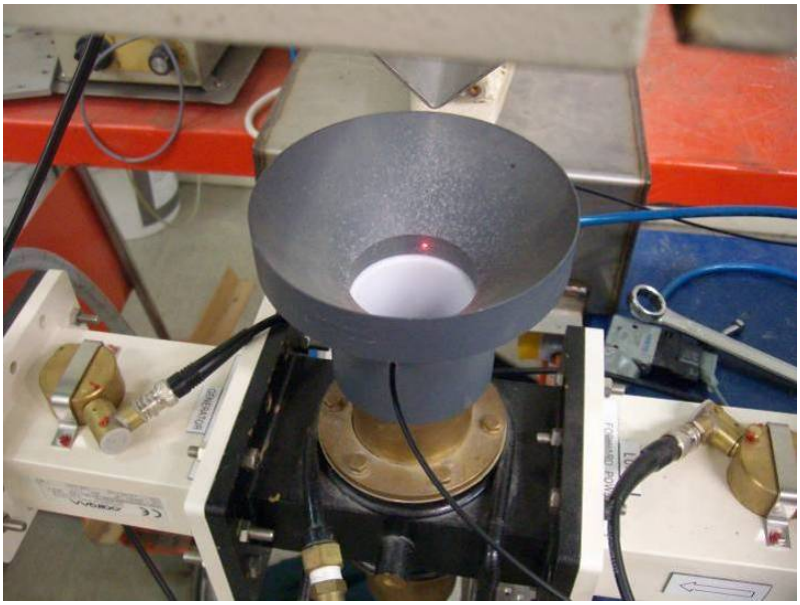

Figure 4-35 Guiding funnel with the infrared detector

From Figure 4-36 to Figure 4-38 the positions of the cubes during testing are shown. The region of interest is labelled in every figure with No.1 and it is in a circular shape, highlighted in bold blue colour.

By comparing positions from three consecutive exposures it can be seen that particles free fall from the feeder influenced the final position within the region of interest. This free fall also made a random choice of one of the six sides of the cube, which would then be presented to the infrared camera.

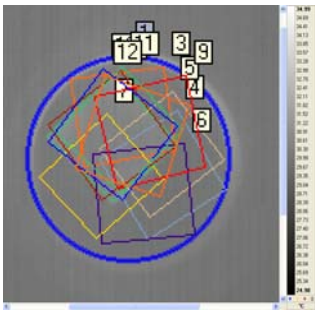

Figure 4-36 First exposure in TWA

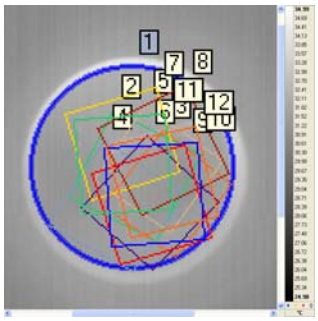

Figure 4-37 Second exposure in TWA

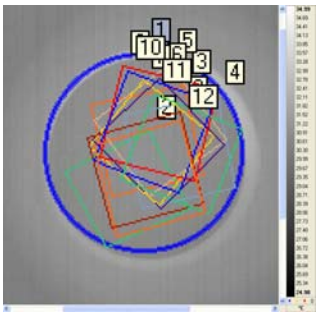

Figure 4-38 Third exposure in TWA

Exposures were repeated three times. During all exposures infrared images were captured in real time allowing detailed data analysis of the temperature profiles for every synthetic particle.

4.7 Results and Discussion

All collected data was analysed by software "Altair" supplied by infrared camera manufacturer Cedip. By placing a boundary around the perimeter of particles a two

dimensional visible surface was selected from the background. From these surfaces software was used to calculate temperatures. Two temperatures were calculated from each particle. The first was the maximum temperature taken from a pixel with the highest measured temperature within the selected surface. The second was the mean temperature calculated as a mean value from all temperatures from all the pixels within the selected surface. To compare experimental data, temperature difference for maximum and mean temperatures were calculated from data before and after microwave exposure. Following abbreviations were taken to represent data.

- For each exposure:

T max= maximum temperature on the surface of the particle

T mean = mean temperature on the surface of the particle

ΔT max = temperature difference for the maximum temperature on the surface of the particle calculated from data before microwave exposure and after microwave exposure

ΔT mean = temperature difference for the mean temperature on the surface of the particle calculated from data before microwave exposure and after microwave exposure

- From repeated exposures:

average ΔT max = mean value for ΔT max from repeated exposures

average ΔT mean = mean value for ΔT mean from repeated exposures

Figure 4-39 shows average ΔT max and average ΔT mean from repeated testing. It can be seen that particles, which were used as tracers (on the graph particles with numbers 3, 5 and 9), have higher temperatures than the rest of the particles, which were made just from the matrix material. The displayed data shows that the highest standard deviation was calculated for the tracer “Cube No.5”. This high standard deviation was caused by presenting different sides of the synthetic particle to the infrared camera. The first exposure with numbers “up” had the side which was furthest from mineral grains and had a cumulative influence of all three grains which resulted with lower values for ΔT max and ΔT mean. The second exposure with numbers “down” had the side which was much closer to the one of the grains which resulted with increased values for ΔT max and ΔT mean.

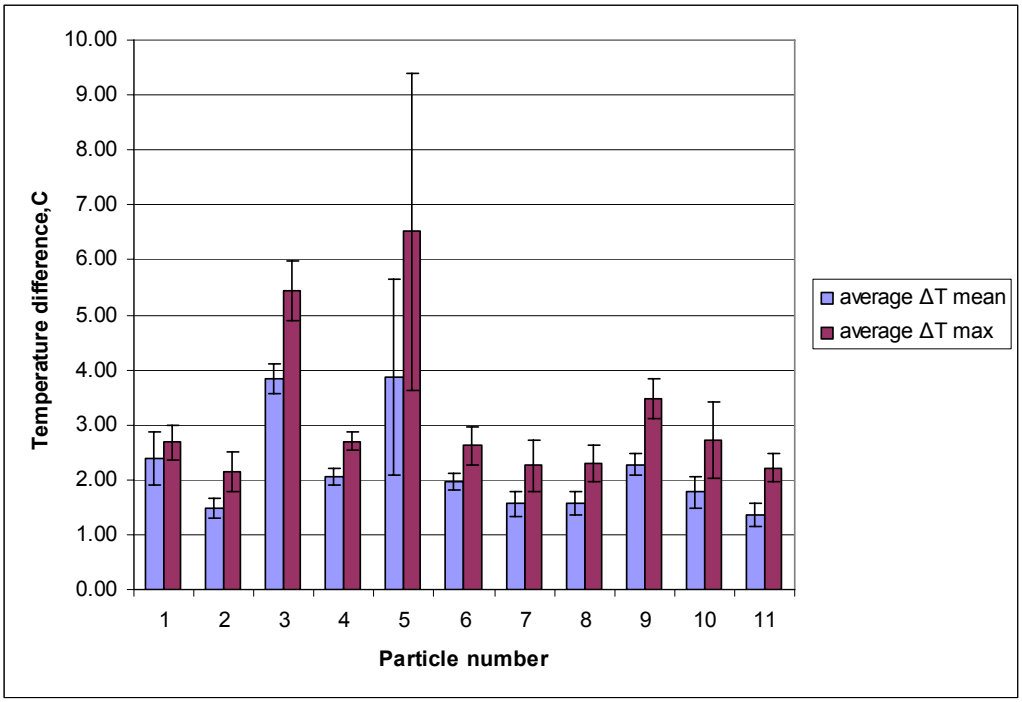

Figure 4-39 Mean values for the temperature differences from repeated exposures with their standard deviations from the multimode oven testing

Tracers "Cube No.3" and "Cube No.9" had much lower standard deviations due to their more symmetrical texture. The lowest average ΔT max from tracers was calculated for the "Cube No.9" caused by the grain which was deeply embedded inside the matrix. Average ΔT max was still above the other synthetic particles without any mineral grains.

Figure 4-40 shows the data for the best case scenario from the multimode oven exposure. For every particle the maximum value from all repeated exposures was chosen for the average ΔT max and average ΔT mean.

The best case scenario was defined as the case when the highest energy transfer was reached in all repeated microwave exposures and measured from the surface closest to the heating minerals. In other words, the particle was coupled at that time to receive the best power transfer during exposure while also having the most favourable orientation to the surface for the infrared temperature measurement.

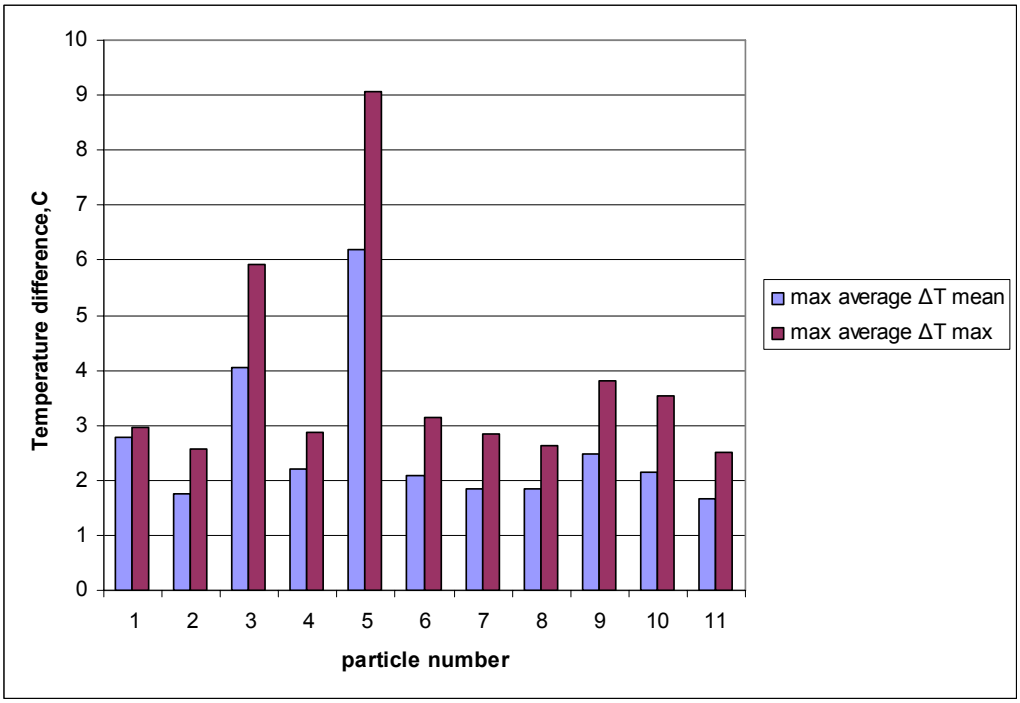

Figure 4-40 The best case scenario for the multimode oven exposure

By analysing data from the microwave exposures in the travelling wave applicator it was straightforward to detect and identify some of the predicted heating patterns on the surface of the synthetic samples from their predefined locations of mineral grains. Figure 4-41 shows four noticeable hot spots caused by produced texture with pyrite.

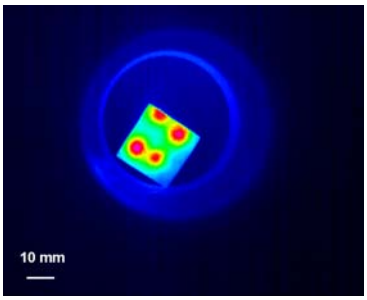

Figure 4-41 The temperature profile for the "Cube No.3"

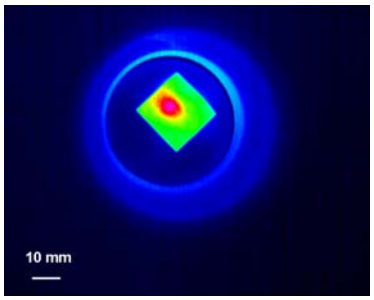

Figure 4-42 The temperature profile for the "Cube No.5"

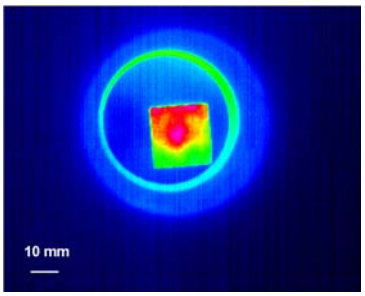

Figure 4-43 The temperature profile for the "Cube No.9"

The temperature profile for the "Cube No.5" can be seen in Figure 4-42 for one of the sides closer to the mineral grain, while the temperature profile for the "Cube No.9" can be seen in Figure 4-43.

For these experimental tests infrared images were collected with 25 frames per second in real time. The region of interest was set to cover the whole surface of the particle holder placed in the middle of the applicator. The region of interest (ROI) was introduced as a quick insight in temperature profile for each particle in real time

during testing. Considering that the position of the particle was influenced by free fall, this was the approach to introduce a constant surface for the analysis. In one of the exposures T max of ROI was influenced by the residual heat from the previously tested particle, as it can be seen in Figure 4-44. In the final data analysis for every particle tested, errors caused by residual heat were removed by placing new ROI in the shape of square around the surface of particle.

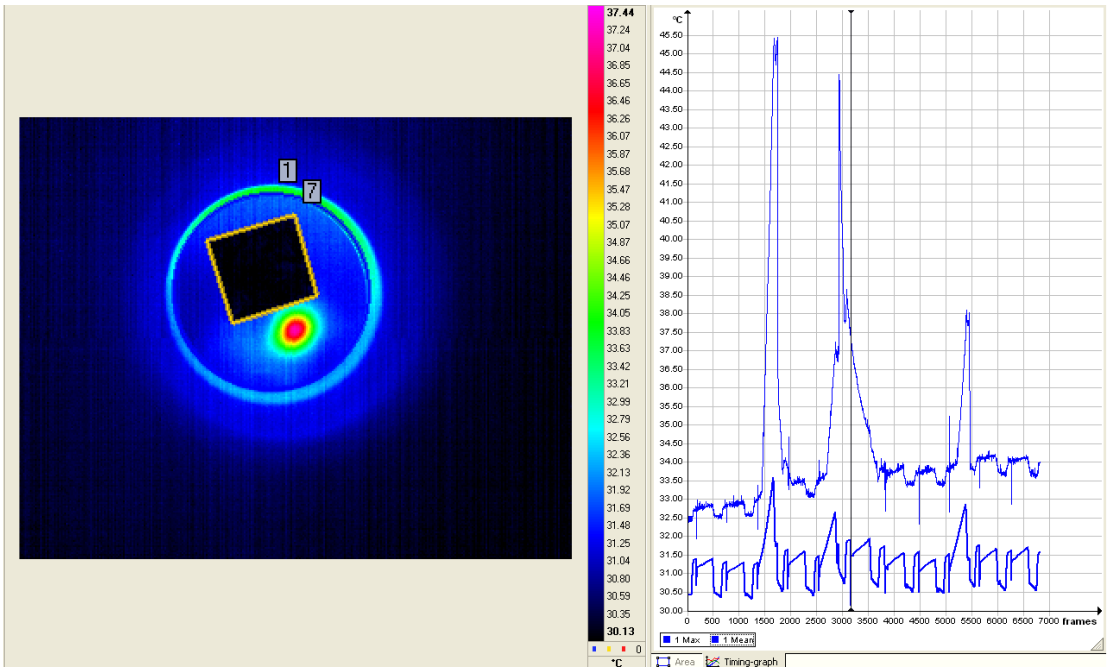

Figure 4-44 For every particle tested, errors caused by residual heat were removed by placing new ROI only on the surface of particle

Figure 4-45 to Figure 4-47 show the change of T max and T mean for the placed region of interest in three repeated exposures. These temperatures were calculated and plotted in time. All eleven temperature peaks indicating each particle exposure to microwave energy in time can be seen and identified. It is very simple to notice that the particles which were used as tracers have much higher peaks than all the others. These temperature peaks can be identified in positions three, five and nine.

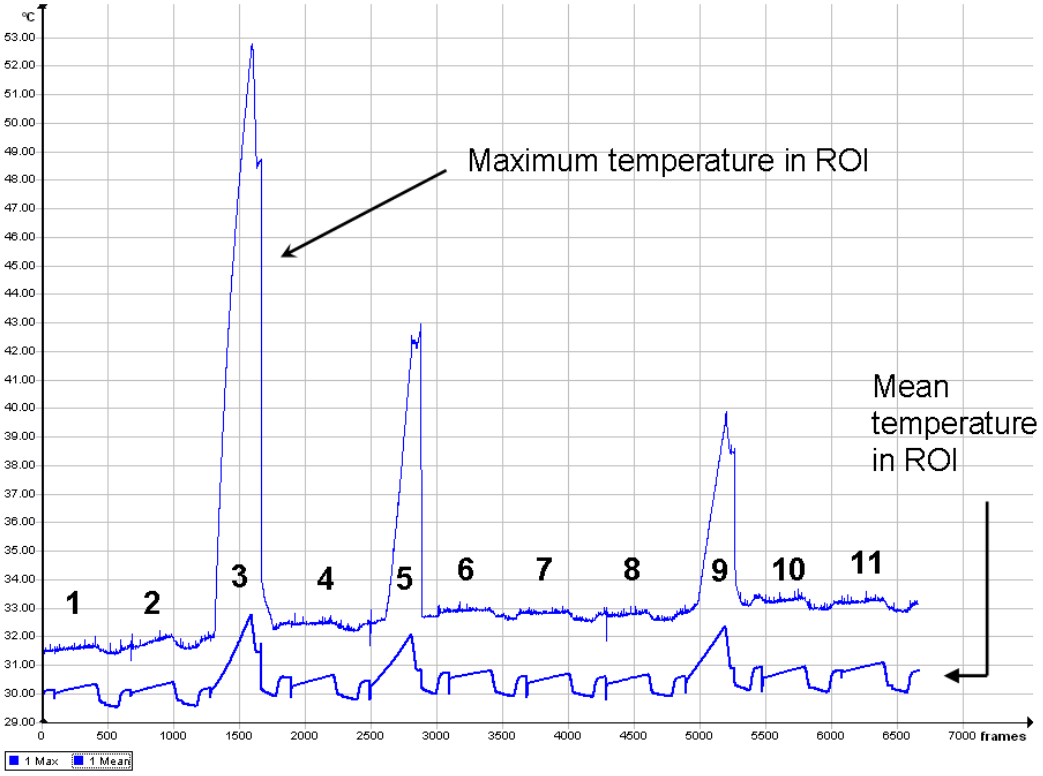

Figure 4-45 First exposure: Maximum and mean temperatures recorded in real time in ROI during first exposure testing.

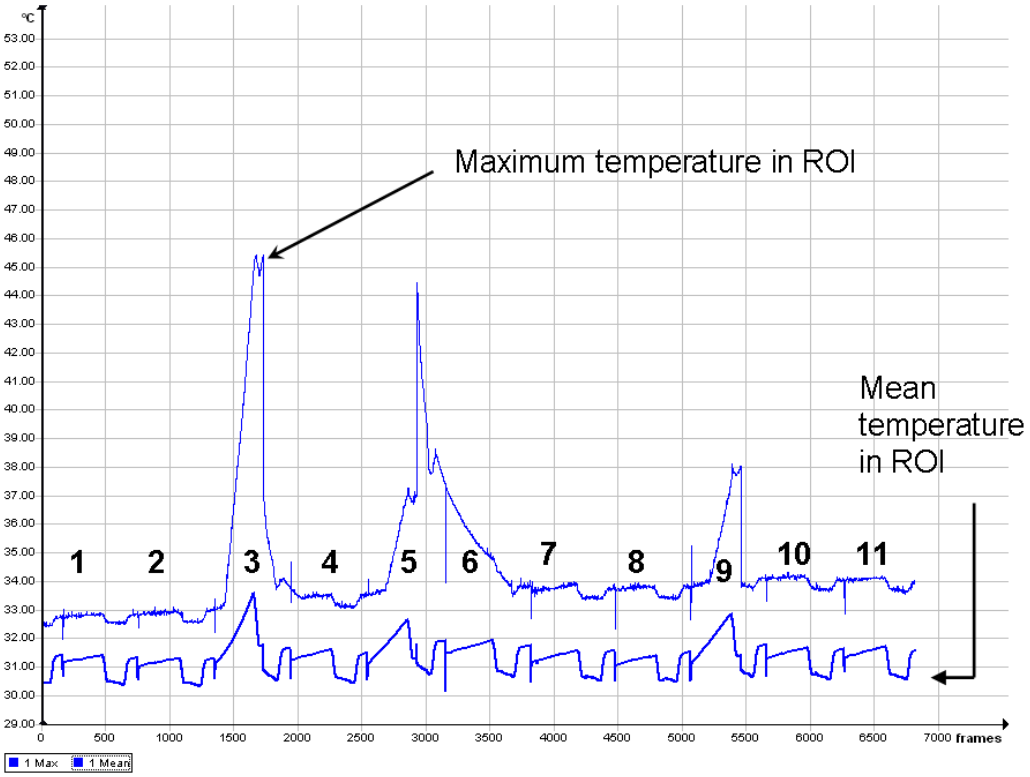

Figure 4-46 Second exposure: Maximum and mean temperatures recorded in real time in ROI during second exposure testing.

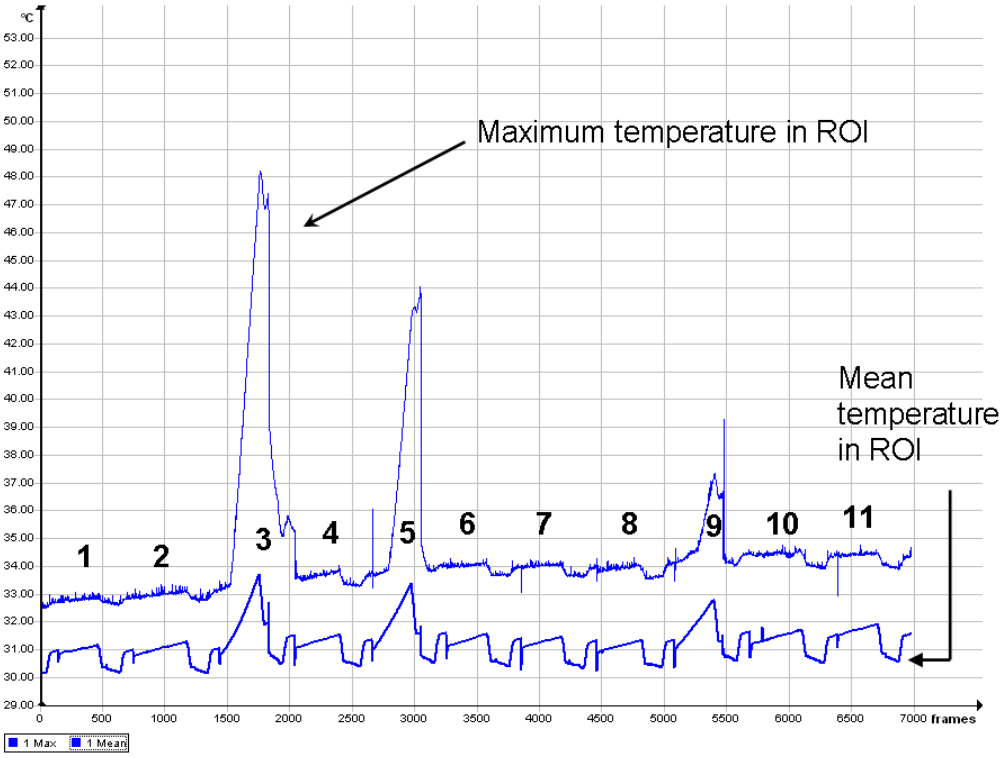

Figure 4-47 Third exposure: Maximum and mean temperatures recorded in real time in ROI during third exposure testing.

Figure 4-48 indicates mean values for the temperature differences from repeated exposures with their standard deviations from the travelling wave applicator testing.

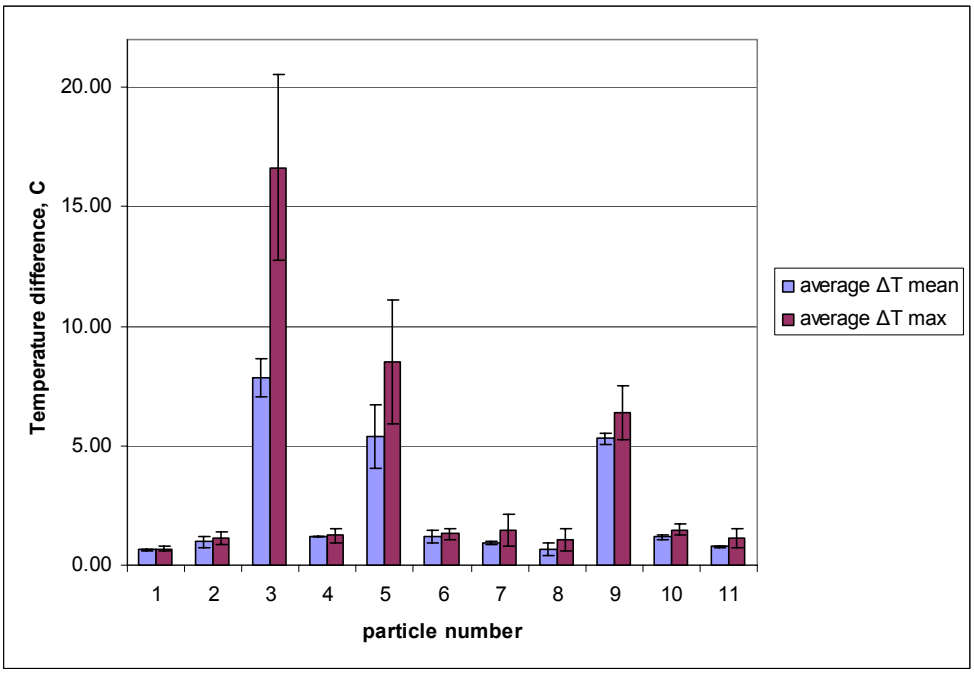

Figure 4-48 Mean values for the temperature differences from repeated exposures with their standard deviations from the TWA testing

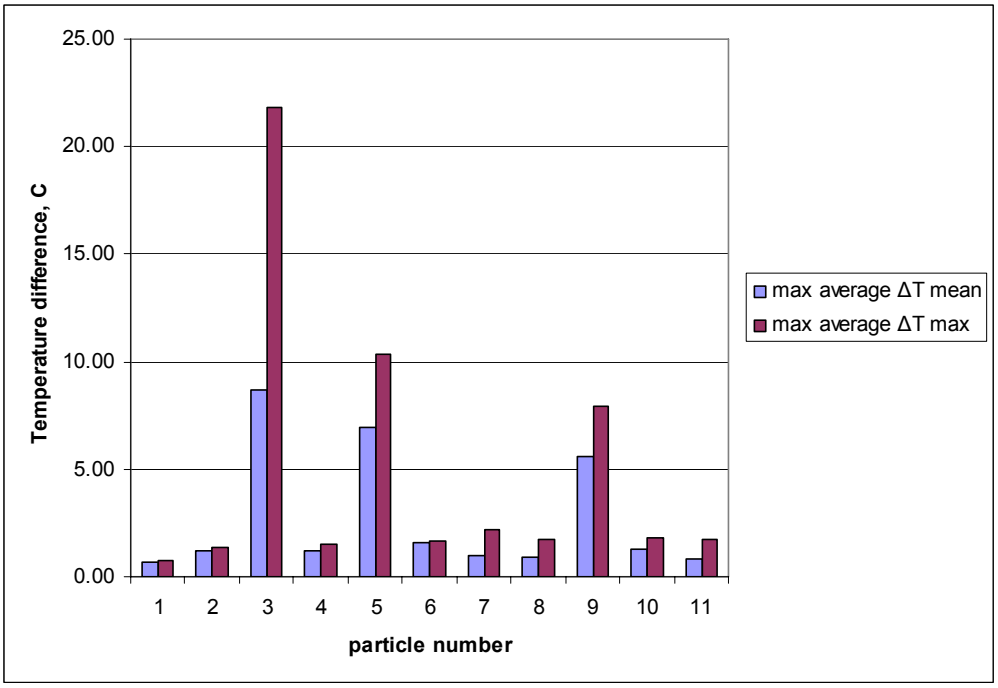

Figure 4-49 The best case scenario for the TWA exposure

Figure 4-49 shows the data from the travelling wave applicator testing. The best case scenario was used to obtain data.

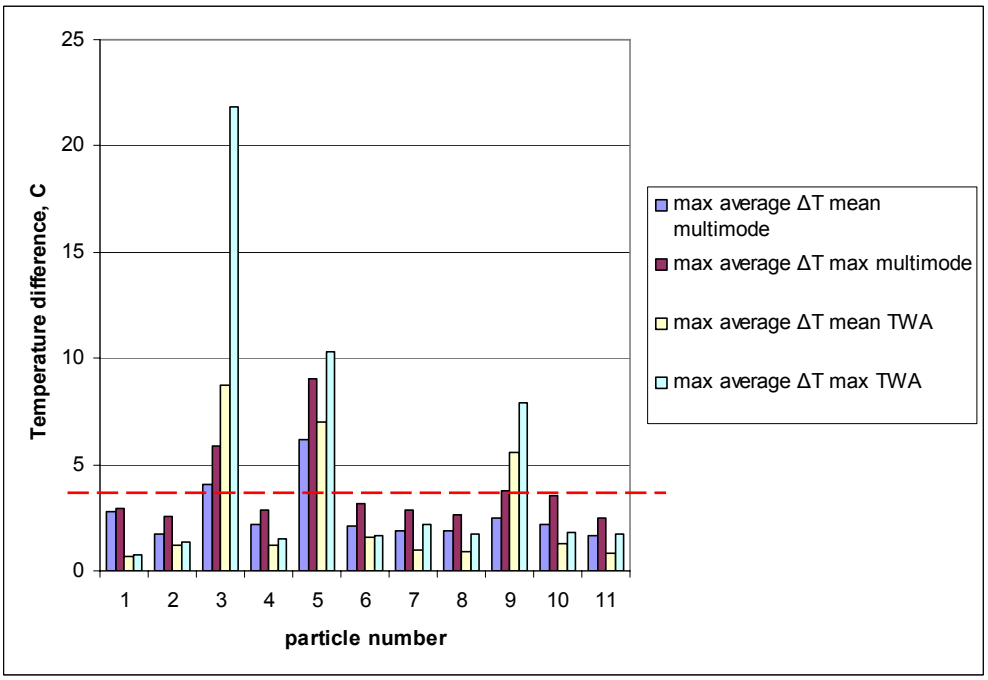

Figure 4-50 Maximum values from all measurements and both systems for average surface temperatures calculated from ROI for synthetic samples

By comparing data from both exposures, presented in Figure 4-50, it can be stated that synthetic particles with created mineral texture had noticeably higher maximum and mean temperature differences. They were compared with the rest of the particles which were created to resemble barren rock particles. It can also be seen that the

temperature difference is strongly dependable upon texture of the heating mineral phases and their proximity to the surface of the particle.

From these two exposures the temperature threshold which is defined by bulk properties of barren synthetic particles can be determined. This temperature threshold can be considered as a base line for the surface temperature variability caused by the matrix material (because the best case scenario was defined and used). By analysing all particles in Figure 4-50, particle number ten can be identified with the highest temperature change for the matrix material. If slightly higher temperature is chosen for selection threshold (indicated with horizontal red line) it will exclude all particles except particles with numbers three, five and nine. The particles which reach higher temperatures indicate presents of the mineral phases within the matrix material as additional heating source.

A barren synthetic particle had better heating response when it was heated up in the group with other particles which increased overall volume of the load during multimode exposure. This effect is explained in more detail in Chapter 3 section 3.9. During individual testing with TWA which was designed to respond to reflected power from introduced external influence, in this case synthetic particle, absence of heating mineral phase caused lower heating response. Throughout same testing, synthetic particle which had a responsive mineral phase was able to absorb more power. This was caused by higher reflected power from the same synthetic particle, which was used by the TWA to achieve better coupling for the power transfer during their testing. Eventually this resulted in much higher heating temperature difference, compared to multimode oven exposure, which can be used as a strong indicator of the present mineral texture.

4.8 Summary

Based on testing synthetic samples following results and observations can be summarised:

- PMMA proved to be good choice of adhesive which allowed testing particles with designed experimental equipment without mechanical damages. This was necessary to achieve repeatable testing.

- Tracers were recognisable in both types of microwave heating experiments, which was previously indicated by testing particles for their dielectric properties using resonant cavity method.
- By using two different types of applicators for created synthetic samples they have become a functioning part of those applicators in two different ways. It has enabled either for barren particles or tracers to have better interaction with electric field. Combined results have provided more accurate selection of temperature threshold defined for bulk properties of matrix material and identification of tracers.

4.9 Particle Characterisation by Image Analysis

4.9.1 Necessity for particle characterisation

One of the challenges with infrared detection is that information is calculated from two-dimensional space. Real information is actually in three-dimensional space. The images of the particles seen in a camera are projected areas which dimensions depend on a particle's orientation when they are placed or fallen on the flat surface. The particles in their most stable orientation tend to present their maximum area to the camera lens, so it can be stated that the projected area of a particle is orientation dependent.

Temperature profiles are created by minerals which are heated by microwaves and the heat is spread by conduction throughout the volume of the particle. The temperatures that can be observed on the surface are a reflection of the texture of the microwave absorbing minerals; their proximity to the surface, the homogeneity of the matrix, and the shape of surface of the matrix.

When synthetic samples were tested they were created to have same shape and proportion to avoid any additional factors which could influence the temperature profiles under the investigation. With real rock particles, (for a chosen testing size) shape and proportions will vary within the boundaries given for that specific size. In some cases specific shape or proportion can be dominant, which can influence temperature profiles. For the real ore particles from different ore types shape factors can be used to investigate whether they have a preference to a specific shape or

proportion for which temperature profiles should be corrected. If two different ore types demonstrate similar distribution in shapes and proportions for the chosen particle size, then it can be stated that the temperature profiles will be mostly dominated by their mineral texture and composition.

4.9.2 Particle shapes

The word 'shape' in common usage refers to two distinct characteristics of particles, form and proportion. The form refers to the degree to which a particle approaches a definite form, such as a cube, tetrahedron or sphere, and the latter by the relative proportions of the particle which distinguish one cuboids, tetrahedron or spheroid from another of the same class (Allen 1997).

Figure 4-51 shows forms and proportions of different particles. Macroscopically, shape may be derived using shape coefficients or shape factors.

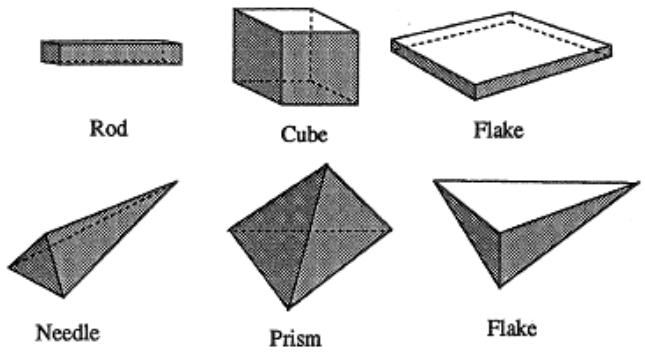

Figure 4-51 Forms and proportions after Allen (1997)

For ore tested, -22.4+19.0 mm sieve diameters were used to select the size for experimental testing and texture investigation. In this case the particle diameter was defined through the sieve diameter which is defined as the width of the minimum square aperture through which the particle will pass.

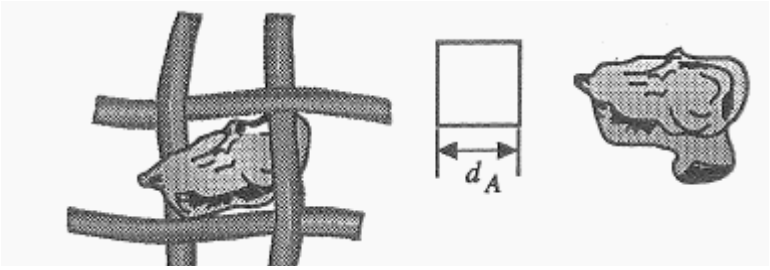

Figure 4-52 Woven wire sieves presents square aperture after Allen (1997)

Woven wire sieves in Figure 4-52 presents a square aperture to the material being sized. In this case it is defined as the projected area diameter of the particle in its plane of greatest stability, $d_A = \sqrt{4A/\pi}$ where d_A is the diameter of a circle with an area equal to that of the projected area of the particle, A.

Particles can be described by using one of the diameters described in Table 4-6. The differences between these dimensions increase as the particle diverges in shape from a sphere. For two-dimensional images the proximity of the image to the outline of a circle is defined by circularity where:

$$Circularity = \frac{(\text{perimeter of particle outline})^2}{4\pi(\text{cross-sectional or projection area of particle outline})}$$

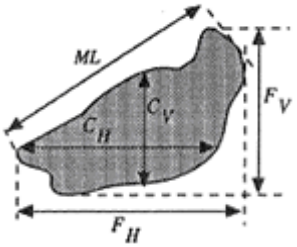

Figure 4-53 Maximum horizontal chord C_H, Maximum vertical chord C_V, Horizontal Feret F_H, Vertical Feret F_V, Maximum length ML after Allen (1997)

Figure 4-53 shows different measured parameters by quantitative image analysis which can be used to calculate shape factors

Table 4-6 Definitions of some diameters after Allen (1997)

d_a	Diameter of a circle having the same projected area as the particle in stable orientation
d_p	Diameter of a circle having the same projected area as the particle in random orientation mean value of $d_p = d_s$ for convex particles
d_c	Diameter of a circle having the same perimeter as the projected outline of the particle
d_A	Width of the minimum square aperture through which the particle will pass
d_F	The distance between pairs of parallel tangents to the projected outline of the particle in some fixed direction
d_M	Cord length, parallel to some fixed direction, which divides the particle projected outline into two equal areas

4.10 Image analysis for QZ Ohio and LRO

Lab View Vision Assistant was used to write the algorithm which is used to perform analysis and gather necessary data. Each step in this algorithm is described in Appendix C. Figure 4-54 and Figure 4-55 show the original images used for analysis.

They present two ore types and all 88 particles used for the second step of experimental investigations. The objective was to compare shape factors such as: perimeter, Waddel disc diameter, elongation factor, Heywood circularity factor and visible area of particles.

Figure 4-54 The original image for QZ-Ohio size -22.4+19.0 mm

Figure 4-55 The original image for LRO size -22.4+19.0 mm

4.11 Calculating mean shape factors for size -22.4+19.0 mm

4.11.1 Perimeter

The perimeter is defined as the length of the outer boundary of the particle. Because the boundary is comprised of discrete pixels, the Vision Assistant subsamples the

boundary points to approximate a smoother, more accurate perimeter. The perimeter is calculated in mm.

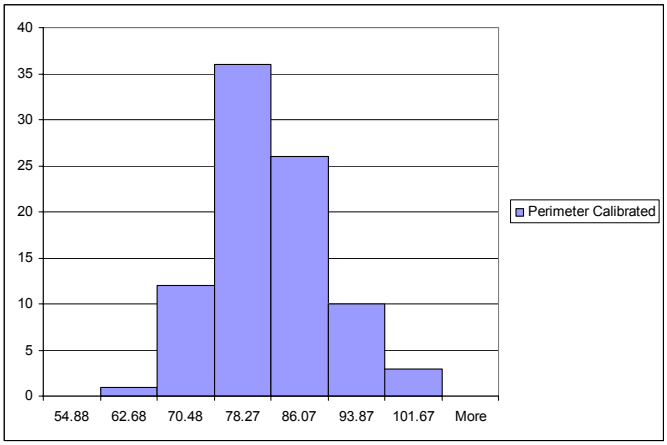

Figure 4-56 Histogram describing Perimeter Calibrated for size -22.4+19.0 mm QZ Ohio

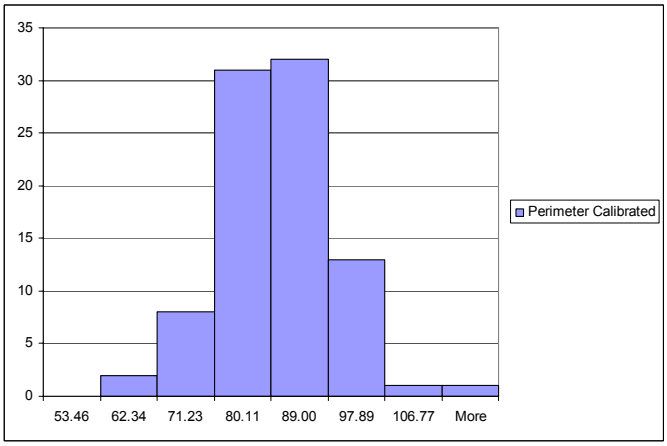

Figure 4-57 Histogram describing Perimeter Calibrated for size -22.4+19.0 mm LRO

4.11.2 Waddel Disk Diameter

Diameter of a disk with the same area as the particle in mm. It is defined as

$$\frac{2\sqrt{particle\_area}}{\sqrt{\pi}}$$

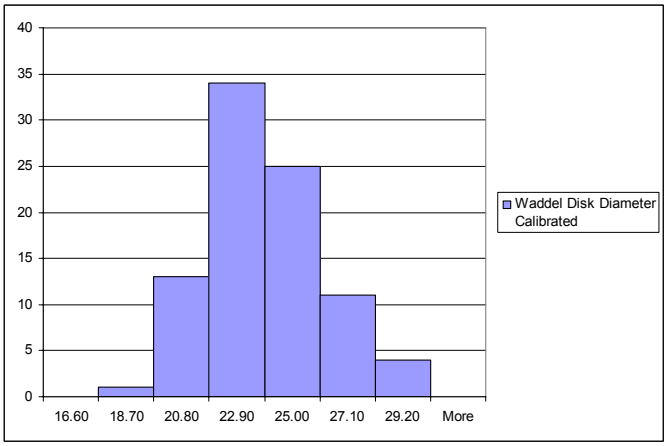

Figure 4-58 Histogram for Waddel Disk Diameter Calibrated for size -22.4+19.0 mm QZ Ohio

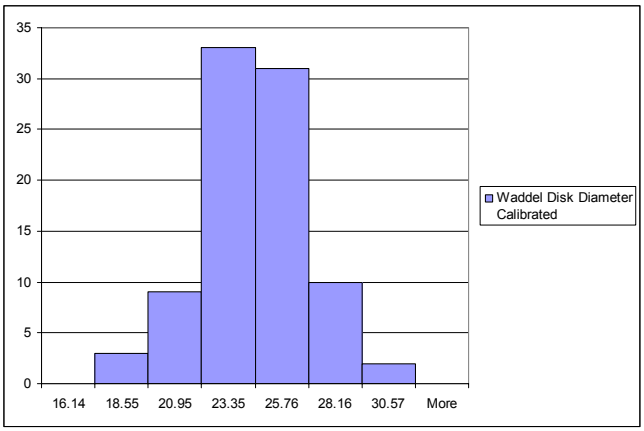

Figure 4-59 Histogram for Waddel Disk Diameter Calibrated for size -22.4+19.0 mm LRO

4.11.3 Elongation Factor

Max Feret Diameter divided by Equivalent Rectangle Short Side (Feret). The more elongated the shape of a particle, the higher its elongation factor.

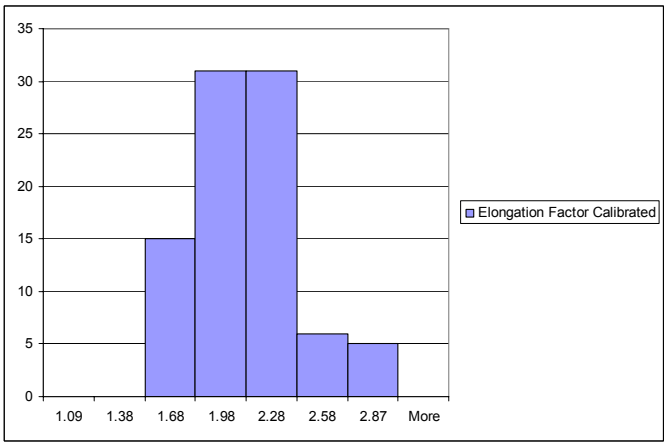

Figure 4-60 Histogram for Elongation Factor Calibrated for size -22.4+19.0 mm QZ Ohio

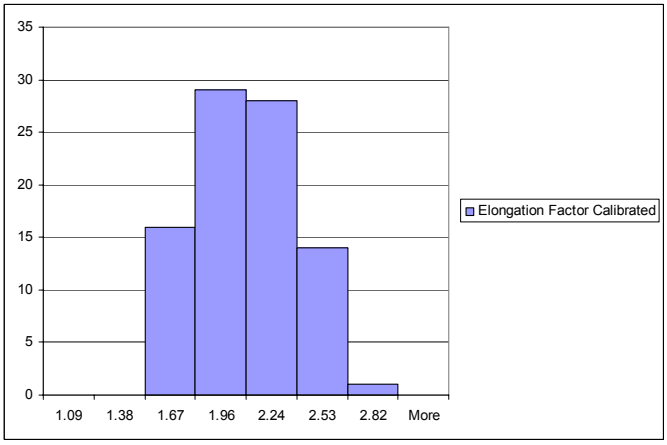

Figure 4-61 Histogram for Elongation Factor Calibrated for size -22.4+19.0 mm LRO

4.11.4 Heywood Circularity Factor

Perimeter divided by the circumference of a circle with the same area. The closer the shape of a particle is to a disk, the closer the Heywood circularity factor to 1.

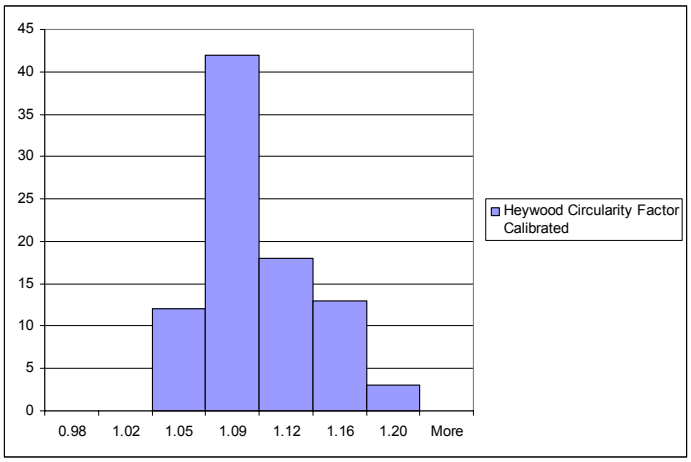

Figure 4-62 Histogram for Heywood circularity factor for size -22.4+19.0 mm QZ Ohio

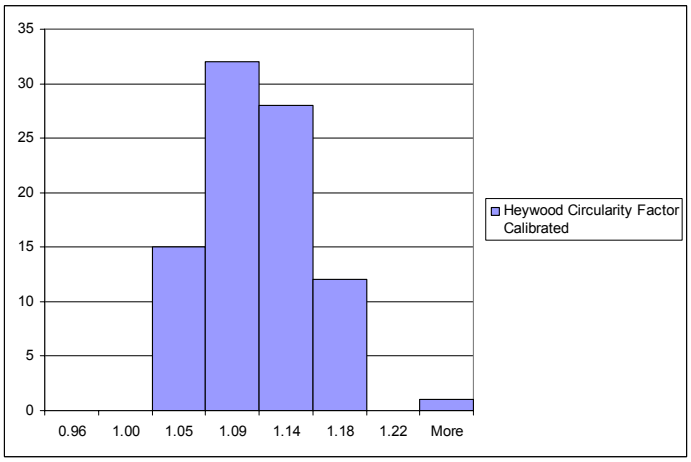

Figure 4-63 Histogram for Heywood circularity factor for size -22.4+19.0 mm LRO

4.11.5 Area

Area of the particle calculated in mm^3

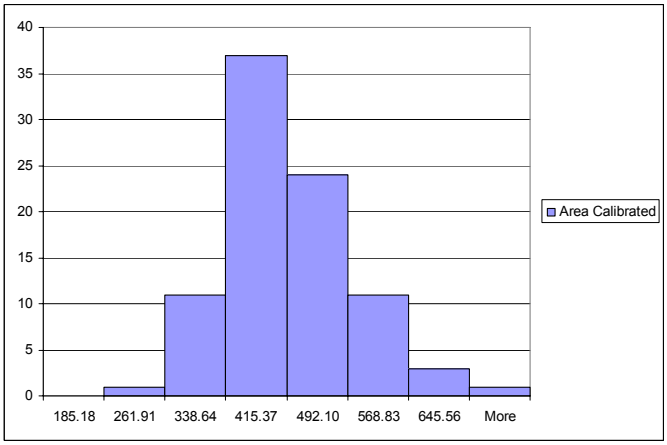

Figure 4-64 Histogram for Area for size -22.4+19.0 mm QZ Ohio

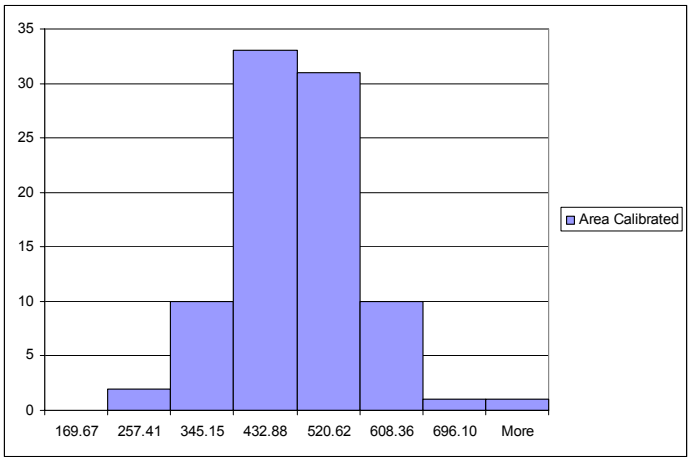

Figure 4-65 Histogram for Area for size -22.4+19.0 mm LRO

4.12 Summary from particle image analysis

Comparing shape factors for the same size -22.4+19.0 mm for two different ore types QZ Ohio and Low Recovery Ore (LRO) the following can be stated:

- LRO ore is slightly larger than QZ Ohio, although they have a very similar distribution between the smallest and the largest particle within analysed particles. Derived from comparing: perimeter, Waddel disc diameter, and visible area of the particle
- QZ Ohio has particles which are slightly elongated compared to LRO particles. Derived from comparing: elongation factor and Heywood circularity factor.

In general, if the distribution in all shape factors for these two ore types is compared for chosen size -22.4+19.0 mm it can be stated that there is no significant difference in shapes and proportions between them. This means that during microwave heating none of the shapes and proportions will influence the temperature profiles to a great extent and that all the difference in heating between them will be influenced by their differences in mineral composition and texture of the minerals they are made of.

Chapter 5-Study of LRO Ore Type

5.1 Introduction

This chapter covers the experimental evaluation of Low Recovery Ore (LRO) for microwave assisted infrared sorting. It was the first, from two ore types, supplied by Bingham Canyon Mine operated by Rio Tinto's Kennecott Utah Copper Corporation. The term, "Low Recovery" refers to the poor recovery of valuable minerals during the mineral concentration process. The LRO was considered to be a "skarn" ore because it contains substantial quantities of common garnet in various forms.

To inquire into basic controlling factors which influence behaviour and creation of temperature profiles, selected particles will be subjected to detail analysis using MLA, X-ray CBT and Optical Microscopy (procedures are covered in more detail in Chapter 3).

The aim of experimental investigations is to detect rock fragments with minerals which interact strongly with microwave energy with two objectives. The first objective is to evaluate potential for sorting using temperature difference after microwave heating and assayed metals grades (with emphasis on copper grade). The second objective is to evaluate potential for sorting determined from mineral textures as in contrast to assayed metal content. In Chapter 4 the exposure of synthetic particles with known textures (of microwave more responsive minerals) showed that it

is advantageous to use both multimode and single mode cavities for better understanding of microwave heating of the ore.

5.2 Overview of the Test Work Procedure and Obtaining Representative Samples

The investigation was carried out in two separate steps. Figure 5-1 shows diagram of preparing the representative sample and the test work procedure.

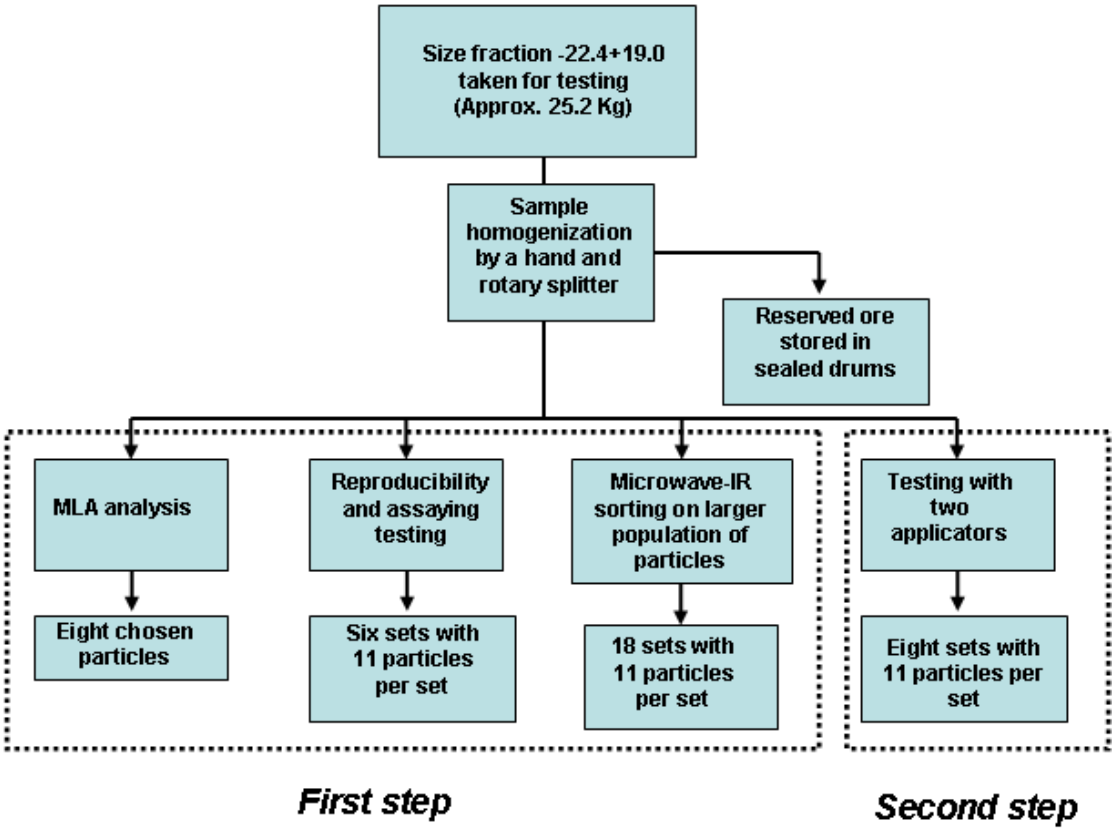

Figure 5-1 Preparation of the sample for the detailed test work which was carried out in several experimental investigations

The first step provides very wide overview and characterisation of the ore tested through three connected experimental investigations. Each experimental investigation had specific objective and according to them the number of particles was increased. This also allowed a very deductive flow of information throughout them.

- ***The first step was divided into three experimental investigations:***

The first experimental investigation was to identify the mineralogical composition of the tested ore with Mineral Liberation Analyser. The objective was to provide an insight into the mineralogical and textural properties which can be correlated to

selective heating processes in an applied microwave field. The particles were carefully examined for any distinct features in texture to ensure that the ore particles selected for MLA examination represented visually most frequent textural features of the bulk ore.

The second experimental investigation had the objective of testing -22.4 + 19.0 mm size fraction of the QZ Ohio ore for reproducibility and separability using multimode excitation in a domestic microwave oven. Sixty-six particles were tested up to six times in different orientations. The mass of each particle was measured before it was pulverised and assayed for copper, iron and molybdenum. Separation graphs which use curves for particle and metal mass as a function of temperature change were created to discuss separability.

Finally, the third experimental investigation had an objective to investigate experimentally simulated (on laboratory scale) the sorting process on the larger population of ore particles. Eighteen sets (189 ore particles) were randomly chosen for multimode microwave exposure. It was decided to expose them only once as they would be exposed in a real microwave apparatus during the sorting process and then perform an assay analysis (of chosen metals) for each ore particle.

- ***The second step was performed in single experimental investigation***

The -22.4 + 19.0 mm size fraction was tested for its textural interaction with an electromagnetic field created in two different microwave applicators. Particles were subjected to individual heating and batch microwave heating in sets. The data collected was used with the objective of creating two temperature curves and enabling discussion of natural separability as a function of mineral texture which causes selective heating.

The Low Recovery Ore was received in 200 l steel drums as a representative sample. The material in the drums was not washed or treated in any other way; it was just selected as a representative sample and divided into four drums for shipment. The ore was spread out on a floor and left to dry under room temperature for a day. In order to obtain representative sample below 90 mm in size some of the larger lumps between

100 mm and 200 mm were handpicked and crushed. Figure 5-2 shows the Gilson Testing Screen used to screen material into fractions. Screening time was set for ten minutes.

Figure 5-2 The Gilson Testing Screen used to screen material into fractions.

Figure 5-3 Rotary Sample Divider

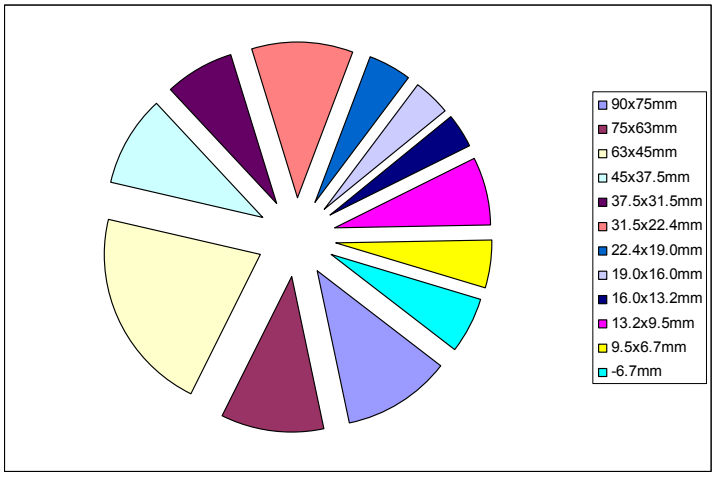

Figure 5-4 Distribution of the material throughout size fractions for the LRO

Figure 5-4 shows distribution of mass through twelve different size fractions after screening. The particle size distribution data is given in Appendix I. By taking into consideration the possible wanted throughputs, energy necessary to achieve separation and natural properties of rock particles as very heterogeneous material, the size fraction -22+19 mm was selected for the detailed test work. The mineral liberation was taken as the first guide to select this size. Kelly & Spottiswood (1995) pointed that the crushing is operation employed to fracture mineral aggregates, and thus induce or increase liberation of minerals. Reducing size also allows easier identification of locked and middling particles by applying sorting technique. On the other hand, size has to be adequate in order to remove as much as possible of the waste minerals for the lowest processing costs. This process favours retaining larger size of particles. The second guide came from the air consumption, which is the most

common medium used for the physical process of separation during sorting. This particle size is typically closer to the lower economic size limit for industrial sorting using compressed air.

A rotary sample divider shown in Figure 5-3 was then used to obtain a homogeneous mixture of the retained ore type by splitting the bulk ore into twelve fractions. Obtained fractions had approximately 2 kg of material. A quarter of initial material was combined by randomly selecting three bags. New combined material was then divided using a smaller hand splitter into bags with approximately 150 g of ore material. For the batch exposure in the microwave multimode domestic oven, it was necessary to obtain eleven particles for testing. For this particular reason, the number of particles in each bag was counted. The bags which already had eleven particles were placed on the side, while bags which had less than eleven particles were combined with bags which had more than eleven particles. To assure random selection of the bags Matlab random function was used. After counting eleven particles in each bag final number of forty one sets was created. Every particle in the set was labelled with the number of the position in multimode cavity and the number of set to which it belongs. The labels enabled easy identification of ore particles during testing and were also used to provide order during “numbers up” and “numbers down” exposures.

5.3 Mineralogical Characterisation of LRO-MLA Results

5.4 Results

The type of the ore tested originates from the Bingham Canyon Mine deposit which is generally described as a porphyry copper ore. It also contains large skarn copper deposits. As Robb (2005) explains: The word "skarn" is an old Swedish term that originally referred to the very hard rocks composed dominantly of calc-silicate minerals (i.e. Ca-rich garnet, pyroxene, amphibole, and epidote) that identify the rather unusual alteration assemblages associated with magnetite and chalcopyrite deposits in that country. It is now widely used to refer to the metasomatic replacement of carbonate rocks (limestone and dolomite) by calc-silicate mineral assemblages during either contact or regional metamorphic processes. Mineral deposits associated

with skarn assemblages are referred to as skarn deposits, and are typically the product of contact metamorphism and metasomatism associated with intrusion of granite into carbonate rocks.

Tested ore was named Low Recovery Ore (LRO) which is considered to be a “skarn” ore because it contains substantial quantities of common garnet in various forms. This garnet was identified with a high content of andradite (calcium iron garnet) which is a strong indicator of skarn mineralisation.

Randomly selected -13.2 + 9.5 mm particles were carefully examined for any distinct features in texture to ensure that the ore particles selected for MLA examination represented visually most frequent textural features of the bulk ore. Eight specimens were examined for this ore type as high polished sections prepared for accurate MLA system measurement.

The Chapter 3, section 3.6 covered and pointed to importance of mineralogy, texture and structure which influence the magnitude of microwave selective heating by producing heating profiles. The following data was processed from the MLA to provide an insight into the mineralogical and textural features which can be correlated to observed heating effects:

- The identity of minerals present in each section examined
- The mineral abundance by surface percentage of each mineral phase
- The grain size distribution of microwave absorbent mineral grains
- The spatial distribution of each mineral phase
- The variation of the above in all the eight specimens which were examined

There were 23 minerals which were identified from MLA scans from all polished sections. They are presented in following table:

Table 5-1 Expected average heating rates as per test conditions described by: a) Harrison (1997) b) Walkiewicz et al. (1988) c) McGill et al.(1988) d) Chen et al. (1984) e) Weert et al. (2011) f) Vorster (2001) g) Kobusheshe (2010) h) Genn (2012)

	Mineral	Chemical formula	Heating rate, ^{o}C/s
1	Amphibole	RSi_4O_{11} R=Mg,Fe,Ca,Na,Li,Ti	--
2	Apatite	$Ca_5(PO_4)_3(F,Cl,OH)$	Poor heater [f]
3	Arsenopyrite	FeAsS	5.83[e]
4	Biotite	$K(Mg,Fe)_3(AlSi_3O_{10})(F,OH)_2$	Unknown (but contains –OH)[g]
5	Bornite	Cu_5FeS_4	11.32[a] Heats readily [d]
6	Calcite	$CaCO_3$	0.6[c]
7	Chalcocite	Cu_2S	1.8[b] 1.43[e]
8	Chalcopyrite	$CuFeS_2$	1.000[a] 15.3[b] 2.85[e]
9	Chlorite	$RClO_2$ R=Na,Mg	--
10	Feldspar	$KAlSi_3O_8 – NaAlSi_3O_8 – CaAl_2Si_2O_8$	0.111[a] 0.2[b]
11	Galena	PbS	2.388[a] 2.3[b] 3.51[e]
12	Garnet *	$X_3Y_2(SiO_4)_3$ X=Ca,Mg,Fe Y=Al,Fe,Cr	Poor heater-medium heater [h]
13	Ilmenite	$FeTiO_3$	A medium heating mineral [a]
14	Magnetite	Fe_3O_4	2.111[a] 7.6[b]
15	Molybdenite	MoS_2	0.4[b] 1.10[e]
16	Olivine	$(Mg, Fe)_2SiO_4$	--
17	Pyrite	FeS_2	1.000[a] 2.5[b] 2.29[e]
18	Pyroxene	$XY(Si,Al)_2O_6$ X=Ca,Na,Fe Y=Cr,Al,Mg,Ti	Poor heater [f]
19	Quartz	SiO_2	0.083[a] 0.2[b] 0.1[c]
20	Rutile	TiO_2	0.75[a]
21	Talc	$Mg_3Si_4O_{10}(OH)_2$	--
22	Tennantite	$Cu_{12}As_4S_{13}$	Difficult to heat when cold [d]
23	Titanite	$CaTiSiO_5$	--

*** For the Garnet estimation was made for the expected heating rate from the dielectric properties measured at 2.47 GHz by Genn (2012) and given in Table 3-6.**

For easier representation some of the minerals were grouped together, so the following grouping was undertaken:

1 Copper Sulphides: Bornite, Chalcopyrite, Chalcocite, Tennantite
2 Other Sulphides: Pyrite, Arsenopyrite
3 Quartz
4 Feldspar
5 Garnet
6 Magnetite
7 Other Forming Minerals: Amphibole, Apatite, Biotite, Calcite, Chlorite, Galena, Ilmenite, Molybdenite, Olivine, Pyroxene, Rutile, Talc, Titanite and Other Minerals

First two groups represent sulphides which have a tendency to respond very well to microwave heating. The first group represented was copper bearing minerals also defined as minerals of interest. The second group was other sulphides, defined as pyrite and arsenopyrite. Quartz and feldspar as common forming rock minerals were not grouped. Garnet and magnetite were also not grouped as minerals whose high content can influence temperature profiles of rock particles. Garnet because of the source of the ore tested and magnetite as responsive oxide which can heat along with sulphides. The last group represent all others rock forming minerals. Their content varies with a scanned surface of the particles. In some cases amount of those minerals can be found with significant surface percentage, while in other cases they are found in small trace or not detected at all.

The following figures from Figure 5-5 to Figure 5-12 will be discussed to present the surface minerals in the eight specimens examined. The full results of all minerals identified in each measured section, which includes the abundance of each mineral or mineral group by surface percentage, are presented in tables and can be found in Appendix F.

The “responsiveness” to microwave heating is based on literature from previous work such as microwave heating studies carried out by: Harrison (1997), Walkiewicz et al. (1988), McGill et al.(1988), Chen et al. (1984), Weert et al. (2011), Vorster (2001) and Kobusheshe (2010).

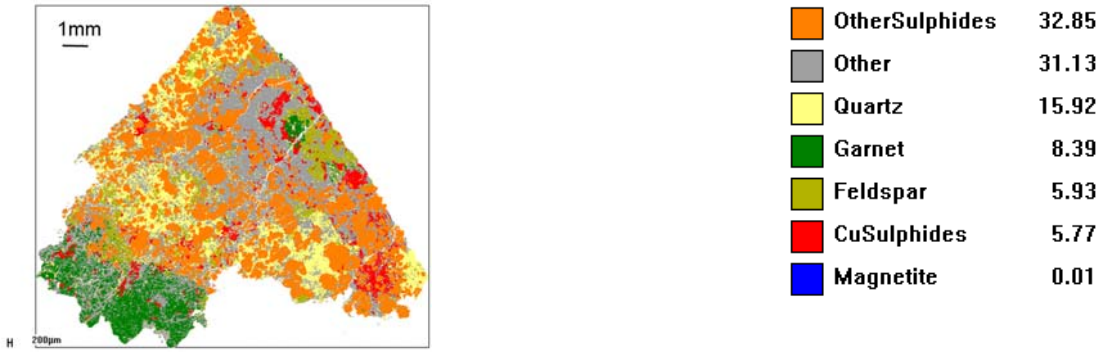

Figure 5-5 Particle No. 1, chosen for the MLA analysis, LRO

Figure 5-5 shows a strong presence of sulphide minerals in the particle No. 1. Various grain sizes from 100 µm up to 2 mm (scale bar estimation) are finely dispersed throughout the whole surface. Copper sulphides are interlocked with pyrite in most cases, although they can be found interlocked with garnet, feldspar and amphibole.

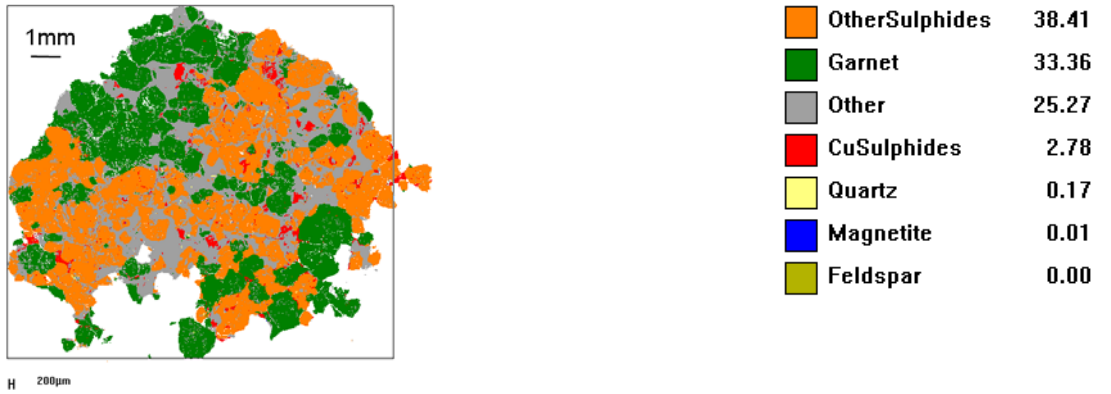

Figure 5-6 Particle No. 2, chosen for the MLA analysis, LRO

Particle No. 2 presented in Figure 5-6 shows pyrite and garnet to be the most dominant minerals with very similar grain sizes and spatial distribution. Grain sizes vary from 500 µm to 3 mm (scale bar estimation) and they are connected by calcite. The chalcopyrite is dominant copper sulphide and it is in most cases interlocked with pyrite and calcite, while grain sizes lower than 200 µm can be found in larger grains of garnet.

Figure 5-7 Particle No. 3, chosen for the MLA analysis, LRO

The most dominant mineral in particle No. 3 is garnet covering about 60% of the surface as we can see in Figure 5-7. Chalcopyrite is mostly associated with pyrite for larger grains above 500 µm. The smaller grains can be found embedded in biotite and amphibole or in garnet.

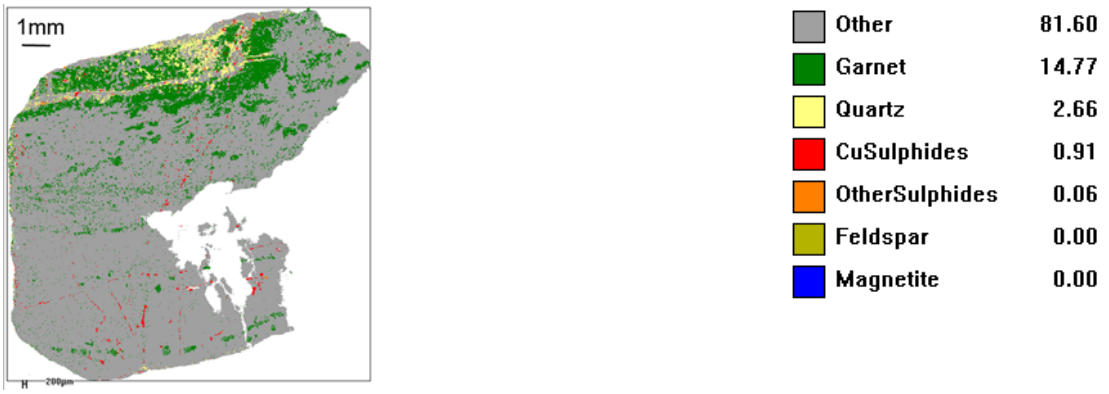

Figure 5-8 Particle No. 4, chosen for the MLA analysis, LRO

Figure 5-8 displays amphibole with calcite, garnet and quartz which make the relatively transparent matrix for the particle No. 4. Although, quartz and garnet form a distinguishable section, garnet can also be found disseminated throughout the large surface of amphibole. In this specimen copper bearing sulphides are present in higher content than other sulphides. They can be identified as tiny seams spread out in different directions with grain sizes around 200 µm.

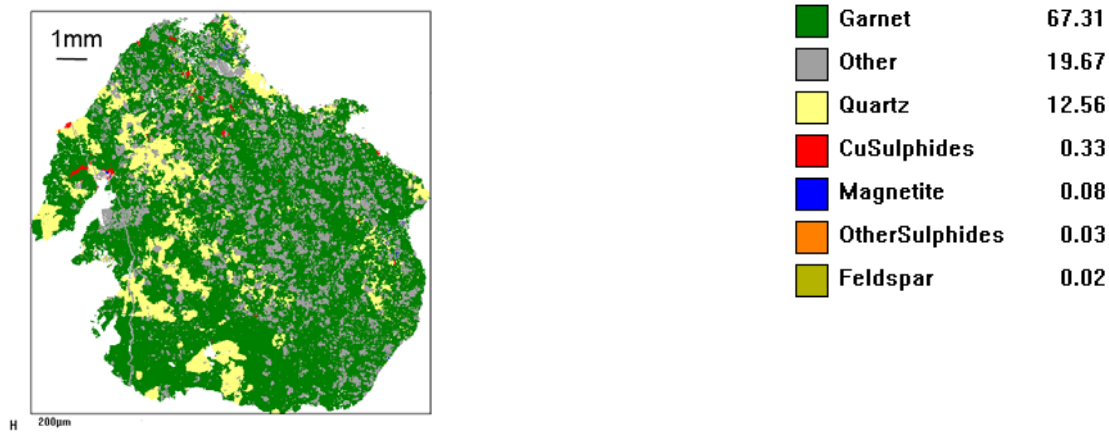

Figure 5-9 Particle No. 5, chosen for the MLA analysis, LRO

Particle No. 5 shows a very high content of garnet as composing mineral for the matrix. Other composing minerals are quartz and calcite which are disseminated in the garnet as we can see in Figure 5-9. Quartz is present in much larger grains compared to calcite. A small content of sulphides is detected in the shape of grains around 200 µm in size and mostly embedded in the calcite.

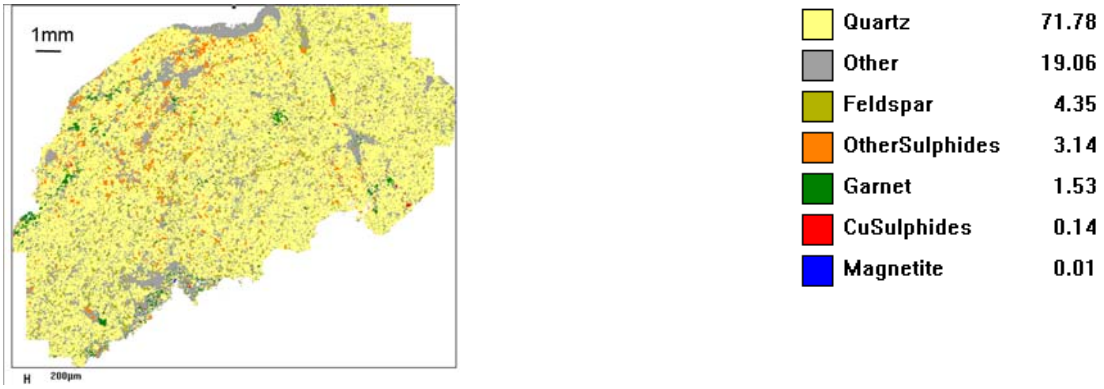

Figure 5-10 Particle No. 6, chosen for the MLA analysis, LRO

Figure 5-10 shows the distribution of mineral phases in particle No. 6. Quartz is the most dominant mineral phase with over 70% while all the other minerals are dispersed. Grain sizes of all the other minerals are very similar and with relatively equal space distribution between them within the quartz. Zones with higher concentration of garnet, amphibole and calcite are present and not larger than 2 mm in diameter. Pyrite is present with the highest content and almost evenly dispersed in quartz matrix.

Figure 5-11 Particle No. 7, chosen for the MLA analysis, LRO

In Figure 5-11 it can be seen that for particle No. 7 major gangue minerals such as feldspar, quartz and biotite, (which are more transparent to microwave energy) form almost 96% of the surface. Chalcopyrite is present in small grains with the spatial distribution between grains from 0.5 to 1 mm.

Figure 5-12 Particle No. 8, chosen for the MLA analysis, LRO

Figure 5-12 shows mineral phases for the particle No. 8. It is made of high content of well dispersed fine grains of pyrite within the quartz and calcite matrix. In some parts the spatial distribution between grains has tendency to decrease making possible to identify those regions where grains almost merge together.

5.5 Summary

As might be expected, the particles show substantial variation. However, the presence of the garnet is a strong indicator of skarn ore. The results of the ore modal mineralogy summarised through MLA investigation shows that the LRO ore contains significant amounts of good absorbers of microwave energy such as pyrite and chalcopyrite. The major gangue minerals which are relatively transparent to microwave energy are quartz, feldspar and calcite with varying content of garnet, amphibole and biotite.

5.6 Microwave Heating and Temperature Characterisation Procedure

Temperature data for the particles in each set was collected using the following procedure. The microwave tray was demarcated into eleven regions. All of the fragments from the set were placed along the circular periphery of the microwave tray in one of the demarcated regions shown in Figure 5-13 a). Before exposure to microwaves, an infrared image of the ore particles was taken using an IR camera with internal cooling system. An IR image before microwave heating was taken to obtain initial temperatures which were usually around room temperature. Figure 5-13 b) shows one of these initial images taken during experimental work.

The infrared camera (manufactured by CEDIP) was mounted on a specially designed camera stand enabling capture of the infrared images directly above the microwave tray. At the same time the camera stand provided constant distance between the camera lens and the glass tray which was taken as one of the settings in supplied software for the camera.

Each batch of ore particles was then heated using 2.45 GHz microwaves in a multimode microwave oven. After heating for 12 seconds, or for the one rotation respectively of the microwave tray, the tray was taken out and a video recording of the tray was started using the CEDIP camera. The overall recording time was 40 seconds after the end of microwave heating. Two time points were chosen to collect data. The first time point was 5 second after microwave exposure. One of the images taken in first time point with clearly distinguishable "hot" and "cold" particles can be seen in Figure 5-13 c). The second time point was 35 seconds later.

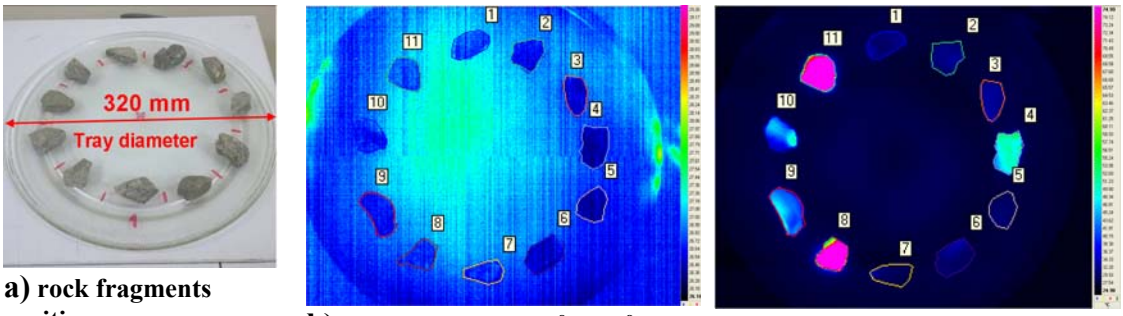

a) rock fragments positions **b) [scale min-max: 26°C-29 °C]** **c) [scale min-max: 25°C-75 °C]**

Figure 5-13 a) The microwave tray was demarcated into eleven regions. b) IR recording before microwave exposure. c) IR recording 5 sec after the end of microwave heating

The images of each particle before microwave exposure, 5 sec after the end of microwave heating and at the end of recording time were analysed using software supplied with the camera to determine:

- change in *average* temperature during heating period and after 5 seconds (Delta T1)
- change in *average* temperature during heating period and after the end of recording time of 40 seconds (Delta T2)
- change in *maximum* temperature during heating period and after 5 seconds (Delta Max T).

The temperature for each particle was calculated by applying a region of interest around the perimeter of the particle. The region of interest enabled separation of visible surface of the particle from the background and calculation of the maximum and mean temperature on the surface of the particle.

5.7 Reproducibility of -22.4 +19.0 mm Particle Selection

The objective was to investigate the reproducibility and validity on a sub-sample for the -22+19 mm size fraction and to identify the amount of variability in results due to the process (as opposed to the particle variability). Six sets were selected at random and subjected to the following procedure.

Each set was subjected to the microwave heating and temperature characterisation procedure six times. The particles and microwave glass tray were allowed sufficient time to cool between each run of the heating procedure. A computer random number generator program was used to randomly match particle numbers to one of the numbered regions on the microwave tray and this determined the initial placement of the particles for each run. In addition, particles were placed with their number facing up for half the runs and down for the other half. This process aimed to duplicate the random orientation of particles on the belt of a sorting machine.

In Figure 5-14 and Figure 5-15 results calculated from sets No. 1 and No. 6 are shown while the results for remaining sets can be found in Appendix G. The temperature change for each particle was calculated by following the earlier described procedure in section 5.6 and values for Delta T1, Delta T2 and Delta Max T are plotted including their standard deviations.

The degree of heating is quite reproducible for “cold” particles but less so for “hot” particles. For example, in the set No. 1 particles No. 3 and No. 4 are identifiable as “cold”. The term “cold” was used because of their slight temperature change which was up to 10 ^{o}C. Some of the particles exhibited much higher temperature change even up to 60 ^{o}C and they were characterised as “hot” as it can be seen in Figure 5-14. This behaviour is expected if the particle’s texture or in other words the physical arrangements of the minerals which interact with microwaves are strong controlling

factors in the degree of heating. The target of the pre-concentration process is to identify and reject barren or "cold" particles.

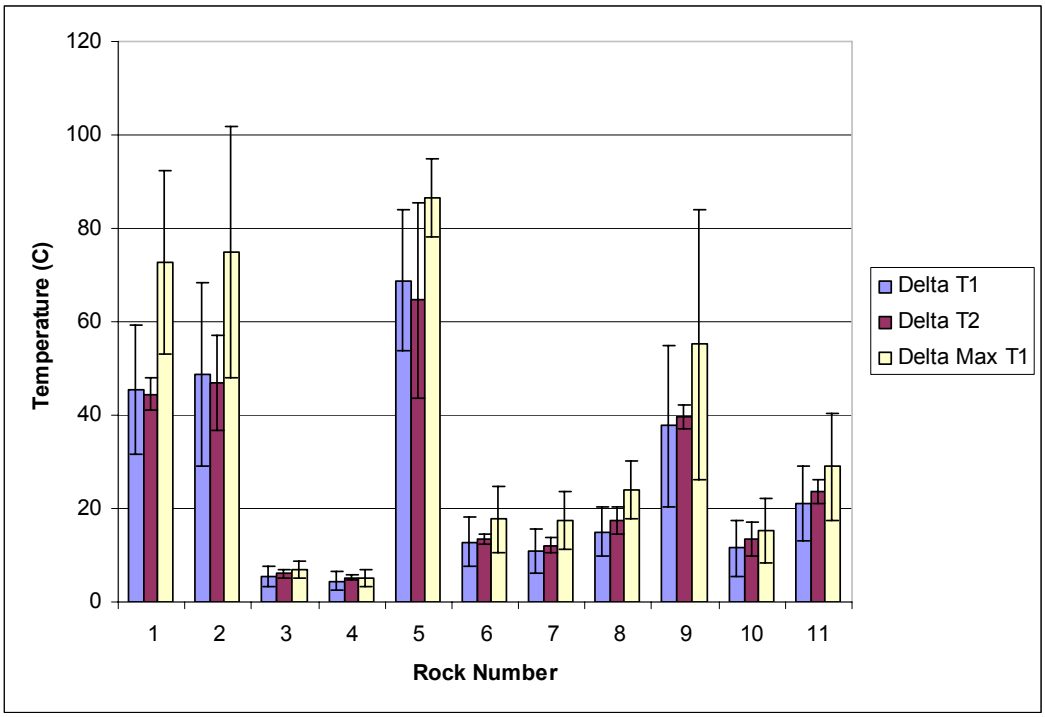

Figure 5-14 Reproducibility temperature change graph for the eleven -22+19 mm particles in set No. 1 for LRO where each particle was tested 6 times in different orientations

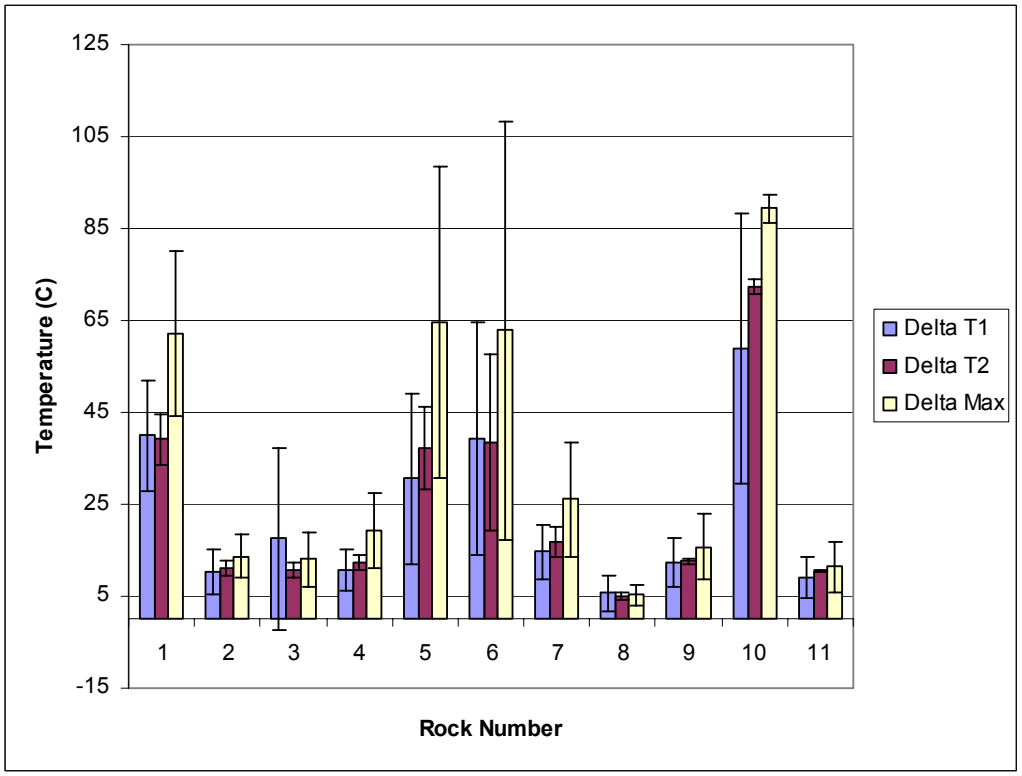

Figure 5-15 Reproducibility temperature change graph for the eleven -22+19 mm particles in set No. 6 for LRO where each particle was tested 6 times in different orientations

In each set tested, it can be seen that "cold" particles were clearly distinguishable with a much smaller standard deviation. In general, the temperature change would be most likely reproducible if the standard deviation from all six exposures had a very small value, regardless of a particle being characterised as "cold" or "hot". The reproducibility can be easily investigated by plotting the values of standard deviations with a population, as it can be seen in Figure 5-16.

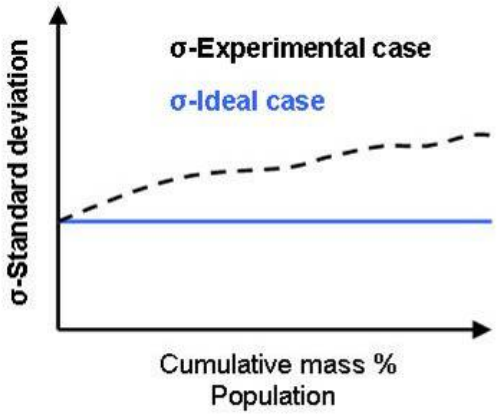

Figure 5-16 Plotted σ -standard deviation vs. population to assess the reproducibility

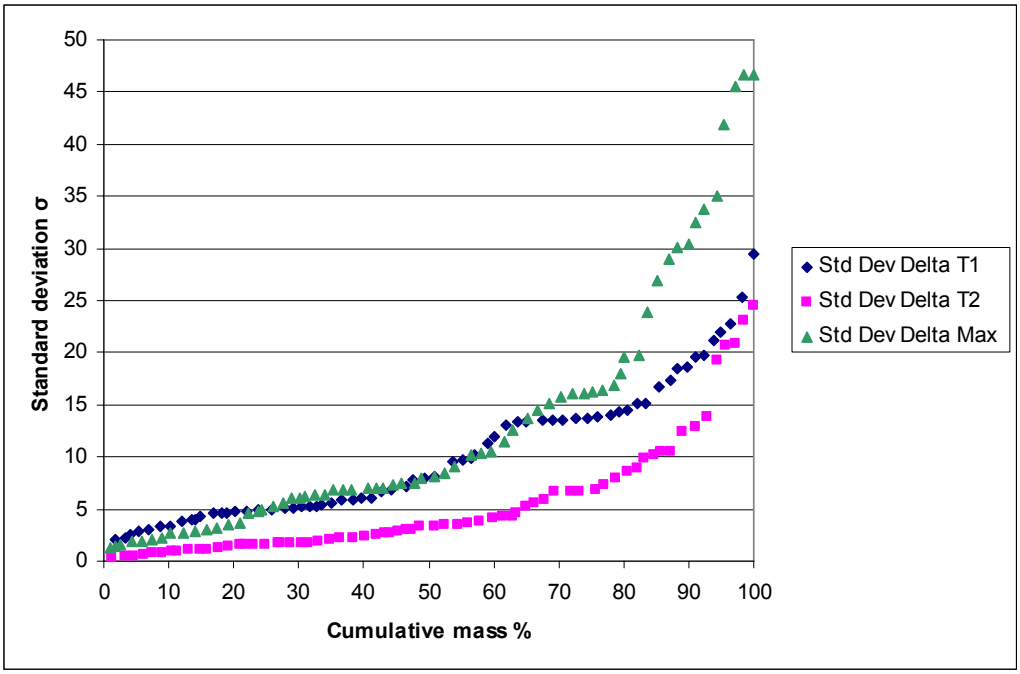

Figure 5-17 Standard deviation from the reproducibility study for the LRO Ore type

Figure 5-17 shows standard deviation from the reproducibility study for the LRO ore type with the population presented through cumulative mass percentage. If it is decided that standard deviation up to 5 ^{o}C is acceptable to describe the reproducible process it can be observed that standard deviation for Delta Max and Delta T1

corresponds to 30 % of mass of the all particles. It also can be noticed that reproducibility increases significantly for the standard deviation of Delta T2, up to 65 % of mass of all particles.

The increase in reproducibility for the temperature change Delta T2 can be explained through the time for which the ore particle had an opportunity to reach temperature equilibrium. As explained in Chapter 3 section 3.6 with selective heating a certain time (depending on the size of the particle) will be necessary for the heat transfer to take place within the whole mass of the particle. In this case, after 35 seconds ore particles had already reached a certain level of temperature equilibrium which reduced the variability in surface temperature change.

5.8 Summary

The analysis shows that substantial variation in mineral phases and their distribution, which was also detected by mineralogical characterisation in section 5.3, had reflected on the standard deviation in the reproducibility study. With the exposures repeated six times data clearly shows that the frequency of smaller standard deviations for the "cold" particles is much higher compared to "hot" ones. This suggests that they can be more easily identified and selected. For defined standard deviation up to 5 ^{o}C it can be stated that approximately a third of the particles had a very reproducible temperature change for the first time point. For the longer time point (Delta T2) this number of particles was more than doubled.

5.9 Potential for Sorting Using Temperature Difference After Microwave Heating and Copper Grade of Low Recovery Ore Particles

5.9.1 Temperature Separation Curves

Determining thresholds for separation is one of the most important challenges in sorting and the pre-concentration process. Although the physical process of separation is more of an engineering problem (depending of desired throughputs), setting the right thresholds which will divide the feed into the concentrate and the gangue minerals requires more systematic study. To investigate the potential of setting the right thresholds, separation curves were created. They present mass and metal rejected as a function of temperature change.

All the rock particles for the reproducibility study were measured to determine their mass and then sent for assaying to quantify the content of copper, iron and molybdenum. The particles were pulverised and sent for independent assaying analysis by AMMTEC Laboratory based in Perth, AU. The copper content was determined by mixed acid digest followed by ICP (Induction Coupled Plasma) and finished with AAS (Atomic Absorption Spectroscopy).

It was found that for the majority of rock particles the content of molybdenum was below 10 ppm. Despite the fact that some of the particles had a higher content of molybdenum, minerals with molybdenum for this particular ore type were taken as contributing factors and not as leading factors in the process of selective heating.

For these separation curves the temperature threshold will change depending on the time chosen to execute physical separation and whether it is decided to sort by average or maximum temperature change. The separation curves were sorted by temperature change for Delta T2, Delta T1 and Delta Max.

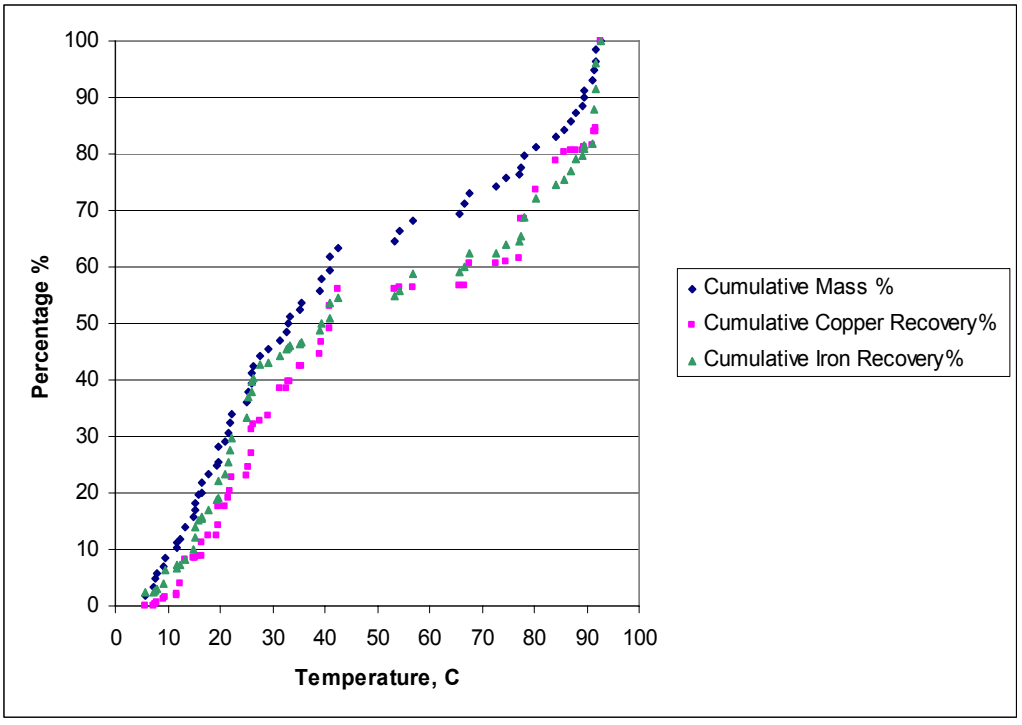

Figure 5-18 Separation curves from reproducibility study six sets sorted by Delta MAX for LRO ore type

Figure 5-18 shows separation curves sorted by temperature change for Delta Max. Cumulative copper and iron recovery curves are compared to cumulative mass to determine temperature change which will define the loss of metal with the mass being

rejected. The separation curves for Delta T2, Delta T1 are given in Appendix G while separation curve for Delta Max (see Figure 5-18) is presented this section since it gave the best separation results.

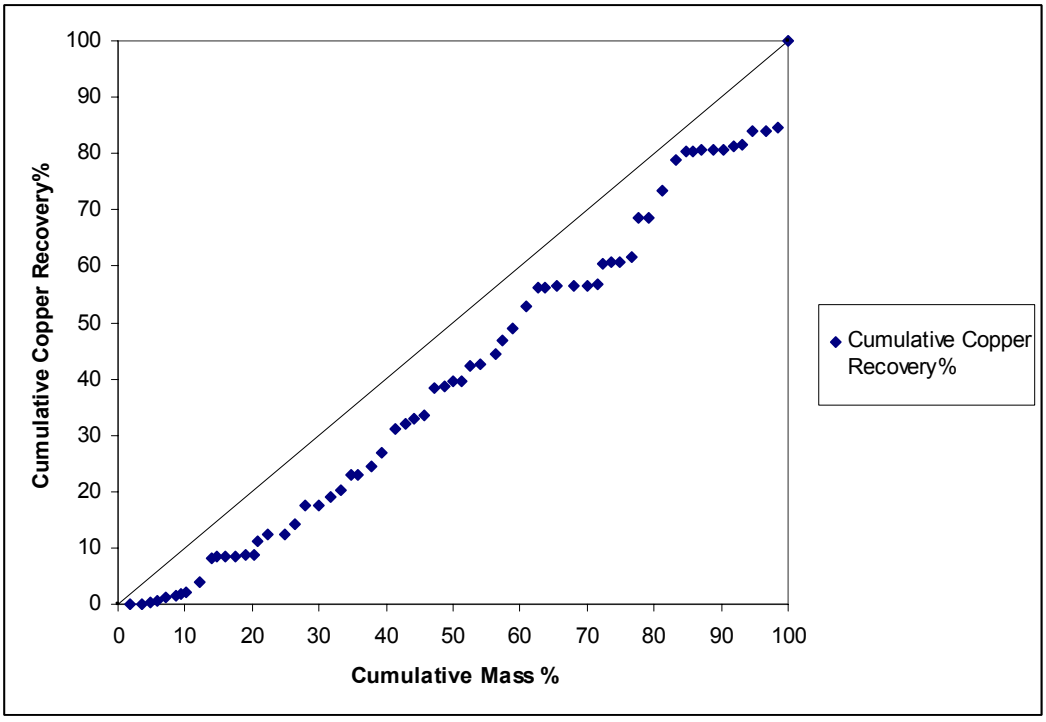

Figure 5-19 Non-linear deviation between the Cumulative Mass % and the Cumulative Copper Recovery % for Delta MAX for LRO ore type.

To choose the best operating point, non-linear deviation between the cumulative copper recovery % and cumulative mass % for Delta Max is presented in Figure 5-19. For this particular ore type the target of the pre-concentration process is to identify and reject barren "cold" particles. According to Cohen (2000) "Rejection of 25 – 30% of the feed mass is usually a minimum requirement for sorting to be economically justifiable". Choosing to reject 30% of mass treated following temperature threshold can be placed: for the Delta MAX with 30% of mass having standard deviation up to 5 ^{o}C temperature change of 20 ^{o}C will reject 30% mass with an approximately 18% loss of overall copper.

The cumulative iron recovery follows mass recovery very closely and about 45% starts to separate. The separation indicates that in the remaining 55% of the mass tested, which corresponds mostly to the hotter particles, the content of iron is increasing. In this case the increased content of iron cannot be correlated only with the presence of a copper bearing minerals. The results for iron content were obtained

from pulverised samples, therefore; they represent overall content of iron whether it comes from sulphides (for example: pyrite, arsenopyrite and chalcopyrite) or oxides (for example: magnetite).

5.10 Temperature Separation Curves for the Larger Population

To investigate further, it was decided to experimentally simulate the sorting process on the larger population of ore particles. Eighteen new sets (189 ore particles) were randomly chosen for multimode microwave exposure. It was decided to expose them only once as they would be exposed in a microwave apparatus during the sorting process.

The particles have been sorted into the order of each measured temperature increase and then plotted for the cumulative mass of copper, iron and total mass against temperature increase (after obtaining assaying results). The separation curves were sorted by temperature change for Delta T2, Delta T1 and Delta Max.

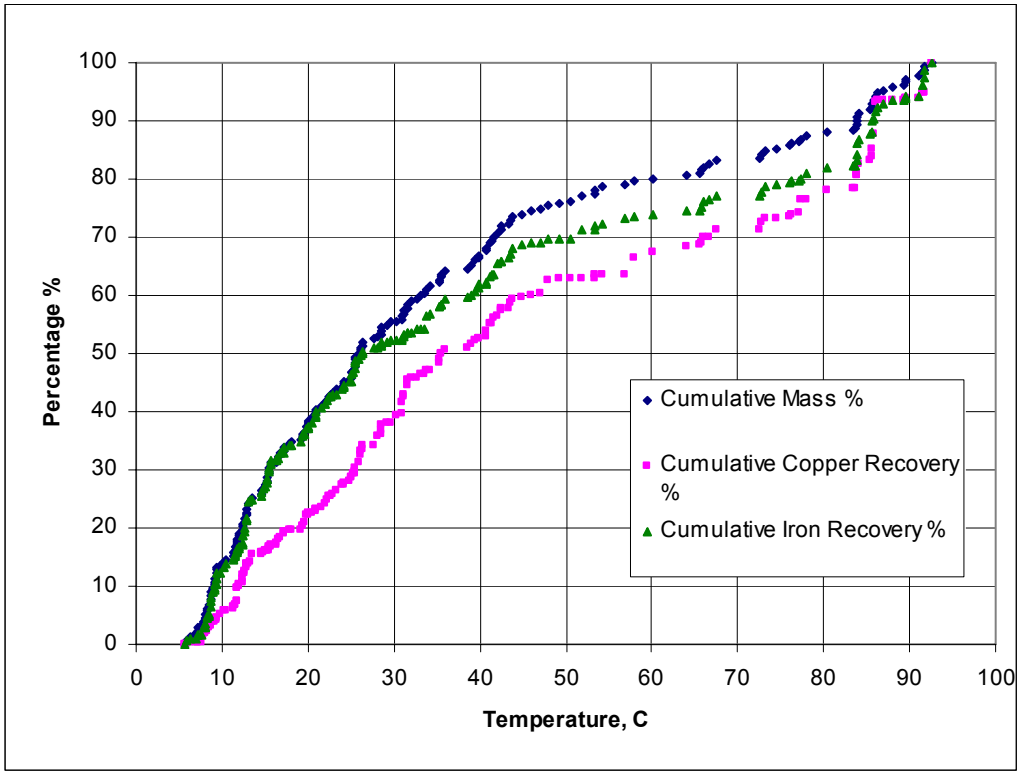

Figure 5-20 Separation curve for LRO (larger population) -22+19 mm size fraction based on Delta Max T

The separation curves for Delta T2, Delta T1 are given in Appendix G while separation curve for Delta Max (see Figure 5-20) is presented this section since it gave the best separation results. To choose the best operating point, non-linear

deviation between the cumulative copper recovery % and cumulative mass % for Delta Max is presented in Figure 5-21.

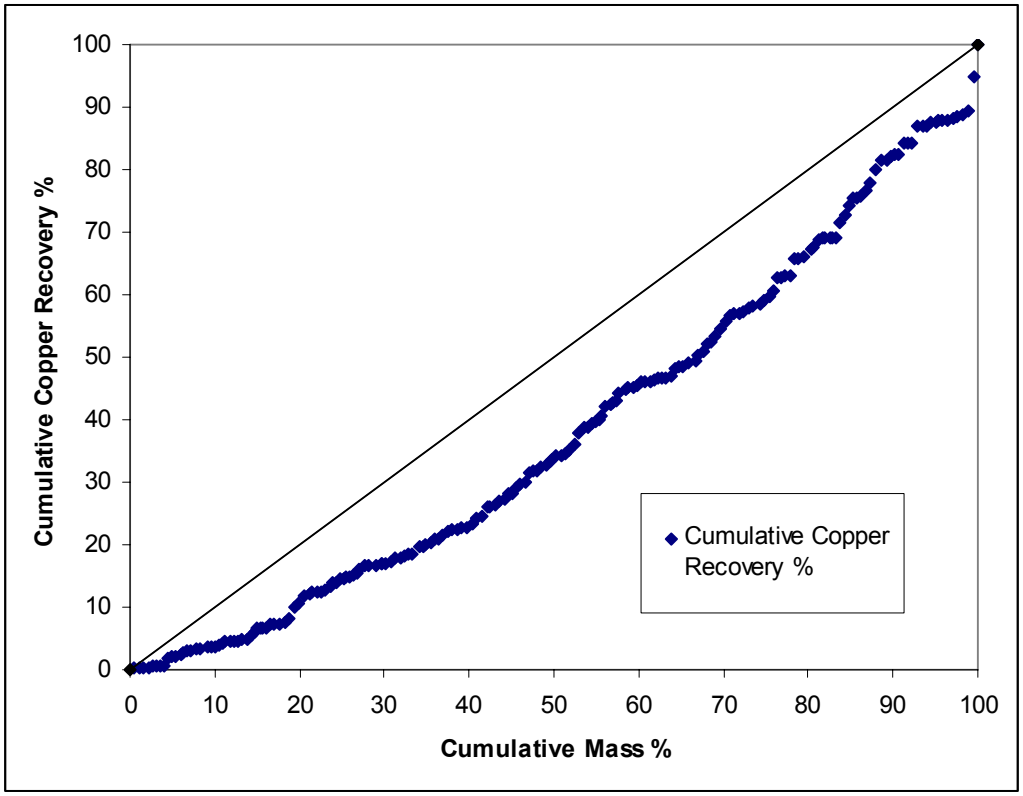

Figure 5-21 Non-linear deviation between the Cumulative Mass % and the Cumulative Copper Recovery % for Delta Max T for LRO ore type (larger population)

Keeping the same goal as in the reproducibility study to reject 30% of mass treated following temperature thresholds can be determined: for the Delta MAX temperature change of 16 ^{o}C will reject 30% mass with nearly 16% loss of overall copper.

Higher content of iron is located in the second half of the mass treated. With the content of molybdenum similar results were discovered to the reproducibility study. For the majority of rock particles content of molybdenum was below 10 ppm.

5.11 Summary

A laboratory method was used to investigate the pre concentration potential of Low Recovery Ore. The separation strategy was developed as the most suitable method to illustrate the level of separability by exposing rock particles to microwave heating and obtaining copper content by assaying. Every ore sorter can be described through a performance curve. This information describes the best separation which can be

achieved with a particular ore sorting machine. The difference between separation by separation curves and sorter performance curve which comes from inherent inefficiency of the sorter has to be acknowledged. For example, in the second testing of eighteen sets of material, particles were heated only one time (as they would be in real sorting machine) and the infrared measurements were taken only from the clearly seen top surfaces of the particles. This limitation will lead to a certain level of inefficiency in operation of the sorter.

For these laboratory tests, the theoretical separator with temperature information from two sides of the particle, which could detect copper content with similar precision to an assaying test, was used. The separation curves indicate that Low Recovery Ore material was reasonably responsive to this strategy in spite of the extremely high variation in the content of the minerals which interacted with microwaves.

For a minimum requirement of 30% mass rejected, temperature change for Delta MAX gave the most promising separation conditions to carry out pre concentration in both laboratory tests. As the particles cool down the efficiency of sorting by selective heating was reduced and the temperature thresholds needed to be reduced to retain the predetermined percentage of rejected mass, as it is shown in Table 5-2.

Table 5-2 Identified thresholds to reject 30% of mass tested

Reproducibility study	Delta MAX	Delta T1	Delta T2
Temperature threshold, ^{o}C	20	15	12
Loss of overall copper, %	18	20	22
The Larger Population study			
Temperature threshold, ^{o}C	16	13	12
Loss of overall copper, %	16	18	20

For Delta MAX and Delta T1 temperature thresholds, in the larger population study, were lower. This can be partially explained by inefficiency in operation of the sorter and partially by standard deviation from the reproducibility study. When particles are presented to an IR camera for temperature measurement with only one side, there will always be a number of particles for which that particular side is an unfavourable side for measurement. The information about the number of those particles can be quantified by implementing a stochastic model. From the reproducibility study it can be noted that for Delta T2 (where reproducibility was much higher, with 65% of mass having standard deviation up to 5 ^{o}C) temperature thresholds are the same. The

differences in values for temperature thresholds for Delta MAX and Delta T1 in the larger population study are still within the standard deviation of 5 ^{o}C which was chosen to describe the reproducible process.

For the real sorting machines, the difference in temperature thresholds from a theoretical sorting machine can be reduced by examining heated particles in free fall with two IR cameras. The side with the higher temperature change should be compared with an arranged temperature threshold.

5.12 Test Procedure for the Experimental Investigation Using Two Types of Microwave Applicators - Second Step

In Chapter 4 the exposure of synthetic particles with designed shapes and textures of microwave more responsive minerals showed that it is advantageous to use both multimode and single mode waveguide for better understanding of microwave interaction with ore particles. In the second step of investigation samples will be analysed with less destroying techniques such as x-ray tomography and optical microscopy. The first step of investigation ended with destroying samples, necessary to perform assaying analysis. The particles will be tested in microwave oven and in TWA which has ability to obtain data in real time from placed ROI, which was used to quickly estimate heating behaviour of tested particles within the each set tested.

5.13 Overview of the Test Procedure

The representative sub sample was prepared for -22.4 + 19.0 mm size fraction. The eight new sets containing eleven particles were randomly chosen from the remaining seventeen sets in this particular size fraction. The detailed procedure of the ore screening and obtaining a representative sample is presented in section 5.2 of this chapter. The particles were tested for textural interaction with an electromagnetic field created in two different microwave applicators. They were subjected to the individual and to the batch microwave heating. The data collected from the particle's temperature profiles were combined to create two temperature curves and analyse separability.

The results of the ore modal mineralogy summarised through MLA examination for the first experimental study revealed that the Low Recovery Ore contains significant amounts of good absorbers of microwave energy such as pyrite and chalcopyrite. This indicated that the test can be carried out with much less energy required. The power applied in the second experimental procedure was half of the power applied in the first experimental procedure.

After microwave exposures, fifteen randomly chosen particles were analysed by high-resolution X-ray computed tomography which was used to obtain information about texture and structure of minerals with higher densities. These minerals were associated with minerals which have a tendency to heat more.

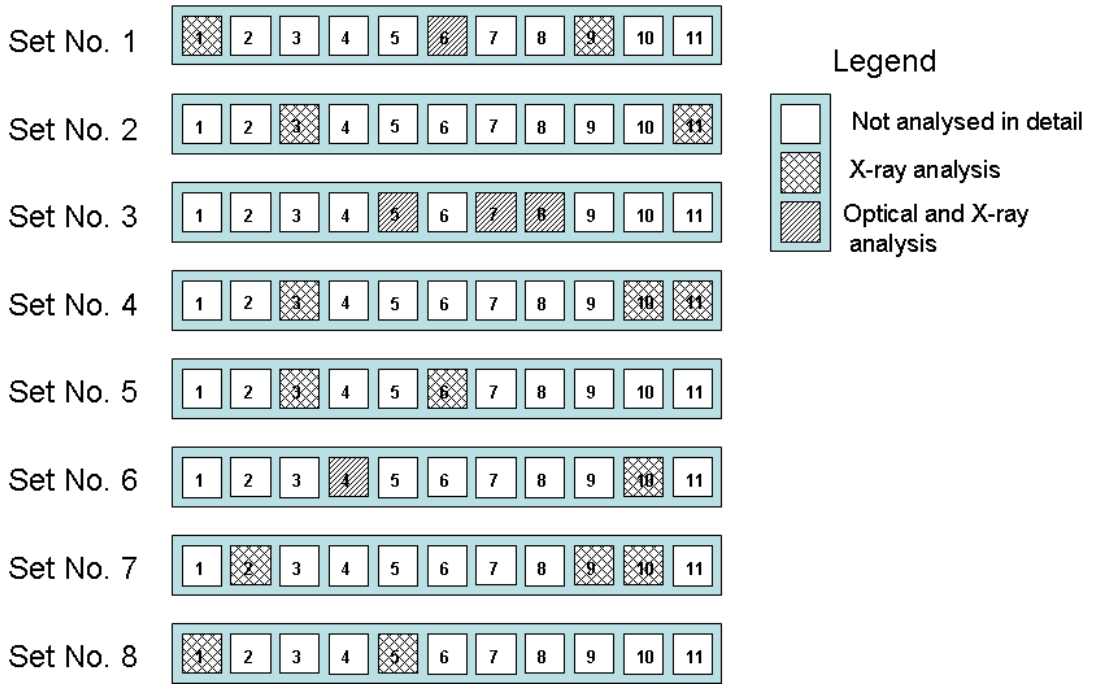

Figure 5-22 Particles randomly chosen for more detail analysis with less destructive techniques such as x-ray tomography and optical microscopy LRO

Five randomly chosen particles were studied in great detail by combining automated mineral identification by optical microscopy along with the high-resolution X-ray computed tomography to identify sulphide minerals. Surfaces for optical microscopy were prepared by cutting particles in half or removing the top part of the whole particle with the aim to primary identifies pyrite and chalcopyrite. Figure 5-22 shows locations of rock particles selected within tested sets and applied technique.

5.14 Exposing "LRO" Particles to Multimode Electromagnetic Field in Microwave Oven

The batch microwave heating was carried out with the same microwave oven used in the first step of experimental investigation. The glass microwave tray was separated into eleven sections for eleven ore particles. Particles were then distributed along the edges of the rotating tray in order to cover the larger area of the tray. This was done to ensure that particles have a greater chance of passing through the multiple modes. During repeated exposures particles were positioned in numbered order, ascending and clockwise. Once allocated on the edge of the tray they did not have any preferred orientation.

Each batch of ore particles were then heated four times alternating their sides with labels placing numbers "up" and numbers "down" in front of infrared camera. Before placing the tray in the oven the infrared snapshot was taken to obtain initial temperatures of the ore particles. Applied power of 600 W was used and after heating for 12 seconds (for the one rotation respectively of the microwave tray) the tray was taken out. The infrared snapshot of the tray was taken after 5 seconds using the CEDIP infrared camera.

5.15 Exposing "LRO" Particles to Electromagnetic Field in the Travelling Wave Applicator

The individual microwave heating of ore particles was done by the travelling wave applicator. Detailed description of TWA is given in Chapter 3 section 3.10. All rock particles were placed in a numbered sequence from one to eleven on the vibratory feeder which can be seen in Figure 5-23 on the left side. Particles were fed one by one into the applicator. The generator was set for 600 W with an exposure time of 12 seconds.

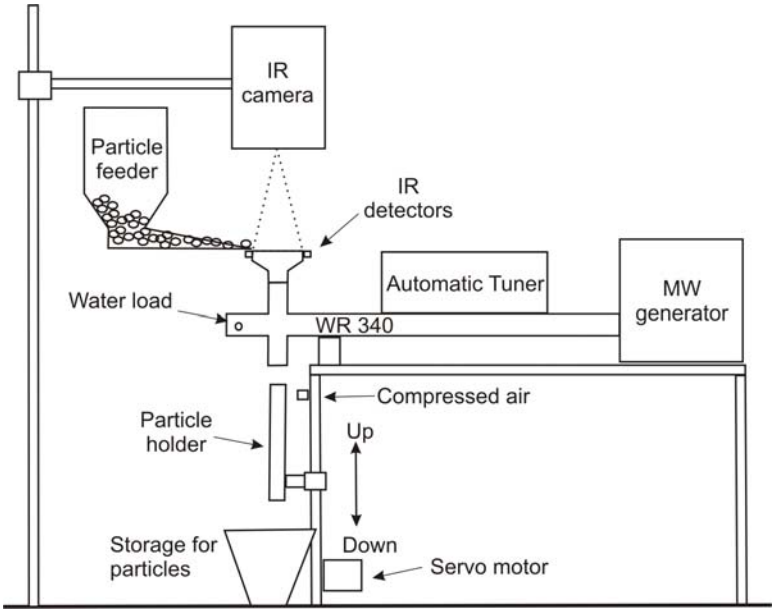

Figure 5-23 TWA used to test Low Recovery Ore

The infrared images were collected with 25 frames per second (in real time) during testing. The region of interest was set to cover up the complete surface of the particle holder (circular shape) placed in the middle of the applicator. The region of interest was introduced as a quick insight in temperature profile for each particle in real time during testing. These temperatures were calculated and plotted in time.

5.16 Experimental Results from Testing Rock Particles in Two Applicators

To compare experimental data, temperature difference for maximum and mean temperatures were calculated from the data before and after microwave exposure. Following abbreviations are taken to represent data:

- ΔT max = temperature difference for the maximum temperature on the surface of the particle calculated from data before microwave exposure and after microwave exposure
- ΔT mean = temperature difference for the mean temperature on the surface of the particle calculated from data before microwave exposure and after microwave exposure
- average ΔT max = mean value for ΔT max calculated from repeated exposures
- average ΔT mean = mean value for ΔT mean calculated from repeated exposures

Results from the TWA exposures are presented as a surface temperature change with the time. The surface temperature change was calculated from region of interest in a shape of the circle (set to cover the whole area of the particle holder). The graphs form three repeated exposures provide a good insight into which particles are highly responsive and which were not so responsive. Finally, every particle temperature change was calculated by placing a new region of interest corresponding to the visible perimeter of the particle. These new values are compared with the values from multimode exposures as average values from repeated testing. Temperature differences are presented in one common graph for every particle within the set.

Five randomly chosen particles were studied in great detail to identify sulphide minerals by combining high-resolution X-ray computed tomography and automated mineral identification by optical microscopy. IR images were studied during heating to identify selective heating and locate responsive minerals. The appropriate planes for optical microscopy were determined by cutting these particles in half in the locations where selective heating took place. The identification was focused primarily to recognize two sulphides; chalcopyrite and pyrite.

To present reconstructed data from the tomography analysis, visualisation software DataViewer ver. 1.4.4 (licensed by SkyScan) was used to view a stack of images in 2D/3D at their original range and resolution. This process enabled the texture to be seen from three different views:

- transaxial view (in the red colour, in x-y plane),
- coronal view (in the green colour, x-z plane),
- sagittal view (in the blue colour, z-y plane).

For every particle tested top left image is used to display coronal view of the selected reconstructed plane. The largest bottom left image is used to see transaxial view which is also chosen to correspond to surface analysis performed by optical microscope. In the top right corner the image of all three chosen planes through the particle can be seen, while the bottom left image is used to display sagittal view.

5.16.1 Set No. 1:

Figure 5-24 shows the temperature change from the region of interest placed to promptly obtain heating rate from every particle exposed to microwave heating in real

time (time is given in 25 frames per second). Data for the first and the second exposure are provided in the Appendix H. On the given graph in Figure 5-24 the top line represents maximum temperature, while the bottom one represents the mean temperature calculated from the visible surface of the particle including the background confined within the ROI. The analysis shows that the change for both temperatures exhibit almost a spike shape, which is produced by a rise in temperature during microwave heating, as well as sudden decrease in temperature after finished microwave exposure, followed by particle ejection from the holder.

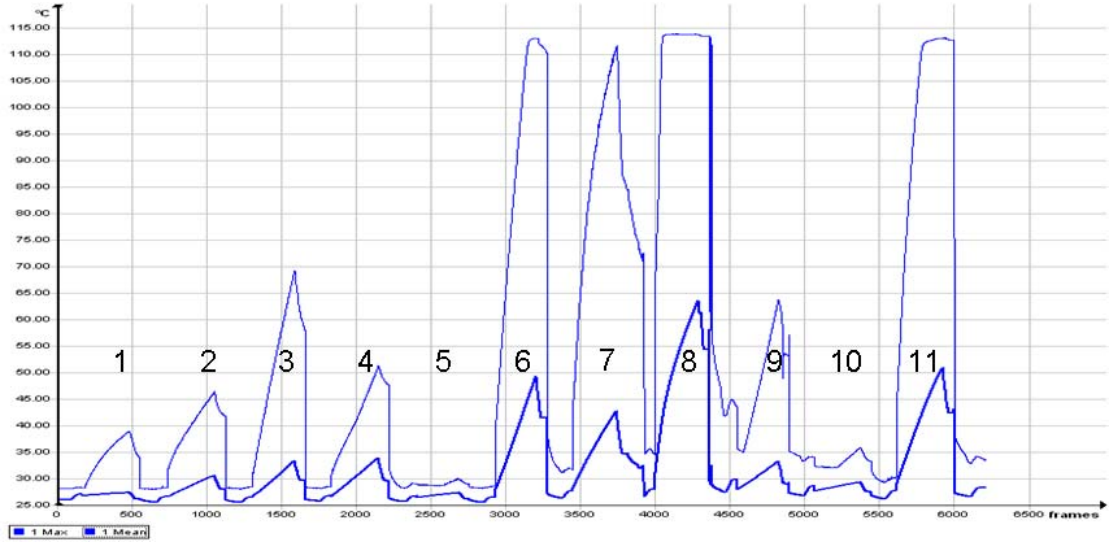

Figure 5-24 Third exposure, timing graph for the set No. 1

From this set particles with No. 1 and No. 9 were selected for analysis with CBT. Figure 5-25 shows x-ray radiogram of particle No. 1 presenting only low density minerals (associated with quartz, biotite and feldspar) which caused a slight increase in temperature change. In Figure 5-26 x-ray radiogram for particle No. 9 clearly reveals the presence of high density minerals (associated with magnetite, pyrite and chalcopyrite). These minerals have responded well to microwave heating causing a steeper increase for mean temperature and a very sharp increase of maximum temperature reaching over 60 ^{o}C. The X-ray radiograms which exhibit texture and structure of these particles under different angle are given in Appendix H for this chapter.

Figure 5-25 X-ray radiogram for particle No. 1 set No. 1

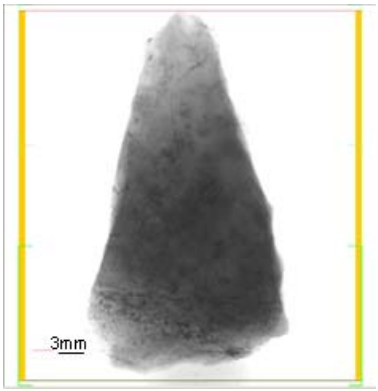

Figure 5-26 X-ray radiogram for particle No. 9 set No. 1

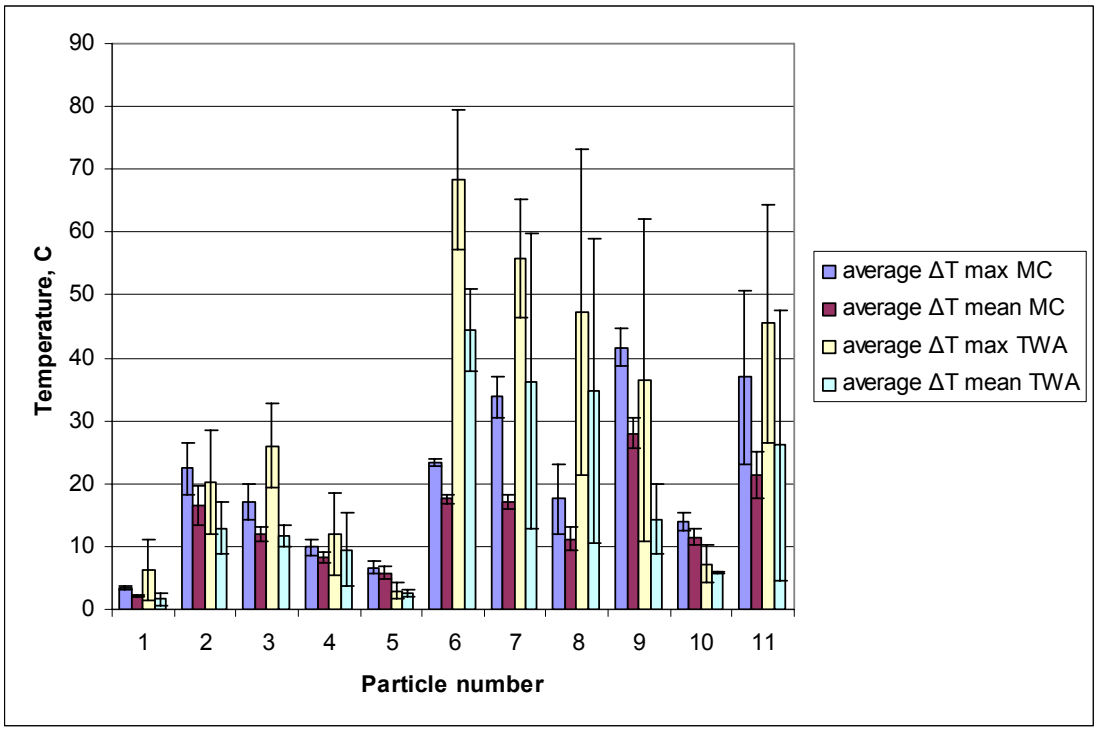

Figure 5-27 Results for the LRO from multimode cavity and travelling wave applicator testing for the set No. 1

Data from all repeated exposures in multimode domestic oven and TWA are compared and presented in Figure 5-27. The data was calculated from new ROI placed to overlap with perimeter around visible surface of particles. As the timing graph of temperature profiles indicate the poorest heating response was for the particle No. 5 which in both types of applicators reached less than 10 ^{o}C (for all temperature changes) followed by particle No. 1. These particles can be considered as barren or less responsive. The rest of the particles exhibited a much higher increase in temperature change, indicating the presence of higher contents of microwave absorbing phases.

In this set, particle No. 6 was chosen for a more detailed study. IR images were examined from TWA testing (the right image in Figure 5-28) with a goal to pinpoint locations on the surface of the particle where temperature has increased significantly, indicating the presence of more responsive minerals. From the Figure 5-28 it can be seen that the particle No. 6 can be classified as “hot” or very responsive. Considering that there was more than one hot location (from IR image), it was decided to cut the particle in half and polish the right side of the particle and arrange the larger surface for the optical microscopy analysis. Following the preparation for optical microscopy the same half of the particle was analysed by high-resolution X-ray computed tomography.

The reconstructed data from the tomography analysis is presented in Figure 5-29. The largest bottom left image is used to see transaxial view which is also chosen to correspond to surface analysis performed by optical microscope. The coronal view (in the top left corner) and the sagittal view (in the bottom right corner) show that there is a presence of disseminated structures of minerals with higher densities.

The transaxial view shows mineral grains which belong to a plane situated very close to the polished top surface. If the locations of the grains were compared with results from optical microscopy (the left image in Figure 5-28) a great deal of grains were identified as chalcopyrite, while the rest of the minerals could be associated with minerals with higher densities such as pyrite, bornite, tennantite or chlorite. All obtained results show a significant presence of heating phases and clearly explain the temperature profile of this particle and why it can be considered as “hot”.

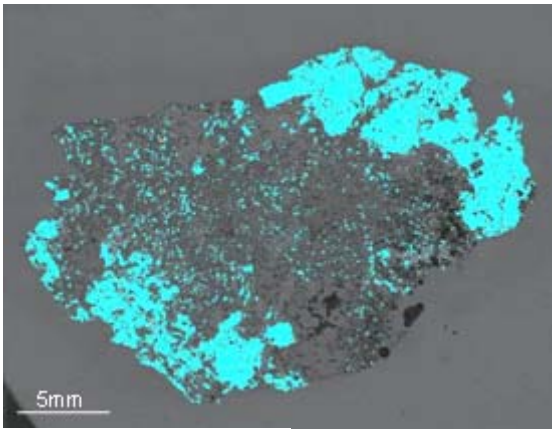

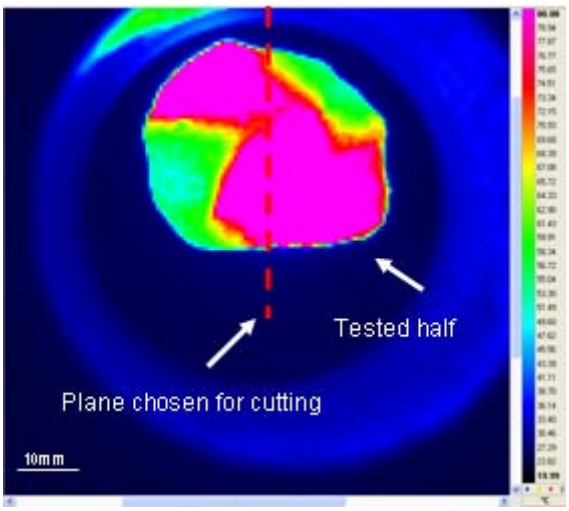

- **Scale min-max: 20 °C-80 °C**
- **From third exposure at the end of 12 s since the beginning of the heating**

Figure 5-28 Optical mineral identification and IR temperature profile for particle No. 6 from the set No.1

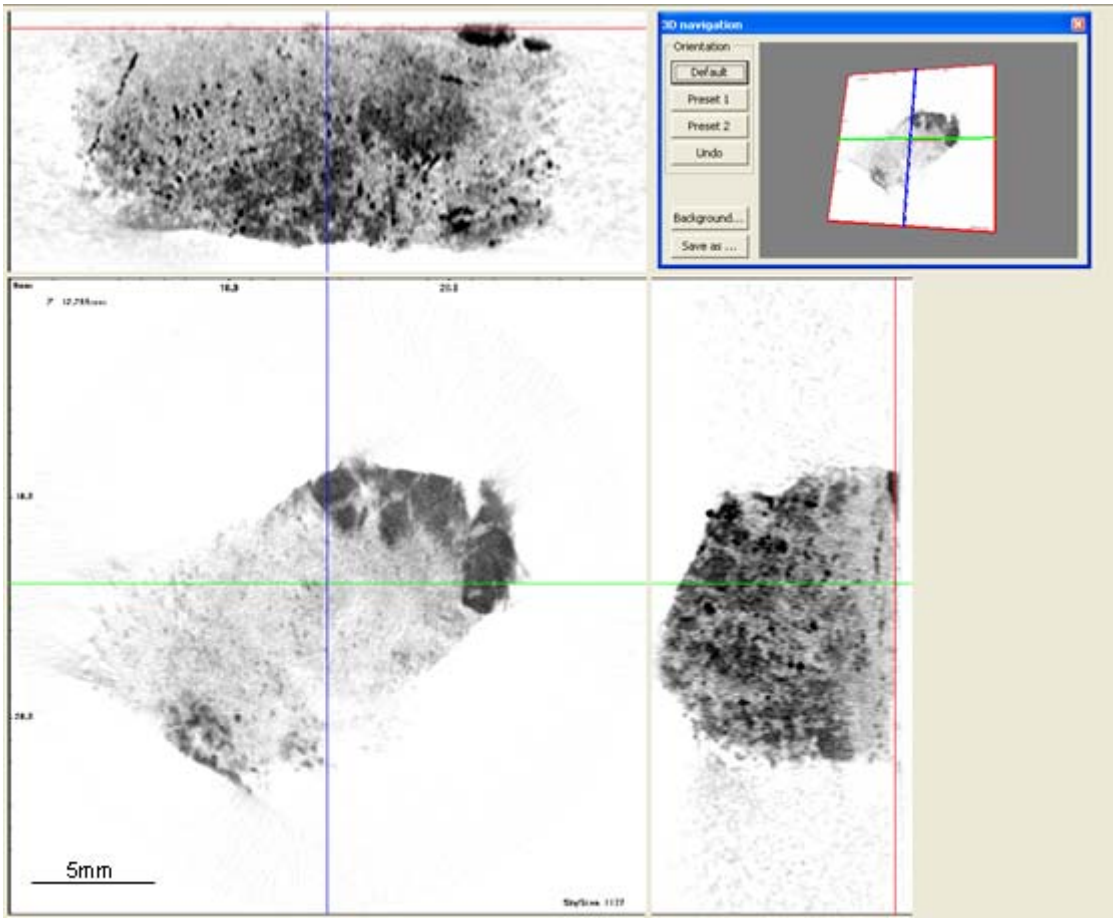

Figure 5-29 X-ray computed tomography analysis for particle No. 6 from the set No.1

5.16.2 Set No. 2:

After testing set No. 2, temperature profiles revealed that the majority of particles reached a very high increase in max temperature. For some of the particles maximum temperature had reached a maximum threshold of the IR camera (115 ^{o}C). The threshold can be identified as a flattened top of the peak (constant temperature in time) in Figure 5-30. With a close examination of the mean temperatures it can be seen that the particles No. 7 and No. 10 can be identified as coldest within the group. Results from the third exposure, are shown in Figure 5-30, displaying temperature change from the circular ROI.

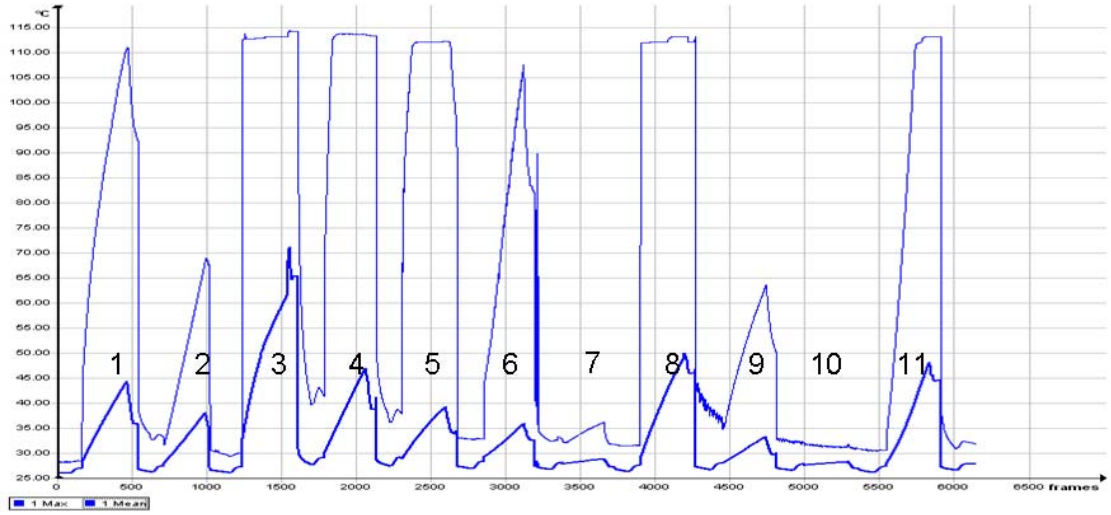

Figure 5-30 Third exposure, timing graph for the set No. 2

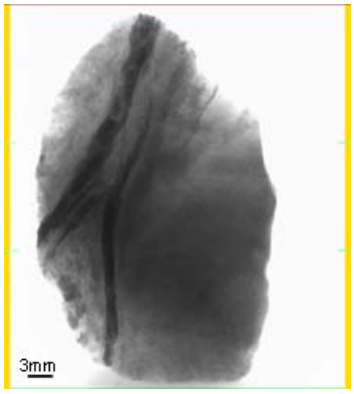

Figure 5-31 X-ray radiogram for particle No. 3 set No. 2

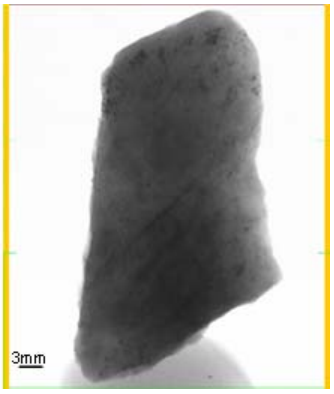

Figure 5-32 X-ray radiogram for particle No. 11 set No. 2

Figure 5-31 and Figure 5-32 show textural differences between particle No. 3 and particle No. 11. The X-ray radiograms which exhibit texture and structure of these particles under a different angle are given in Appendix H. The first particle is made of low density minerals with an embedded vein like shape of higher density minerals,

while the second particle presence of higher density minerals can be identified in disseminated grains.

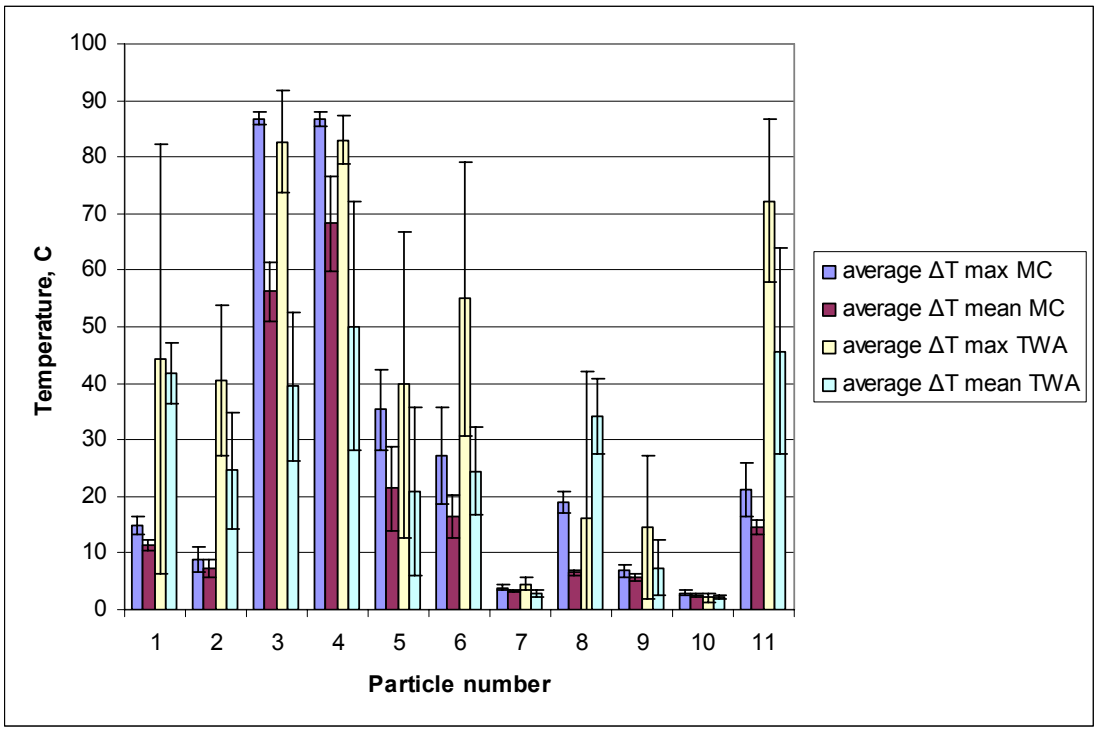

Figure 5-33 Results for the LRO from multimode cavity and travelling wave applicator testing for the set No. 2

By combining information from x-ray radiograms with calculated data from repeated testing showed in Figure 5-33, it is simple to associate good heating responses with particle No. 3 and particle No. 11.

5.16.3 Set No. 3:

Temperature profiles from ROI for the set No. 3 are given Figure 5-34. Particles with No. 1, 4, 5, 6 and 11 can be easily identified as not so responsive or "cold".

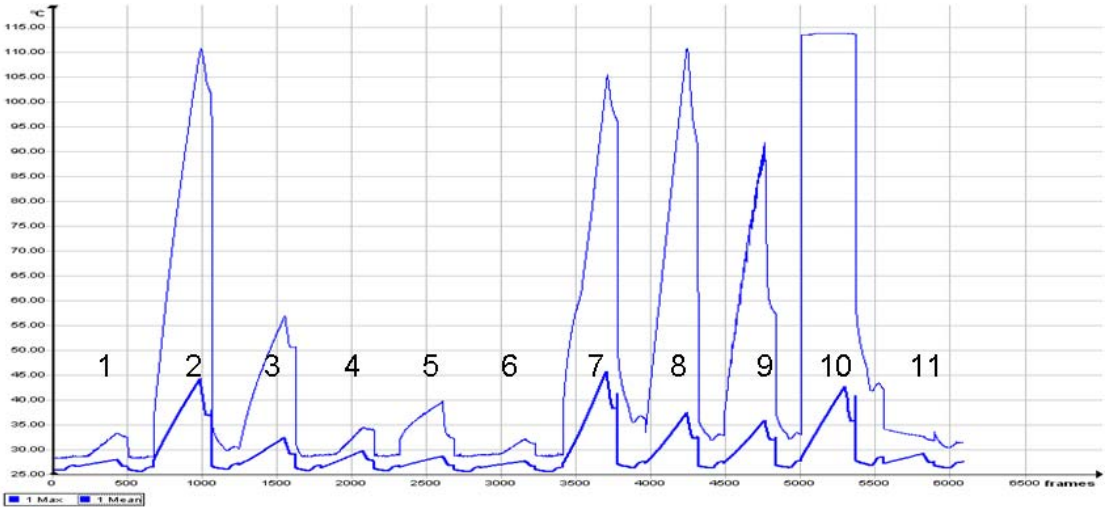

Figure 5-34 Third exposure, timing graph for the set No. 3

The presented data for the repeated exposures in Figure 5-35 shows that the remaining particles had responded well to microwave heating and can be considered as “hot”. The particles No. 3 and 10 exhibited much higher temperature change during multimode cavity exposures in comparison to TWA testing. Two scenarios can be given to explain the behaviour of these particles which are still in agreement with the “best case scenario” defined in Chapter 4, section 4.7. The first is derived from experimental testing conditions. Considering that repeated multimode testing was done prior TWA testing, these particular particles had already responded well to heating which might cause alteration of some physical properties of very responsive minerals. This change then consequently influenced less responsive coupling in TWA and eventually lower temperature change. The second is derived from properties of the particles such as shape and form. Experimental equipment for TWA was designed to feed particles one by one with a free fall into the particle holder placed in the middle of the WR 340 waveguide. For some particles, shape would create preference of specific visible surface which was unfavourable to completely detect heating profiles when they fell from the feeder and assumed their most stable positions.

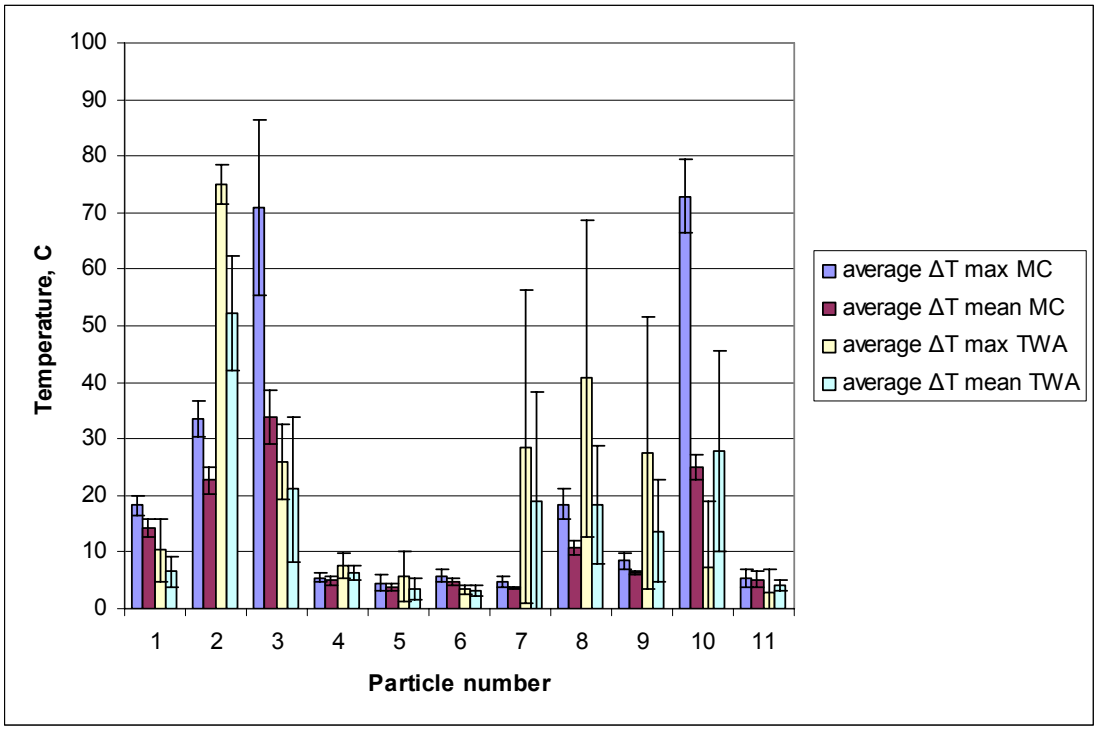

Figure 5-35 Results for the LRO from multimode cavity and travelling wave applicator testing for the Set No. 3

Two particles were chosen for more detailed analysis. These are particle No. 5 and particle No. 8. IR image during heating for the particle No. 5 demonstrated the results

of more uniform heating during repeated exposures, although one half of the particle had higher temperature gradients then the other (as seen in the right image in Figure 5-36). The particle was cut in the middle and the chosen half was polished and prepared for optical microscope analysis (results are given the left image in Figure 5-36). The results from x-ray computed tomography shows a presence of embedded minerals of higher density which are scattered within the matrix of lower density. There are some areas of matrix with a higher density which also contributed to no uniform heat distribution through matrix. When the transaxial view in Figure 5-37 was analysed along with optical results it demonstrated that embedded minerals are identified as grains of very responsive chalcopyrite. With the location of the grains and their size (they can be estimated from scale bar) this particle can be now clearly identified as barren particle.

For the particle No. 11 which was also analysed in great detail, the IR image revealed a spot on the surface of the particle with a much higher temperature gradient identifying the presence of microwave responsive minerals. This spot can be seen in the right image of the Figure 5-38. The particle was cut in the middle and the chosen half was polished and prepared for further analysis. The coronal and sagittal view after computed tomographic reconstruction (shown in Figure 5-39) displayed a presence of a very large vein like structure embedded in the middle of the particle. It also showed that this structure was mostly surrounded with matrix material with a higher density. A part of that structure was exposed to optical microscopy identification which identified chalcopyrite as a dominant mineral with very small inclusions of pyrite.

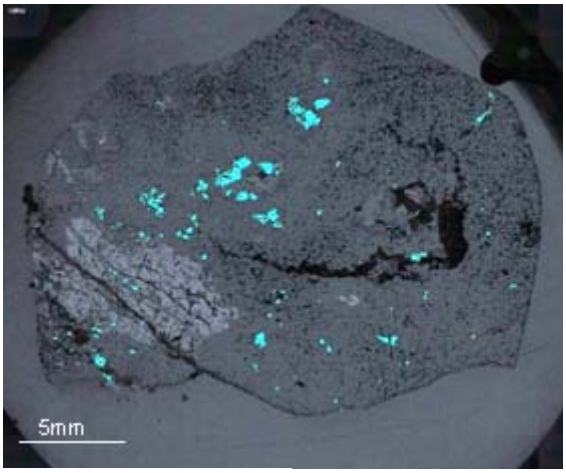

Chalcopyrite
Pyrite

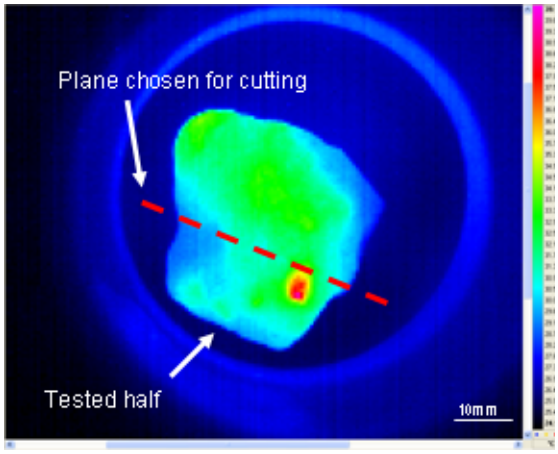

- **Scale min-max: 25°C-40 °C**
- **From third exposure at the end of 12 s since the beginning of the heating**

Figure 5-36 Optical mineral identification and IR temperature profile for particle No. 5 from the set No.3

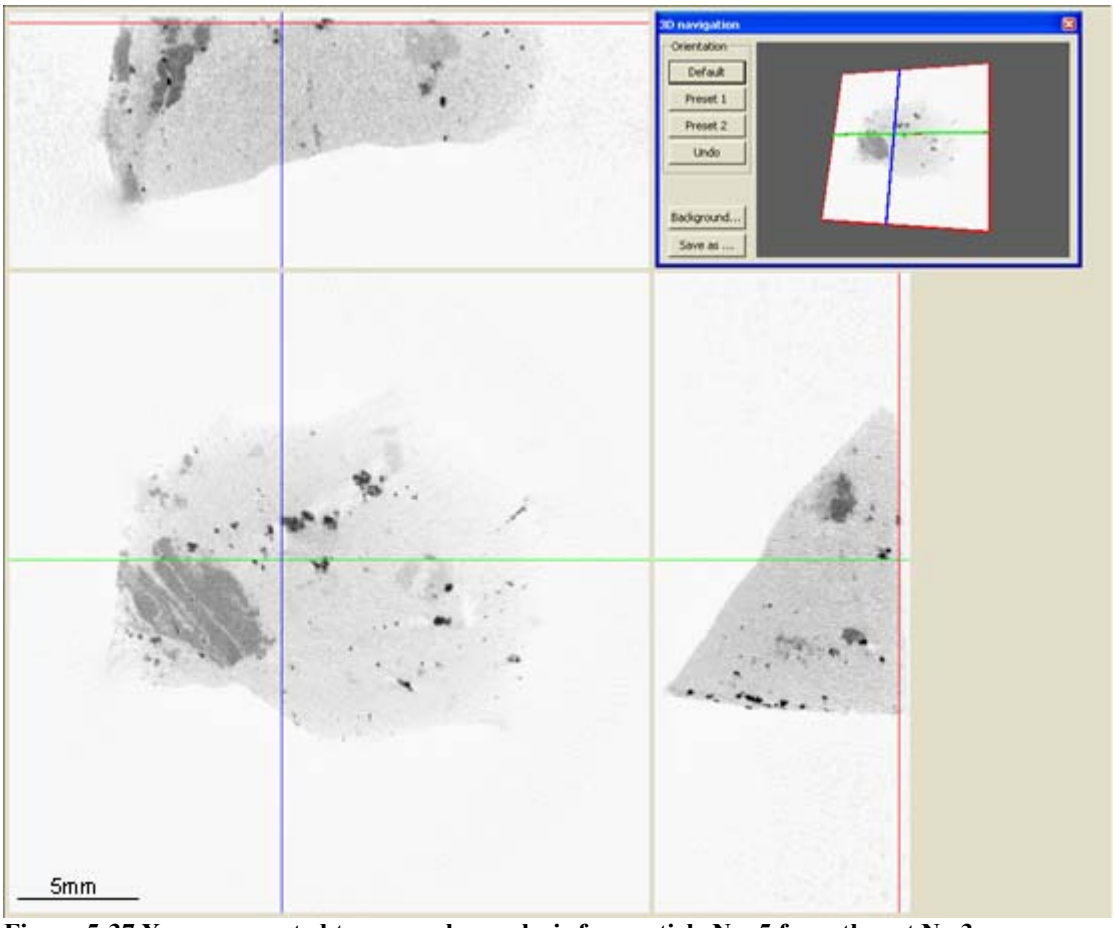

Figure 5-37 X-ray computed tomography analysis for particle No. 5 from the set No.3

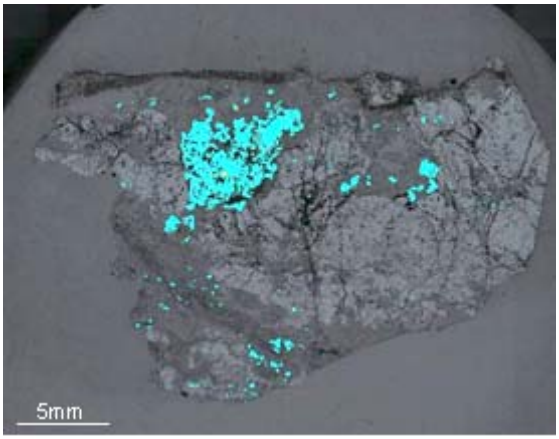

Chalcopyrite
Pyrite

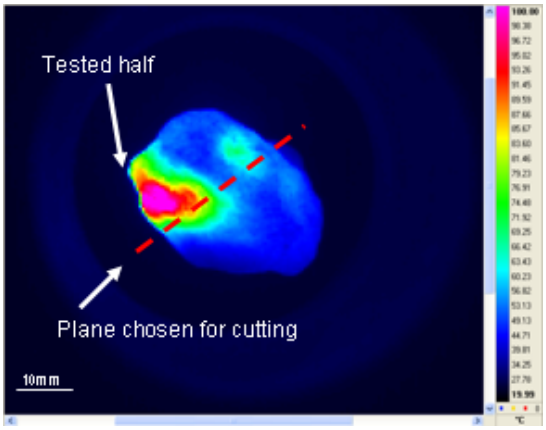

- **Scale min-max: 20°C-100 °C**
- **From third exposure at the end of 12 s since the beginning of the heating**

Figure 5-38 Optical mineral identification and IR temperature profile for particle No. 8 from the set No.3

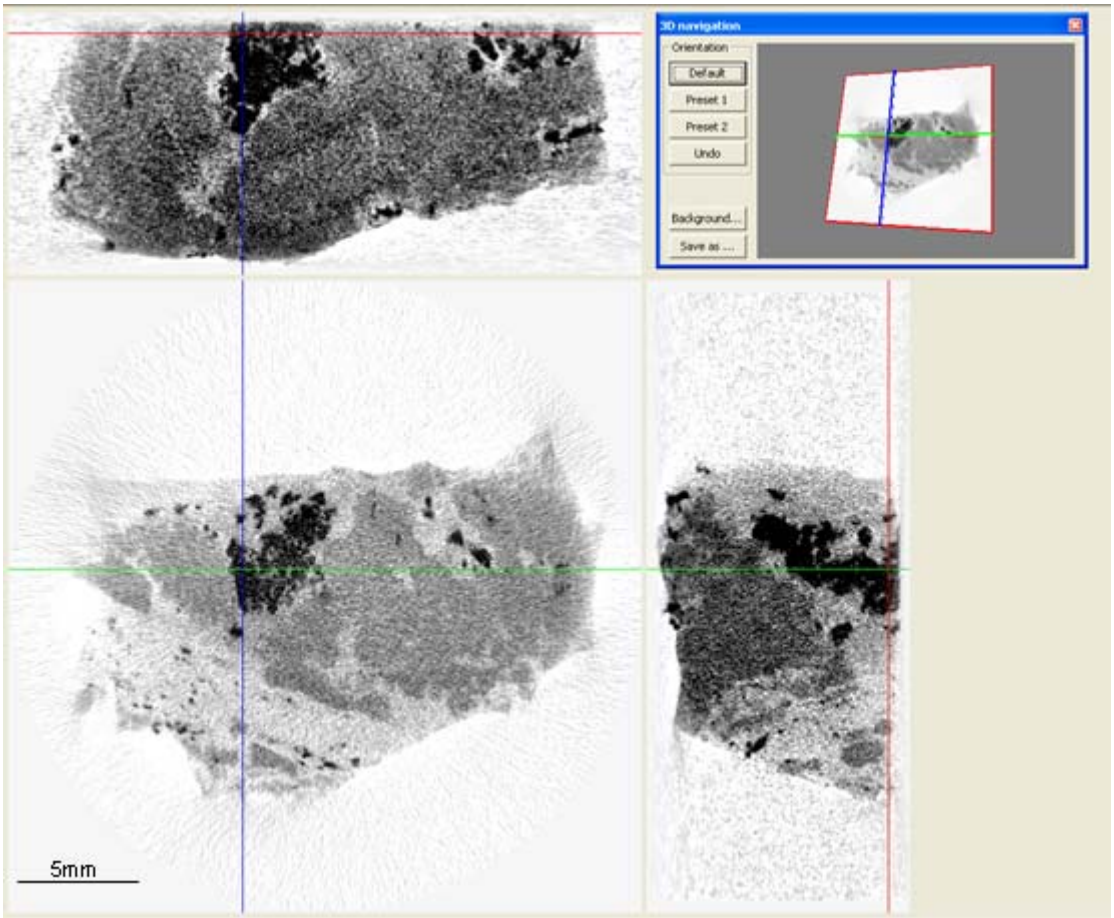

Figure 5-39 X-ray computed tomography analysis for particle No. 8 from the set No.3

5.16.4 Set No. 4:

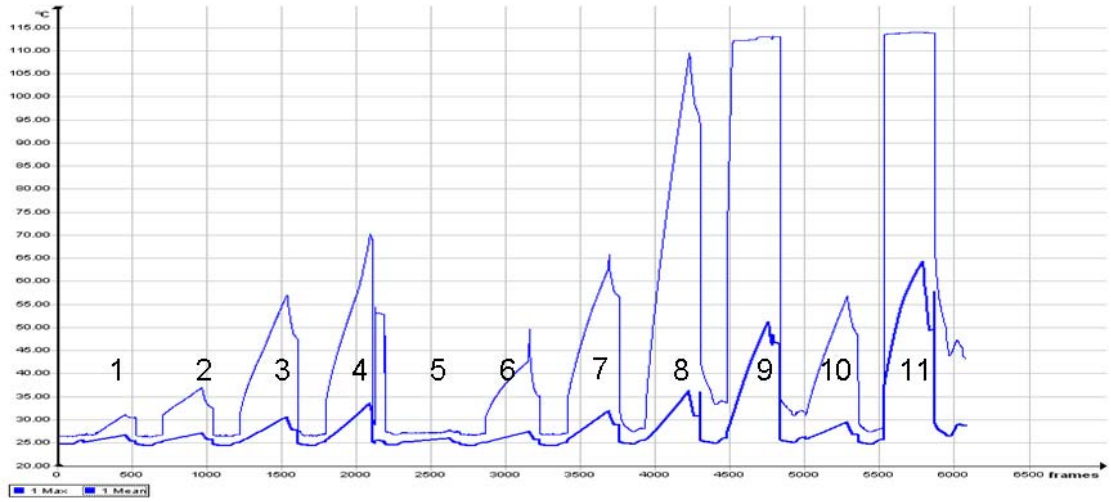

Figure 5-40 First exposure, timing graph for the set No. 4

Figure 5-40 shows quickly obtained heating rates from particles within the ROI exposed to microwave heating in real time. For this particular set, three particles were randomly chosen for analysis using a SkyScan 1172 Cone Beam X-ray micro-tomograph.

By acquiring x-ray radiograms which are given in Figure 5-41, Figure 5-42 and Figure 5-43 shows that particles No. 10 and 11 have presence of mineral structure which is absent in the particle No. 3.

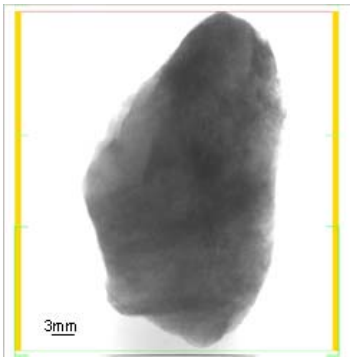

Figure 5-41 X-ray radiogram for particle No. 3 set No. 4

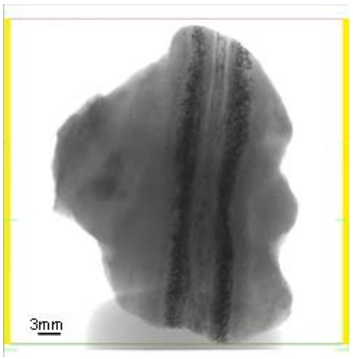

Figure 5-42 X-ray radiogram for particle No. 10 set No. 4

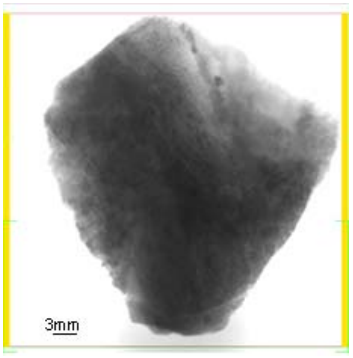

Figure 5-43 X-ray radiogram for particle No. 11 set No. 4

The absence of higher density mineral structure inside particle No. 3 caused a small temperature difference as shown in Figure 5-44. Two of the better responding particles had higher temperature changes in multimode cavity exposures compared to TWA exposures. These particles are No. 8 and 11 (explanation for these results is provided in the description of the Set No. 4).

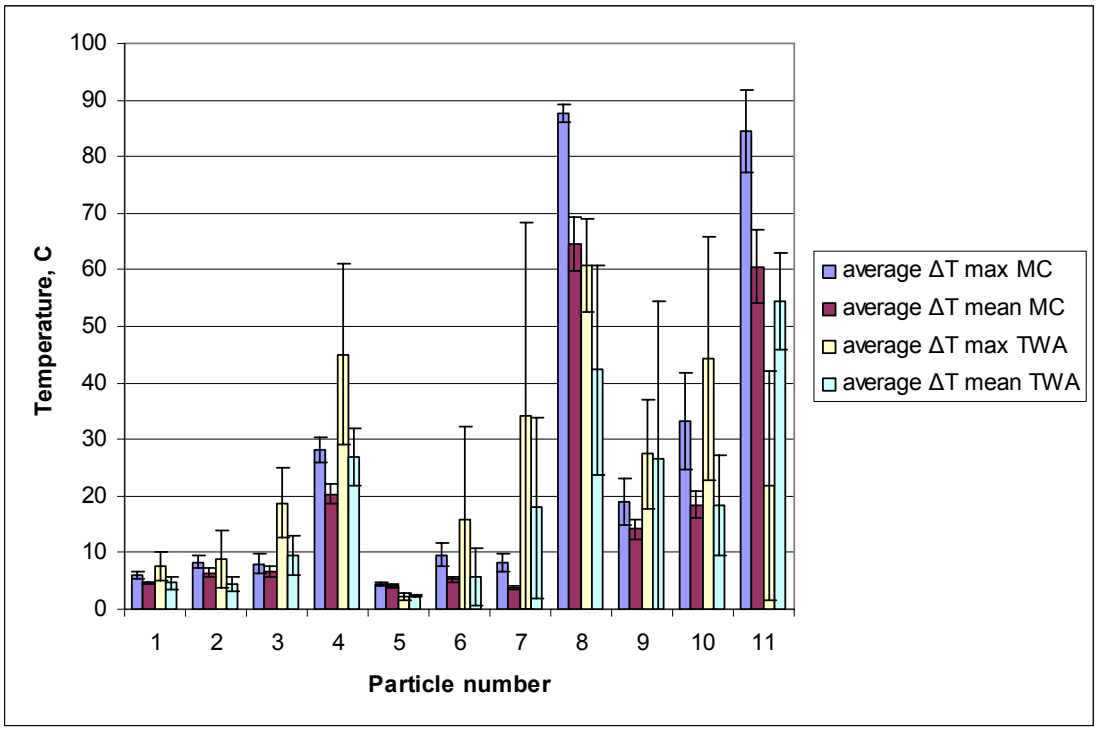

Figure 5-44 Results for the LRO from multimode cavity and travelling wave applicator testing for the Set No. 4

5.16.5 Set No. 5:

Individual testing of all eleven rock particles in the TWA and their heating response for the set No. 5 can be assessed with a temperature graph presented in Figure 5-45.

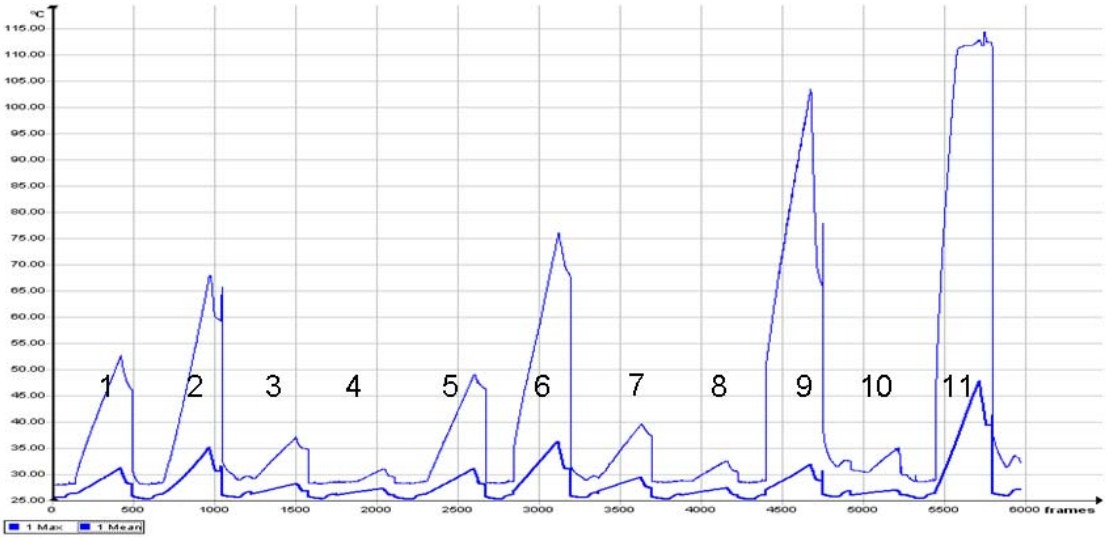

Figure 5-45 Third exposure, timing graph for the set No. 5

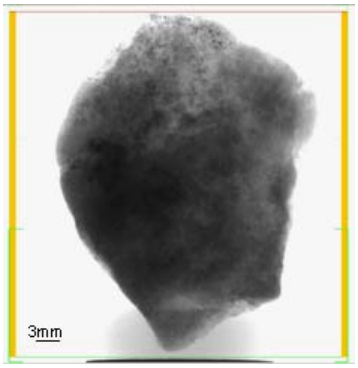

Figure 5-46 X-ray radiogram for particle No. 3 set No. 5

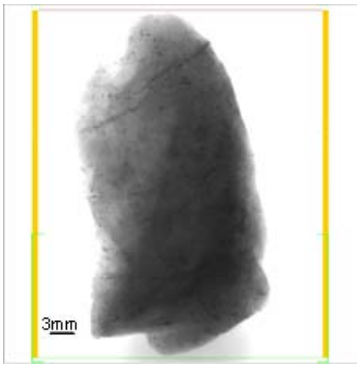

Figure 5-47 X-ray radiogram for particle No. 6 set No. 5

Similarly as in the previous set, two randomly chosen particles were x-ray scanned to produce their radiograms which can provide information about presence and distribution of mineral phases without destroying rock particles.

Figure 5-46 shows a presence of dispersed minerals with higher densities, although variation in the matrix minerals can be noticed as well in particle No.3. The x-ray radiogram for particle No.6 displayed a presence of minerals with higher density located in a thin layer (see top part of the Figure 5-47) and less variation in the matrix minerals.

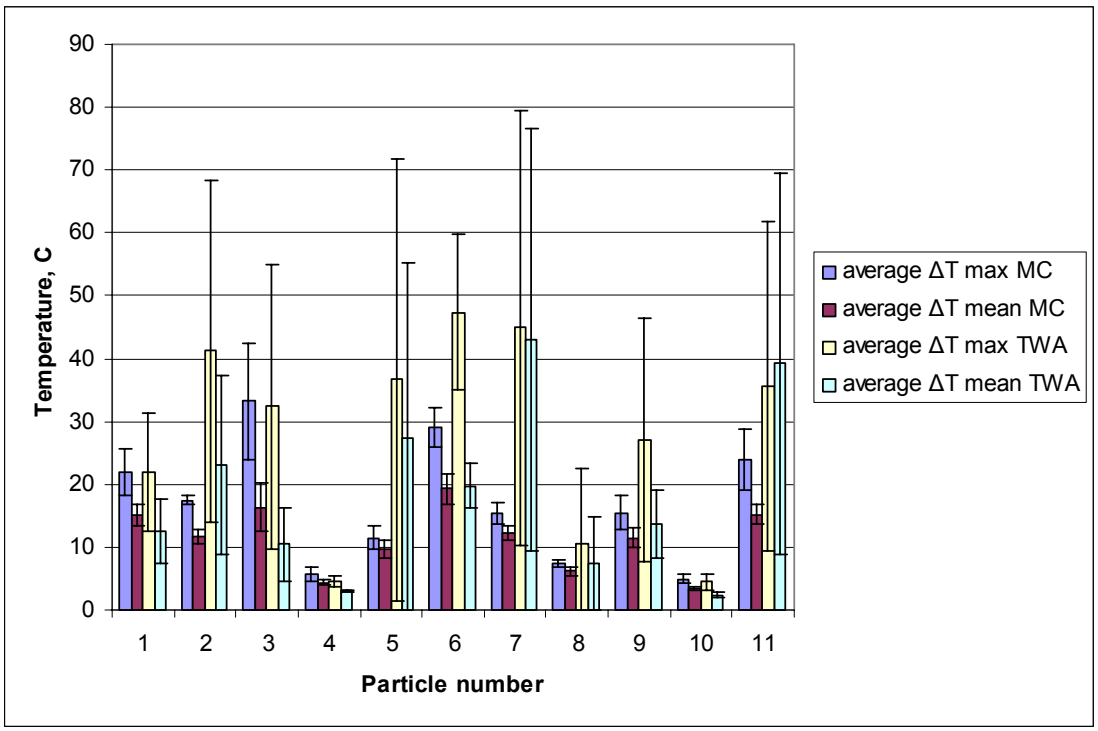

Figure 5-48 Results for the LRO from multimode cavity and travelling wave applicator testing for the set No. 5

By analysing data from the Figure 5-48, particles No. 3 and 6 can be identified as "hot" within this tested set of rocks particles.

5.16.6 Set No. 6:

Within the tested set No. 6 it can be seen that more than half of the particles can be considered as "cold" with a slight increase in temperature change (observing timing graph for the maximum temperature in Figure 5-49).

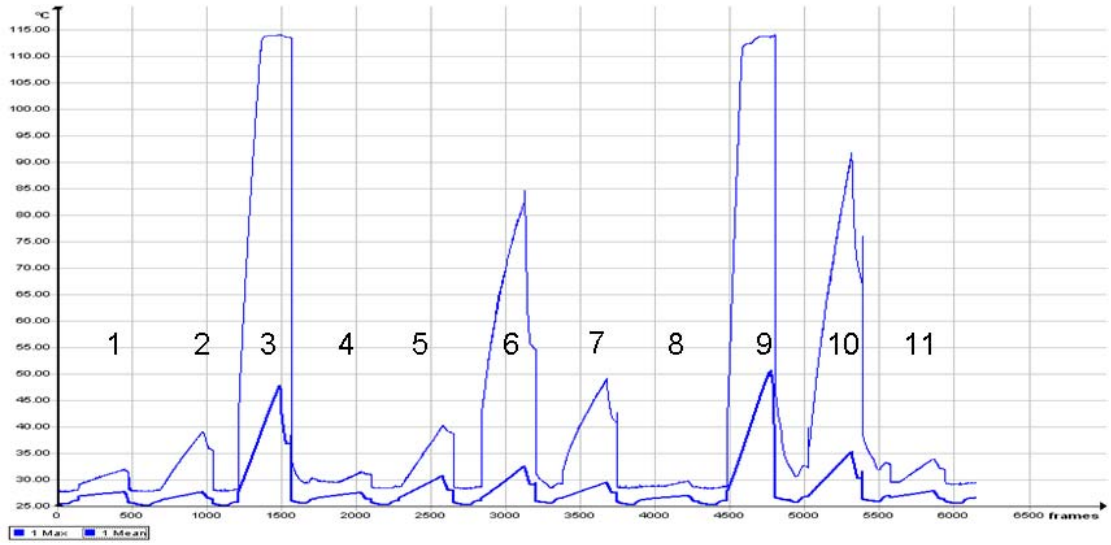

Figure 5-49 Third exposure, timing graph the set No. 6

By examining textural features from the randomly chosen particle, x-ray radiogram (displayed in Figure 5-50), shows that the particle No. 10 consists of dispersed grains of high density minerals similar in size and with approximately even spatial distribution.

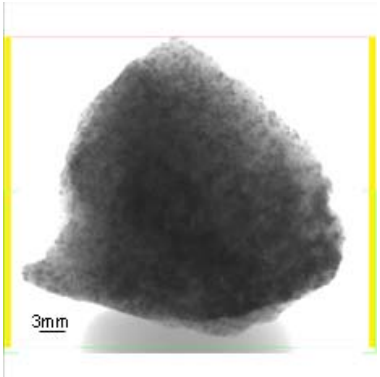

Figure 5-50 X-ray radiogram for particle No. 10 set No. 6

Exploring calculated mean values which are given in Figure 5-51 it can be seen that repeated heating confirmed that majority of exposed particles had lower temperature changes which indicated lower contents of responsive minerals.

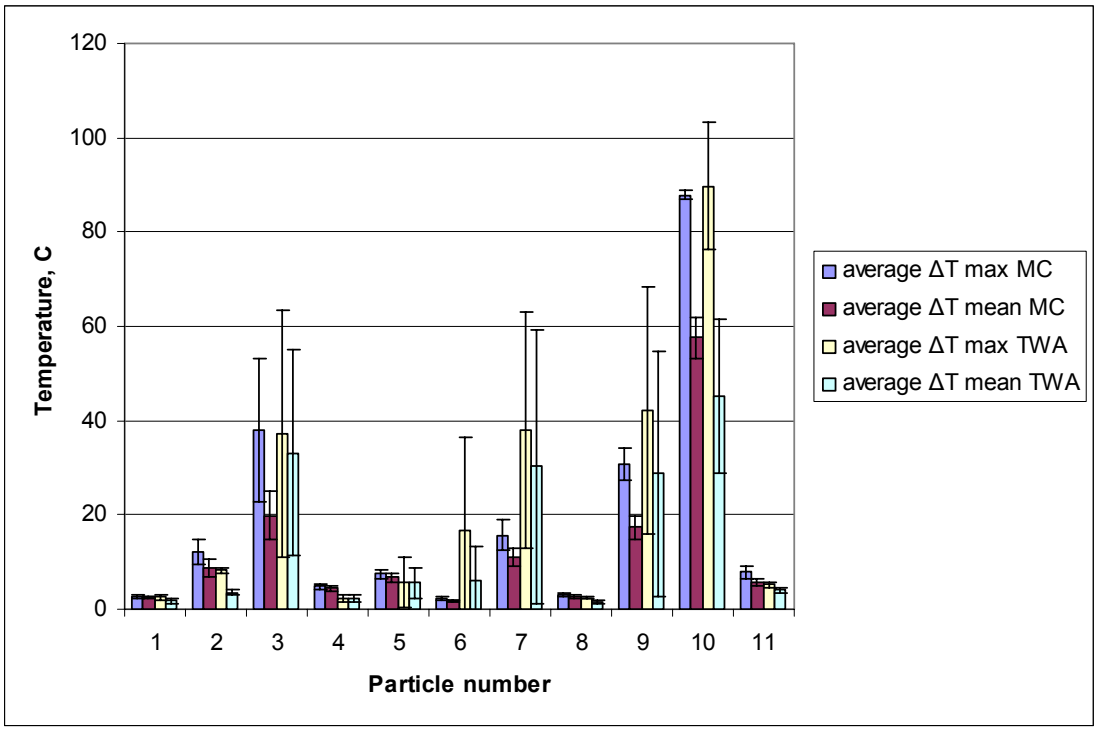

Figure 5-51 Results for the LRO from multimode cavity and travelling wave applicator testing for the set No. 6

Particle No. 4 was analysed in more detail. Figure 5-52 shows the infrared image on the right which presents only a slight and very even increase of the surface temperature. With no observed localised heating it was decided to cut the particle in two pieces and prepare one half for further examination. After polishing one section and using optical microscopy, small mineral grains of chalcopyrite were identified with the larger grain in the middle. The same larger grain was identified with tomography analysis (see transaxial view in Figure 5-53), tomography data also revealed that by examining coronal view (in the top left corner) and the sagittal view (in the bottom right corner) the depth of that grain was not very big and that it was mostly localised in a very thin layer close to the plane were the particle was cut. Other smaller grains were very well dispersed with a large distance between them. The analysis shows why the low content of minerals and their distribution did not create any localised heating and why this particle can be considered as less responsive.

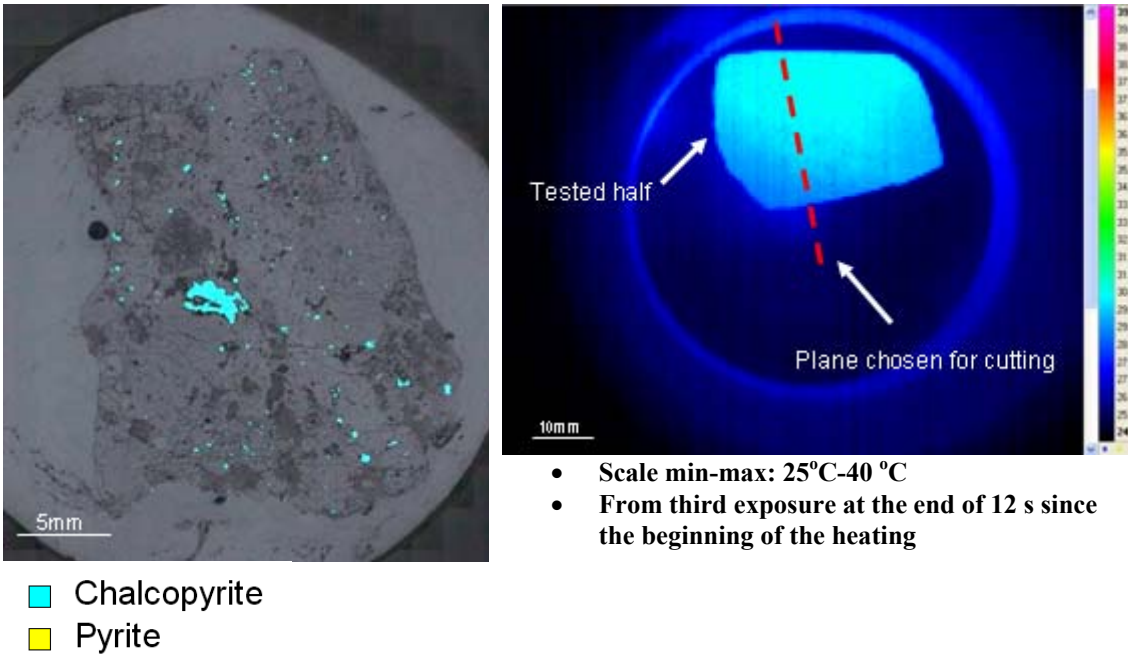

- **Scale min-max: 25°C-40 °C**
- **From third exposure at the end of 12 s since the beginning of the heating**

Figure 5-52 Optical mineral identification and IR temperature profile for particle No. 4 from the set No.6

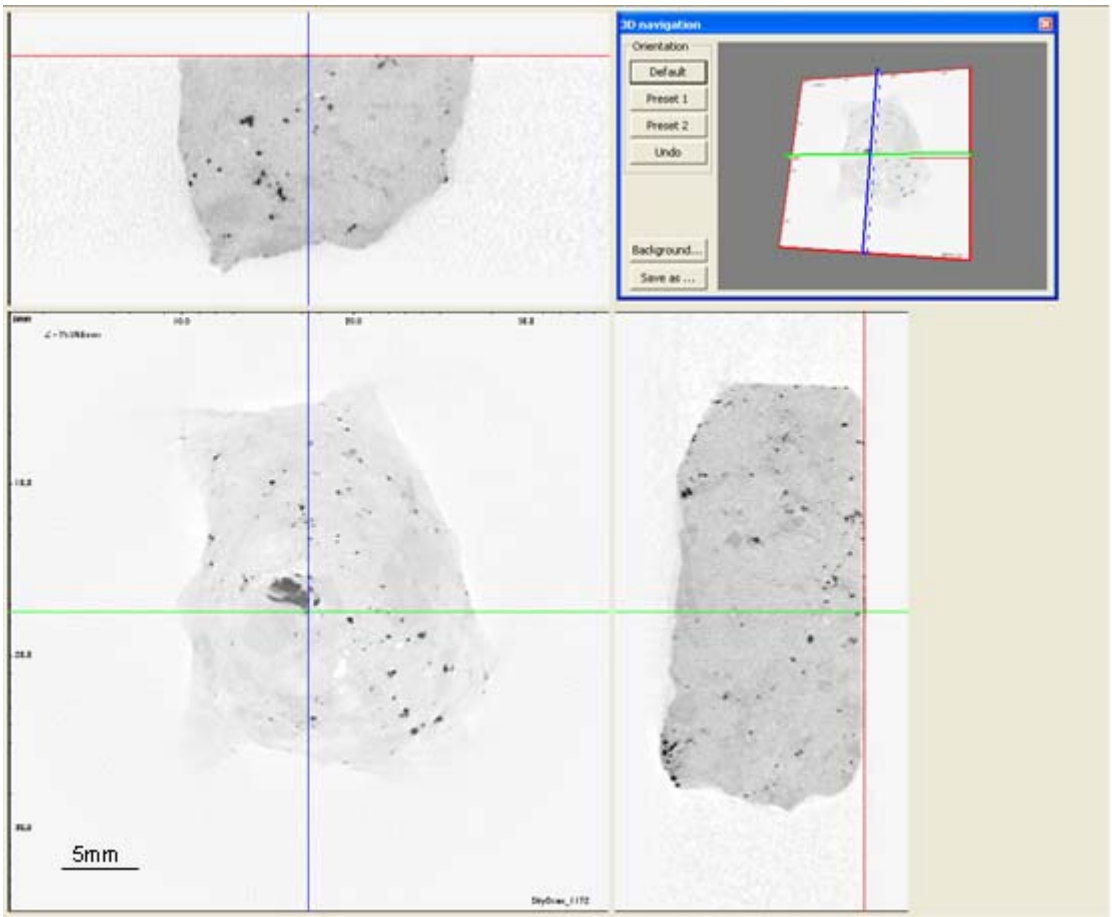

Figure 5-53 X-ray computed tomography analysis for particle No. 4 from the set No.6

5.16.7 Set No. 7:

During the repetitive testing of the set No. 7 all timing graphs showed a presence of responsive particles to microwave heating. Figure 5-54 shows the locations of the peaks of maximum and mean temperature from the ROI from the third exposure (remaining timing graphs are provided in the Appendix H).

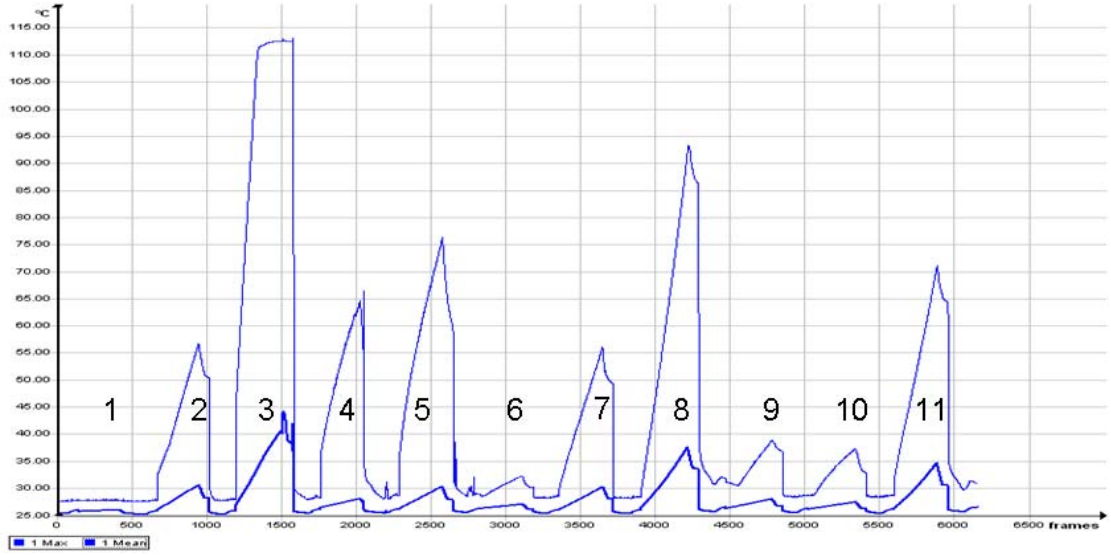

Figure 5-54 Third exposure, timing graph for the set No. 7

Four particles from this set were analysed in more details. Three were analysed just by CBT while for the fourth more information was obtained through optical microscopy. Figure 5-55, Figure 5-56 and Figure 5-57 show X-ray radiograms and demonstrates that particles No. 2 and 9 have a presence of mineral structure with higher densities which is absent in the particle No. 10 when compared.

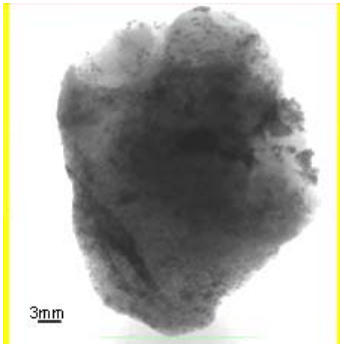

Figure 5-55 X-ray radiogram for particle No. 2 set No. 7

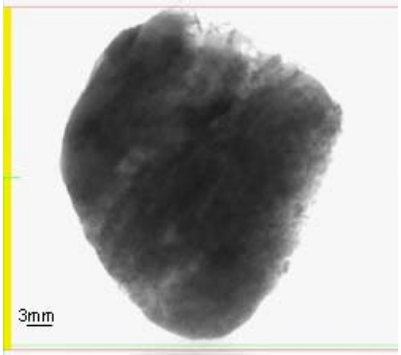

Figure 5-56 X-ray radiogram for particle No. 9 set No. 7

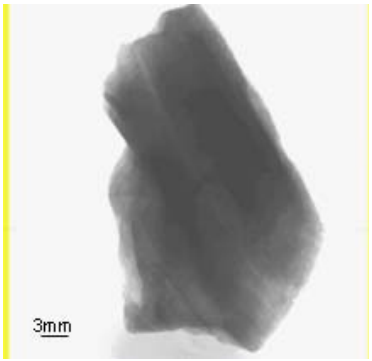

Figure 5-57 X-ray radiogram for particle No. 10 set No. 7

From the calculated mean values which can be seen in Figure 5-58, particles with No. 1, 6 and 10 showed a temperature difference less than 10 ^{o}C and they could be separated as “cold” particles. X-ray radiogram for particle No. 10 confirmed the

absence of minerals with higher densities which were associated with microwave strong absorbing minerals.

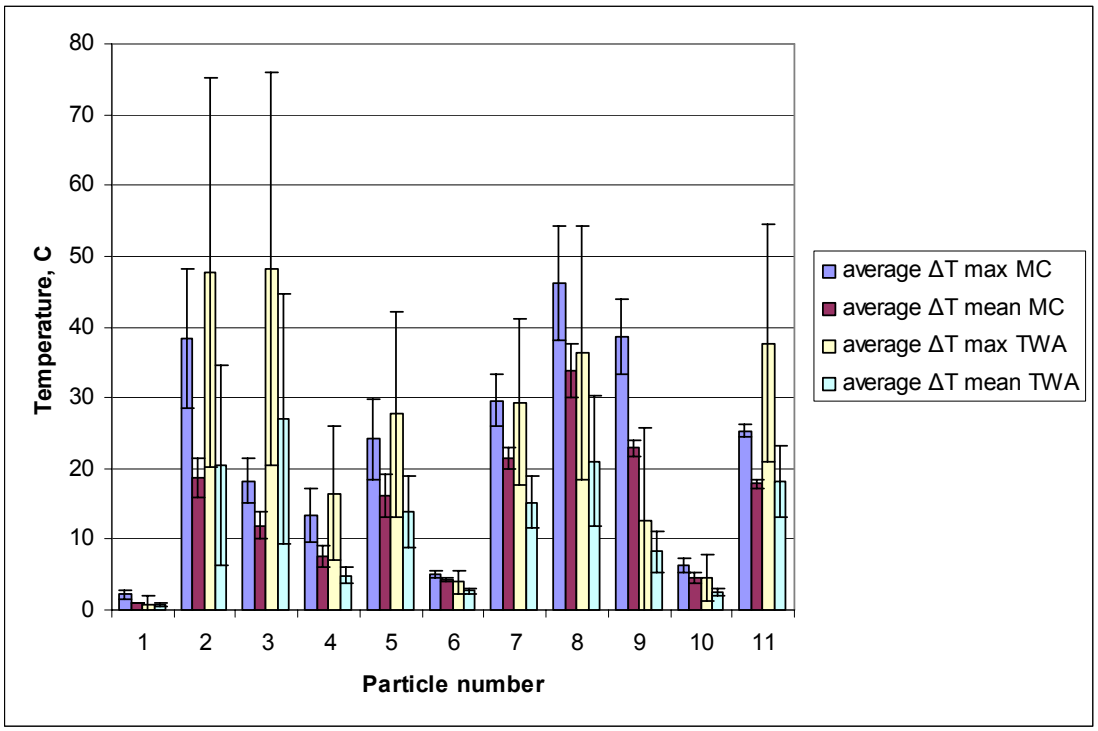

Figure 5-58 Results for the LRO from multimode cavity and travelling wave applicator testing for the set No. 7

The obtained infrared image from heating for particle No. 3 showed a very concentrated hot spot close to the edge of the particle (as seen in the right image in Figure 5-59). The particle was cut in the middle and the chosen half which had localised heating was polished and prepared for optical microscope analysis (results are given the left image in Figure 5-59). It can be seen that both pyrite and chalcopyrite were identified with pyrite being more abundant. The transaxial view (from x-ray computed tomography presented in Figure 5-60) shows that the detected structure which can be correlated to chalcopyrite and pyrite in a large portion was located at the surface of the particle which created a good detectable response. CBT data also shows that there are two dominant minerals with different densities from which the matrix material was composed.

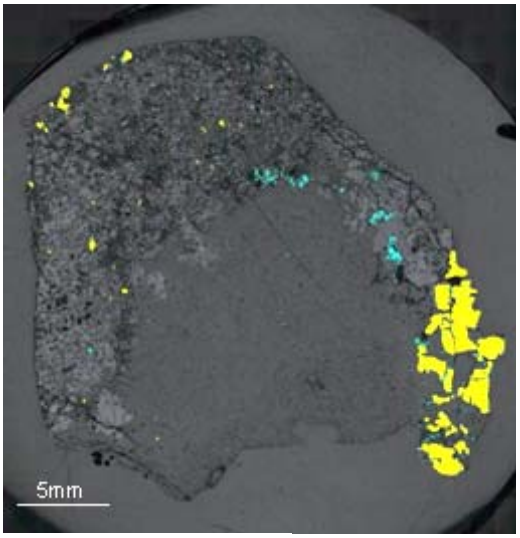

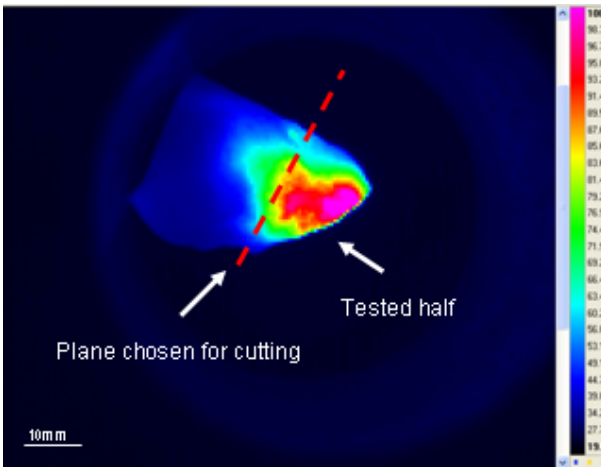

- **Scale min-max: 20°C-100 °C**
- **From third exposure at the end of 12 s since the beginning of the heating**

Chalcopyrite
Pyrite

Figure 5-59 Optical mineral identification and IR temperature profile for particle No. 4 from the set No.6

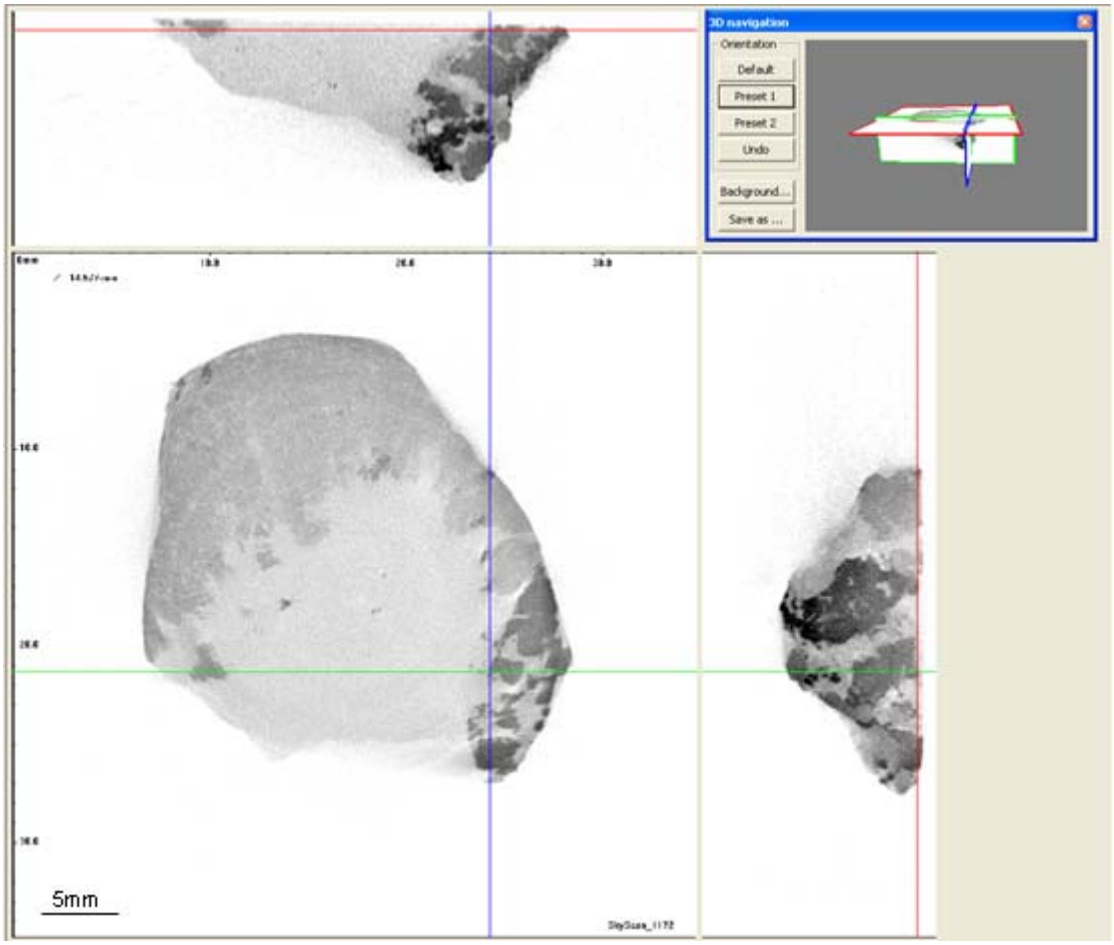

Figure 5-60 X-ray computed tomography analysis for particle No. 3 from the set No.7

5.16.8 Set No. 8:

The timing graph for the last set tested is shown in Figure 5-61. The circular ROI placed to quickly assess temperature change on the timing graph had identified particle No. 1 as the most non responsive heated particle from set No.8.

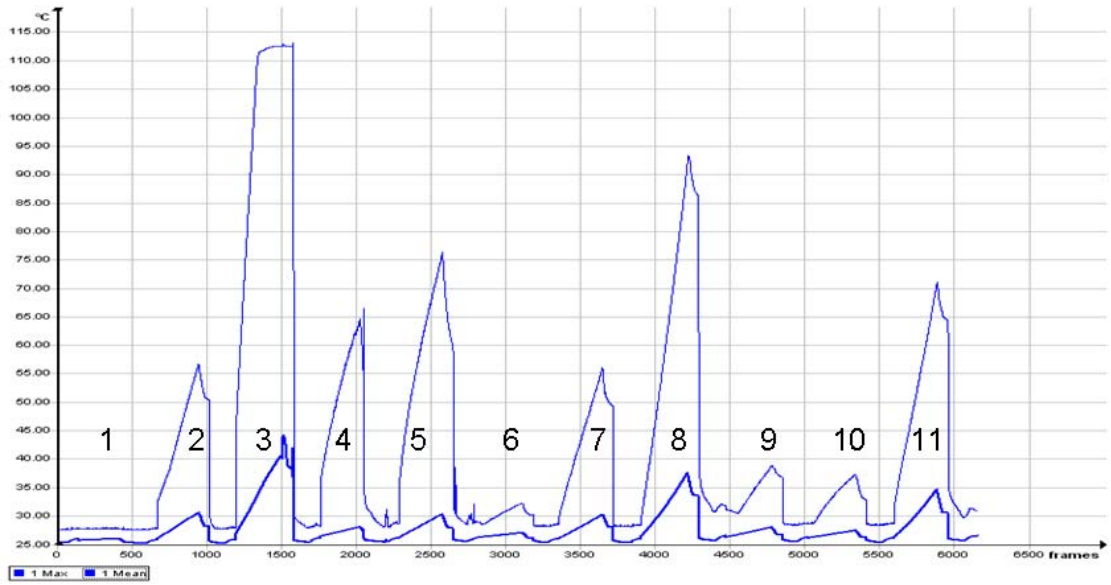

Figure 5-61 Third exposure, timing graph for the set No. 8

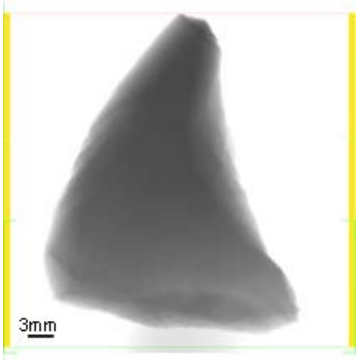

Figure 5-62 X-ray radiogram for particle No. 1 set No. 8

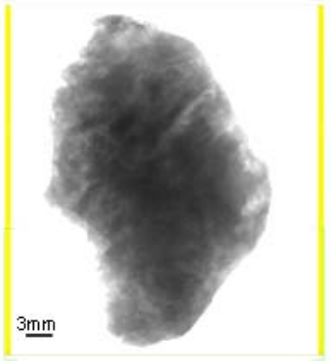

Figure 5-63 X-ray radiogram for particle No. 5 set No. 8

The X-ray radiogram for the particle No. 1 (see Figure 5-62) shows a very uniform matrix of the particle, without any minerals of higher densities. By examining textural features, displayed in Figure 5-63, it can be seen that particle No. 5 consists of a matrix with the presence of mineral structures with higher densities throughout the volume of the particle. Following their mean temperatures after repeated microwave testing in Figure 5-64 it is easy to associate particle No.2 with less responsive and particle No. 5 with more responsive ore particles.

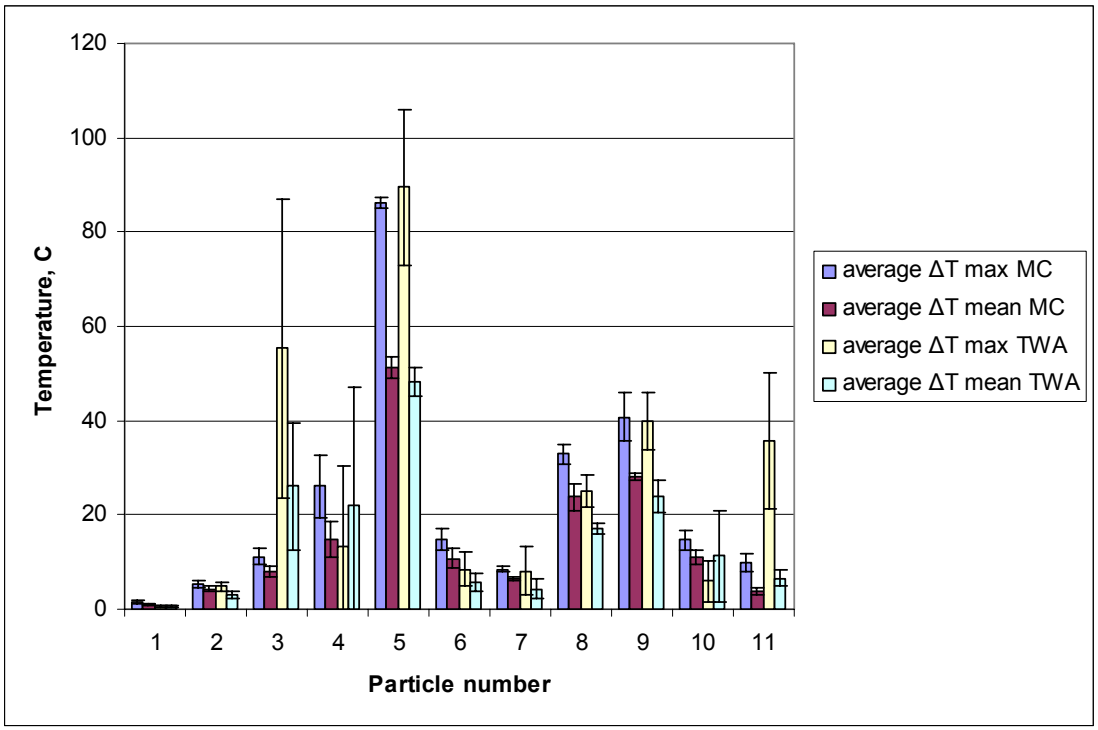

Figure 5-64 Results for the LRO from multimode cavity and travelling wave applicator testing for the set No. 8

5.17 Reduction in Power Applied for the Second Experimental Investigation

The results of the ore mineralogy obtained through MLA examination for the first experimental study, presented that the Low Recovery Ore contains significant amounts of good absorbers of microwave energy, such as pyrite and chalcopyrite. This indicated that the test can be carried out with much less energy required. The power applied in the second experimental procedure was reduced from 1.2 kW to the 600 W.

In Figure 5-65 it can be seen that the temperature change (ΔT mean) for the population which was chosen for the second step of experimental testing is below the temperature curves created from the first step of experimental testing. Temperature curves for the population of 88 and 198 particles were created from ΔT mean calculated from the first exposure with the labels up, while the temperature curve for the population of 66 particles was created from average ΔT mean from the six repeated exposures. Reduction in power applied clearly contributed to lower temperature changes.

Taking into consideration that all particles had to be tested in two applicators by using reduced applied power, the chance of overheating some of the very responsive particles would also be reduced.

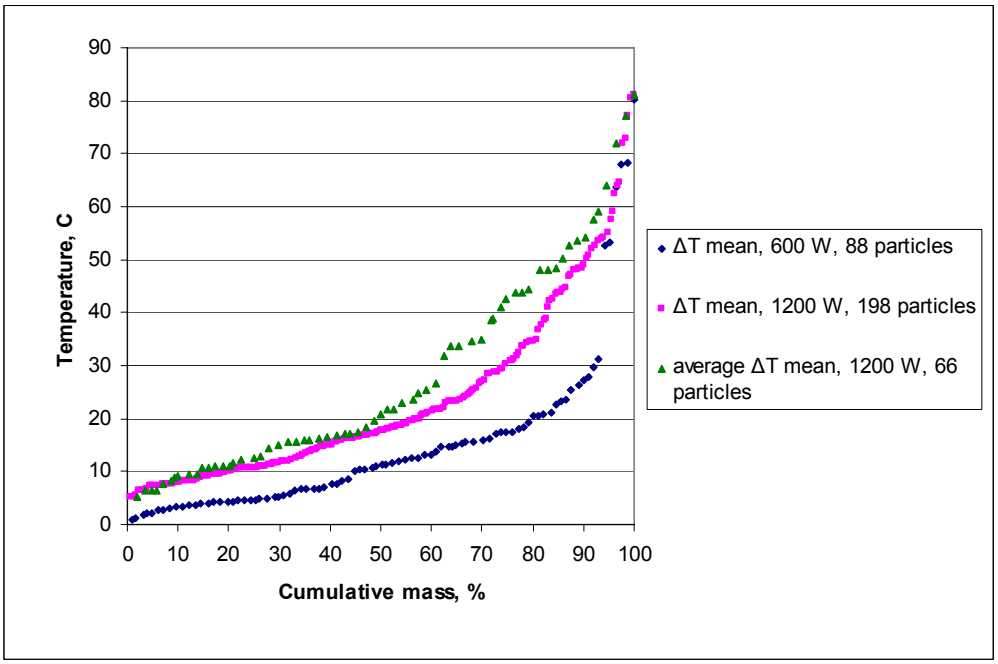

Figure 5-65 Temperature change for the three populations of LRO particles treated with two different applied powers

5.18 Determining a Temperature Threshold for Barren or "Cold" Ore Particles

The results from every set tested, showed that "cold" particles were clearly distinguishable with a lesser temperature change. The term "cold" was used to describe barren ore particles which did not have a high content of very responsive mineral phases to microwave heating. A comparable outcome was achieved through experimental testing with synthetic samples presented in Chapter 4. The synthetic particles with created and well defined mineral texture had noticeably higher maximum and mean temperature differences compared to the rest of the particles which were created to resemble barren rock particles. From the results obtained it can be seen that the temperature difference is strongly dependent upon the texture of the heating mineral phases and the proximity of the heated phase to the surface of the particle.

To determine the temperature threshold for the "cold" ore particles the best case scenario was used. This case was defined for the highest energy transfer reached in all repeated microwave exposures and the ΔT mean measured from the surface closest to the heating minerals. In other words, the particle was coupled at that time to receive the best power transfer during exposure while also having the most favourable orientation of the surface for the infrared temperature measurement. Maximum temperature from all repeated exposures for ΔT mean was calculated and plotted against cumulative mass. This was carried out for both applicators as displayed in Figure 5-66.

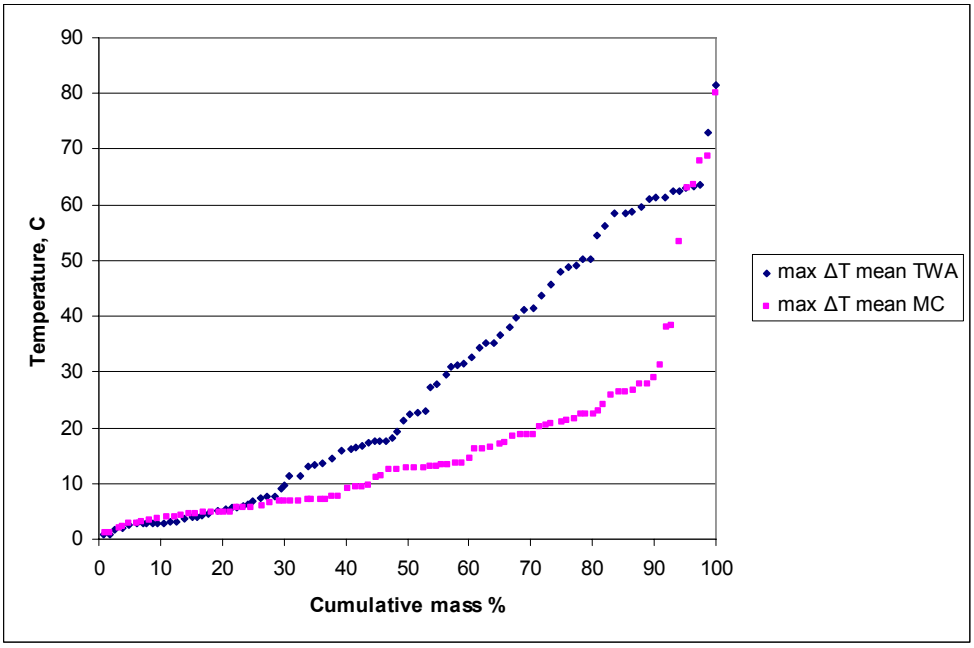

Figure 5-66 Temperature threshold for the "Cold" ore particles from the LRO

The barren ore particles were heated much more during multimode exposures. The better heating response was achieved when the ore particles were heated up in the group which increased overall volume of the load. During individual testing of the particles with the TWA, which was designed to respond to reflected power from introduced external influence, the absence of heating mineral phase caused lower heating response.

The ore particles which had a responsive mineral phase were able to absorb more of applied power. This was caused by higher reflected power from the same ore particles, which was used by the TWA to achieve better coupling with automatic

tuning. Eventually this resulted in a much higher heating temperature difference which was used as a strong indication of present mineral texture.

From these two exposures the temperature threshold which is defined by bulk properties of barren ore particles can be determined as seen in Figure 5-67. It can be considered as a base line for the surface temperature variability caused by the matrix material. The particles which reach higher temperatures indicate the presence of mineral phases within the matrix material as an additional heating source.

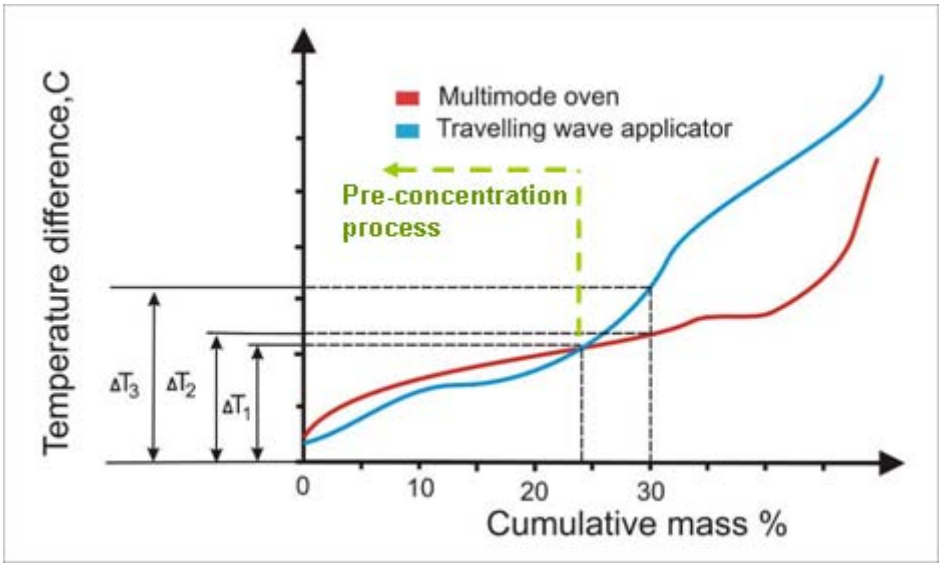

Figure 5-67 Determining temperature threshold for the "cold" ore particles

For this particular ore type the target of the pre-concentration process is to identify and reject barren "cold" particles. To achieve that, a minimum of 30% of the feed mass will have to be rejected to be economically justifiable. The temperature threshold was obtained as a highest temperature change closest to the predetermined mass percentage for the sorting in a multimode oven. In Figure 5-67 , ΔT_2 represents this threshold and for the value of ΔT_2=6.90^{o}C, 31.2% of the feed mass that can be rejected. For the same percentage temperature threshold using TWA, will be ΔT_3=11.26 ^{o}C.

The temperature threshold ΔT_1 has to be calculated only from the particles which were cold during testing in both types of microwave applicators. For this laboratory testing identification of "cold" particles was achieved sorting particles within ΔT_2 threshold

by their max ΔT mean. Data before sorting and after sorting can be found in Appendix H. The overlapping "cold" particles in both types of cavities are shown in Table 5-3:

Set number	Multimode cavity (particle No.)	TWA (particle No.)	Number of overlapping particles
1	1	1, 5, 10	1
2	7, 9, 10	7, 10	2
3	4, 5, 6, 7	6, 5, 11	3
4	1, 5, 6, 7	1, 2, 5	2
5	4, 8, 10	4, 10	2
6	1, 4, 6, 8, 11	1, 2, 4, 8, 11	4
7	1, 6, 10	1, 4, 6, 10	3
8	1, 2, 7, 11	1, 4, 6, 10	1
Overall No. of the particles in 30% of mass	27	25	18
% overlapping from the group	66.67	72.00	

Table 5-3 Overlapping barren "cold" particles in both types of cavities

By implementing percentage for the overlapping cold particles from the multimode cavity on the 31.2% of the feed mass, new experimental value for the temperature threshold can be determined ΔT_1=4.90^{o}C for the 20.80% of the feed mass.

5.19 Summary

The results confirmed that majority of tested particles (about 80%) exhibited a significant increase in temperature change, which is in agreement with experimental results from the first step of experimental investigations. The results of controlled laboratory testing on the same eight sets of rocks demonstrated that combining temperature curves from microwave exposure in two applicators can be used to set threshold for less responsive particles which can be removed by the pre-concentration process.

5.20 General Summary for Low Recovery Ore (LRO)

To address the aims and objectives from the beginning of this chapter, which was to detect rock fragments with minerals which interact with microwaves, Low Recovery Ore was tested in two steps. The first step involved mineralogical characterisation, reproducibility and separability testing followed by testing of the larger particle

population. The major findings from the first step of investigation can be summarised as follows:

The results of the ore mineralogical characterisation, presented through MLA investigation shows that the Low Recovery Ore contains the presence of good absorbers of microwave energy such as pyrite and chalcopyrite. The copper sulphides are interlocked with pyrite in most cases, although they can be found interlocked with garnet, feldspar and amphibole. The size of mineral grains (mostly chalcopyrite and pyrite) varies to a great extent from 50 μm to 3 mm (scale bar estimation).

The substantial variation in mineral phases and their distribution had reflected on the standard deviation in the reproducibility study. With the exposures repeated six times data clearly shows that the frequency of smaller standard deviations for the "cold" particles is much higher compared to "hot" particles. This suggests that they can be more easily identified and selected. For defined standard deviation up to 5 ^{o}C it can be stated that approximately third of the particles had a very reproducible temperature change for the first time point or Delta T1. For the longer time point (Delta T2) this number of particles was more than 65%.

To investigate the potential of setting the right thresholds, separation curves were created. They present mass and metal rejected as a function of temperature change. For a minimum requirement of 30% mass rejected, temperature change for Delta MAX gave the most promising separation conditions to carry out pre concentration in both laboratory tests. From the reproducibility study with the temperature threshold Delta MAX of 20 ^{o}C it is possible to reject 30% of mass tested with a loss of overall copper of 18 %. The same 30% of ore mass can be rejected from larger population testing by using temperature threshold Delta MAX of 20 ^{o}C with the 16 % of overall copper loss. The differences between thresholds for Delta MAX are still within the standard deviation of 5 ^{o}C which was chosen to describe the reproducible process. If the temperature threshold Delta T2 is chosen it would have the same value of 12 ^{o}C with increased overall copper loss of 20 % and more from both studies.

In the second step of the investigation the data collected was used to discuss natural separability as a function of mineral texture which causes selective heating (as in contrast to assayed metal content). The results of controlled laboratory testing in the first step of investigations demonstrated a large number of very responsive ore particles which indicated that applied power can be reduced for the second step of experimental investigations. By combining temperature curves from microwave exposure in two applicators temperature threshold for pre-concentration process can be determined without destroying rock particles. The 20.80% of the feed mass can be rejected having absence of mineral texture which causes selective heating by setting the temperature threshold to $\Delta T_1=4.90^oC$.

Chapter 6-Study of QZ Ohio Ore Type

6.1 Introduction

The main aim of this chapter is to investigate sortability of quartzite copper ore from Bingham Canyon Mine operated by Rio Tinto's Kennecott Utah Copper Corporation using microwave heating in combination with an IR detector.

The goal is to detect rock fragments with minerals, which interact strongly with microwaves. The obtained ore sample was received as quartzite ore with the description name "QZ OHIO". A description of the ore, test work procedure and techniques used to carry out several experimental investigations will be described here.

To provide some insight into the underlying control factors for sortability, selected particles have been subjected to detailed microanalysis using the JK Mineral Liberation Analyser (MLA), a SkyScan 1172 Cone Beam X-ray micro-tomograph (CBT) and Leica DM 6000 Optical Microscope. The detailed descriptions of how they were utilised are given in Chapter 3 section 3.12.

6.2 Overview of the Test Work Procedure and Obtaining Representative Samples

Figure 6-1 shows size distribution within the bulk sample received from the Bingham Canyon Mine site in USA. The particle size distribution data is given in Appendix I.

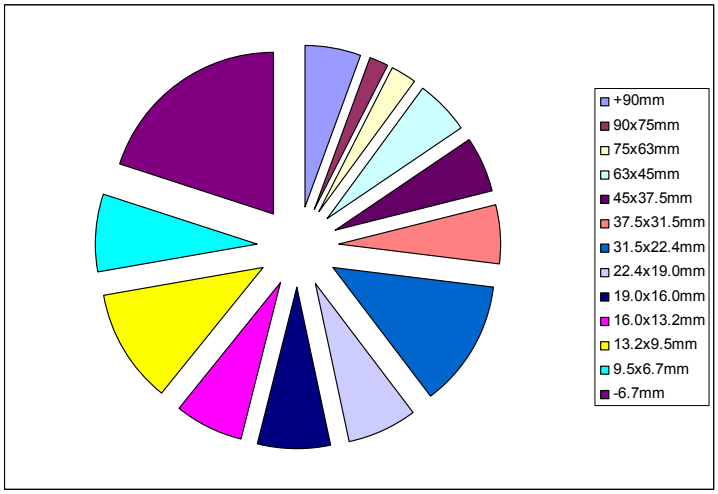

Figure 6-1 Distribution of the material throughout size fractions for the QZ Ohio

The investigation was carried out in two separate steps as shown in Figure 6-2.

The first step was divided into three experimental investigations:

The first experimental investigation involved the selection of particles for MLA examination. Particles were carefully examined for any distinct characteristics in texture, to ensure that they represented visually the most frequent textural features of the bulk ore. The objective was to provide an insight into the mineralogical and textural properties which can be correlated to selective heating processes in an applied microwave field.

The second experimental investigation had the objective of testing -22.4 + 19.0 mm size fraction of the QZ Ohio ore for reproducibility and separability using multimode excitation in a domestic microwave oven. Sixty-six particles were tested up to six times in different orientations. The mass of each particle was measured before it was pulverised and assayed for copper, iron and molybdenum. Separation graphs which use curves for particle and metal mass as a function of temperature change were created to discuss separability.

Finally the third experimental investigation had an objective to further investigate: if "QZ Ohio" ore type was amenable to sorting, whether the copper content (and content molybdenum as other metal of commercial interest) will follow the distribution within

sorted groups. The flotation response was investigated under controlled conditions in hot, medium and cold group formed after microwave/IR sorting.

The second step was performed in single experimental investigation:

The -22.4 + 19.0 mm size fraction was tested for its textural interaction with an electromagnetic field created in two different microwave applicators. Particles were subjected to batch microwave heating in sets and individual heating. The data collected was used with the objective of creating two temperature curves and enabling discussion of natural separability as a function of mineral texture which causes selective heating.

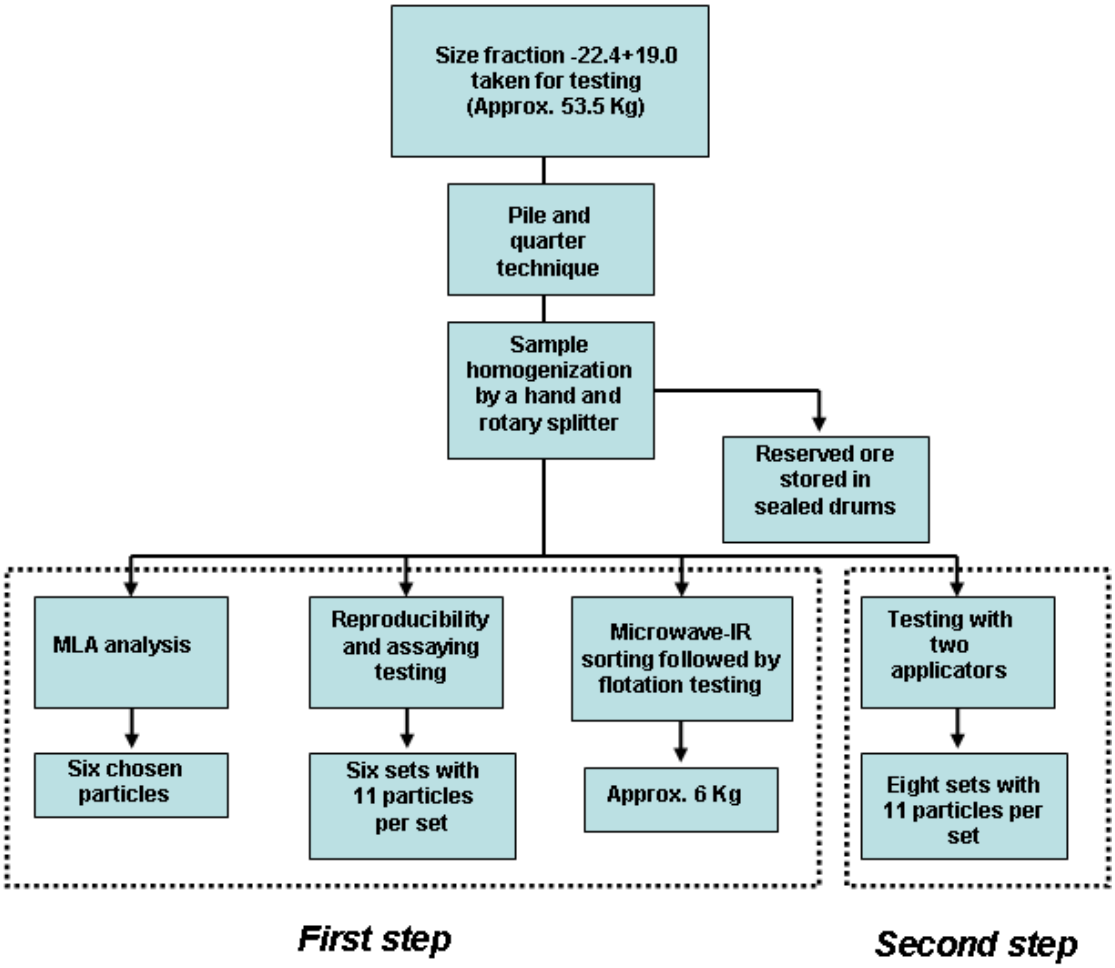

Figure 6-2 Preparation of the sample for the detailed test work which was carried out in several experimental investigations

The QZ Ohio ore was received in 200 l steel drums as a representative sample. The material in the drums was not washed or treated in any other way; it was just selected

as a representative sample and divided into six drums for shipment. The ore was spread out on a floor and left to dry under room temperature for a day. The Gilson Testing Screen was used to screen material into fractions and the screening time was set for ten minutes.

The -22+19 mm fraction was selected for the detailed test work. The mineral liberation was taken as the first guide to select this size. Kelly & Spottiswood (1995) stated that the crushing is operation employed to fracture mineral aggregates, and thus induce or increase liberation of the minerals. Reducing size also allows easier identification of locked and middling particles by applying a sorting technique. On the other hand, ore particle size has to be adequate in order to remove as much as possible of the waste minerals for the lowest processing costs. This process favours retaining larger size of particles.

The second guide came from the air consumption, which is the most common medium used for the physical process of separation during sorting. This particle size is typically closer to the lower economic size limit for industrial sorting using compressed air.

To start the sample preparation cone and quarter method was used to reduce the initial sample (Lowrie & Society for Mining 2002). The sample was piled into a cone shape with a flattened top, and the cone divided into quarters. Two opposite quarters were omitted from further preparation. A rotary sample divider was then used to obtain a homogeneous mixture of the retained two quarters by splitting the bulk ore into twelve fractions. Obtained fractions had approximately 2.2 kg of material. A third of initial material was combined by randomly selecting four bags. New combined material was then divided using a smaller hand splitter into the bags with approximately 150 g of ore material. For the batch exposure in the microwave multimode domestic oven, it was necessary to obtain eleven particles for testing. For this particular reason, the number of particles in each bag was counted. The bags which already had eleven particles were placed on the side, while bags which had less than eleven particles were combined with bags which had more than eleven particles. To assure random selection of the bags Matlab's random function was used. Every

particle in the bag was labelled with the number for the position in multimode cavity and the number of bag to which it belongs. The labels enabled easy identification of ore particles during testing and were also used to provide order during "numbers up" and "numbers down" microwave exposures.

6.3 Mineralogical Characterisation of OZ Ohio Ore - MLA Results

The ore tested originates from the Bingham Canyon Mine operated by Rio Tinto's Kennecott Utah Copper Corporation deposit which is described as a porphyry copper ore.

The tested ore was named "QZ OHIO" which is considered to be a quartzite ore with the bulk copper content around 0.25% which is below current Bingham Canyon Mine economic percentage to be treated as ore. It is of great interest if this ore type can be upgraded through sorting technology (up to 0.35% of copper content) and then treated as economic ore.

Randomly selected (using Matlab software) -13.2 + 9.5 mm particles, were carefully examined for any distinct features in texture to ensure that the ore particles selected for MLA examination represented visually the most frequent textural features of the bulk ore. Six specimens were examined for this ore type as high polished sections prepared for accurate MLA system measurement.

It was stated earlier (in Chapter three Section 3.6) that mineralogy, texture and structure, influence the magnitude of microwave selective heating creating heating profiles. The following data was processed from the MLA to enable an insight into the mineralogical and textural features which can be correlated to observed heating effects:

- The identity of minerals present in each section examined
- The mineral abundance by surface percentage of each mineral phase
- The grain size distribution of microwave absorbent mineral grains
- The spatial distribution of each mineral phase
- The variation of the above in all the eight specimens which were examined

There were 22 minerals which were identified from MLA scans from all polished sections. They are presented in following list:

Table 6-1 Expected average heating rates as per test conditions described by: a) Harrison (1997) b) Walkiewicz et al. (1988) c) McGill et al.(1988) d) Chen et al. (1984) e) Weert et al. (2011) f) Vorster (2001) g) Kobusheshe (2010) h) Genn (2012)

	Mineral	Chemical formula	Heating rate, ^{o}C/s
1	Amphibole	RSi_4O_{11} R=Mg,Fe,Ca,Na,Li,Ti	--
2	Apatite	$Ca_5(PO_4)_3(F,Cl,OH)$	Poor heater [f]
3	Arsenopyrite	FeAsS	5.83[e]
4	Biotite	$K(Mg,Fe)_3(AlSi_3O_{10})(F,OH)_2$	Unknown (but contains –OH) [g]
5	Bornite	Cu_5FeS_4	11.32[a] Heats readily [d]
6	Calcite	$CaCO_3$	0.6[c]
7	Chalcocite	Cu_2S	1.8[b] 1.43[e]
8	Chalcopyrite	$CuFeS_2$	1.000[a] 15.3[b] 2.85[e]
9	Chlorite	$RClO_2$ R=Na,Mg	--
10	Feldspar	$KAlSi_3O_8 – NaAlSi_3O_8 – CaAl_2Si_2O_8$	0.111[a] 0.2[b]
11	Galena	PbS	2.388[a] 2.3[b] 3.51[e]
12	Garnet *	$X_3Y_2(SiO_4)_3$ X=Ca,Mg,Fe Y=Al,Fe,Cr	Poor heater-medium heater [h]
13	Magnetite	Fe_3O_4	2.111[a] 7.6[b]
14	Molybdenite	MoS_2	0.4[b] 1.10[e]
15	Olivine	$(Mg, Fe)_2SiO_4$	--
16	Pyrite	FeS_2	1.000[a] 2.5[b] 2.29[e]
17	Pyroxene	$XY(Si,Al)_2O_6$ X=Ca,Na,Fe Y=Cr,Al,Mg,Ti	Poor heater [f]
18	Quartz	SiO_2	0.083[a] 0.2[b] 0.1[c]
19	Rutile	TiO_2	0.75[a]
20	Talc	$Mg_3Si_4O_{10}(OH)_2$	--
21	Tennantite	$Cu_{12}As_4S_{13}$	Difficult to heat when cold [d]
22	Titanite	$CaTiSiO_5$	--

*** For the Garnet estimation was made for the expected heating rate from the dielectric properties measured at 2.47 GHz by Genn (2012) and given in Table 3-6.**

For easier representation some of the minerals were grouped together, so the following grouping was undertaken:

1 Copper Sulphides: Bornite, Chalcopyrite, Chalcocite, Tennantite

2 Other Sulphides: Pyrite, Arsenopyrite

3 Quartz

4 Feldspar

5 Garnet

6 Magnetite

7 Other Forming Minerals: Amphibole, Apatite, Biotite, Calcite, Chlorite, Galena, Molybdenite, Olivine, Pyroxene, Rutile, Talc, Titanite and Other Minerals

The first two groups represent sulphides which have a tendency to respond very well to microwave heating. The first group represented was copper bearing minerals also defined as minerals of our interest. The second group was other sulphides, defined as pyrite and arsenopyrite. Quartz and feldspar as common forming rock minerals were not grouped. Garnet and magnetite were also not grouped as minerals whose high content can influence temperature profiles of rock particles. Garnet because of its tendency to heat and magnetite as responsive oxide which can heat along with sulphides. The last group represent all other rock forming minerals. Their content varies with a scanned surface of the particles. In some cases the amount of those minerals can be found with significant surface percentage, while in other cases they are found in small trace or not detected at all.

The following figures (from Figure 6-3 to Figure 6-8) will be discussed to present the surface minerals in the six particles examined. The full results of all minerals identified in each measured section, which includes the abundance of each mineral or mineral group by surface percentage, are presented in tables and can be found in Appendix J.

The “responsiveness” to microwave heating is based on literature from previous work such as microwave heating studies carried out by: Harrison (1997), Walkiewicz et al. (1988), McGill et al.(1988), Chen et al. (1984), Weert et al. (2011) and Vorster (2001).

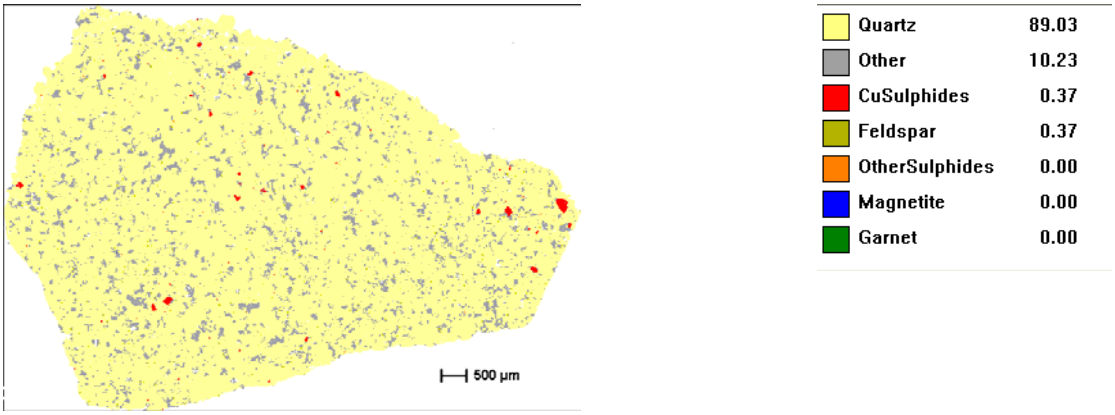

Figure 6-3 Particle one, chosen for the MLA analysis, QZ Ohio

In Figure 6-3 it can be seen that gangue minerals such as quartz and biotite, (which are more transparent to microwave energy then chalcopyrite or pyrite) form almost 98% of the surface. Chalcopyrite is present in small grains with the grains dimensions from 50 to 400 µm (estimation from scale bar).

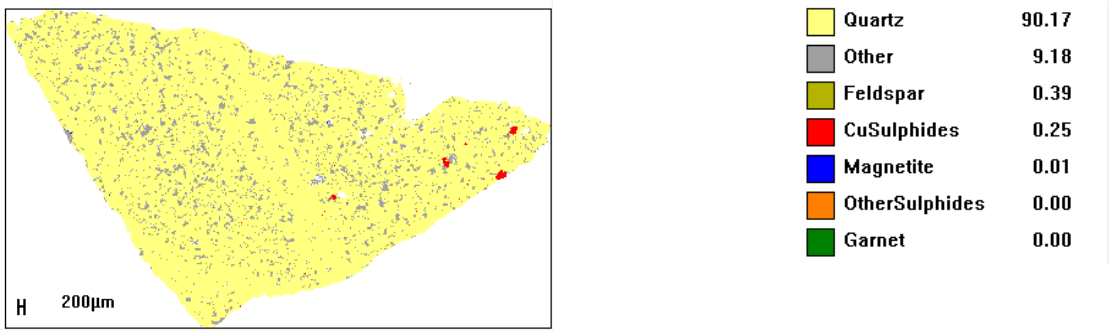

Figure 6-4 Particle two chosen for the MLA analysis, QZ Ohio

Figure 6-4 shows mineral phases for the particle two, and indicates that quartz and biotite (refer to Appendix J for more detailed information about surface % of other forming minerals) are the most dominant matrix minerals. The smaller grain size of copper sulphides is present with diameters between 50 and 100 µm (scale bar estimation).

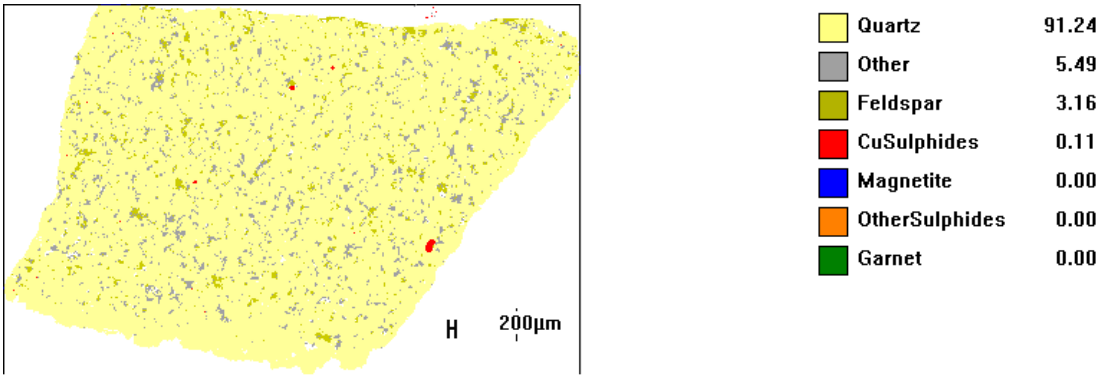

Figure 6-5 Particle three chosen for the MLA analysis, QZ Ohio

Particle three, compared to the previous two has grains of the copper sulphides with similar dimensions but much lower content is detected. As shown in Figure 6-5 Quartz is still the most dominant matrix forming mineral.

Figure 6-6 Particle four chosen for the MLA analysis, QZ Ohio

Particle four, represented in Figure 6-6 revealed a high absence of copper sulphides as major heating phases. Magnetite is present within the quartz and feldspar matrix and in disseminated grains with dimensions between from 50 to 150 µm (scale bar estimation).

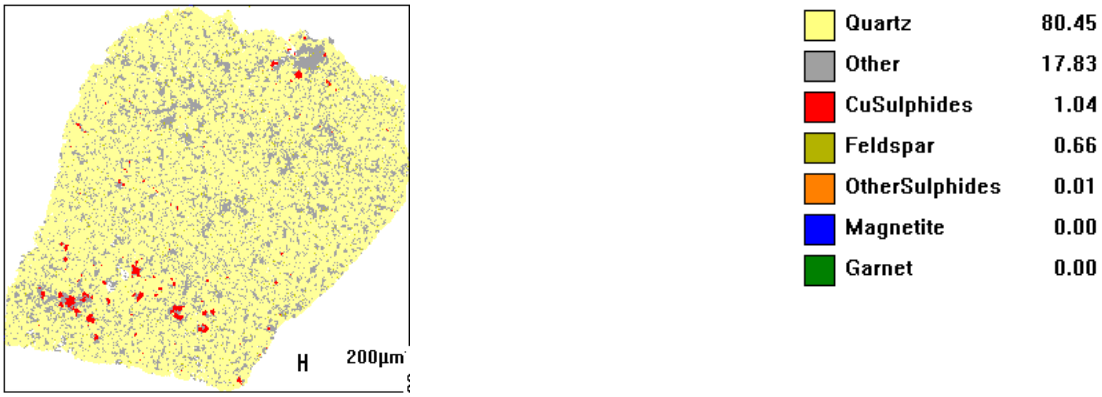

Figure 6-7 Particle five chosen for the MLA analysis, QZ Ohio

A high presence of copper sulphides clustered in two areas, seen at the top and bottom of Figure 6-7, show some grain sizes larger than 200 µm. In the rest of the surrounding quartz and feldspar matrix, much smaller and disseminated grains can be spotted.

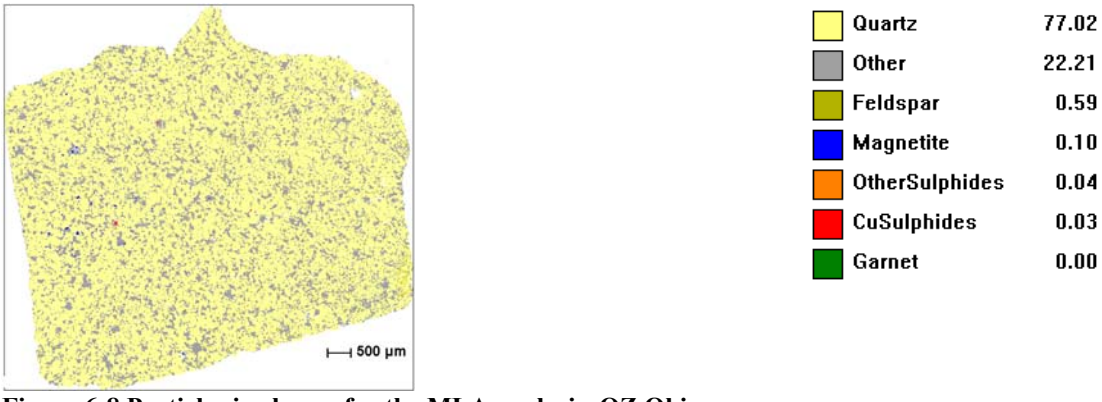

Figure 6-8 Particle six chosen for the MLA analysis, QZ Ohio

Figure 6-8 shows particle six which has the largest amount of biotite that is almost evenly dispersed throughout the quartz. Magnetite and sulphides are present in grains not larger than 50 µm.

6.4 Summary

Observing and analysing all surfaces from chosen particles it can be seen that they exhibit substantial similarity in their mineralogy. The results of the ore modal mineralogy summarised through MLA investigation show that the QZ Ohio ore contains presence of good absorbers of microwave energy such as magnetite, pyrite and chalcopyrite. These minerals are usually dispersed within the matrix made of very large content of quartz interlocked with biotite, feldspar and sometimes chlorite. The presence of mineral grains (mostly chalcopyrite and pyrite) larger than 200 μm is detected. In some tested samples clustered grain forms of chalcopyrite are present in several different locations.

6.5 Microwave Heating and Temperature Characterisation Procedure

The second experimental investigation tested the -22.4 + 19.0 mm size fraction of the QZ Ohio ore for reproducibility and separability using multimode excitation in a domestic multimode microwave oven. The established procedure which was used to test reproducibility for "LRO" ore type was repeated. The procedure is described in more detail in Chapter 5. Here, only the brief summary of the procedure will be given.

All heating was carried out using a "Sharp" domestic microwave oven Model 380-J. After screening, the mass of each rock particle in the -22+19 mm size fraction was measured and the particles were randomly grouped into sets, with approximately constant mass in each set. Each set contained 11 particles prepared for batch microwave heating.

A randomly chosen (with Matlab software) sub-set of six sets was subjected to "reproducibility tests". All particles which were subjected to microwave testing were uniquely identified by a number on the particle and their set number.

Temperature data was collected before and after microwave exposure for the particles in each set. The microwave tray was demarcated into eleven regions. All of the particles from the set were placed along the circular periphery of the microwave tray in one of the demarcated regions. Before microwave heating, an infrared image of the

particles was taken using a "CEDIP "IR- camera. This camera records images in the 2-5 μm infrared spectrums. Each group of samples are then heated using 2.45 GHz multi-mode microwave oven with applied power of 1.2 kW. After heating for 12 seconds, or for the one rotation respectively of the microwave tray, the tray was taken out and a video recording of the tray was initiated using the software supplied with infrared camera. Recording continued until 40 seconds after the end of microwave heating to enable the thermal bloom to develop and a steady state to be reached.

The images of each particle before microwave heating, 5 seconds after the end of microwave heating and 40 seconds after the end of microwave heating were analysed using software supplied with the camera to determine:

- change in *average* temperature during heating period and after 5 seconds (Delta T1)
- change in *average* temperature during heating period and after the end of recording time (Delta T2)
- change in *maximum* temperature during heating period and after 5 seconds (Delta Max T).

Temperature for every particle was calculated, by applying a region of interest around the perimeter of the particle. The region of interest enabled separation of the visible surface of the particle from the background and to calculate the maximum and mean temperature on the surface of the particle.

6.6 Reproducibility Testing for QZ Ohio Ore Type

The aim was to investigate the validity and reproducibility on a sub sample for the -22+19 mm size fraction and to identify the amount of variability in the results due to the procedure (as opposed to the particle variability). Six sets or sets were selected at random and subjected to the detailed testing.

Each set was subjected to the microwave heating and temperature characterisation procedure six times. Particles were allowed sufficient time to cool between each run of the procedure. During repeatable testing particles were placed with their number

facing up for half the runs and down for the other half. This process aimed to duplicate the random orientation of particles on the belt of a theoretical sorting machine. In addition, a computer program was used to generate random numbers which matched particle numbers to one of the numbered regions on the microwave tray and this determined the initial placement of the particles for each run.

The results from the reproducibility study will be commented by discussing data from sets three and four which are presented in Figure 6-9 and Figure 6-10. The graphs for four other sets of the -22+19 mm size fraction are provided in Appendix K for this chapter. It can be seen that set three had one very responsive particle which reached almost six times higher the average surface temperature, compared to the rest of the particles. Standard deviation is found to be the largest for the maximum surface temperature, followed by the average temperature after 5 seconds and finally reducing to a smallest value for an average temperature after 40 seconds. The described trend is present for most particles in all tested sets.

The data for the set four shows very uniform values of surface temperatures with an average temperature after 5 seconds below 2^{o}C and maximum temperature above 2.5 ^{o}C. Only particle eleven reached nearly double the values of temperatures compared to all the others particles. This set of particles can be used as a good example of set with a majority of "cold" particles taking into the consideration their poor response to microwave heating.

As shown in Figure 5-16, the degree of heating is highly reproducible if the standard deviation has a small and constant value throughout its population (presented in blue horizontal line for theoretical case). This performance is expected if the particle's orientation and texture i.e. the physical arrangement of the minerals which interact with microwaves are strong controlling factors in the degree of heating. The QZ Ohio ore is well disseminated and has much lower concentrations of microwave reactive minerals than the skarn ore type (LRO) previously tested and presented in the earlier chapter. As might be expected, the variation even in the higher grade particles is much less.

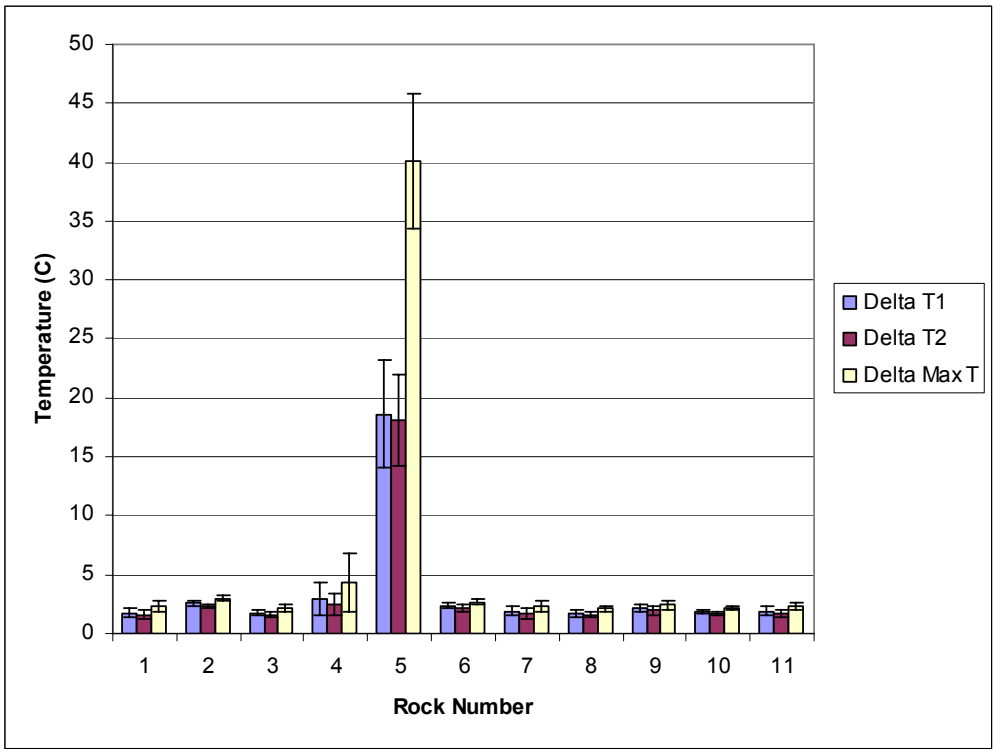

Figure 6-9 Reproducibility temperature change graph for the eleven -22+19 mm particles in set three where each particle was tested 6 times in different orientations

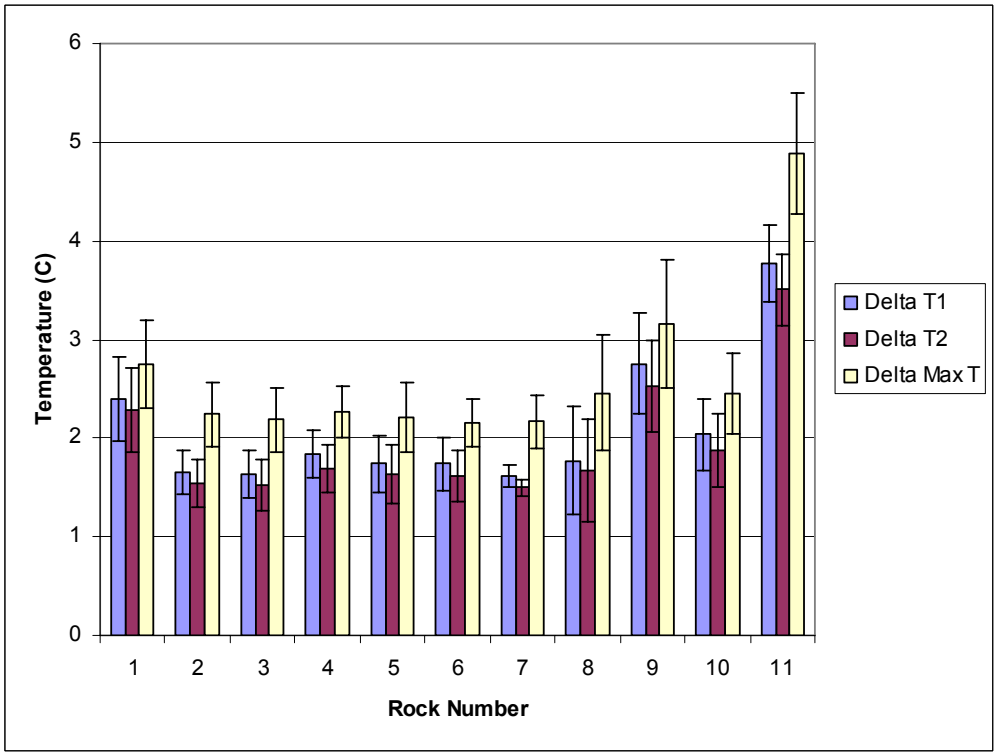

Figure 6-10 Reproducibility temperature change graph for the eleven -22+19 mm particles in set four where each particle was tested 6 times in different orientations

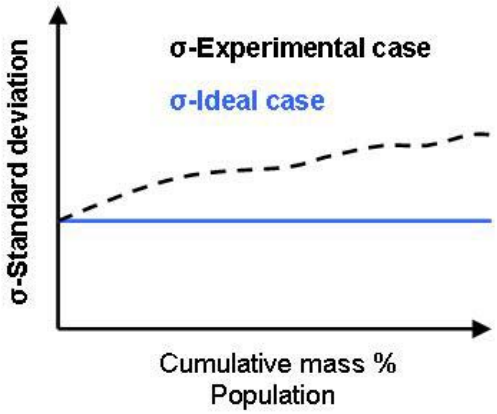

Figure 6-11 Plotted σ -standard deviation vs. population to assess the reproducibility

In Figure 6-12 the standard deviation can be seen from the reproducibility study for the QZ Ohio ore type with the population presented through cumulative mass percentage. The values from particles are very constant and small which resulted in formation of almost straight horizontal line (just as for theoretical ideal case) demonstrating that the reproducibility for this particular ore type is very high.

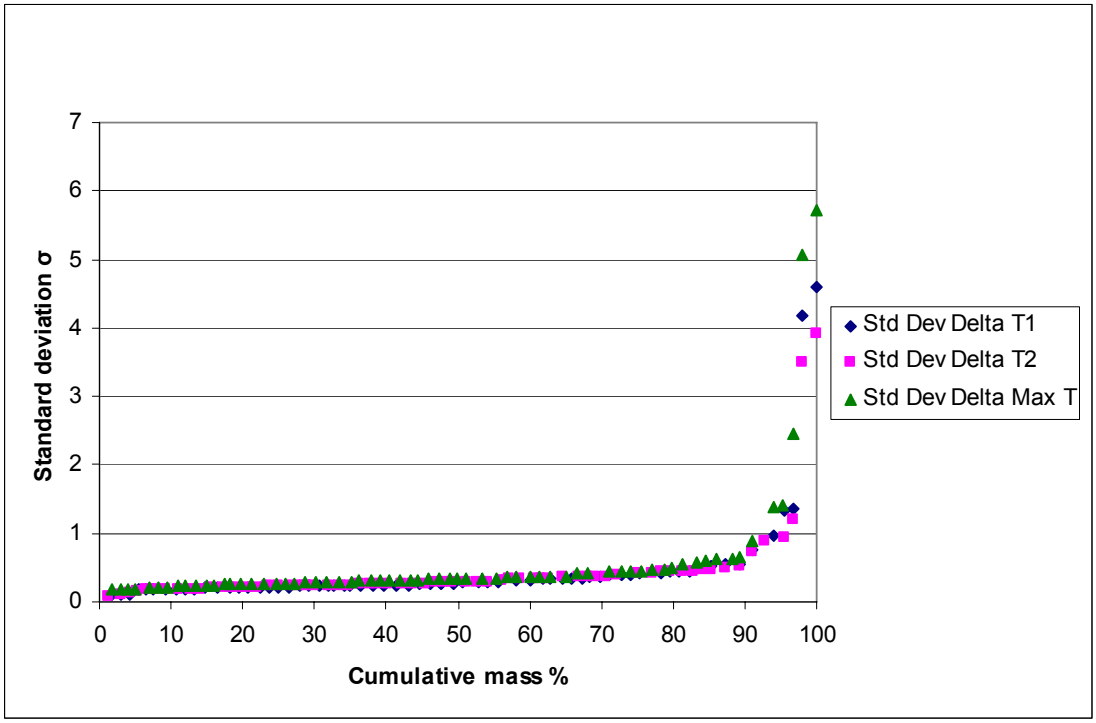

Figure 6-12 Plotted σ -standard deviation vs. population to assess the reproducibility for the QZ Ohio Ore type

If it is decided that standard deviation up to 0.5 ^{o}C is acceptable to describe the reproducible process it can be observed that the 70 % of mass of the all particles and their standard deviation for Delta T1, Delta T2 and Delta Max T will be defined as very reproducible.

6.7 Summary

It is clearly presented that the existence of very uniform and very transparent matrix, which was tested in this case of QZ Ohio ore type, had an effect by increasing repeatability. Particles which had responsive minerals were easily reheated and reached similar temperatures which caused smaller values for standard deviation and at the same time contributed to the repeatability of microwave heating of the overall population.

6.8 Potential for Sorting Using Temperature Difference After Microwave Heating and Copper Grade of QZ Ohio Ore Particles

6.8.1 Temperature Separation Curves

The amenability of an ore type to be sorted by microwave excitation followed by infrared measurement of the temperature change has been assessed by ranking particles according to their temperature change (Delta) at various times after heating and to the "hottest pixel" in the ROI of the image of each particle at those times. The basic potential for separation has been estimated using the copper assay of each particle.

Setting the right thresholds which will divide the feed into the concentrate and the gangue minerals requires a more systematic study. Therefore, to investigate the potential of setting the right thresholds, separation curves were created. They present mass and metal rejected as a function of temperature change.

All the rock particles for the reproducibility study were measured to determine their mass and then sent for assaying to quantify the content of copper, iron and molybdenum. The particles were pulverised and sent for independent assaying analysis by AMMTEC Laboratory based in Perth, AU. The copper content was determined by mixed acid digest followed by ICP (Induction Coupled Plasma) and finished with AAS (Atomic Absorption Spectroscopy).

It was found that for the selected rock particles the content of molybdenum was between 10 and 1950 ppm. The average content of all tested particles was 344 ppm

with a very large standard deviation of 394 ppm which points to a very uneven distribution of molybdenum throughout the tested sample. Despite the fact that some of the particles had a significant content of molybdenum metal detected, minerals with molybdenum for this particular ore type were taken as contributing factors and not as leading factors in the process of selective heating.

The separation curves were sorted by temperature change for Delta T2, Delta T1 and Delta Max. For these separation curves the temperature threshold will change depending on the time chosen to execute physical separation and whether it is decided to sort by average or maximum temperature change. Figure 6-13 shows separation curves sorted by temperature change for Delta Max.

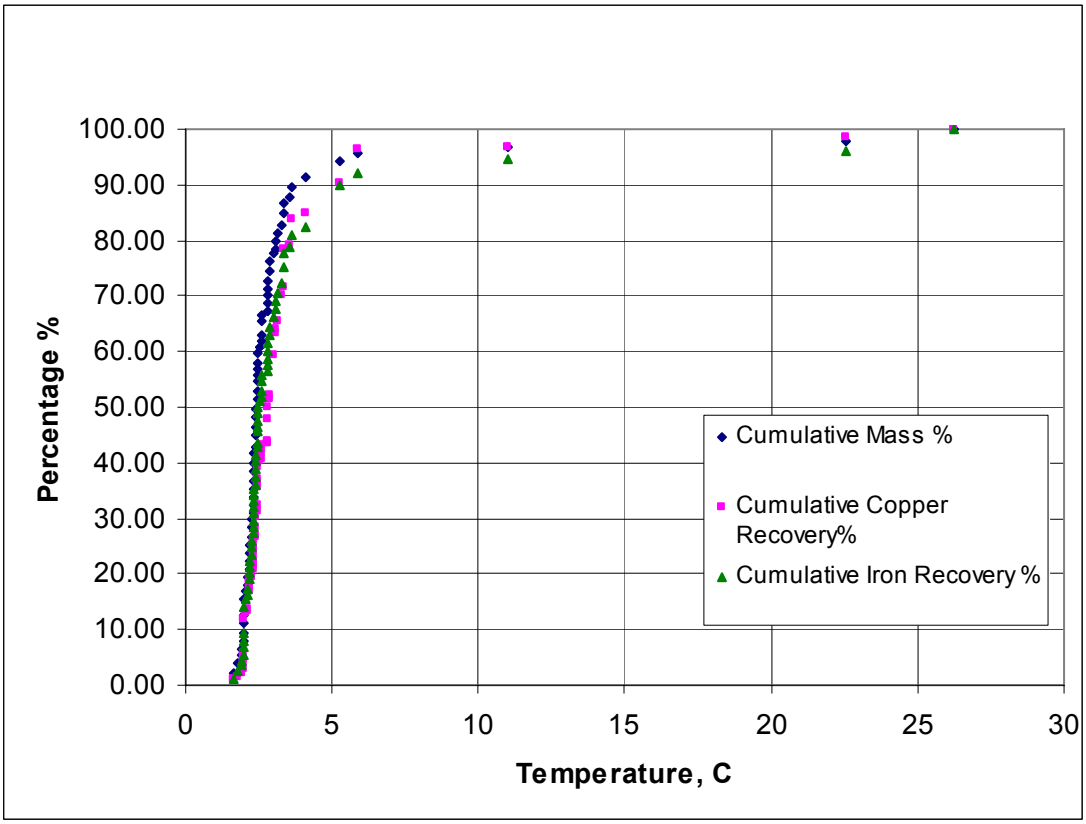

Figure 6-13 Separation curves for QZ OHIO -22.4 +19.0 mm size fraction based on Delta Max T

Cumulative copper and iron recovery curves are compared to cumulative mass to determine temperature change which will define the loss of metal with the mass being rejected. The separation curves for Delta T2, Delta T1 are given in Appendix K while separation curve for Delta Max (see Figure 6-13) is presented this section since it gave the best separation results.

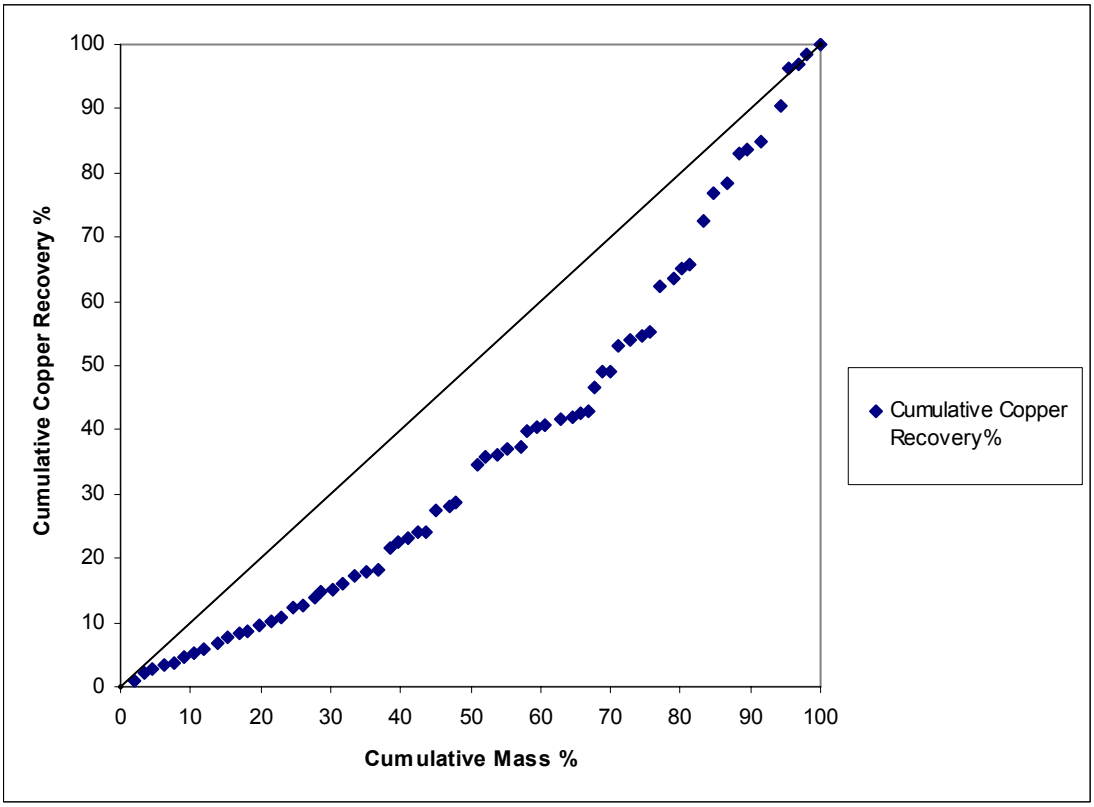

Figure 6-14 Non-linear deviation between the Cumulative Mass % and the Cumulative Copper Recovery % for Delta Max T for QZ OHIO ore type

To choose the best operating point, non-linear deviation between the cumulative copper recovery % and cumulative mass % for Delta Max is presented in Figure 6-14. According to Cohen (2000) "Rejection of 25 – 30% of the feed mass is usually a minimum requirement for sorting to be economically justifiable." Taking this into the consideration and that for this particular ore type 30 to 40 % of mass demonstrated larger temperature changes, the sorting process would be operated as a scavenging process with the aim to remove hot particles which would contain microwave responsive minerals. Choosing to remove 30% of the feed mass treated, following temperature thresholds can be placed: for the Delta Max T temperature change above 2.6 ^{o}C will scavenge 30% mass with close to 50% of overall copper.

The cumulative iron recovery follows mass recovery very closely and at about 55% it starts to separate. The separation indicates that in the remaining 45% of the mass tested, which corresponds mostly to the hotter particles, the content of iron is increasing. In this case the increased content of iron cannot be correlated only with the presence of a copper bearing minerals. The results for iron content were obtained from pulverised samples therefore; they represent overall content of iron whether it

comes from sulphides (e.g. pyrite, arsenopyrite and chalcopyrite) or oxides (e.g. magnetite).

6.8.2 Summary

A separation strategy was developed as a most suitable method to illustrate the level of separability by exposing rock particles to microwave heating and obtaining copper content by assaying. The laboratory method was used to investigate the sorting potential (operated as scavenging process) of QZ Ohio ore. Every ore sorter can be described through a performance curve. This information describes the best separation which can be achieved with a particular ore sorting machine. The difference between separation by separation curves and sorter performance curve which comes from build-in inefficiency of the sorter has to be acknowledged.

For this laboratory method, the theoretical separator with temperature information from two sides of the particle which could detect copper content with similar precision to an assaying test was used. The separation curves indicate that QZ Ohio ore material was responsive to scavenging strategy which had goal to separate all particles with higher temperature difference then set threshold. For a minimum requirement of 30% mass separated, temperature difference for Delta Max T gave the most promising separation conditions to carry out sorting in the laboratory tests.

As the particles cool down the efficiency of sorting by selective heating was reduced and the temperature thresholds needed to be reduced to retain the pre-determined percentage of scavenged mass, as shown in Table 6-2.

Table 6-2 Identified thresholds to scavenge 30% of mass tested

Reproducibility study	Delta Max T	Delta T1	Delta T2
Temperature threshold, ^{o}C	2.6	2.3	2.1
Regained overall copper, %	50	49	48

The QZ Ohio ore was sourced as a low copper grade material with an average bulk copper grade of 0.25%. It is of great interest if this ore type can be upgraded through sorting technology up to 0.35% of copper content and treated as economic ore. After plotting separation curves, copper grade frequency distribution for QZ Ohio ore was analysed and shown in Figure 6-15.

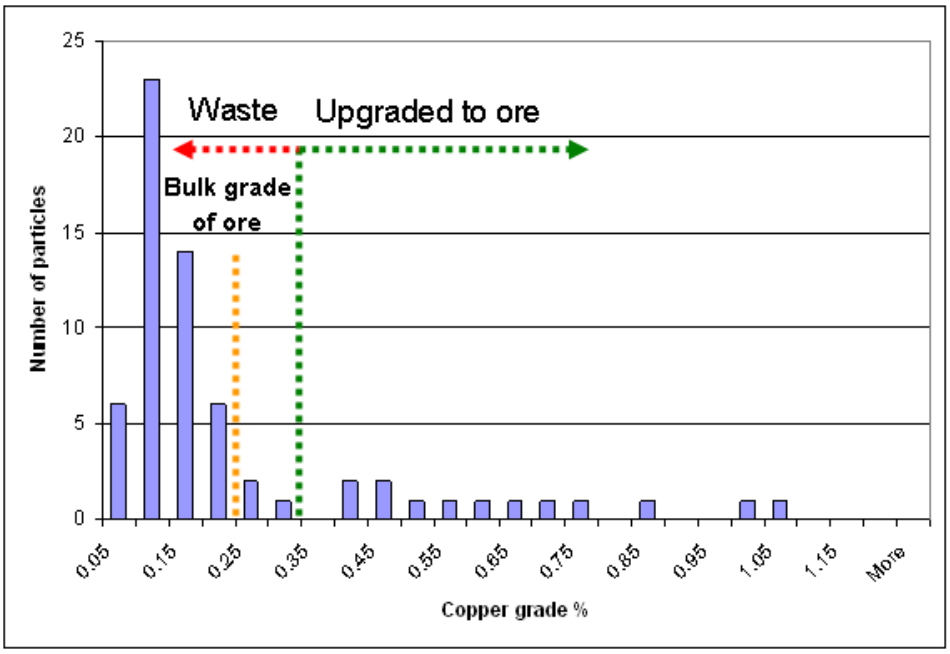

Figure 6-15 Copper grade frequency distribution for QZ Ohio ore type

Data from the histogram shows that the majority of assayed ore particles are below the set threshold for them to be considered as ore and this can be easily correlated to a majority of cold particles. Within the scavenged mass, 20% mass can be upgraded to have copper content of 0.35% and more. If the threshold is lowered to be just above bulk grade of ore then an additional increase of 4% can be achieved.

6.9 Flotation Testing of Microwave Sorted Ore

The main aim of this section is to investigate the content of copper after sorting the QZ Ohio ore in three selected fractions (hot, medium and cold), by performing preliminary flotation testing under controlled operating conditions. Along with copper, the content of molybdenum was also investigated. The unprocessed (UP) material, which was tested under the same flotation conditions, was used as a control. Flotation testing was performed by JKMRC Pilot Plant Flotation Laboratory. The utilised flotation cell and the conditions are described in the following sections.

6.9.1 Preparation of the material

The Figure 6-16 shows the temperature profile for particles of -22.4 +19.0 mm QZ Ohio plotted in terms of temperature change Delta T_2 against cumulative mass from cold to hot. All particles were labelled and treated in microwave domestic multimode oven for 12 seconds at the 1.2 kW. The procedure of exposing particles and acquiring temperature measurements are described in detail in Section 5.6 of Chapter 5.

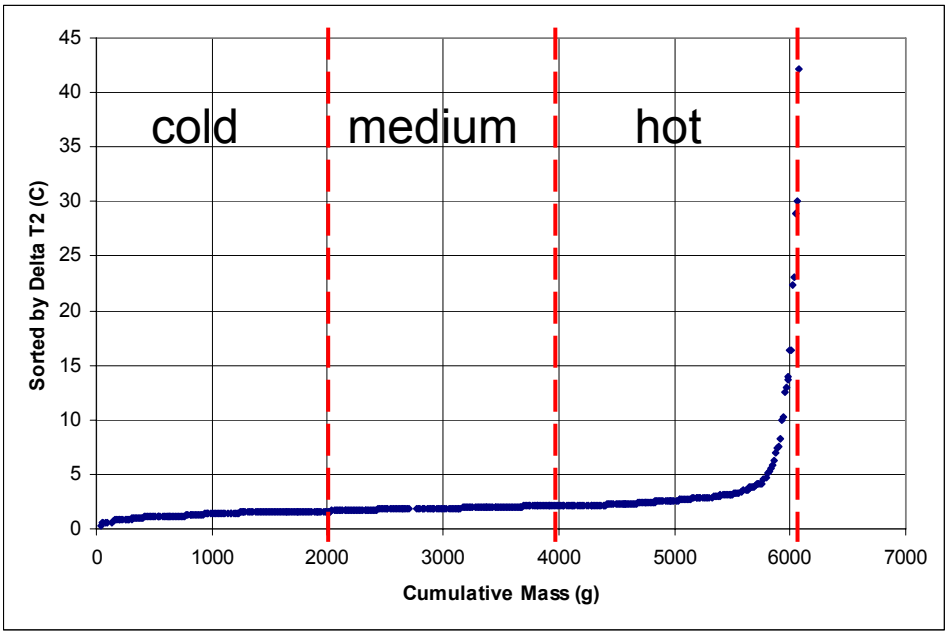

Figure 6-16 – Cumulative mass-temperature curve for -22 +19 mm QZOHIO

The approximate mass of 6 kg was then divided into three fractions of approximately 2 kg representing a hot fraction with the highest temperature change, the medium with the slighter temperature change and the cold fraction. All three fractions were split into two different groups for the two different grinding times (the first 10 min and the

second 15 min). By selecting every second rock from the curve for one group an even distribution of hotter particles was achieved throughout the groups.

The diagram for preparation of the material for the flotation testing is shown in Figure 6-17. The selection provided six flotation tests which were complemented with two more for the unprocessed material. During the preparation of approximately 6 kg, for microwave treatment and sorting, a sub-sample of approximately 2 kg was prepared following the same procedure for the unprocessed material. By splitting the representatively unprocessed fraction in half, two groups were obtained for 10 and 15 minute grinding.

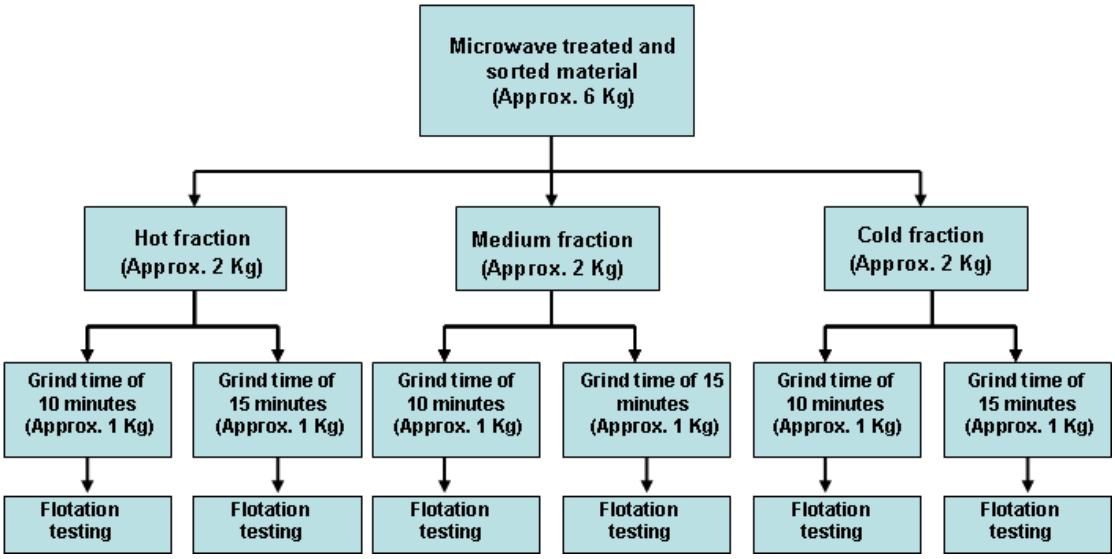

Figure 6-17 Diagram of the material split after microwave treatment and sorting

All groups were prepared for the flotation testing after grinding to investigate how much of the sulphide minerals can be recovered under controlled conditions. To investigate copper recovery from the floated material all samples were sent for independent assaying by AMMTEC Laboratory based in Perth, AU.

6.9.2 Procedure and Flotation Apparatus

A review by Bruckard et al. (2011) found that the flotation response of ground minerals can be influenced by the grinding conditions used. This include interaction of the minerals with the grinding media, the generation or presence of oxyhydroxide species in the pulp, the effects of any added reagents or chemicals, and the type of grinding method employed. To achieve controlled conditions for this particular testing

all these influences were considered. The choice for some came from consultation with the sponsor.

The metallurgical performance of any separation technique is influenced by mineral liberation. The locking characteristics and the liberation of the minerals in an ore are mainly dictated by the grain size of the minerals. Kelly and Spottiswood (1995) commented that the interaction between minerals and reagents and the effect of the reagents on the surface of the minerals is the first important condition for a successful flotation process. The second is of a physical-mechanical nature and determined by the flotation machine characteristics.

The results obtained from the mineralogical characterization study using MLA (in the section 6.3 of this chapter) on the ore showed that the grain size of copper bearing sulphide and sulphides particles was fine (from 100 to 200 µm) and fine grinding was required to achieve a high degree of liberation of minerals. In this study, for achieving the desired 75% passing size (P75) the conventional rod mill grinding technique was used. For determining the best grind size and achieving a higher degree of liberation size between 100 and 200 µm was targeted. The grinding experiments were conducted using a laboratory-scale 260 mm (L) × 205 mm (D) rod mill with a charge of 15 rods. The mill and rods were made of stainless steel and they can be seen in Figure 6-18.

Figure 6-18 Rod mill used to grind samples for 10 and 15 minutes

Figure 6-19 The standard JKMRC flotation cell

After wet grinding, the samples were wet sieved to determine 75% passing size. This was done by plotting the cumulative passing percentage of the mass with the sieve sizes used for screening. The linear interpolation between the two closest sieve sizes was used to calculate values for the P75. Figure 6-20 shows linear interpolation for the hot fraction and the group which was grinded for 10 minutes. For all the other groups their mass distributions and their linear interpolations can be found in Appendix L.

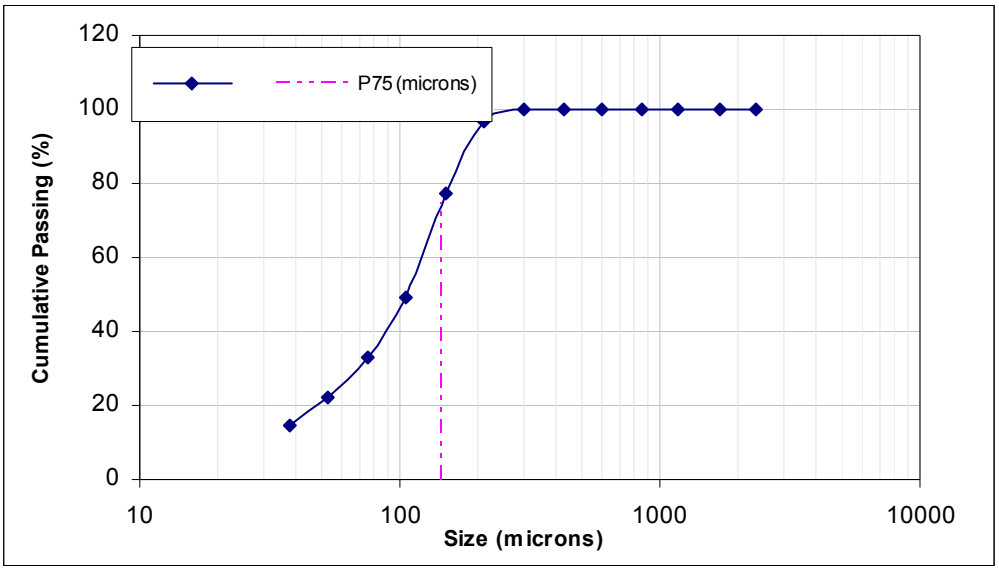

Figure 6-20 The passing size (P75) for the hotter fraction after 10 minute grind time

The 75% passing size (P75) for each temperature category and the unprocessed rocks are shown in Table 6-3.

Table 6-3 Grind product sizes (P75) for different temperature categories and untreated -22 +19 mm QZOHIO

Grind time (min)	P75 (µm) Hot	P75 (µm) Medium	P75 (µm) Cold	P75 (µm) Unprocessed
10	146	158	160	181
15	121	127	132	144

The passing size is smaller for the hotter rocks for both of the grinding times. The colder rocks also have a smaller passing size than the unprocessed rocks for this size fraction which tends to indicate that the microwave test procedure might weaken the ore. However, there is not enough evidence that this was the major factor for the smaller passing size. It might be that an increase in grindability in the hot group is related to the specific minerals species present, particle size of the specific minerals and also the degree of dissemination. The content of sulphide minerals should be

higher in the hot group as a result of sorting and this may be reflected in different breakage characteristics when compared to medium and cold groups.

All of the flotation experiments were carried out in a 5-litre, bottom-driven JKMRC batch flotation cell (Figure 6-19) which is also used for the commercial testing of froth performance. In this cell, air is injected through the stator on the top of the impeller. The air flow rate, air pressure and impeller speed were controlled constantly during the experiments. At 10 second intervals, using the scraper, all the froth was swept with a single brisk stroke from the rear of the cell to the overflow into the collection container.

Some of the operating conditions for this flotation testing were chosen by the sponsor to be similar to the operating conditions in the real operation. To summarise, all conditions used during flotation testing are presented in tables from Table 6-4 to Table 6-7.

Table 6-4 Pre-Grind reagent additions used to prepare material for flotation

pH Modifier	$Ca(OH)_2$
Concentration	5%
Target pH	10.2
Amount Added	1000µl
Mo promoter	Diesel
Concentration	Neat
Amount Added	21µl

Ore supplier uses a non-standard molybdenum promoter ("Burner Oil"). As the "Burner Oil" was not available, with the approval from sponsor, standard automotive diesel was used as a molybdenum promoter.

Table 6-5 Grind conditions

Sample Mass (g):	Approx. 1000.00
Charge Mass (g):	11020.00
Water Mass (g):	Approx. 500.00
RPM:	76
Grind Time (min):	10
Water Source:	Pilot Plant

Table 6-6 Test conditions

Cell Size (L):	5
Air Rate (L/min):	10
Froth Pull (s)	10
Air Press.(kPa):	200
Froth Depth (cm)	1
Water source:	Pilot Plant tap water
Conditioning time per reagent added (min)	1

Table 6-7 Float chemistry used during flotation tests

pH Modifier	$Ca(OH)_2$
Concentration	5.00%
Amount Added	6ml
Collector	S8989
Concentration	Neat
Amount Added	18µl
Frother	MIBC
Concentration	Neat
Amount Added	210µl

Initial readings after grinding showed satisfactory values of pH around the targeted value of 10.2. In Table 6-7 it can be seen that commercial collector AERO® S 9889 produced by CYTEC was used along with the most common frother methyl isobutyl carbinol (MIBC) to promote separation of sulphide minerals.

6.10 Results from Flotation Testing

As a result of sorting in three fractions the highest content of sulphide minerals should be in the hot fraction followed by the content in medium fraction and finishing with the most barren cold fraction. From Figure 6-21 and Figure 6-22 by observing all floated groups it can be seen that the hot group has separated from the rest of the groups. This is evident for both grinding times which demonstrate that the most sulphides minerals in the mass recovered originated from the particles which had the good response to microwave heating. The experimental data for all calculations can be found in Appendix L.

When the obtained results of treated fractions are compared with the results from unprocessed fraction it shows that they all follow increase in mass recovery with time. In addition, it demonstrates that their sequence is a function of distribution and content of heating phases within the particles which comprise the particular group.

From the Figure 6-16 it can be seen that the temperature difference between cold and medium fraction is minimal. This small difference can also be noticed in Figure 6-21 and Figure 6-22 with the higher cumulative mass recovery percentage for the medium fraction.

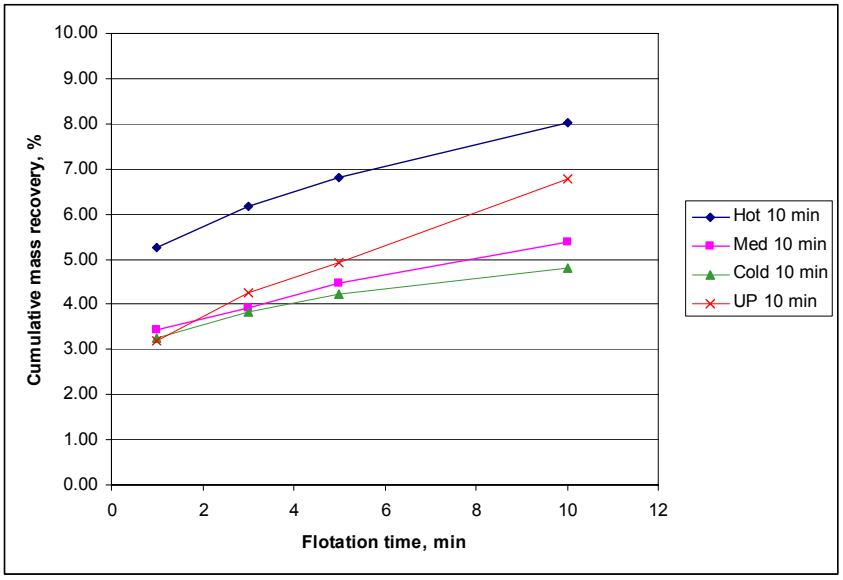

Figure 6-21 Flotation recovery for 10 min grind time

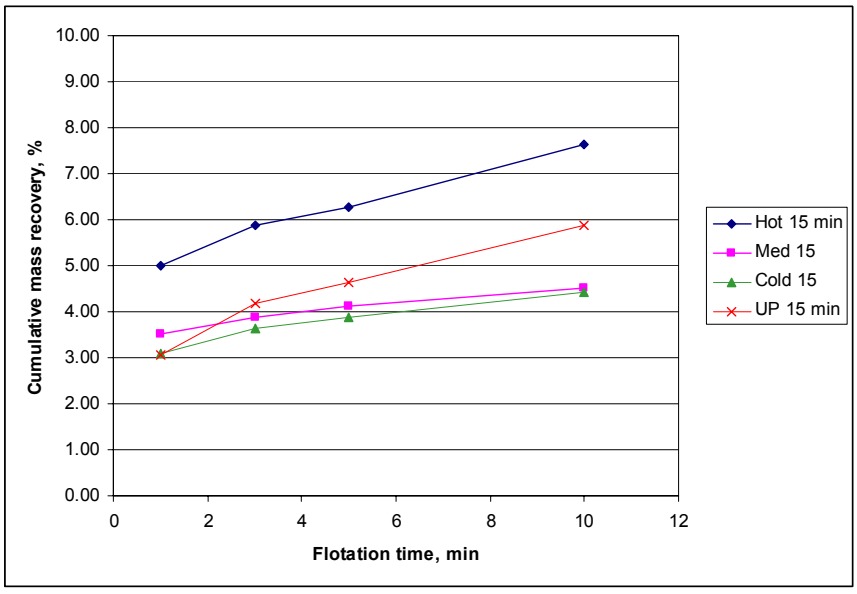

Figure 6-22 Flotation recovery for 15 min grind time

Data for UP fraction, which is not sorted and in that context represents all three fractions, at the very beginning (first minute during flotation time) has values close to cold and the medium fractions. This can be explained through the higher influence of the existing medium and cold phase within the UP fraction. As the flotation time passes (third, fifth and tenth minute) values for cumulative mass recovery for UP fraction increases gradually distinguishing them from the medium and cold fraction;

here the influence of the hot fraction is more evident. All of the obtained results show that unprocessed material used as control is in the right sequence and its values are between values of hot and cold fraction which were selected as extremes for tested ore types.

To determine copper content in the concentrates from the froth and in the tailings samples from flotation testing, they were sent for independent assaying analysis by AMMTEC Laboratory based in Perth, AU. The copper content was determined by mixed acid digest followed by ICP (Induction Coupled Plasma) and finished with AAS (Atomic Absorption Spectroscopy).

Table 6-8 Copper content obtained through assaying and used to calculate final mass in each concentrate and final recovered copper content in each group grinded for 10 minutes

	Copper (ppm)			
	Flotation time (min)	Hot	Med	Cold
Concentrate 1	1	47600	35800	24400
Concentrate 2	3	12300	22600	7750
Concentrate 3	5	3470	2490	1710
Concentrate 4	10	1580	990	1140
Tail		190	120	90
	Copper (g)			
	Flotation time (min)	Hot	Med	Cold
Concentrate 1	1	2.49	1.23	0.79
Concentrate 2	3	0.11	0.11	0.04
Concentrate 3	5	0.02	0.01	0.01
Concentrate 4	10	0.02	0.01	0.01
Cu lost in Tail		0.17	0.11	0.09
Total without Tail		***2.64***	***1.36***	***0.85***

Table 6-9 Copper content obtained through assaying and used to calculate final mass in each concentrate and final recovered copper content in each group grinded for 15 minutes

	Copper (ppm)			
	Flotation time (min)	Hot	Med	Cold
Concentrate 1	1	41300	28400	28600
Concentrate 2	3	19500	14000	15000
Concentrate 3	5	3750	2740	3150
Concentrate 4	10	950	1870	1490
Tail		180	90	100
	Copper (g)			
	Flotation time (min)	Hot	Med	Cold
Concentrate 1	1	2.04	0.91	0.88
Concentrate 2	3	0.17	0.05	0.08
Concentrate 3	5	0.01	0.01	0.01
Concentrate 4	10	0.01	0.01	0.01
Cu lost in Tail		0.16	0.08	0.09
Total without Tail		***2.24***	***0.97***	***0.97***

From Table 6-8 and Table 6-9 it can be seen that after sorting the largest amount of copper recovered it is from the hot fraction followed by the medium and the cold fraction. The location of the copper can be discussed by plotting cumulative copper recovery from all copper content with flotation time as seen in Figure 6-23 and Figure 6-24 for different grind times. The data for these calculations are shown in Appendix L.

The results for the shorter grinding time in general demonstrate better copper recovery when compared with the longer grinding time. As the flotation time increases the cumulative copper recovery becomes the highest for the hot group as expected.

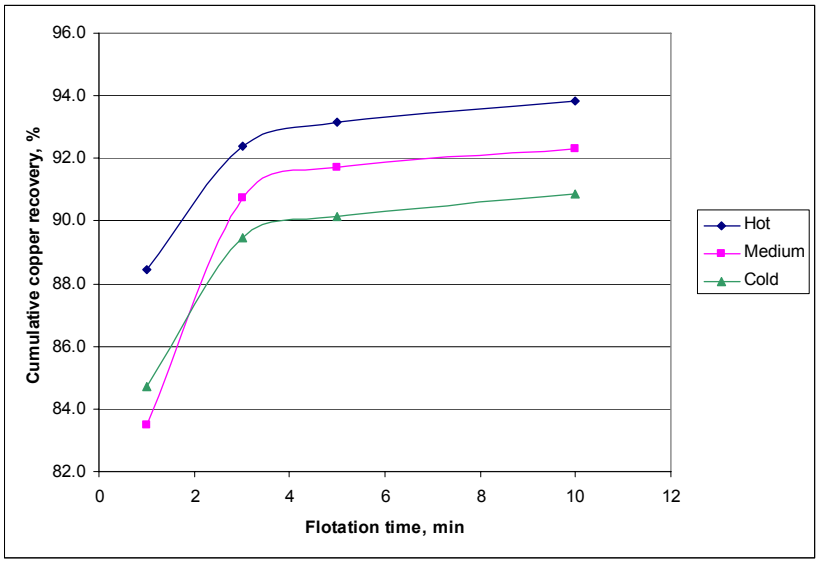

Figure 6-23 The cumulative copper recovery for 10 min grind time

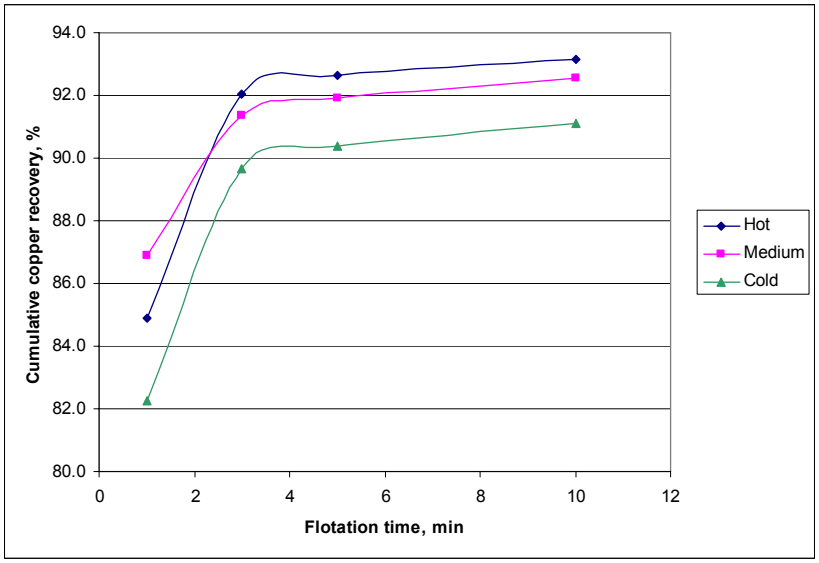

Figure 6-24 The cumulative copper recovery for 15 min grind time

The content of molybdenum was also investigated as a commercially valuable metal. The results obtained from the mineralogical characterization study using MLA showed that the grain size of molybdenum were very small (less than 50 μm). It was mostly found as very well dispersed and with the surface percentage around 0.1%. Minerals with molybdenum for this study were considered not to be the major minerals for selective heating but contributing minerals taking into account their content and distribution. Data for recovered molybdenum content in each group is presented in the Table 6-10 for 10 minutes grinding time and in Table 6-11 for 15 minutes grinding time. It can be seen that for a longer grinding time which resulted with smaller P75, recovered molybdenum content follows the pattern of copper by having the highest content of molybdenum in the hot group. In the case of samples grinded for 10 minutes the highest recovered molybdenum content was in the cold group.

Table 6-10 Molybdenum content obtained through assaying and used to calculate final mass in each concentrate and final recovered molybdenum content in each group grinded for 10 minutes

	Molybdenum (ppm)			
	Flotation time (min)	Hot	Med	Cold
Concentrate 1	1	6370	9560	19600
Concentrate 2	3	1530	7700	4470
Concentrate 3	5	560	940	870
Concentrate 4	10	240	290	520
Tail		30	30	20
	Molybdenum (g)			
	Flotation time (min)	Hot	Med	Cold
Concentrate 1	1	0.333	0.329	0.636
Concentrate 2	3	0.014	0.037	0.026
Concentrate 3	5	0.003	0.005	0.003
Concentrate 4	10	0.003	0.003	0.003
Cu lost in Tail		0.027	0.028	0.019
Total without Tail		***0.35***	***0.37***	***0.67***

The unprocessed material, which was tested under the same flotation conditions, was used as a control. Data for the copper and the molybdenum content is presented in Table 6-12. It can be seen that in the case of copper, a shorter grinding time resulted in a much better recovery, while for molybdenum a longer grinding time only slightly increased the recovery.

Table 6-11 Molybdenum content obtained through assaying and used to calculate final mass in each concentrate and final recovered molybdenum content in each group grinded for 15 minutes

		Molybdenum (ppm)		
	Flotation time (min)	Hot	Med	Cold
Concentrate 1	1	13200	7240	6410
Concentrate 2	3	6450	3090	3320
Concentrate 3	5	1490	740	670
Concentrate 4	10	430	550	440
Tail		60	40	40
		Molybdenum, (g)		
	Flotation time (min)	Hot	Med	Cold
Concentrate 1	1	0.651	0.232	0.197
Concentrate 2	3	0.057	0.010	0.017
Concentrate 3	5	0.006	0.002	0.002
Concentrate 4	10	0.006	0.002	0.002
Tail		0.055	0.035	0.038
Total without Tail		***0.77***	***0.28***	***0.26***

Table 6-12 Copper and molybdenum content obtained through assaying and used to calculate final mass in each concentrate and final recovered copper and molybdenum content for unprocessed material grinded for 10 and 15 minutes

Grinding time		10 min		15 min	
	Flotation time (min)	Cu (ppm)	Mo (ppm)	Cu (ppm)	Mo (ppm)
Concentrate 1	1	53000	8410	27100	5830
Concentrate 2	3	17400	3050	30500	8320
Concentrate 3	5	2100	270	2130	530
Concentrate 4	10	770	120	630	190
Tail		140	20	110	40
Grinding time		10 min		15 min	
	Flotation time (min)	Cu (g)	Mo (g)	Cu (g)	Mo (g)
Concentrate 1	1	1.68	0.27	0.83	0.18
Concentrate 2	3	0.18	0.03	0.35	0.09
Concentrate 3	5	0.01	0.00	0.01	0.00
Concentrate 4	10	0.01	0.00	0.01	0.00
Cu lost in Tail		0.13	0.02	0.10	0.04
Total without Tail		***1.89***	***0.30***	***1.20***	***0.32***

6.11 Summary

This section has described the investigation of the copper content after sorting the QZ Ohio ore in three selected fractions: hot, medium and cold. The type of grinding media, the size reduction method employed, pre-conditioning stages prior to flotation, and reagent interactions during grinding (and conditioning) were chosen for the flotation process so that the ore composition in the fractions could be investigated.

For the -22.4+19.0 mm size fraction tested, the hot and medium fractions are generally of higher grade and indicate a substantial improvement in recovery of copper and molybdenum compared with the cold fraction, except that the molybdenum recovery for the 10 minute grind time is higher in the colder fraction. By comparing data with the unprocessed material it shows that there is an improvement in molybdenum recovery in the hot fraction with the largest difference achieved through finer grinding.

Nevertheless, the copper results revealed that the shorter (coarser) grind time delivered much better improvements in recovery in the hot and medium fractions (these fractions were of interest because valuable minerals were located there) when compared with the cold fraction.

In scavenging mode (of the theoretical sorter) the hottest one third could be accepted with a recovery of more than half the metal and substantial grade improvement for copper and molybdenum for both grind times.

In pre-concentration mode (of the theoretical sorter), the coldest one third of the mass could be rejected for the loss of about 18% of the metal for the 15 minute grind time and 24% of the metal for the 10 minute grind time.

6.12 Test Procedure for the Experimental Investigation Using Two Types of Microwave Applicators - Second Step

The first step of the investigation ended with destroying samples, necessary to perform assaying analysis, in the second step of investigation samples were analysed with more of conserving techniques such as x-ray tomography and optical microscopy. New sets of particles were tested in a microwave oven and in TWA that had ability to obtain data in real time from ROI. This was used to quickly estimate heating behaviour of tested particles within the every set tested.

6.12.1 Overview of the Test Procedure

The representative sample was prepared for -22.4 + 19.0 mm size fraction. The eight new sets containing eleven particles were randomly chosen from the remaining sub-sample in this particular size fraction after preparation for the first step of experimental investigations. The detailed procedure of the ore screening and obtaining a representative sample is presented in section 6.2 in this chapter. The particles were tested for textural interaction with an electromagnetic field created in two different microwave applicators. They were subjected to batch microwave heating in the domestic multimode oven and individual testing in the TWA. The data collected from the particle's temperature profiles were combined to create two temperature curves and analyse separability.

The results of the MLA examination for the first experimental study revealed that the QZ Ohio ore contains good absorbers of microwave energy such as pyrite and chalcopyrite which are embedded in the quartz matrix (usually interlocked with biotite, feldspar and sometimes chlorite). For the majority of particles heating phases were mostly well dispersed, while for some they could be found in clusters forming a plain or vein like structure. For this reason the power applied in the second step was 1.2 kW same as in reproducibility and flotation study.

After microwave exposures, fifteen randomly chosen particles were analysed by high-resolution X-ray computed tomography which was used to obtain information about texture and structure of minerals with higher densities. These minerals were

associated with minerals which have a tendency to heat more. Five randomly chosen particles were studied in great detail by combining an automated mineral identification by optical microscopy and X-ray computed tomography to identify sulphide minerals. Surfaces for optical microscopy were prepared by cutting particles in half or removing the top part of the whole particle with the aim to primary identifies pyrite and chalcopyrite. Figure 6-25 shows locations of rock particles selected within tested sets and technique applied.

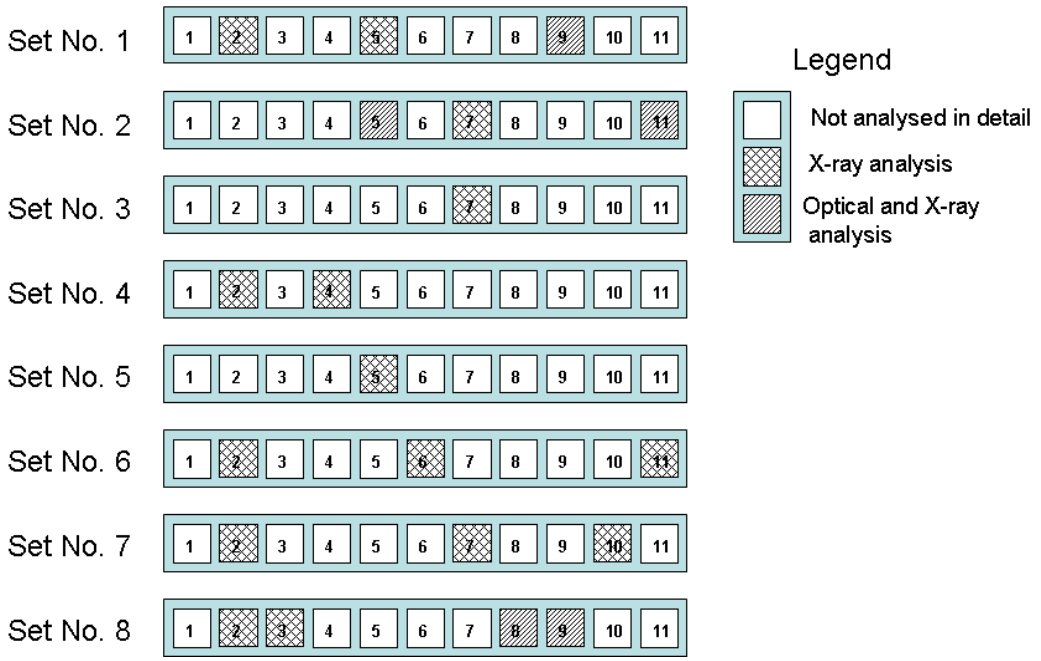

Figure 6-25 Particles randomly chosen for more detail analysis with less destructive techniques such as x-ray tomography and optical microscopy

6.12.2 Exposing "QZ Ohio" Particles to Multimode Electromagnetic Field in Microwave Oven

The batch microwave heating was carried out with the same microwave oven used in the first study. The glass microwave tray was separated into eleven sections for eleven ore particles. Those same particles were then distributed along the edges of the rotating tray in order to cover the larger area of the tray. This was done to ensure that particles have a greater chance of passing through multiple modes. During repeated exposures, particles were positioned in numbered, ascending and clockwise order. Once allocated on the edge of the tray they did not have any preferred orientation.

Each batch of ore particles was then heated four times alternating their sides with labels placing numbers “up” and numbers “down” in front of infrared camera. Before placing the tray in the oven, the infrared snapshot was taken to obtain initial temperatures of the ore particles. An applied power of 1200 W was used and after heating for 12 seconds (for the one rotation respectively of the microwave tray) the tray was taken out. The infrared snapshot of the tray was taken after 5 seconds using the CEDIP infrared camera.

6.12.3 Exposing “QZ Ohio” to Electromagnetic Field in the Travelling Wave Applicator

The individual microwave heating of ore particles was carried out by the travelling wave applicator. A detailed description of TWA is given in Chapter 3 section 3.10. All rock particles were placed in a numbered sequence from one to eleven on the vibratory feeder which can be seen in Figure 5-23 on the left side. Particles were fed one by one into the applicator. The generator was set for 1200 W with an exposure time of 12 seconds.

During testing infrared images were collected with 25 frames per second in real time. The region of interest was set to cover the whole surface of the particle holder placed in the middle of the applicator. The region of interest was introduced as a quick insight in temperature profile for every particle in real time during testing. These temperatures are calculated and plotted in time.

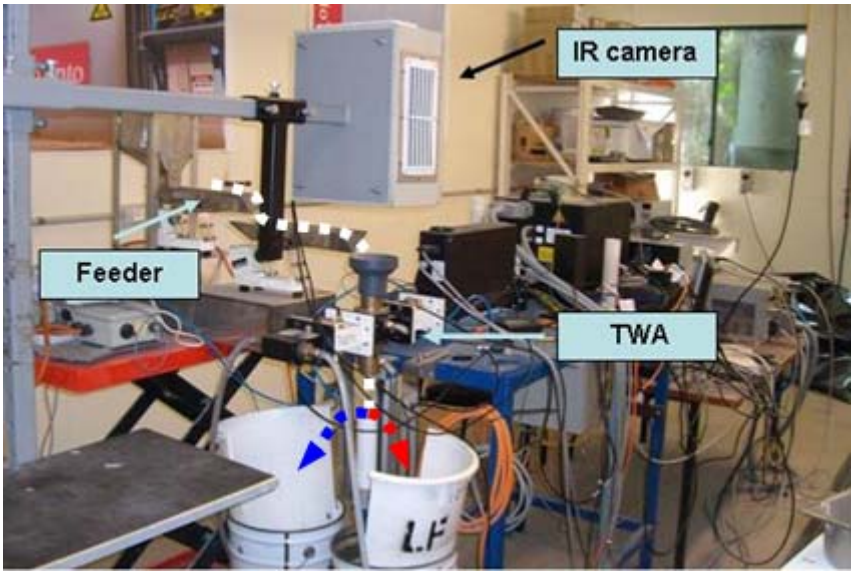

Figure 6-26 TWA used to test Low Recovery Ore

6.13 Experimental Results from Testing Rock Particles in Two Applicators

To compare experimental data, the temperature difference for maximum and mean temperatures were calculated from data before and after microwave exposure. Following abbreviations were taken to represent data:

- ΔT max = temperature difference for the maximum temperature on the surface of the particle calculated from data before microwave exposure and after microwave exposure
- ΔT mean = temperature difference for the mean temperature on the surface of the particle calculated from data before microwave exposure and after microwave exposure
- average ΔT max = mean value for ΔT max calculated from repeated exposures
- average ΔT mean = mean value for ΔT mean calculated from repeated exposures

Results from the TWA exposures are presented as a surface temperature change as a function of time. The surface temperature change was calculated from region of interest in a shape of circle set to cover the whole area of particle holder. The graphs form the three repeated exposures provide a good insight into responsive and non-responsive particles (the graphs from all repeated exposures are given in Appendix M). Finally, for every particle temperature change was calculated by placing new region of interest corresponding to the visible perimeter of the particle. These new values are compared with the values from multimode exposures as an average value from repeated testing. Temperature differences are presented in one common graph for each particle within the set.

Five randomly chosen particles were studied in great detail to identify sulphide minerals by combining a high-resolution X-ray computed tomography and an automated mineral identification by optical microscopy. IR images were studied during heating to identify selective heating and locate responsive minerals. The appropriate planes for optical microscopy were determined by cutting these particles in half in the locations where selective heating took place. The identification was focused primarily to recognize two sulphides; chalcopyrite and pyrite.

To present reconstructed data from the tomography analysis, visualisation software DataViewer ver. 1.4.4 (licensed by SkyScan) was used to view a stack of images in 2D/3D at their original range and resolution. This process enabled the texture to be seen from three different views:

- transaxial view (in the red colour, in x-y plane),
- coronal view (in the green colour, x-z plane),
- sagittal view (in the blue colour, z-y plane).

For every particle tested top left image is used to display coronal view of the selected reconstructed plane. The largest bottom left image is used to see transaxial view which is also chosen to correspond to surface analysis performed by optical microscope. In the top right corner the image of all three chosen planes through the particle can be seen, while the bottom left image is used to display sagittal view.

6.13.1 Set No. 1:

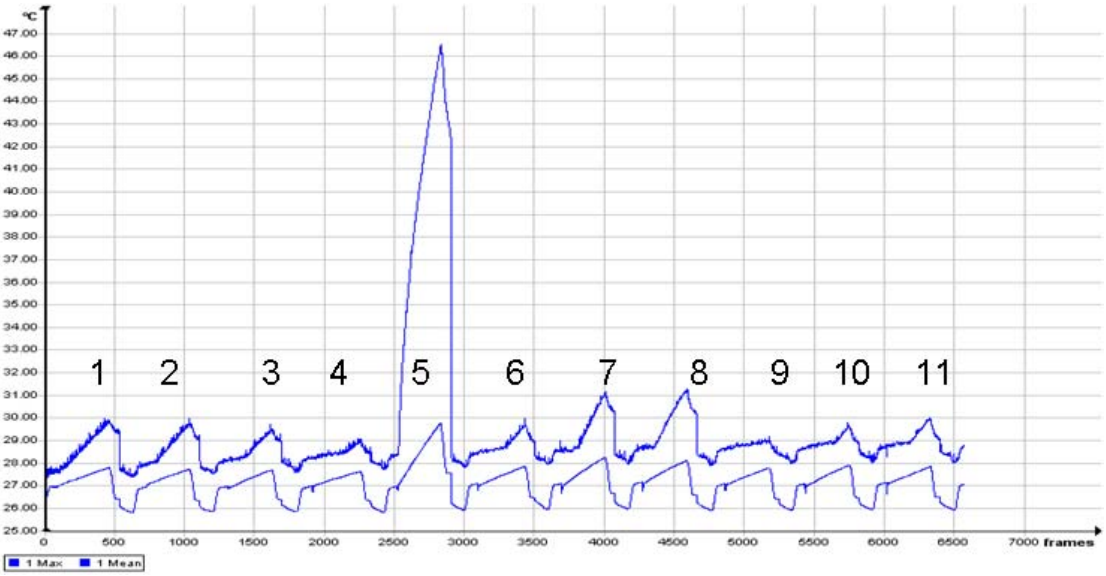

Figure 6-27 Third exposure, timing graph for set no.1

Figure 6-27 shows the temperature change from the ROI, placed to quickly obtain a heating rate from every particle exposed to microwave heating in real time (time is given in 25 frames per second). The top line represents the maximum temperature, while the bottom one represents the mean temperature, calculated from the visible surface of the particle including the background confined within the ROI. It can be

clearly seen that the change for both temperatures exhibit almost a meandering shape, produced by the increase in temperature (during microwave heating) and followed by a sudden decrease (after stopped particle heating and ejection from the holder).

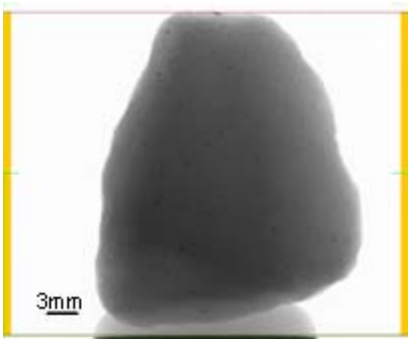

Figure 6-28 X-ray radiogram for particle No. 2

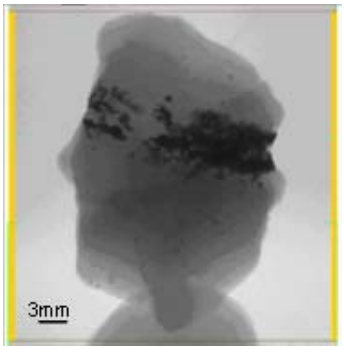

Figure 6-29 X-ray radiogram for particle No. 5

By observing all eleven peaks, specified with numbers for each particle, it can be seen that the best heating response was detected for particle No. 5. Figure 6-28 shows x-ray radiogram of particle No. 2 presenting only low density minerals (associated with quartz, biotite and feldspar) which caused a slight increase in temperature change. In Figure 6-29 x-ray radiogram for particle No. 5 clearly reveals a presence of high density minerals (associated with magnetite, pyrite and chalcopyrite). These minerals have responded well to microwave heating causing a steeper increase for mean temperature and a very sharp increase of maximum temperature reaching over 46 ^{o}C. X-ray radiograms exhibit texture and structure of these particles under different angles, and they are given in Appendix M of this chapter.

Data from all repeated exposures in a multimode domestic oven and TWA are compared and presented in Figure 6-30. As the timing graph of temperature profiles indicated the best heating response was for particle No. 5 and also had the largest standard deviation from repeated measurements in both types of applicators. The rest of the particles exhibited a slight increase in temperature change showing an absence of higher contents of microwave absorbing phases. From this set, particle No. 9 was chosen for a more detailed study. IR images were examined from TWA testing (the right image in Figure 6-31) with a goal to pinpoint locations on the surface of the particle where temperature had increased significantly, signifying the presence of more responsive minerals. From Figure 6-30 it can be seen that the particle No. 9 can be classified as “cold” or less responsive. Considering that from IR images there was no specific hot locations, it was decided to cut and polish the top of the whole particle

and in that manner prepares a larger surface for the optical microscopy analysis. Following the preparation for optical microscopy the same particle was analysed by high-resolution X-ray computed tomography.

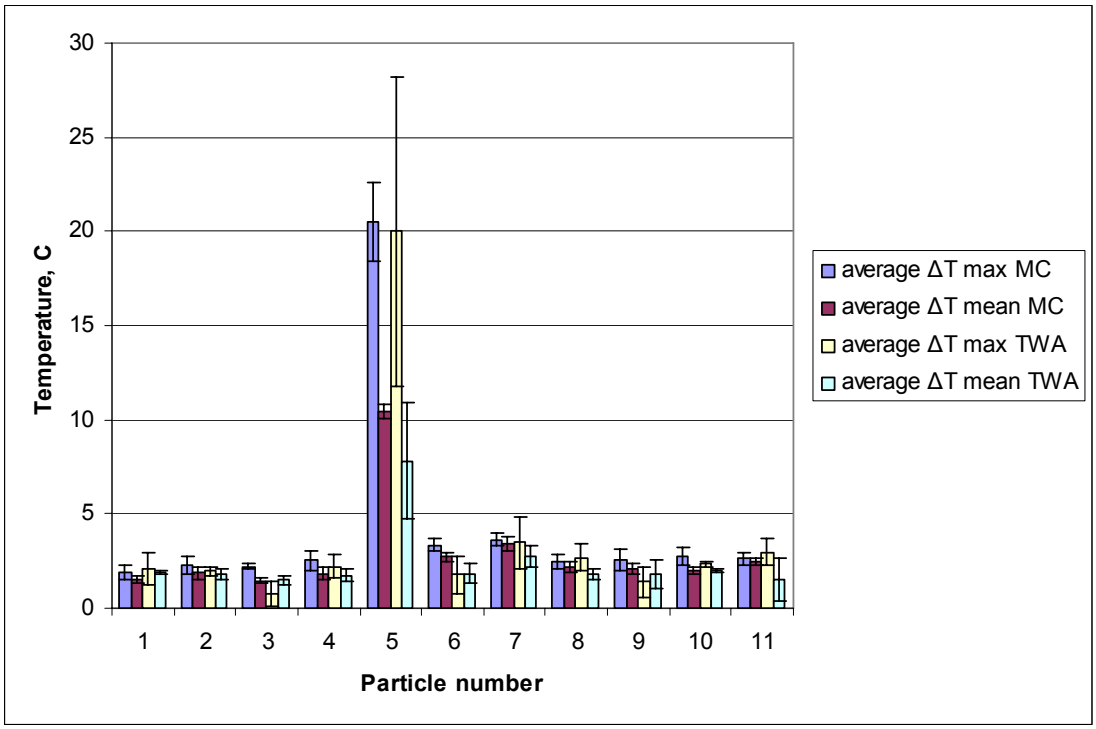

Figure 6-30 Compared results for MC and TWA for the set No.1

The reconstructed data from the tomography analysis is presented in Figure 6-32. The largest bottom left image is used to see transaxial view which is also chosen to correspond to surface analysis performed by optical microscope. The coronal view (in the top left corner) and the sagittal view (in the bottom right corner) show that there is not a presence of large grains or structures of minerals with higher densities.

The transaxial view shows mineral grains which belong to a plane situated very close to a polished top surface. If the locations of the grains were compared with results from optical microscopy (the left image in Figure 6-31) only some of them were identified as chalcopyrite, while the rest of the minerals were minerals with higher densities such as bornite, tennantite or chlorite.

All obtained results show a significant absence of heating phases and clearly explain temperature profile of this particle and why it can be considered as “cold”.

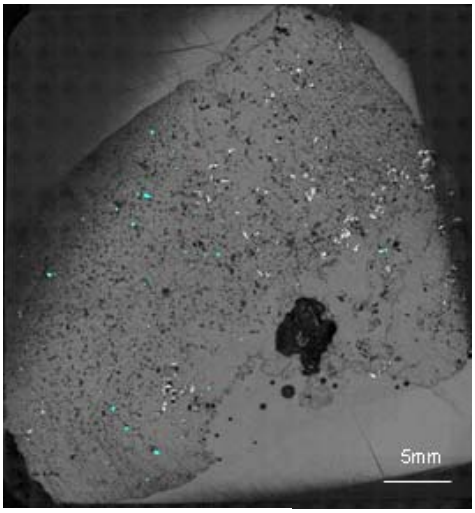

Chalcopyrite
Pyrite

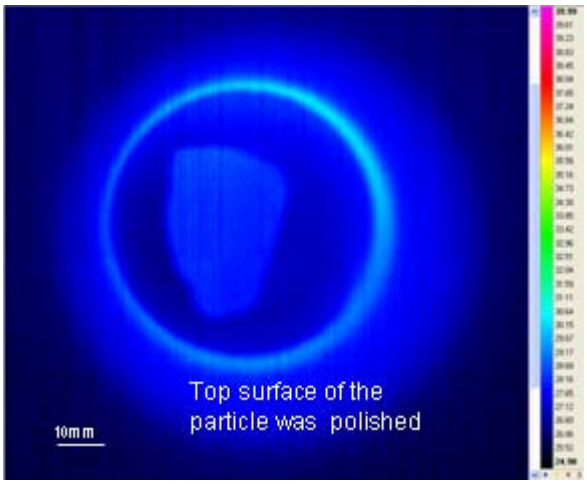

- **Scale min-max: 25°C-40 °C**
- **From third exposure at the end of 12 s since the beginning of the heating**

Figure 6-31 Optical mineral identification and IR temperature profile for particle No. 9 from the set No.1

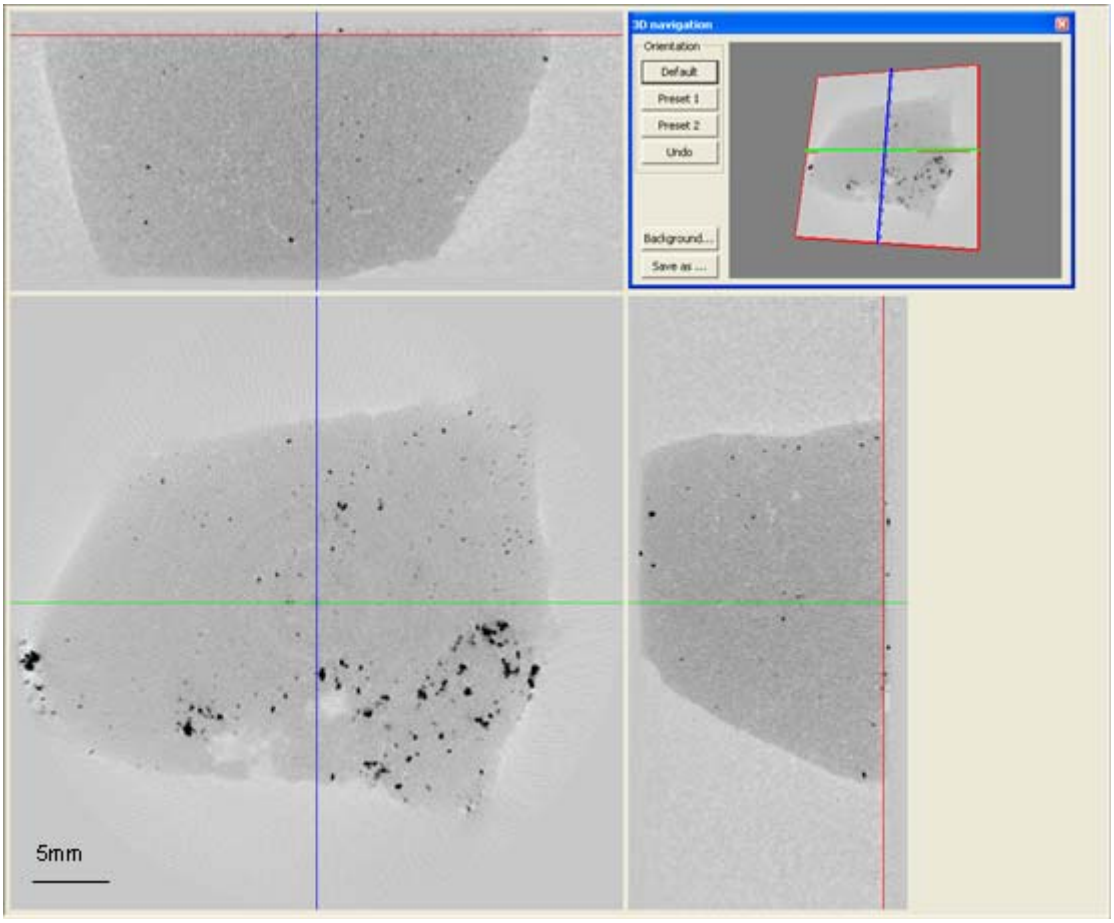

Figure 6-32 X-ray computed tomography analysis for particle No. 9 from the set No.1

6.13.2 Set No. 2:

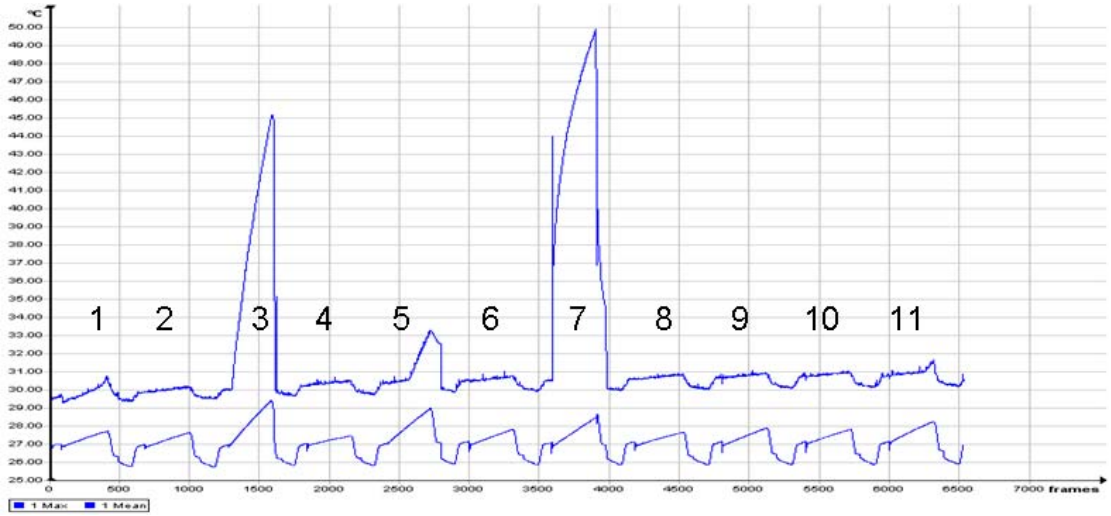

Figure 6-33 Third exposure, timing graph for set No.2

Temperature profiles from ROI for the set No.2 are given in Figure 6-33. Data for the first and the second exposure are provided in the Appendix M. Particles with No. 3, 5, and 7 can be easily identified as very responsive.

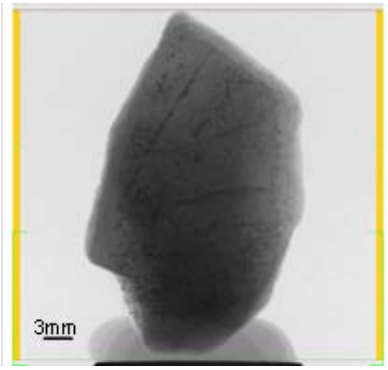

Figure 6-34 X-ray radiogram for particle No. 7

It can be seen from Figure 6-34 that particle No. 7 is interwoven with microwave responsive minerals which form couple of thin planes. One of these planes can be identified as a straight line at the left side of the particle. The other x-ray radiograms demonstrate this texture under different angles and they are provided in the Appendix M.

The presented data in Figure 6-35 for repeated exposures, shows that the particles with No. 3, 5, and 7 can be considered as “hot” because they did reach temperature difference almost three times more than the rest of the particles. It shows that for the

rest of the particles average temperature difference was about 2 ^{o}C with the exception of particle No. 11 which was almost two times higher.

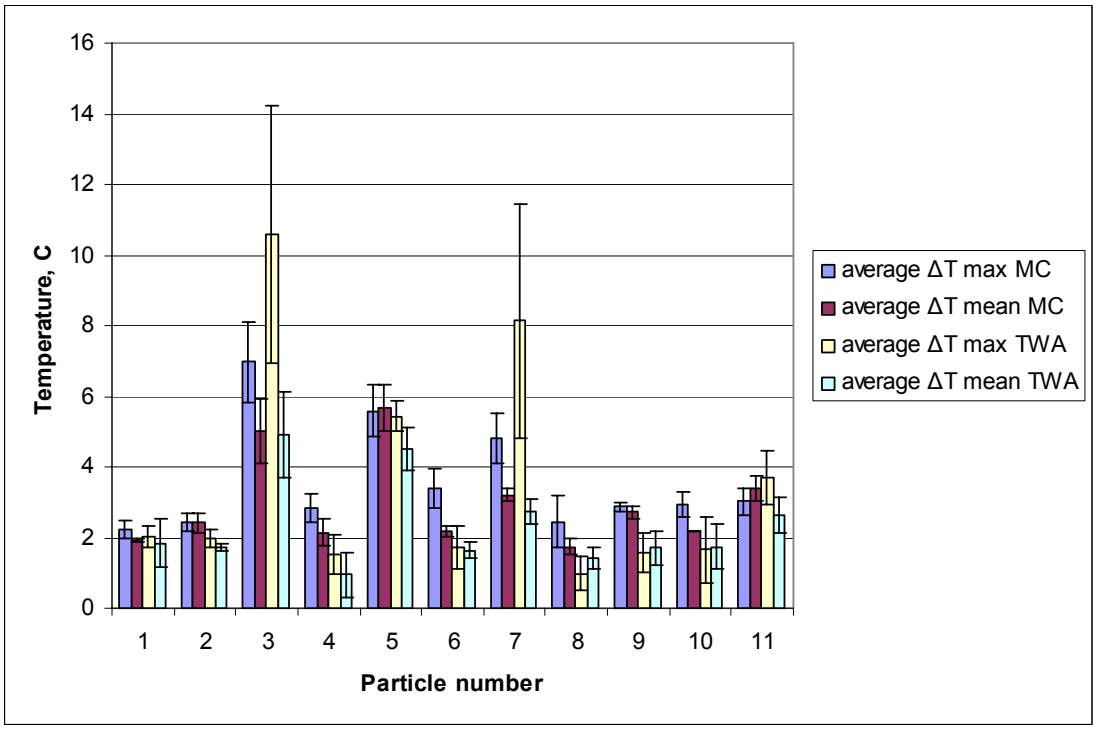

Figure 6-35 Compared results for MC and TWA for the set No. 2

Two particles were chosen for a more detailed analysis. These were particle No. 5 and particle No. 11. An IR image during heating for the particle No. 5, demonstrated results of more uniform heating during repeated exposures, although one half of the particle had higher temperature gradients then the other (as seen in the right image in Figure 6-36). The particle was cut in the middle and the chosen half was polished and prepared for optical microscope analysis (results are given the left image in Figure 6-36). The results from x-ray computed tomography showed a presence of embedded minerals of a higher density which are scattered within the matrix of lower density. When the transaxial view in Figure 6-37 was analysed along with optical results it showed that embedded minerals are identified as grains of very responsive pyrite. A similar distribution of mineral grains was identified in samples used for surface MLA analysis.

For the particle No. 11 which was also analysed in great detail, IR image revealed a spot on the surface of the particle with much higher temperature gradient identifying a

presence of microwave responsive minerals. This spot can be seen in the right image of the Figure 6-38.

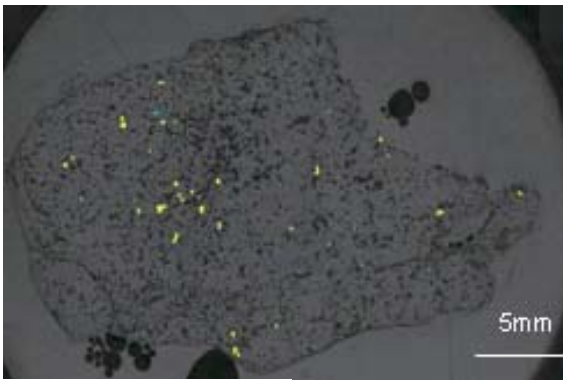

Chalcopyrite
Pyrite

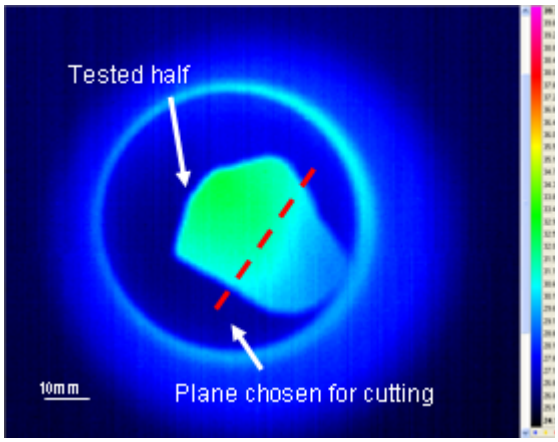

- **Scale min-max: 25°C-40 °C**
- **From third exposure at the end of 12 s since the beginning of the heating**

Figure 6-36 Optical mineral identification and IR temperature profile for particle No. 5 from the set No.2

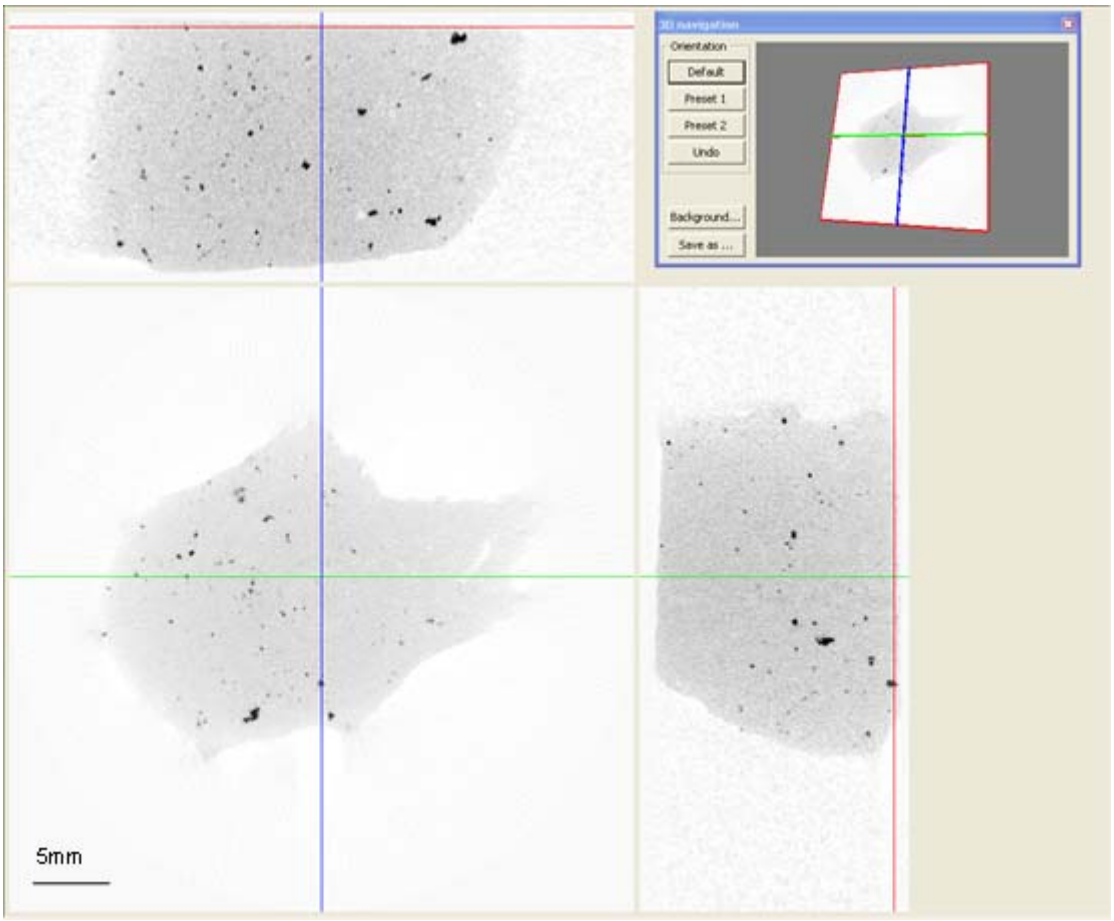

Figure 6-37 X-ray computed tomography analysis for particle No. 5 from the set No.2

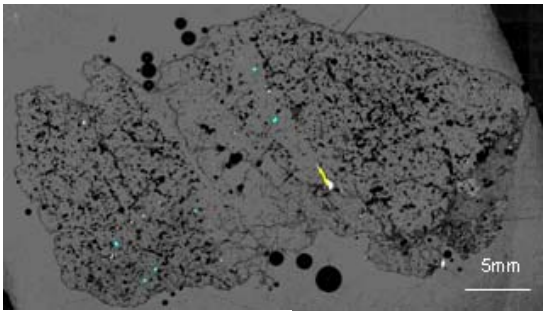

Chalcopyrite
Pyrite

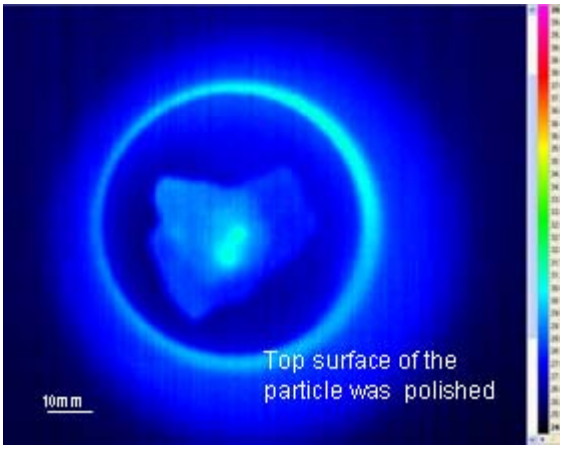

- **Scale min-max: 25°C-40 °C**
- **From third exposure at the end of 12 s since the beginning of the heating**

Figure 6-38 Optical mineral identification and IR temperature profile for particle No. 11 from the set No.2

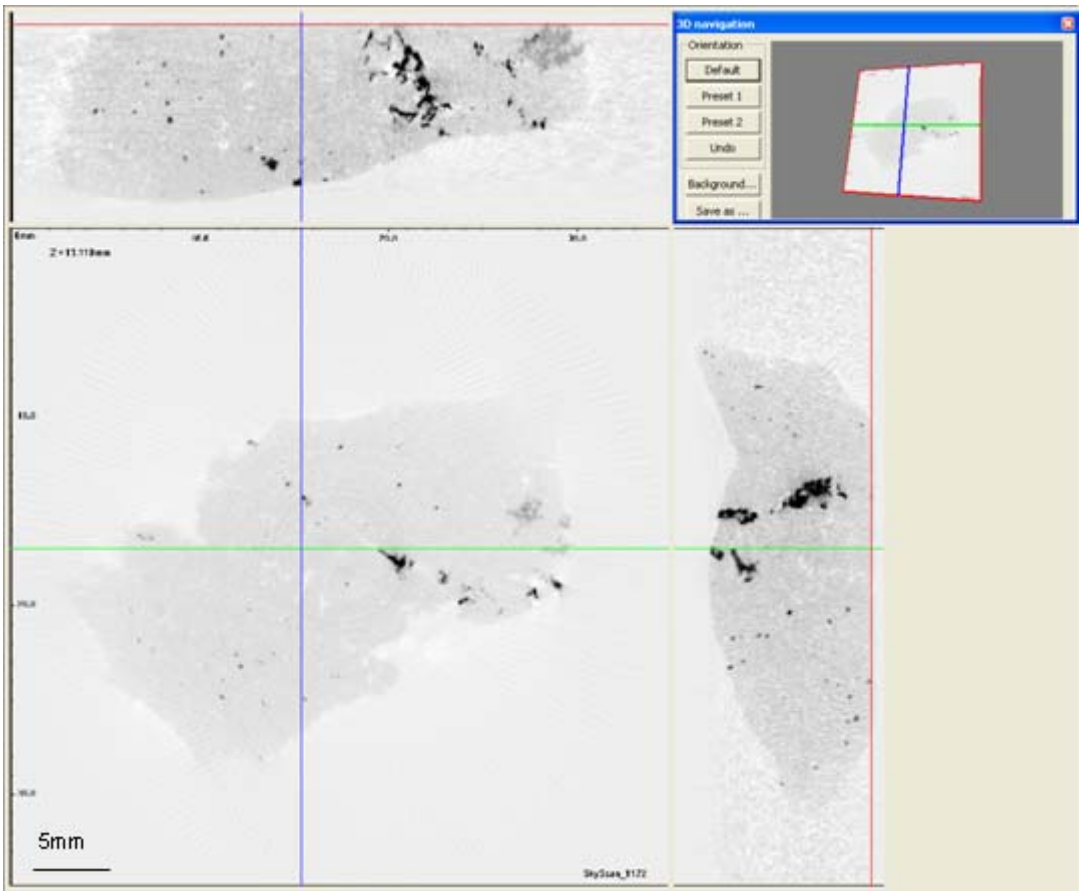

Figure 6-39 X-ray computed tomography analysis for particle No. 11 from the set No.2

To prepare particles for the mineral identification by optical microscopy, the top surface of the whole particle was removed and polished. The coronal and sagittal view after computed tomographic reconstruction (shown in Figure 6-39) displayed the presence of a very thin vein like structure embedded in the middle of the particle.

Only the top of that structure was exposed to optical microscopy identification which identified pyrite as a dominant mineral. Chalcopyrite was also identified in much smaller grains and on the larger spatial distance from the vein.

6.13.3 Set No. 3:

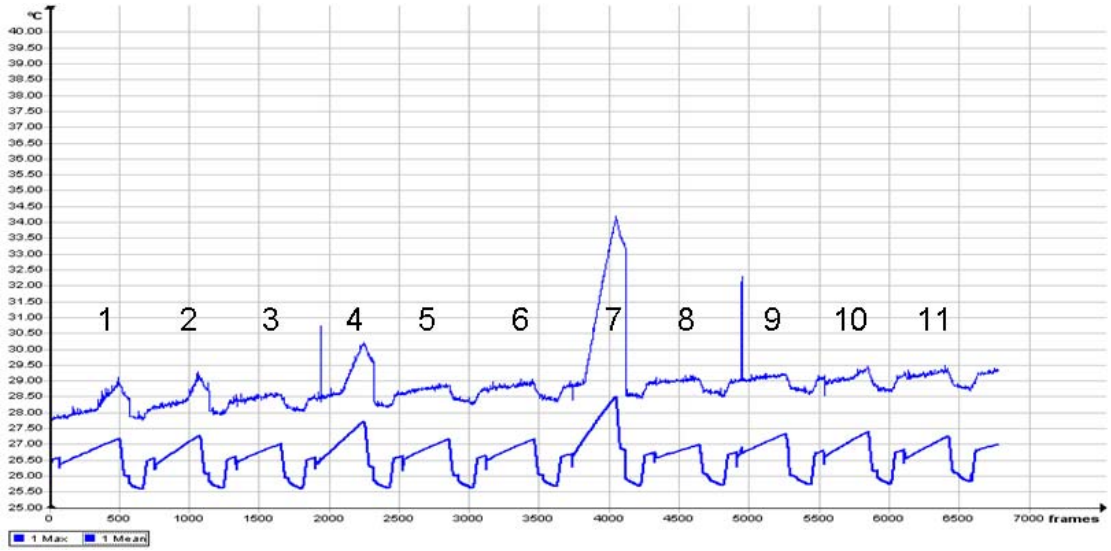

Figure 6-40 Third exposure, timing graph for set No.3

Within the tested set No. 3 it can be seen that the highest temperature change was detected with exposure of particle No.7 (observing timing graph for the maximum temperature in Figure 6-40). There was slight increase for the particle No. 4 which in addition can be seen on the timing graph for the mean temperature.

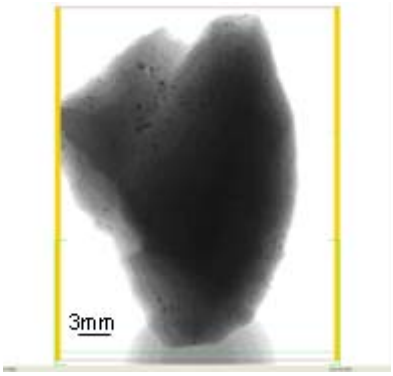

Figure 6-41 X-ray radiogram for particle No. 7

Examining textural features, from x-ray radiogram (displayed in Figure 6-41), it demonstrates that the particle No. 7 consists of dispersed grains of high density minerals similar in size and with even spatial distribution.

Exploring calculated mean values presented in Figure 6-42 it can be said that during exposure in multimode domestic oven particles had reached temperature difference in average higher than 2 ^{o}C, while in the case of TWA exposures these values were on average below 2 ^{o}C.

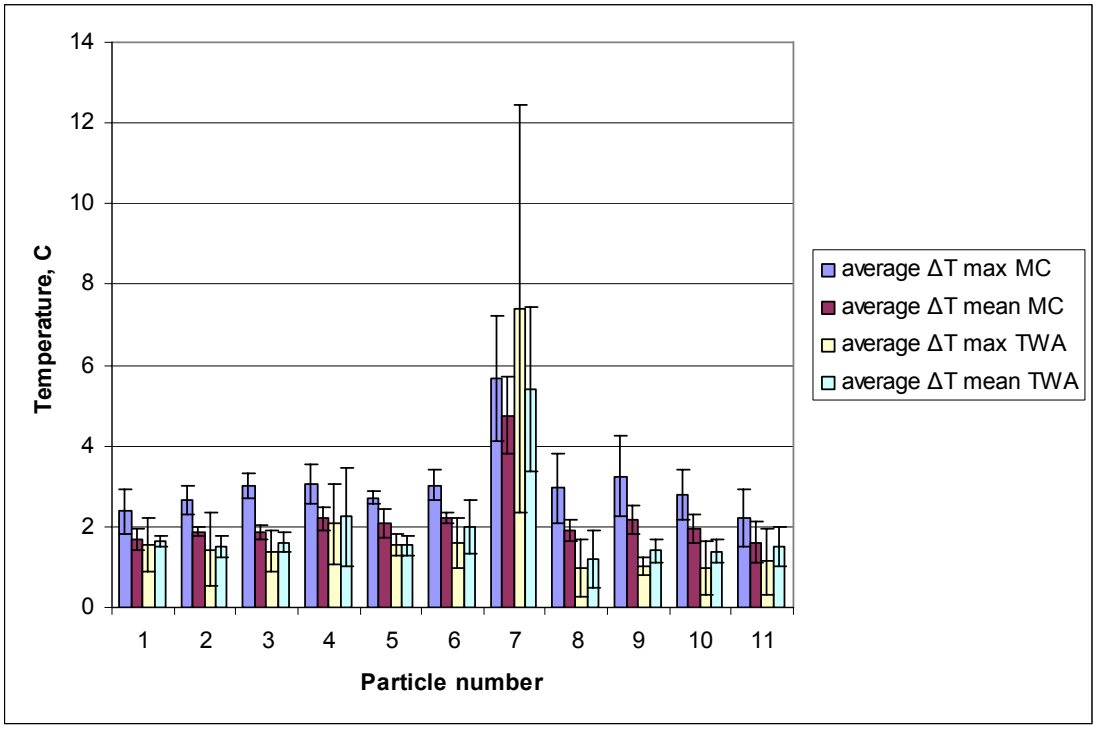

Figure 6-42 Compared results for MC and TWA for the set No. 3

6.13.4 Set No. 4:

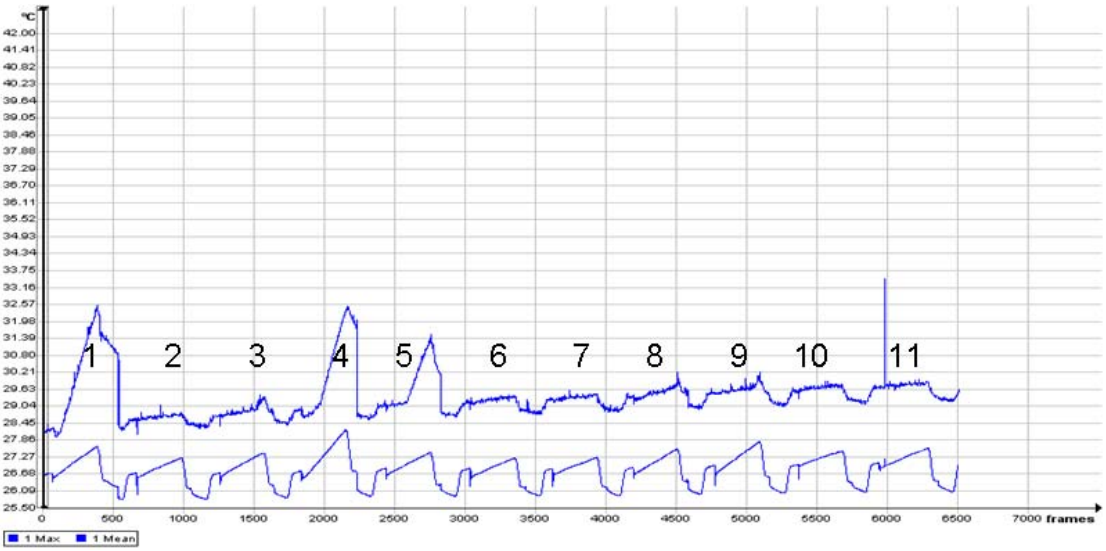

Figure 6-43 Third exposure, timing graph for set No. 4

After testing set No. 4, temperature profiles revealed an increase in max temperature in a couple of particles, although with close examination of mean temperatures it can

be seen that the best response was with particle No.4. Results from third exposure, are given in Figure 6-43.

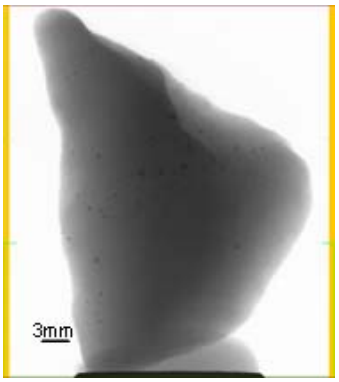

Figure 6-44 X-ray radiogram for particle No. 2

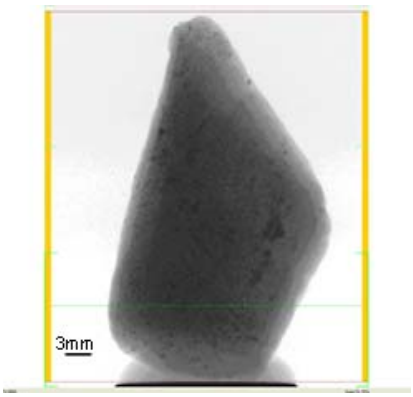

Figure 6-45 X-ray radiogram for particle No. 4

Figure 6-44 and Figure 6-45 show textural differences between particle No. 2 and particle No. 4. The first particle is completely made of low density minerals while in the second particle a presence of higher density minerals can be identified.

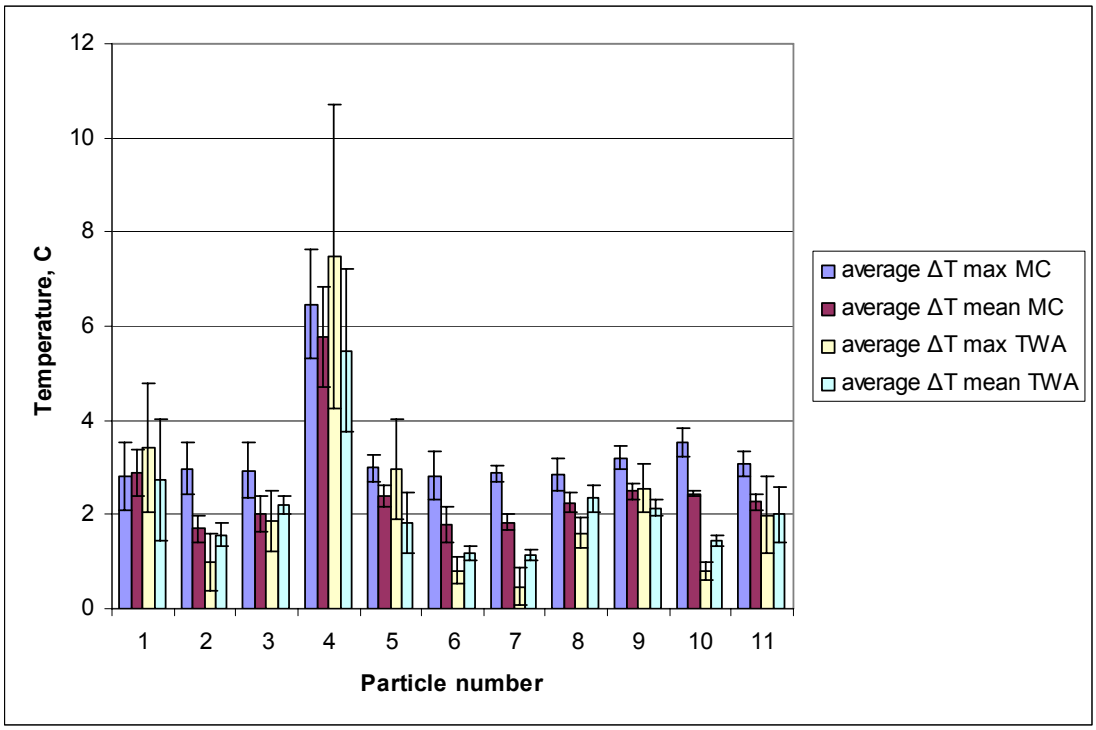

Figure 6-46 Compared results for MC and TWA for the set No. 4

By combining information from x-ray radiograms with calculated data from repeated testing in Figure 6-46 it is easy to associate a poor heating response with particle No. 2 and a good heating response with particle No. 4.

6.13.5 Set No. 5:

During repetitive testing of set No. 5 all timing graphs showed a presence of responsive particles to microwave heating. In Figure 6-47 the locations of the peaks of maximum and mean temperature from the ROI in positions 1, 5 and 10 clearly point to responsive particles.

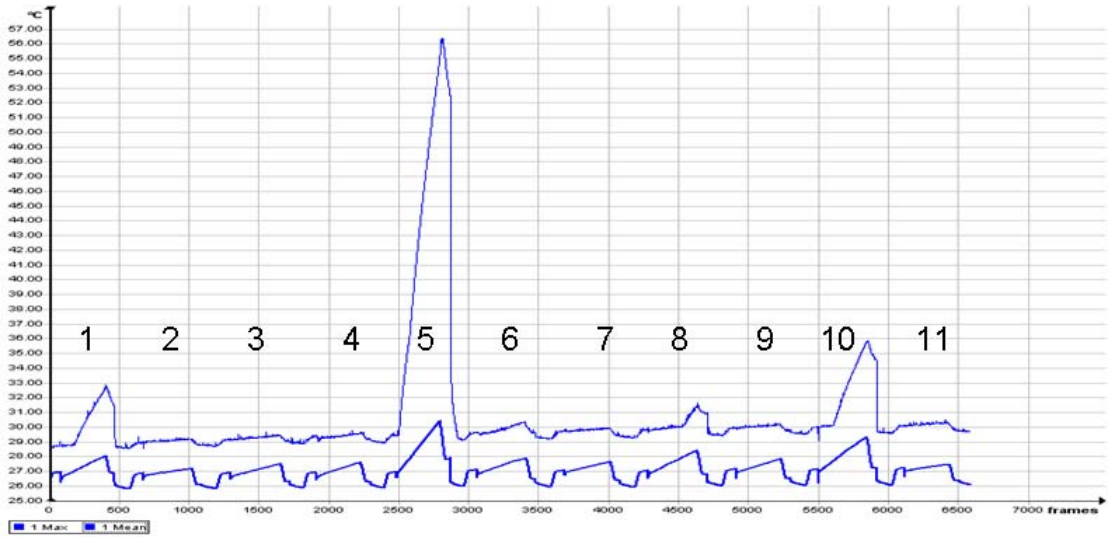

Figure 6-47 Third exposure, timing graph for set No. 5

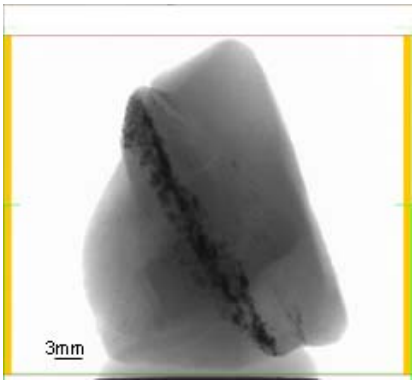

Figure 6-48 X-ray radiogram for particle No. 5

Figure 6-48 shows a high concentration of very responsive minerals within particle No. 5 which are distributed along the particular plane located almost in the middle of the particle (refer to the Appendix M for the X-ray radiograms taken under different viewing positions). The presence of this kind of structure clearly displays why particle No. 5 had such a good response.

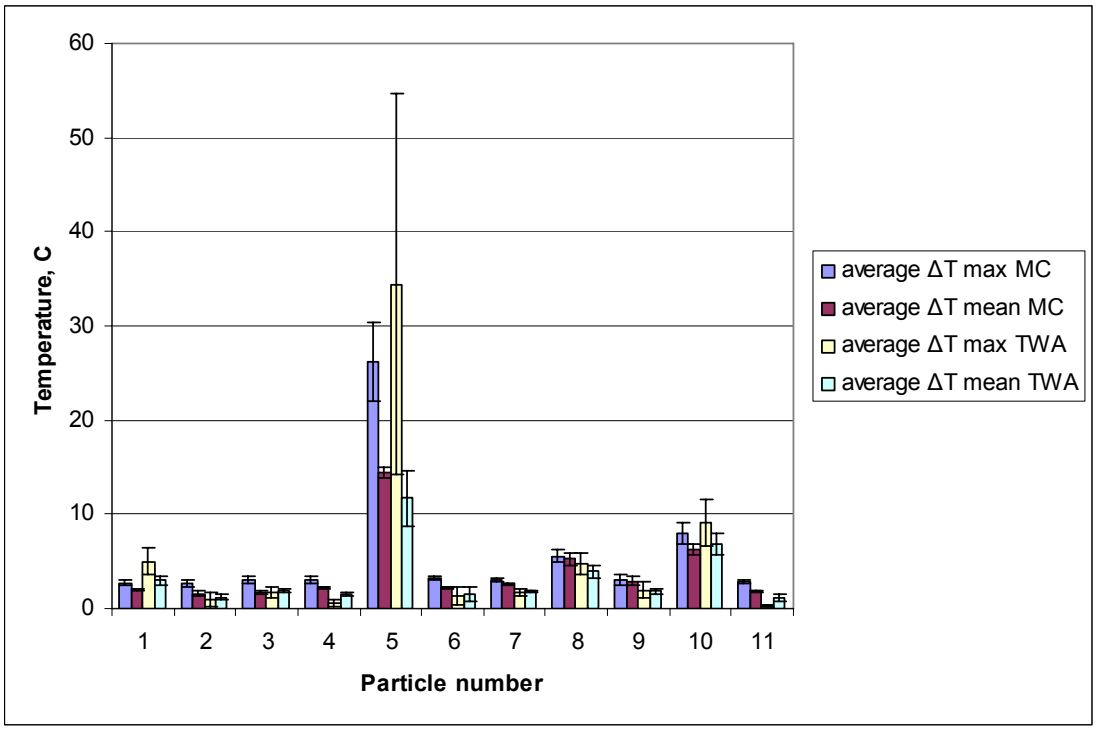

Figure 6-49 Compared results for MC and TWA for the set No. 5

In Figure 6-49 it can be seen that the average ΔT max for particle No. 5 reached 34 ^{o}C during tests with TWA and 26 ^{o}C with multimode domestic oven. These results support earlier observations about influence of texture in forming temperature profiles.

6.13.6 Set No. 6:

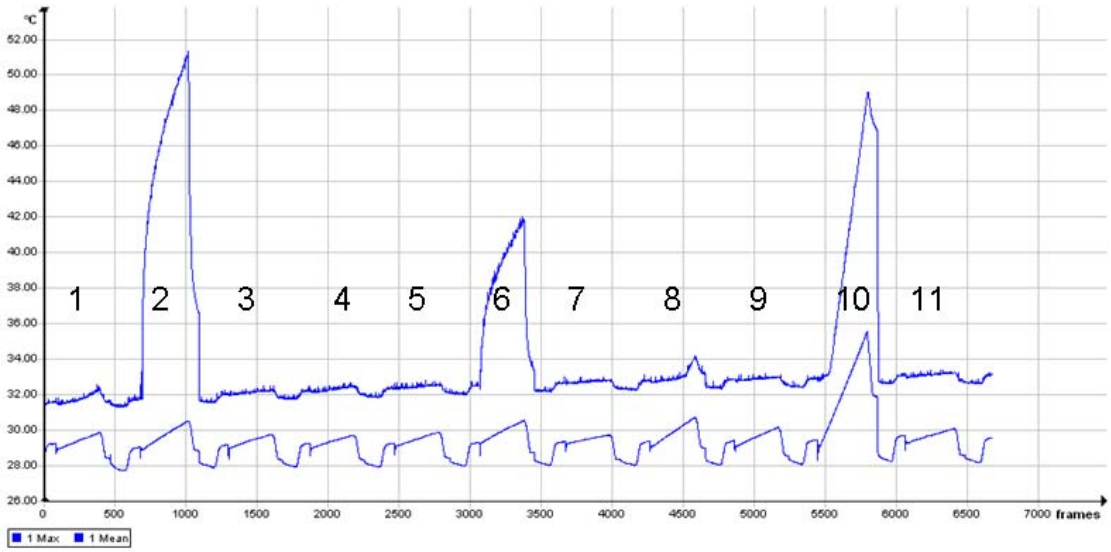

Figure 6-50 Second exposure, timing graph for set No. 6

Figure 6-50 shows quickly obtained heating rates from particles within the ROI exposed to microwave heating in real time. For this particular set, three particles were

randomly chosen for analysis using a SkyScan 1172 Cone Beam X-ray micro-tomograph.

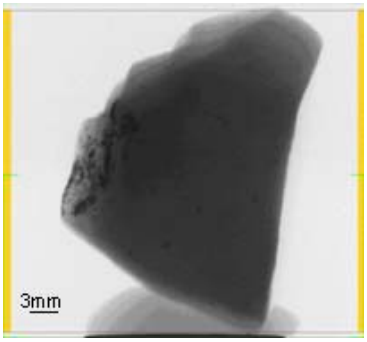

Figure 6-51 X-ray radiogram for particle No. 2

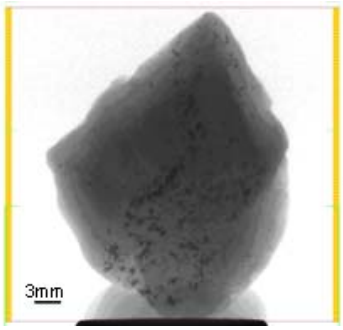

Figure 6-52 X-ray radiogram for particle No. 6

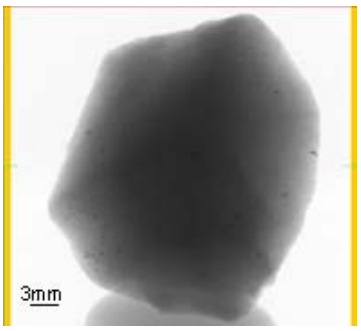

Figure 6-53 X-ray radiogram for particle No. 11

By acquiring x-ray radiograms which are given in Figure 6-51, Figure 6-52 and Figure 6-53 show that particles No. 2 and 6 have presence of mineral structures which is absent in the particle No. 11.

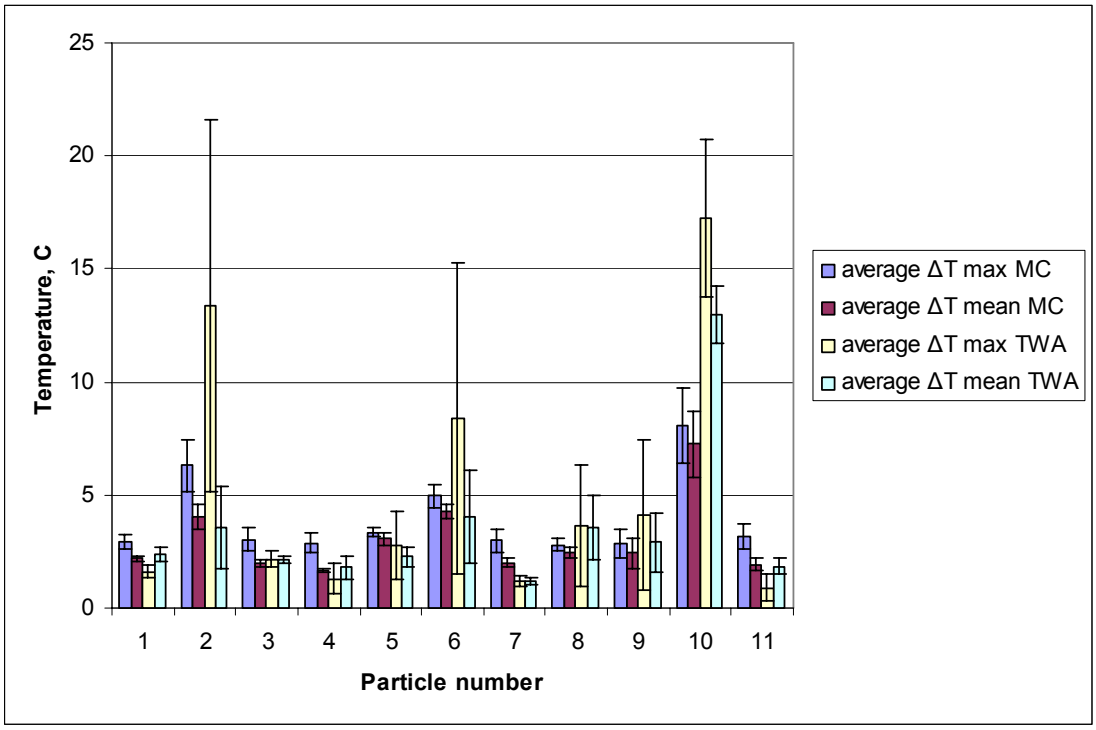

Figure 6-54 Compared results for MC and TWA for the set No. 6

The absence of higher density mineral structure inside particle No. 11 caused small temperature difference as it can be seen in Figure 6-54.

6.13.7 Set No. 7:

Individual testing of all eleven rock particles in the TWA and the heating response for set No. 7 can be assessed with the temperature graph presented in Figure 6-55.

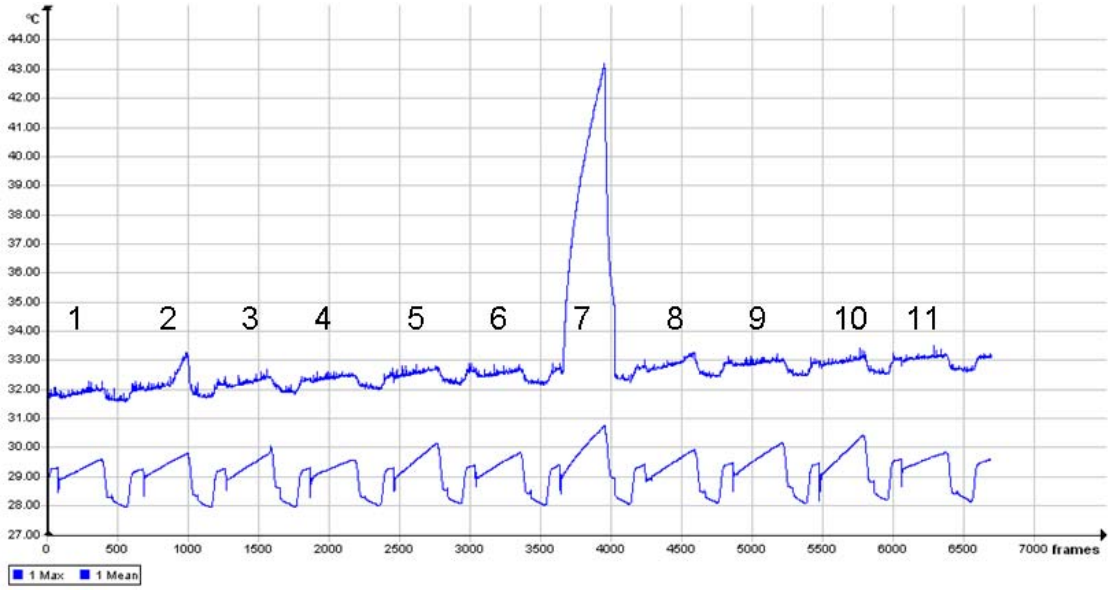

Figure 6-55 Second exposure, timing graph for set no.7

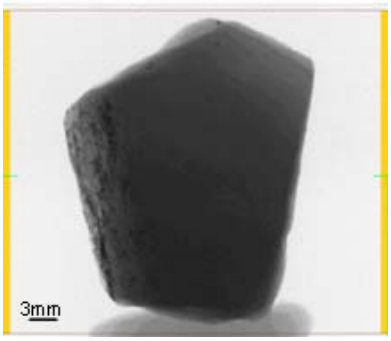

Figure 6-56 X-ray radiogram for particle No. 2

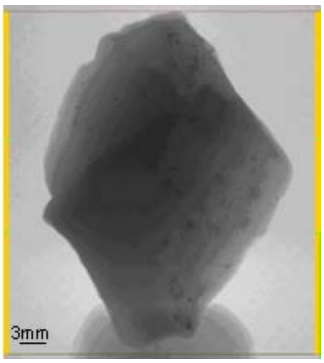

Figure 6-57X-ray radiogram for particle No. 7

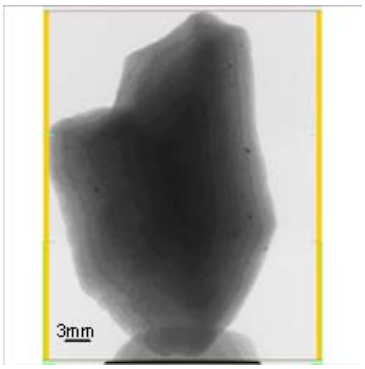

Figure 6-58 X-ray radiogram for particle No.10

As same as in the previous set, three randomly chosen particles were x-ray, and scanned to produce their radiograms, which provided information about the presence and distribution of mineral phases without destroying rock particles.

Figure 6-56 shows a strong presence of mineral structure on the one side of the particle No. 2 very close to the surface. It shows that for this particular particle and similar to this one, there will be both a favourable and unfavourable side. It depends which side falls in front of the IR detector (during the second exposure it was the unfavourable side). Particle No.7 also displayed a presence of minerals with higher density while in particle No.10 there was none.

By observing data from the Figure 6-59, particles No. 2 and 7 can be identified as "hot" within this tested set of rocks.

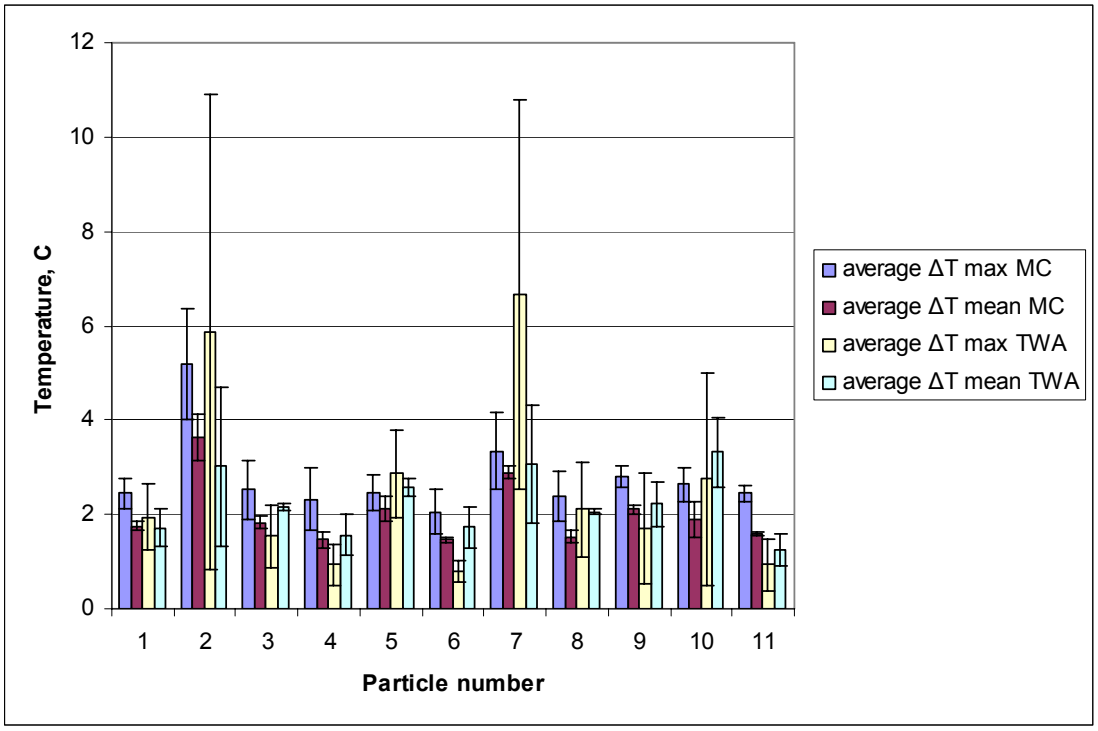

Figure 6-59 Compared results for MC and TWA for the set No. 7

6.13.8 Set No. 8:

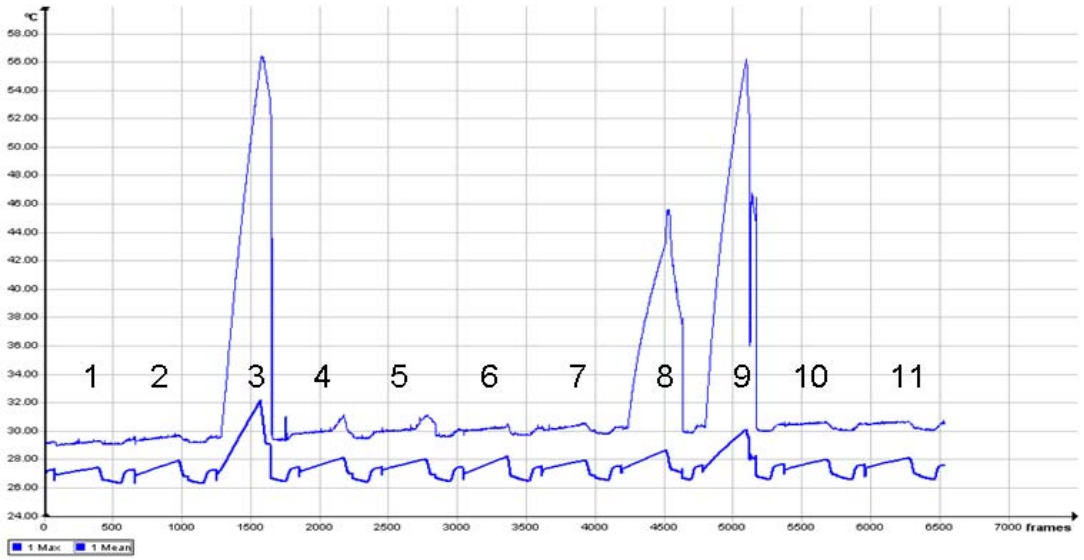

Figure 6-60 Third exposure, timing graph for set No. 8

The timing graph for the last set tested as shown in Figure 6-60. The highest temperature change was detected with exposure of particles No. 3, 8 and 9. Four particles from this set were chosen for a closer study.

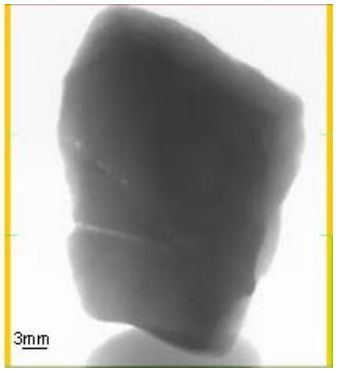

Figure 6-61 X-ray radiogram for particle No. 2

Figure 6-62 X-ray radiogram for particle No. 3

It was observed that particle No.2 is made of low density minerals shown in Figure 6-61. By examining textural features, displayed in Figure 6-62, it appears that the particle No. 3 consists of dispersed grains of high density minerals similar in size and with even spatial distribution. Following their mean temperatures after repeated microwave testing in Figure 6-63 it is easy to associate particle No.2 with "cold" and No. 3 with "hot".

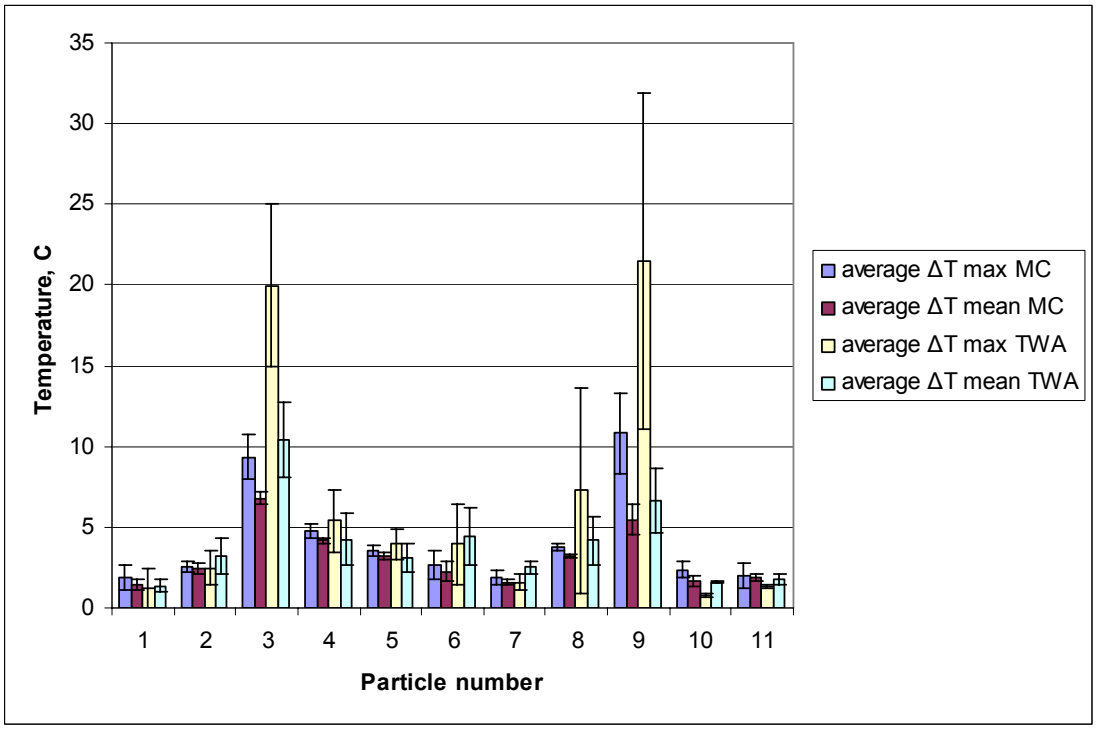

Figure 6-63 Compared results for MC and TWA for the set No. 8

The remaining chosen two were studied in greater detail. These are particle No. 8 and particle No. 9. The IR image during heating for particle No. 8 revealed a very

concentrated hot spot close to the edge of particle (as seen in the right image in Figure 6-36). In this particular IR image, the particle had fallen vertically and the hot spot was located at the left side. The particle was cut in the middle and the chosen half was polished and prepared for optical microscope analysis (results are given the left image in Figure 6-64). The transaxial view (from x-ray computed tomography presented in Figure 6-65) is analysed along with optical results and demonstrated that embedded minerals are identified as very responsive chalcopyrite. The matrix of this particular particle was also with a higher density, indicating higher content of biotite or feldspar interlocked with quartz.

For the particle No. 11 the IR image revealed a spot on the surface of the particle with a much higher temperature gradient, identifying the presence of microwave responsive minerals. This spot can be seen in the right image of the Figure 6-66. It was decided to cut the particle in the middle close to the location of the hot spot. The coronal and sagittal view after computed tomographic reconstruction (shown in Figure 6-67) displayed a presence of closely sized inclusions which are nearly connected to resemble more vein-like structure. Only the top of that structure was exposed to optical microscopy identification which identified pyrite and chalcopyrite as dominant minerals.

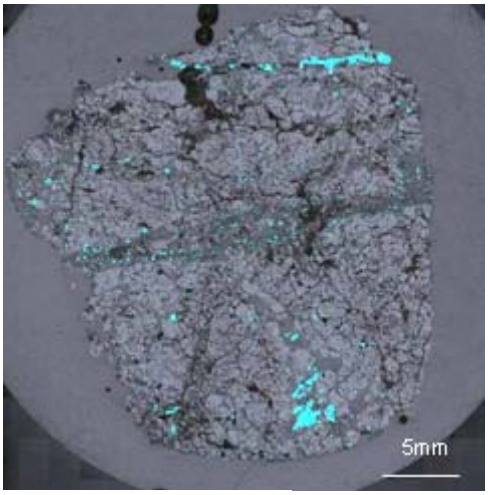

Chalcopyrite
Pyrite

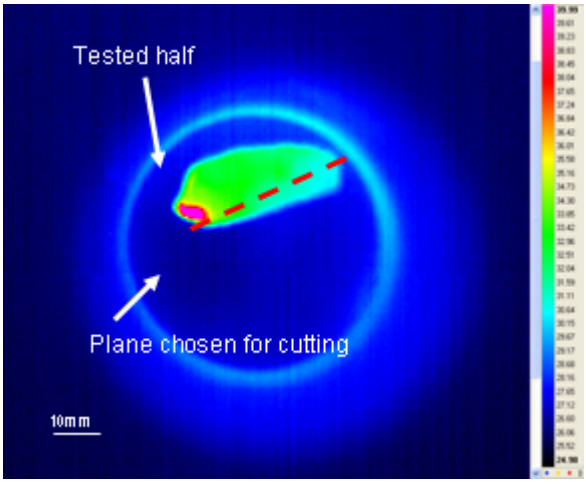

- **Scale min-max: 25°C-40 °C**
- **From third exposure at the end of 12 s since the beginning of the heating**

Figure 6-64 Optical mineral identification and IR temperature profile for particle No. 8 from the set No.8

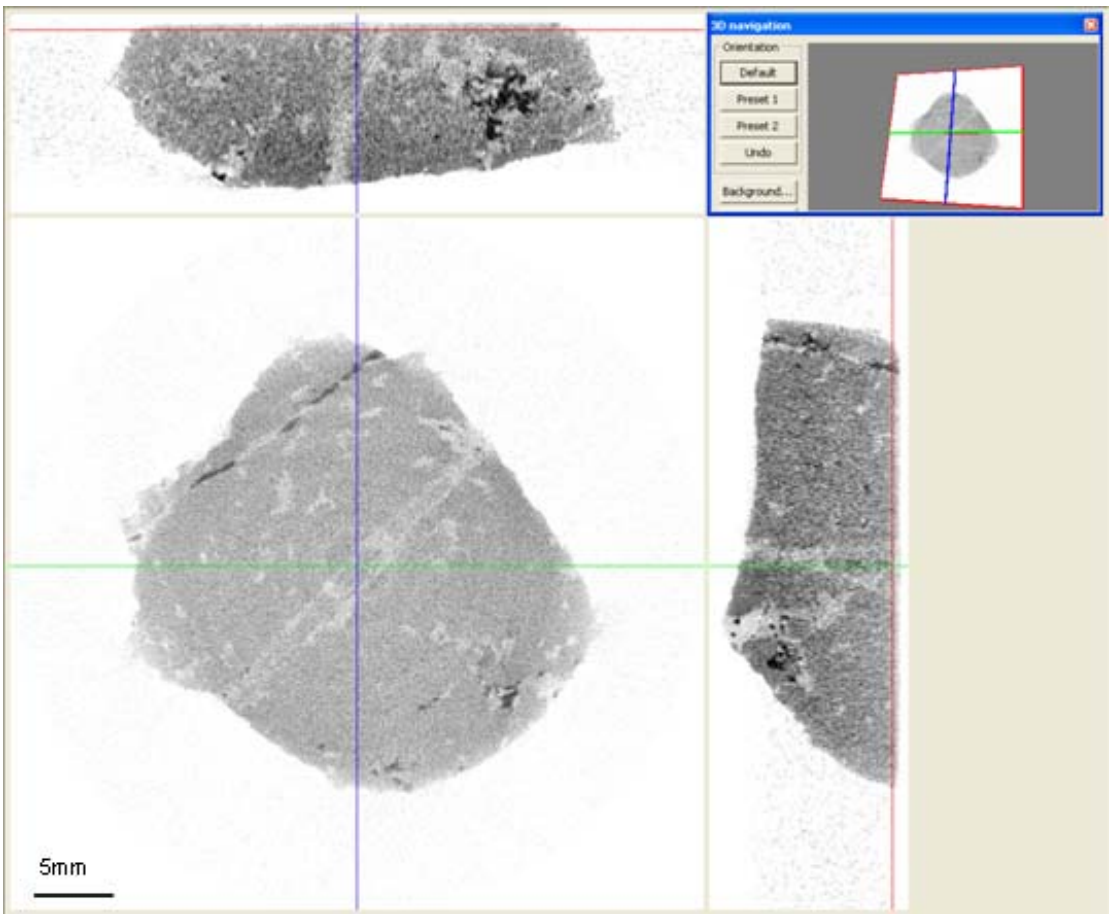

Figure 6-65 X-ray computed tomography analysis for particle No. 8 from the set No.8

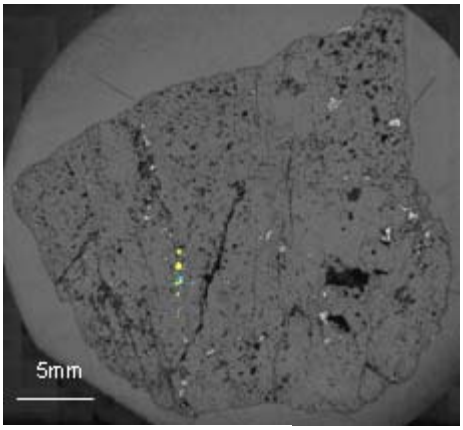

Chalcopyrite
Pyrite

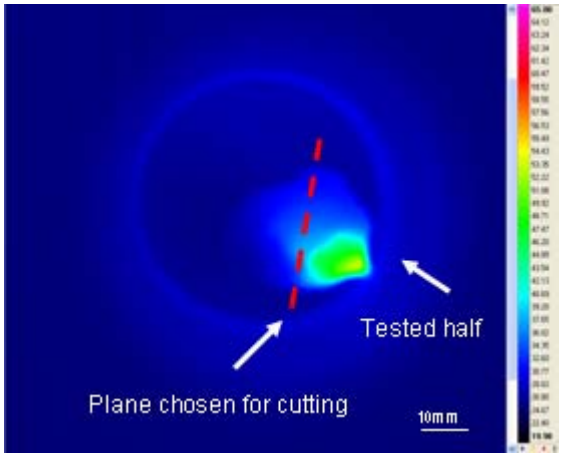

- **Scale min-max: 20°C-65 °C**
- **From third exposure at the end of 12 s since the beginning of the heating**

Figure 6-66 Optical mineral identification and IR temperature profile for particle No. 9 from the set No.8

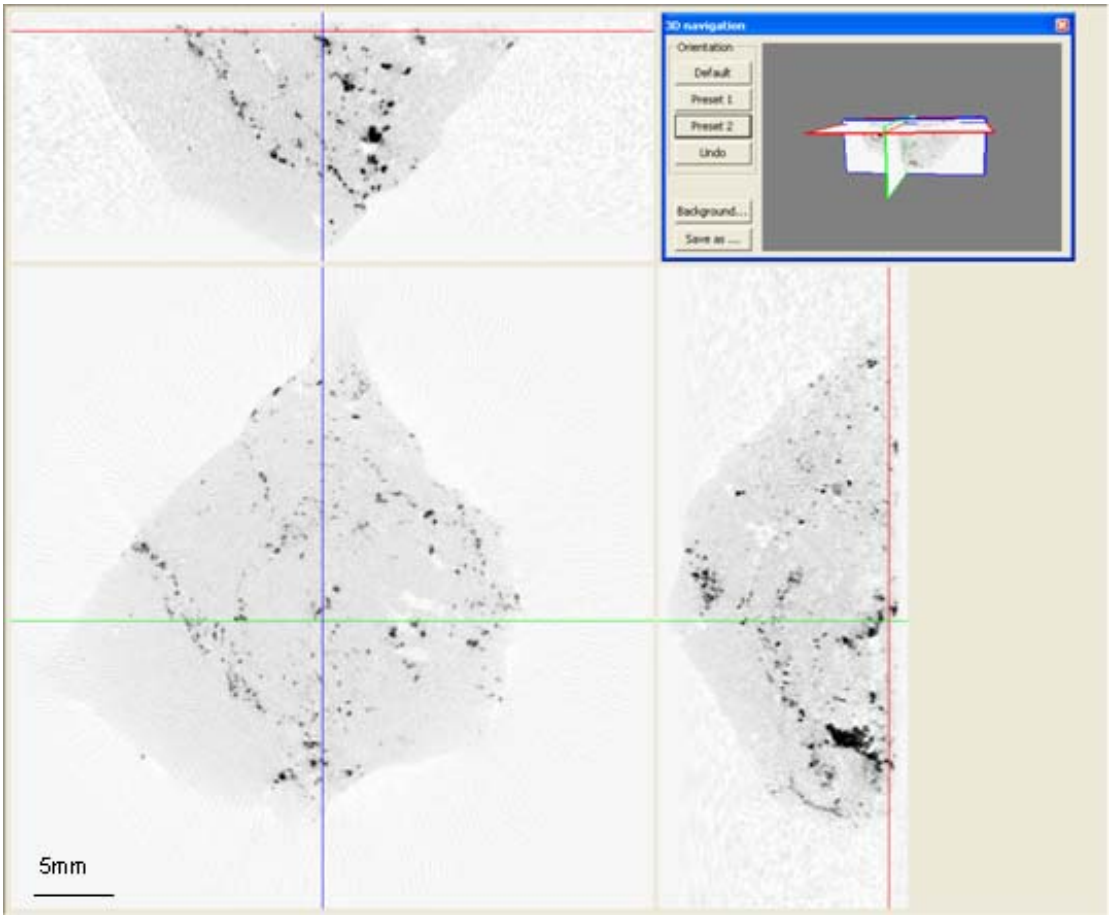

Figure 6-67 X-ray computed tomography analysis for particle No. 9 from the set No.8

6.14 Summary

After analysing eight sets under the same conditions, repetitive testing revealed similar results to the reproducibility study. The "cold" particles had undergone to a

slight increase in temperature while "hot" had a much greater temperature difference. This behaviour was also confirmed by observing a change of the surface temperature in real time. A sharp increase in temperature was associated with the presence of microwave responsive minerals. These minerals were additionally identified by data from x-ray tomography and optical microscopy.

6.15 Determining a Temperature Threshold for the "Hot" Ore Particles

The term "hot" is used to describe very responsive ore particles which have a high content of mineral phases which can be easily heated by microwave energy. A similar outcome was achieved through experimental testing with synthetic samples presented in Chapter 4**.** The synthetic particles with created and well defined mineral textures had noticeably a higher maximum and mean temperature difference compared to the rest of the particles which were created to resemble barren rock particles. From the results obtained it was confirmed that the temperature difference is strongly dependent upon the texture of the heating mineral phases and their proximity to the surface of the particle.

To determine temperature threshold for the "hot" ore particles the best case scenario was used. This case was defined for the highest energy transfer reached in all repeated microwave exposures and the ΔT mean measured from the surface closest to the heating minerals. In other words, the particle was coupled at that time to receive the best power transfer during exposure while also having the most favourable orientation of the surface for the infrared temperature measurement. Maximum from all repeated exposures for ΔT mean was calculated and plotted with cumulative mass. This was carried out for both applicators as displayed in Figure 5-66.

The barren ore particles were heated much more during multimode exposures. The better heating response was achieved when the ore particles were heated up in the group which increased overall volume of the load. During individual testing of the particles with the TWA, which was designed to respond to reflected power from introduced external influence, absence of the heating mineral phase caused a lower heating response.

The ore particles which had a responsive mineral phase were able to absorb more of applied power. This was caused by higher reflected power from the same ore particles, which was used by the TWA to achieve better coupling with automatic tuning. Eventually this resulted in a much higher heating temperature difference which was used as a strong indication of the mineral texture present.

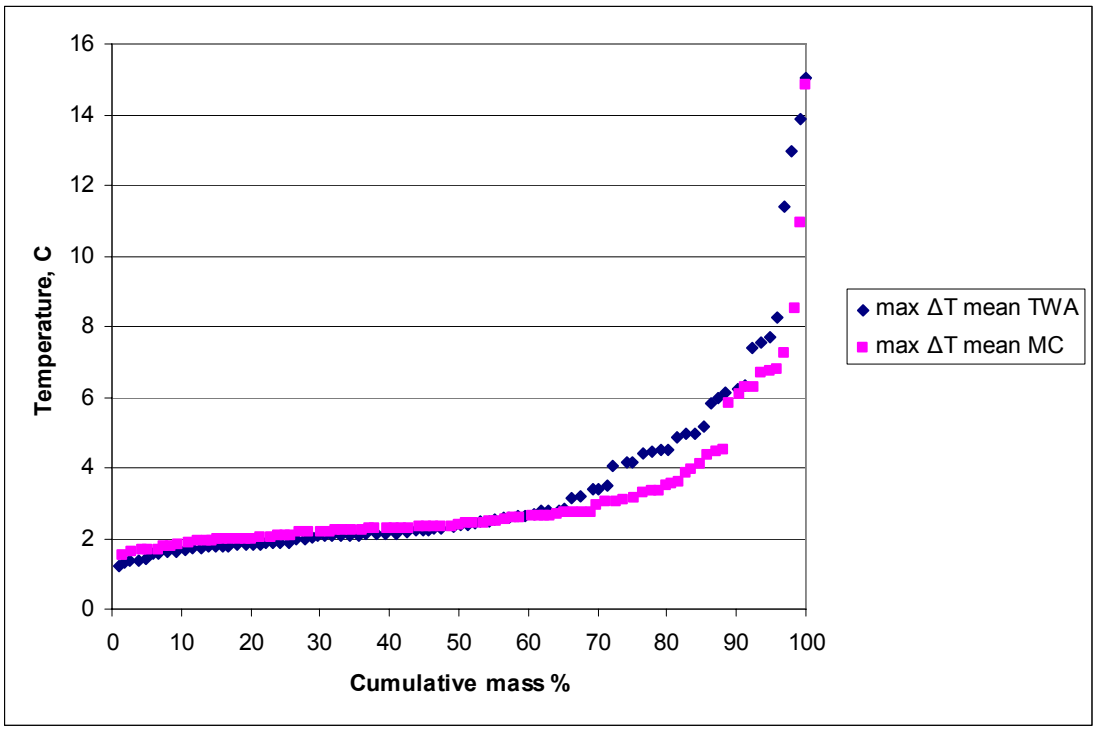

Figure 6-68 Temperature threshold for the "hot" ore particles from the QZ Ohio

From these two exposures the temperature threshold which is defined by bulk properties of barren ore particles can be determined as shown Figure 6-68. It can be considered as a base line for the surface temperature variability caused by the matrix material and at the same time points to the beginning for the scavenging process. The particles which reach higher temperatures indicate the presence of mineral phases within the matrix material as an additional heating source.

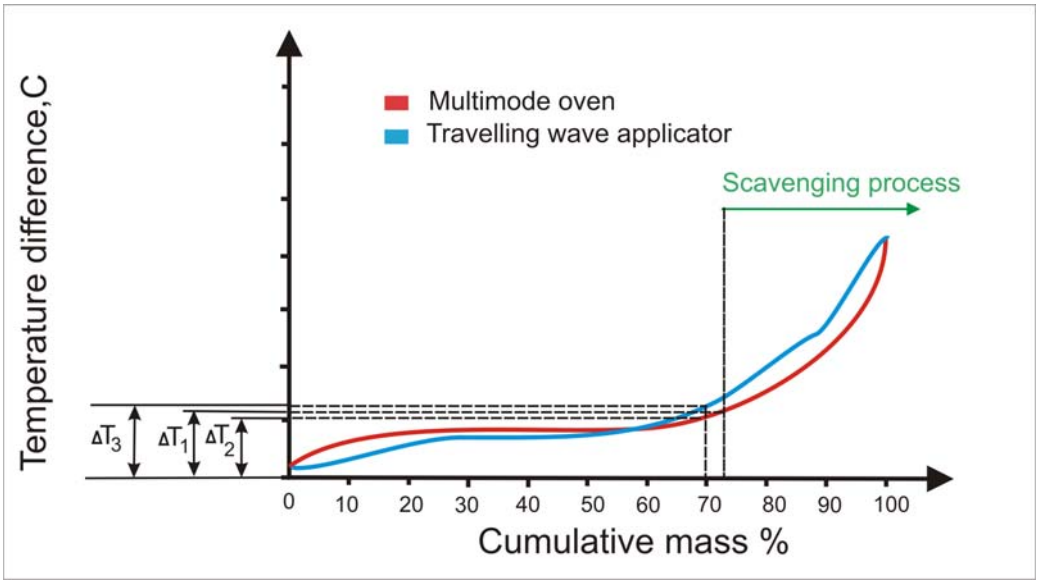

Figure 6-69 Determining temperature threshold for the "hot" ore particles

For this particular ore type the target of the scavenging process is to identify and select "hot" particles. To achieve that, a minimum of 30% of the feed mass will have to be selected to be economically justifiable. The temperature threshold was obtained as a highest temperature change closest to the predetermined mass percentage for the sorting in multimode oven. In Figure 6-69 , ΔT_2.represents this threshold and for the value of ΔT_2=2.96^{o}C, 30.17% of the feed mass can be rejected. For the same percentage temperature threshold using TWA, will be ΔT_3=3.37 ^{o}C.

The temperature threshold ΔT_1 has to be calculated only from the particles which were hot during testing in both types of microwave applicators. For this laboratory testing identification of "hot" particles was achieved by sorting particles within ΔT_2 threshold by their max ΔT mean. Data before sorting and after sorting can be found in Appendix M. The overlapping "hot" particles in both types of cavities are shown in Table 6-13.

By implementing the percentage for the overlapping hot particles from the TWA cavity on the 30.17% of the feed mass, new experimental value for the temperature threshold can be determined as ΔT_1=3.12^{o}C for the 24.58% of the feed mass.

Table 6-13 Overlapping particles in both types of cavities

Set number	Multimode cavity (particle No.)	TWA (particle No.)	Number of overlapping particles
1	5, 6, 7	5, 7	2
2	3, 5, 7, 9, 11	3, 5	2
3	7	4, 7	1
4	1, 4	1, 4	2
5	5, 8, 9, 10	1, 5, 8, 10	3
6	2, 6, 9, 10	2, 6, 8, 9, 10	4
7	2, 7	2, 7, 10	2
8	3, 4, 5, 6, 8, 9	2, 3, 4, 5, 6, 8, 9	6
Overall No. of the particles in 30% of mass	28	27	22
% overlapping from the group	78.57	81.48	

6.16 Summary

The results of controlled laboratory testing on the eight sets of rocks clearly demonstrated that combining temperature curves from microwave exposure in two applicators can be used to set a threshold for the scavenging process. The results also demonstrated that majority of the tested particles (about 60%) exhibited a slight increase in temperature change, which is in agreement with experimental results from the first step of experimental investigations.

General Summary for Low Grade Quartzite Ore – QZ OHIO (16)

To address the goal from the beginning of this chapter, which is to detect rock fragments with minerals which interact with microwaves, low grade quartzite ore "QZ Ohio" was tested in two steps. The first step involved MLA analysis, repeatability and separability testing followed by flotation testing. The major findings from the first step of investigation can be summarised as follows:

The results of the ore modal mineralogy presented through MLA investigation show that the QZ Ohio ore contains the presence of good absorbers of microwave energy such as magnetite, pyrite and chalcopyrite. These minerals are usually dispersed within the matrix made of a very large content of quartz interlocked with biotite, feldspar and sometimes chlorite. The presence of mineral grains (mostly chalcopyrite and pyrite) larger than 200 μm is detected. In some tested samples clustered grain forms of chalcopyrite are present in several different locations.

The repeatability investigation clearly demonstrated that the existence of very uniform and very transparent matrix (which was tested in this case of QZ Ohio ore type) had an effect of increasing repeatability. Particles which had responsive minerals were easily reheated and reached similar temperatures which caused lower values of standard deviation and at the same time contributed to the repeatability of microwave heating of the overall population.

With temperature separation curves, an ideal separation could scavenge 30% of the mass with a gain of 50% of the copper for the Delta Max T temperature change above 2.6 ^{o}C. The baselines for both metals of economic interest are at mineralised waste (values for the bulk properties in the obtained ore type 0.25% for Cu and 1000ppm for Mo) which would probably be stockpiled and not processed. However, the sorted products would be above a notional cut-off grade of 0.35% Cu and could contribute to metal production.

The flotation performance of both the hot and medium products is improved in line with the grade improvement. Two grinding times used were 10 and 15 min. The

copper results clearly show that the shorter (coarser) grind time delivers much better improvements in recovery in the hot and medium fractions (these fractions are of interest because the valuable minerals are located there) when compared with the cold fraction.

In the second step of the investigation the data collected was used to discuss natural separability as a function of mineral texture which causes selective heating. The results of controlled laboratory testing also clearly demonstrated that combining temperature curves from microwave exposure in two applicators it can be used to set a threshold for the scavenging process without destroying rock particles. For the temperature threshold $\Delta T_1=3.12^oC$ (determined from mineral texture as in contrast to assayed metal content) 24.58% of the feed mass can be selected having a mineral texture which causes selective heating.

Chapter 7- Conclusions and Recommendations for Future Work

7.1 Introduction

Research developments in the last two decades have highlighted the potential for microwave heating to provide an important step change in ore processing. Microwave selective heating used for sorting is still however, not used commercially in the mining and mineral industry and it belongs to a class of technologies which are still under new development and evaluation. This thesis investigates the conditions under which this process is technically effective and can potentially move to the next stage.

A detailed investigation was conducted to understand the reasons for selective heating of ore particles and how infrared sensing can be used as an identification technique to discriminate particles. In this research, it is hypothesized that: "*The texture in addition to composition of minerals within ore particles, especially microwave absorbing minerals, has a significant effect on the creation of the temperature profiles which are used to evaluate selectivity and potential for the mineral sorting.*" To test the hypothesis, significant sets of experiments were conducted to investigate in detail factors such as: particle shape and proportion, mineral composition and most importantly the textures of the minerals which have tendency to heat quickly when exposed to microwave energy. In the earlier reviewed studies, (including the study for this thesis), it was found that copper sulphide bearing minerals respond well to microwave heating. If these minerals are present in ore particles with less responsive

gangue minerals (such as quartz, feldspar and calcite) the overall surface temperature will increase enabling their identification with infrared detection. The sorting of microwave responsive minerals from two types of complex ores from Bingham Canyon Mine gave very promising results. The main findings and derived conclusions of this research are summarised in the following section.

7.2 Major Findings and Conclusions

Findings from synthetic particle analysis

In this part of the study the effects of different factors on microwave heating of ore particles were considered. These include the influences of dielectric and thermal properties of minerals, applied power, and textural features such as absorbent phase grain size and absorbent phase dissemination. The aim of this part of the study was to better understand the influences of these factors on the heating rates and temperature profiles of the ore particles. For this purpose the synthetic ore particles with defined shapes and known properties were engineered and tested. The resonant cavity used for heating, proved to be suitable to measure bulk dielectric properties of synthetic rock particles. The difference in dielectric properties between synthetic samples (cubes) used as tracers and the samples without minerals was easily measured.

The results showed that barren synthetic particles had better heating response when they were heated up in a group with other particles, which increased the overall volume of the load during exposure in a multimode cavity. In addition, individual testing with a TWA (which was designed to respond to reflected power from introduced external influence) showed that an absence of a heating mineral phase caused lower heating response. The synthetic particles which had responsive mineral phase were able to absorb more power during individual testing with a TWA because of better coupling and therefore power transfer during their testing. Eventually, this resulted in a much higher heating temperature difference compared to exposure in a multimode oven which can then be used as a strong indication of present mineral texture.

By comparing data from both exposures, it can be concluded that synthetic particles with created mineral textures had noticeably higher maximum and mean temperature differences on their measured surfaces. They were compared with the rest of the particles which were created to resemble barren rock particles. These results lead to the conclusion that by exposing synthetic particles in these two different applicators it is possible to set a temperature threshold which is defined by bulk properties of barren synthetic particles. This temperature threshold can be considered as a base line for the surface temperature variability caused by the matrix material (in the case of ore particles variability caused by the composition and texture of less microwave responsive gangue minerals). The particles which reach higher temperatures indicate a presence of the mineral phases as additional heating source within the matrix material. Previously reviewed studies of microwave assisted liberation showed that ores with coarser grain sizes (of microwave reactive minerals) respond better to microwave treatment having higher extent of damage between mineral phases. For microwave assisted sorting the results from synthetic samples also demonstrated that the proximity of responsive mineral phase to the particle surface is very important. All tracers were made with same mineral content and the tracer which had the mineral grains closest to its surface had the highest temperature difference.

Findings from particle analysis by image analysis

When synthetic samples were tested they were created to have the same shape and proportions to avoid any additional factors which could influence the temperature profiles under the investigation. Two ore types supplied from the Bingham Canyon Mine were chosen for testing and it was important to determine how much the shape and proportion will vary within the boundaries given for specific size chosen for microwave exposure. In some cases for a specific ore type the shape or proportion can be dominant, which can influence temperature profiles. By comparing shape factors for the same size -22.4+19.0 mm of QZ Ohio and LRO data showed that LRO ore was slightly larger than QZ Ohio, although they had a very similar distribution between the smallest and the largest particle within analysed population. Also, QZ Ohio had particles which were slightly elongated compared to LRO particles. In conclusion, it can be stated that there is no significant difference in shapes and proportions between

them for chosen testing size and that temperature profiles will be more dominated by their mineral texture and composition.

Findings for LRO ore type

The results of the ore modal mineralogy summarised through MLA investigation revealed that the LRO ore contains significant amounts of good absorbers of microwave energy such as pyrite and chalcopyrite. The particles also exposed a substantial variation in distribution of minerals and mineral grain sizes. The presence of the garnet was a strong indicator of skarn ore. The major gangue minerals (relatively transparent to microwave energy) were: quartz, feldspar and calcite with varying content of garnet, amphibole and biotite.

The -22.4 + 19.0 mm size fraction of the Low Recovery Ore was tested for repeatability and separability using multimode excitation in a domestic microwave oven. Sixty-six particles were tested up to six times in different orientations. The standard deviation from the repeatability study for the LRO ore type was presented through cumulative mass percentage. The results indicated that cold particles were clearly distinguishable with a much smaller standard deviation. From the analysed results it can be concluded that there is a substantial variation in content and distribution of good absorbers such as pyrite and chalcopyrite contributed to a higher standard deviation for a majority of the rock particles.

All particles were sent for assaying and along with obtained content of copper, separation temperature curves were created. They were used to assess the best separation strategy. Temperature threshold measuring Delta MAX (or change in *maximum* temperature during heating period and after 5 seconds) gave the most promising option. For the Delta MAX with 30% of mass having standard deviation up to 5 ^{o}C temperature change of 20 ^{o}C would reject 30% mass with an 18% loss of overall copper. Analysed data showed that this particular ore type is a good candidate for a case where microwave assisted sorting can be used for pre-concentration process.

Furthermore, testing was expanded to a larger population of rock particles by a factor of three compared to a previous reproducibility study. In this case temperatures were measured only from one side (with labels facing infrared detector) as opposed to the reproducibility study, where mean values from measurements with labels "up" and "down" were taken. The temperature threshold measuring Delta MAX temperature change of 16 ^{o}C would reject 30% mass with a 16% loss of overall copper. It can be stated that for the Delta MAX temperature threshold, in the larger population study, was lower. This can be partially explained by inefficiency in operation of the defined "theoretical" sorter and partially by standard deviation from the reproducibility study. A threshold of 20 ^{o}C from reproducibility study was determined for 30% of mass with standard deviation up to 5 ^{o}C, so threshold of 16 ^{o}C is within 20 ^{o}C± 5 ^{o}C defined for the same 30% of mass from reproducibility testing.

The Low Recovery Ore contained significant amounts of good absorbers of microwave energy, such as pyrite and chalcopyrite. This indicated that the test can be carried out with much less energy required. The power applied in the second step of experimental investigation was reduced from 1.2 kW to the 600 W. It can be stated that with the lower applied power lower temperature threshold can be placed for ore types which have more responsive mineral phases.

To determine temperature threshold for the "cold" ore particles which were defined by choosing a pre-concentration process, experimental investigation was continued by heating ore particles in two types of applicators. By following experimental methodology, validated on synthetic samples, the data was collected and used with the objective to create two temperature curves and discuss natural separability as a function of mineral texture which causes selective heating. For the 600 W of applied power temperature threshold of ΔT_1=4.90 ^{o}C would reject 20.80 % of the feed mass defined as "cold" ore particles. To achieve similar economically valuable percentage from the first step of investigation the temperature threshold of ΔT_1=6.90 ^{o}C would reject 31.20 % of the feed mass with the loss of 10.40 % ore particles with responsive texture.

From both steps of experimental investigations, it can be concluded that Low Recovery Ore can be sorted by selecting a pre-concentration process. Economically justifiable 30 % of mass feed can be sorted by using microwave heating of ore particles and classification by infrared detector.

Findings for QZ Ohio ore type

The mineralogical characterisation performed by MLA upon QZ Ohio ore showed the presence of mineral phases such as magnetite, pyrite and chalcopyrite. All these detected minerals are good absorbers of microwave energy. The dimensions of mineral grains (mostly chalcopyrite and pyrite) were estimated to be larger than 200 μm. In some tested samples clustered forms of chalcopyrite grains were present in several different locations. These minerals were usually dispersed within the matrix made of very large content of quartz interlocked with biotite, feldspar and sometimes chlorite.

The repeatability investigation clearly presented that the existence of very uniform and very transparent matrix, which was found in this case of QZ Ohio ore type, had an effect by increasing repeatability. Particles which had responsive minerals were easily reheated and reached similar higher temperatures. This caused smaller values for standard deviation and at the same time contributed to the repeatability of microwave heating of overall tested population.

From the repeatability investigation all particles were sent for assaying and with the obtained content of copper, separation temperature curves were created. With temperature separation curves, an ideal separation could scavenge 30% of the mass with a gain of 50% of the copper for the Delta Max T temperature change above 2.6 ^{o}C. Within the scavenged mass, 20% mass can be upgraded to have copper content of 0.35% and more and contribute to metal production. The baselines for both copper and molybdenum within provided ore was at the values of mineralised waste (0.25% for Cu and 1000 ppm for Mo). It can be stated that the for this ore type sorting as a scavenging process could achieve with an economic upgrade.

Experimental investigation extended with flotation testing under controlled operating conditions. The objective was to investigate the content of copper after sorting the QZ Ohio ore in three selected fractions: hot, medium and cold. The flotation performance of both the hot and medium products was improved in line with the grade improvement. Two grinding times were used 10 and 15 min. The copper results show that the shorter (coarser) grind time delivers much better improvements in recovery in hot and medium fractions (these fractions are of our interest because valuable minerals are located there) when compared with the cold fraction.

In the second step of the investigation the data collected was used to discuss natural separability as a function of mineral texture which causes selective heating. The results of controlled laboratory testing clearly demonstrated that combining temperature curves from microwave exposure in two applicators can be used to set a threshold for the scavenging process without destroying rock particles. For the temperature threshold $\Delta T_1=3.12^oC$ (determined from mineral texture as in contrast to assayed metal content) 24.58% of the feed mass can be selected having mineral texture which causes selective heating. From both stages of the experimental investigations, it can be concluded that QZ Ohio ore can be sorted by a selecting scavenging process.

Summarising overall results it can be stated: both approaches of microwave heating (the first with multimode cavity and the second with waveguide applicator) in conjunction with infrared detection can be applied for different ore types. Every ore type will have its own separation curve which will be a function of applied power, mineral composition and mineral textures.

7.3 Recommendations for Future Work

A domestic multimode oven used for this experimental research could be upgraded with an industrial multimode oven which can be engineered to allow automation of the particle preparation and data collection during and after microwave exposures.

With a similar approach of measuring surface temperatures, measuring dielectric properties of particles in sets and individually can be performed. The correlation with their heating responses can be further investigated in this manner.

Further automation during the detection step could include inspection of ore particles from multiple angles to complete the data for temperature profiles. By using multi sensors founded to simultaneously detect several features, having different detection principles, the efficiency and accuracy of the sorting process can be improved and the possibility to discriminate between copper bearing and non-copper bearing minerals can be accomplished.

Once the best recovery-grade ratio is determined (for a good ore candidate) larger-scale/pilot tests should be conducted. Then, after the prediction of "theoretical" sorter performance, the "real" sorter performance can be accurately predicted when extensive test work at set throughput on full sized sorting machines, using a representative feed properly crushed and screening are performed.

The combination of electromagnetic and thermal processes could be modelled very effectively using a "multi-physics" FEM package such as COMSOL or ANSYS. This modelling approach can be used to study virtual ore type which can be then associated with a realistic ore. The modelling results of the virtual ore type then can be used to mathematically interpolate and predict best operating conditions for the real ore.

References

Agilent 2008, *Technical Overview 85070E Dielectric Probe Kit 200 MHz to 50 GHz* Agilent Technologies, USA.

Allen, T 1997, *Particle size measurement*, 5th ed. edn, Chapman & Hall, London ; Weinheim :.

Arai, H, Binner, JGP & Cross, TE 1995, 'Use of mixture equations for estimating theoretical complex permittivities from measurements on porous or powder ceramic specimens', *Japanese Journal of Applied Physics, Part 1 (Regular Papers & Short Notes)*, vol. 34, no. 12A, pp. 6463-7.

Assael, M, Antoniadis, K & Wu, J 2008, 'New Measurements of the Thermal Conductivity of PMMA, BK7, and Pyrex 7740 up to 450K', *International Journal of Thermophysics*, vol. 29, no. 4, pp. 1257-66.

Assael, M, Botsios, S, Gialou, K & Metaxa, I 2005, 'Thermal Conductivity of Polymethyl Methacrylate (PMMA) and Borosilicate Crown Glass BK7', *International Journal of Thermophysics*, vol. 26, no. 5, pp. 1595-605.

Bergmann, C 2009, *Developments in Ore Sorting Technologies*, <http://www.mintek.co.za/Mintek75/Proceedings/M02-Bergmann.pdf>.

Berry, R, Walters, SG & McMahon, C 2008, 'Automated mineral identification by optical microscopy', Brisbane, QLD, Australia.

Birch, AF & Clark, H 1940, 'The thermal conductivity of rocks and its dependence upon temperature and composition', *American Journal of Science*, vol. 238, no. 8, pp. 529-58.

Blaine, RL & Cassel, RB *Precision and Bias of the ASTM Test E1952 for Thermal Conductivity by Modulated Temperature DSC1*, TA256, TA Instruments.

Böhme, RC 1983, 'The development of a radiometric sorter for South African gold ores', *The International Journal of Applied Radiation and Isotopes*, vol. 34, no. 1, pp. 417-28.

Bradshaw, SL, W. 2007, 'Techno-Economic Considerations in the Commercial Microwave Processing of Mineral Ores', *Journal of Microwave Power & Electromagnetic Energy*, vol. 40, no. 4, pp. 228-40.

Bruckard, WJ, Sparrow, GJ & Woodcock, JT 2011, 'A review of the effects of the grinding environment on the flotation of copper sulphides', *International Journal of Mineral Processing*, vol. 100, no. 1-2, pp. 1-13.

Burfoot, D, James, S, AM Foster, KP Self, TJ Wilkins & I Phillips 1990, 'Uniformity of reheating in domestic microwave ovens.' in Field RW & Howell JA (eds), *Process Engineering in the Food Industry: 2 Convenience Foods and Quality Assurance*, Elsevier Science, pp. 33-44.

Cheesman, HB, Carl 2006, 'Scale Up Issues on Mineral Optical Sorting Plants: Bridging the Gaps in Sorting Quality', paper presented to Sensorgestutzte Sortierung 2006 "Sensor Based Sorting 2006", Aachen Germany.

Chen, TT, Dutrizac, JE, Haque, KE, Wyslouzil, W & Kashyap, S 1984, 'The relative transparency of minerals to microwave radiation', *Canadian Metallurgical Quarterly*, vol. 23, no. 3, pp. 349-51.

Church, RH, Webb, WE & Salsman, JB 1988, *Dielectric properties of low-loss minerals*.

Clauser, C & Huenges, E 1995, 'Thermal conductivity of rocks and minerals', *AGU Reference Shelf*, vol. 3, pp. 105-26.

Cohen, HE, 2000, *Solid–Solid Separation, Introduction*, Ullmann's Encyclopedia of Industrial Chemistry, Wiley-VCH Verlag GmbH & Co. KGaA.

Cumbane, A 2003, 'Microwave treatment of Minerals and Ores: Dielectric properties of minerals The effect of microwave radiation on the grindability and mineral liberation', Ph.D. thesis, The University of Nottingham.

Czichos, H, Saito, T, Smith, L, Schumacher, B, Bach, H-G, Spitzer, P & Obrzut, J 2006, 'Electrical Properties', in Springer Handbook of Materials Measurement Methods, Springer Berlin Heidelberg, pp. 431-84.

de Jong, T 2005, 'Automatic sorting of minerals', paper presented to Automation in mining, mineral and metal processing 2004 (MMM'04) Nancy France.

Death, DL, Pollard, LJ & Rogers, CA 2005, 'Mid-infrared reflectance measurements using a DPSS OPO for on-line determination of mineralogy for ore sorting and characterisation', paper presented to Lasers and Electro-Optics Society, 2005. LEOS 2005. The 18th Annual Meeting of the IEEE, 22-28 Oct. 2005.

Denison, C, Carlson, WD & Ketcham, RA 1997, 'Three-dimensional quantitative textural analysis of metamorphic rocks using high-resolution computed X-ray tomography; Part I, Methods and techniques', *Journal of Metamorphic Geology*, vol. 15, no. 1, pp. 29-44.

Djordjevic, N 2007, *Mineral detection method for use in e.g. rock fragments, involves applying pulsed microwave radiation at lower power densities to material such as rock fragment to identify mineral in that material*, WO2007051225-A1 Univ Queensland (Uyqu), Australia.

Dyer, SA 2001, *Survey of instrumentation and measurement*, Wiley, New York :.

Feher, LE 2009, *Industrial Microwave Sources at ISM Frequencies*, Energy Efficient Microwave Systems.

Gaft, M, Reisfeld, R & Panczer, G 2005, 'Minerals Radiometric Sorting', in *Modern Luminescence Spectroscopy of Minerals and Materials*, Springer Berlin Heidelberg, pp. 281-314.

Genn, G 2012, 'Novel Tecniques in Ore Classification and Sorting', Unpublished PhD thesis, University of Queensland.

Goetz, AFH, Curtiss, B & Shiley, DA 2009, 'Rapid gangue mineral concentration measurement over conveyors by NIR reflectance spectroscopy', *Minerals Engineering*, vol. 22, no. 5, pp. 490-9.

Gu, Y 1998, *Rapid Mineral Liberation Analysis Using the JKMRC/Philips MLA*, Mineralogy for Mineral Processing Engineers Workshop, Minerals Processing '98, Cape Town, SA.

---- 2003, 'Automated Scanning Electron Microscope Based Mineral Liberation Analysis. An Introduction to JKMRC/FEI Mineral Liberation Analyser', *Journal of Minerals & Materials Characterization & Engineering*, vol. 2, no. 1, pp. 33-41.

Gu, Y, Gay, S, Guerney, P & Napier-Munn, T 1998, 'Measuring and Modelling Mineral Liberation with the JKMRC/Philips MLA', paper presented to Minerals Processing, Cape Town, SA.

Harrison, PC 1997 'A fundamental study of the heating effect of 2.45GHz microwave radiation on minerals ', Ph.D. thesis,The University of Birmingham

Hartner, R, 2011 Integration and Analysis of Optical and MLA-based Microscopy for Optimisation of Geometallurgical Modelling and Ore Deposit Characterisation', Ph.D. thesis, The University of Queensland.

Horai, K-I & Baldridge, S 1972, 'Thermal conductivity of nineteen igneous rocks, I application of the needle probe method to the measurement of the thermal

conductivity of rock', *Physics of the Earth and Planetary Interiors*, vol. 5, pp. 151-6.

IEC 2010, *IEC 60705 Household microwave ovens - Methods for measuring performance* International Electrotechnical Commission (IEC) Publications, Geneva.

James S.J., Foster, AM, Phillips, IC, Wilkins, TJ, Swain M.J. & D., B 1994, *Effects on Microwave Power-Output of Size of Load, Continuous (intermittent) Use. Position of Load and Variation in Mains Supply Voltage Microwave Science Series Report No 11.*, MAFF Publications London.

Jelinek, RV, Linford, HB, McMahon, EK & Schutz, PW 1949, 'Dielectric Heating of Granular Materials', *Industrial & Engineering Chemistry*, vol. 41, no. 4, pp. 852-6.

Kelly, EG & Spottiswood, DJ 1995, *Introduction to mineral processing*, Australian Mineral Foundation, [Adelaide, S. Aust.] :.

Ketcham, RA & Carlson, WD 2001, 'Acquisition, optimization and interpretation of X-ray computed tomographic imagery: applications to the geosciences', *Computers & Geosciences*, vol. 27, no. 4, pp. 381-400.

Ketelhodt, L & Bergmann, C 2010, 'Dual energy X-ray transmission sorting of coal', *The Journal of The Southern African Institute of Mining and Metallurgy*, vol. 110 p. 8.

Ketelhodt, L & Jacobs, J 2006, 'Optical Sorting of Tanzanite Concentrate', paper presented to Sensorgestutzte Sortierung 2006 "Sensor Based Sorting 2006", Aachen, Germany.

Keys, NJ, Gordon, RJ & Peveret, NF 1974, 'Photometric sorting of ore on a South African gold mine', *Journal of the South African Institute of Mining and Metallurgy*, no. 2, p. 9.

Kingman, SW, Vorster, W & Rowson, NA 2000, 'The influence of mineralogy on microwave assisted grinding', *Minerals Engineering*, vol. 13, no. 3, pp. 313-27.

Kleine, C & Wotruba, H 2010, 'Test Work on High Throughput Diamond Tracer Recovery from Alluvial Recovery Tailings with a Containerised Optical Sorter Under Real Production Conditions', paper presented to XXV International Mineral Processing Congress IMPC, Brisbane, Australia.

Kobusheshe, J 2010, 'Microwave enhanced processing of ores', Ph.D. thesis, The University of Nottingham.

Kuilman, W 2006, 'DE-XRT sorting of coal', paper presented to Sensor Based Sorting conference Aachen, Germany, 29 – 30 March 2006.

Kyle, JR, Mote, AS & Ketcham, RA 2008, 'High-resolution X-ray computed tomography studies of Grasberg porphyry Cu-Au ores, Papua, Indonesia', *Mineralium Deposita*, vol. 43, no. 5, pp. 519-32.

LabView 2011, Application Design Patterns: State Machines, National Instruments, 2011, <http://zone.ni.com/devzone/cda/tut/p/id/3024>.

Landau, LD & Lifshitz, EM 1960, Electrodynamics of Continuous Media, vol. 8, Pergamon Press, Oxford, England, .

Lew A, Krutzik P O, Hartm E & Chamberlin A R (2002), Increasing rates of reaction: microwave-assisted organic synthesis for combinatorial chemistry, *Journal of Combinatorial Chemistry*, 4(2): 95-105.

Lowrie, RL & Society for Mining, MaE 2002, SME mining reference handbook, Society for Mining, Metallurgy, and Exploration.

McGill, SL, Walkiewicz, JW & Smyres, GA 1988, *The Effects of Power Level on the Microwave Heating of Selected Chemicals and Minerals*, MRS Proceedings, 124 , 247 doi:10.1557/PROC-124-247

Mehdizadeh, M 2009, Microwave/RF Applicators and Probes for Material Heating, Sensing, and Plasma Generation : A Design Guide, Elsevier Science & Technology, Burlington, MA, USA.

Meredith, RJ 1998, *Engineers' handbook of industrial microwave heating*, Institution of Electrical Engineers, London :.

Metaxas, AC & Meredith, RJ 1983, *Industrial microwave heating*, P. Peregrinus on behalf of the Institution of Electrical Engineers, London, UK :.

Miller, VR, Nash, RW & Schwaneke, AE 1978, 'Preconcentration of Native Copper and Porphyry Copper Ores by Electronic Sorting', *Minerals Engineering*, p. 1194.

MIT *MIT Online Database*, Massachusetts Institute of Technology, 2011, <http://www.mit.edu/~6.777/matprops/pmma.htm>.

Naval Air Warfare Center Weapons Div Point Mugu, CA 1997, Electronic Warfare and Radar Systems Engineering Handbook, Storming Media.

NIST 2010, *XCOM: Photon Cross Sections Database*, <http://physics.nist.gov/PhysRefData/Xcom/Text/XCOM.html>.

Parkhomenko, EI 1967, *Electrical properties of rocks*, Plenum Press, New York :.

Pirard, E 2004, 'Multispectral imaging of ore minerals in optical microscopy', *Mineralogical Magazine*, vol. 68, no. 2, pp. 323-33.

Pozar, DM 1997, *Microwave engineering*, 2nd ed. edn, Wiley, New York :.

Ralph, J 2011, *Hematite mindat.org - the mineral and locality database*, Site hosted & developed by Jolyon Ralph, <http://www.mindat.org/min-1856.html>.

Robb, LJ 2005, *Introduction to ore-forming processes*, Blackwell Pub.

Robben, M, Buxton, M, Dalmijn, W, Wotruba, H & Balthasar, D 2010, 'Near-Infrared Spectroscopy (NIRS) Sorting in the Upgrading and Processing of Skorpion Non-Sulfi de Zinc Ore', paper presented to XXV International Mineral Processing Congress – IMPC 2010, Brisbane, Australia.

Sahyoun, C 2004 'The effect of microwave radiation on the liberation of minerals from ores ', Ph.D. thesis, The University of Birmingham

Salsman, JB, Williamson, RL, Tolley, WK & Rice, DA 1996, 'Short-pulse microwave treatment of disseminated sulfide ores', *Minerals Engineering*, vol. 9, no. 1, pp. 43-54.

Salter, JD, Nordin, L & Downing, BJ 1989, *Kimberlite-gabbro sorting by use of microwave attenuation: development from the laboratory to a 100 t/h plant*, De Beers diamond Research Lab, Johannesburg.

Salter, JD & Wyatt, NPG 1991, 'Sorting in the minerals industry: Past, present and future', *Minerals Engineering*, vol. 4, no. 7-11, pp. 779-96.

Sass, JH, Lachenbruch, AH, Moses, TH, Jr. & Morgan, P 1992, 'Heat flow from a scientific research well at Cajon Pass, California', *Journal of Geophysical Research*, vol. 97, no. B4, pp. 5017-30.

Schodde, RC 2010, The Declining Discovery Rate – What is the Real Story?, Presentation to the AMIRA International's Exploration Managers Conference, Yarra Valley, Victoria.

Schon, JH 1995, *Physical properties of rocks : fundamentals and principles of petrophysics*, Pergamon Press, Oxford :.

Schubert, H & Regier, M 2005, *The microwave processing of foods*, Woodhead Publishing, Cambridge :.

Scott, G 2006, 'Microwave Pretreatment of a Low Grade Copper Ore to Enhance Milling Performance and Liberation', Master thesis, The University of Stellenbosch.

Sivamohan, R & Forssberg, E 1991, 'Electronic sorting and other preconcentration methods', *Minerals Engineering*, vol. 4, no. 7-11, pp. 797-814.

Smith , DB 1990, 'Cone-beam tomography: recent advances and a tutorial review', *Optical Engineering*, vol. 29, no. 5, pp. 524-34.

Standard ASTM 2010, *ASTM Standard D2520-01 Standard Test Methods for Complex Permittivity (Dielectric Constant) of Solid Electrical Insulating Materials at Microwave Frequencies and Temperatures to 1650°C DOI: 10.1520/D2520-01,www.astm.org.*

Stock, SR 1999, 'X-ray microtomography of materials', *International Materials Reviews*, vol. 44, no. 4, pp. 141-64.

Stratton, JA 1941, *Electromagnetic Theory*, McGraw-Hill:.

Thomas, LC 1999, *Heat transfer : professional version*, 2nd ed. edn, Capstone Pub., Tulsa, Oklahoma USA. :.

Tsuchiyama, A, Hanamoto, T, Nakashima, Y & Nakano, T 2000, 'Quantitative evaluation of attenuation contrasts of minerals by using a medical X-ray CT scanner', *Journal of Mineralogical and Petrological Sciences*, vol. 95, no. 6, pp. 125-37.

von Hippel, AR 1954, *Dielectrics and waves*, John Wiley and Sons; Chapman and Hall.

Vorster, W 2001, 'The effect of microwave radiation on mineral processing', Ph.D. Thesis The University of Birmingham

Walkiewicz, JW, Kazonich, G & McGill, SL 1988, 'Microwave Heating Characteristics of Selected Minerals and Compounds ', *Minerals and Metallurgical Processing*, vol. 5, no. 1, pp. 39-42.

Wang, J, Carson, JK, North, MF & Cleland, DJ 2006, 'A new approach to modelling the effective thermal conductivity of heterogeneous materials', *International Journal of Heat and Mass Transfer*, vol. 49, no. 17-18, pp. 3075-83.

Waples, D & Waples, J 2004, 'A Review and Evaluation of Specific Heat Capacities of Rocks, Minerals, and Subsurface Fluids. Part 2: Fluids and Porous Rocks', *Natural Resources Research*, vol. 13, no. 2, pp. 123-30.

Waples, DW & Waples, JS 2004, 'A review and evaluation of specific heat capacities of rocks, minerals, and subsurface fluids; Part 1, Minerals and nonporous rocks', *Natural Resources Research (New York, N.Y.)*, vol. 13, no. 2, pp. 97-122.

Weert, GV & Kondos, P 2007, 'Infrared recognition of high sulphide and carbonaceous rocks after microwave heating', paper presented to 39th CMP Conf. Proceedings, Ottawa, Jan. 23-25.

Weert, GV, Kondos, P & Gluck, E 2009, 'Upgrading Molybdenite Ores between Mine and Mill Using Microwave/Infrared (MW/IR) Sorting Technology', paper presented to 41st Annual Meeting of the Canadian Mineral Processors, Ottawa, Ontario, Canada, January 20 to 22, 2009.

Weert, GV, Kondos, P & Wang, O 2011, 'Microwave heating of sulphide minerals as a function of their size and spatial distribution', *Canadian Institute of Mining CIM Journal*, vol. 2. No. 3.

Wright, R, Cocks, F, Vaniman, D, Blake, R & Meek, T 1989, 'Thermal processing of ilmenite and titania-doped haematite using microwave energy', *Journal of Materials Science*, vol. 24, no. 4, pp. 1337-42.

Yussuf, AA, Sbarski, I, Solomon, M, Tran, N & Hayes, JP 2007, 'Sealing of polymeric-microfluidic devices by using high frequency electromagnetic field and screen printing technique', *Journal of Materials Processing Technology*, vol. 189, no. 1-3, pp. 401-8.

Appendices

Appendix A

Implementation of the Engineering Design for the Travelling Wave Applicator

This appendix is dedicated to provide more details regarding the design of the travelling wave applicator used in the experiment. Components used to build applicator came from different manufactures (Sairem, Festo, Ocean Controls...) and the main problem was to build universal controlling platform. For that purpose LabView graphical programming environment was used. It offered integration of hardware devices, data processing, data storing and visualisation of data at the same time. Although LabView graphical programming environment is using intuitive graphical icons and wires that look like a flowchart which is easy to follow, some knowledge of graphical or LabView programming is required for this section.

The Figure App. A-1 shows project structure used to organise LabView code and virtual instruments (VI). Three groups can be seen: state VI's, controls and sub VI's which are all dependable by main VI's.

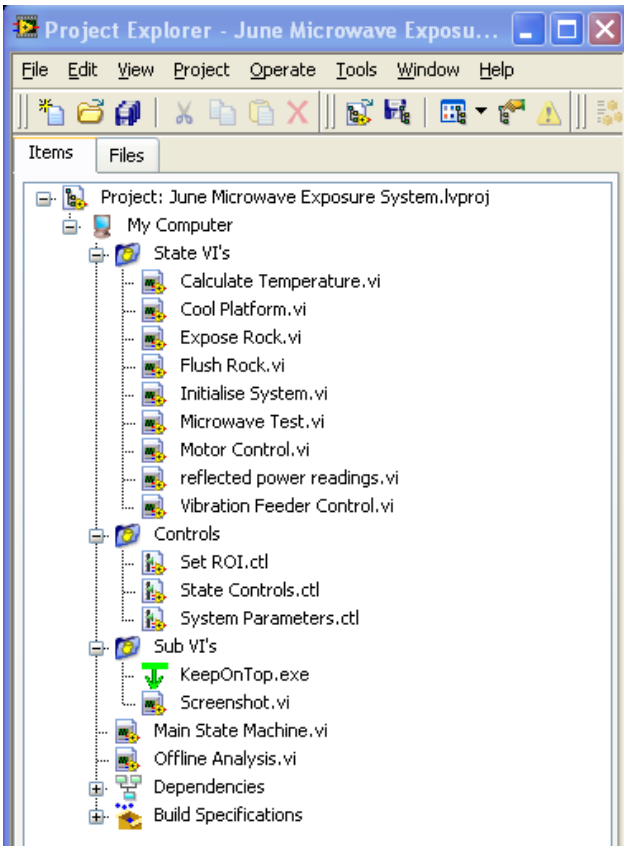

Figure App. A-1 Project structure used to organise LabView code

Main State Machine VI has a structure of state machine which code can be seen in Figure App. A-2 and it is set to initial or default state. Depending on inputs, states will change accordingly to inputs and proper state sub VI will be executed.

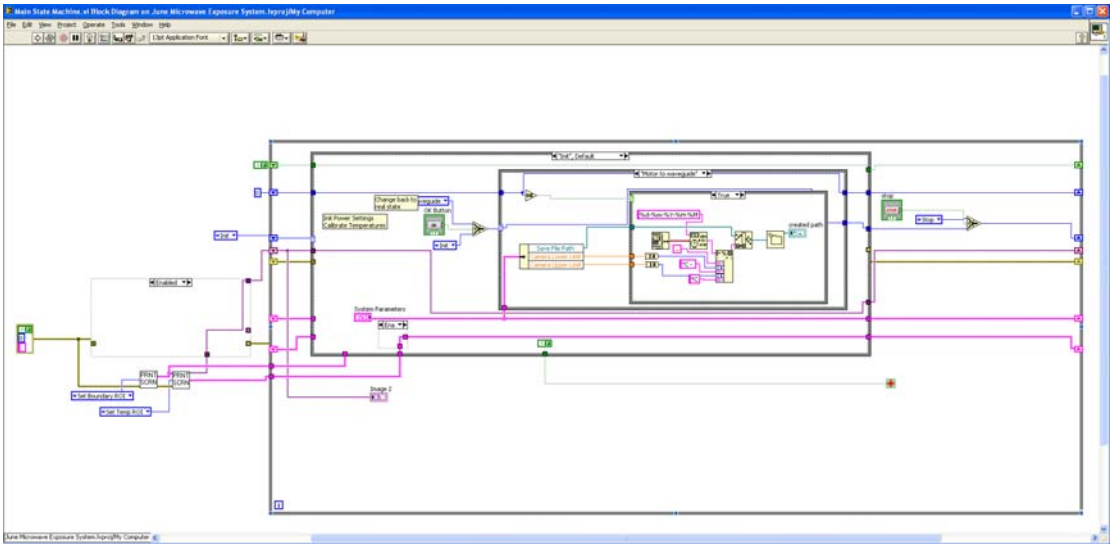

Figure App. A-2 Initial Default state

In Figure App. A-3 user interface which is designed to allow easy manipulation of parameters before testing can be seen. In the top right side, we can see temperature display for maximum, mean and minimum temperature from region of interest (ROI) and bottom display for forward and reflected power. ROI is defined through control window positioned on the left bottom side.

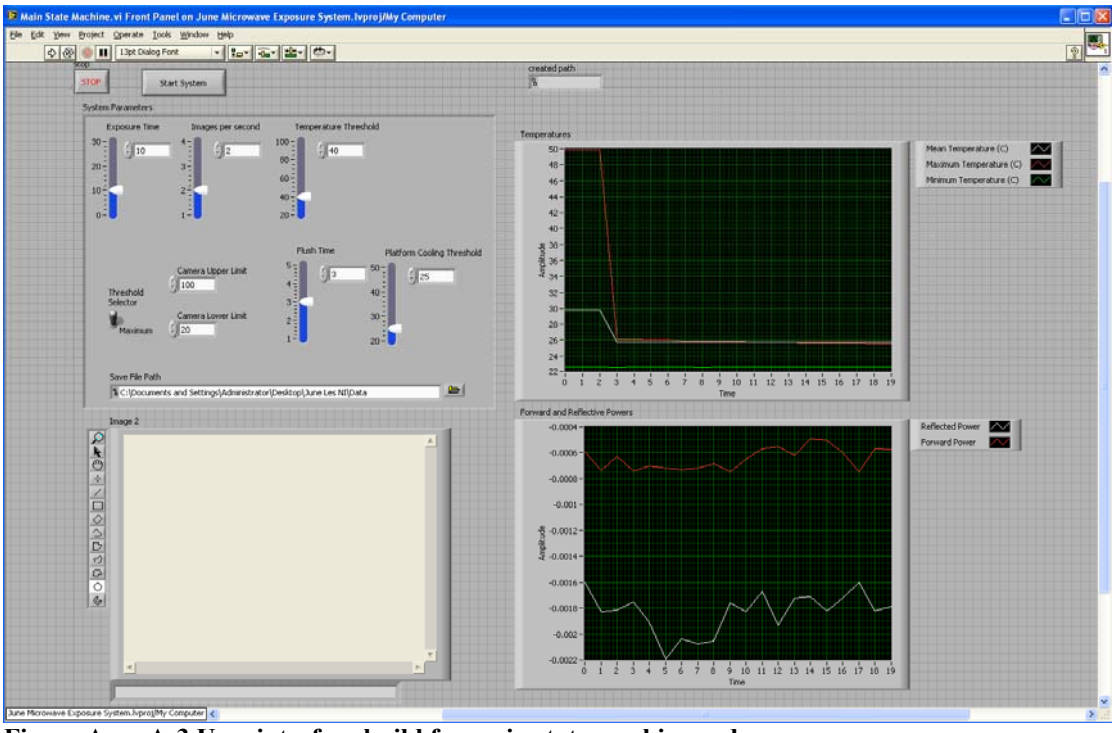

Figure App. A-3 User interface build for main state machine code

In Figure App. A-4 it can be seen that controls for automatic tuner, microwave generator and user interface for state machine are in same place for convenient usage by the operator.

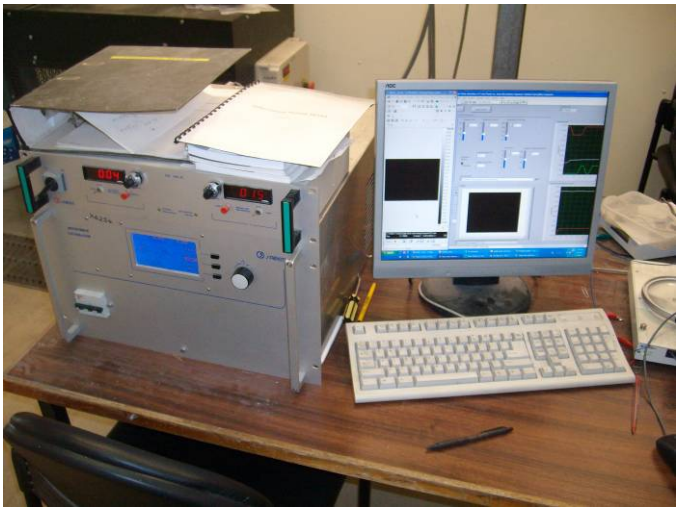

Figure App. A-4 Microwave control system with LabView user interface control

Following order of the executions in the state machine presented in Figure 3-35 in Chapter 3 adequate hardware and supporting LabView code will be explained.

After initial state set parameters we can see that next state is particle holder to waveguide. The Figure App. A-5 shows the particle holder which is here in "flush" position used to sort particles to hot or cold group. This state is set as default when testing is started. In order to hold the particles it needs to be moved up in second position which is in the middle of the applicator.

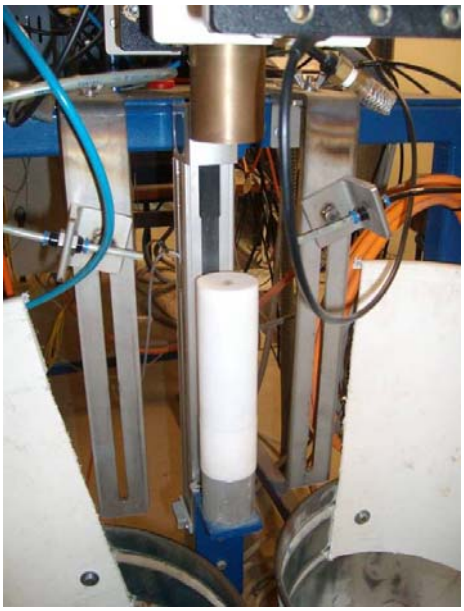

Figure App. A-5 Particle holder made out Teflon®

Particle holder is positioned up or down by servo motor manufactured by FESTO. This motor is controlled by its own FESTO controller which operates on 24V and requires four bit input for control. In Figure App. A-6 we can see code used to

generate those four bits to FESTO controller and in Figure App. A-7 we can see the FESTO controller. Problem of difference between supplied voltage from LabView DAQ card and required 24V for FESTO was solved by using relays manufactured by Ocean Controls.

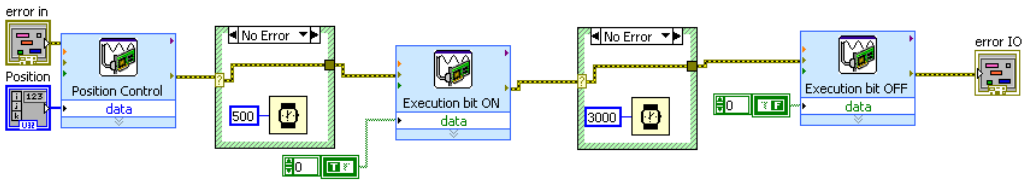

Figure App. A-6 Motor control

Figure App. A-7 FESTO controller connected to LabView DAQ card used to run servo motor

Next state is feeding particles to a travelling wave applicator by two serial vibratory feeders. Those feeders are presented in Figure App. A-8 and the code is given in Figure App. A-9.

Figure App. A-8 Two vibratory feeders with different speeds used to supply continuous flow of particles one by one

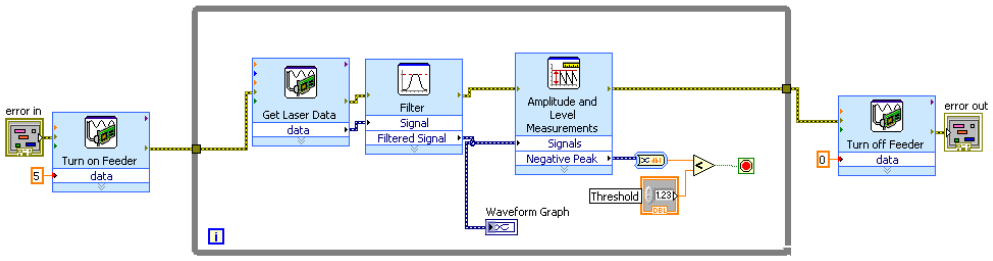

Figure App. A-9 Vibration Feeder control

This state is conditioned by signal created from IR sensor manufactured by FESTO. Spike of voltage is generated when object breaks the infrared beam. State is looping which means that both vibratory feeders are working and moving particles toward funnel with IR sensor. Once the particle breaks the beam feeders are stopped and condition to move to following state is enabled. Funnel is made to guide fall of particles as much as possible to the middle of particle holder which is important for repeatability in the experiment.

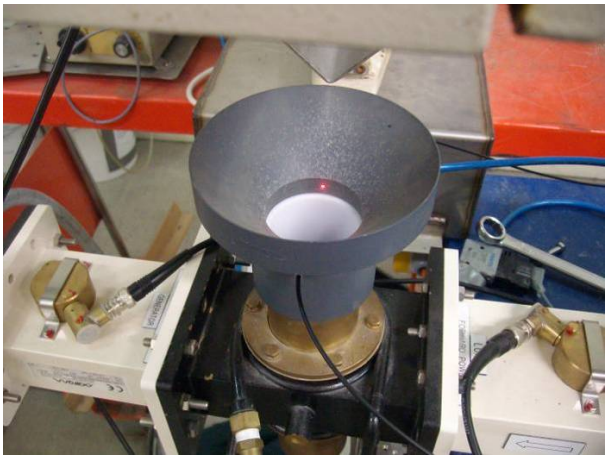

Figure App. A-10 Guiding funnel with IR sensor

Integration of IR sensor, funnel and vibratory feeders made possible to test particles in sequence and treat them one by one. Speed of vibration had to be tested before microwave testing and tuned to specific particle size or ore type.

When particle is positioned in applicator exposure to microwave power is defined by previously set parameters. This state is executing multiple sub VI's which are used to calculate temperatures from region of interest and collect and store data. Figure App. A-11 shows LabView code for expose rock to microwave state. Initialise System, Screenshot and Calculate temperature are used to communicate with IR camera (manufactured by CEDIP). They are used to obtain image, apply region of interest and calculate temperatures. Microwave test and Reflected power readings are sub VI's which are used to perform quick calibration and readings of forward and reflected power. Those sub VI's are given from Figure App. A-12 to Figure App. A-16 respectively.

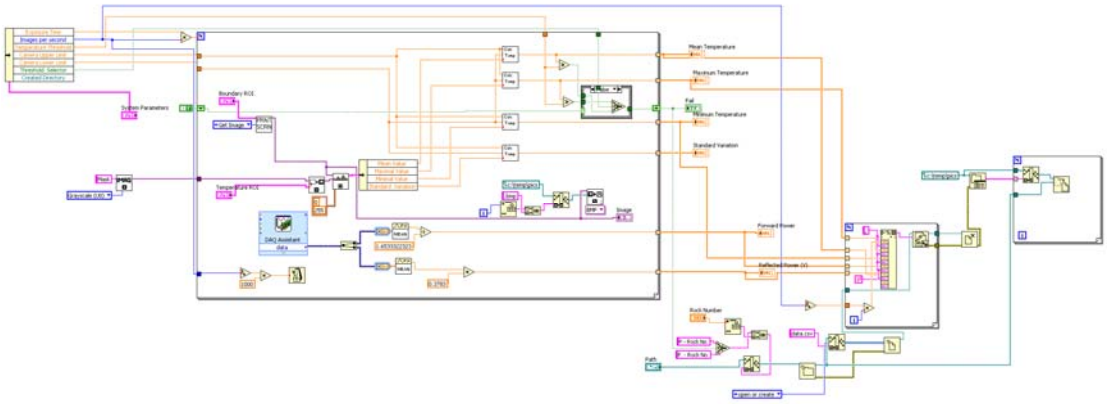

Figure App. A-11 Expose rock

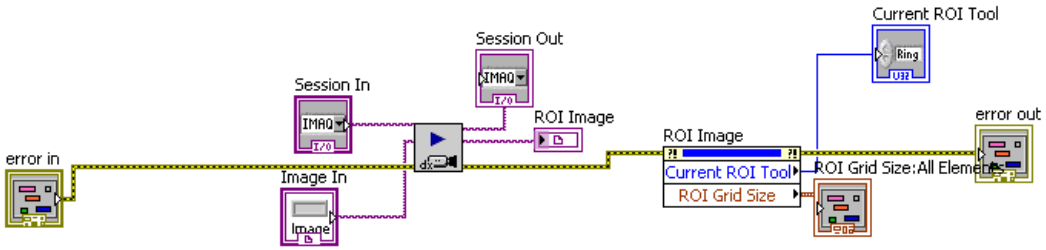

Figure App. A-12 Initialise System

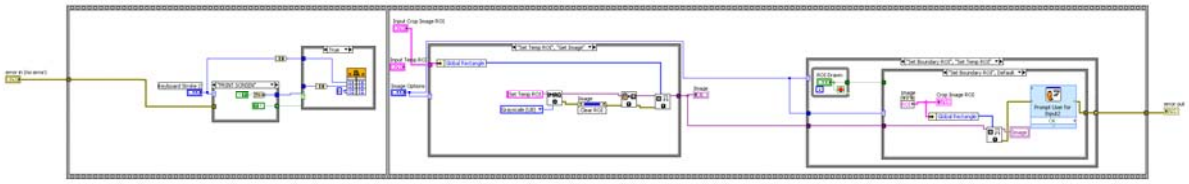

Figure App. A-13 Screenshot

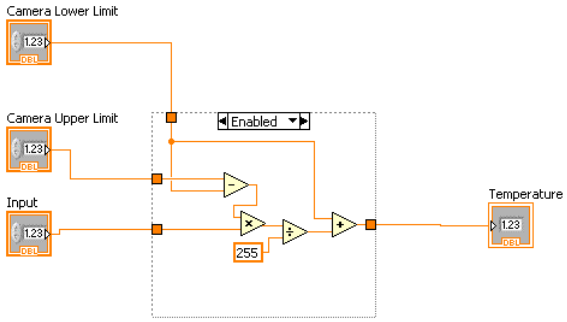

Figure App. A-14 Calculate temperature

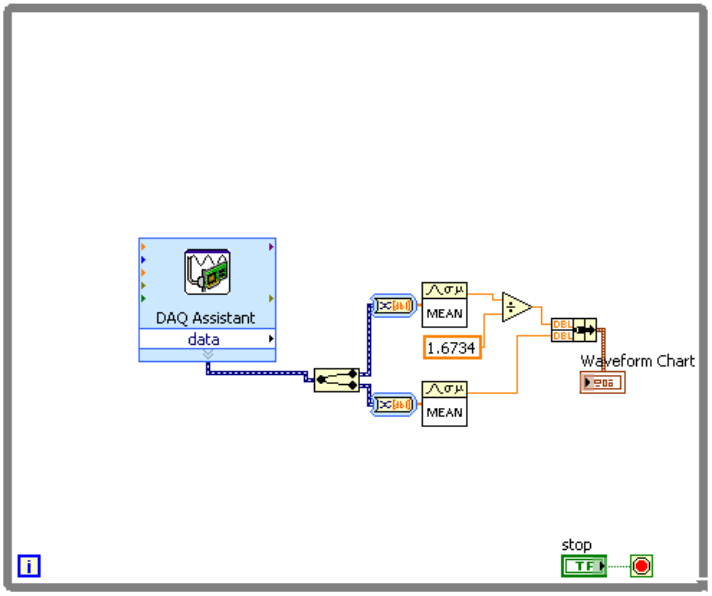

Figure App. A-15 Microwave test

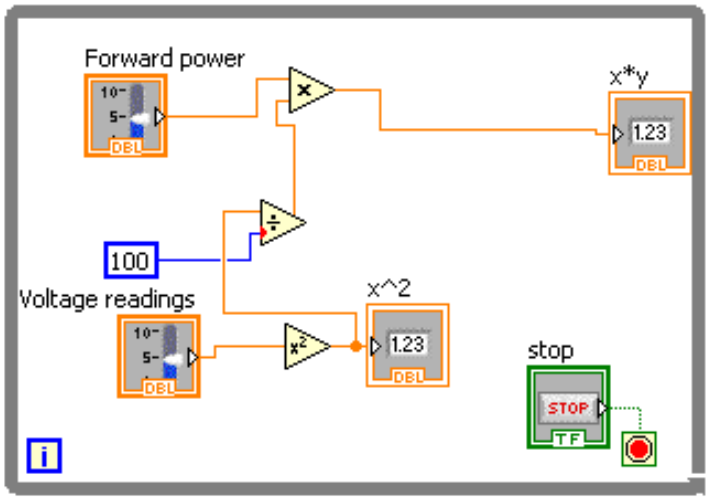

Figure App. A-16 Reflected power readings

After microwave exposure particle is lowered down from applicator to flush position. In this state compressed air is used to flush particle to the cold or the hot group by a compressed air using solenoid valves (manufactured by FESTO). Figure App. A-17 shows code used for this state.

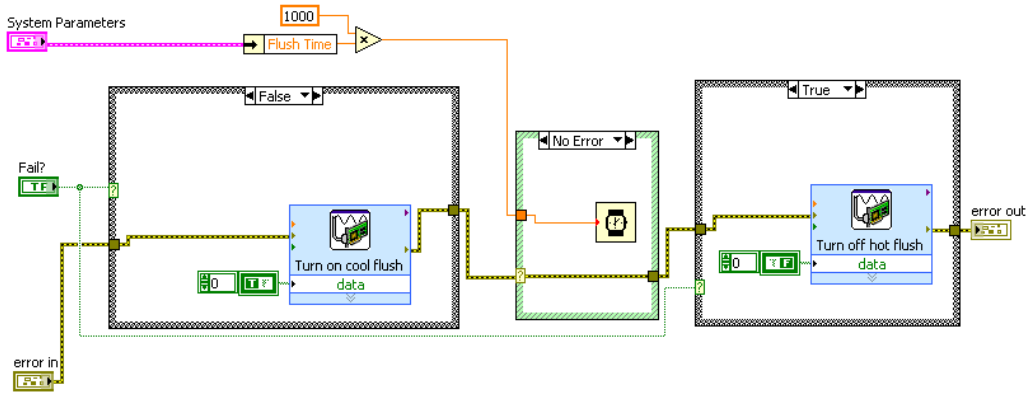

Figure App. A-17 Flush rock

In the last state, before new cycle starts again any residual heat is removed by cooling the platform from. Teflon® is used for particle holder because it has low thermal conductivity and temperature increase after contact with heated particle is reduced by using forced convection cooling with compressed air. Figure App. A-18 shows the

code for that state. Air was used by opening cold and hot flush at the same time for set period.

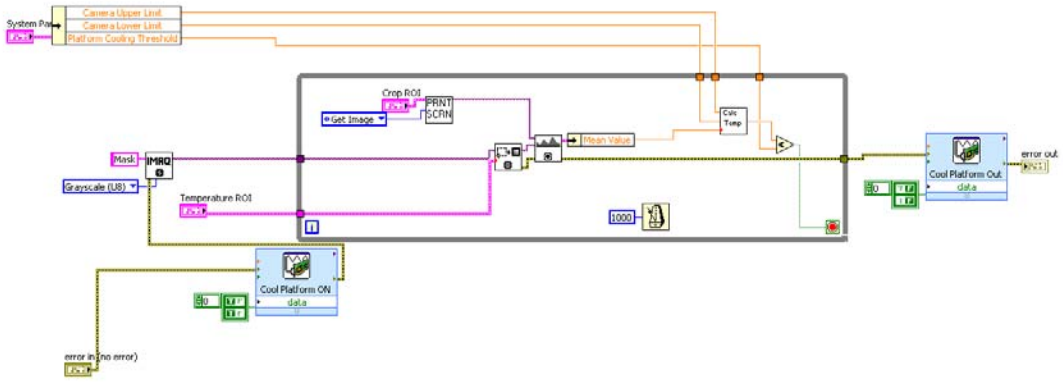

Figure App. A-18 Cool platform

In Figure App. A-19 National Instruments DAQ NI USB-6221 card can be seen which was used for the acquisition of data and execution of LabView code during experiment.

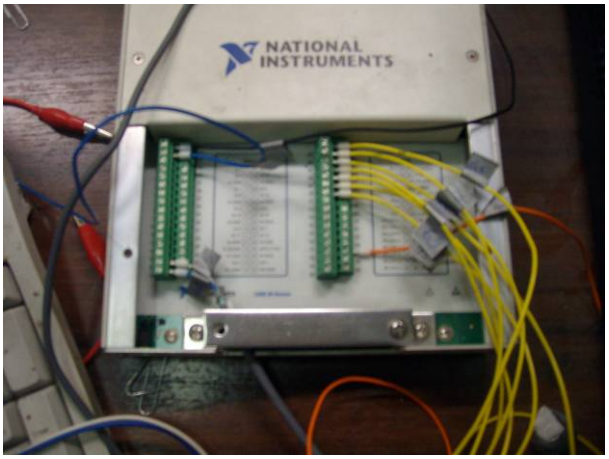

Figure App. A-19 National Instruments DAQ NI USB-6221 card

Appendix B

Recommendations and Considerations for Calculating Coefficient of the Heat Transfer for the Particles on the Conveyor Belt

After heating in microwave applicators particles will fall on conveyor belt which is used to transport them to a location for further separation according their temperature.

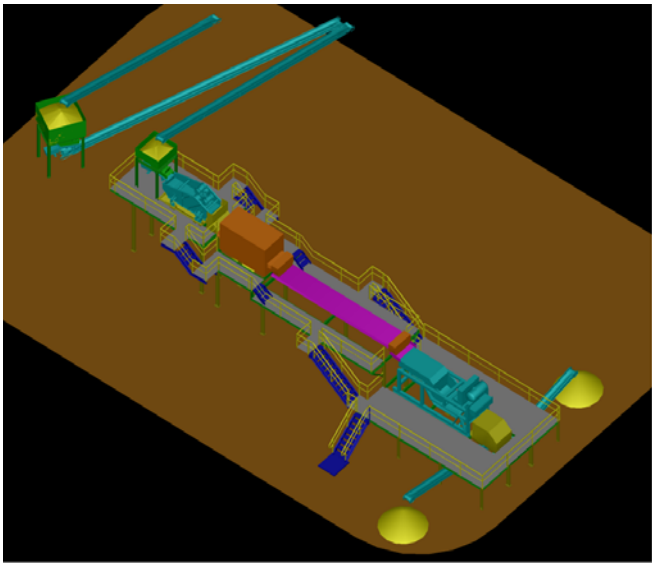

Figure App. B-1 Conveyor belt for transporting particles from microwave applicator to sorting location.

As it can be seen on Figure App. B-1 particles will spend certain amount of time on conveyor belt and they will be exposed to cooling effect of surrounding air.

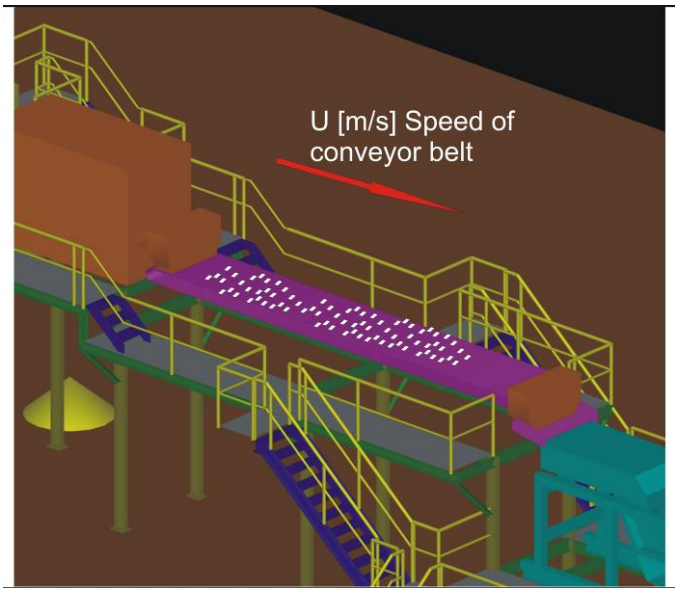

Figure App. B-2 Under the premise that speed of conveyor belt is equal to a speed of air over particles and conveyor belt

Rock particles are losing heat over their surfaces through conduction and convection. In most cases, depending on particle shape, surface area for convection is much larger than surface for conduction, and why it is necessary to calculate heat transfer coefficient.

Heat transfer coefficient is used in calculating the heat transfer, between a fluid and a solid and it can be calculated from a dimensionless Nusselt number.
The Nusselt number is the ratio of convective to conductive heat transfer across (normal to) the boundary.

$$\mathrm{Nu} = \frac{\mathrm{hL}}{\mathrm{k_f}}$$

Where:

- L = characteristic length
- k_f = thermal conductivity of the fluid
- h = convective heat transfer coefficient

The Nusselt number is the function in this particular problem of two dimensionless numbers, Reynolds number (Re), and Prandtl number (Pr).

The Reynolds number Re is a dimensionless number that gives a measure of the ratio of inertial forces over viscous forces. In boundary layer flow over a flat plate, experiments can confirm that, after a certain length of flow, a laminar boundary layer will become unstable and become turbulent. This instability occurs across different scales and with different fluids, usually when, $\mathrm{Re}_x \approx 5 \cdot 10^5$ where x is the distance from the leading edge of the flat plate, and the flow velocity is the 'free stream' velocity of the fluid outside the boundary layer.

$$\mathrm{Re}_x = \frac{\rho L U}{\mu} = \frac{L U}{\nu}$$

Where:

- U is the mean fluid velocity (m/s)
- *L* is a characteristic linear dimension, (travelled length of fluid, or hydraulic radius when dealing with river systems) (m)
- μ is the dynamic viscosity of the fluid (Pa·s or N·s/m² or kg/m·s)
- ν is the kinematic viscosity (ν = μ / *ρ*) (m²/s)

- ρ is the density of the fluid (kg/m³)

The Prandtl number Pr is a dimensionless number approximating the ratio of momentum diffusivity (kinematic viscosity) and thermal diffusivity.

$$\mathrm{Pr} = \frac{\nu}{\alpha} = \frac{c_p \mu}{k}$$

Where:

- ν : kinematic viscosity, ν = μ / ρ, (m^2/s)
- α : thermal diffusivity, α = k / (ρc_p), (m^2/s)
- μ : dynamic viscosity, (Pa s)
- k: thermal conductivity, (W/(m K))
- c_p : specific heat, (J/(kg K))

In order to determine Re number average velocity over the surface of particles needs to be determined. Re number will tell us whether the flow is laminar or turbulent. Certain assumptions are taken in this calculation.

Assumptions

In Figure App. B-3 we can see how shapes of particles of particular size (-22.4+19.0 mm) can be different. Passing through air on conveyor belt all this different shapes will interact in a different way with air, so choosing some average size and shape is favourable. Simplification of their shapes will simplify solution to the problem.

Figure App. B-3 Shapes of real particles

- Cubes with side of a=22.4 mm were chosen to represent simplified realistic particles. Bottom of the cube is not exposed to the fluid and that side is considered to exchange heat over conduction.
- Sides of cubes are represented with average temperature
- Shape of cube is represented with flat surfaces so model for forced convection over flat surfaces is chosen
- Heat flux is constant over surfaces in a very short amount of time which correspond with previous assumption with average temperature on the surface
- Velocity of air is equal to velocity of conveyor belt. Speed of air is set to U=5m/s.

Numerical modelling of air flow

Air flow over the particles and conveyor belt was simulated with CFX form Ansys. CFX is a commercial Computational Fluid Dynamics (CFD) program, used to simulate fluid flow in a variety of applications. Speed of air is set to U=5m/s.

Shear Stress Transport (SST) turbulence model was used because of its highly accurate predictions of flow separation.

To take full advantage of SST air as an ideal fluid is used. Pressure is set to 1 atm , temperature is set to 27 ºC and air is considered to be dry.

Geometry and spacing between particles considerations

For all cases, assumption is taken. First particle is not in the shadow of other particles, it is on distance long enough so that interaction of others particles with fluid is minimised before.

Simple labelling of sides is introduced for better explanation of average velocity on them.

Three consecutive particles evenly spaced-Case No. 1

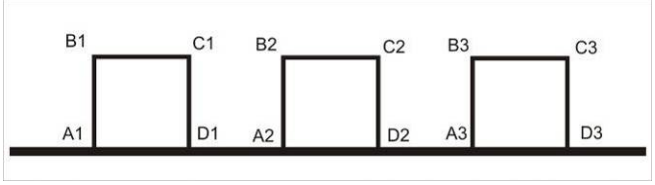

Figure App. B-4 Case No.1

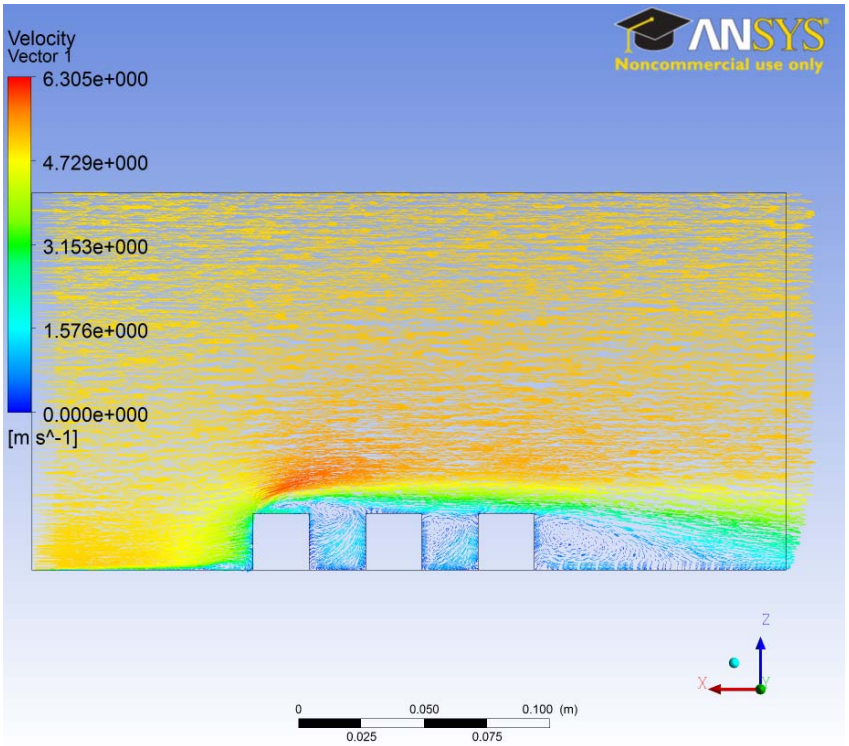

Figure App. B-5Velocity vector plotted over particles for case No.1

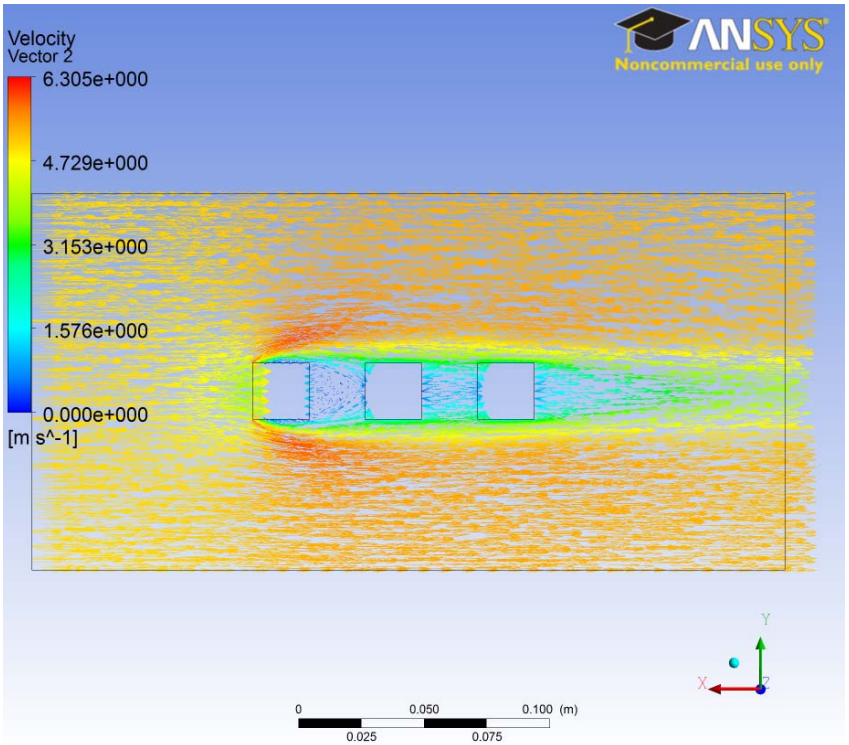

Figure App. B-6 Velocity vector plotted in horizontal plane equal to the height of particles for case No.1

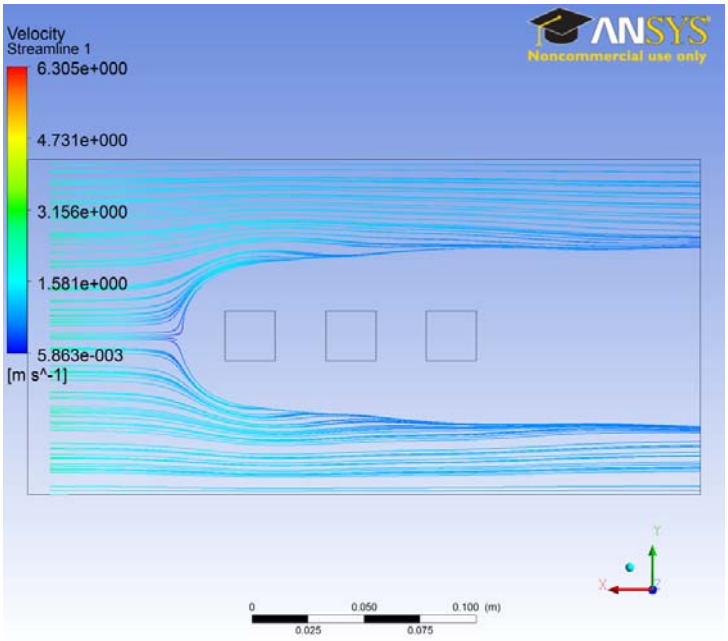

Figure App. B-7 Velocity streamline plotted over particles for case 1

This case simplified in Figure App. B-4 investigates three consecutive particles evenly spaced. Space between particles is equal to cube side. Table App. B-1 shows the average velocity change on sides caused by geometry and spacing between particles.

Table App. B-1 Velocity change caused by geometry and spacing between particles for the casse No. 1

Particle / Side	A1B1	B1C1	C1D1	Sideways (in this model, for both sides)
First	2/3U	0.5U	0	2/3U
Particle / Side	A2B2	B2C2	C2D2	Sideways (in this model, for both sides)
Second	1/3U	1/3U	0	2/3U
Particle / Side	A3B3	B3C3	C3D3	Sideways (in this model, for both sides)
Third	1/3U	0.5U	0	2/3U

It can be seen that particle in the middle experience the highest velocity decrease. Creation of velocity dead zones is observed on all particles C1D1, C2D2 and C3D3 correspondingly.

By observing velocity streamlines in Figure App. B-7 we can see that first particle is creating interaction zone approximately equal to 1.5 cube side in radius.

Two particles on the distance equal to 3a-Case No. 2

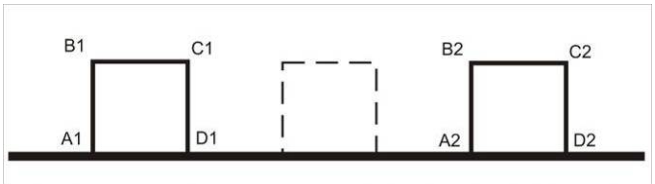

Figure App. B-8 Case No.2

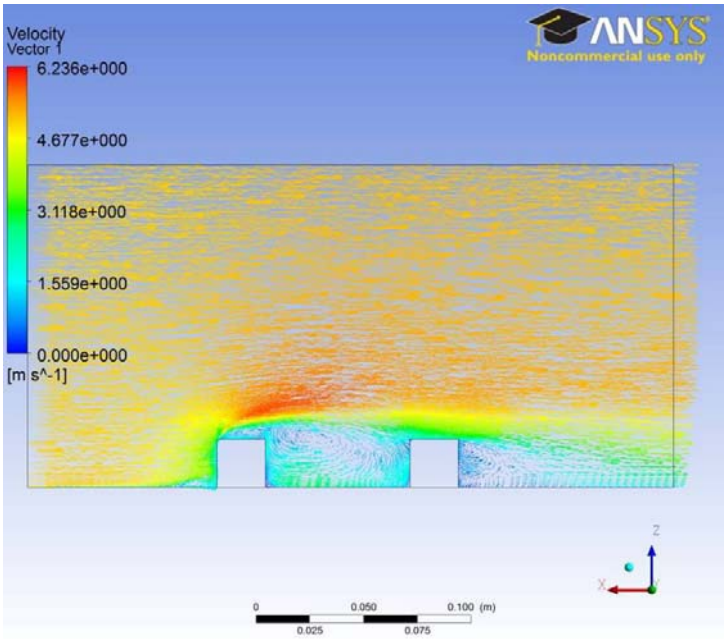

Figure App. B-9 Velocity vector plotted over particles for case No.2

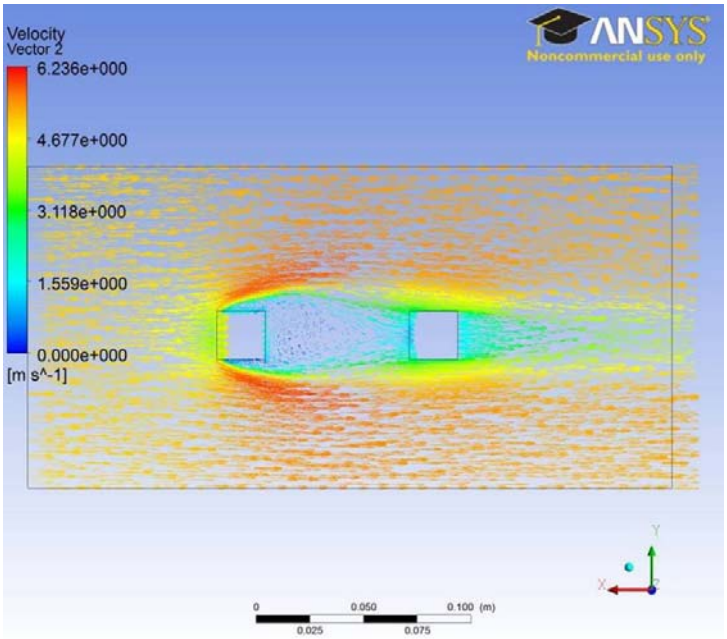

Figure App. B-10 Velocity vector plotted in horizontal plane equal to the height of particles for case 2

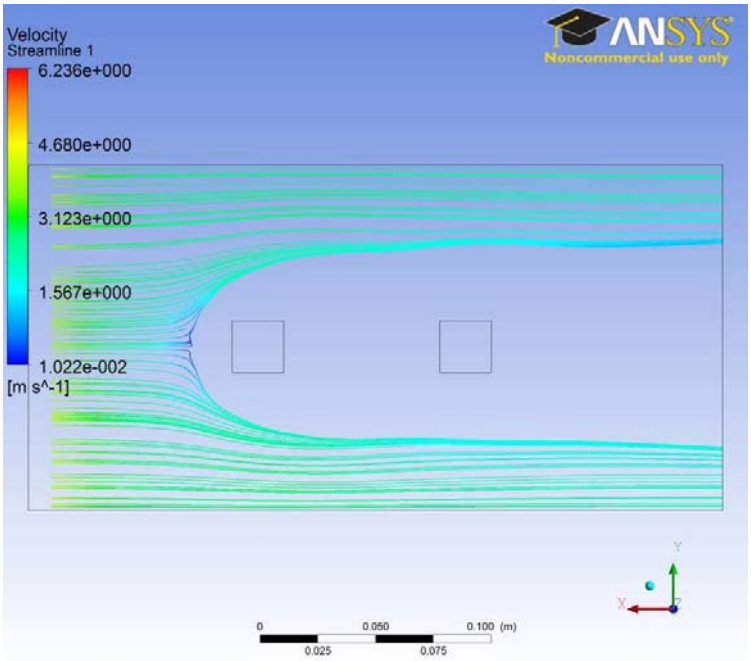

Figure App. B-11 Velocity streamline plotted over particles for case 2

The case No.2 simplified in Figure App. B-8By investigates two consecutive particles and much longer distance between them, this can represent case where time delay happened or one of the particles is missing, in a case of evenly spaced particles. Space between particles is equal to 3a. Table App. B-2 shows the average velocity change on sides caused by geometry and spacing between particles.

Table App. B-2 Velocity change caused by geometry and spacing between particles for the casse No. 2

Particle / Side	A1B1	B1C1	C1D1	Sideways (in this model, for both sides)
First	2/3U	0.5U	1/3U	1/3U
Particle / Side	A2B2	B2C2	C2D2	Sideways (in this model, for both sides)
Second	0.5U	0.5U	0	2/3U

It can be seen that increased distance caused decay of death zone on the first particle and higher recirculation of fluid in a space between them. On the second particle increase on both sides A2B2 and B2C2 is noticeable while the side C2D2 is the only one with velocity death zone in this case.

By observing velocity streamlines in Figure App. B-10 we can see that first particle is creating interaction zone which is not that different from case No. 1.

Smaller particle in front of larger particle-Case No. 3

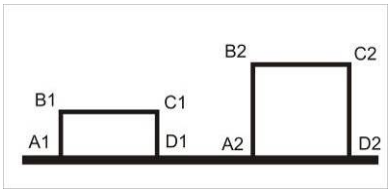

Figure App. B-12 Case No.3

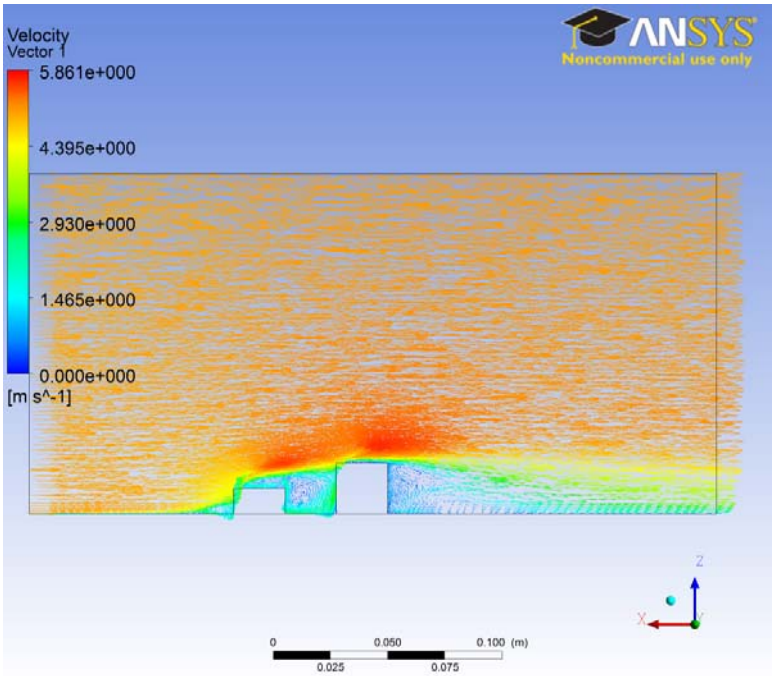

Figure App. B-13 Velocity vector plotted over particles for the case No.3

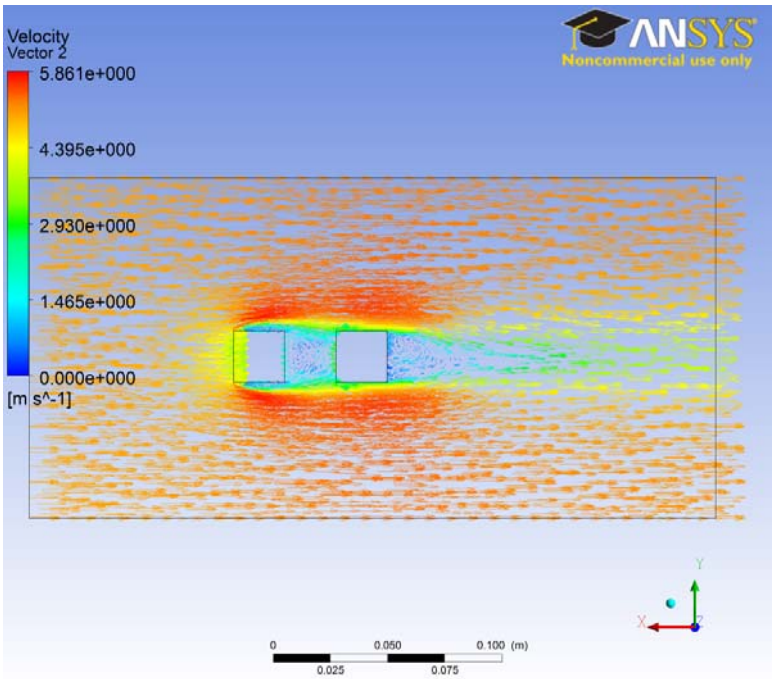

Figure App. B-14 Velocity vector plotted in horizontal plane equal to the height of the smallest particle for the case No.3

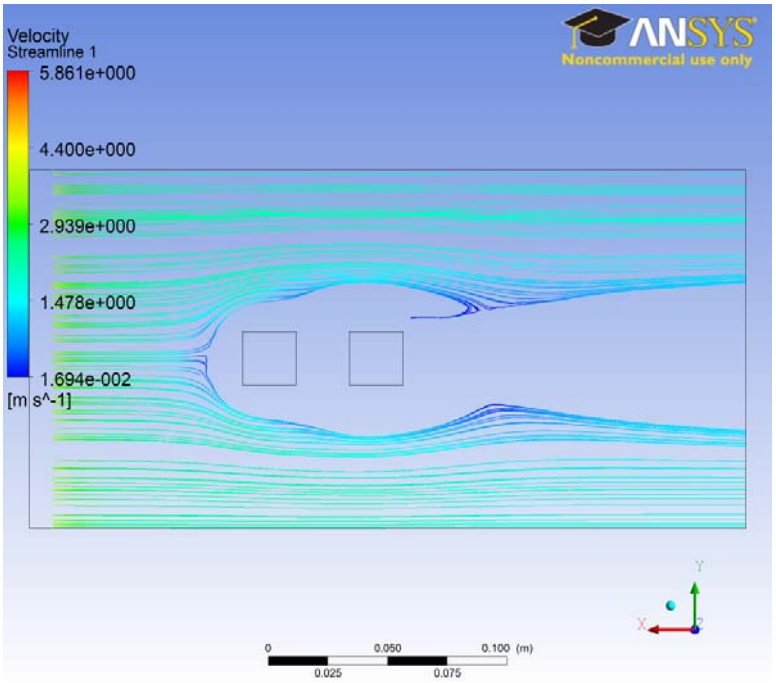

Figure App. B-15 Velocity streamline plotted over particles for the case No.3

This case simplified in Figure App. B-12 investigates two consecutive particles where height of the first particle is half of the height of second one or a/2. Space between particles is equal to a. Table App. B-3 shows the average velocity change on sides caused by geometry and spacing between particles.

Table App. B-3 Velocity change caused by geometry and spacing between particles for the casse No. 3

Particle / Side	A1B1	B1C1	C1D1	Sideways (in this model, for both sides)
First	1/3U	1/3U	1/3U	1/3U
Particle / Side	A2B2	B2C2	C2D2	Sideways (in this model, for both sides)
Second	0.5U	1/3U	0	2/3U

It can be seen that by reducing height of first particle in half, velocity dead zone on side B1C1 is disappearing and that there is almost uniform velocity on all sides of particle.

On the second particle increase on side A2B2 is noticeable while the biggest increase is sideways.

By observing velocity streamlines in Figure App. B-15 we can see that first particle is creating interaction zone which is much smaller than the second particle.

Larger particle in front of smaller particle-Case No. 4

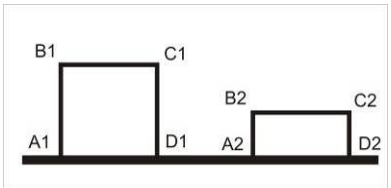

Figure App. B-16 Case No.4

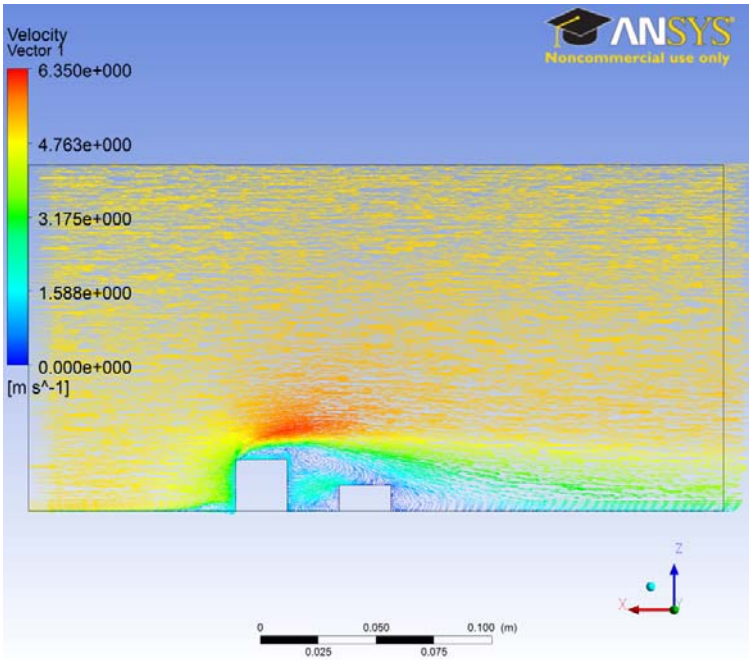

Figure App. B-17 Velocity vector plotted over particles for the case No. 4

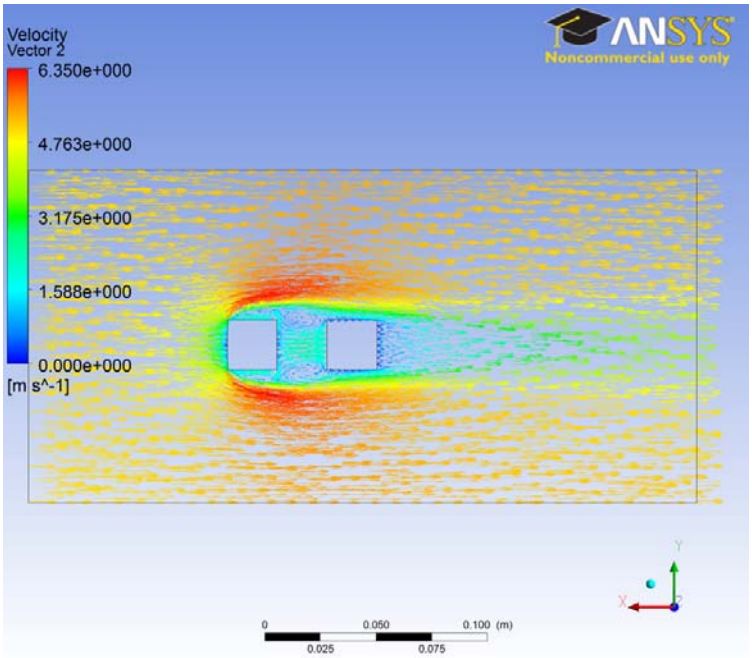

Figure App. B-18 Velocity vector plotted in horizontal plane equal to the height of smallest particle for the case No. 4

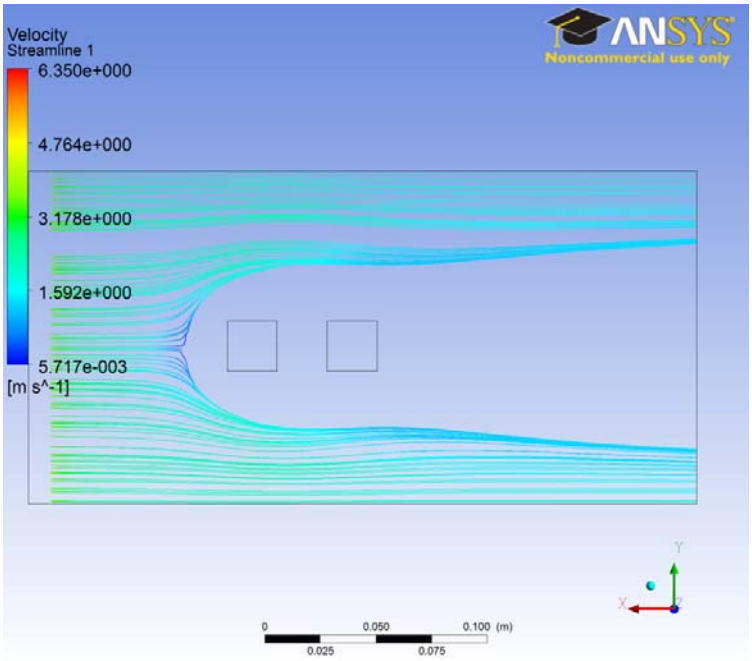

Figure App. B-19 Velocity streamline plotted over particles for the case No. 4

This case simplified in Figure App. B-16 investigates two consecutive particles where height of the second particle is half of the height of first one or a/2. Space between particles is equal to a. Table App. B-4 shows the average velocity change on sides caused by geometry and spacing between particles.

Table App. B-4 Velocity change caused by geometry and spacing between particles for the casse No. 4

Particle / Side	A1B1	B1C1	C1D1	Sideways (in this model, for both sides)
First	2/3U	1/3U	1/3U	1/3U
Particle / Side	A2B2	B2C2	C2D2	Sideways (in this model, for both sides)
Second	0U	0U	0	1/3U

It can be seen that by reducing height of second particle in half place second particle entirely in velocity dead zone of first one. Velocity on side C1D1 is increased slightly caused by some recirculation from a top edge of side A2B2.

Observing velocity streamlines in Figure App. B-19. It can be seen that first particle is creating interaction zone which is similar to case No. 1.

Analysis

Taking all cases in consideration, we can see that in average on overall surfaces of particles, there is decrease of velocity for about 50% except in case No. 4 where second particle was in velocity dead zone of first particle.

Using Table A-C-5 from (Thomas 1999) we obtain data for air at 27 ºC:

ρ= 1.18 (kg/m³)

ν = 1.57 x 10^{-5} (m^2/s)

μ =1.85 x 10^{-5} (Pa s)

k = 0.0262 (W/(m K))

Pr=0.708

Nu number is dependent on location and whether the flow is laminar or turbulent. To see what kind of flow we have, we need to calculate Re number.

Using half of air speed which is taken as an average speed on almost all surfaces on particle, Re number is calculated.

$$\mathrm{Re} = \frac{aU}{\nu} = 3.566 \text{ x } 10^3$$

Comparing value to criteria for flow over flat plate Re<1 x 10^5 which tells us that flow is definitely laminar. Using Equation 8-92 from Thomas (1999) for laminar boundary layer flow with uniform wall flux heating Nu number can be approximated with:

$Nu = 0.45\,\mathrm{Re}^{1/2}\,\mathrm{Pr}^{1/3}$ for condition $0.464 \le \mathrm{Pr}$ which is met in this case.

Nu=23.953, now we can calculate convective heat transfer coefficient from $\mathrm{Nu} = \frac{\mathrm{hL}}{\mathrm{k_f}}$.

Average convective heat transfer coefficient is h=28.01 W/(m^2ºC)

Recommendations

Optimum spacing

In order to prevent heat dissipation into surrounding fluid, space between particles should not exceed more than one length of cube side used to simplify particle geometry.

Average convective heat transfer coefficient

Assumption is used that heat flux is constant over the flat surface; this is closer for a case of highly disseminated texture of minerals which are heated by microwave energy. For vein like or more concentrated texture of minerals which will have more localised heating higher errors can be expected.

Appendix C

The Calibration of the Images

Vision Assistant can calibrate images containing linear, perspective, or nonlinear distortions in order to return accurate measurements. The Image Calibration step calibrates images so that inspection results are returned in real-world units.

Calibrating an image is a two-step process:

1. The first is an offline step during which you specify the type of calibration, the calibration parameters, and the real-world unit in which you want to express measurements.
2. The second step of the calibration process applies the computed calibration to the image during the inspection process. This step is represented in the inspection as the Image Calibration step.

Vision Assistant supports three types of calibration, which depend on the position of the camera in relation to the object under inspection and the type of lens used in the application**:** Simple Calibration**,** Calibration Using User-Defined Points**,** and Grid Calibration.

In this measurement a digital camera was placed directly above the centre of the background. Additional light was applied to avoid creation of shadows and a flash from the digital camera was used to make a clear contrast between the background and the particles. The digital camera was placed 65 cm perpendicular to the background plane. A simple calibration was chosen to create the X-Y coordinate system and input values which will convert pixels into real word dimensions. In Figure App. C-1 the image calibration with X-Y coordinate system can be seen.

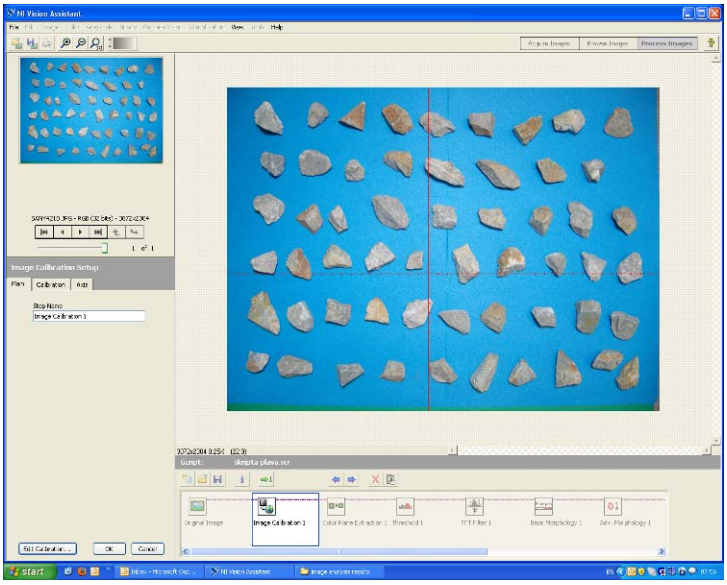

Figure App. C-1 Image calibration

Colour Plane Extraction

It extracts one of the three colour planes (Red, Green, Blue, Hue, Saturation, Luminance, Value, and Intensity) from an image.

- **RGB – Red Plane**—Extracts the red plane from an RGB image.
- **RGB – Green Plane**—Extracts the green plane from an RGB image.
- **RGB – Blue Plane**—Extracts the blue plane from an RGB image.

After colour plane extraction we can see results in Figure App. C-2.

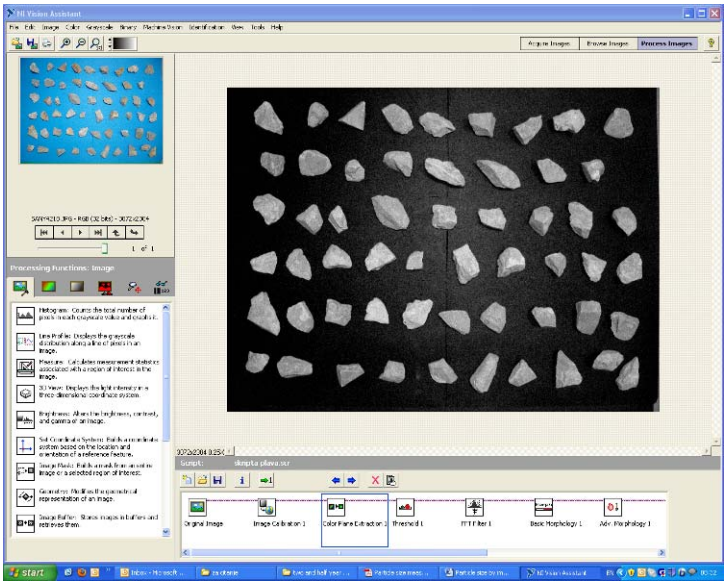

Figure App. C-2 Colour plane extraction

Threshold

Threshold was used to separate significant structures in an image from the rest of the image. Thresholding sets all pixels within the **Threshold Range** to 1 and sets all other pixels in the image to 0. The resulting image is a binary image which we can be seen in Figure App. C-3.

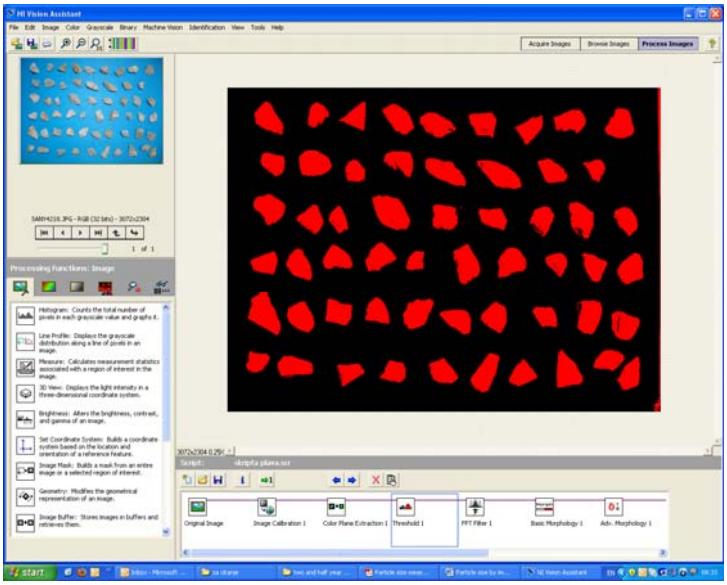

Figure App. C-3 Threshold

FFT Filter

This function applies a frequency filter to the image. This function performs three steps. First, it finds the fast Fourier transform (FFT) of the source image, which is a complex image. Then the function filters (truncates or attenuates) the complex image. Finally, it computes the inverse FFT. Generally, the FFT Filter is used to compute backgrounds in order to correct light drifts. We can see the background enhancement in Figure App. C-4.

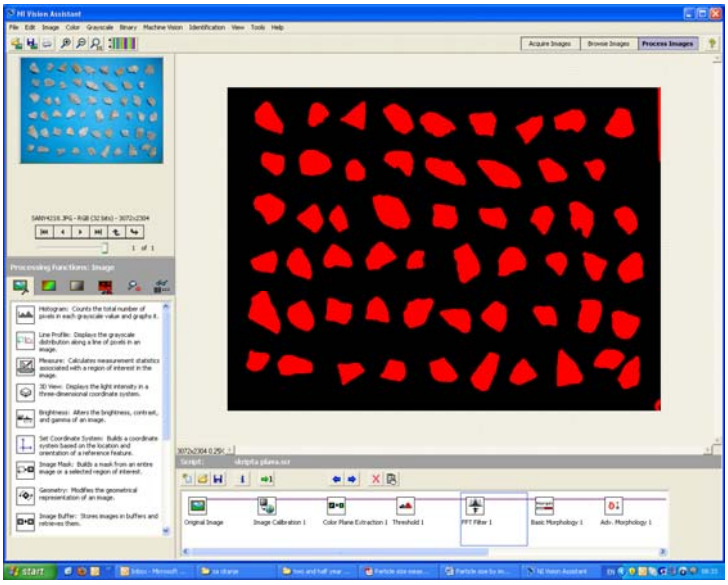

Figure App. C-4 FFT filter

Basic Morphology

The basis morphology affects the shape of particles in binary images. Each particle or region is affected on an individual basis. It was used for tasks such as expanding or reducing objects, filling holes, closing particles, or smoothing boundaries. These tasks are to delineate objects and prepare images for quantitative analysis.

Dilate objects was used. Eliminates tiny holes isolated in objects and expands the contour of the objects based on the structuring element. Dilation makes objects larger. Effects can be seen in Figure App. C-5.

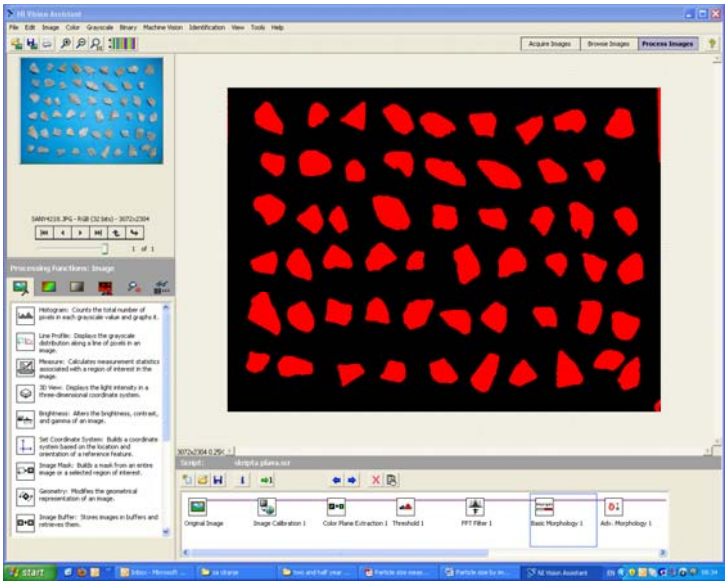

Figure App. C-5 Basic Morphology Dilate

Advanced Morphology

The advanced morphology was used to perform high-level operations on particles in binary images. These can be used for tasks such as removing small particles from an image, removing border objects and labelling particles in an image.

Removing small objects: Removes small objects. A small object is defined by the number of erosions (specified in **Iterations**) needed to remove the object. Figure App. C-6 shows the result.

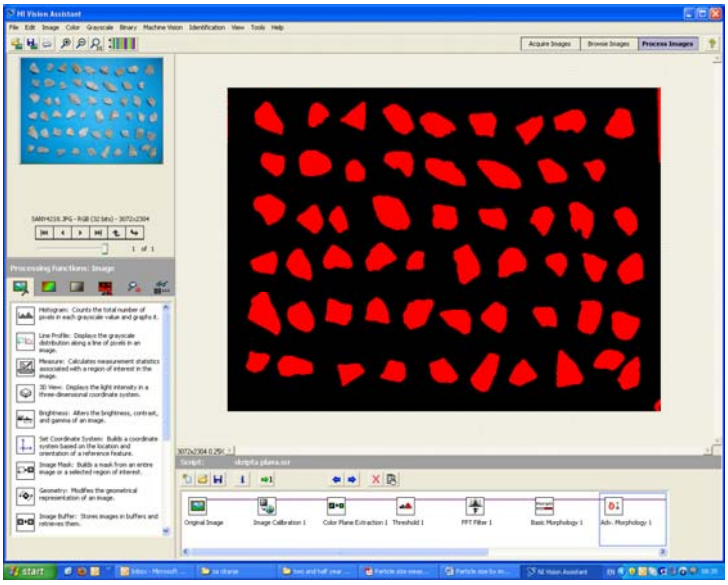

Figure App. C-6 Advanced Morphology Remove small objects

Removing border objects: Eliminates particles that touch the borders of an image. Figure App. C-7 is without border objects.

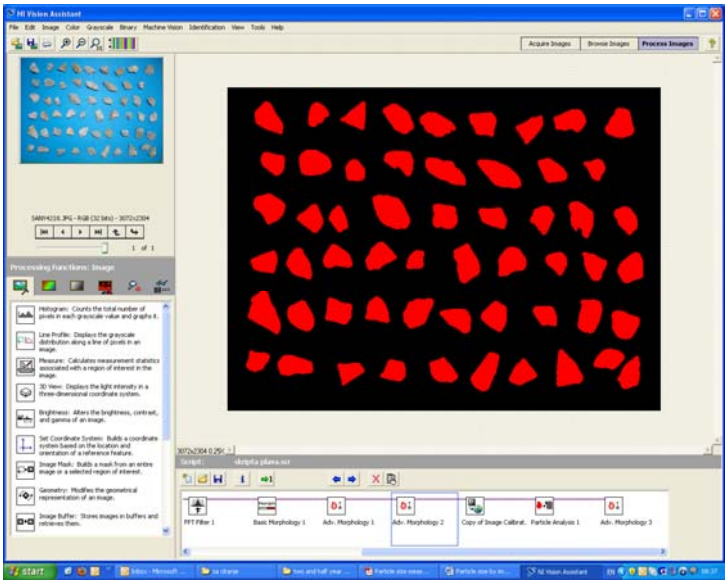

Figure App. C-7 Advanced Morphology Remove border objects

Labelling objects: Produces a labelled image using greyscale values equal to the number of objects in the image plus the greyscale 0 used in the background area. Figure App. C-8 shows us labelled particles for much easier identification.

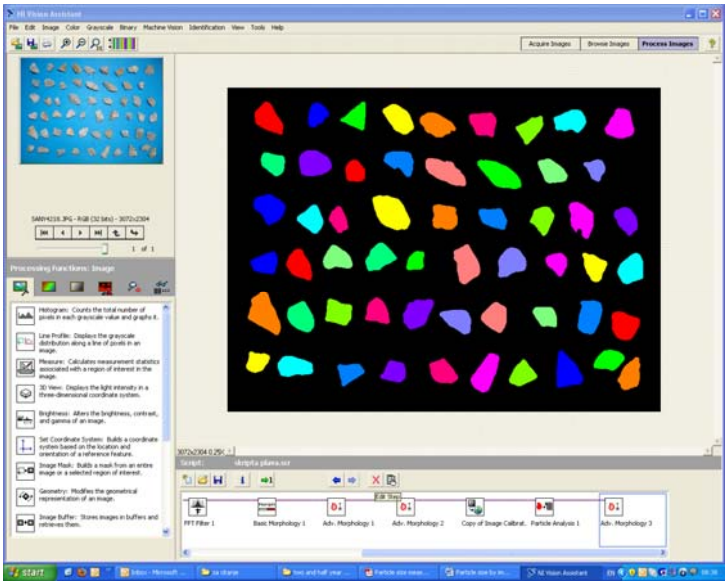

Figure App. C-8 Advanced Morphology label objects

Appendix D

Perimeter

Table App. D-1 Histogram values describing Perimeter Calibrated for size -22.4+19.0 mm QZ Ohio

Perimeter Calibrated			
average	bin	*Bin*	*Frequency*
78.27	54.88	54.88	0
stdev	62.68	62.68	1
7.80	70.48	70.48	12
	78.27	78.27	36
	86.07	86.07	26
	93.87	93.87	10
	101.67	101.67	3
		More	0

Table App. D-2 Histogram values describing Perimeter Calibrated for size -22.4+19.0 mm LRO

Perimeter Calibrated			
average	bin	*Bin*	*Frequency*
80.11	53.46	53.46	0
stdev	62.34	62.34	2
8.89	71.23	71.23	8
	80.11	80.11	31
	89.00	89.00	32
	97.89	97.89	13
	106.77	106.77	1
		More	1

Waddel Disk Diameter

Table App. D-3 Histogram values describing Waddel Disk Diameter for size -22.4+19.0 mm QZ Ohio

Waddel Disk Diameter Calibrated			
average	bin	*Bin*	*Frequency*
22.90	16.60	16.60	0
stdev	18.70	18.70	1
2.10	20.80	20.80	13
	22.90	22.90	34
	25.00	25.00	25
	27.10	27.10	11
	29.20	29.20	4
		More	0

Table App. D-4 Histogram values describing Waddel Disk Diameter for size -22.4+19.0 mm LRO

Waddel Disk Diameter Calibrated			
average	bin	*Bin*	*Frequency*
23.35	16.14	16.14	0
stdev	18.55	18.55	3
2.40	20.95	20.95	9
	23.35	23.35	33
	25.76	25.76	31
	28.16	28.16	10
	30.57	30.57	2
		More	0

Elongation Factor

Table App. D-5 Histogram values for Elongation Factor Calibrated for size -22.4+19.0 mm QZ Ohio

Elongation Factor Calibrated			
average	bin	*Bin*	*Frequency*
1.98	1.09	1.09	0
stdev	1.38	1.38	0
0.30	1.68	1.68	15
	1.98	1.98	31
	2.28	2.28	31
	2.58	2.58	6
	2.87	2.87	5
		More	0

Table App. D-6 Histogram values for Elongation Factor Calibrated for size -22.4+19.0 mm LRO

Elongation Factor Calibrated			
average	bin	*Bin*	*Frequency*
1.96	1.09	1.09	0
stdev	1.38	1.38	0
0.29	1.67	1.67	16
	1.96	1.96	29
	2.24	2.24	28
	2.53	2.53	14
	2.82	2.82	1
		More	0

Heywood Circularity Factor

Table App. D-7 Histogram values for Heywood circularity factor for size -22.4+19.0 mm QZ Ohio

Heywood Circularity Factor Calibrated			
average	bin	*Bin*	*Frequency*
1.09	0.98	0.98	0
stdev	1.02	1.02	0
0.04	1.05	1.05	12
	1.09	1.09	42
	1.12	1.12	18
	1.16	1.16	13
	1.20	1.20	3
		More	0

Table App. D-8 Histogram values for Heywood circularity factor for size -22.4+19.0 mm LRO

Heywood Circularity Factor Calibrated			
average	bin	*Bin*	*Frequency*
1.09	0.96	0.96	0
stdev	1.00	1.00	0
0.04	1.05	1.05	15
	1.09	1.09	32
	1.14	1.14	28
	1.18	1.18	12
	1.22	1.22	0
		More	1

Area

Table App. D-9 Histogram values for Area for size -22.4+19.0 mm QZ Ohio

Area Calibrated			
average	bin	*Bin*	*Frequency*
415.37	185.18	185.18	0
stdev	261.91	261.91	1
76.73	338.64	338.64	11
	415.37	415.37	37
	492.10	492.10	24
	568.83	568.83	11
	645.56	645.56	3
		More	1

Table App. D-10 Histogram values for Area for size -22.4+19.0 mm LRO

Area Calibrated			
average	bin	*Bin*	*Frequency*
432.88	169.67	169.67	0
stdev	257.41	257.41	2
87.74	345.15	345.15	10
	432.88	432.88	33
	520.62	520.62	31
	608.36	608.36	10
	696.10	696.10	1
		More	1

Appendix E

Dielectric Properties of the Materials Used to Create Synthetic Samples for the Testing

Dielectric Probe Kit 85070E from Agilent Technologies was used to determine the dielectric properties, complex permittivity, of materials used to create synthetic samples. In Agilent Technical Overview (Agilent 2008) information is provided, that a complete system is based on a network analyser, which measures the material's response to RF or microwave energy. The probe transmits a signal into the material under test.

A high temperature probe is used with these requirements which are given in Table App. E-1:

Table App. E-1 Probe Characteristics Table from (Agilent 2008)

Requirement	**Range or assumption**
Frequency Range (nominal)	200 MHz to 20 GHz with network analyser
Temperature Range	–40 to +200 °C
Temperature Slew Rate	< 10 degrees/minute
Immersible length (approximate)	35 mm
Connector	3.5 mm male
Repeatability and resolution	Two to four times better than accuracy
Material under test assumptions	Material is "infinite" in size, non-magnetic ($\mu_r^* = 1$), isotropic (uniform orientation), and homogeneous (uniform composition) Solids have a single, smooth, flat surface with gap-free contact at the probe face.
Sample size requirements	Diameter: > 20 mm Thickness: $> \frac{20}{\sqrt{\varepsilon\left\vert_r^*\right\vert}}$ mm Granule size: < 0.3 mm
Expected Value requirements	Maximum recommended ε_r': < 100 Minimum recommended loss tangent > 0.05 Not recommended for low loss (loss tangent < 0.5) materials with $\varepsilon_r' > 5$
Accuracy (typical)	Dielectric constant, $\varepsilon_r' = \varepsilon_r'$ $\pm 0.05\vert \varepsilon_r^* \vert$. $\varepsilon_r'' = \varepsilon_r'' \pm 0.05\vert \varepsilon_r^* \vert$

Table App. E-2 Data from measuring dielectric constant ε' and dielectric loss factor ε'' for Poly (methyl methacrylate) in the frequency range 2.0-3.0 GHz and room temperature of 23 ^{o}C

	First Measurment		Second Measurment		Third Measurment		Fourth Measurment	
Frequency	e'	e''	e'	e''	e'	e''	e'	e''
2E+09	2.3561	-0.0114	2.3813	-0.0124	2.3731	-0.0154	2.3561	-0.0114
2.01E+09	2.3204	0.0164	2.3519	0.0157	2.3437	0.0119	2.3204	0.0164
2.02E+09	2.2942	0.0356	2.3279	0.0325	2.3116	0.0324	2.2942	0.0356
2.03E+09	2.2956	0.0372	2.3275	0.0363	2.3075	0.0348	2.2956	0.0372
2.04E+09	2.3357	0.0236	2.3629	0.0231	2.3467	0.0255	2.3357	0.0236
2.05E+09	2.3945	0.0122	2.4174	0.0117	2.4132	0.0133	2.3945	0.0122
2.06E+09	2.4517	0.0062	2.464	0.0113	2.4708	0.0091	2.4517	0.0062
2.07E+09	2.4519	0.02	2.4727	0.0219	2.4705	0.0234	2.4519	0.02
2.08E+09	2.4062	0.0302	2.4331	0.031	2.4345	0.0297	2.4062	0.0302
2.09E+09	2.3365	0.0306	2.3619	0.036	2.3687	0.0281	2.3365	0.0306
2.1E+09	2.289	0.0182	2.3195	0.0164	2.3171	0.0142	2.289	0.0182
2.11E+09	2.2882	-0.0078	2.3147	-0.0106	2.3168	-0.0097	2.2882	-0.0078
2.12E+09	2.3207	-0.022	2.3413	-0.0218	2.3533	-0.0216	2.3207	-0.022
2.13E+09	2.375	-0.0192	2.3839	-0.0073	2.3906	-0.0096	2.375	-0.0192
2.14E+09	2.3957	0.0085	2.398	0.0285	2.4089	0.0245	2.3957	0.0085
2.15E+09	2.3721	0.0517	2.3923	0.0623	2.3931	0.0614	2.3721	0.0517
2.16E+09	2.3529	0.0677	2.3788	0.0762	2.3706	0.0754	2.3529	0.0677
2.17E+09	2.348	0.057	2.3784	0.0589	2.3725	0.0573	2.348	0.057
2.18E+09	2.3683	0.0261	2.3927	0.0273	2.3908	0.026	2.3683	0.0261
2.19E+09	2.399	-0.0081	2.4075	-0.0014	2.412	-0.0007	2.399	-0.0081
2.2E+09	2.3981	-0.0188	2.4095	-0.0095	2.4023	-0.0079	2.3981	-0.0188
2.21E+09	2.3627	-0.015	2.3636	0.0068	2.3789	-0.0065	2.3627	-0.015
2.22E+09	2.2957	0.0186	2.3149	0.0275	2.3173	0.0213	2.2957	0.0186
2.23E+09	2.2684	0.0286	2.2945	0.0354	2.2906	0.0298	2.2684	0.0286
2.24E+09	2.2889	0.0286	2.3193	0.03	2.308	0.0297	2.2889	0.0286
2.25E+09	2.3566	0.0212	2.3779	0.022	2.375	0.023	2.3566	0.0212
2.26E+09	2.4344	0.0169	2.4343	0.0242	2.4442	0.0227	2.4344	0.0169
2.27E+09	2.4526	0.0299	2.4507	0.039	2.4566	0.0356	2.4526	0.0299
2.28E+09	2.4185	0.0438	2.4147	0.0567	2.4395	0.0388	2.4185	0.0438
2.29E+09	2.3428	0.0481	2.3587	0.0586	2.3563	0.0519	2.3428	0.0481
2.3E+09	2.2808	0.0303	2.3124	0.0368	2.2992	0.0308	2.2808	0.0303
2.31E+09	2.2713	0.0024	2.3036	0.004	2.287	0.0045	2.2713	0.0024
2.32E+09	2.3048	-0.02	2.3281	-0.0207	2.3179	-0.0193	2.3048	-0.02
2.33E+09	2.3519	-0.0211	2.361	-0.0203	2.3725	-0.0214	2.3519	-0.0211
2.34E+09	2.3693	0.0034	2.372	0.0065	2.3792	0.0051	2.3693	0.0034
2.35E+09	2.3642	0.0312	2.3629	0.0435	2.3679	0.0396	2.3642	0.0312
2.36E+09	2.3331	0.0549	2.345	0.0666	2.3434	0.0618	2.3331	0.0549
2.37E+09	2.3236	0.055	2.3467	0.062	2.3326	0.0588	2.3236	0.055
2.38E+09	2.3441	0.0345	2.3675	0.036	2.3507	0.0356	2.3441	0.0345
2.39E+09	2.3766	0.0088	2.3939	0.007	2.3806	0.0081	2.3766	0.0088
2.4E+09	2.3938	-0.0069	2.4036	-0.0066	2.3874	-0.0073	2.3938	-0.0069
2.41E+09	2.3688	-0.0026	2.3736	0.0004	2.3565	-0.0021	2.3688	-0.0026
2.42E+09	2.324	0.0058	2.3258	0.0163	2.3076	0.0124	2.324	0.0058
2.43E+09	2.2727	0.0205	2.2914	0.0284	2.2711	0.0268	2.2727	0.0205
2.44E+09	2.2656	0.0233	2.2987	0.0279	2.2784	0.0272	2.2656	0.0233
2.45E+09	2.309	0.016	2.3421	0.0165	2.3231	0.0169	2.309	0.016
2.46E+09	2.3696	0.0093	2.398	0.0082	2.3828	0.0079	2.3696	0.0093
2.47E+09	2.4279	0.0055	2.4232	0.0117	2.4116	0.0096	2.4279	0.0055
2.48E+09	2.4125	0.0191	2.4026	0.0271	2.3994	0.0263	2.4125	0.0191
2.49E+09	2.3589	0.0345	2.3579	0.0425	2.3569	0.0408	2.3589	0.0345
2.5E+09	2.3	0.0396	2.3173	0.0473	2.3218	0.0412	2.3	0.0396

Table App. E-3 Data from measuring dielectric constant ε' and dielectric loss factor ε'' for Quartz sand in the frequency range 2.0-3.0 GHz and room temperature of 23 °C

	First Measurment		Second Measurment		Third Measurment		Fourth Measurment	
Frequency	e'	e''	e'	e''	e'	e''	e'	e''
2E+09	2.8204	0.0198	2.874	0.0116	2.8827	-0.0276	2.8005	-0.0061
2.01E+09	2.834	0.0286	2.8773	0.016	2.88	-0.0269	2.7963	-0.0062
2.02E+09	2.8155	0.0385	2.8681	0.0274	2.8455	-0.0023	2.7674	0.0109
2.03E+09	2.7789	0.0461	2.8475	0.0417	2.8106	0.0293	2.732	0.0314
2.04E+09	2.7714	0.0436	2.8306	0.0478	2.7989	0.0434	2.7148	0.0439
2.05E+09	2.788	0.0383	2.835	0.0467	2.8166	0.0337	2.7253	0.0418
2.06E+09	2.8212	0.0326	2.8586	0.0393	2.8549	0.0079	2.7576	0.0285
2.07E+09	2.8479	0.0313	2.8795	0.03	2.8822	-0.0161	2.7828	0.013
2.08E+09	2.8507	0.0347	2.8881	0.0239	2.8806	-0.0212	2.7854	0.0043
2.09E+09	2.8431	0.0367	2.8782	0.0228	2.8551	-0.0074	2.7637	0.0065
2.1E+09	2.8276	0.0332	2.8518	0.0233	2.8173	0.0128	2.7328	0.015
2.11E+09	2.811	0.0274	2.8257	0.0246	2.7974	0.0224	2.7148	0.0211
2.12E+09	2.8051	0.0262	2.8173	0.0284	2.806	0.0167	2.7196	0.0257
2.13E+09	2.8003	0.0314	2.8193	0.0345	2.8346	0.0045	2.7384	0.0259
2.14E+09	2.8089	0.0427	2.8325	0.0419	2.8597	-0.0008	2.7579	0.0267
2.15E+09	2.8114	0.0535	2.8308	0.0493	2.8557	0.0076	2.7649	0.0272
2.16E+09	2.805	0.0593	2.8258	0.0529	2.8324	0.0257	2.7513	0.0333
2.17E+09	2.8034	0.0512	2.8201	0.0465	2.8137	0.0345	2.7344	0.0367
2.18E+09	2.8123	0.0386	2.8223	0.0377	2.82	0.0303	2.732	0.033
2.19E+09	2.8228	0.0261	2.8358	0.0261	2.8497	0.0079	2.757	0.0211
2.2E+09	2.8318	0.0224	2.8485	0.0203	2.883	-0.0138	2.7983	0.0017
2.21E+09	2.8319	0.0282	2.8526	0.0191	2.8882	-0.022	2.8168	-0.0115
2.22E+09	2.8119	0.0396	2.8447	0.0269	2.8594	-0.007	2.7964	-0.0026
2.23E+09	2.7761	0.046	2.8175	0.0355	2.8129	0.0167	2.7501	0.0168
2.24E+09	2.7478	0.0485	2.7868	0.0438	2.7757	0.038	2.7128	0.035
2.25E+09	2.7451	0.0444	2.774	0.0469	2.7735	0.0403	2.7073	0.0391
2.26E+09	2.7648	0.0404	2.7855	0.045	2.8023	0.0222	2.7365	0.0282
2.27E+09	2.7987	0.0377	2.8123	0.0393	2.8465	0.0003	2.7833	0.0074
2.28E+09	2.8227	0.0395	2.8402	0.033	2.8723	-0.0096	2.8082	-0.0107
2.29E+09	2.8268	0.0431	2.8485	0.0307	2.8604	-0.0018	2.802	-0.0025
2.3E+09	2.8135	0.0421	2.8361	0.0283	2.8257	0.0147	2.7737	0.0113
2.31E+09	2.7981	0.0381	2.8118	0.0297	2.8008	0.0262	2.7478	0.0255
2.32E+09	2.7937	0.031	2.7997	0.0301	2.803	0.0245	2.7462	0.0239
2.33E+09	2.7934	0.0261	2.8054	0.0285	2.8284	0.0117	2.7692	0.0089
2.34E+09	2.7889	0.0238	2.81	0.0244	2.8498	-0.0027	2.7872	-0.0078
2.35E+09	2.7676	0.0242	2.8106	0.0193	2.8448	-0.0078	2.7859	-0.0188
2.36E+09	2.7469	0.0235	2.8029	0.0179	2.8184	-0.0018	2.7581	-0.0112
2.37E+09	2.7399	0.0227	2.793	0.018	2.7892	0.0108	2.7308	0.0071
2.38E+09	2.7617	0.0244	2.8	0.0219	2.7863	0.0201	2.7297	0.0192
2.39E+09	2.7931	0.028	2.8207	0.0268	2.8107	0.0198	2.7622	0.0184
2.4E+09	2.8204	0.0297	2.8454	0.0292	2.8538	0.0087	2.8048	0.0044
2.41E+09	2.8252	0.0287	2.8576	0.0262	2.8808	-0.0027	2.824	-0.0082
2.42E+09	2.8069	0.0207	2.8491	0.0222	2.8629	-0.0067	2.7998	-0.0069
2.43E+09	2.7759	0.0128	2.8219	0.0166	2.8152	-0.0009	2.7526	-0.0018
2.44E+09	2.7535	0.0119	2.7941	0.0162	2.7708	0.0116	2.714	0.0109
2.45E+09	2.7647	0.0161	2.7854	0.021	2.7653	0.0214	2.7097	0.0213
2.46E+09	2.8031	0.02	2.8068	0.0241	2.8086	0.0171	2.7468	0.0176
2.47E+09	2.8338	0.0216	2.8423	0.0233	2.8628	0.0036	2.806	-0.0024
2.48E+09	2.8563	0.018	2.8713	0.0151	2.896	-0.0153	2.8403	-0.0229
2.49E+09	2.8519	0.0086	2.8786	0.006	2.8781	-0.022	2.8238	-0.0236
2.5E+09	2.8244	0.005	2.8547	0.0041	2.8214	-0.0085	2.7765	-0.0102

Table App. E-4 Data from measuring dielectric constant ε' and dielectric loss factor ε'' for Pyrite in the frequency range 2.0-3.0 GHz and room temperature of 23 °C

	First Measurment		Second Measurment		Third Measurment		Fourth Measurment	
Frequency	e'	e''	e'	e''	e'	e''	e'	e''
2E+09	22.0558	8.6858	21.0635	6.7793	26.5979	15.2999	24.8334	13.1336
2.01E+09	22.0419	8.7682	20.9476	6.6578	26.5552	15.2598	24.8271	13.0709
2.02E+09	22.0061	8.8599	20.7231	6.4659	26.491	15.2295	24.8143	13.0144
2.03E+09	21.9658	8.9027	20.4899	6.2986	26.4344	15.2037	24.799	13.0005
2.04E+09	21.9319	8.8157	19.4821	5.5412	26.411	15.1851	24.773	12.9486
2.05E+09	21.9364	8.7722	19.2004	5.3638	26.4237	15.1536	24.7408	12.9139
2.06E+09	21.9497	8.4858	19.1159	5.2849	26.4557	15.1012	24.7238	12.8518
2.07E+09	21.9549	8.4076	19.1039	5.2536	26.4644	15.0486	24.7144	12.845
2.08E+09	21.9559	8.4279	19.2361	5.3131	26.4452	14.9906	24.7207	12.8282
2.09E+09	21.9173	8.458	19.3461	5.3743	26.3871	14.955	24.7106	12.7854
2.1E+09	21.8698	8.4967	19.0263	5.1589	26.3271	14.9385	24.6857	12.7952
2.11E+09	21.8232	8.4178	19.0786	5.2118	26.2919	14.9088	24.6589	12.8277
2.12E+09	21.8112	8.3081	19.2319	5.3356	26.2963	14.8793	24.62	12.8799
2.13E+09	21.8093	8.2382	18.8998	5.1254	26.3051	14.8424	24.5767	12.9086
2.14E+09	21.8254	8.2083	18.2399	4.7034	26.3196	14.8133	24.5865	12.8622
2.15E+09	21.8133	8.0675	14.8439	3.058	26.2964	14.7881	24.6222	12.6846
2.16E+09	21.7795	8.0404	10.7526	1.5355	26.2576	14.7616	24.6187	12.6919
2.17E+09	21.7231	7.8688	9.8708	1.2724	26.2267	14.7342	24.6066	12.724
2.18E+09	21.6451	7.6197	9.5411	1.1832	26.2233	14.7065	24.5869	12.7281
2.19E+09	21.6817	7.741	10.0404	1.3021	26.2355	14.6657	24.5762	12.5398
2.2E+09	21.6965	7.7595	10.2583	1.3628	26.2408	14.6222	24.544	12.2637
2.21E+09	21.6547	7.5988	10.6278	1.4667	26.2178	14.5757	24.4984	12.2677
2.22E+09	21.5959	7.5796	10.09	1.3374	26.1572	14.5479	24.5139	12.045
2.23E+09	21.5438	7.6297	10.438	1.4357	26.0916	14.5339	24.5657	11.8187
2.24E+09	21.4919	7.5804	10.9765	1.5911	26.0527	14.5298	24.518	11.7389
2.25E+09	21.4615	7.4796	10.3304	1.4163	26.058	14.5052	24.4311	11.6875
2.26E+09	21.5131	7.538	10.0443	1.3379	26.0814	14.4679	24.3994	11.9016
2.27E+09	21.4859	7.3825	10.0825	1.339	26.1143	14.4107	24.383	12.0283
2.28E+09	21.4789	7.3553	10.8158	1.5304	26.1083	14.3644	24.3804	11.9811
2.29E+09	21.4863	7.419	10.8302	1.5274	26.069	14.3273	24.4107	11.8195
2.3E+09	21.4659	7.5023	11.1375	1.6136	26.0169	14.2933	24.394	11.867
2.31E+09	21.4373	7.4796	11.5451	1.7405	25.9896	14.2822	24.3697	11.769
2.32E+09	21.4456	7.5197	11.5162	1.7366	25.9772	14.2612	24.3122	11.8358
2.33E+09	21.4753	7.5271	11.9596	1.8791	25.9931	14.2333	24.3054	11.9933
2.34E+09	21.4423	7.3959	12.2142	1.9605	25.993	14.1951	24.2861	11.994
2.35E+09	21.4136	7.3995	12.3947	2.0167	25.9662	14.1562	24.2886	11.9686
2.36E+09	21.3759	7.3923	12.7516	2.134	25.9258	14.1333	24.306	11.9106
2.37E+09	21.3249	7.329	13.1932	2.2912	25.8963	14.1306	24.3085	11.9018
2.38E+09	21.3026	7.278	14.1617	2.6714	25.8955	14.117	24.2999	11.8656
2.39E+09	21.3037	7.2401	15.4995	3.2596	25.9176	14.109	24.2687	11.15
2.4E+09	21.3341	7.2302	15.9026	3.4427	25.9417	14.0657	24.2309	11.218
2.41E+09	21.2888	7.1819	15.7884	3.3905	25.9275	14.0151	24.2122	11.4474
2.42E+09	21.2862	7.2133	15.6533	3.3258	25.8738	13.9764	24.1766	11.4473
2.43E+09	21.2634	7.2543	15.5523	3.2845	25.8074	13.9609	24.1582	11.5044
2.44E+09	21.1654	7.1584	15.4424	3.2373	25.773	13.9595	24.1549	11.4727
2.45E+09	21.1817	7.1935	14.9764	3.0349	25.7751	13.9537	24.1485	11.3961
2.46E+09	21.1809	7.1451	14.8133	2.9572	25.8235	13.9318	24.1545	11.4196
2.47E+09	21.1731	7.0897	14.1554	2.6743	25.8619	13.8887	24.1544	11.4316
2.48E+09	21.2082	7.0896	13.9043	2.556	25.8622	13.845	24.1556	11.4101
2.49E+09	21.1937	7.08	12.5435	2.0433	25.8121	13.8093	24.1354	11.4597
2.5E+09	21.0262	6.9523	12.3144	1.9716	25.7493	13.7987	24.1116	11.5029

Data from the literature:

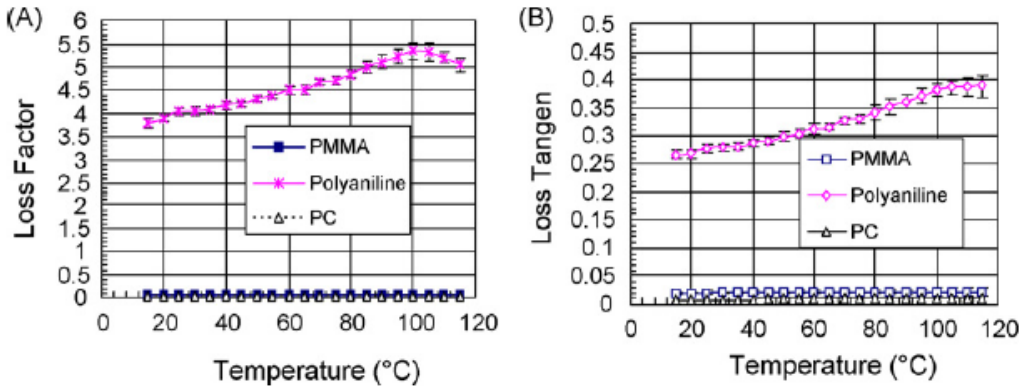

Figure App. E-1 (A) Loss factor vs. temperature for polyaniline, PC and PMMA and (B) loss tangent vs. temperature for polyaniline, PC and PMMA, from the work of Yussuf et al. (2007)

Appendix F

Mineralogical Investigation of the LRO ore type

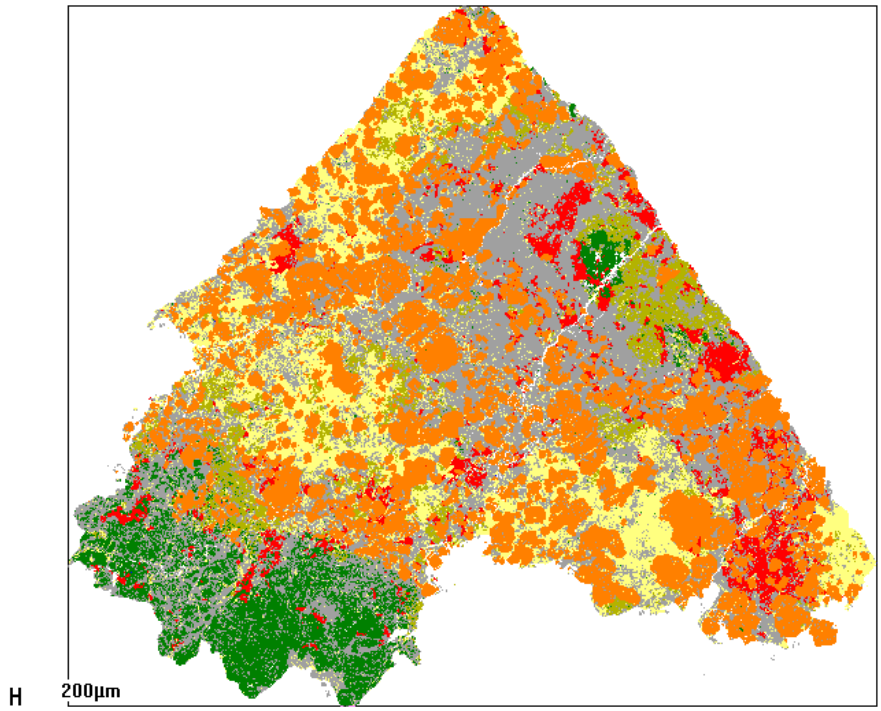

Figure App. F-1 Sample No. 1 from LRO ore type

OtherSulphides	32.85
Other	31.13
Quartz	15.92
Garnet	8.39
Feldspar	5.93
CuSulphides	5.77
Magnetite	0.01

Table App. F-1 Mineral content represented in surface percentage

Copper Sulphides	**Surface %**	**Other Forming Minerals**	**Surface %**
Bornite	<0.01	Amphibole	21.76
Chalcopyrite	5.77	Apatite	2.48
Chalcocite	<0.01	Biotite	0.80
Tennantite	<0.01	Calcite	2.39
		Chlorite	1.49
Other Sulphides		Galena	<0.01
Pyrite	32.82	Ilmenite	<0.01
Arsenopyrite	0.03	Molybdenite	<0.01
		Olivine	0.03
Quartz	15.92	Pyroxene	0.62
Feldspar	5.93	Rutile	<0.01
		Talc	0.03
Garnet	8.39	Titanite	0.33
Magnetite	0.01	Other Minerals	1.21

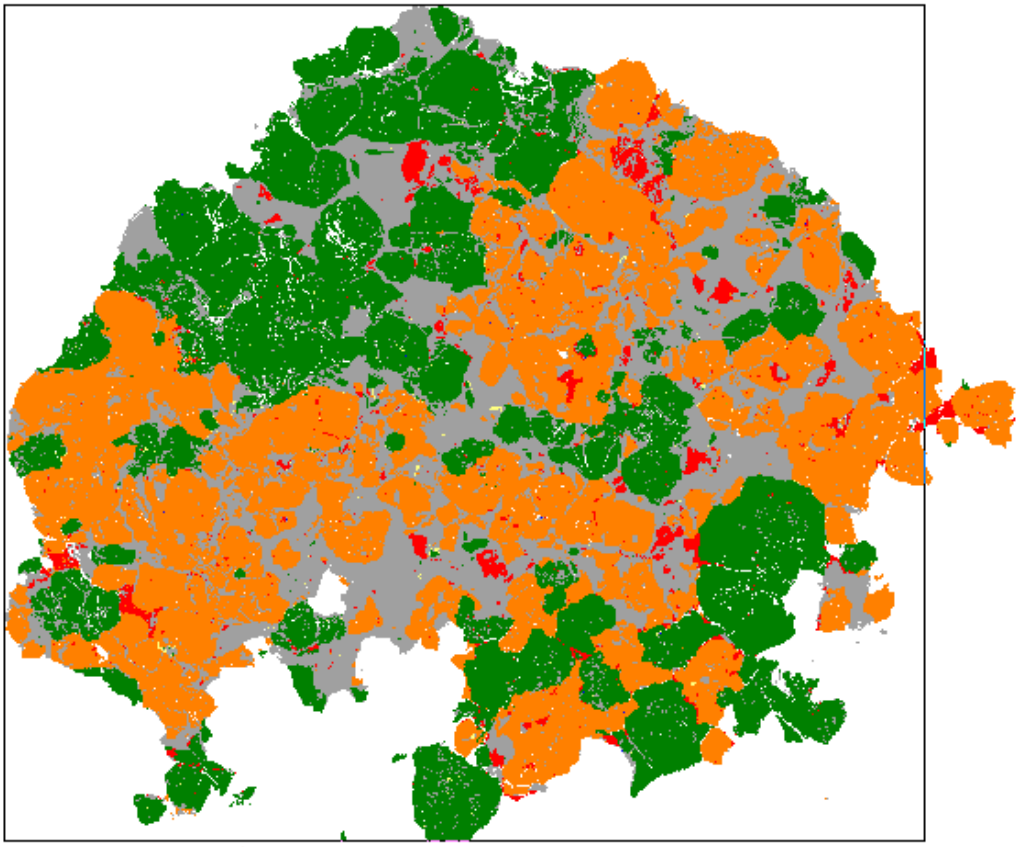

H 200µm

Figure App. F-2 Sample No. 2 from LRO ore type

OtherSulphides	38.41
Garnet	33.36
Other	25.27
CuSulphides	2.78
Quartz	0.17
Magnetite	0.01
Feldspar	0.00

Table App. F-2 Mineral content represented in surface percentage

Copper Sulphides	**Surface %**	**Other Forming Minerals**	**Surface %**
Bornite	<0.01	Amphibole	0.22
Chalcopyrite	2.78	Apatite	0.57
Chalcocite	<0.01	Biotite	<0.01
Tennantite	<0.01	Calcite	23.76
		Chlorite	0.01
Other Sulphides		Galena	0.07
Pyrite	38.35	Ilmenite	Not present
Arsenopyrite	0.06	Molybdenite	<0.01
		Olivine	<0.01
Quartz	0.17	Pyroxene	0.17
Feldspar	<0.01	Rutile	<0.01
		Talc	<0.01
Garnet	33.36	Titanite	<0.01
Magnetite	0.01	Other Minerals	0.47

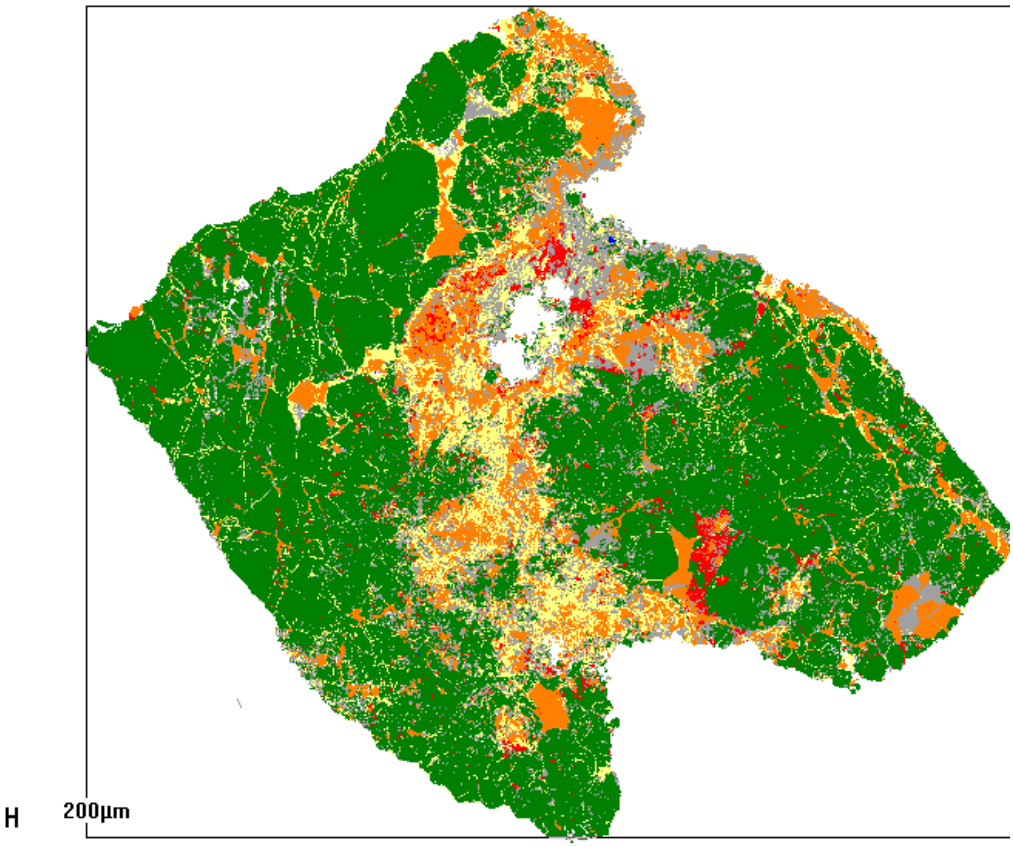

Figure App. F-3 Sample No. 3 from LRO ore type

Garnet	59.34
Other	13.81
OtherSulphides	12.57
Quartz	11.67
CuSulphides	2.53
Feldspar	0.07
Magnetite	0.01

Table App. F-3 Mineral content represented in surface percentage

Copper Sulphides	**Surface %**	**Other Forming Minerals**	**Surface %**
Bornite	0.02	Amphibole	5.23
Chalcopyrite	2.50	Apatite	0.48
Chalcocite	0.01	Biotite	3.67
Tennantite	<0.01	Calcite	0.36
		Chlorite	1.17
Other Sulphides		Galena	<0.01
Pyrite	12.56	Ilmenite	Not present
Arsenopyrite	<0.01	Molybdenite	<0.01
		Olivine	0.02
Quartz	11.67	Pyroxene	1.73
Feldspar	0.07	Rutile	<0.01
		Talc	0.16
Garnet	59.34	Titanite	0.01
Magnetite	0.01	Other Minerals	0.98

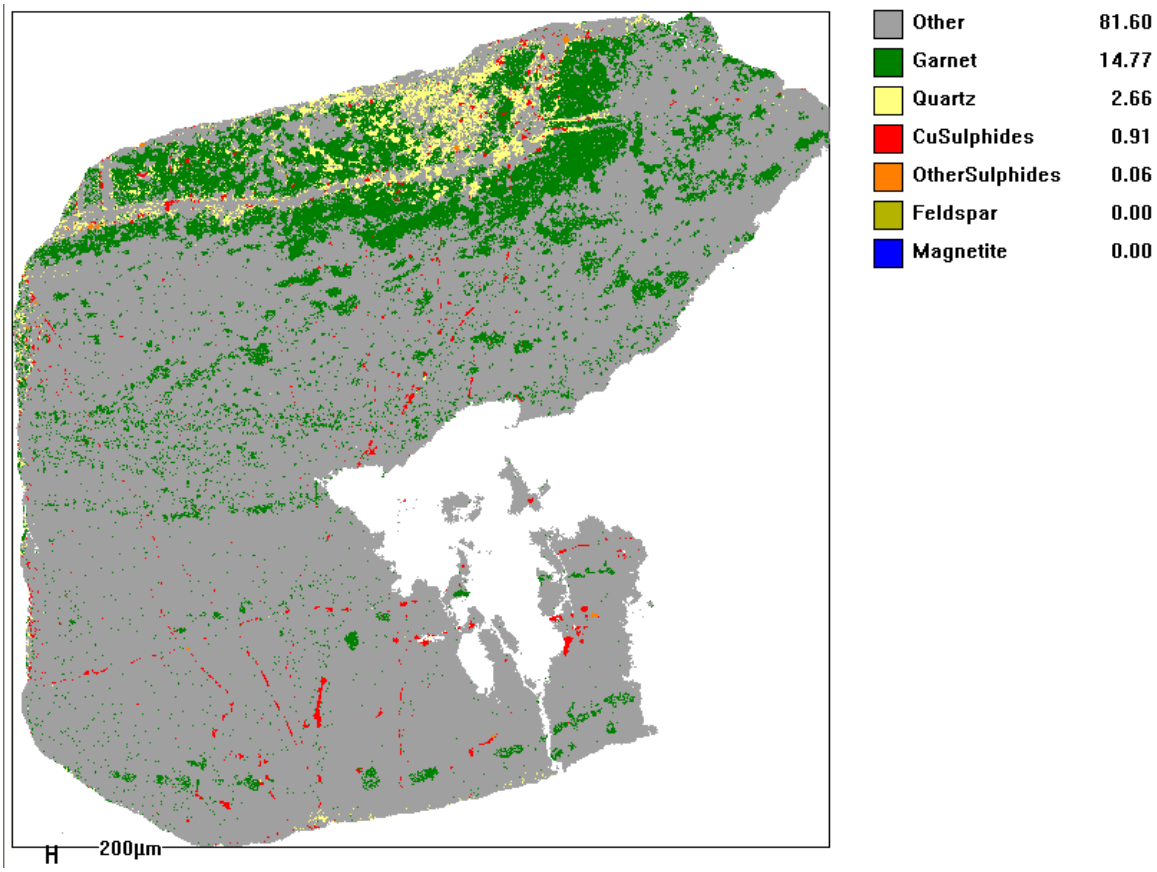

Figure App. F-4 Sample No. 4 from LRO ore type

Table App. F-4 Mineral content represented in surface percentage

Copper Sulphides	**Surface %**	**Other Forming Minerals**	**Surface %**
Bornite	<0.01	Amphibole	71.59
Chalcopyrite	0.91	Apatite	0.58
Chalcocite	<0.01	Biotite	0.04
Tennantite	<0.01	Calcite	6.82
		Chlorite	0.07
Other Sulphides		Galena	<0.01
Pyrite	0.06	Ilmenite	Not present
Arsenopyrite	<0.01	Molybdenite	<0.01
		Olivine	<0.01
Quartz	2.66	Pyroxene	0.94
Feldspar	<0.01	Rutile	0.12
		Talc	0.19
Garnet	14.77	Titanite	0.01
Magnetite	<0.01	Other Minerals	1.35

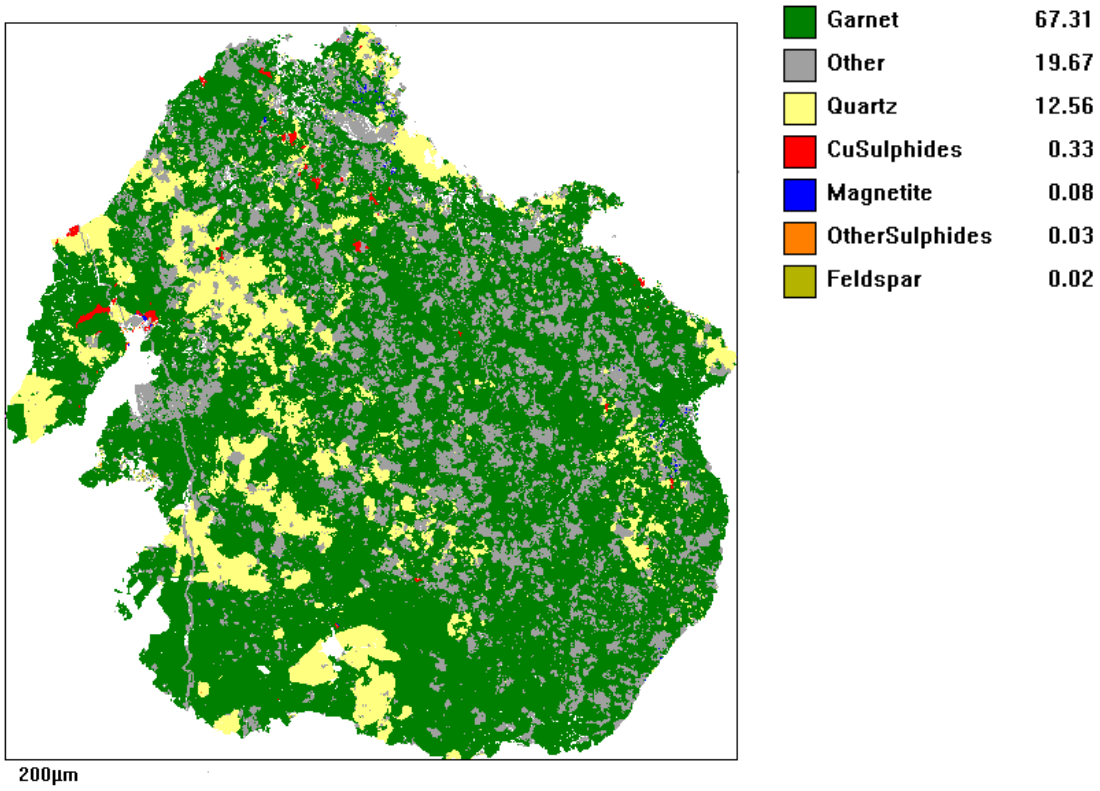

Figure App. F-5 Sample No. 5 from LRO ore type

Copper Sulphides	**Surface %**	**Other Forming Minerals**	**Surface %**
Bornite	<0.01	Amphibole	1.71
Chalcopyrite	0.33	Apatite	1.58
Chalcocite	<0.01	Biotite	0.01
Tennantite	<0.01	Calcite	13.36
		Chlorite	0.21
Other Sulphides		Galena	<0.01
Pyrite	0.03	Ilmenite	Not present
Arsenopyrite	<0.01	Molybdenite	<0.01
		Olivine	0.41
Quartz	12.56	Pyroxene	1.04
Feldspar	0.02	Rutile	<0.01
		Talc	<0.01
Garnet	67.31	Titanite	<0.01
Magnetite	0.08	Other Minerals	1.33

Table App. F-5 Mineral content represented in surface percentage

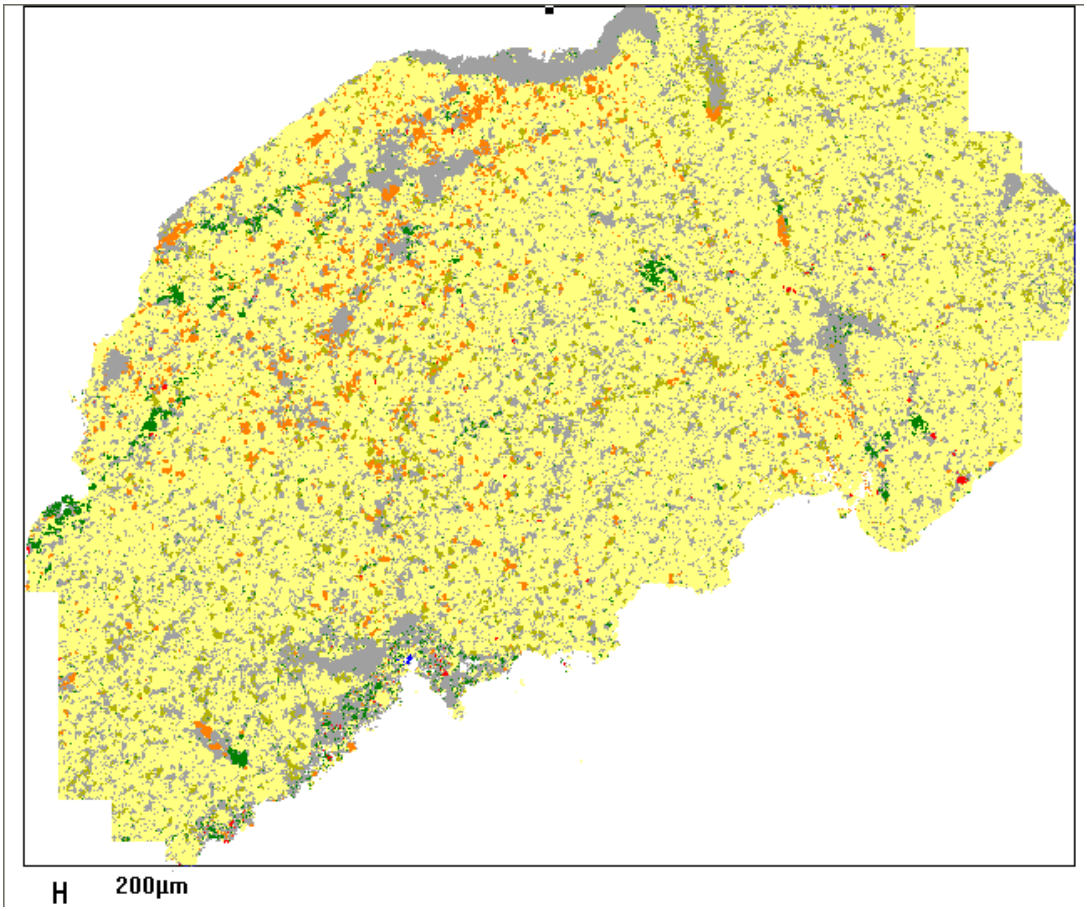

Figure App. F-6 Sample No. 6 from LRO ore type

Quartz	71.78
Other	19.06
Feldspar	4.35
OtherSulphides	3.14
Garnet	1.53
CuSulphides	0.14
Magnetite	0.01

Table App. F-6 Mineral content represented in surface percentage

Copper Sulphides	**Surface %**	**Other Forming Minerals**	**Surface %**
Bornite	<0.01	Amphibole	8.18
Chalcopyrite	0.13	Apatite	0.06
Chalcocite	<0.01	Biotite	0.09
Tennantite	<0.01	Calcite	9.39
		Chlorite	0.14
Other Sulphides		Galena	<0.01
Pyrite	3.13	Ilmenite	Not present
Arsenopyrite	<0.01	Molybdenite	<0.01
		Olivine	0.01
Quartz	71.78	Pyroxene	0.47
Feldspar	4.35	Rutile	<0.01
		Talc	0.01
Garnet	1.53	Titanite	0.08
Magnetite	0.01	Other Minerals	0.63

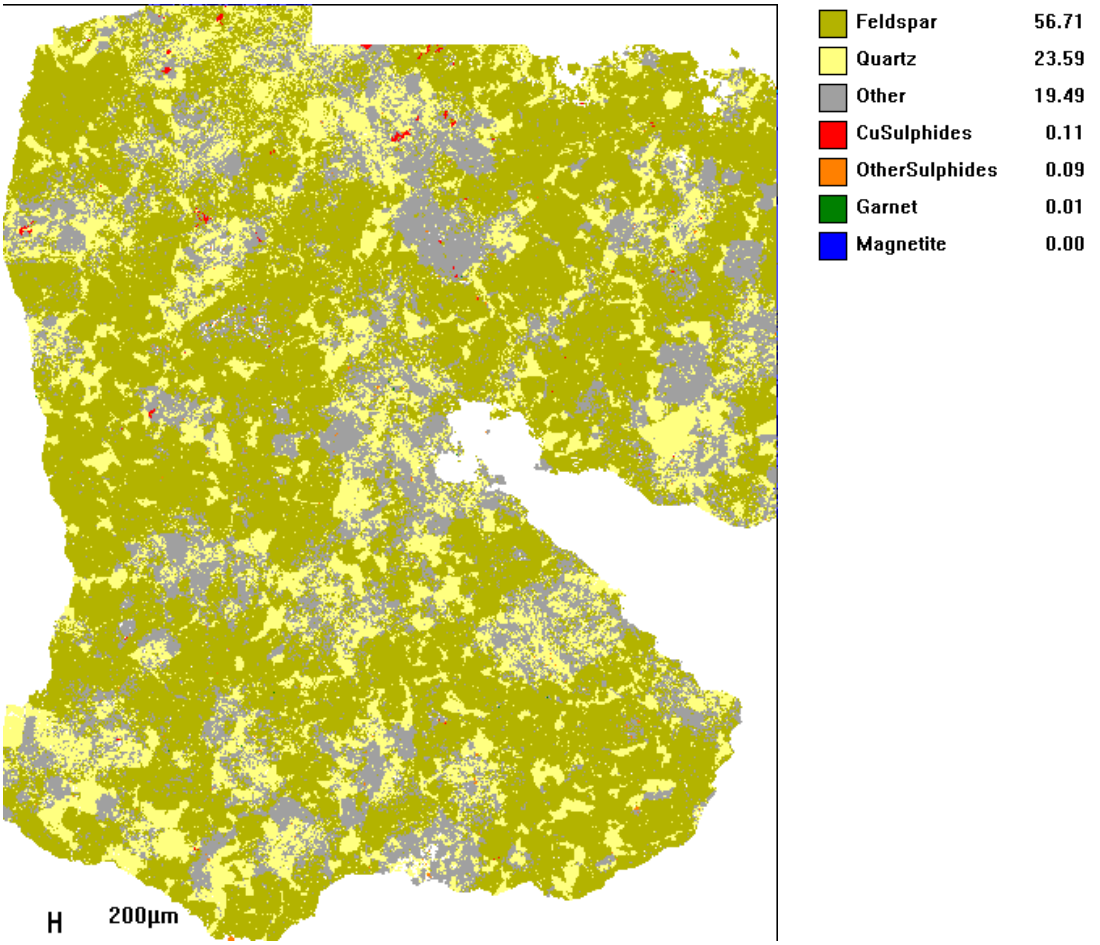

Figure App. F-7 Sample No. 7 from LRO ore type

Table App. F-7 Mineral content represented in surface percentage

Copper Sulphides	**Surface %**	**Other Forming Minerals**	**Surface %**
Bornite	0.01	Amphibole	0.09
Chalcopyrite	0.10	Apatite	0.66
Chalcocite	<0.01	Biotite	16.43
Tennantite	<0.01	Calcite	0.01
		Chlorite	0.36
Other Sulphides		Galena	<0.01
Pyrite	0.09	Ilmenite	<0.01
Arsenopyrite	<0.01	Molybdenite	<0.01
		Olivine	0.01
Quartz	23.59	Pyroxene	0.04
Feldspar	56.71	Rutile	0.12
		Talc	<0.01
Garnet	0.01	Titanite	<0.01
Magnetite	<0.01	Other Minerals	1.78

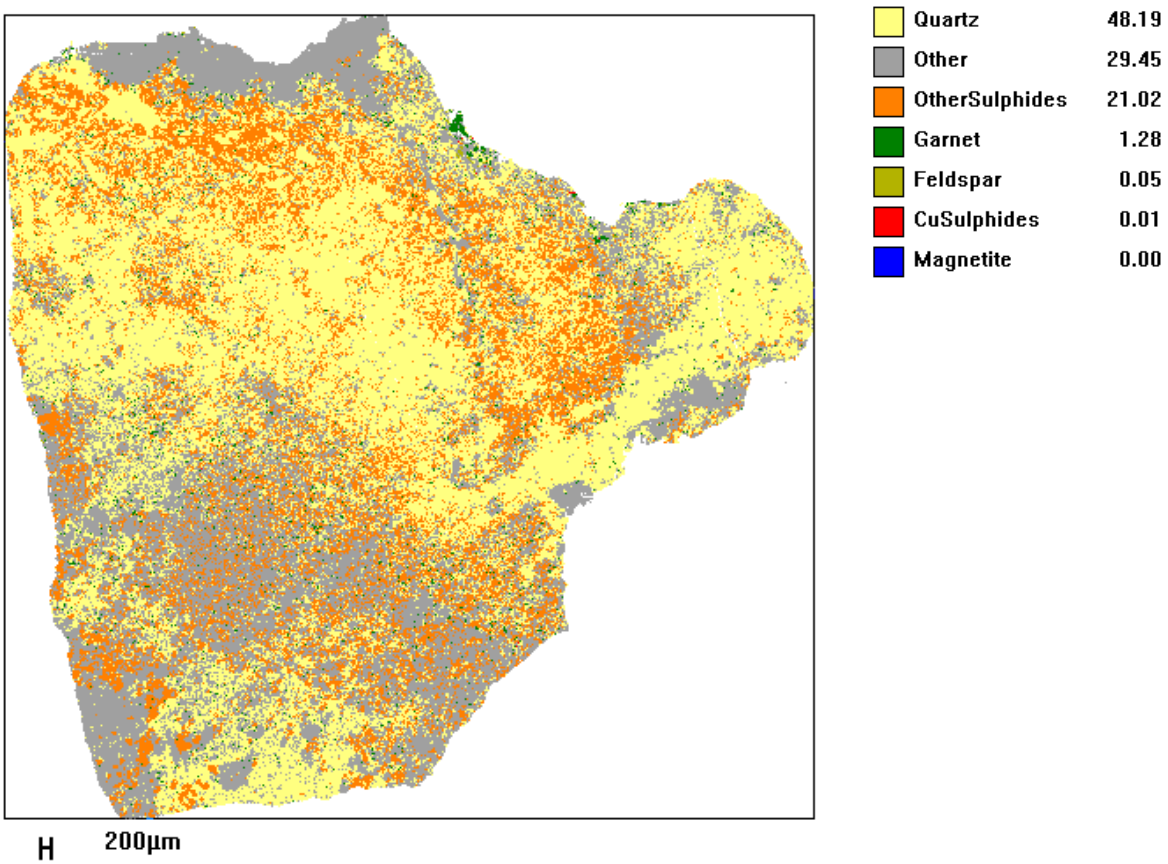

Figure App. F-8 Sample No. 8 from LRO ore type

Table App. F-8 Mineral content represented in surface percentage

Copper Sulphides	**Surface %**	**Other Forming Minerals**	**Surface %**
Bornite	<0.01	Amphibole	1.14
Chalcopyrite	0.01	Apatite	0.32
Chalcocite	<0.01	Biotite	0.05
Tennantite	<0.01	Calcite	20.54
		Chlorite	2.40
Other Sulphides		Galena	Not present
Pyrite	21.01	Ilmenite	Not present
Arsenopyrite	0.01	Molybdenite	<0.01
		Olivine	0.01
Quartz	48.19	Pyroxene	3.01
Feldspar	0.05	Rutile	<0.01
		Talc	0.48
Garnet	1.28	Titanite	<0.01
Magnetite	<0.01	Other Minerals	1.49

Appendix G

Reproducibility Testing for the LRO Ore Type

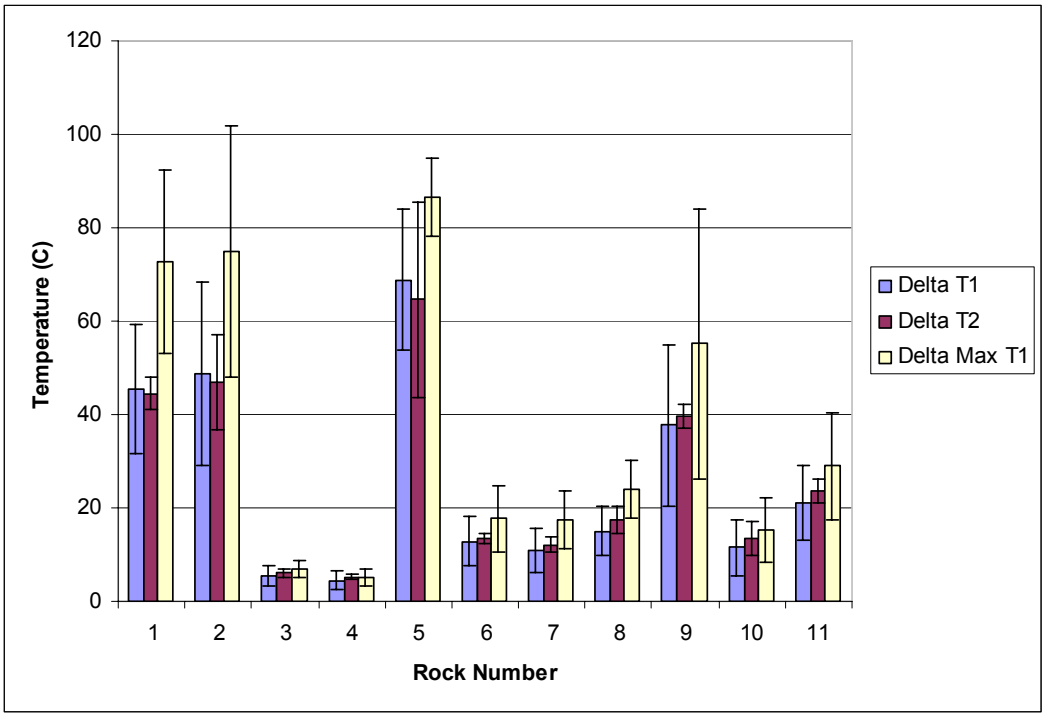

Figure App. G-1 Reproducibility temperature change graph for the eleven -22+19 mm particles in set No. 1 where each particle was tested 6 times in different orientations

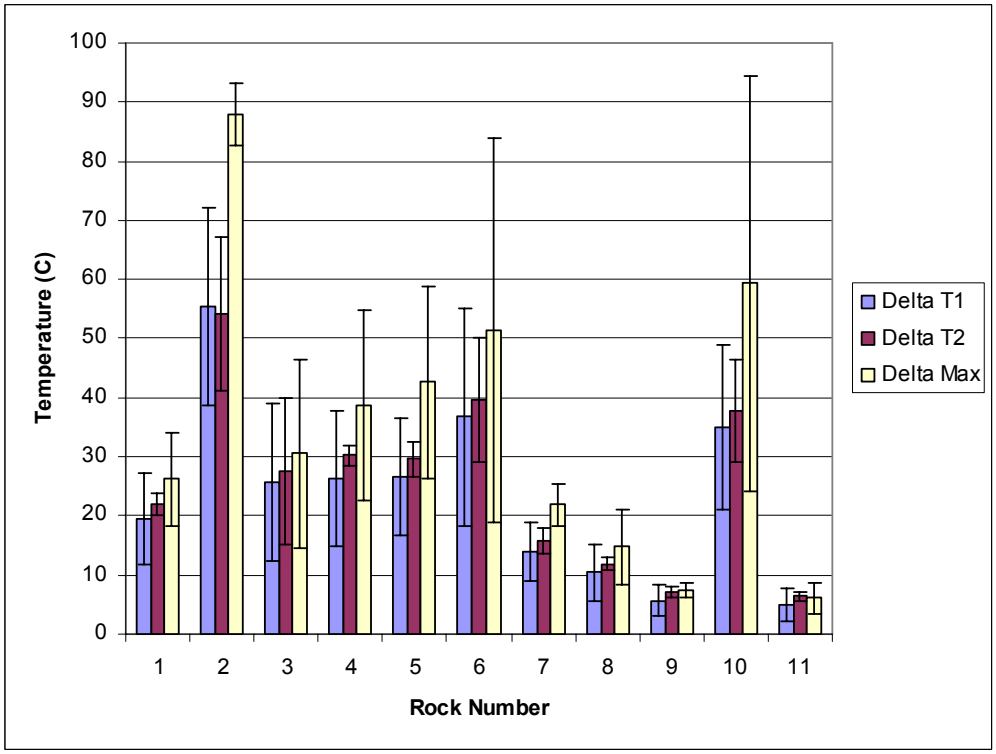

Figure App. G-2 Reproducibility temperature change graph for the eleven -22+19 mm particles in set No. 2 where each particle was tested 6 times in different orientations

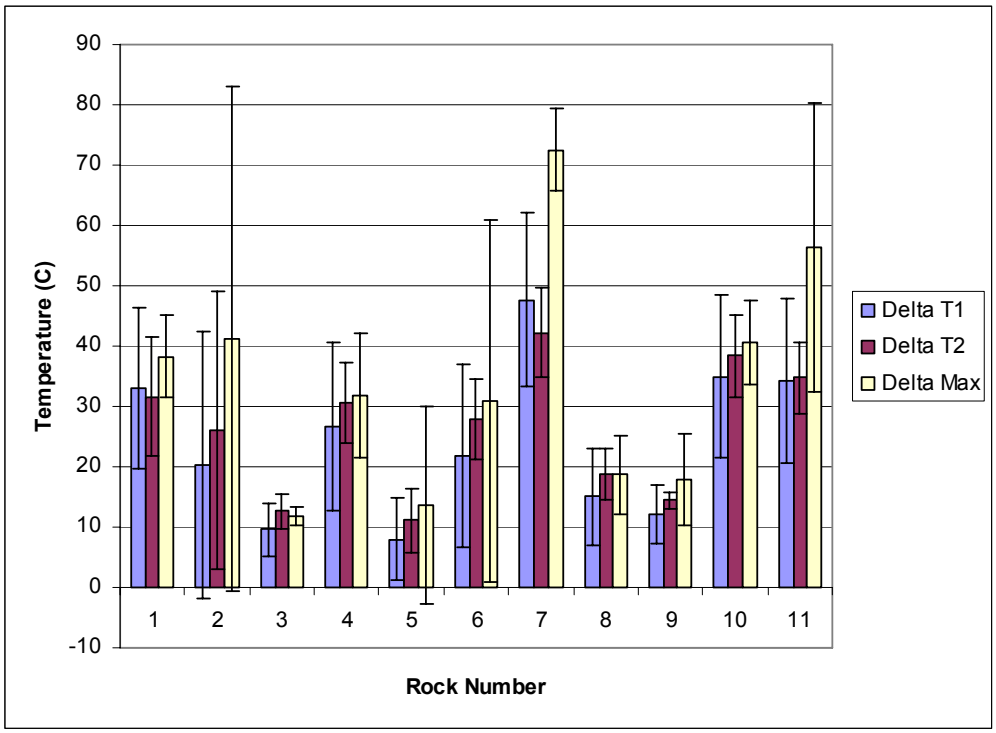

Figure App. G-3 Reproducibility temperature change graph for the eleven -22+19 mm particles in set No. 3 where each particle was tested 6 times in different orientations

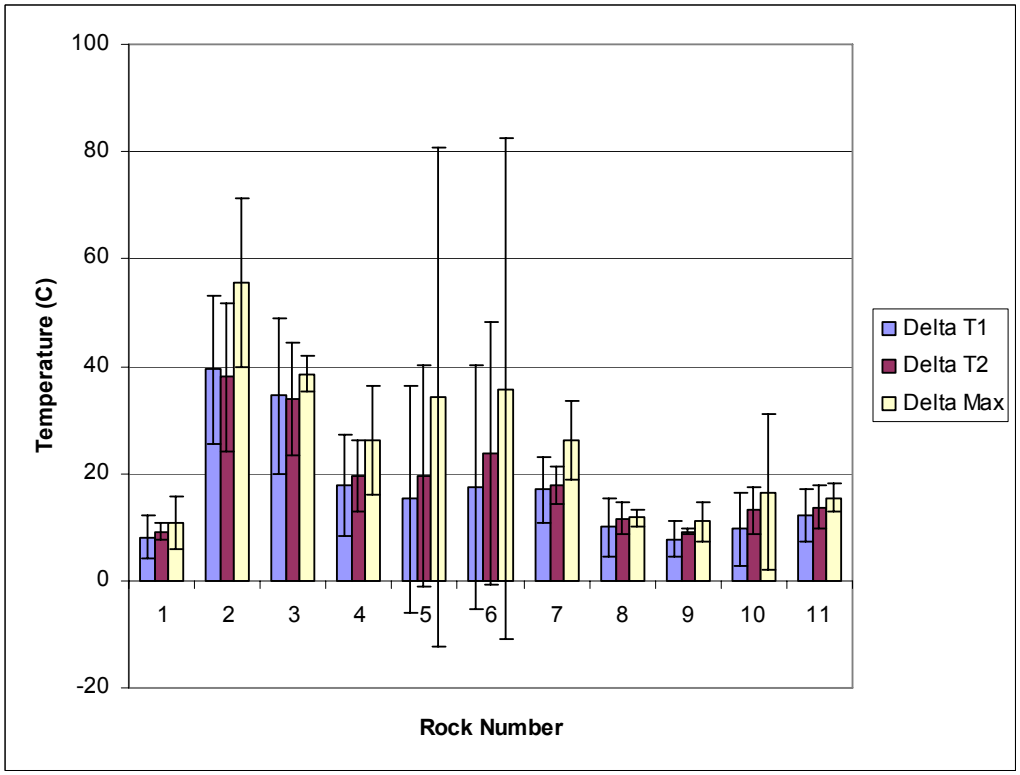

Figure App. G-4 Reproducibility temperature change graph for the eleven -22+19 mm particles in set No. 4 where each particle was tested 6 times in different orientations

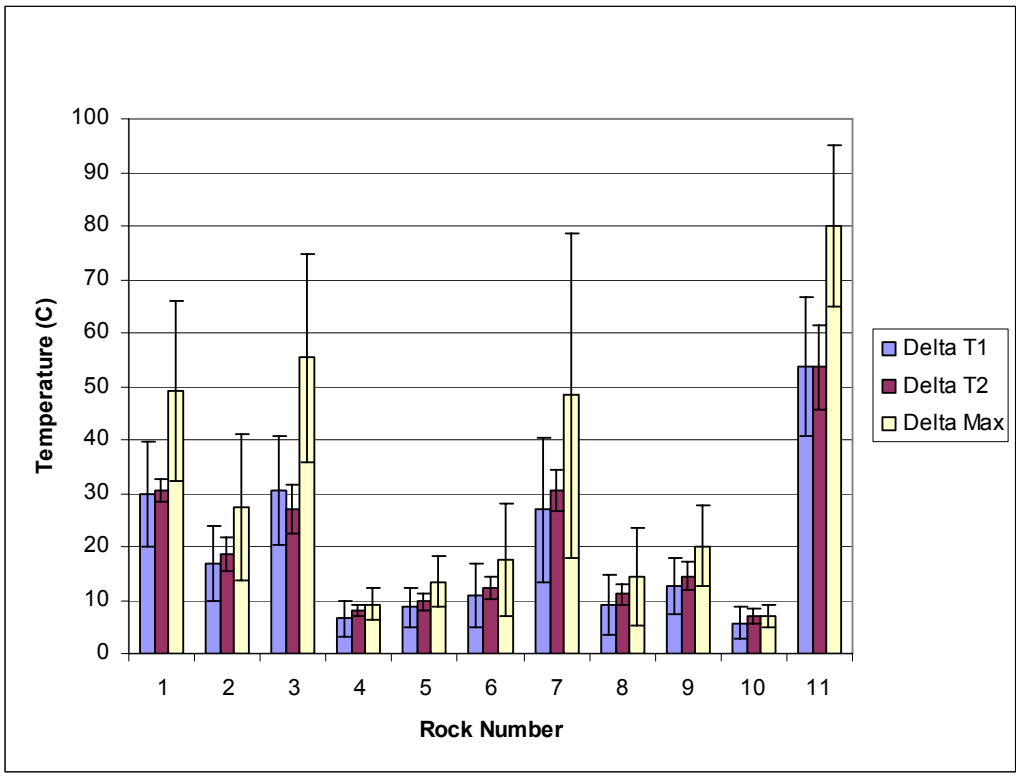

Figure App. G-5 Reproducibility temperature change graph for the eleven -22+19 mm particles in set No. 5 where each particle was tested 6 times in different orientations

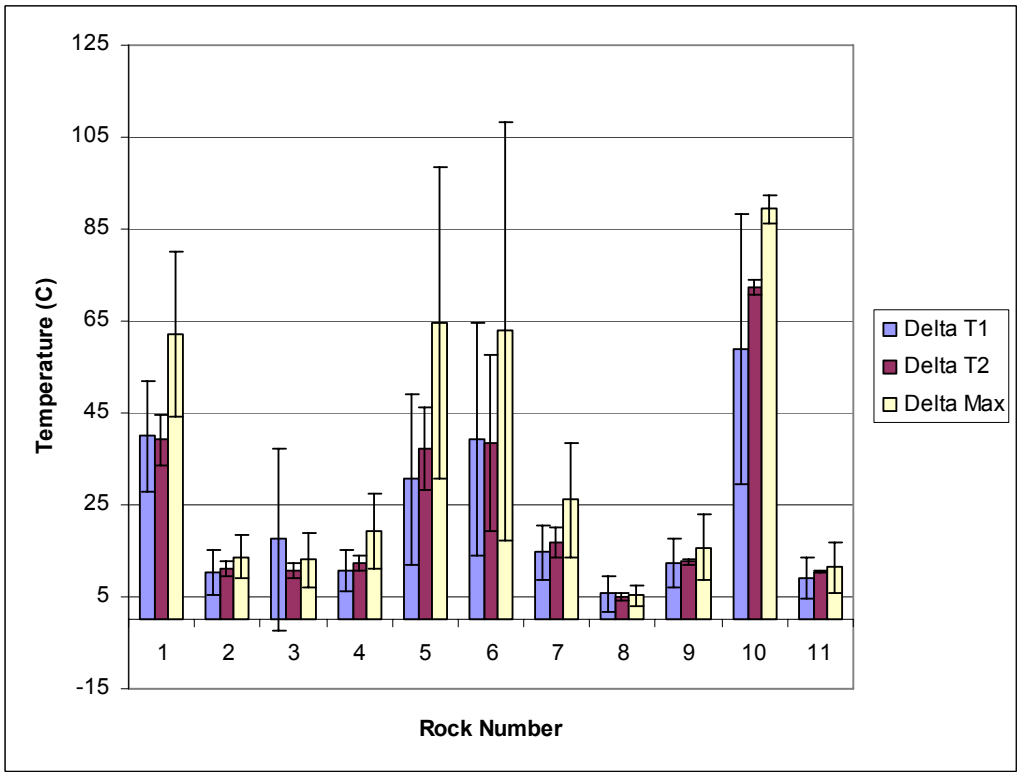

Figure App. G-6 Reproducibility temperature change graph for the eleven -22+19 mm particles in set No. 6 where each particle was tested 6 times in different orientations

Sub Sample No	Position Number	Rock Number durin testing	Rock Number	Rock Mass (g)	Cu Assay %	Fe Assay %	Delta Max T1	Cumulative Mass %	Cumulative Copper Recovery %	Cumulative Iron Recovery %
1	1	8	1	18.23	0.038	8.400	5.810	1.843	0.113	2.374
1	2	3	2	15.71	0.010	0.240	7.290	3.431	0.139	2.432
1	2	9	3	13.81	0.060	1.300	7.700	4.828	0.275	2.711
1	8	11	4	9.35	0.249	1.580	8.080	5.773	0.653	2.940
1	4	10	5	11.96	0.361	4.970	9.150	6.982	1.356	3.861
1	2	4	6	15.51	0.012	10.500	9.430	8.550	1.385	6.385
1	8	8	7	17.4	0.197	1.390	11.600	10.309	1.945	6.760
1	3	3	8	7.54	0.047	3.110	11.830	11.072	2.003	7.124
1	11	11	9	8.85	1.330	2.030	12.440	11.966	3.920	7.402
1	9	9	10	20.19	1.260	2.070	13.470	14.008	8.062	8.050
2	5	2	11	15.99	0.154	7.760	14.850	15.624	8.464	9.974
2	6	3	12	12.63	0.022	10.400	15.230	16.901	8.510	12.010
2	8	11	13	12.7	0.042	9.470	15.230	18.185	8.596	13.874
2	1	1	14	13.68	0.096	6.650	15.770	19.568	8.809	15.285
2	4	3	15	4.06	0.102	1.760	16.380	19.979	8.877	15.395
2	6	5	16	17.61	0.852	1.080	16.630	21.759	11.319	15.690
2	9	9	17	16.08	0.408	4.720	17.780	23.385	12.387	16.867
2	9	7	18	13.2	0.034	9.320	19.220	24.719	12.459	18.774
2	4	4	19	7.17	1.400	2.020	19.670	25.444	14.094	18.998
2	5	6	20	25.86	0.819	7.430	19.760	28.059	17.542	21.977
2	11	8	21	10.26	0.076	8.060	20.940	29.096	17.669	23.259
3	5	8	22	16.19	0.503	8.570	21.490	30.733	18.994	25.410
3	7	10	23	15.47	0.530	8.700	21.960	32.297	20.329	27.496
3	7	4	24	15.87	0.971	8.600	22.180	33.902	22.838	29.612
3	5	7	25	20.15	0.063	11.500	25.090	35.939	23.044	33.204
3	8	8	26	18.99	0.465	13.100	25.470	37.859	24.482	37.060
3	9	9	27	14.98	0.962	3.940	26.000	39.373	26.828	37.975
3	10	9	28	19.53	1.340	5.740	26.060	41.348	31.090	39.713
3	8	6	29	11.93	0.524	2.770	26.460	42.554	32.108	40.225
3	4	8	30	15.43	0.274	10.200	27.600	44.114	32.797	42.665
3	7	7	31	13.07	0.379	2.540	29.090	45.435	33.604	43.179
3	5	5	32	15.33	1.930	4.130	31.510	46.985	38.422	44.161
4	10	10	33	15.11	0.055	5.290	32.650	48.513	38.557	45.400
4	1	1	34	15.35	0.434	1.900	33.080	50.065	39.643	45.852
4	1	1	35	11.5	0.045	0.882	33.460	51.227	39.728	46.009
4	11	7	36	10.59	1.550	2.720	35.340	52.298	42.401	46.456
4	3	11	37	13.89	0.060	1.570	35.610	53.702	42.537	46.794
4	1	2	38	18.86	0.614	6.520	38.970	55.609	44.423	48.700
4	3	3	39	22.03	0.633	3.880	39.370	57.836	46.696	50.025
4	10	10	40	14.36	0.972	4.140	40.830	59.288	48.968	50.947
4	4	4	41	25.15	0.989	6.540	41.100	61.831	53.020	53.497
4	10	5	42	15.7	1.200	4.900	42.440	63.418	56.088	54.689
4	3	4	43	10.89	0.013	1.450	53.400	64.519	56.110	54.934
5	7	1	44	18.94	0.093	3.300	54.300	66.434	56.396	55.903
5	6	6	45	17.39	0.015	10.500	56.760	68.192	56.439	58.733
5	2	2	46	13.13	0.073	1.130	65.600	69.520	56.594	58.963
5	11	9	47	17.53	0.028	3.470	66.560	71.292	56.674	59.906
5	2	1	48	16.95	1.390	9.060	67.610	73.006	60.511	62.287
5	3	7	49	11.68	0.116	1.000	72.550	74.187	60.733	62.468
5	9	3	50	16.69	0.019	5.340	74.510	75.874	60.784	63.849
5	7	7	51	5.96	0.895	5.990	77.100	76.477	61.653	64.403
5	8	1	52	12.35	3.420	5.500	77.310	77.725	68.531	65.456
5	11	11	53	20.7	0.010	10.800	77.950	79.818	68.564	68.921
5	9	10	54	14.51	2.090	13.600	80.370	81.285	73.503	71.980
6	6	6	55	18.67	1.710	8.510	84.140	83.173	78.702	74.443
6	3	6	56	10.57	1.000	5.330	85.670	84.241	80.424	75.317
6	5	5	57	15.83	0.028	6.460	86.840	85.842	80.495	76.902
6	4	5	58	13.1	0.012	10.400	88.010	87.166	80.519	79.014
6	6	6	59	13.74	0.061	3.480	89.280	88.555	80.655	79.755
6	2	2	60	15.55	0.042	4.860	89.530	90.127	80.762	80.927
6	11	11	61	11.76	0.288	3.450	89.570	91.316	81.313	81.556
6	10	10	62	17.49	0.069	0.935	91.000	93.085	81.509	81.809
6	1	2	63	18.48	0.835	20.800	91.570	94.953	84.021	87.768
6	7	2	64	14.91	0.005	15.600	91.660	96.460	84.034	91.373
6	10	5	65	19.8	0.189	15.200	91.730	98.462	84.643	96.039
1	10	5	66	15.21	6.200	16.800	92.620	100.000	100.000	100.000

Figure App. G-7 Data for separation curves from reproducibility study six sets sorted by Delta T1 for LRO ore type

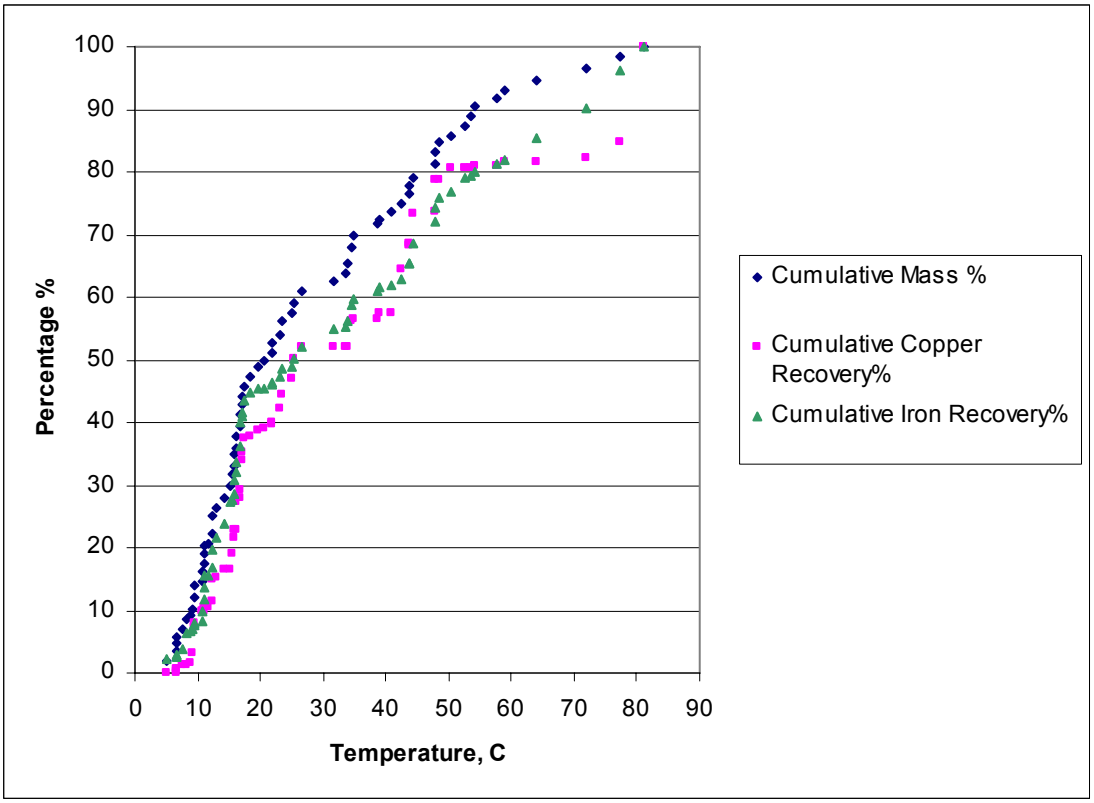

Figure App. G-8 Separation curves from reproducibility study six sets sorted by Delta T1 for LRO ore type

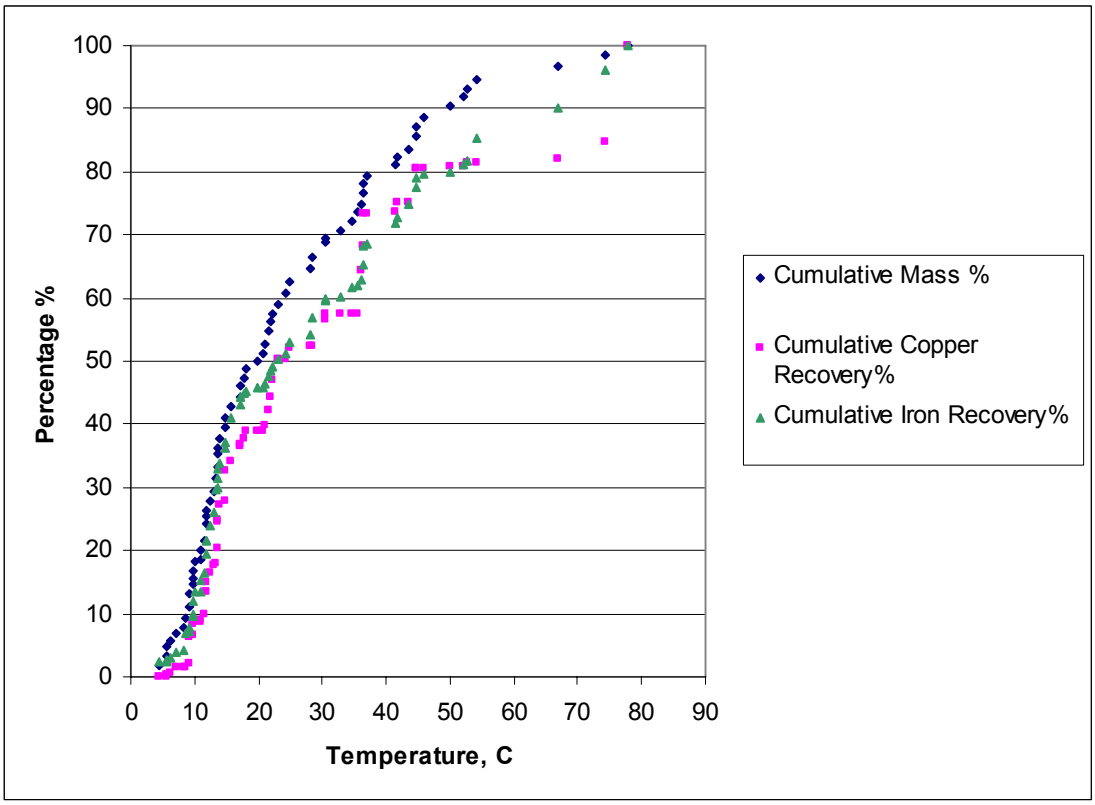

Figure App. G-9 Separation curves from reproducibility study six sets sorted by Delta T2 for LRO ore type

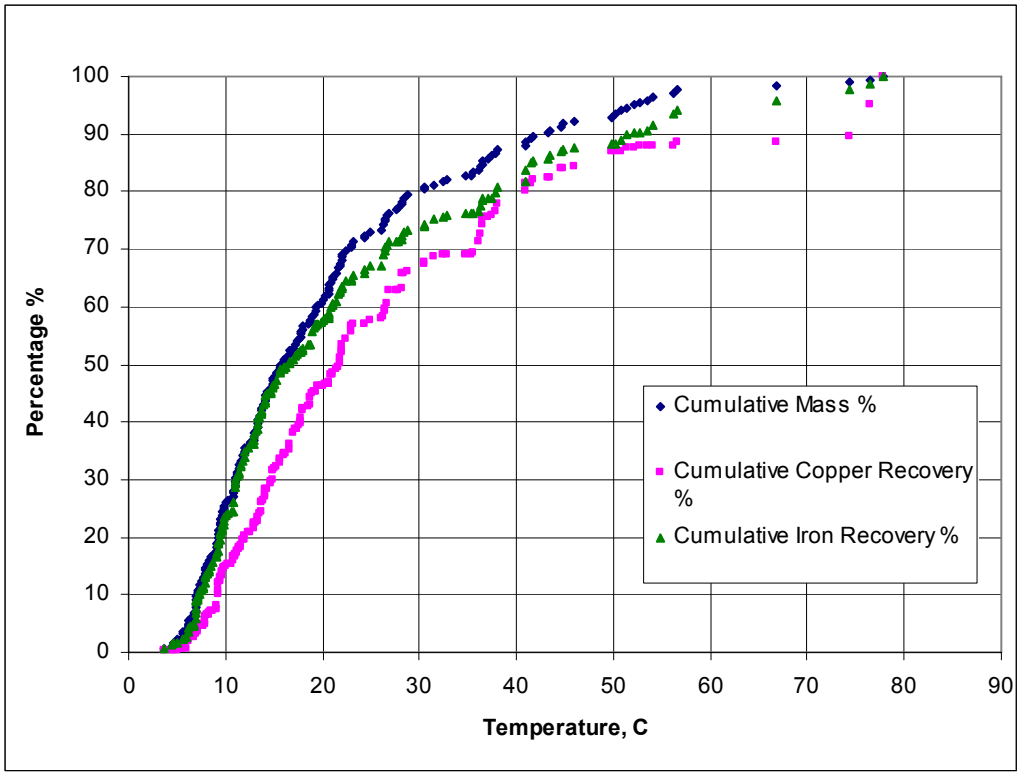

Figure App. G-10 Separation curve for LRO (larger population) -22+19 mm size fraction based on Delta T2

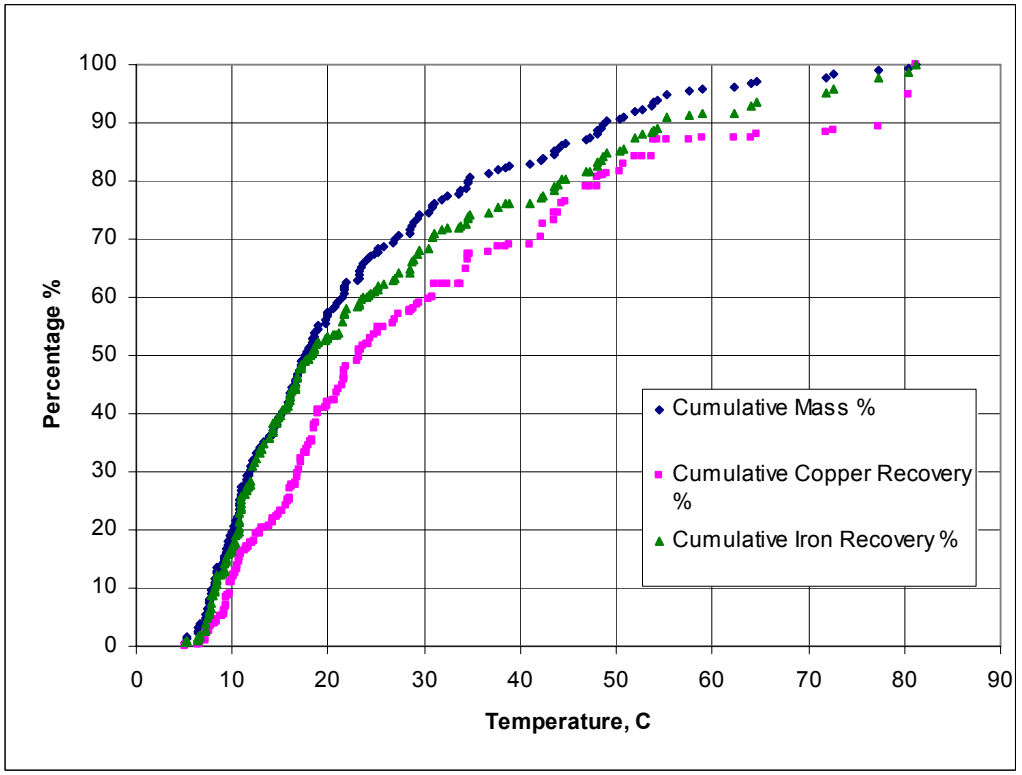

Figure App. G-11 Separation curve for LRO (larger population)-22+19 mm size fraction based on Delta T1

Appendix H

Set No. 1:

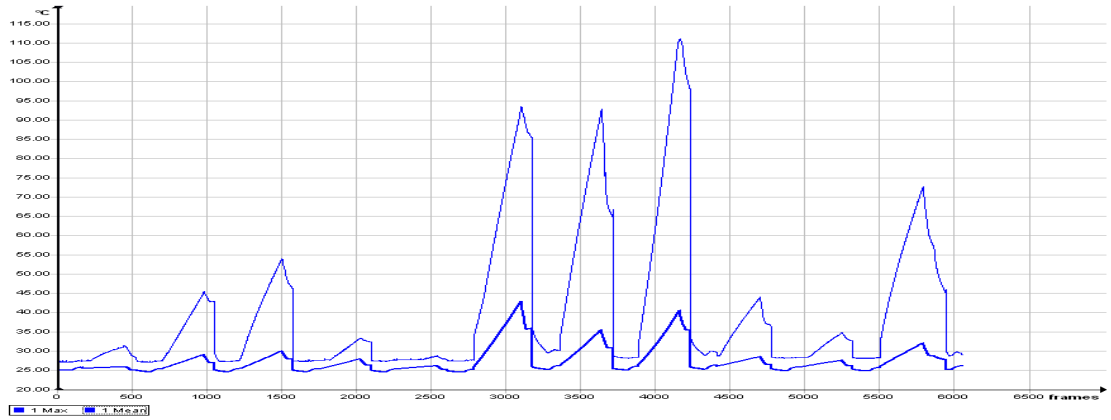

Figure App. H-1 First exposure, timing graph for the set No. 1

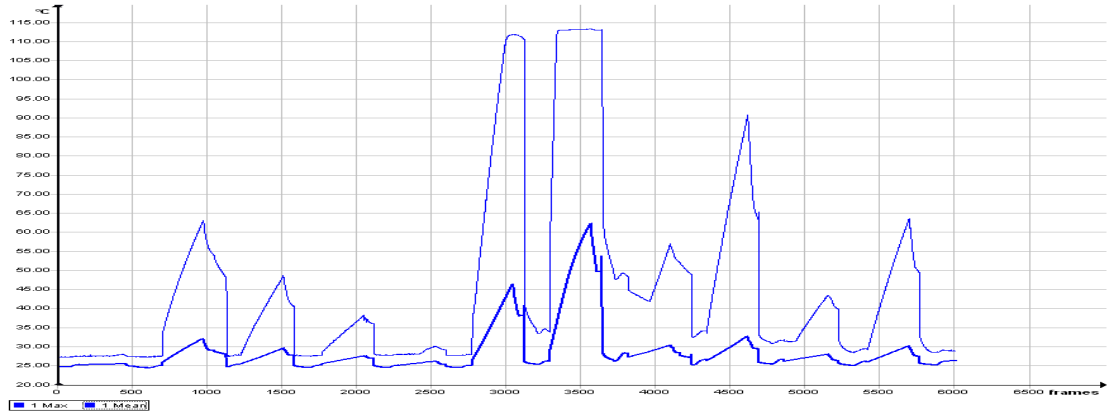

Figure App. H-2 Second exposure, timing graph for the set No. 1

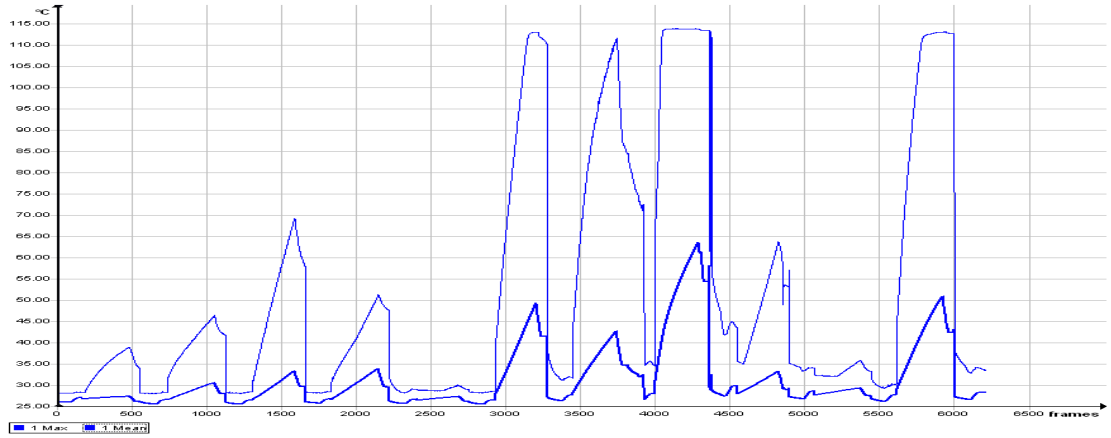

Figure App. H-3 Third exposure, timing graph for the set No. 1

Tomography Analysis for Some of the Particles in the Set No. 1:

Tomography analysis of some of the cold particles:

Particle No. 1 Set No. 1

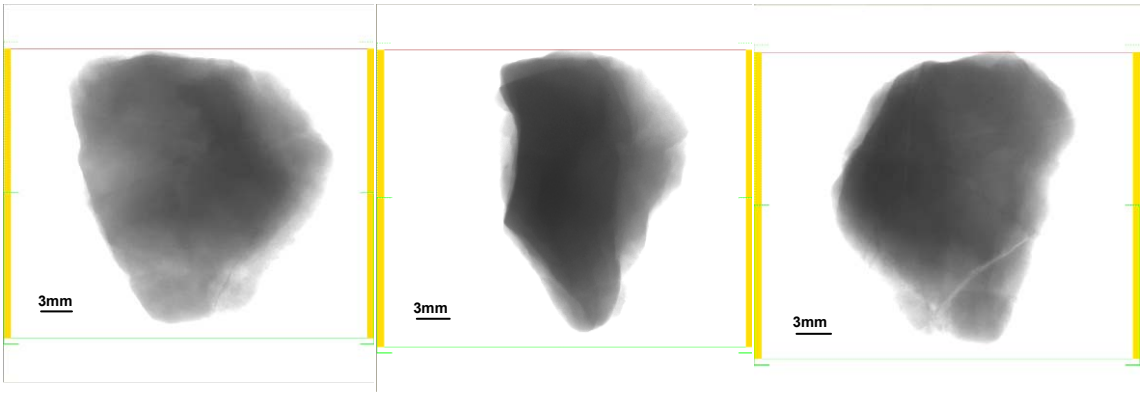

Position 0 deg **Position 90 deg** **Position 120 deg**

Figure App. H-4 LRO Ore Particle No. 1 Set No. 1

Tomography analysis of some of the hot particles:

Particle No. 9 Set No. 1

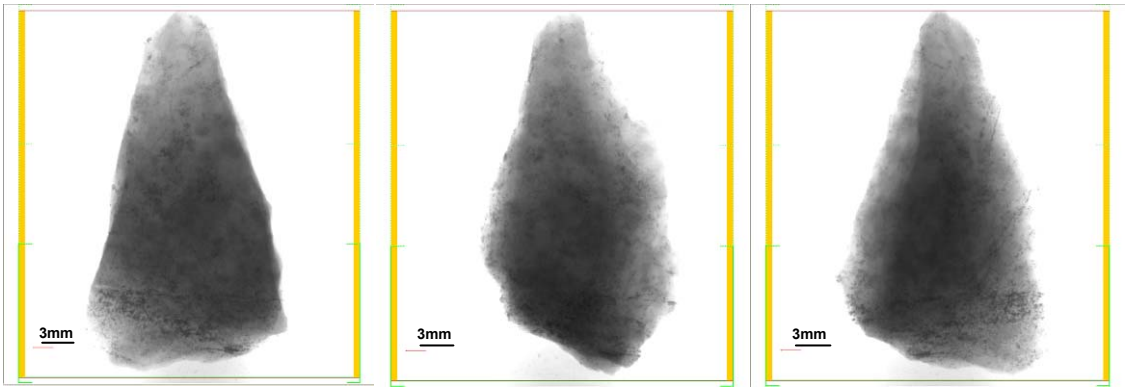

Position 0 deg **Position 45 deg** **Position 110 deg**

Figure App. H-5 LRO Ore Particle No. 9 Set No. 1

Set No. 2:

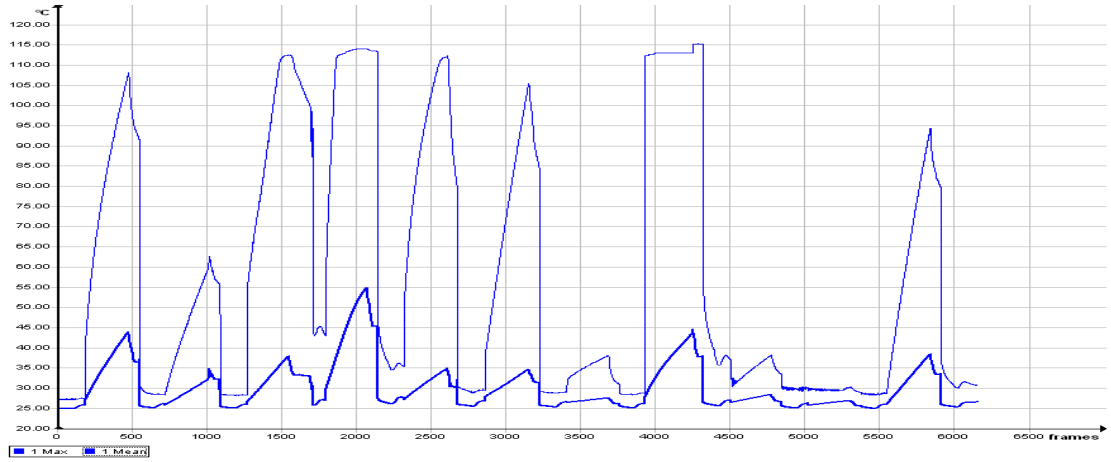

Figure App. H-6 First exposure, timing graph for the set No. 2

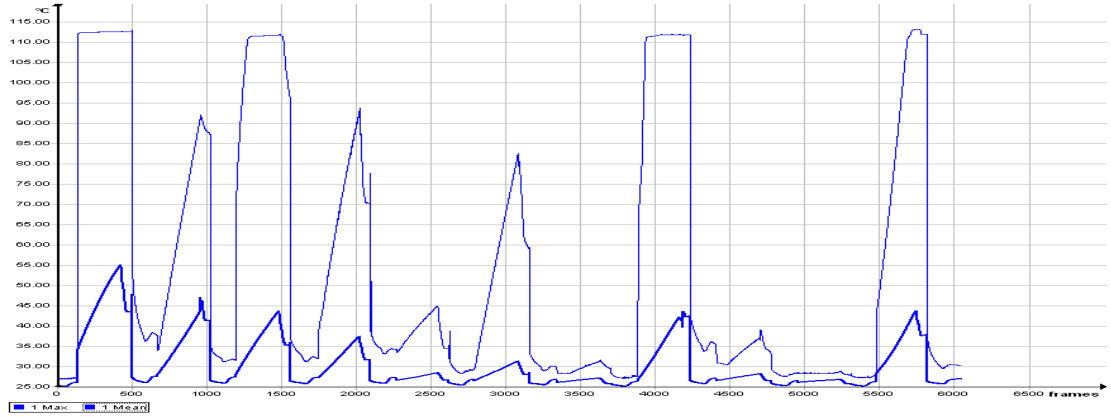

Figure App. H-7 Second exposure, timing graph for the set No. 2

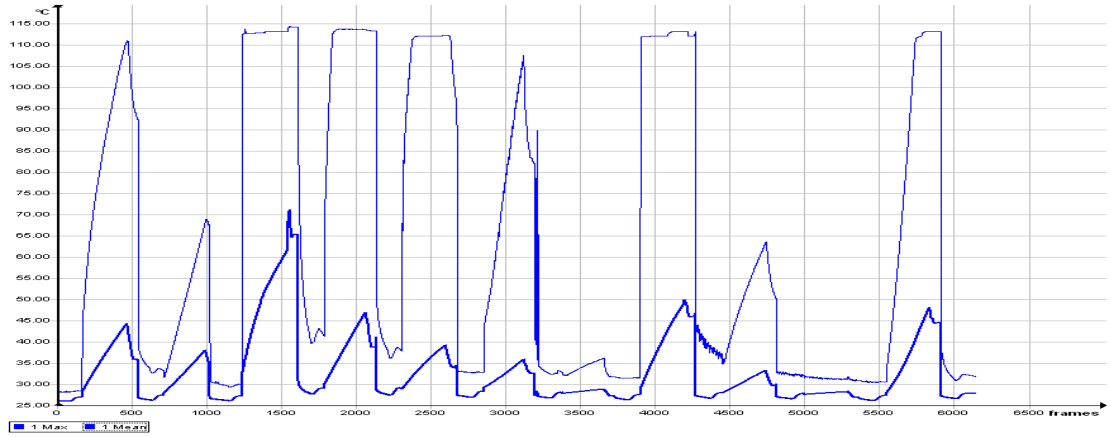

Figure App. H-8 Third exposure, timing graph for the set No. 2

Tomography Analysis for Some of the Particles in the Set No. 2:

Tomography analysis of some of the hot particles:

Particle No. 3 Set No. 2

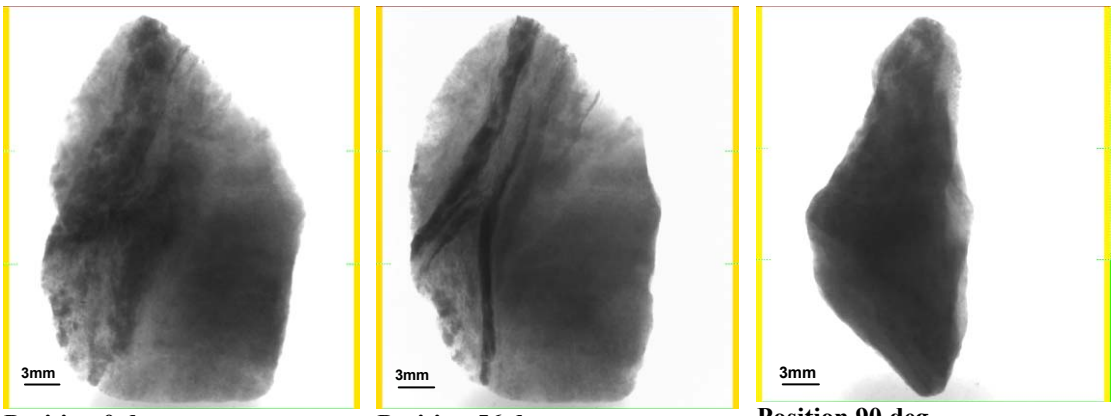

Position 0 deg **Position 56 deg** **Position 90 deg**

Figure App. H-9 LRO Ore Particle No. 3 Set No. 2

Particle No. 11 Set No. 2

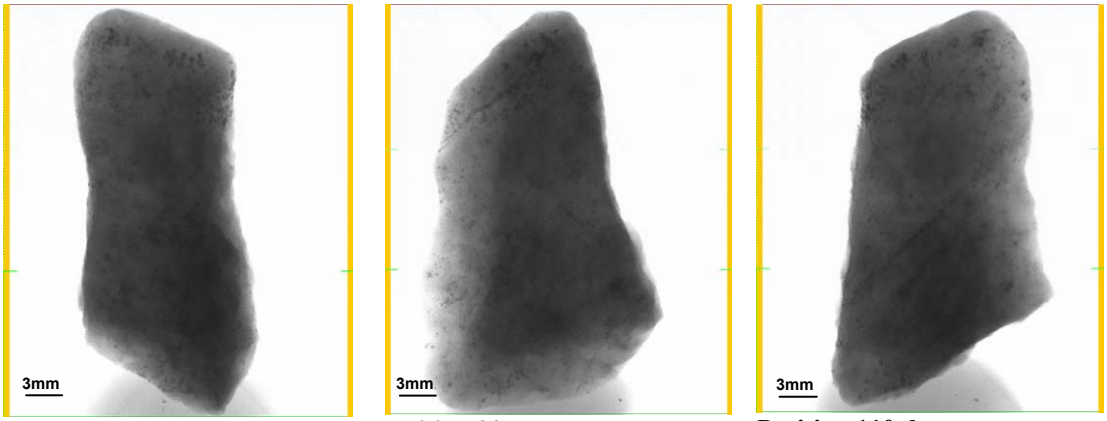

Position 0 deg **Position 90 deg** **Position 110 deg**

Figure App. H-10 LRO Ore Particle No. 11 Set No. 2

Set No. 3:

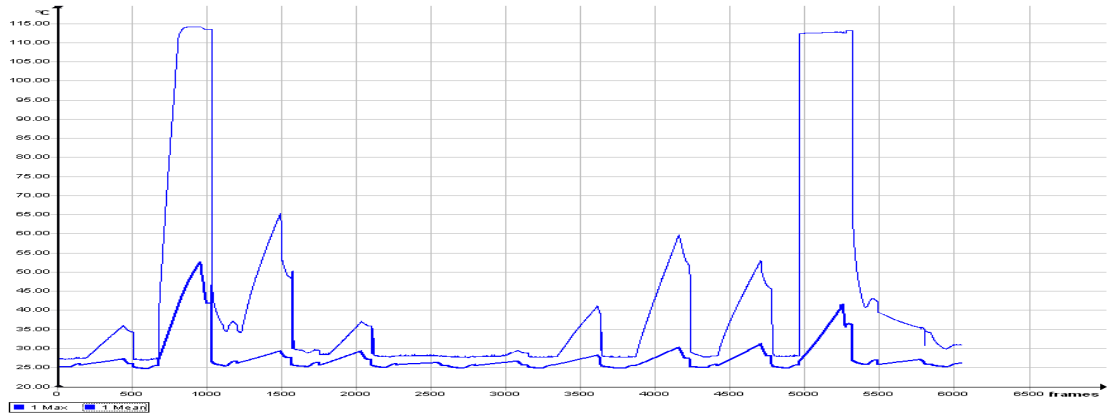

Figure App. H-11 First exposure, timing graph the set No. 3

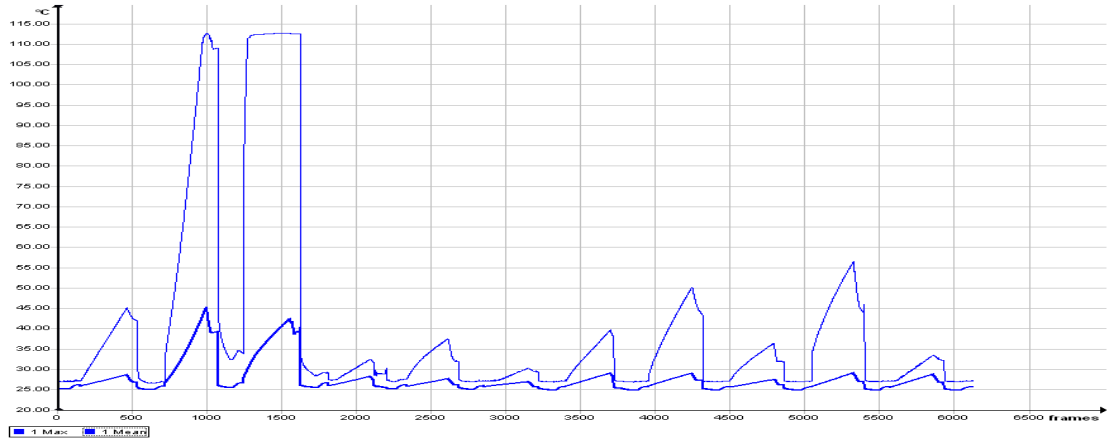

Figure App. H-12Second exposure, timing graph for the set No. 3

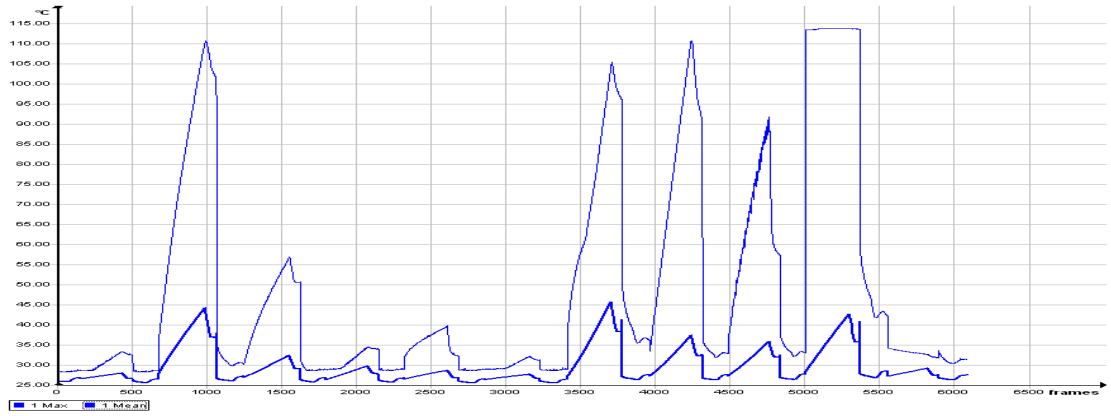

Figure App. H-13Third exposure, timing graph for the set No. 3

Set No. 4:

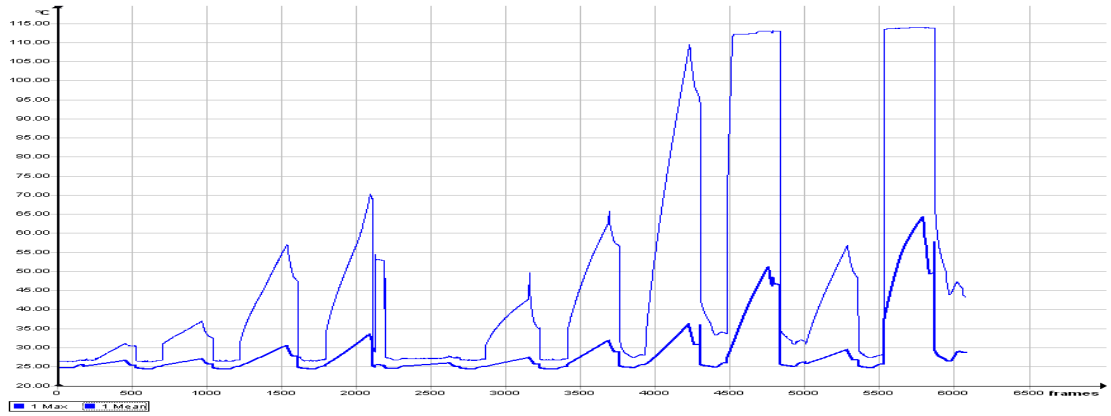

Figure App. H-14 First exposure, timing graph for the set No. 4

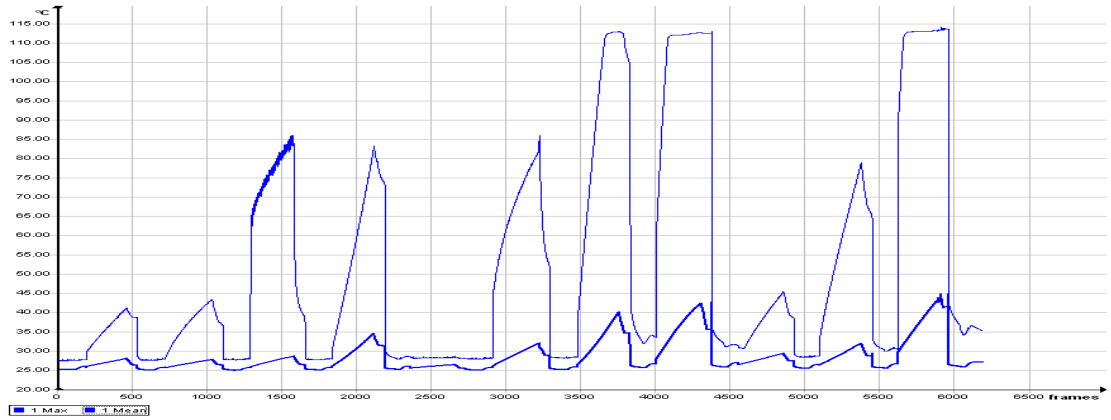

Figure App. H-15 Second exposure, timing graph for the set No. 4

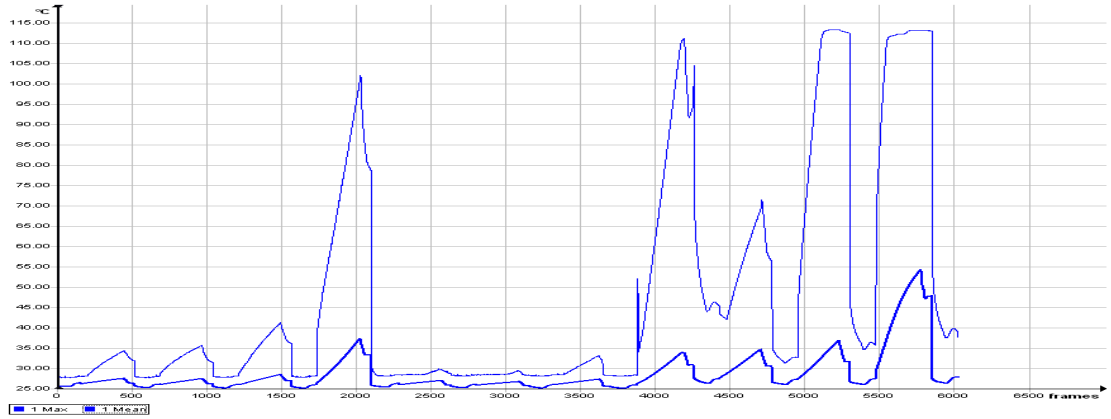

Figure App. H-16 Third exposure, timing graph for the set No. 4

Tomography analysis of some of the cold particles:

Particle No. 3 Set No. 4

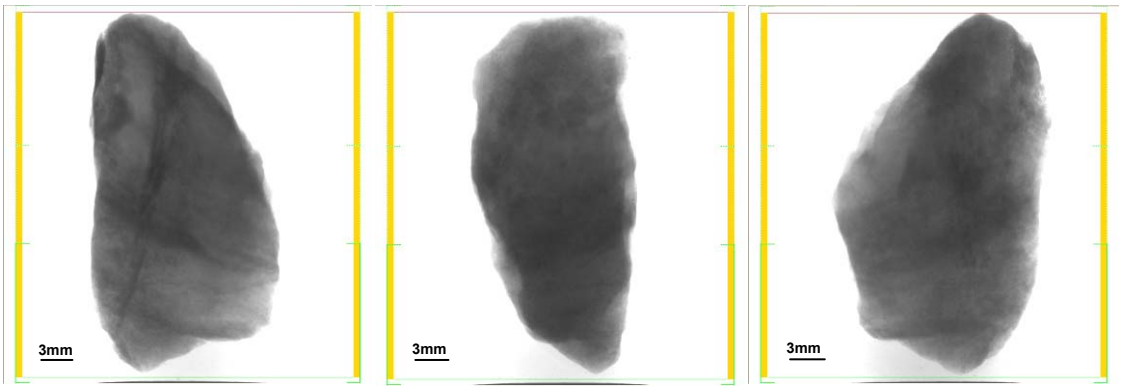

Position 0 deg **Position 90 deg** **Position110 deg**

Figure App. H-17 LRO Ore Particle No. 3 Set No. 4

Tomography analysis of some of the hot particles:

Particle No. 10 Set No. 4

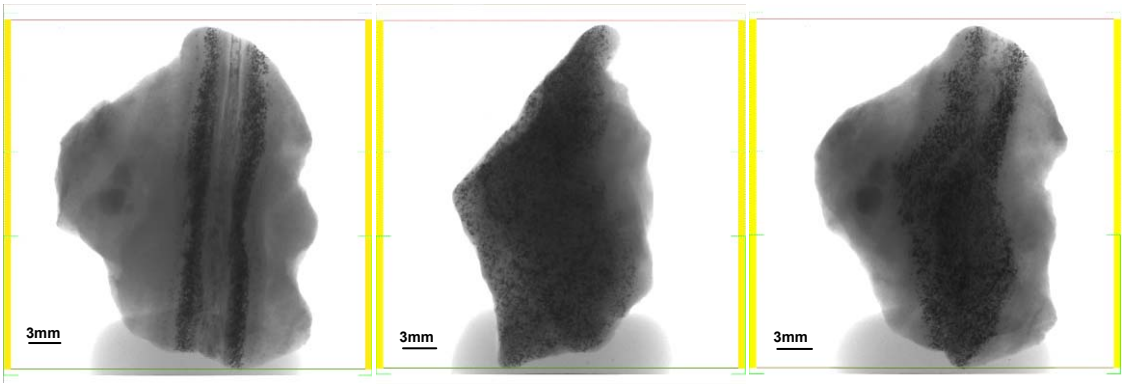

Position 0 deg **Position 90 deg** **Position 120 deg**

Figure App. H-18 LRO Ore Particle No. 10 Set No. 4

Particle No. 11 Set No. 4

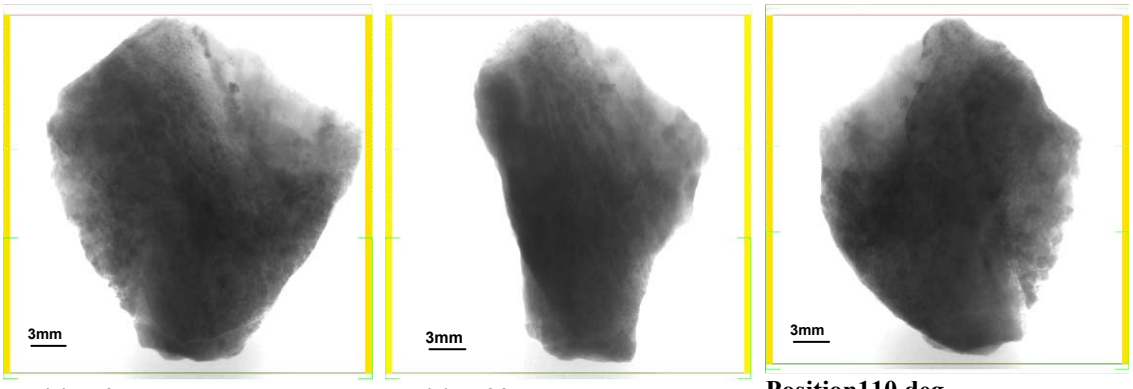

Position 0 deg **Position 90 deg** **Position110 deg**

Figure App. H-19 LRO Ore Particle No. 11 Set No. 4

Set No. 5:

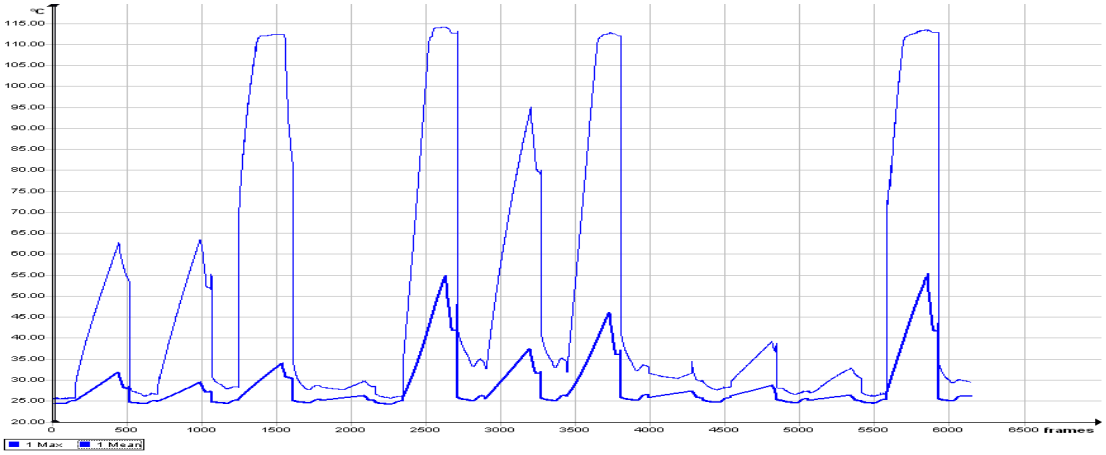

Figure App. H-20 First exposure, timing graph for the set No.5

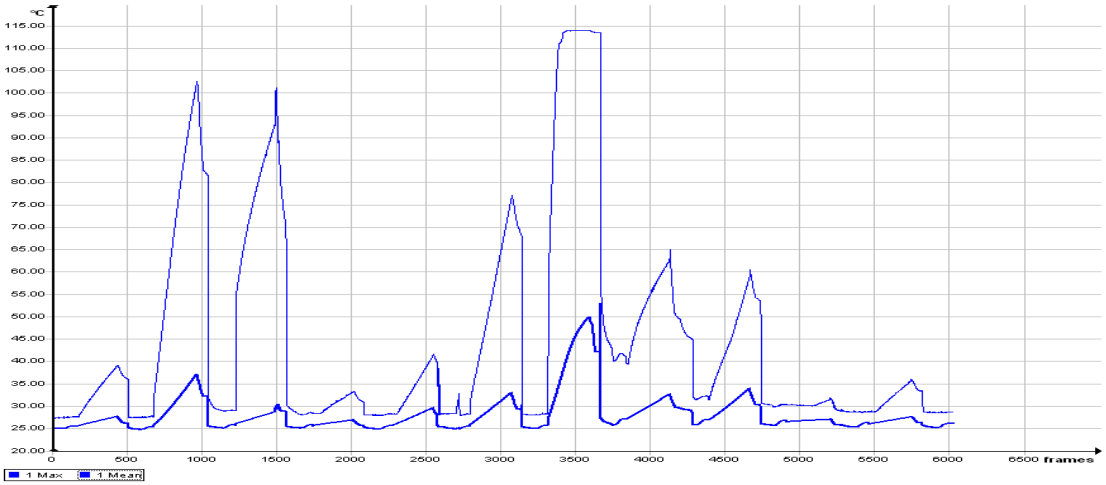

Figure App. H-21 Second exposure, timing graph for the set No.5

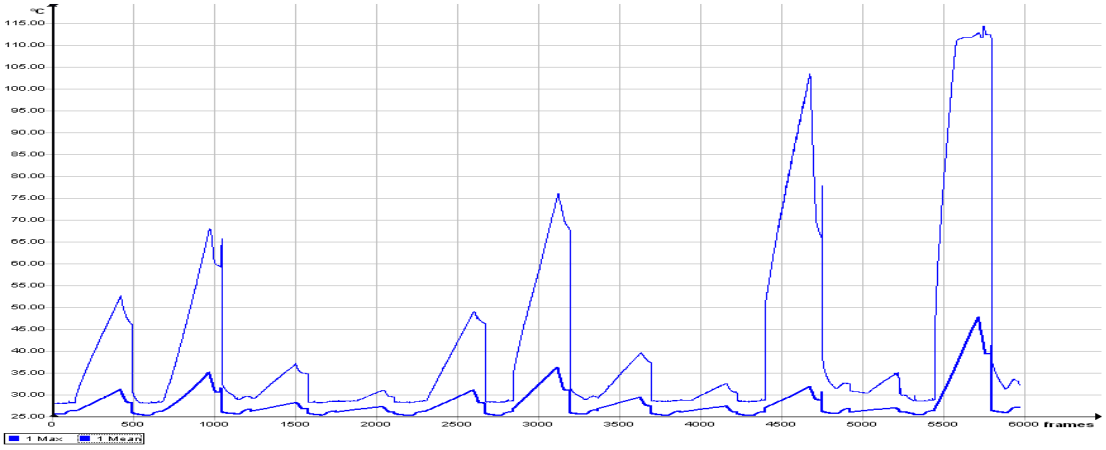

Figure App. H-22 Third exposure, timing graph for the set No. 5

Particle No. 3 Set No. 5

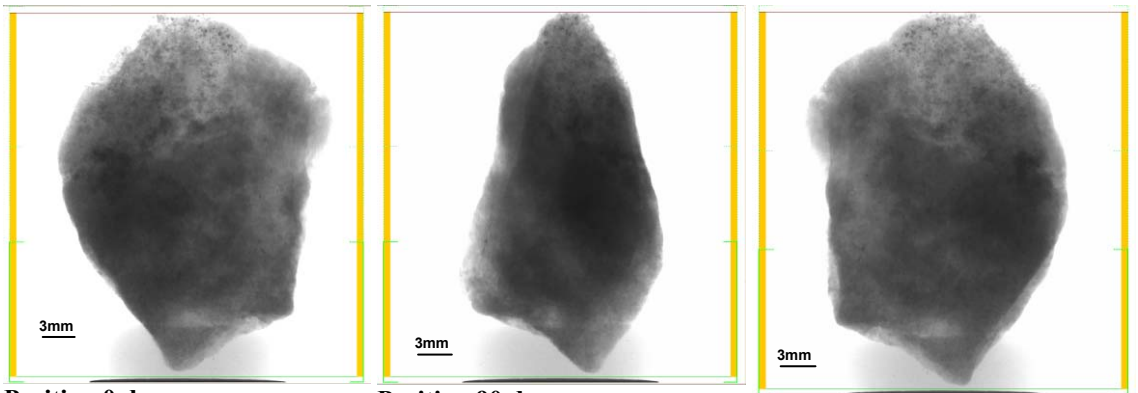

Position 0 deg **Position 90 deg** **Position120 deg**

Figure App. H-23 LRO Ore Particle No. 3 Set No. 5

Particle No. 6 Set No. 5

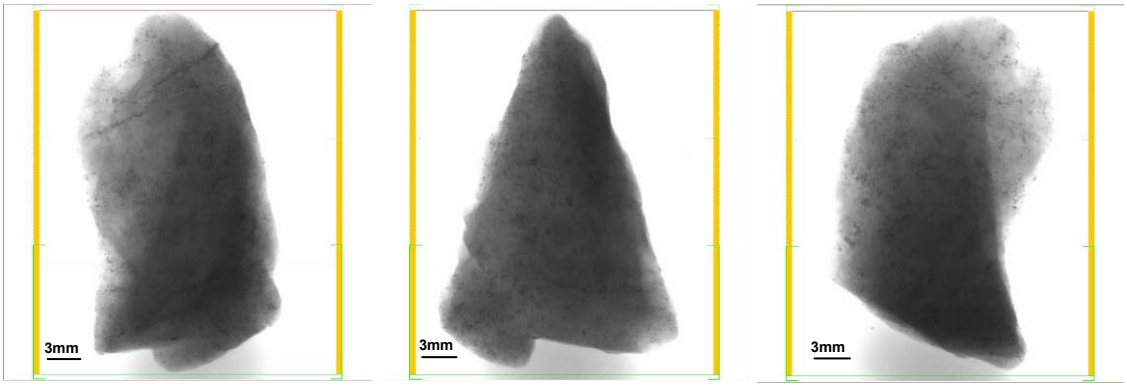

Position 0 deg **Position 90 deg** **Position110 deg**

Figure App. H-24 LRO Ore Particle No. 6 Set No. 5

Set No. 6:

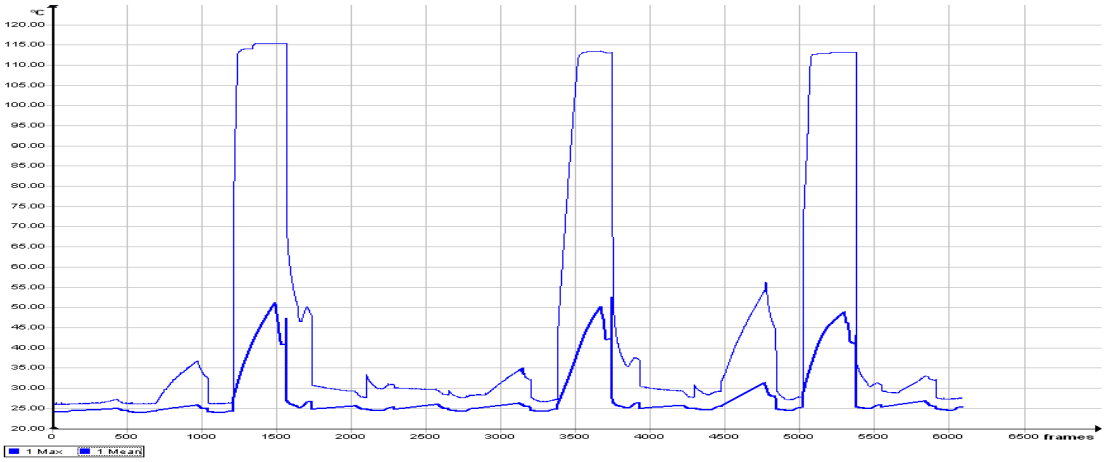

Figure App. H-25 First exposure, timing graph for the set No. 6

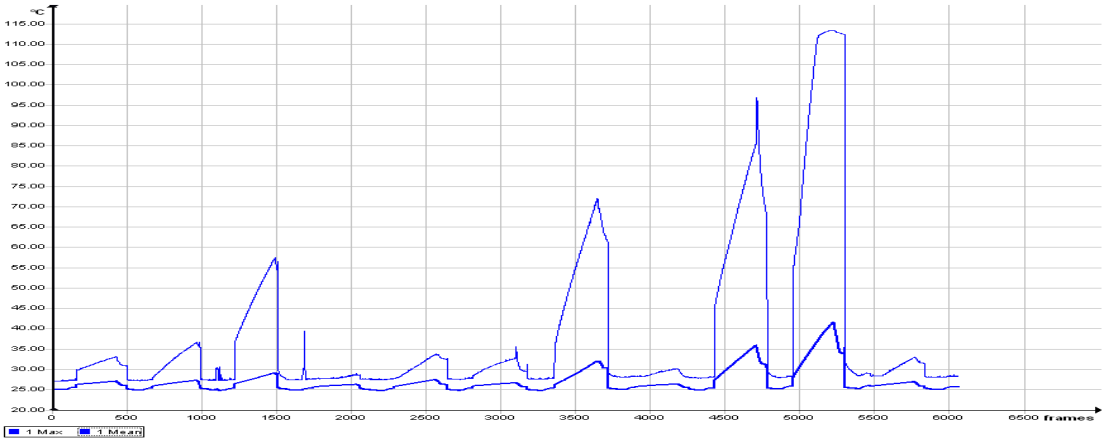

Figure App. H-26 Second exposure, timing graph the set No. 6

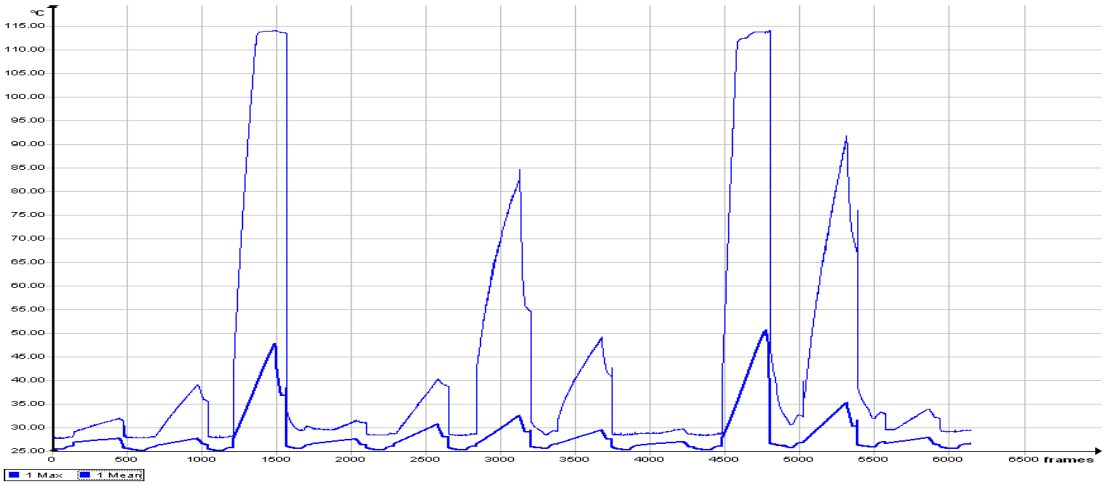

Figure App. H-27 Third exposure, timing graph the set No. 6

Particle No. 10 Set No. 6

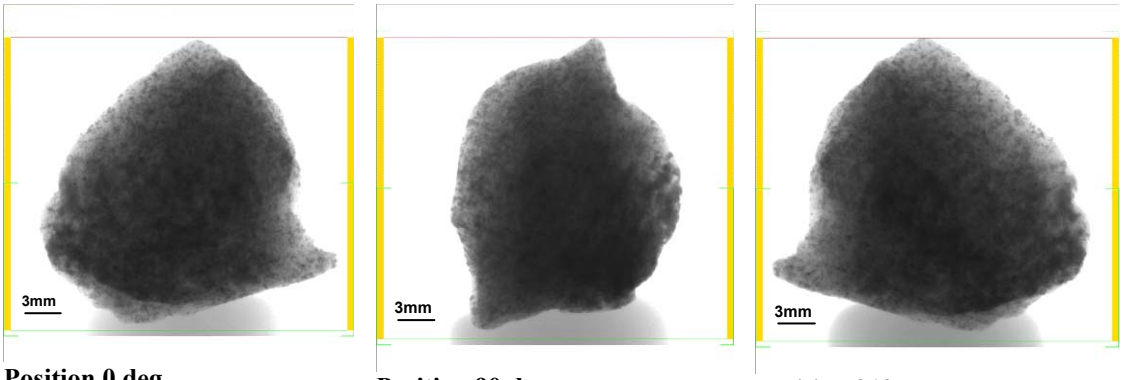

Position 0 deg **Position 90 deg** **Position 212 deg**

Figure App. H-28 LRO Ore Particle No. 10 Set No. 6

Set No. 7:

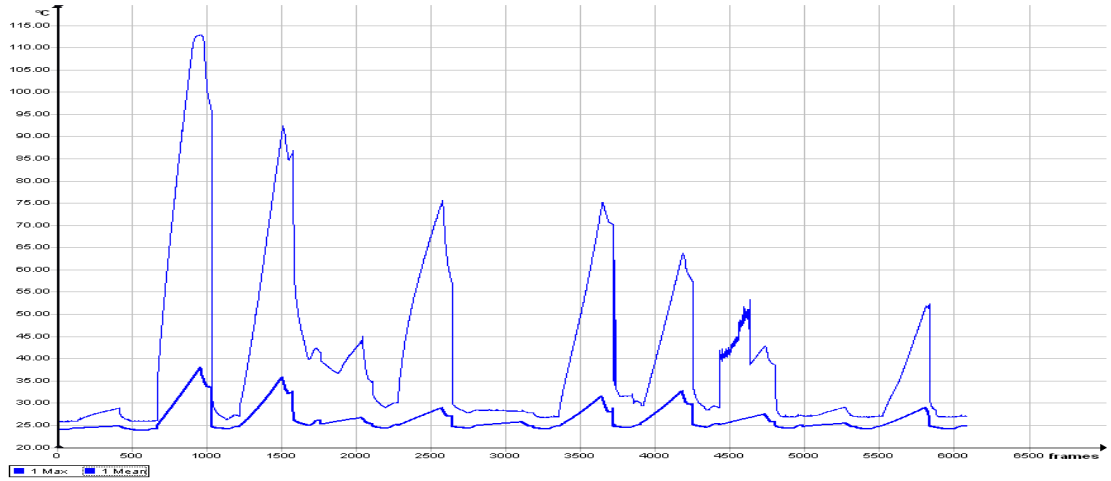

Figure App. H-29 First exposure, timing graph for the set No. 7

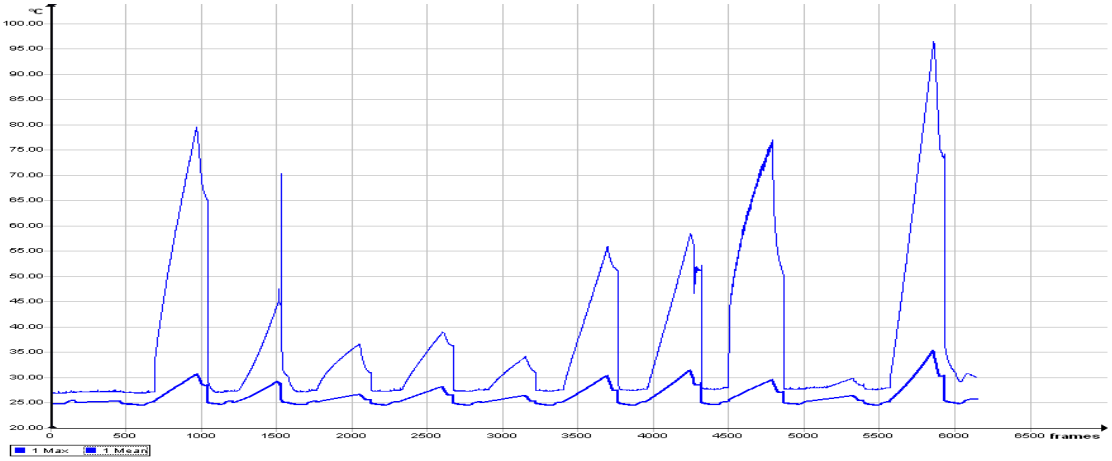

Figure App. H-30 Second exposure, timing graph for the set No. 7

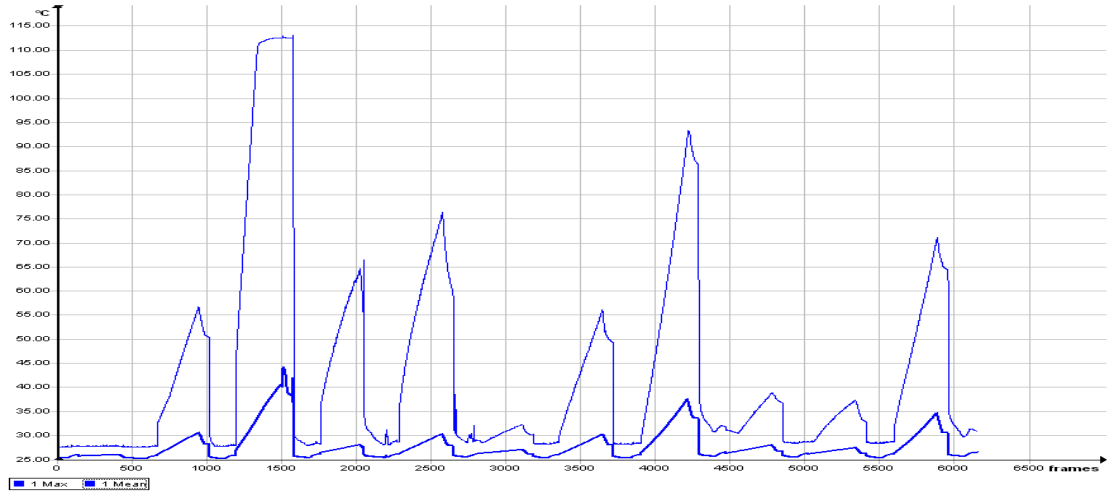

Figure App. H-31 Third exposure, timing graph for the set No. 7

Tomography analysis of some of the hot particles:

Particle No. 2 Set No. 7

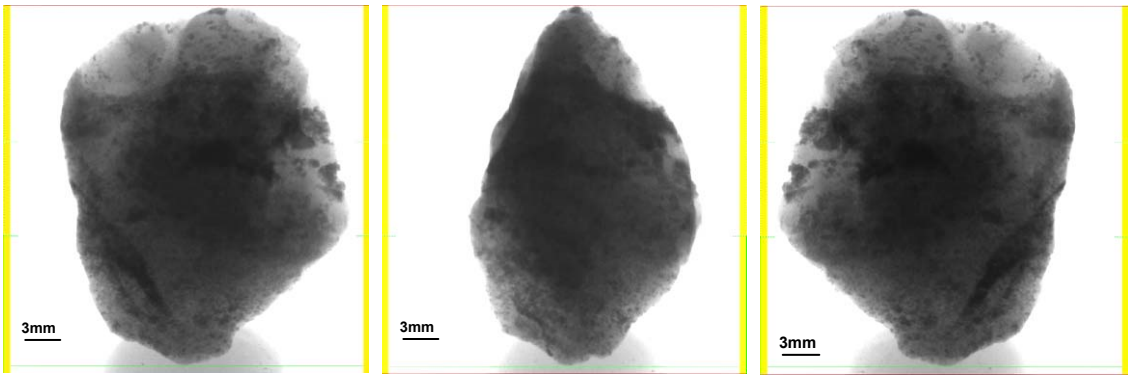

Position 0 deg **Position 45 deg** **Position 180 deg**

Figure App. H-32 LRO Ore Particle No. 2 Set No. 7

Particle No. 9 Set No. 7

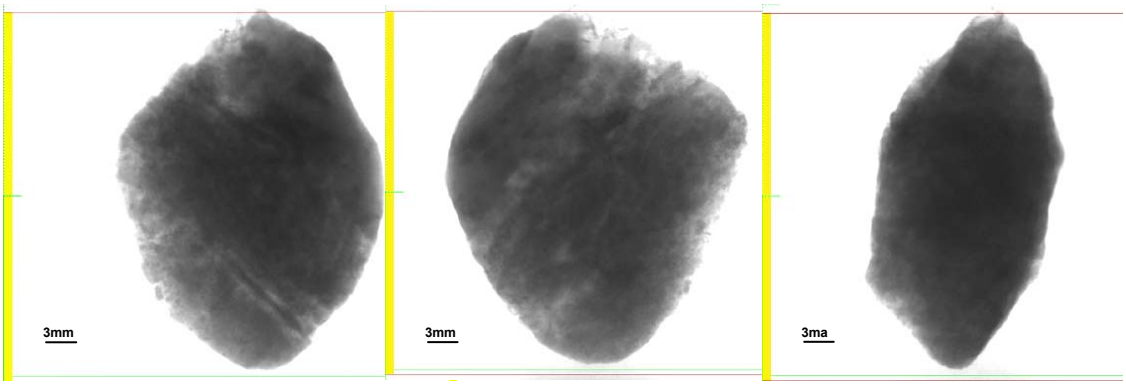

Position 40 deg **Position 180 deg** **Position 280 deg**

Figure App. H-33 LRO Ore Particle No. 9 Set No. 7

Tomography analysis of some of the cold particles:

Particle No. 10 Set No. 7

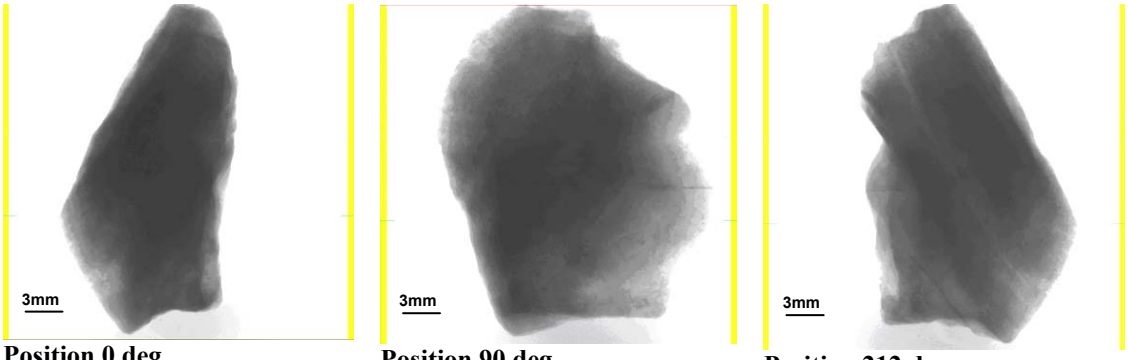

Position 0 deg **Position 90 deg** **Position 212 deg**

Figure App. H-34 LRO Ore Particle No. 10 Set No. 7

Set No. 8:

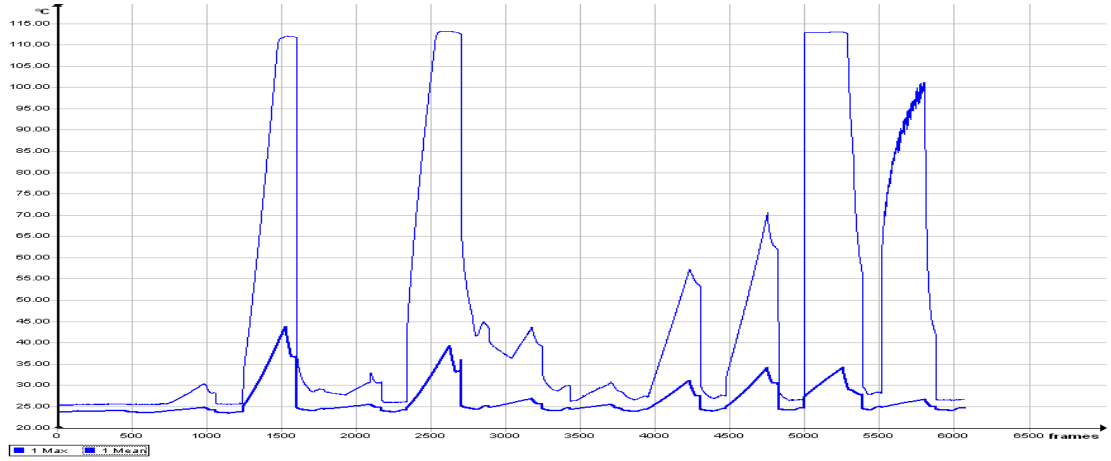

Figure App. H-35 First exposure, timing graph for the set No. 8

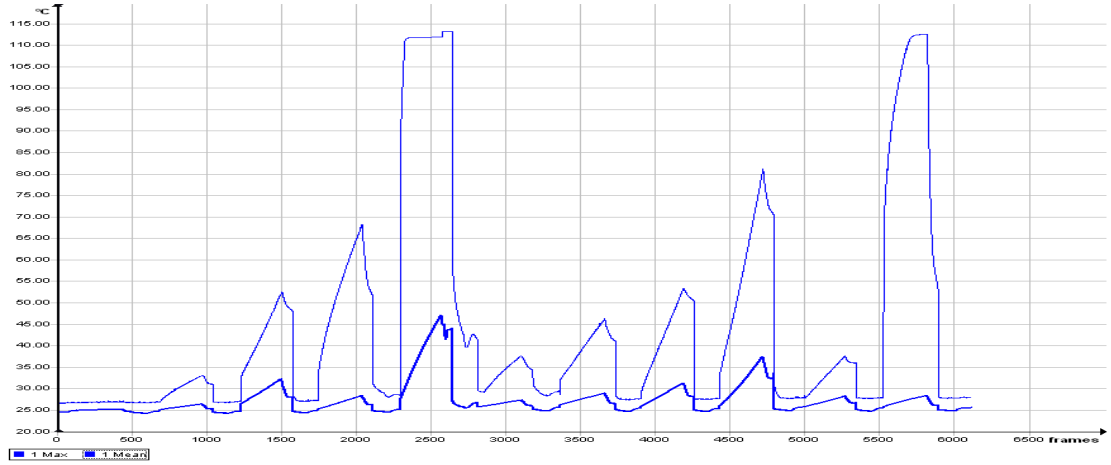

Figure App. H-36Second exposure, timing graph for the set No. 8

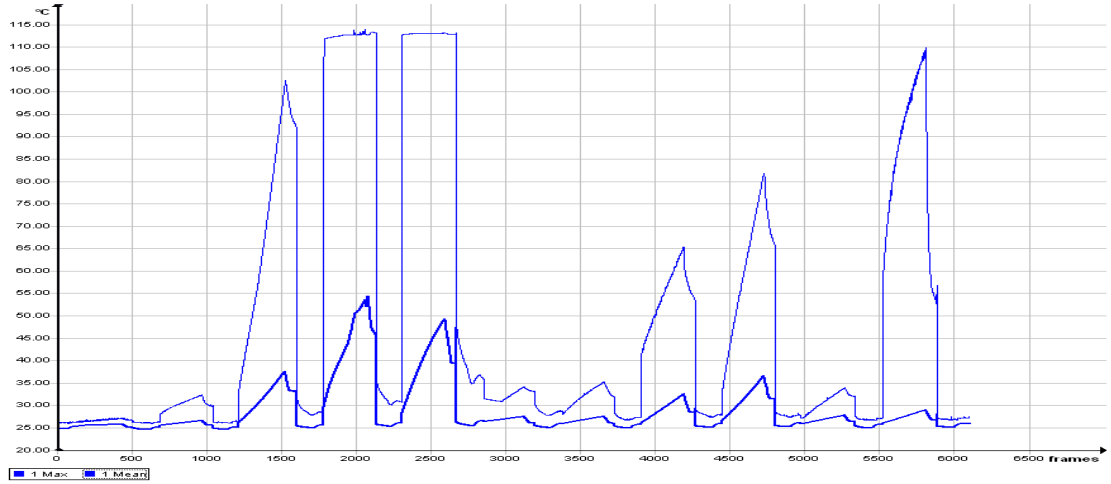

Figure App. H-37 Third exposure, timing graph for the set No.. 8

Tomography analysis of some of the cold particles:

Particle No. 1 Set No. 8

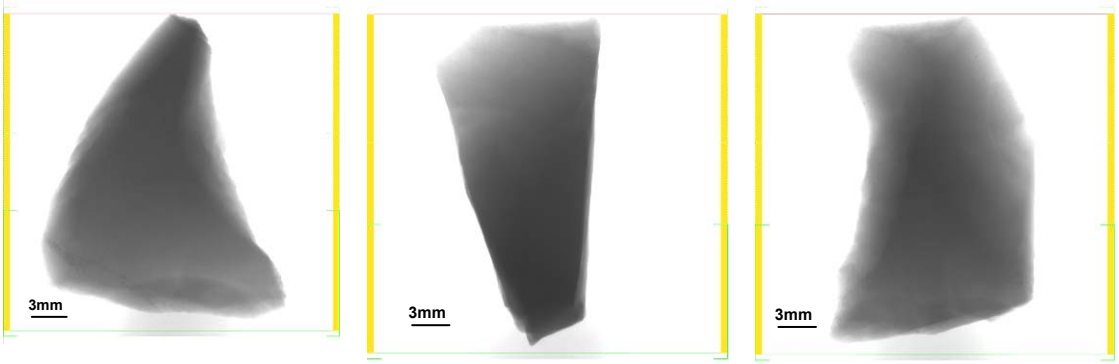

Position 0 deg **Position 90 deg** **Position 180 deg**

Figure App. H-38 LRO Ore Particle No. 1 Set No. 8

Tomography analysis of some of the hot particles:

Particle No. 5 Set No. 8

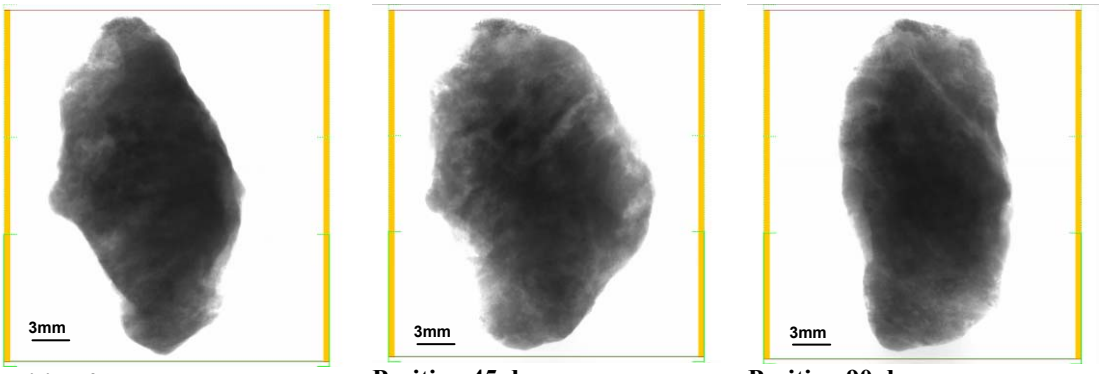

Position 0 deg **Position 45 deg** **Position 90 deg**

Figure App. H-39 LRO Ore Particle No. 5 Set No. 8

Overlapping particles in both types of cavities

Table App. H-1 Before sorting by max ΔT mean for the LRO ore type:

	Multimode Cavity							Single Mode Cavity						
	particle nur	bag	max delta t	mass of pa	Cumulative	Cumulative mass%		particle nur	bag	max delta t	mass of pa	Cumulative	Cumulative
1	1	8	1.21	11.99	11.99	0.770942		1	8	0.76	11.99	11.99	0.770942
2	2	8	4.75	19.7	31.69	2.037628		2	8	3.97	19.7	31.69	2.037628
3	3	8	9.52	15.91	47.6	3.060621		3	8	39.62	15.91	47.6	3.060621
4	4	8	18.67	16.34	63.94	4.111263		4	8	50.34	16.34	63.94	4.111263
5	5	8	53.38	19.27	83.21	5.3503		5	8	56.26	19.27	83.21	5.3503
6	6	8	13.68	14.9	98.11	6.308351		6	8	7.64	14.9	98.11	6.308351
7	7	8	6.79	13.03	111.14	7.146164		7	8	6.86	13.03	111.14	7.146164
8	8	8	26.5	14.14	125.28	8.055348		8	8	18.26	14.14	125.28	8.055348
9	9	8	29.06	16.6	141.88	9.122708		9	8	27.74	16.6	141.88	9.122708
10	10	8	13.2	15.99	157.87	10.15084		10	8	22.46	15.99	157.87	10.15084
11	11	8	4.74	17.88	175.75	11.30051		11	8	7.76	17.88	175.75	11.30051
12	1	7	1.05	15.29	191.04	12.28363		1	7	0.91	15.29	191.04	12.28363
13	2	7	22.39	15.42	206.46	13.27512		2	7	36.74	15.42	206.46	13.27512
14	3	7	14.6	23.29	229.75	14.77264		3	7	45.7	23.29	229.75	14.77264
15	4	7	9.45	14.93	244.68	15.73262		4	7	5.82	14.93	244.68	15.73262
16	5	7	20.67	13.29	257.97	16.58715		5	7	17.69	13.29	257.97	16.58715
17	6	7	4.45	18.11	276.08	17.7516		6	7	3.01	18.11	276.08	17.7516
18	7	7	22.97	12.91	288.99	18.5817		7	7	19.37	12.91	288.99	18.5817
19	8	7	38.27	14.53	303.52	19.51596		8	7	31.51	14.53	303.52	19.51596
20	9	7	24.24	12.56	316.08	20.32355		9	7	11.26	12.56	316.08	20.32355
21	10	7	5.55	16.11	332.19	21.3594		10	7	2.94	16.11	332.19	21.3594
22	11	7	18.62	17.43	349.62	22.48013		11	7	21.43	17.43	349.62	22.48013
23	1	6	2.84	19.14	368.76	23.71081		1	6	2.09	19.14	368.76	23.71081
24	2	6	11.24	11.37	380.13	24.44189		2	6	4.29	11.37	380.13	24.44189
25	3	6	26.43	21.83	401.96	25.84553		3	6	48.7	21.83	401.96	25.84553
26	4	6	4.81	15.26	417.22	26.82673		4	6	2.95	15.26	417.22	26.82673
27	5	6	7.7	15.83	433.05	27.84458		5	6	9.11	15.83	433.05	27.84458
28	6	6	2.12	23.33	456.38	29.34467		6	6	14.37	23.33	456.38	29.34467
29	7	6	13.18	17.84	474.22	30.49176		7	6	63.33	17.84	474.22	30.49176
30	8	6	3.12	12.19	486.41	31.27556		8	6	1.67	12.19	486.41	31.27556
31	9	6	20.93	28.96	515.37	33.13765		9	6	58.43	28.96	515.37	33.13765
32	10	6	62.98	18.26	533.63	34.31175		10	6	58.67	18.26	533.63	34.31175
33	11	6	6.9	16.17	549.8	35.35146		11	6	4.47	16.17	549.8	35.35146
34	1	5	17.45	13.9	563.7	36.24521		1	5	16.78	13.9	563.7	36.24521
35	2	5	12.9	22.08	585.78	37.66493		2	5	38.12	22.08	585.78	37.66493
36	3	5	20.07	14.47	600.25	38.59533		3	5	16.57	14.47	600.25	38.59533
37	4	5	4.66	15.82	616.07	39.61254		4	5	3.1	15.82	616.07	39.61254
38	5	5	11.21	20.85	636.92	40.95316		5	5	59.52	20.85	636.92	40.95316
39	6	5	21.5	21.36	658.28	42.32659		6	5	23.01	21.36	658.28	42.32659
40	7	5	13.29	18.95	677.23	43.54505		7	5	73.04	18.95	677.23	43.54505
41	8	5	6.78	24.78	702.01	45.13837		8	5	15.82	24.78	702.01	45.13837
42	9	5	13.54	17.87	719.88	46.28739		9	5	17.35	17.87	719.88	46.28739
43	10	5	3.75	20.71	740.59	47.61902		10	5	2.71	20.71	740.59	47.61902
44	11	5	17.11	22.03	762.62	49.03552		11	5	61.38	22.03	762.62	49.03552
45	1	4	4.91	14.91	777.53	49.99421		1	4	5.96	14.91	777.53	49.99421
46	2	4	7.14	12.18	789.71	50.77737		2	4	5.73	12.18	789.71	50.77737
47	3	4	7.6	16.61	806.32	51.84537		3	4	13.45	16.61	806.32	51.84537
48	4	4	22.55	16.69	823.01	52.91852		4	4	31.11	16.69	823.01	52.91852
49	5	4	4.4	15.39	838.4	53.90808		5	4	2.45	15.39	838.4	53.90808
50	6	4	5.98	26.67	865.07	55.62293		6	4	11.38	26.67	865.07	55.62293
51	7	4	4.05	20.99	886.06	56.97256		7	4	35.3	20.99	886.06	56.97256
52	8	4	68.71	20.36	906.42	58.28168		8	4	62.36	20.36	906.42	58.28168
53	9	4	16.27	21.79	928.21	59.68275		9	4	58.41	21.79	928.21	59.68275
54	10	4	21.36	11.76	939.97	60.4389		10	4	27.25	11.76	939.97	60.4389
55	11	4	67.85	16.26	956.23	61.4844		11	4	63.11	16.26	956.23	61.4844
56	1	3	16.08	10.42	966.65	62.15439		1	3	9.72	10.42	966.65	62.15439
57	2	3	25.78	18.2	984.85	63.32463		2	3	63.58	18.2	984.85	63.32463
58	3	3	38.15	15.85	1000.7	64.34377		3	3	35.15	15.85	1000.7	64.34377
59	4	3	5.7	21.77	1022.47	65.74355		4	3	7.35	21.77	1022.47	65.74355
60	5	3	4.72	21.53	1044	67.1279		5	3	5.45	21.53	1044	67.1279
61	6	3	5.55	13.8	1057.8	68.01523		6	3	4.06	13.8	1057.8	68.01523
62	7	3	4.02	24.26	1082.06	69.57511		7	3	41.45	24.26	1082.06	69.57511
63	8	3	12.49	21.56	1103.62	70.9614		8	3	29.53	21.56	1103.62	70.9614
64	9	3	6.91	18.78	1122.4	72.16893		9	3	22.61	18.78	1122.4	72.16893
65	10	3	27.76	18.54	1140.94	73.36102		10	3	43.8	18.54	1140.94	73.36102
66	11	3	7.1	23.65	1164.59	74.88169		11	3	5.03	23.65	1164.59	74.88169
67	1	2	12.69	22.6	1187.19	76.33484		1	2	48.05	22.6	1187.19	76.33484
68	2	2	9.3	22.47	1209.66	77.77964		2	2	34.43	22.47	1209.66	77.77964
69	3	2	63.71	16.59	1226.25	78.84635		3	2	54.65	16.59	1226.25	78.84635
70	4	2	80.1	19.29	1245.54	80.08667		4	2	81.54	19.29	1245.54	80.08667
71	5	2	27.83	18.85	1264.39	81.29871		5	2	32.71	18.85	1264.39	81.29871
72	6	2	22.29	12.59	1276.98	82.10823		6	2	31.03	12.59	1276.98	82.10823
73	7	2	3.38	19.26	1296.24	83.34662		7	2	3.71	19.26	1296.24	83.34662
74	8	2	7.07	22.83	1319.07	84.81456		8	2	41.26	22.83	1319.07	84.81456
75	9	2	6.46	21.28	1340.35	86.18284		9	2	12.93	21.28	1340.35	86.18284
76	10	2	2.77	16.16	1356.51	87.22191		10	2	2.72	16.16	1356.51	87.22191
77	11	2	16.43	18.24	1374.75	88.39472		11	2	61.35	18.24	1374.75	88.39472
78	1	1	2.24	10.17	1384.92	89.04864		1	1	2.75	10.17	1384.92	89.04864
79	2	1	20.52	16.04	1400.96	90.07999		2	1	17.55	16.04	1400.96	90.07999
80	3	1	12.52	19.48	1420.44	91.33253		3	1	13.64	19.48	1420.44	91.33253
81	4	1	9.01	20.97	1441.41	92.68087		4	1	16.17	20.97	1441.41	92.68087
82	5	1	7.07	9.87	1451.28	93.3155		5	1	2.94	9.87	1451.28	93.3155
83	6	1	18.6	19.74	1471.02	94.58476		6	1	48.98	19.74	1471.02	94.58476
84	7	1	18.37	18.31	1489.33	95.76207		7	1	62.43	18.31	1489.33	95.76207
85	8	1	12.82	20	1509.33	97.04804		8	1	61.15	20	1509.33	97.04804
86	9	1	31.33	14.9	1524.23	98.0061		9	1	17.72	14.9	1524.23	98.0061
87	10	1	13.27	10.71	1534.94	98.69474		10	1	6.15	10.71	1534.94	98.69474
88	11	1	26.66	20.3	1555.24	100		11	1	50.37	20.3	1555.24	100

Table App. H-2 After sorting by max ΔT mean LRO ore type:

	Multimode Cavity particle nur	bag	max delta t	mass of pa	Cumulative	Cumulative mass%	
1	1	7	1.05	15.29	15.29	0.983128	
2	1	8	1.21	11.99	27.28	1.75407	
3	6	6	2.12	23.33	50.61	3.25416	
4	1	1	2.24	10.17	60.78	3.908078	
5	10	2	2.77	16.16	76.94	4.947146	
6	1	6	2.84	19.14	96.08	6.177825	
7	8	6	3.12	12.19	108.27	6.961627	
8	7	2	3.38	19.26	127.53	8.200021	
9	10	5	3.75	20.71	148.24	9.531648	
10	7	3	4.02	24.26	172.5	11.09154	
11	7	4	4.05	20.99	193.49	12.44117	
12	5	4	4.4	15.39	208.88	13.43072	
13	6	7	4.45	18.11	226.99	14.59518	6.90 oC
14	4	5	4.66	15.82	242.81	15.61238	
15	5	3	4.72	21.53	264.34	16.99673	
16	11	8	4.74	17.88	282.22	18.1464	
17	2	8	4.75	19.7	301.92	19.41308	
18	4	6	4.81	15.26	317.18	20.39428	
19	1	4	4.91	14.91	332.09	21.35297	
20	10	7	5.55	16.11	348.2	22.38883	
21	6	3	5.55	13.8	362	23.27615	
22	4	3	5.7	21.77	383.77	24.67593	
23	6	4	5.98	26.67	410.44	26.39078	
24	9	2	6.46	21.28	431.72	27.75906	
25	8	5	6.78	24.78	456.5	29.35238	
26	7	8	6.79	13.03	469.53	30.1902	
27	11	6	6.9	16.17	485.7	31.22991	
28	9	3	6.91	18.78	504.48	32.43744	
29	8	2	7.07	22.83	527.31	33.90538	
30	5	1	7.07	9.87	537.18	34.54001	
31	11	3	7.1	23.65	560.83	36.06067	
32	2	4	7.14	12.18	573.01	36.84383	
33	3	4	7.6	16.61	589.62	37.91183	
34	5	6	7.7	15.83	605.45	38.92968	
35	4	1	9.01	20.97	626.42	40.27803	
36	2	2	9.3	22.47	648.89	41.72282	
37	4	7	9.45	14.93	663.82	42.6828	
38	3	8	9.52	15.91	679.73	43.70579	
39	5	5	11.21	20.85	700.58	45.04642	
40	2	6	11.24	11.37	711.95	45.7775	
41	8	3	12.49	21.56	733.51	47.16378	
42	3	1	12.52	19.48	752.99	48.41632	
43	1	2	12.69	22.6	775.59	49.86947	
44	8	1	12.82	20	795.59	51.15545	
45	2	5	12.9	22.08	817.67	52.57517	
46	7	6	13.18	17.84	835.51	53.72226	
47	10	8	13.2	15.99	851.5	54.75039	
48	10	1	13.27	10.71	862.21	55.43903	
49	7	5	13.29	18.95	881.16	56.65749	
50	9	5	13.54	17.87	899.03	57.80651	
51	6	8	13.68	14.9	913.93	58.76456	
52	3	7	14.6	23.29	937.22	60.26208	
53	1	3	16.08	10.42	947.64	60.93207	
54	9	4	16.27	21.79	969.43	62.33314	
55	11	2	16.43	18.24	987.67	63.50595	
56	11	5	17.11	22.03	1009.7	64.92246	
57	1	5	17.45	13.9	1023.6	65.81621	
58	7	1	18.37	18.31	1041.91	66.99352	
59	6	1	18.6	19.74	1061.65	68.26278	
60	11	7	18.62	17.43	1079.08	69.3835	
61	4	8	18.67	16.34	1095.42	70.43415	
62	3	5	20.07	14.47	1109.89	71.36455	
63	2	1	20.52	16.04	1125.93	72.3959	
64	5	7	20.67	13.29	1139.22	73.25043	
65	9	6	20.93	28.96	1168.18	75.11252	
66	10	4	21.36	11.76	1179.94	75.86868	
67	6	5	21.5	21.36	1201.3	77.2421	
68	6	2	22.29	12.59	1213.89	78.05162	
69	2	7	22.39	15.42	1229.31	79.04311	
70	4	4	22.55	16.69	1246	80.11625	
71	7	7	22.97	12.91	1258.91	80.94635	
72	9	7	24.24	12.56	1271.47	81.75394	
73	2	3	25.78	18.2	1289.67	82.92418	
74	3	6	26.43	21.83	1311.5	84.32782	
75	8	8	26.5	14.14	1325.64	85.23701	
76	11	1	26.66	20.3	1345.94	86.54227	
77	10	3	27.76	18.54	1364.48	87.73437	
78	5	2	27.83	18.85	1383.33	88.9464	
79	9	8	29.06	16.6	1399.93	90.01376	
80	9	1	31.33	14.9	1414.83	90.97181	
81	3	3	38.15	15.85	1430.68	91.99095	
82	8	7	38.27	14.53	1445.21	92.92521	
83	5	8	53.38	19.27	1464.48	94.16424	
84	10	6	62.98	18.26	1482.74	95.33834	
85	3	2	63.71	16.59	1499.33	96.40506	
86	11	4	67.85	16.26	1515.59	97.45055	
87	8	4	68.71	20.36	1535.95	98.75968	
88	4	2	80.1	19.29	1555.24	100	

	Single Mode Cavity particle nur	bag	max delta t	mass of pa	Cumulative	Cumulative mass%	
	1	8	0.76	11.99	11.99	0.770942	
	1	7	0.91	15.29	27.28	1.75407	
	8	6	1.67	12.19	39.47	2.537872	
	1	6	2.09	19.14	58.61	3.76855	
	5	4	2.45	15.39	74	4.758108	
	10	5	2.71	20.71	94.71	6.089735	
	10	2	2.72	16.16	110.87	7.128803	
	1	1	2.75	10.17	121.04	7.782722	
	10	7	2.94	16.11	137.15	8.818575	
	5	1	2.94	9.87	147.02	9.453203	
	4	6	2.95	15.26	162.28	10.4344	
	6	7	3.01	18.11	180.39	11.59885	
	4	5	3.1	15.82	196.21	12.61606	6.90 oC
	7	2	3.71	19.26	215.47	13.85445	
	2	8	3.97	19.7	235.17	15.12114	
	6	3	4.06	13.8	248.97	16.00846	
	2	6	4.29	11.37	260.34	16.73954	
	11	6	4.47	16.17	276.51	17.77925	
	11	3	5.03	23.65	300.16	19.29992	
	5	3	5.45	21.53	321.69	20.68427	
	2	4	5.73	12.18	333.87	21.46743	
	4	7	5.82	14.93	348.8	22.42741	
	1	4	5.96	14.91	363.71	23.3861	
	10	1	6.15	10.71	374.42	24.07474	
	7	8	6.86	13.03	387.45	24.91255	
	4	3	7.35	21.77	409.22	26.31234	
	6	8	7.64	14.9	424.12	27.27039	
	11	8	7.76	17.88	442	28.42005	
	5	6	9.11	15.83	457.83	29.4379	
	1	3	9.72	10.42	468.25	30.10789	
	9	7	11.26	12.56	480.81	30.91549	
	6	4	11.38	26.67	507.48	32.63033	
	9	2	12.93	21.28	528.76	33.99861	
	3	4	13.45	16.61	545.37	35.06661	
	3	1	13.64	19.48	564.85	36.31915	
	6	6	14.37	23.33	588.18	37.81924	
	8	5	15.82	24.78	612.96	39.41257	
	4	1	16.17	20.97	633.93	40.76091	
	3	5	16.57	14.47	648.4	41.69131	
	1	5	16.78	13.9	662.3	42.58507	
	9	5	17.35	17.87	680.17	43.73409	
	2	1	17.55	16.04	696.21	44.76544	
	5	7	17.69	13.29	709.5	45.61997	
	9	1	17.72	14.9	724.4	46.57802	
	8	8	18.26	14.14	738.54	47.4872	
	7	7	19.37	12.91	751.45	48.3173	
	11	7	21.43	17.43	768.88	49.43803	
	10	8	22.46	15.99	784.87	50.46617	
	9	3	22.61	18.78	803.65	51.6737	
	6	5	23.01	21.36	825.01	53.04712	
	10	4	27.25	11.76	836.77	53.80327	
	9	8	27.74	16.6	853.37	54.87063	
	8	3	29.53	21.56	874.93	56.25691	
	6	2	31.03	12.59	887.52	57.06643	
	4	4	31.11	16.69	904.21	58.13958	
	8	7	31.51	14.53	918.74	59.07384	
	5	2	32.71	18.85	937.59	60.28587	
	2	2	34.43	22.47	960.06	61.73067	
	3	3	35.15	15.85	975.91	62.7498	
	7	4	35.3	20.99	996.9	64.09943	
	2	7	36.74	15.42	1012.32	65.09092	
	2	5	38.12	22.08	1034.4	66.51064	
	3	8	39.62	15.91	1050.31	67.53363	
	8	2	41.26	22.83	1073.14	69.00157	
	7	3	41.45	24.26	1097.4	70.56146	
	10	3	43.8	18.54	1115.94	71.75356	
	3	7	45.7	23.29	1139.23	73.25107	
	1	2	48.05	22.6	1161.83	74.70423	
	3	6	48.7	21.83	1183.66	76.10787	
	6	1	48.98	19.74	1203.4	77.37713	
	4	8	50.34	16.34	1219.74	78.42777	
	11	1	50.37	20.3	1240.04	79.73303	
	3	2	54.65	16.59	1256.63	80.79975	
	5	8	56.26	19.27	1275.9	82.03879	
	9	4	58.41	21.79	1297.69	83.43985	
	9	6	58.43	28.96	1326.65	85.30195	
	10	6	58.67	18.26	1344.91	86.47604	
	5	5	59.52	20.85	1365.76	87.81667	
	8	1	61.15	20	1385.76	89.10265	
	11	2	61.35	18.24	1404	90.27546	
	11	5	61.38	22.03	1426.03	91.69196	
	8	4	62.36	20.36	1446.39	93.00108	
	7	1	62.43	18.31	1464.7	94.17839	
	11	4	63.11	16.26	1480.96	95.22389	
	7	6	63.33	17.84	1498.8	96.37098	
	2	3	63.58	18.2	1517	97.54122	
	7	5	73.04	18.95	1535.95	98.75968	
	4	2	81.54	19.29	1555.24	100	

Appendix I

Table App. I-1 Mass retained within selected size fractions after screening obtained LRO ore sample

LRO Size Distribution		
Size Fraction	**Mass (Kg)**	**% Retained**
+90mm	0	0.0
90x75mm	61.38	11.0
75x63mm	59.8	10.7
63x45mm	119.08	21.4
45x37.5mm	52.56	9.4
37.5x31.5mm	40.32	7.2
31.5x22.4mm	58.6	10.5
22.4x19.0mm	25.2	4.5
19.0x16.0mm	21.42	3.8
16.0x13.2mm	19.12	3.4
13.2x9.5mm	39.72	7.1
9.5x6.7mm	27.46	4.9
-6.7mm	32.52	5.8
Total	557.18	100.0

Table App. I-2 Mass retained within selected size fractions after screening obtained QZ Ohio ore sample

Size Fraction	**Mass (Kg)**	**% Retained**
+90mm	43.86	5.7%
90x75mm	14.9	1.9%
75x63mm	19.36	2.5%
63x45mm	42.12	5.5%
45x37.5mm	42.16	5.5%
37.5x31.5mm	45.22	5.9%
31.5x22.4mm	99.86	12.9%
22.4x19.0mm	53.52	6.9%
19.0x16.0mm	55.46	7.2%
16.0x13.2mm	52.32	6.8%
13.2x9.5mm	88.66	11.5%
9.5x6.7mm	58.96	7.6%
-6.7mm	155.22	20.1%
Total	771.62	100.0%

Appendix J

Mineralogical Investigation of the QZ Ohio Ore Type

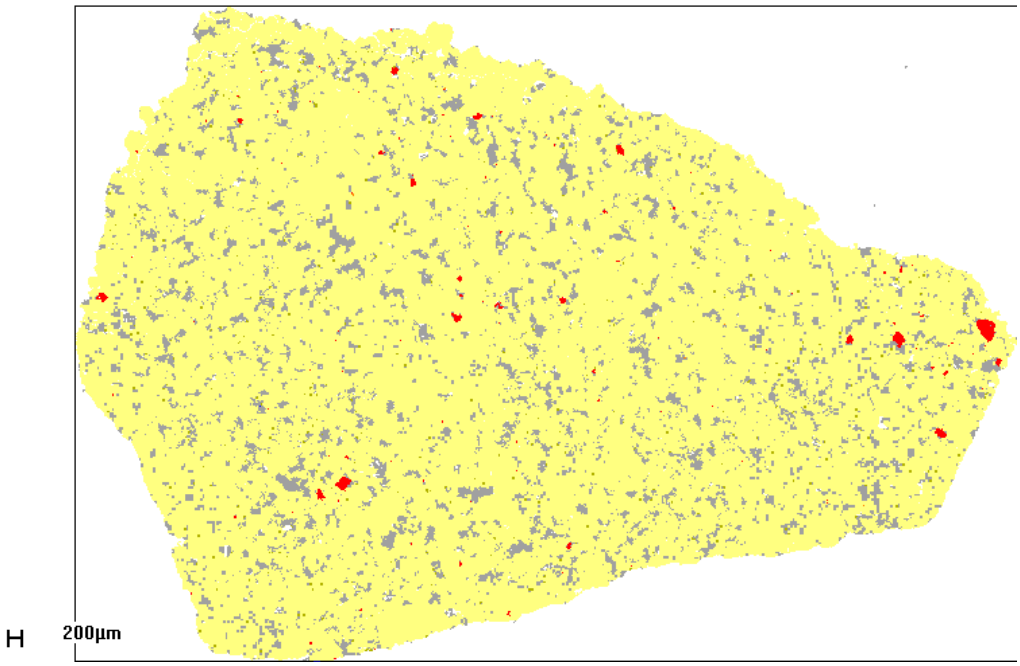

Figure App. J-1 Sample No. 1

Quartz	89.03
Other	10.23
CuSulphides	0.37
Feldspar	0.37
OtherSulphides	0.00
Magnetite	0.00
Garnet	0.00

Table App. J-1 Mineral content represented in surface percentage

Copper Sulphides	**Surface %**	**Other Forming Minerals**	**Surface %**
Bornite	0.11	Amphibole	0.03
Chalcopyrite	0.26	Apatite	0.01
Chalcocite	Not present	Biotite	9.17
Tennantite	Not present	Calcite	<0.01
		Chlorite	0.01
Other Sulphides		Galena	Not present
Pyrite	<0.01	Ilmenite	Not present
Arsenopyrite	Not present	Molybdenite	<0.01
		Olivine	<0.01
Quartz	89.03	Pyroxene	<0.01
Feldspar	0.37	Rutile	<0.01
		Talc	0.01
Garnet	<0.01	Titanite	<0.01
Magnetite	Not present	Other Minerals	0.98

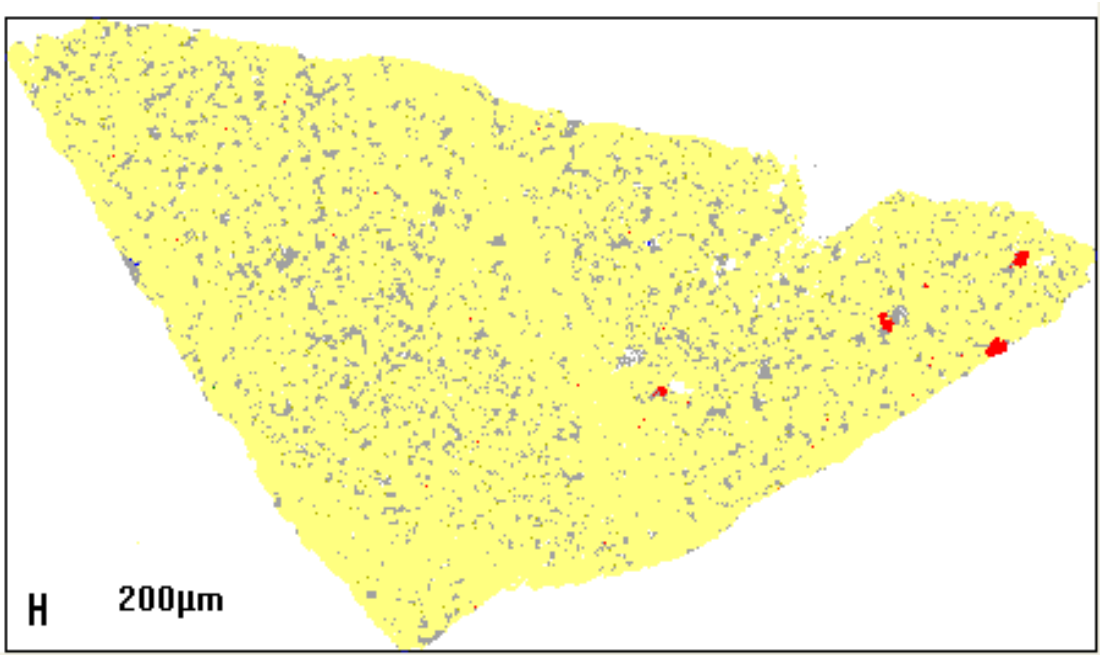

Figure App. J-2 Sample No. 2

Quartz	90.17
Other	9.18
Feldspar	0.39
CuSulphides	0.25
Magnetite	0.01
OtherSulphides	0.00
Garnet	0.00

Table App. J-2 Mineral content represented in surface percentage

Copper Sulphides	**Surface %**	**Other Forming Minerals**	**Surface %**
Bornite	0.10	Amphibole	0.03
Chalcopyrite	0.15	Apatite	0.01
Chalcocite	<0.01	Biotite	8.03
Tennantite	<0.01	Calcite	0.02
		Chlorite	<0.01
Other Sulphides		Galena	Not present
Pyrite	<0.01	Ilmenite	Not present
Arsenopyrite	Not present	Molybdenite	0.11
		Olivine	<0.01
Quartz	90.17	Pyroxene	<0.01
Feldspar	0.39	Rutile	<0.01
		Talc	0.01
Garnet	<0.01	Titanite	<0.01
Magnetite	0.01	Other Minerals	0.96

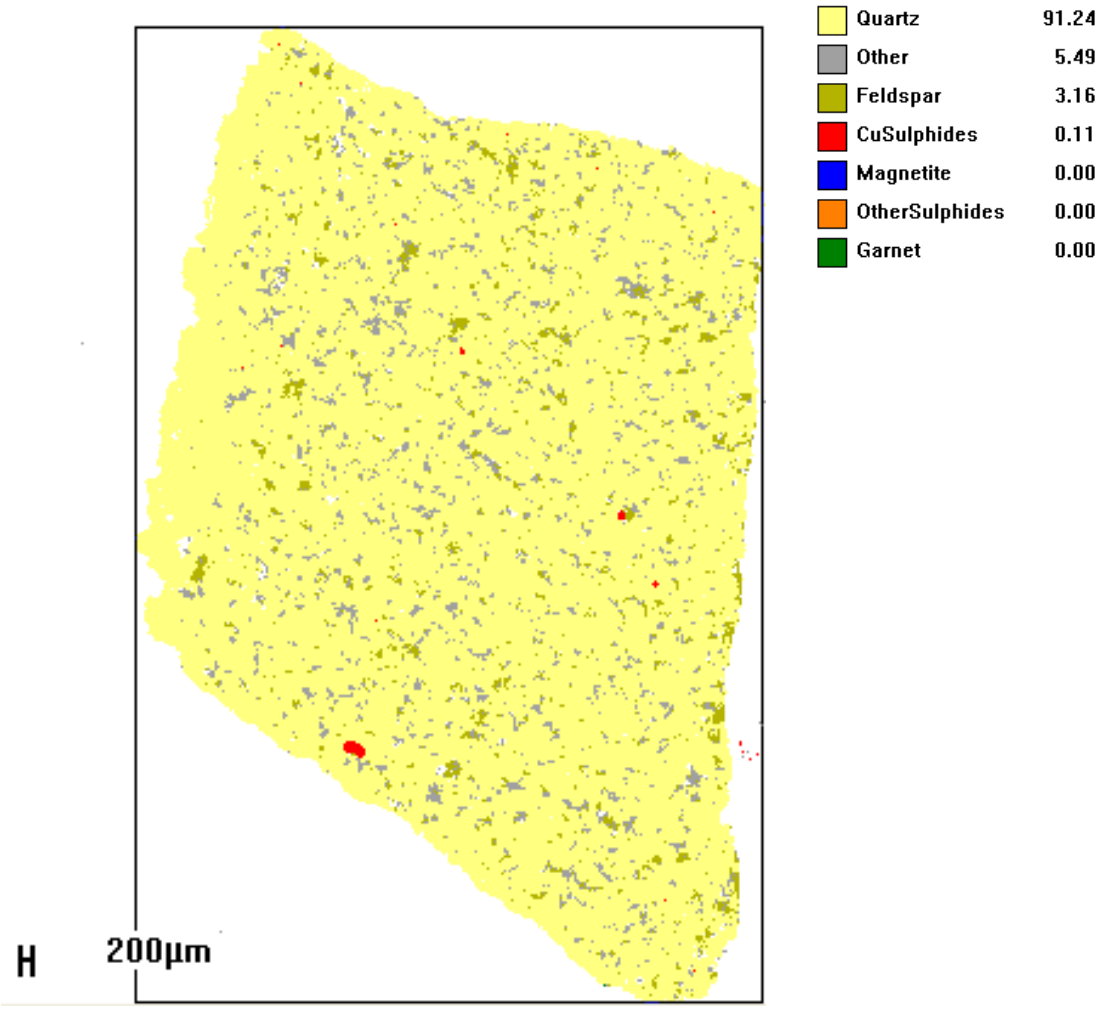

Figure App. J-3 Sample No. 3

Table App. J-3 Mineral content represented in surface percentage

Copper Sulphides	**Surface %**	**Other Forming Minerals**	**Surface %**
Bornite	0.02	Amphibole	0.01
Chalcopyrite	0.09	Apatite	0.01
Chalcocite	<0.01	Biotite	4.21
Tennantite	<0.01	Calcite	<0.01
		Chlorite	0.01
Other Sulphides		Galena	<0.01
Pyrite	<0.01	Ilmenite	Not present
Arsenopyrite	Not present	Molybdenite	<0.01
		Olivine	0.01
Quartz	91.24	Pyroxene	0.01
Feldspar	3.16	Rutile	<0.01
		Talc	<0.01
Garnet	<0.01	Titanite	<0.01
Magnetite	<0.01	Other Minerals	1.23

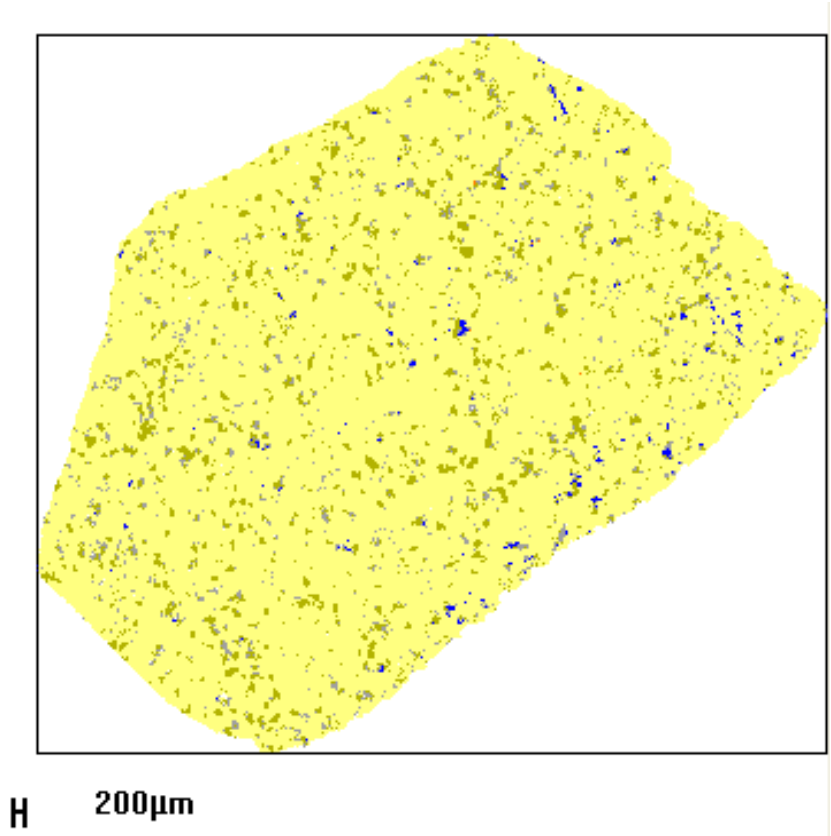

Figure App. J-4 Sample No. 4

Quartz	90.12
Feldspar	6.78
Other	2.64
Magnetite	0.45
OtherSulphides	0.01
Garnet	0.00

Table App. J-4 Mineral content represented in surface percentage

Copper Sulphides	**Surface %**	**Other Forming Minerals**	**Surface %**
Bornite	<0.01	Amphibole	0.63
Chalcopyrite	<0.01	Apatite	0.02
Chalcocite	<0.01	Biotite	0.22
Tennantite	<0.01	Calcite	<0.01
		Chlorite	0.23
Other Sulphides		Galena	<0.01
Pyrite	0.01	Ilmenite	Not present
Arsenopyrite	Not present	Molybdenite	0.11
		Olivine	0.15
Quartz	90.12	Pyroxene	0.02
Feldspar	6.78	Rutile	0.01
		Talc	<0.01
Garnet	<0.01	Titanite	<0.01
Magnetite	0.45	Other Minerals	1.36

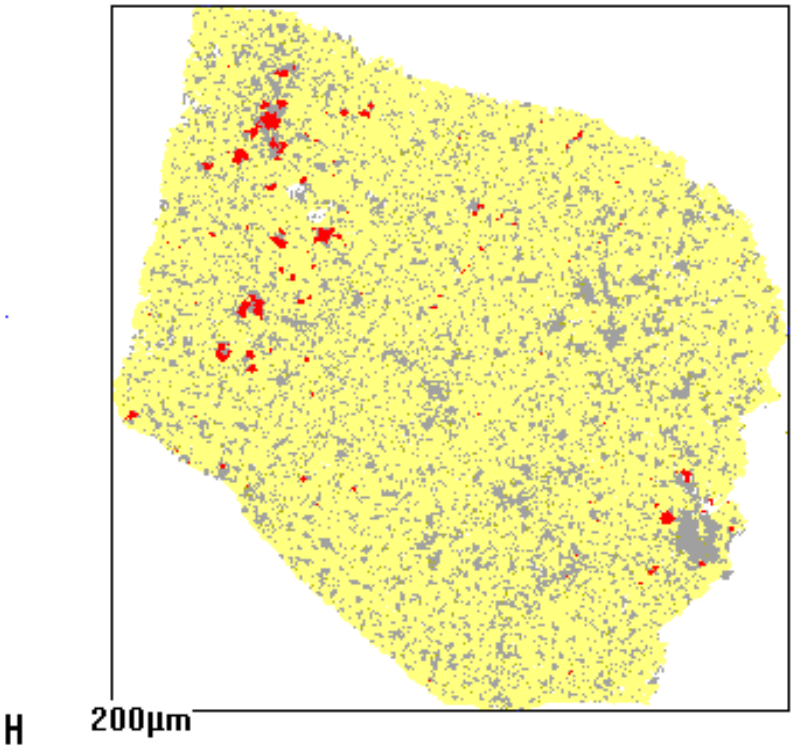

Figure App. J-5 Sample No. 5

Quartz	80.45
Other	17.83
CuSulphides	1.04
Feldspar	0.66
OtherSulphides	0.01
Magnetite	0.00
Garnet	0.00

Table App. J-5 Mineral content represented in surface percentage

Copper Sulphides	**Surface %**	**Other Forming Minerals**	**Surface %**
Bornite	0.18	Amphibole	0.20
Chalcopyrite	0.86	Apatite	0.08
Chalcocite	<0.01	Biotite	14.67
Tennantite	<0.01	Calcite	0.01
		Chlorite	1.77
Other Sulphides		Galena	<0.01
Pyrite	0.01	Ilmenite	Not present
Arsenopyrite	Not present	Molybdenite	0.11
		Olivine	0.02
Quartz	80.45	Pyroxene	0.02
Feldspar	0.66	Rutile	<0.01
		Talc	0.01
Garnet	<0.01	Titanite	<0.01
Magnetite	<0.01	Other Minerals	1.05

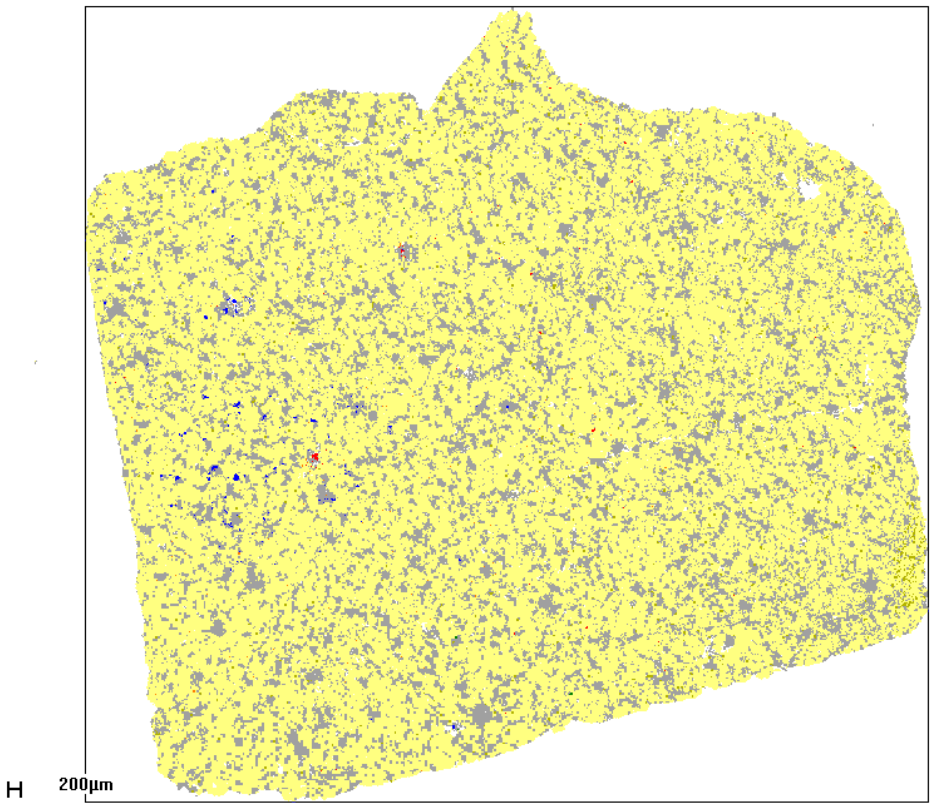

Figure App. J-6 Sample No. 6

Quartz	77.02
Other	22.21
Feldspar	0.59
Magnetite	0.10
OtherSulphides	0.04
CuSulphides	0.03
Garnet	0.00

Table App. J-6 Mineral content represented in surface percentage

Copper Sulphides	**Surface %**	**Other Forming Minerals**	**Surface %**
Bornite	<0.01	Amphibole	0.41
Chalcopyrite	0.03	Apatite	0.11
Chalcocite	<0.01	Biotite	12.88
Tennantite	<0.01	Calcite	0.01
		Chlorite	5.54
Other Sulphides		Galena	<0.01
Pyrite	0.04	Ilmenite	Not present
Arsenopyrite	<0.01	Molybdenite	0.11
		Olivine	0.23
Quartz	77.02	Pyroxene	0.46
Feldspar	0.59	Rutile	<0.01
		Talc	0.16
Garnet	<0.01	Titanite	<0.01
Magnetite	0.10	Other Minerals	2.40

Appendix K

Reproducibility Testing for the QZ Ohio Ore Type

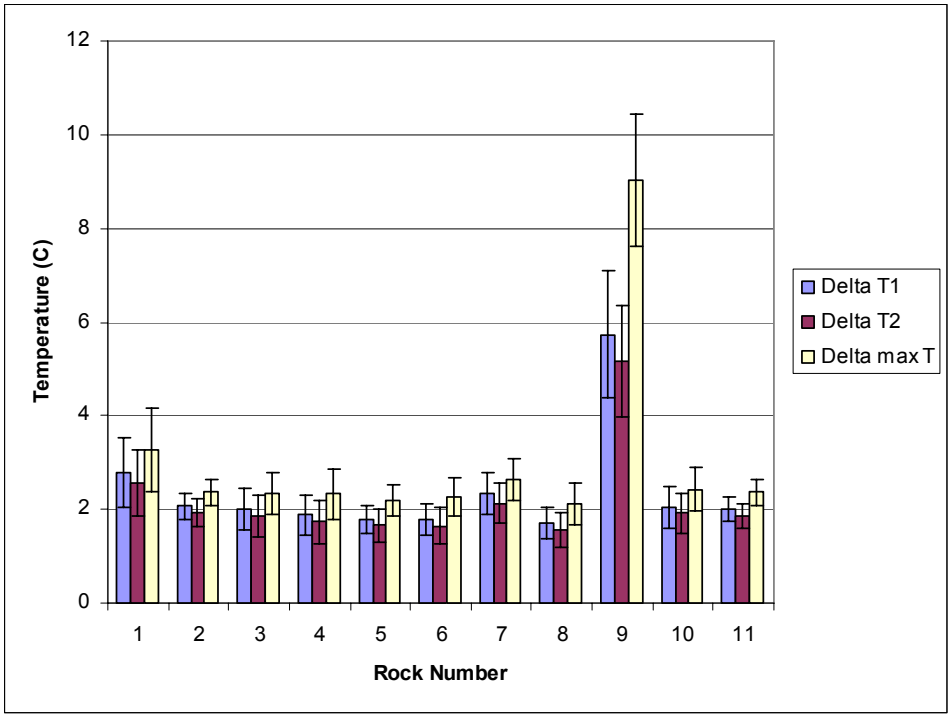

Figure App. K-1 Reproducibility temperature change graph for the eleven -22+19 mm particles in set one where each particle was tested 6 times in different orientations

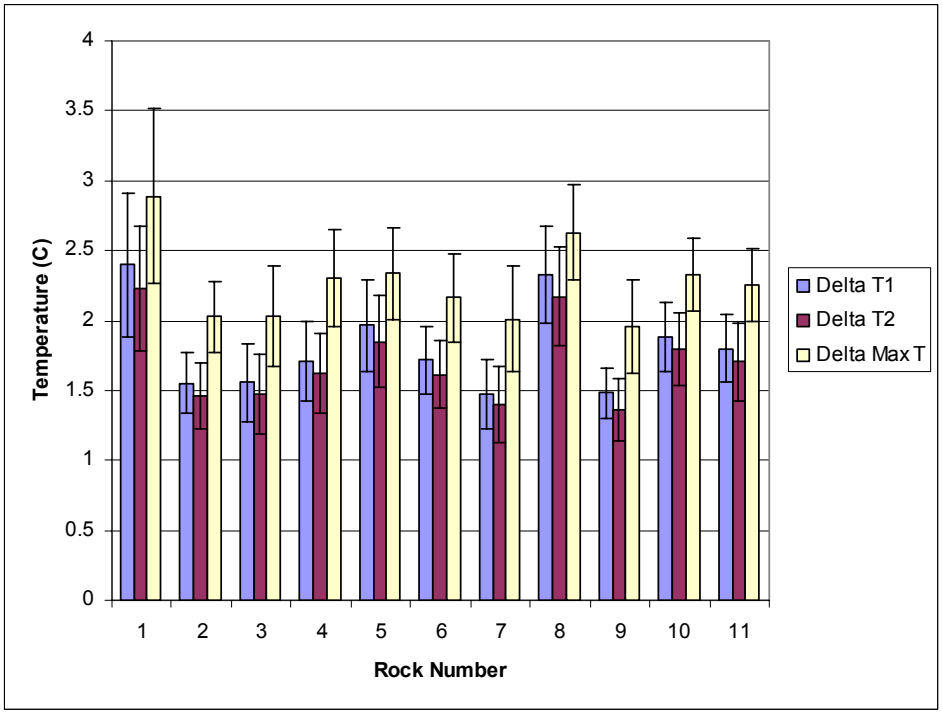

Figure App. K-2Reproducibility temperature change graph for the eleven -22+19 mm particles in set two where each particle was tested 6 times in different orientations

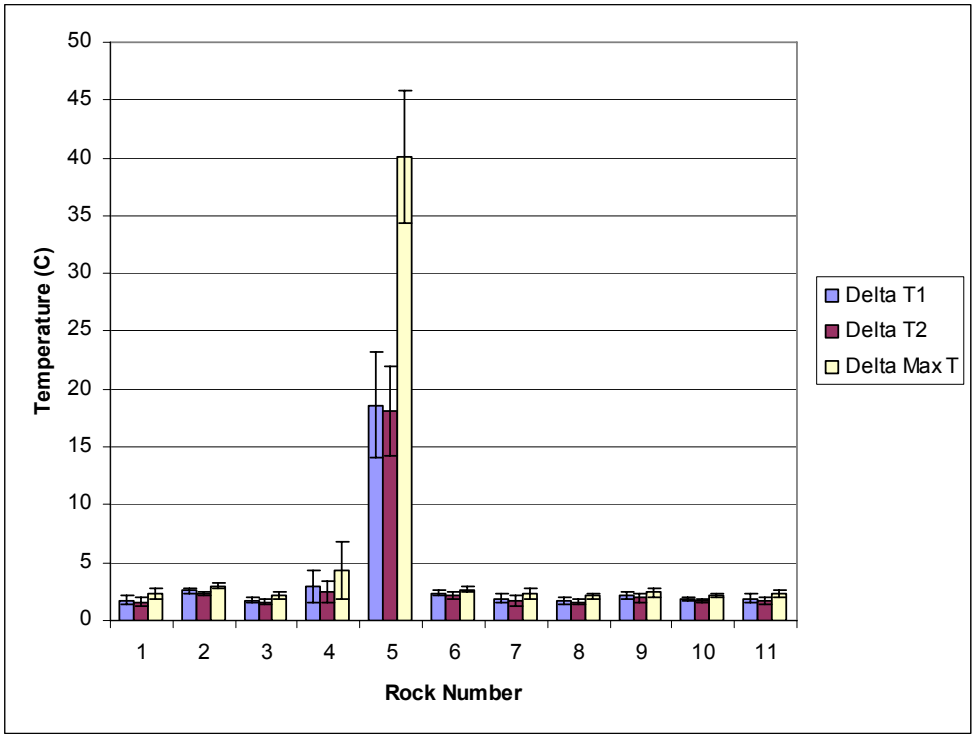

Figure App. K-3 Reproducibility temperature change graph for the eleven -22+19 mm particles in set three where each particle was tested 6 times in different orientations

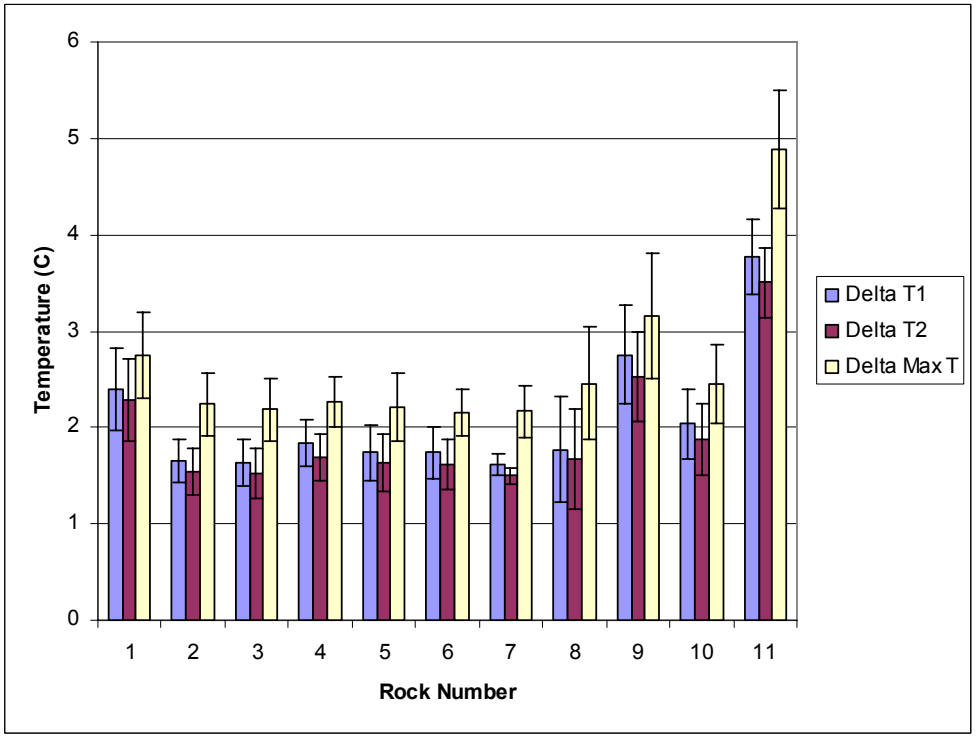

Figure App. K-4 Reproducibility temperature change graph for the eleven -22+19 mm particles in set four where each particle was tested 6 times in different orientations

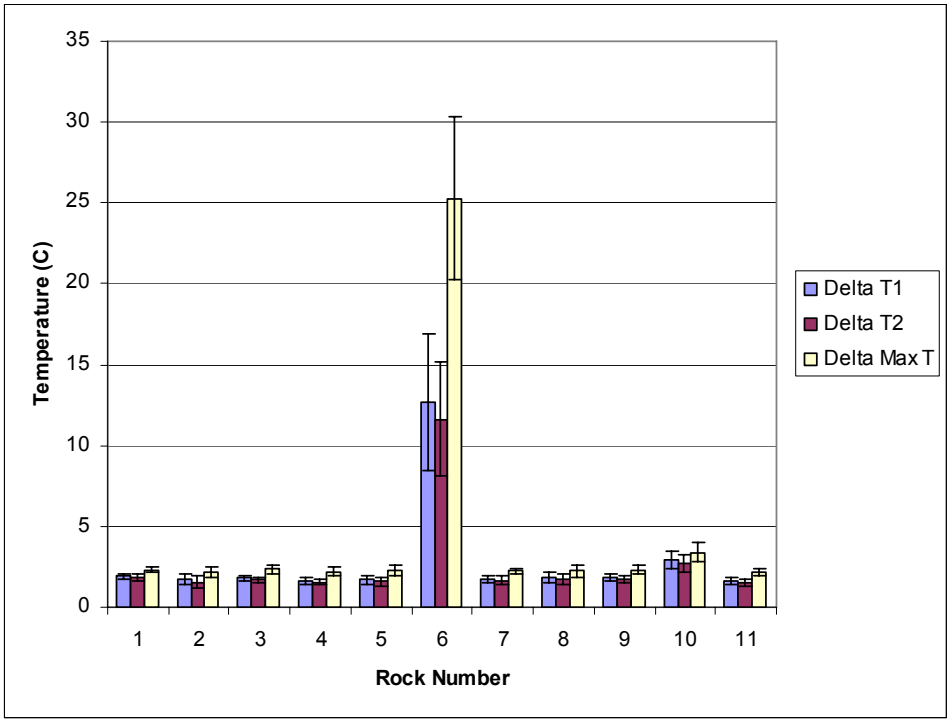

Figure App. K-5 Reproducibility temperature change graph for the eleven -22+19 mm particles in set five where each particle was tested 6 times in different orientations

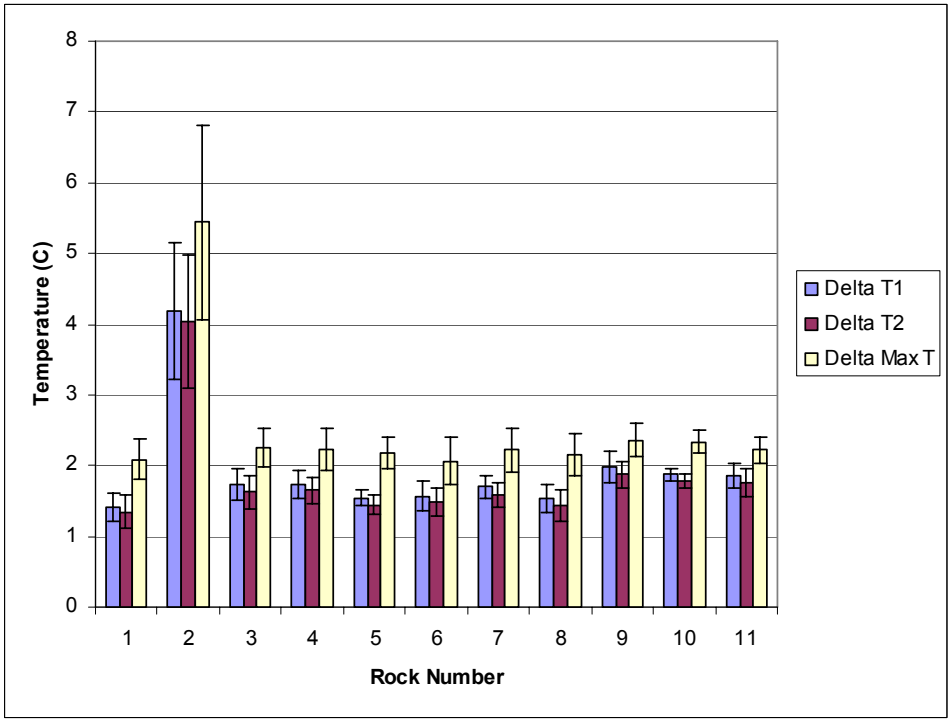

Figure App. K-6 Reproducibility temperature change graph for the eleven -22+19 mm particles in set six where each particle was tested 6 times in different orientations

Sub Sample No	Position Number	Rock Number durin testing	Rock Number	Rock Mass (g)	Rock density (g/cm3)	Cu Assay %	Fe Assay %	Delta Max T1	Cumulative Mass %	Cumulative Copper Recovery%	Cumulative Iron Recovery %
28	9	8	1	18.5	2.569	0.093	0.520	1.630	2.018	0.929	1.145
11	1	10	2	16.49	2.589	0.057	0.640	1.930	3.818	1.436	2.400
28	10	5	3	13.57	2.620	0.089	0.650	1.980	5.298	2.088	3.450
32	1	5	4	11.51	2.622	0.037	0.740	1.950	6.554	2.317	4.463
7	10	9	5	13.3	2.628	0.086	0.700	2.010	8.005	2.935	5.571
20	10	3	6	13.59	2.613	0.120	0.720	1.950	9.488	3.815	6.735
11	2	8	7	16.31	2.614	0.109	0.690	2.010	11.267	4.774	8.074
20	1	7	8	11.86	2.573	0.176	0.820	1.800	12.561	5.901	9.231
20	2	1	9	27.8	2.527	0.402	1.470	2.430	15.594	11.932	14.093
11	6	3	10	11.28	7.139	0.142	0.910	1.900	16.825	12.796	15.314
11	10	1	11	10	2.591	0.087	0.750	3.160	17.916	13.266	16.206
2	1	6	12	14.09	2.609	0.051	0.720	2.250	19.453	13.654	17.413
7	3	6	13	11.84	2.580	0.527	1.140	2.400	20.745	17.021	19.019
7	8	7	14	15.67	2.586	0.075	0.630	2.320	22.455	17.655	20.194
7	4	3	15	12.32	2.556	0.117	0.720	2.360	23.799	18.433	21.249
32	5	8	16	13.52	2.580	0.063	0.730	2.130	25.274	18.893	22.423
7	9	2	17	12.44	2.534	0.068	0.730	2.140	26.631	19.349	23.504
32	4	1	18	15.35	2.521	0.027	0.670	2.330	28.306	19.573	24.727
28	1	11	19	13.72	2.608	0.058	0.720	2.440	29.803	20.002	25.902
32	8	6	20	9.75	2.621	0.137	1.200	2.270	30.867	20.723	27.294
20	11	6	21	14.17	2.629	0.095	0.710	2.160	32.412	21.450	28.491
28	7	4	22	12.85	2.596	0.069	0.740	2.210	33.814	21.928	29.623
2	2	3	23	13.79	2.597	0.135	0.700	2.310	35.319	22.933	30.771
7	1	11	24	13.84	2.631	0.167	0.740	2.250	36.829	24.180	31.990
2	3	11	25	13.78	2.571	0.039	0.700	2.290	38.332	24.470	33.137
32	6	4	26	14.95	2.551	0.085	0.660	2.440	39.964	25.156	34.311
11	9	4	27	14.79	2.572	0.136	0.610	2.020	41.577	26.242	35.385
32	2	7	28	11.78	2.550	0.032	0.540	2.370	42.862	26.445	36.141
7	7	4	29	19.57	2.585	0.062	0.540	2.420	44.998	27.100	37.399
32	7	9	30	14.16	2.637	0.169	0.920	2.310	46.543	28.391	38.949
32	9	10	31	14.92	2.546	0.209	0.710	2.210	48.170	30.074	40.209
20	4	5	32	12.7	2.581	0.086	0.720	2.480	49.556	30.664	41.297
11	5	7	33	16.72	2.576	0.081	0.680	2.180	51.380	31.395	42.649
20	3	2	34	13.77	2.588	0.109	0.610	2.350	52.883	32.205	43.649
7	5	10	35	16.69	2.572	0.371	0.990	2.330	54.703	35.546	45.615
11	3	11	36	9.47	2.566	0.171	0.700	2.340	55.737	36.420	46.403
32	10	11	37	9.65	2.573	0.102	0.860	2.560	56.790	36.951	47.391
7	2	5	38	9.1	2.615	0.486	1.290	2.460	57.782	39.338	48.787
28	8	9	39	16.77	2.620	0.052	0.670	2.450	59.612	39.809	50.124
2	9	4	40	12.23	2.591	0.072	0.680	2.880	60.946	40.284	51.113
20	7	4	41	7.95	2.548	0.079	0.800	2.420	61.814	40.623	51.870
28	3	1	42	11.45	2.556	0.193	0.760	2.430	63.063	41.815	52.905
11	7	9	43	20.83	2.597	0.063	0.710	2.610	65.336	42.524	54.665
32	3	3	44	10.43	2.627	0.110	0.770	2.630	66.474	43.143	55.621
28	5	3	45	8.58	2.592	0.053	0.760	2.810	67.410	43.388	56.396
28	4	7	46	10.42	2.560	0.041	0.820	2.630	68.547	43.619	57.413
2	6	5	47	14.39	2.588	0.041	0.710	2.610	70.117	43.937	58.628
20	5	9	48	10.39	2.778	0.700	1.210	2.820	71.250	47.862	60.124
2	11	10	49	11.65	2.589	0.353	1.100	2.800	72.521	50.082	61.649
2	5	8	50	16.92	2.595	0.140	0.700	3.050	74.367	51.360	63.058
28	6	2	51	16.5	2.594	0.093	0.640	2.820	76.167	52.188	64.314
11	11	2	52	12.61	2.542	1.050	1.160	3.010	77.543	59.334	66.055
11	4	6	53	8.62	2.620	0.850	1.430	2.790	78.484	63.288	67.521
2	8	2	54	14.05	2.592	0.104	0.840	2.840	80.017	64.076	68.925
2	4	7	55	12.08	2.565	0.240	1.170	3.060	81.335	65.641	70.607
20	8	10	56	13.48	2.597	0.612	1.110	3.320	82.805	70.093	72.387
28	2	10	57	18.95	2.544	0.137	1.230	3.330	84.873	71.494	75.160
2	7	1	58	16.85	2.596	0.745	1.310	3.310	86.711	78.269	77.786
7	6	8	59	10.5	2.586	0.150	0.740	3.650	87.857	79.119	78.711
7	11	1	60	14.99	2.576	0.573	1.290	3.580	89.492	83.754	81.011
20	6	8	61	18.76	2.606	0.100	0.690	4.120	91.539	84.767	82.551
32	11	2	62	25.39	2.626	0.406	2.470	5.280	94.309	90.330	90.013
20	9	11	63	11.03	2.614	0.996	1.580	5.870	95.513	96.259	92.086
2	10	9	64	11.64	2.536	0.089	1.720	11.010	96.783	96.818	94.468
28	11	6	65	11.35	2.489	0.275	1.140	22.520	98.021	98.502	96.007
11	8	5	66	18.14	2.534	0.153	1.850	26.270	100.000	100.000	100.000

Figure App. K-7- Data for separation curves for QZ OHIO -22.4 +19.0 mm size fraction based on Delta MAX T

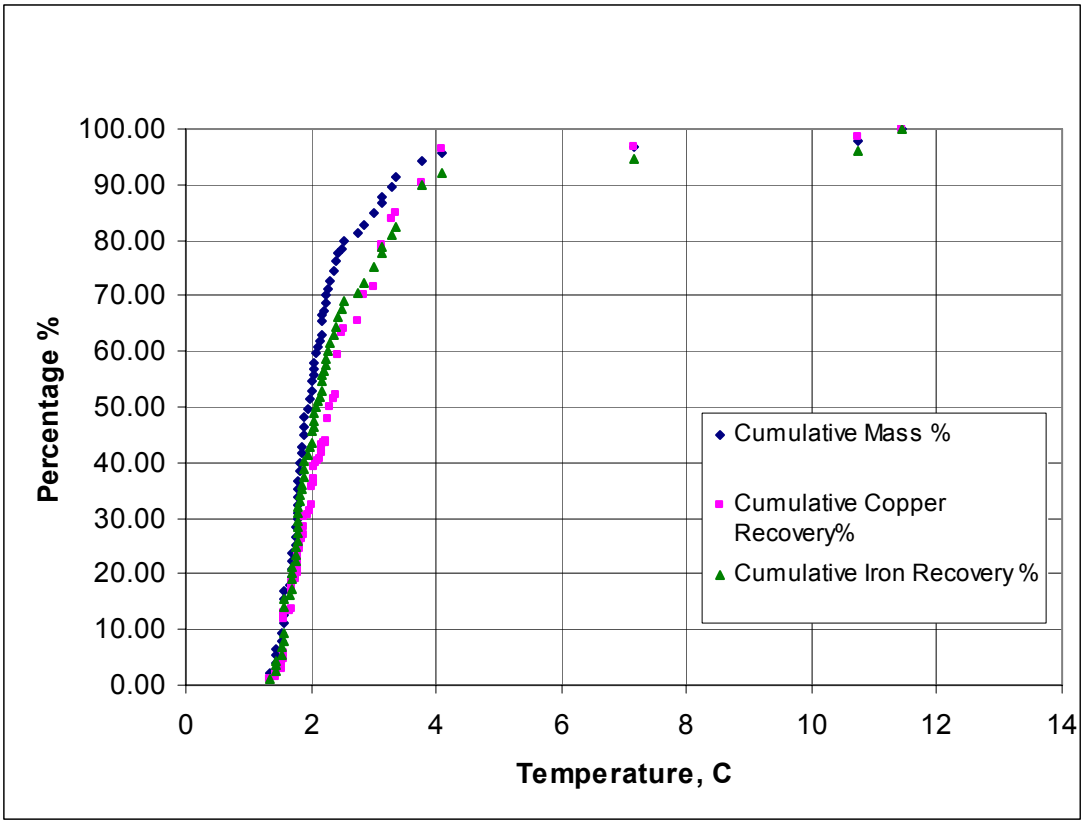

Figure App. K-8- Separation curves for QZ OHIO -22.4 +19.0 mm size fraction based on Delta T1

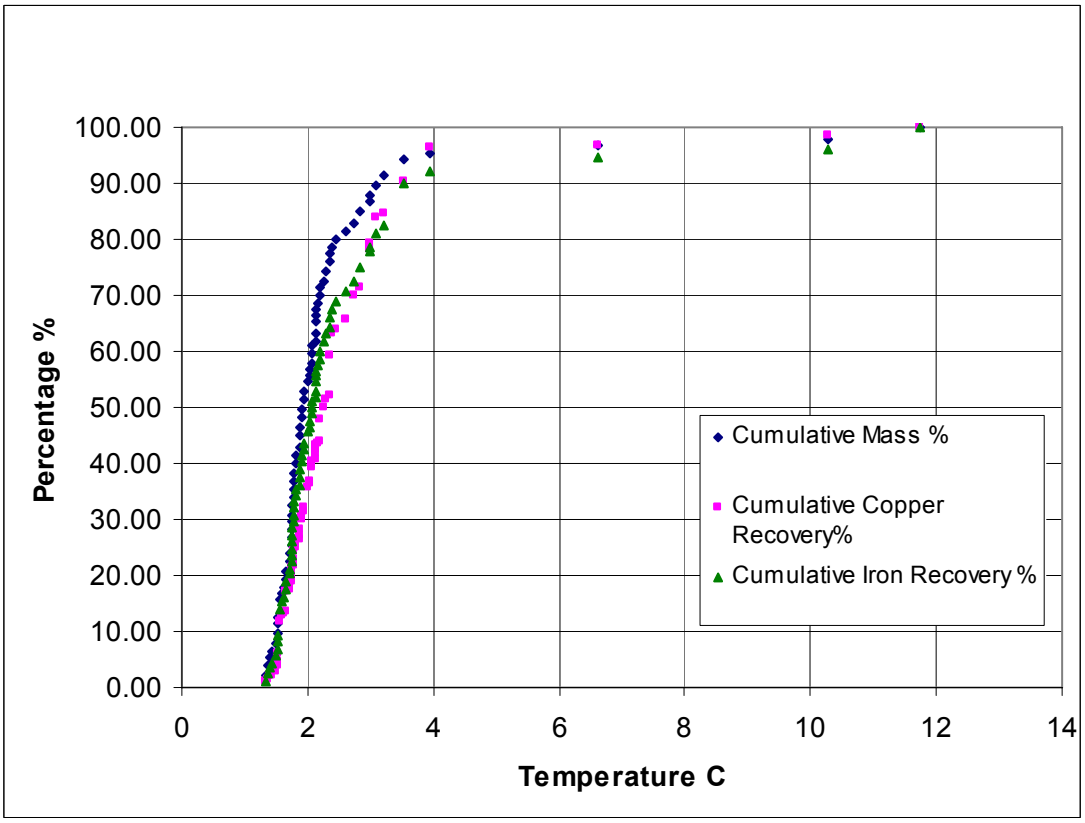

Figure App. K-9 Separation curves for QZ OHIO -22.4 +19.0 mm size fraction based on Delta T2

Appendix L

Calculated Flotation Results

Table App. L-1 Flotation results for mass and cumulative mass % from concentrates for the groups grinded for 10 minutes

Mass, g					
	Flotation time (min)	Hot	Med	Cold	UP
Concentrate 1	1	52.22	34.38	32.47	31.75
Concentrate 2	3	9.03	4.75	5.71	10.54
Concentrate 3	5	6.06	5.56	3.80	6.40
Concentrate 4	10	12.16	8.99	5.97	18.46
Tail		910.80	946.23	948.15	924.71
Total		990.27	999.91	996.10	991.86
Cumulative mass % from concentrates					
	Flotation time (min)	Hot	Med	Cold	UP
Concentrate 1	1	5.27	3.44	3.26	3.20
Concentrate 2	3	6.19	3.91	3.83	4.26
Concentrate 3	5	6.80	4.47	4.21	4.91
Concentrate 4	10	8.03	5.37	4.81	6.77

Table App. L-2 Flotation results for mass and cumulative mass % from concentrates for the groups grinded for 15 minutes

Mass, g					
	Flotation time (min)	Hot	Med	Cold	UP
Concentrate 1	1	49.35	32.10	30.69	30.72
Concentrate 2	3	8.78	3.35	5.26	11.40
Concentrate 3	5	3.74	2.15	2.55	4.47
Concentrate 4	10	13.52	3.55	5.21	12.44
Tail		911.14	869.98	947.16	947.38
Total		986.53	911.13	990.87	1006.41
Cumulative mass % from concentrates					
	Flotation time (min)	Hot	Med	Cold	UP
Concentrate 1	1	5.00	3.52	3.10	3.05
Concentrate 2	3	5.89	3.89	3.63	4.19
Concentrate 3	5	6.27	4.13	3.89	4.63
Concentrate 4	10	7.64	4.52	4.41	5.87

Table App. L-3 Cumulative Copper Recovery (%)grinded for 10 minutes

	Flotation time (min)	Hot	Medium	Cold
Concentrate 1	1	88.5	83.5	84.7
Concentrate 2	3	92.4	90.8	89.5
Concentrate 3	5	93.2	91.7	90.1
Concentrate 4	10	93.8	92.3	90.9

Table App. L-4 Cumulative Copper Recovery (%) grinded for 15 minutes

	Flotation time (min)	Hot	Medium	Cold
Concentrate 1	1	84.9	86.9	82.3
Concentrate 2	3	92.0	91.3	89.6
Concentrate 3	5	92.6	91.9	90.4
Concentrate 4	10	93.2	92.5	91.1

The Linear Interpolation for 75% Passing Size (P75) for the hot, medium, cold fraction and unprocessed material at different grinding times

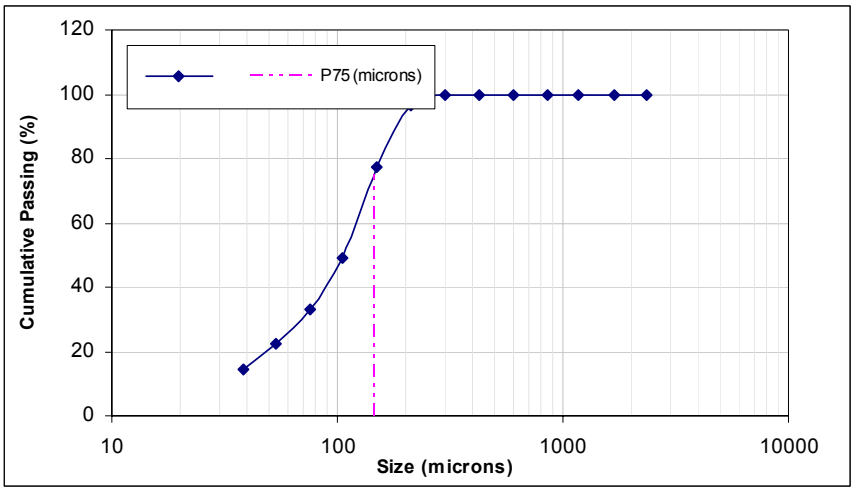

Figure App. L-1 Linear interpolation for P75 for the hot fraction at 10 minutes grind. P75=146 µm

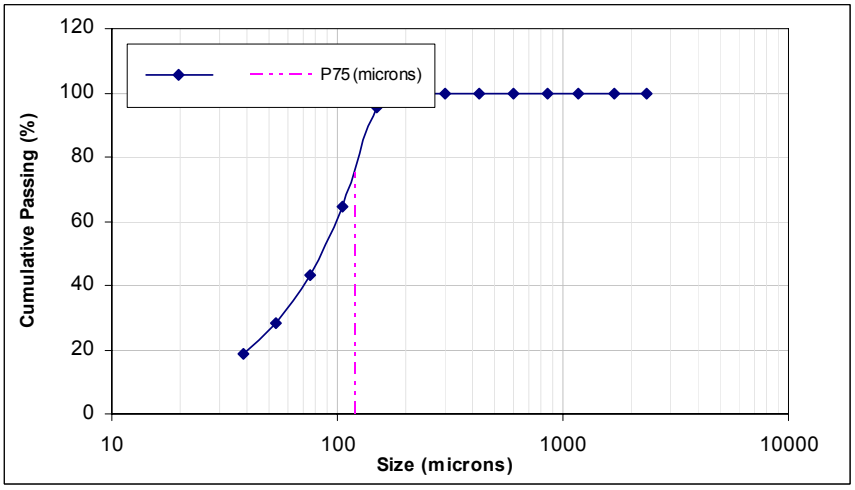

Figure App. L-2 Linear interpolation for P75 for the hot fraction at 15 minutes grind. P75=121 µm

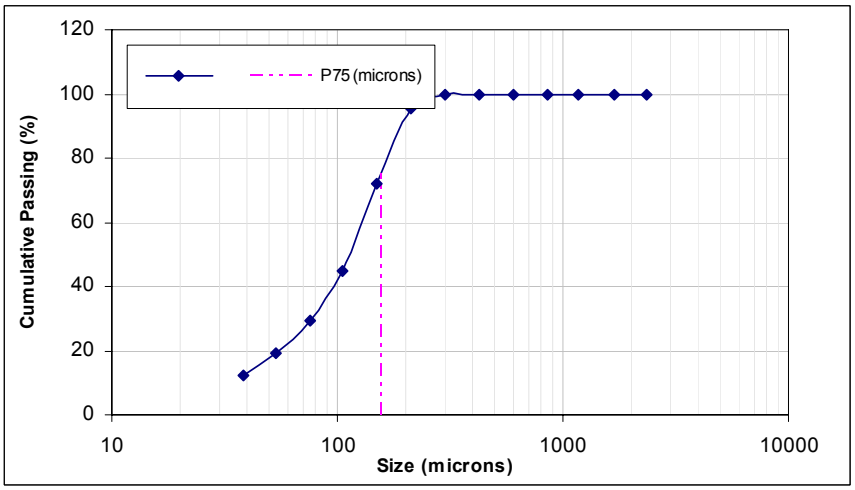

Figure App. L-3 Linear interpolation for P75 for the medium fraction at 10 minutes grind. P75=158 µm

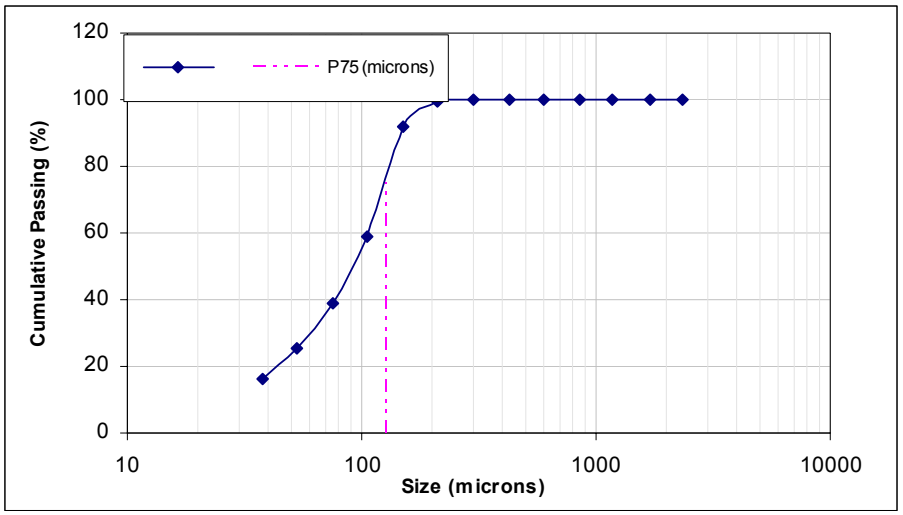

Figure App. L-4Linear interpolation for P75 for the medium fraction at 15 minutes grind. P75=127 µm

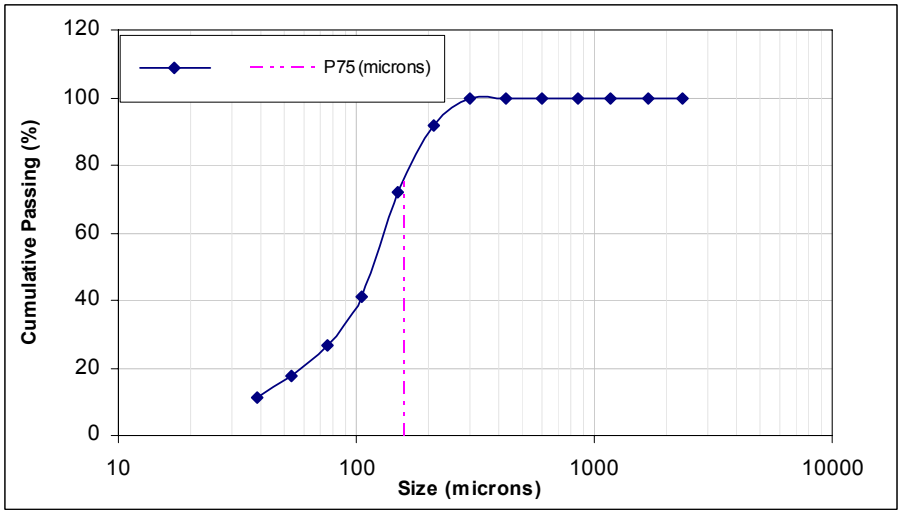

Figure App. L-5 Linear interpolation for P75 for the cold fraction at 10 minutes grind. P75=160 µm

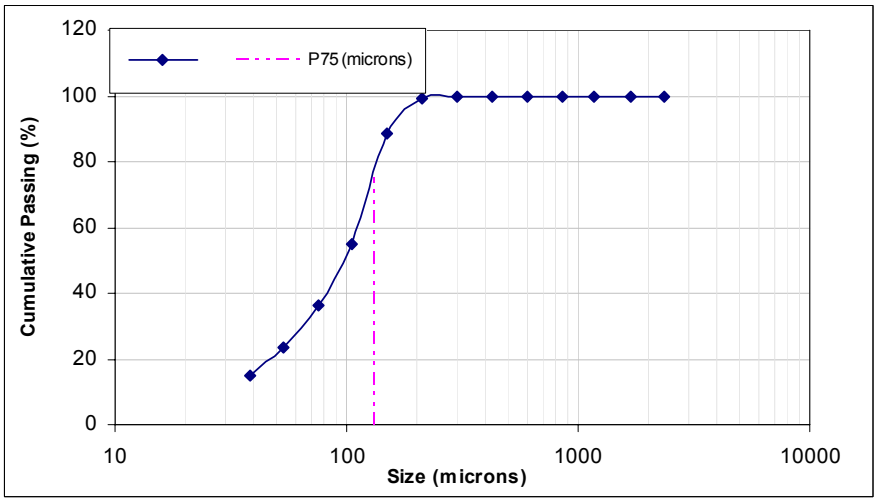

Figure App. L-6Linear interpolation for P75 for the cold fraction at 15 minutes grind. P75=132 µm

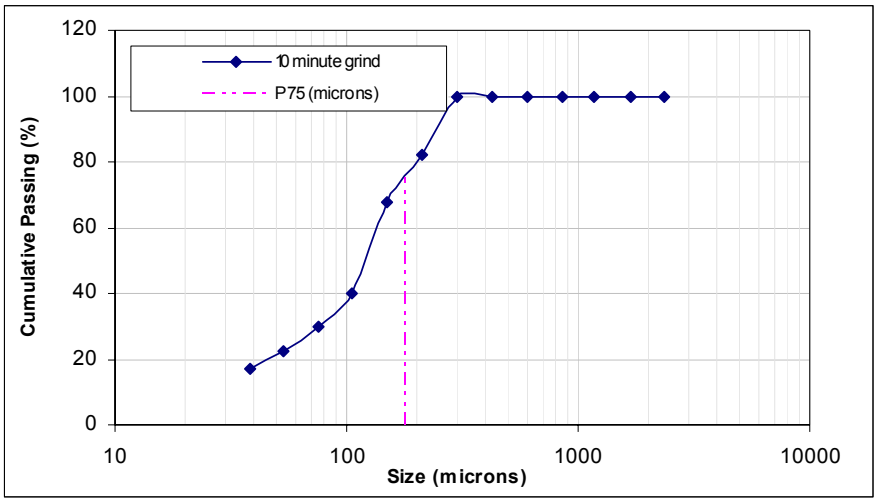

Figure App. L-7 Linear interpolation for P75 for the unprocessed material at 10 minutes grind. P75=181 µm

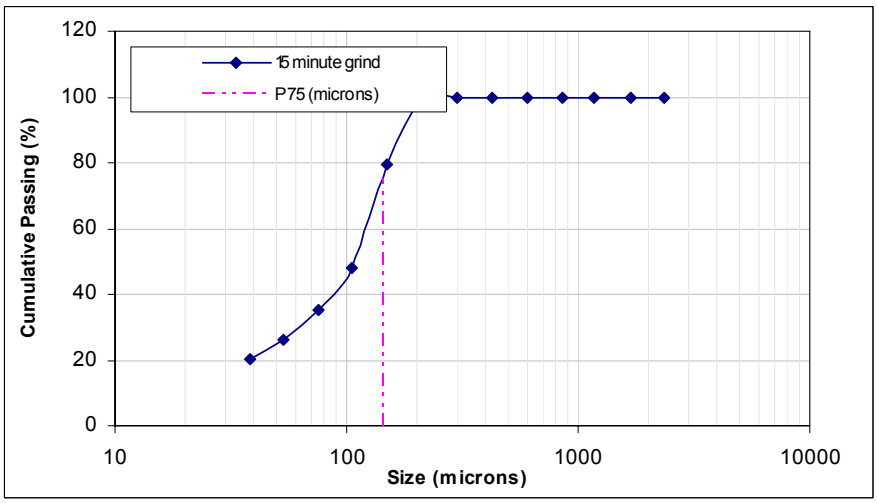

Figure App. L-8 Linear interpolation for P75 for the unprocessed material at 10 minutes grind. P75=144 µm

Flotation results

Flotation Logsheet

Operator:	Cameron

Grind Conditions		Pre-Grind Reagent Addition	
Test:	JK2731-1	pH Modifier	Ca(OH)2
Sample Mass (g):	994.00	Conc	5%
Charge Mass (g):	11020.00	Target pH	10.2
Water Mass (g):	489.58	Amount Added	1000µl
RPM:	76		Diesel
Grind Time (min):	15	Conc	Neat
Water Source:	Pilot Plant	Amount Added	21µl

Test Conditions			
Test:	JK2381-823	Date:	24/08/2009
Cell Size (L):	5	RPM:	1000
Air Rate (L/min):	10	Froth Depth (cm):	1
Froth Pull (s)	10	Water Source:	Pilot Plant
Air Press.(kPa):	200	Conditioning Time:	3

Float Chemistry		pH.	Eh.
Initial Reading After Grind		8.16	234
pH Modifier	Ca(OH)2		
Conc	5.00%	9.95	113
Add	6ml		
Collector	S8989		
Conc	Neat	9.98	106
Add	18µl		
Frother	MIBC		
Conc	Neat	9.97	103
Add	210µl		
Tail		8.92	177

Sample	Time (min)	Water Initial Wt	Water Final Wt	Tray Wt	Wet Wt	Total Dry Wt	Paper Wt	Dry Wt
(#)		g	g	g	g	(g)	(g)	(g)
Conc 1	1	1021.29	950.09	159	1059.02	56.54	7.19	49.35
Conc 2	3	970.43	806.28	157.2	678.55	16.02	7.24	8.78
Conc 3	5	968.4	852.4	157.5	509.08	10.9	7.16	3.74
Conc 4	10	850.21	554.8	158.4	836.67	20.76	7.24	13.52
Tail		480.31	292.18	9508.9	14474.2	918.22	7.08	911.14
Total								**986.53**

Notes:

Additional Water: 1050.23g

Table App. L-5 QZ Ohio Hot grinded for 15 min

Table App. L-6 QZ Ohio Medium grinded for 15 min

Flotation Logsheet

Operator:	Cameron

Grind Conditions		Pre-Grind Reagent Addition	
Test:	JK2731-1	pH Modifier	Ca(OH)2
Sample Mass (g):	917.00	Conc	5%
Charge Mass (g):	11020.00	Target pH	10.2
Water Mass (g):	451.66	Amount Added	1000µl
RPM:	76		Diesel
Grind Time (min):	15	Conc	Neat
Water Source:	Pilot Plant	Amount Added	21µl

Test Conditions			
Test:	JK2381-824	Date:	24/08/2009
Cell Size (L):	5	RPM:	1000
Air Rate (L/min):	10	Froth Depth (cm):	1
Froth Pull (s)	10	Water Source:	Pilot Plant
Air Press.(kPa):	200	Conditioning Time:	3

Float Chemistry		pH.	Eh.
Initial Reading After Grind		8.13	221
pH Modifier	Ca(OH)2	10.26	72
Conc	5.00%		
Add	6ml		
Collector	S8989	10.37	70
Conc	Neat		
Add	18µl		
Frother	MIBC	10.35	71
Conc	Neat		
Add	210µl		
Tail		9.09	168

Sample	Time (min)	Water Initial Wt	Water Final Wt	Tray Wt	Wet Wt	Total Dry Wt	Paper Wt	Dry Wt
(#)		g	g	g	g	(g)	(g)	(g)
Conc 1	1	950.09	855.08	159	1047.16	39.28	7.18	32.1
Conc 2	3	806.28	658.02	157.2	583.14	10.47	7.12	3.35
Conc 3	5	852.4	717.24	157.5	545.42	9.4	7.25	2.15
Conc 4	10	1116.38	847.44	158.4	747.82	10.75	7.2	3.55
Tail		591.47	355.75	9508.9	14595	877.21	7.23	869.98
Total								**911.13**

Notes:

Additional Water: 956.64 g

Table App. L-7 QZ Ohio Cold grinded for 15 min

Flotation Logsheet

Operator:	Cameron

Grind Conditions		Pre-Grind Reagent Addition	
Test:	JK2731-1	pH Modifier	Ca(OH)2
Sample Mass (g):	990.00	Conc	5%
Charge Mass (g):	11020.00	Target pH	10.2
Water Mass (g):	487.61	Amount Added	1000µl
RPM:	76		Diesel
Grind Time (min):	15	Conc	Neat
Water Source:	Pilot Plant	Amount Added	21µl

Test Conditions			
Test:	JK2381-825	Date:	24/08/2009
Cell Size (L):	5	RPM:	1000
Air Rate (L/min):	10	Froth Depth (cm):	1
Froth Pull (s)	10	Water Source:	Pilot Plant
Air Press.(kPa):	200	Conditioning Time:	3

Float Chemistry		pH.	Eh.
Initial Reading After Grind		8.07	234
pH Modifier	Ca(OH)2	10.14	80
Conc	5.00%		
Add	6ml		
Collector	S8989	10.2	78
Conc	Neat		
Add	18µl		
Frother	MIBC	10.2	77
Conc	Neat		
Add	210µl		
Tail		8.94	174

Sample	Time (min)	Water Initial Wt	Water Final Wt	Tray Wt	Wet Wt	Total Dry Wt	Paper Wt	Dry Wt
(#)		g	g	g	g	(g)	(g)	(g)
Conc 1	1	1120.32	1021.93	159	1004.25	37.83	7.14	30.69
Conc 2	3	1118.73	977.64	157.2	641.22	12.45	7.19	5.26
Conc 3	5	1120.57	985.69	157.5	523.46	9.67	7.12	2.55
Conc 4	10	1120.72	834.6	158.4	823.17	12.44	7.23	5.21
Tail		597.96	441.37	9508.9	14500.1	954.25	7.09	947.16
Total								**990.87**

Notes:

Additional Water: 925.24 g

Table App. L-8 QZ Ohio not treated grinded for 15 min

Flotation Logsheet

Operator:	Cameron

Grind Conditions		Pre-Grind Reagent Addition	
Test:	JK2731-1	pH Modifier	Ca(OH)2
Sample Mass (g):	1000.00	Conc	5%
Charge Mass (g):	11020.00	Target pH	10.2
Water Mass (g):	492.54	Amount Added	1000µl
RPM:	76		Diesel
Grind Time (min):	15	Conc	Neat
Water Source:	Pilot Plant	Amount Added	21µl

Test Conditions			
Test:	JK2381-809	Date:	19/08/2009
Cell Size (L):	5	RPM:	1000
Air Rate (L/min):	10	Froth Depth (cm):	1
Froth Pull (s)	10	Water Source:	Pilot Plant
Air Press.(kPa):	200	Conditioning Time:	3

Float Chemistry		pH.	Eh.
Initial Reading After Grind		8.26	187
pH Modifier	Ca(OH)2	10.19	75
Conc	5.00%		
Add	6ml		
Collector	S8989	10.18	79
Conc	Neat		
Add	18µl		
Frother	MIBC	10.14	83
Conc	Neat		
Add	210µl		
Tail		9.03	164

Sample	Time (min)	Water Initial Wt	Water Final Wt	Tray Wt	Wet Wt	Total Dry Wt	Paper Wt	Dry Wt
(#)		g	g	g	g	(g)	(g)	(g)
Conc 1	1	1007.27	903.61	159	906.04	37.68	6.96	30.72
Conc 2	3	965.26	780.75	157.2	774.83	18.64	7.24	11.4
Conc 3	5	987.21	822.38	157.5	554.75	11.46	6.99	4.47
Conc 4	10	796.68	347.46	158.4	816.49	19.63	7.19	12.44
Tail		425.63	321.59	9508.9	14493.9	954.4	7.02	947.38
Total								**1006.41**

Notes:

Additional Water: 977.65 g

Table App. L-9 QZ Ohio Hot grinded for 10 min

Flotation Logsheet

Operator:	Cameron

Grind Conditions		Pre-Grind Reagent Addition	
Test:	JK2731-1	pH Modifier	Ca(OH)2
Sample Mass (g):	1000.00	Conc	5%
Charge Mass (g):	11020.00	Target pH	10.2
Water Mass (g):	492.54	Amount Added	1000µl
RPM:	76		Diesel
Grind Time (min):	10	Conc	Neat
Water Source:	Pilot Plant	Amount Added	21µl

Test Conditions			
Test:	JK2381-820	Date:	21/08/2009
Cell Size (L):	5	RPM:	1000
Air Rate (L/min):	10	Froth Depth (cm):	1
Froth Pull (s)	10	Water Source:	Pilot Plant
Air Press.(kPa):	200	Conditioning Time:	3

Float Chemistry		pH.	Eh.
Initial Reading After Grind		8.11	263
pH Modifier	Ca(OH)2	10.2	86
Conc	5.00%		
Add	6ml		
Collector	S8989	10.27	79
Conc	Neat		
Add	18µl		
Frother	MIBC	10.26	84
Conc	Neat		
Add	210µl		
Tail		9.16	174

Sample	Time (min)	Water Initial Wt	Water Final Wt	Tray Wt	Wet Wt	Total Dry Wt	Paper Wt	Dry Wt
(#)		g	g	g	g	(g)	(g)	(g)
Conc 1	1	1116.97	1000.22	159	1133.7	59.54	7.32	52.22
Conc 2	3	1108.49	945.02	157.2	708.15	16.26	7.23	9.03
Conc 3	5	1115.82	963.4	157.5	576.3	13.33	7.27	6.06
Conc 4	10	1114.33	833.52	158.4	837.3	19.38	7.22	12.16
Tail		592.35	407.7	9508.9	14538	918.05	7.25	910.8
Total								**990.27**

Notes:

Additional Water: 1118.47g

Table App. L-10 QZ Ohio Medium grinded for 10 min

Flotation Logsheet

Operator:	Cameron

Grind Conditions		Pre-Grind Reagent Addition	
Test:	JK2731-1	pH Modifier	Ca(OH)2
Sample Mass (g):	1000.00	Conc	5%
Charge Mass (g):	11020.00	Target pH	10.2
Water Mass (g):	492.54	Amount Added	1000µl
RPM:	76		Diesel
Grind Time (min):	10	Conc	Neat
Water Source:	Pilot Plant	Amount Added	21µl

Test Conditions			
Test:	JK2381-821	Date:	21/08/2009
Cell Size (L):	5	RPM:	1000
Air Rate (L/min):	10	Froth Depth (cm):	1
Froth Pull (s)	10	Water Source:	Pilot Plant
Air Press.(kPa):	200	Conditioning Time:	3

Float Chemistry		pH.	Eh.
Initial Reading After Grind		8.09	232
pH Modifier	Ca(OH)2	10.25	75
Conc	5.00%		
Add	6ml		
Collector	S8989	10.21	82
Conc	Neat		
Add	18µl		
Frother	MIBC	10.18	86
Conc	Neat		
Add	210µl		
Tail		9.01	177

Sample	Time (min)	Water Initial Wt	Water Final Wt	Tray Wt	Wet Wt	Total Dry Wt	Paper Wt	Dry Wt
(#)		g	g	g	g	(g)	(g)	(g)
Conc 1	1	1000.22	893.46	159	1093.35	41.61	7.23	34.38
Conc 2	3	945.02	785.71	157.2	581.85	12	7.25	4.75
Conc 3	5	963.4	814.67	157.5	572.9	12.74	7.18	5.56
Conc 4	10	833.52	495.92	158.4	930.65	16.26	7.27	8.99
Tail		407.7	230.02	9508.9	14528	953.4	7.17	946.23
Total								**999.91**

Notes:

Additional Water: 1088.98g

Table App. L-11 QZ Ohio Cold grinded for 10 min

Flotation Logsheet

Operator:	Cameron

Grind Conditions		Pre-Grind Reagent Addition	
Test:	JK2731-1	pH Modifier	Ca(OH)2
Sample Mass (g):	1000.00	Conc	5%
Charge Mass (g):	11020.00	Target pH	10.2
Water Mass (g):	492.54	Amount Added	1000µl
RPM:	76		Diesel
Grind Time (min):	10	Conc	Neat
Water Source:	Pilot Plant	Amount Added	21µl

Test Conditions			
Test:	JK2381-822	Date:	21/08/2009
Cell Size (L):	5	RPM:	1000
Air Rate (L/min):	10	Froth Depth (cm):	1
Froth Pull (s)	10	Water Source:	Pilot Plant
Air Press.(kPa):	200	Conditioning Time:	3

Float Chemistry		pH.	Eh.
Initial Reading After Grind		8.12	260
pH Modifier	Ca(OH)2	10.27	88
Conc	5.00%		
Add	6ml		
Collector	S8989	10.32	85
Conc	Neat		
Add	18µl		
Frother	MIBC	10.29	86
Conc	Neat		
Add	210µl		
Tail		9.04	177

Sample	Time (min)	Water Initial Wt	Water Final Wt	Tray Wt	Wet Wt	Total Dry Wt	Paper Wt	Dry Wt
(#)		g	g	g	g	(g)	(g)	(g)
Conc 1	1	1112.55	1021.29	159	1081.29	39.61	7.14	32.47
Conc 2	3	1116.74	970.43	157.2	650.72	12.87	7.16	5.71
Conc 3	5	1118.45	988.4	157.5	550.42	11.13	7.33	3.8
Conc 4	10	1116.39	850.21	158.4	777.05	13.19	7.22	5.97
Tail		595.27	480.31	9508.9	14517	955.46	7.31	948.15
Total								**996.1**

Notes:

Additional Water: 999.62 g

Table App. L-12 QZ Ohio not treated grinded for 10 min

Flotation Logsheet

Operator:	Cameron

Grind Conditions		Pre-Grind Reagent Addition	
Test:	JK2731-1	pH Modifier	Ca(OH)2
Sample Mass (g):	1000.00	Conc	5%
Charge Mass (g):	11020.00	Target pH	10.2
Water Mass (g):	492.54	Amount Added	1000µl
RPM:	76		Diesel
Grind Time (min):	10	Conc	Neat
Water Source:	Pilot Plant	Amount Added	21µl

Test Conditions			
Test:	JK2381-808	Date:	19/08/2009
Cell Size (L):	5	RPM:	1000
Air Rate (L/min):	10	Froth Depth (cm):	1
Froth Pull (s)	10	Water Source:	Pilot Plant
Air Press.(kPa):	200	Conditioning Time:	3

Float Chemistry		pH.	Eh.
Initial Reading After Grind		8.27	214
pH Modifier	Ca(OH)2	10.44	70
Conc	5.00%		
Add	6ml		
Collector	S8989	10.51	65
Conc	Neat		
Add	18µl		
Frother	MIBC	10.48	69
Conc	Neat		
Add	210µl		
Tail		9.43	148

Sample	Time (min)	Water Initial Wt	Water Final Wt	Tray Wt	Wet Wt	Total Dry Wt	Paper Wt	Dry Wt
(#)		g	g	g	g	(g)	(g)	(g)
Conc 1	1	1114.25	1007.27	159	805.06	38.99	7.24	31.75
Conc 2	3	1114.61	965.26	157.2	652.06	17.57	7.03	10.54
Conc 3	5	1116.27	987.21	157.5	511.23	13.73	7.33	6.4
Conc 4	10	1115.69	796.68	158.4	936.16	25.47	7.01	18.46
Tail		574.28	425.63	9508.9	14556.4	931.92	7.21	924.71
Total								**991.86**

Notes:

Additional Water: 722.55 g

Appendix M

Set No 1:

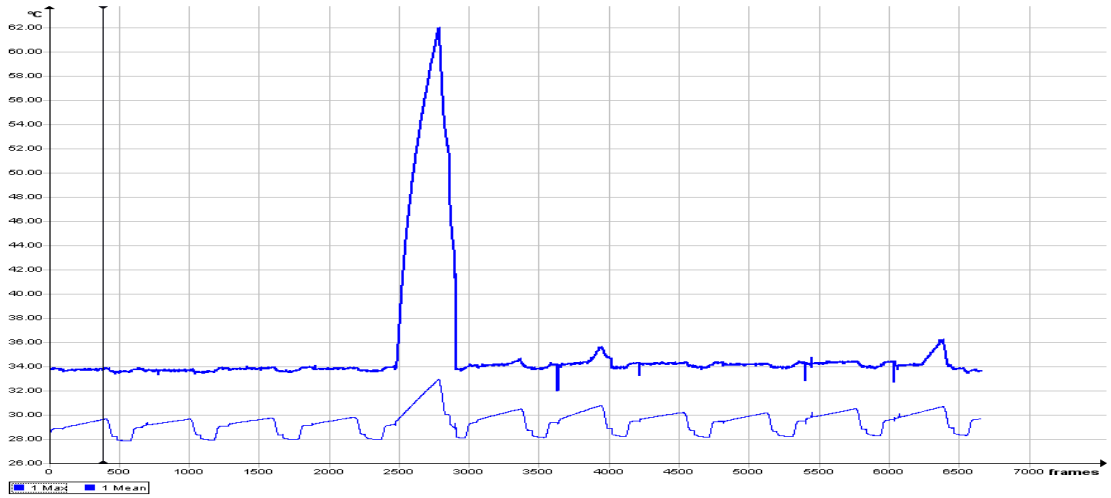

Figure App. M-1 First exposure, timing graph for the set No. 1

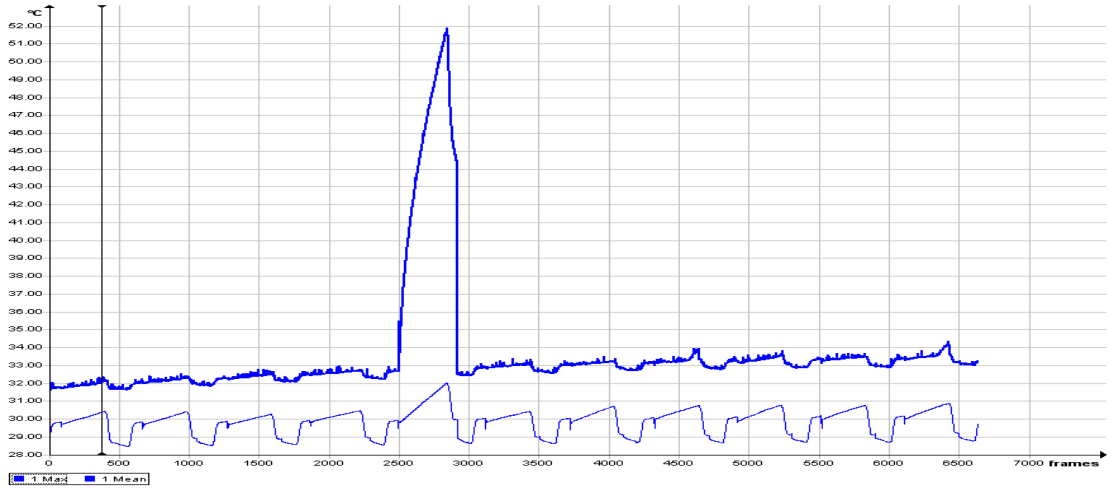

Figure App. M-2 Second exposure, timing graph for the set No. 1

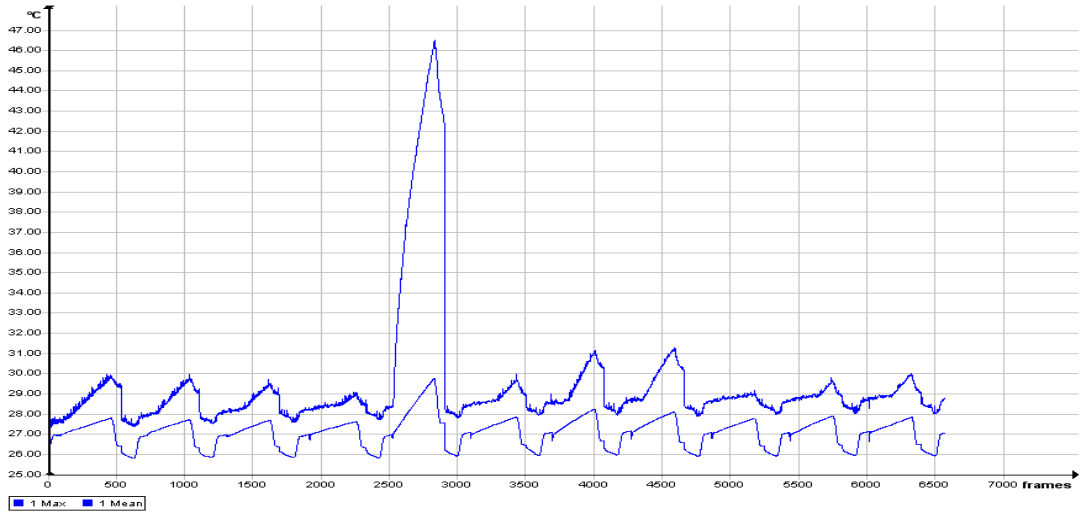

Figure App. M-3 Third exposure, timing graph for the set No. 1

Tomography analysis of some of the hot particles:

Particle No. 5 Set No. 1

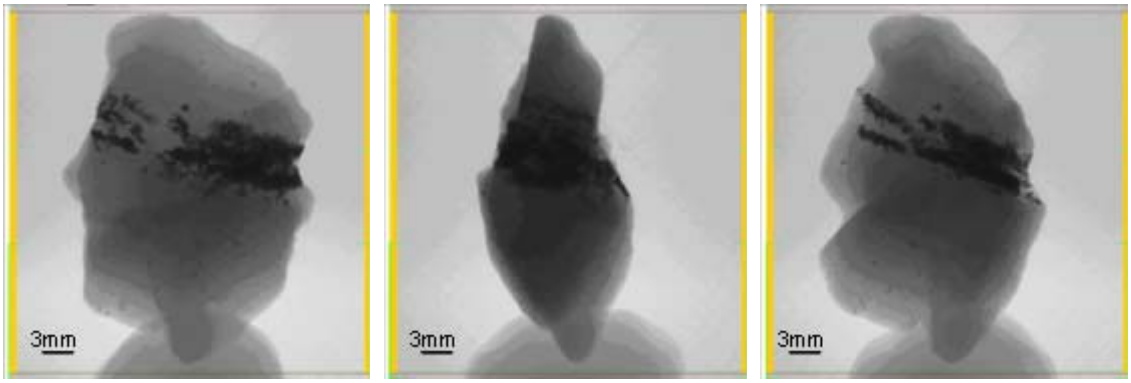

Position 0 deg **Position 45 deg** **Position 180 deg**

Figure App. M-4 QZ Ohio Ore Particle No. 5 Set No. 1

Tomography analysis of some of the cold particles:

Particle No. 2 Set No. 1

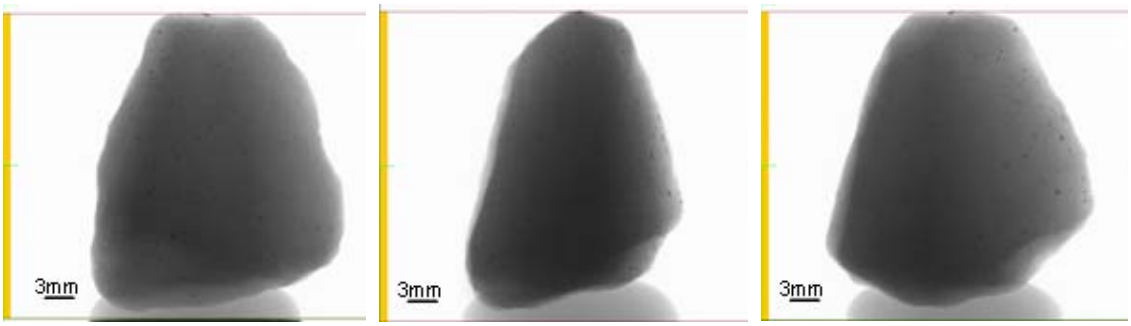

Position 0 deg **Position 45 deg** **Position 180 deg**

Figure App. M-5 QZ Ohio Ore Particle No. 2 Set No. 1

Set No 2:

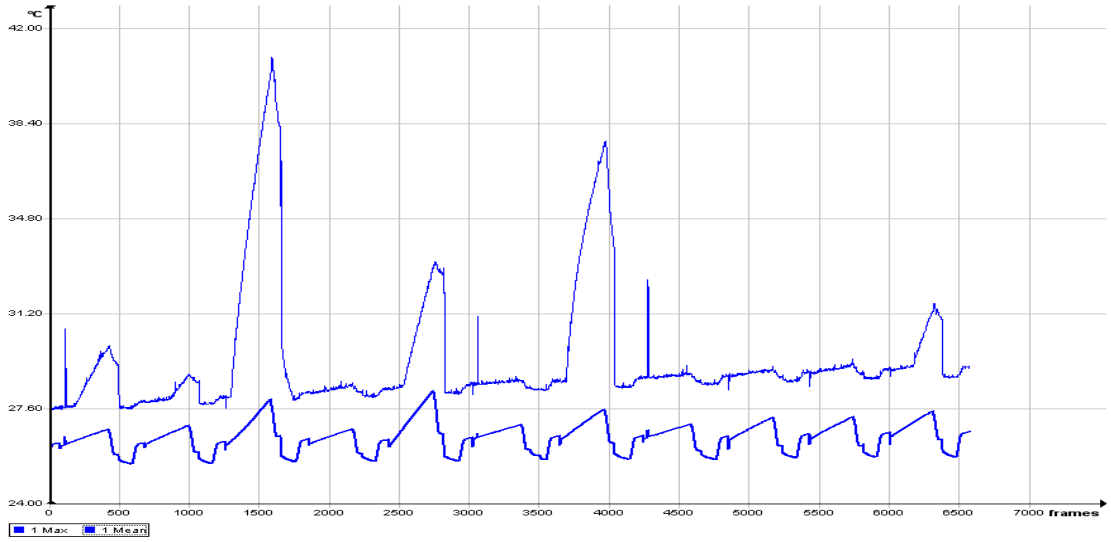

Figure App. M-6 First exposure, timing graph for the set No. 2

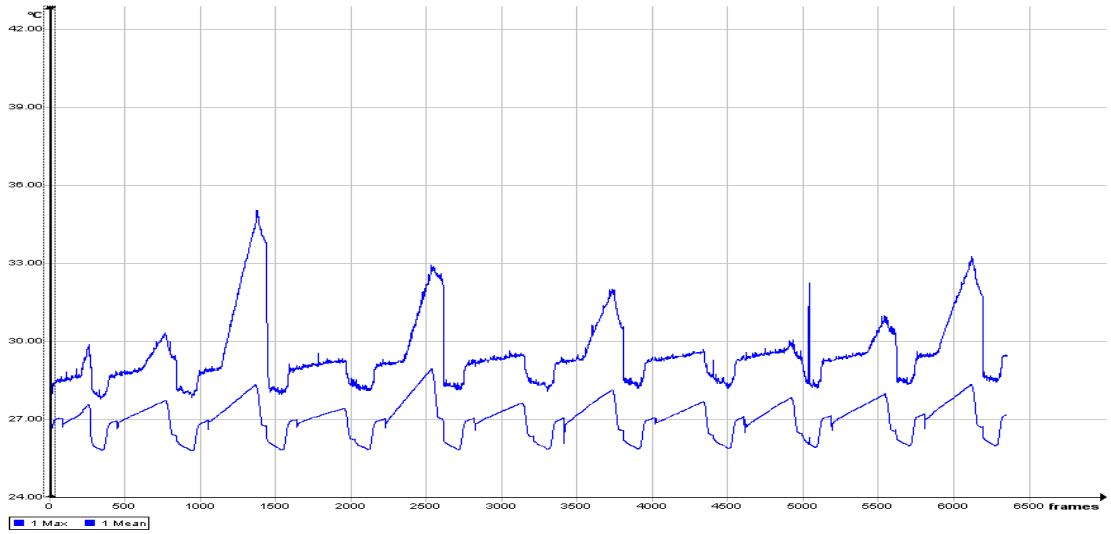

Figure App. M-7 Second exposure, timing graph for the set No. 2

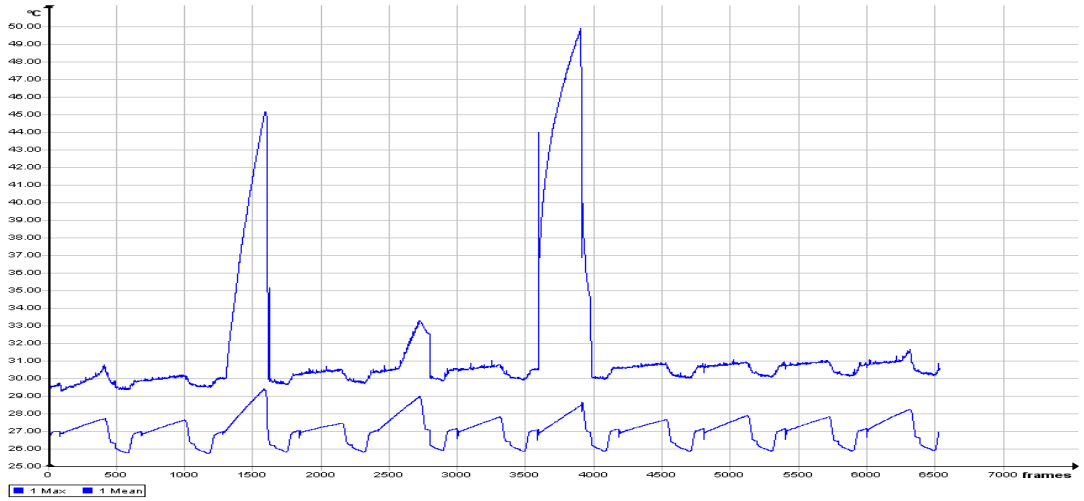

Figure App. M-8 Third exposure, timing graph for the set No. 2

Tomography analysis of some of the hot particles:

Particle No. 7 Set No. 2

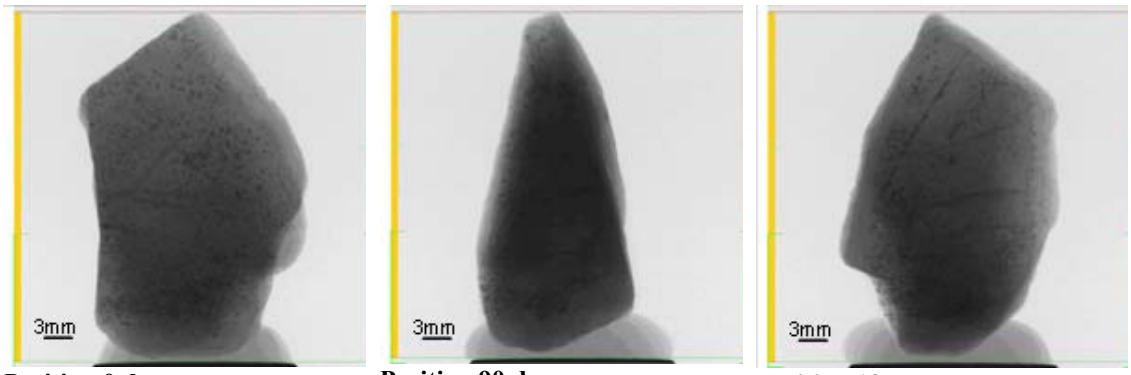

Position 0 deg **Position 90 deg** **Position 135 deg**

Figure App. M-9 QZ Ohio Ore Particle No. 7 Set No. 2

Set No 3:

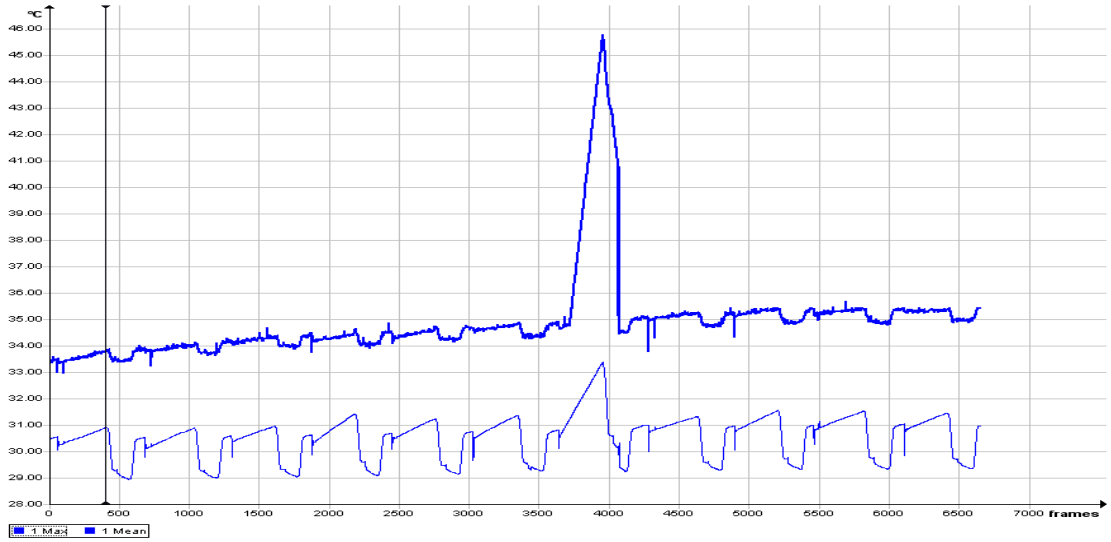

Figure App. M-10 First exposure, timing graph for set no. 3

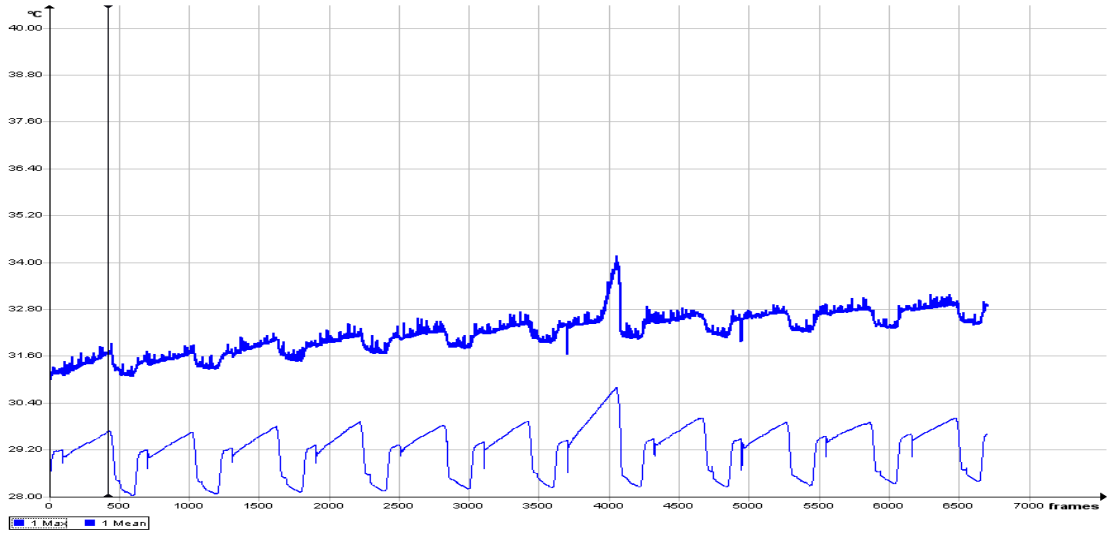

Figure App. M-11 Second exposure, timing graph for set no.3

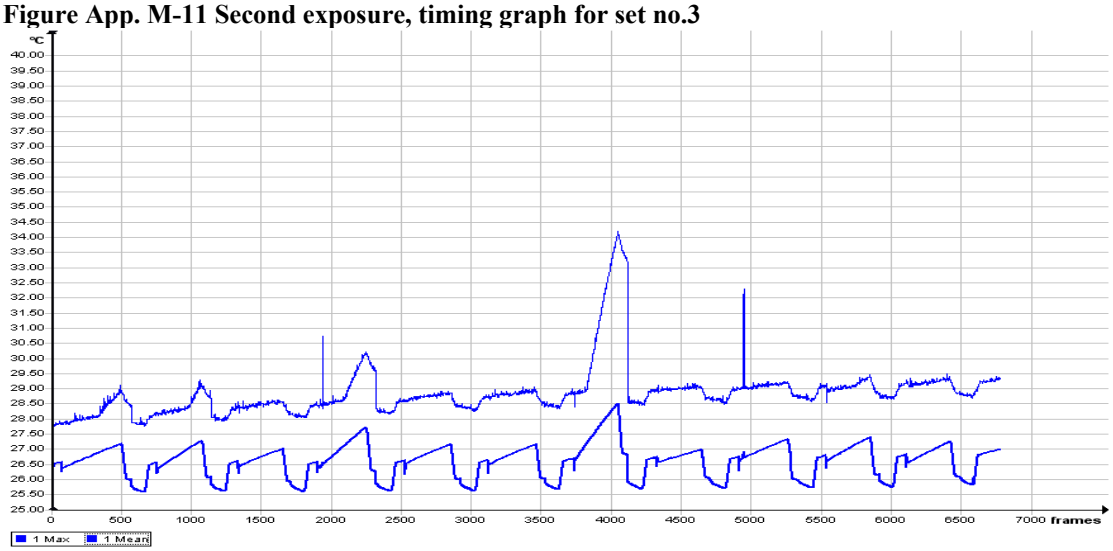

Figure App. M-12 Third exposure, timing graph for set no 3

Tomography analysis of some of the hot particles:

Particle No. 7 Set No. 3

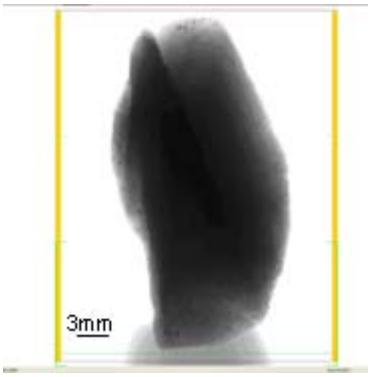

Position 0 deg

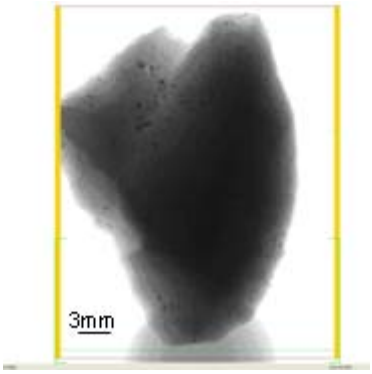

Position 45 deg

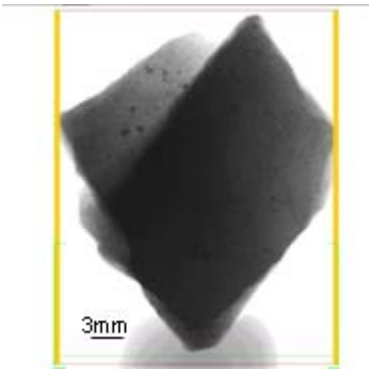

Position 90 deg

Figure App. M-13 QZ Ohio Ore Particle No. 7 Set No. 3

Set No 4:

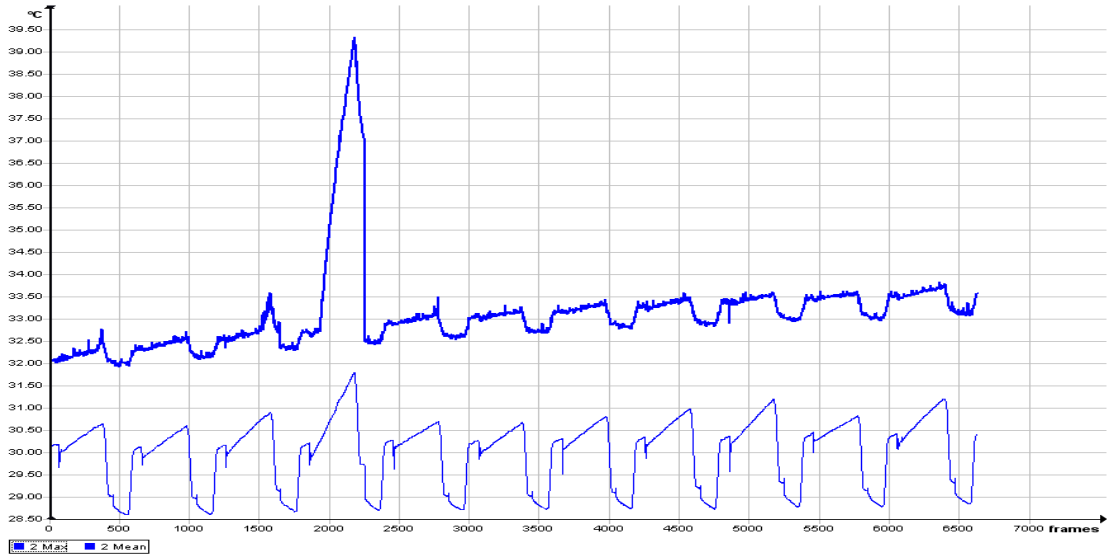

Figure App. M-14 First exposure, timing graph for set no. 4

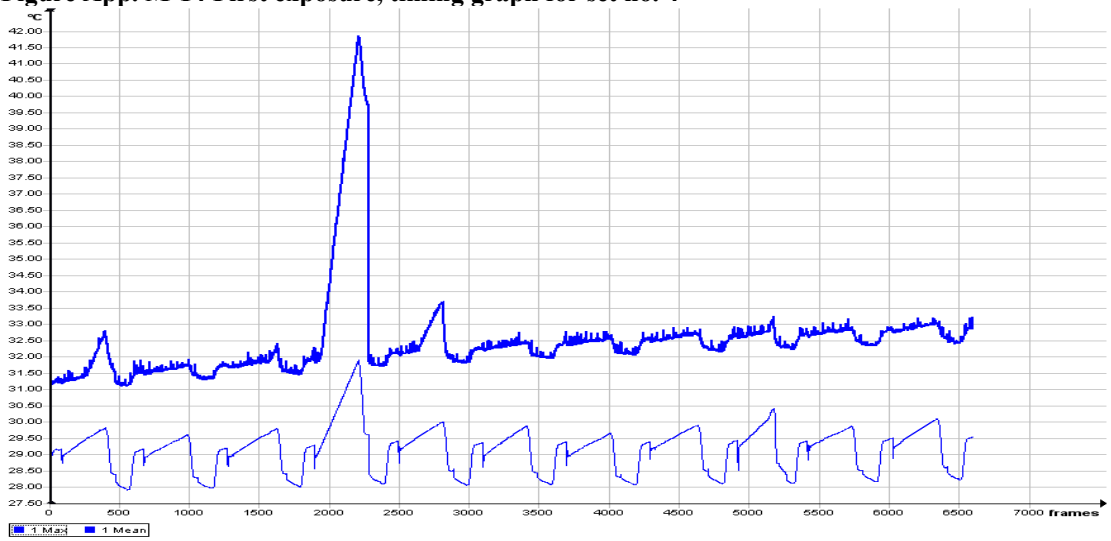

Figure App. M-15 Second exposure, timing graph for set no.4

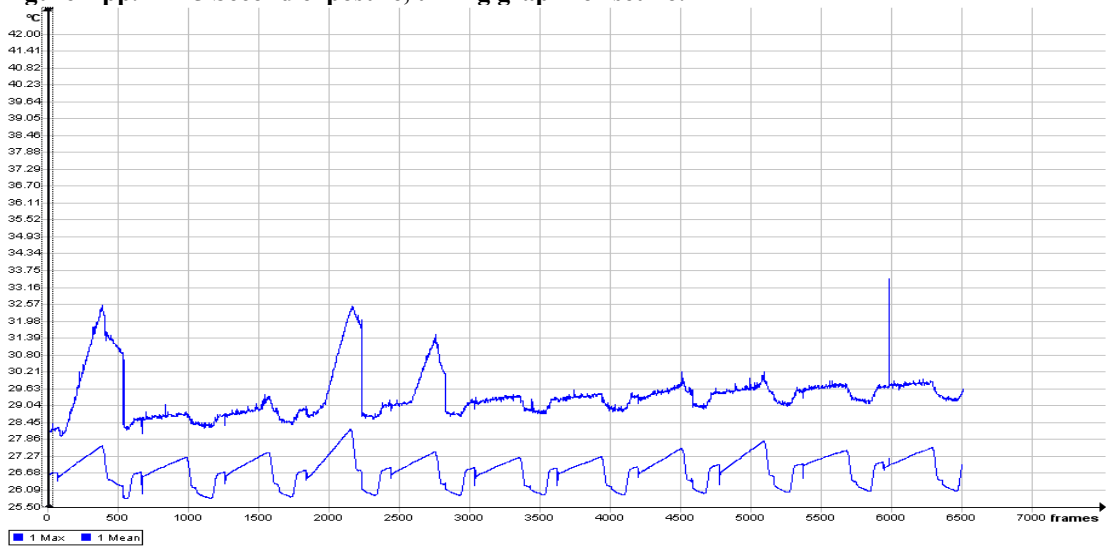

Figure App. M-16 Third exposure, timing graph for set no 4

Tomography analysis of some of the hot particles:

Particle No. 4 Set No. 4

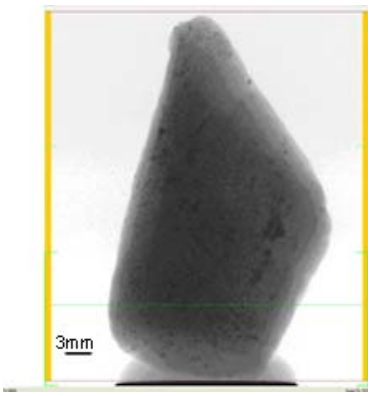

Position 0 deg

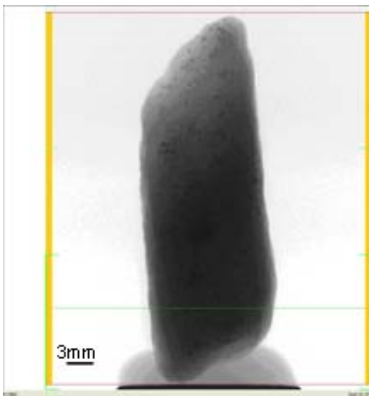

Position 90 deg

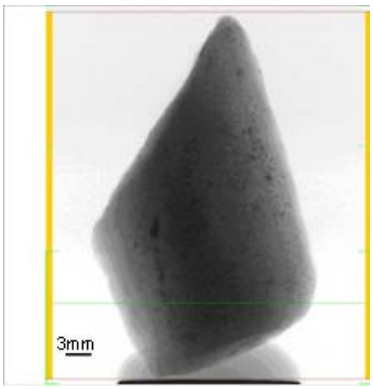

Position 90 deg

Figure App. M-17 QZ Ohio Ore Particle No. 4 Set No. 4

Tomography analysis of some of the cold particles:

Particle No. 2 Set No. 4

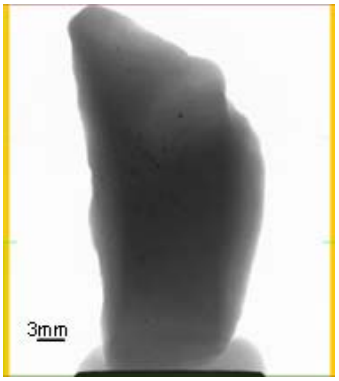

Position 0 deg

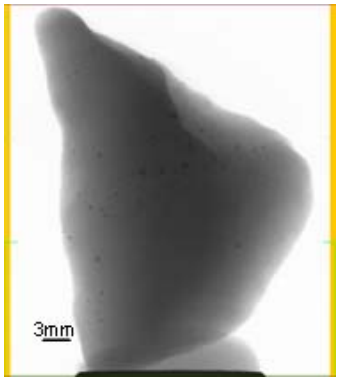

Position 45 deg

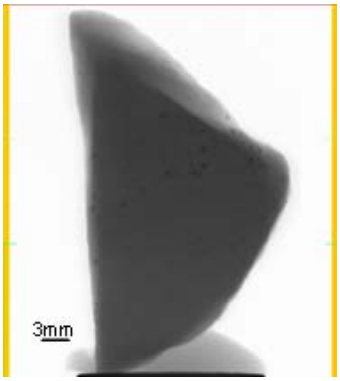

Position 90 deg

Figure App. M-18 QZ Ohio Ore Particle No. 2 Set No. 4

Set No 5:

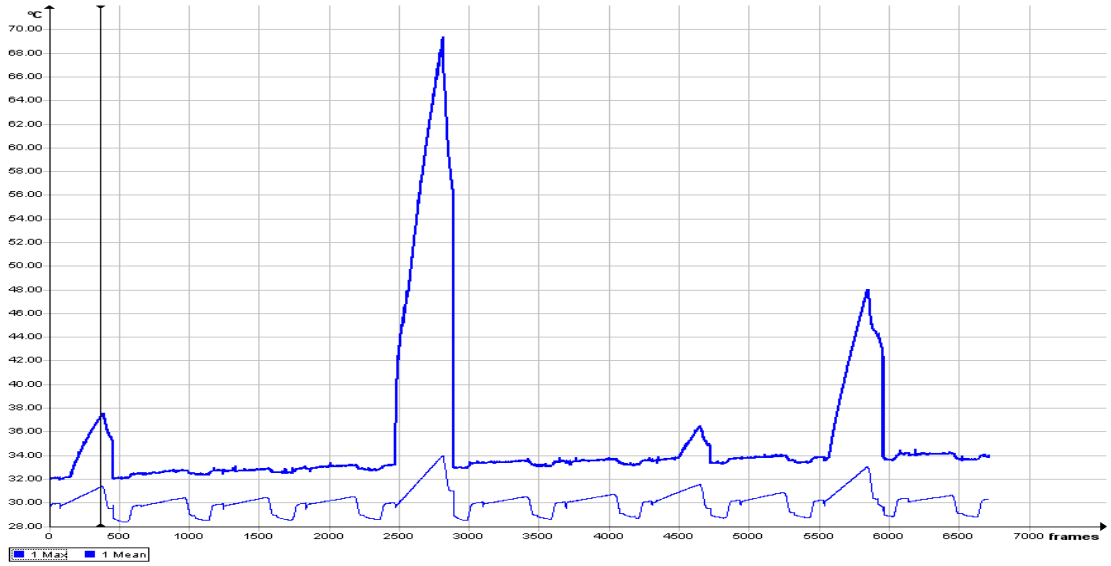

Figure App. M-19 First exposure, timing graph for set no. 5

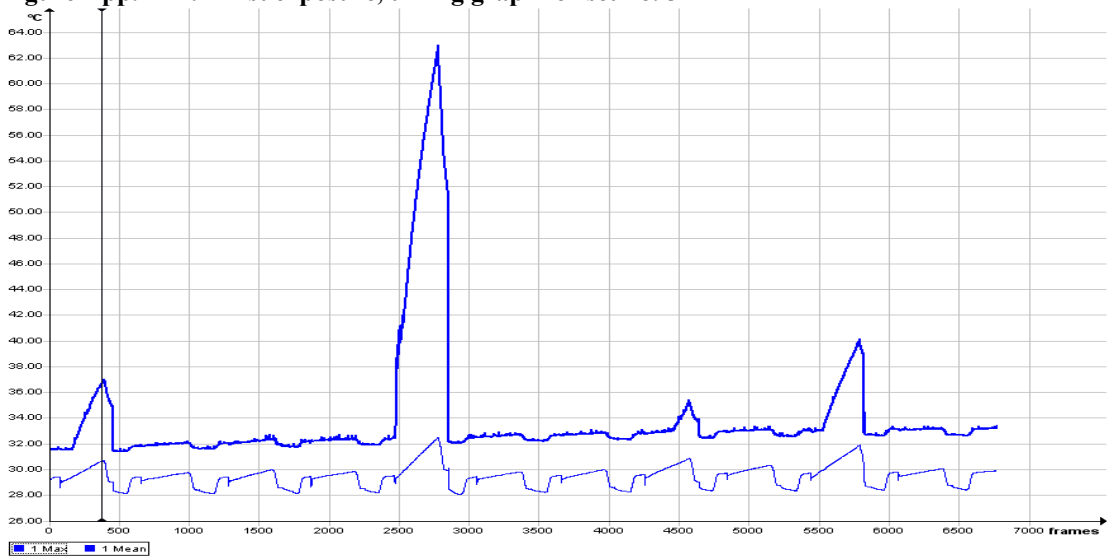

Figure App. M-20Second exposure, timing graph for set no.5

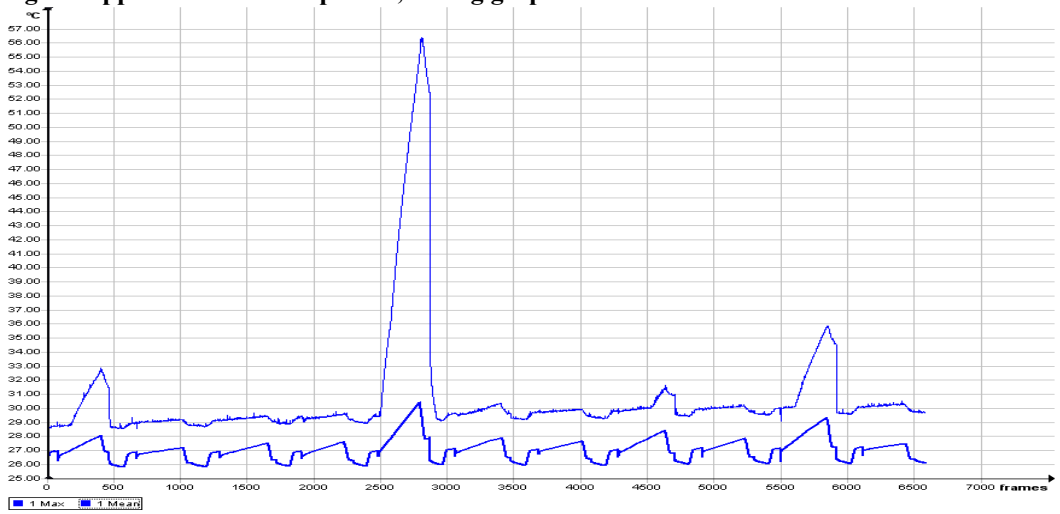

Figure App. M-21 Third exposure, timing graph for set no.5

Tomography analysis of some of the hot particles:

Particle No. 5 Set No. 5

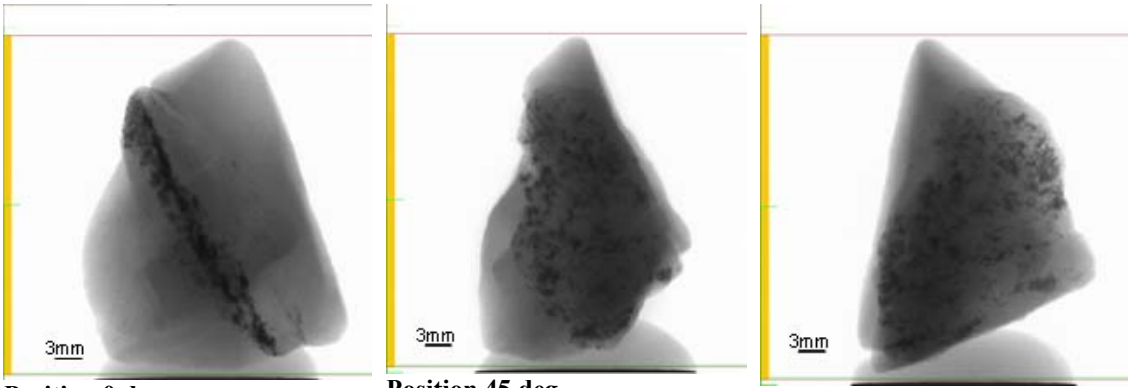

Position 0 deg **Position 45 deg** **Position 90 deg**

Figure App. M-22 QZ Ohio Ore Particle No. 5 Set No. 5

Set No 6:

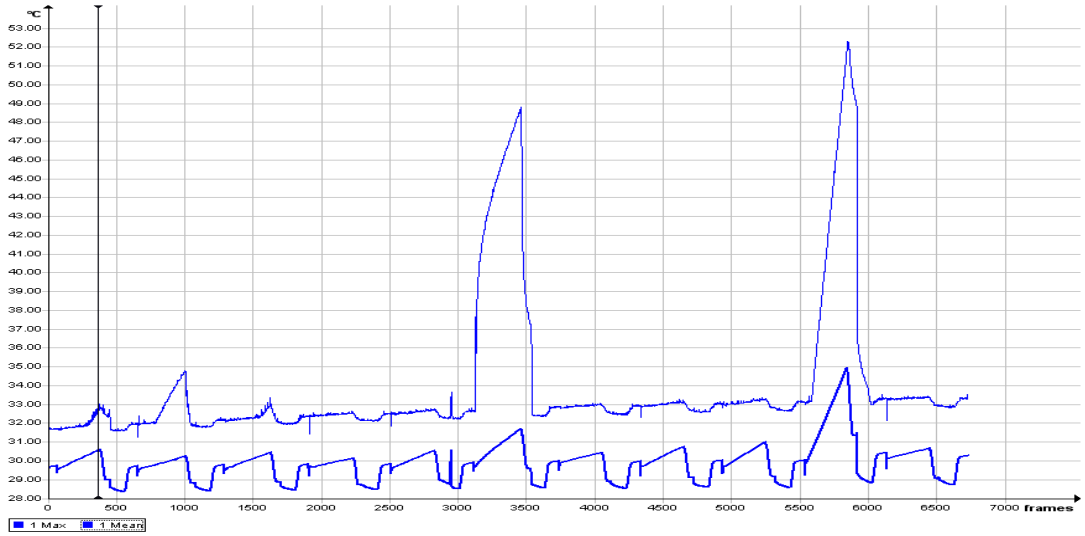

Figure App. M-23 First exposure, timing graph for set no. 6

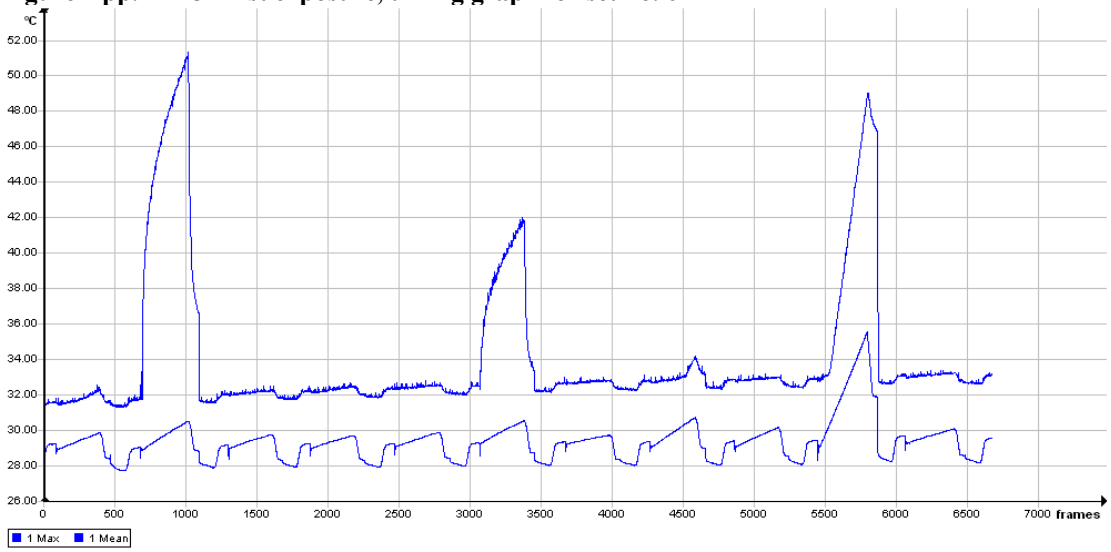

Figure App. M-24 Second exposure, timing graph for set no.6

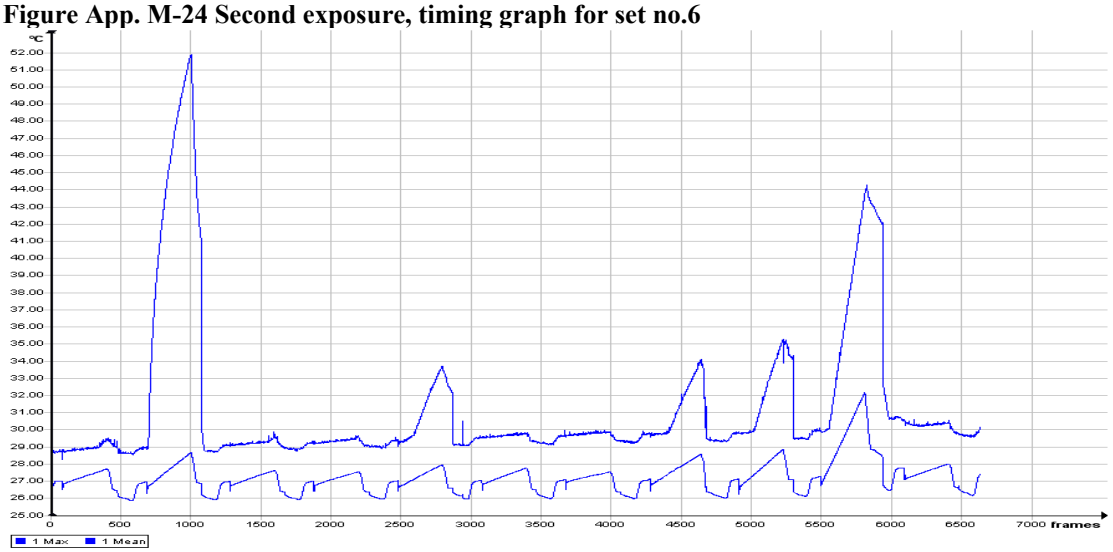

Figure App. M-25 Third exposure, timing graph for set no.6

Tomography analysis of some of the hot particles:

Particle No. 2 Set No. 6

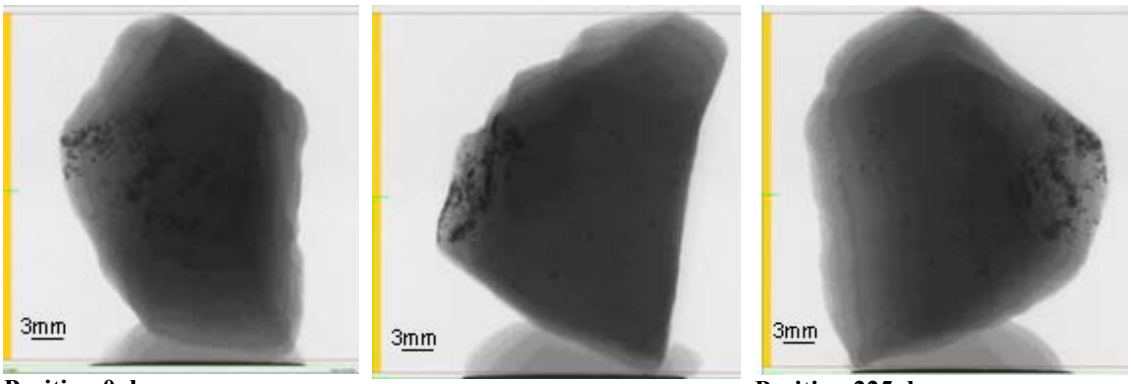

Position 0 deg **Position 90 deg** **Position 225 deg**

Figure App. M-26 QZ Ohio Ore Particle No. 2 Set No. 6

Particle No. 6 Set No. 6

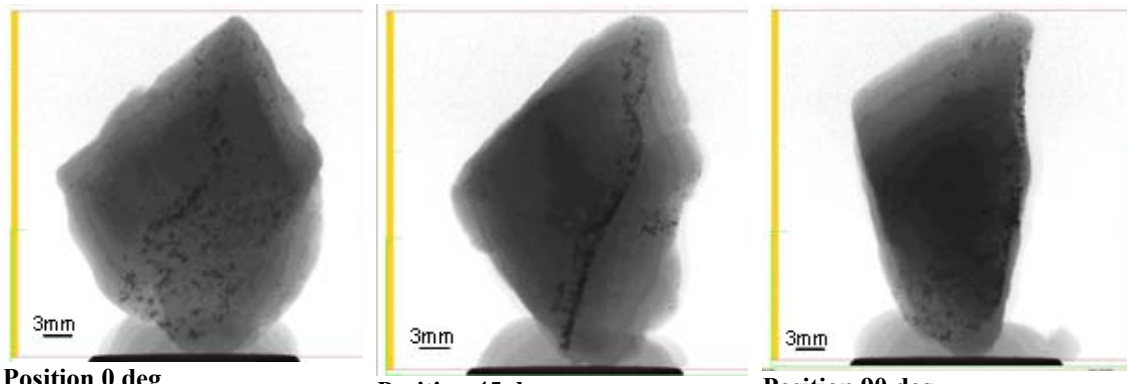

Position 0 deg **Position 45 deg** **Position 90 deg**

Figure App. M-27 QZ Ohio Ore Particle No. 6 Set No. 6

Tomography analysis of some of the cold particles:

Particle No. 11 Set No. 6

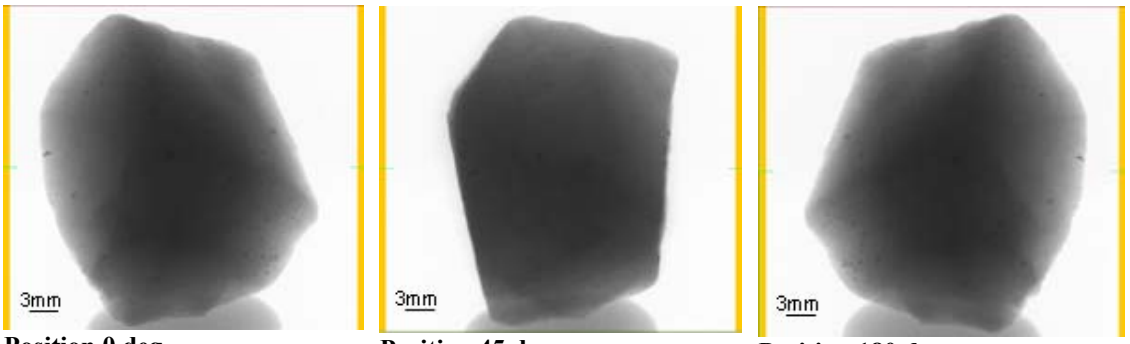

Position 0 deg **Position 45 deg** **Position 180 deg**

Figure App. M-28 QZ Ohio Ore Particle No. 11 Set No. 6

Set No 7:

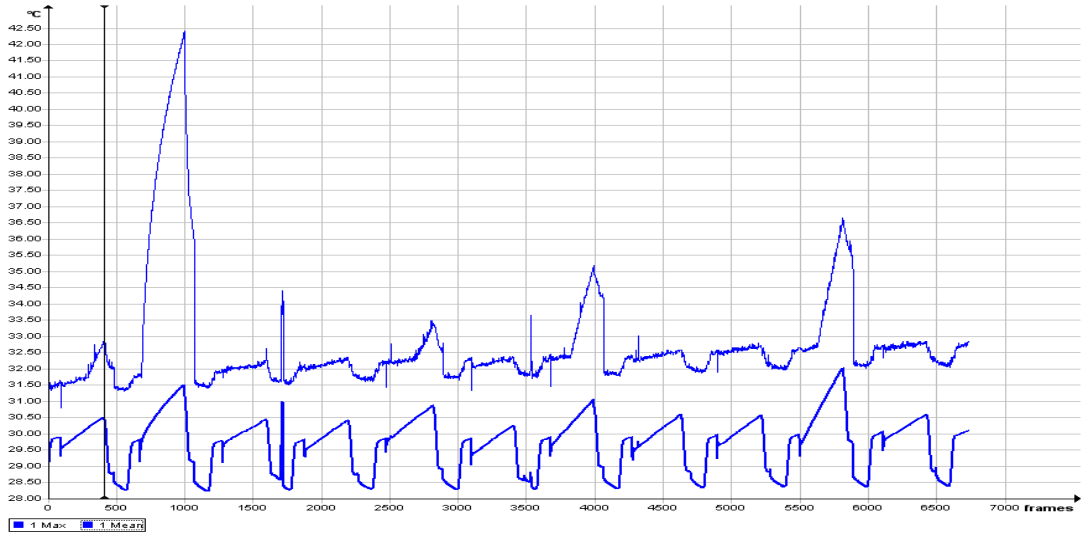

Figure App. M-29 First exposure, timing graph for set no. 7

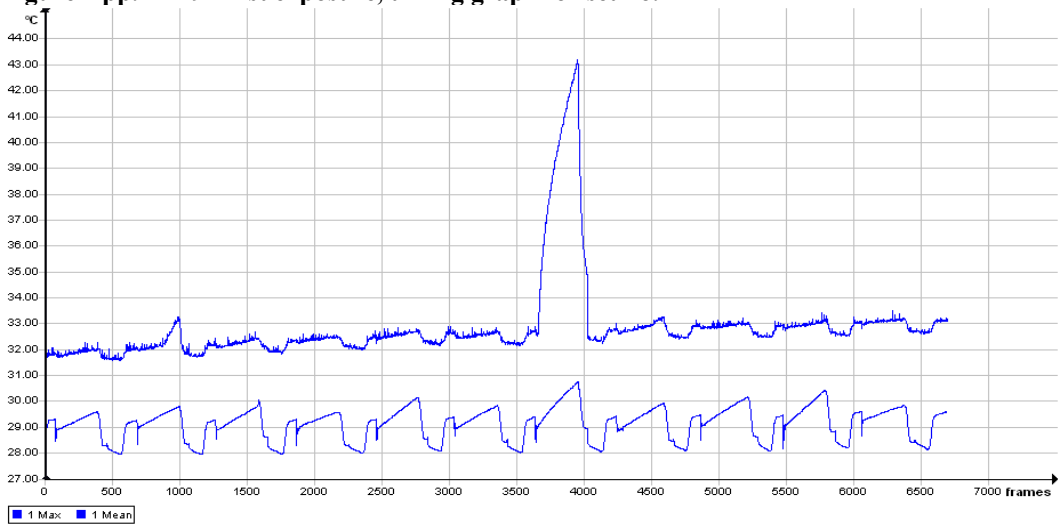

Figure App. M-30 Second exposure, timing graph for set no.7

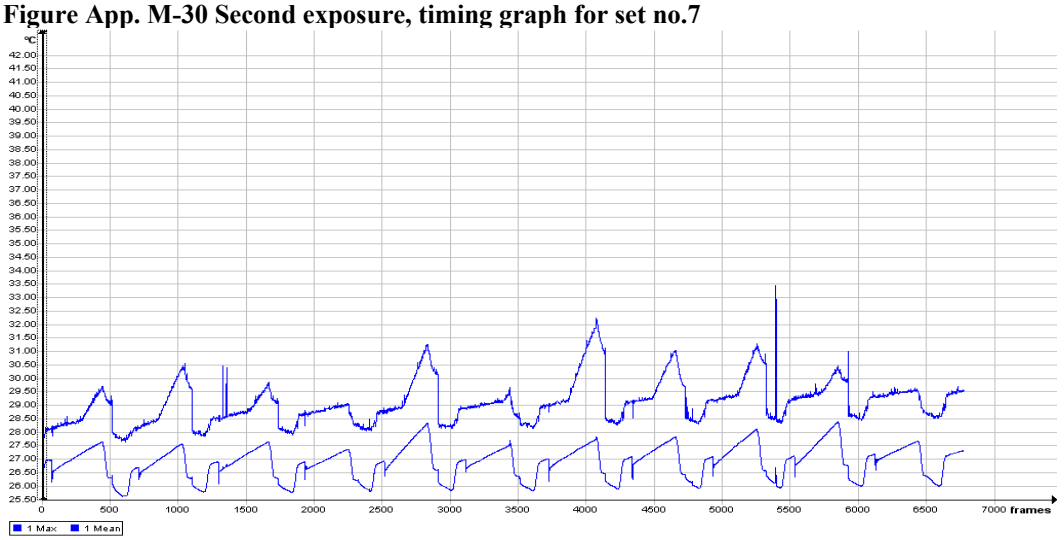

Figure App. M-31 Third exposure, timing graph for set no.7

Tomography analysis of some of the hot particles:

Particle No. 2 Set No. 7

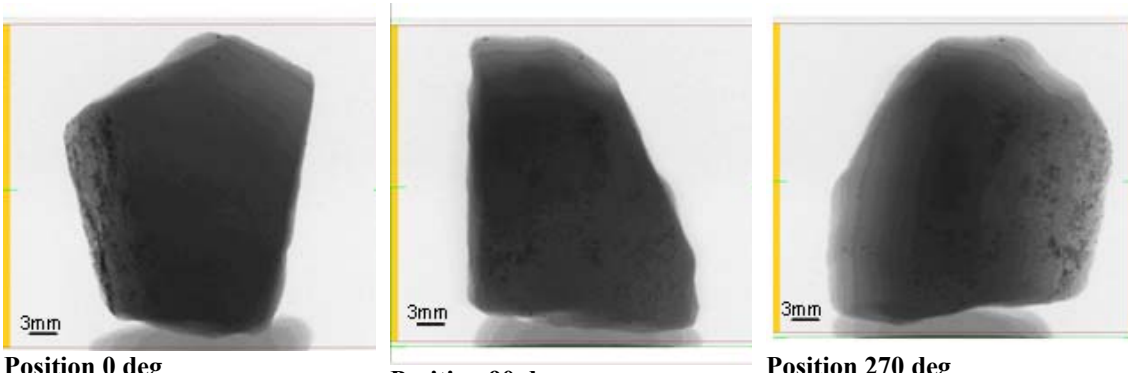

Position 0 deg **Position 90 deg** **Position 270 deg**

Figure App. M-32 QZ Ohio Ore Particle No. 2 Set No. 7

Particle No. 7 Set No. 7

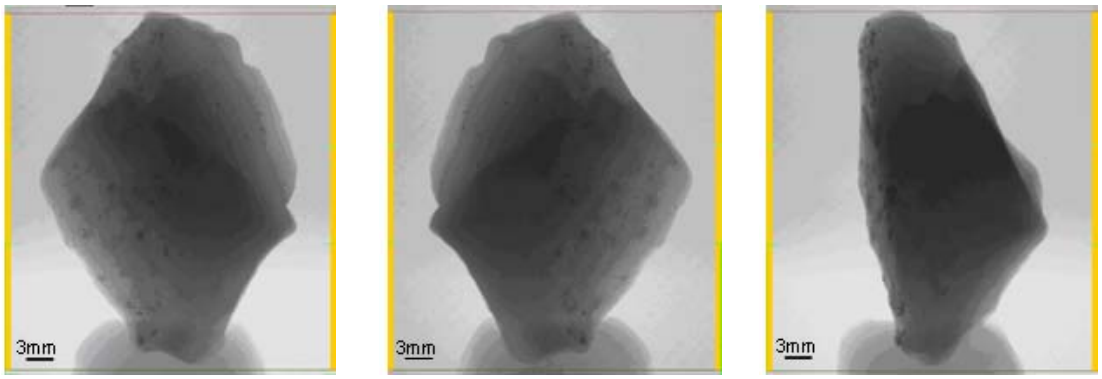

Position 0 deg **Position 180 deg** **Position 90 deg**

Figure App. M-33 QZ Ohio Ore Particle No. 7 Set No.7

Tomography analysis of some of the cold particles:

Particle No. 10 Set No. 7

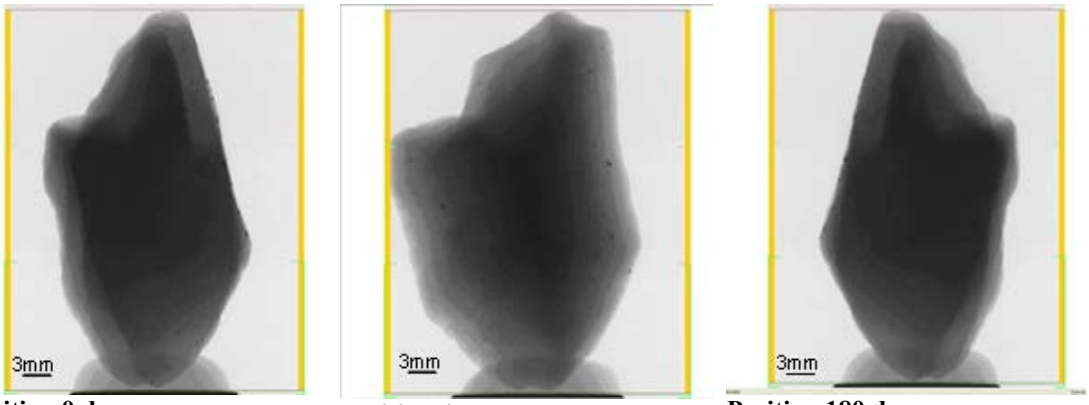

Position 0 deg **Position 45 deg** **Position 180 deg**

Figure App. M-34 QZ Ohio Ore Particle No. 10 Set No. 7

Set No 8:

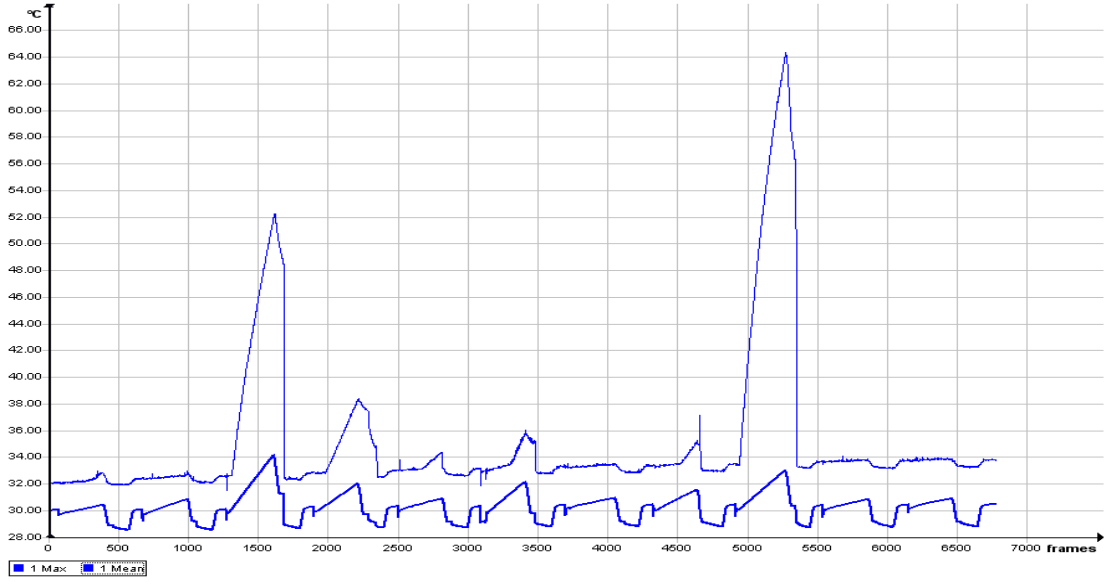

Figure App. M-35 First exposure, timing graph for set no. 8

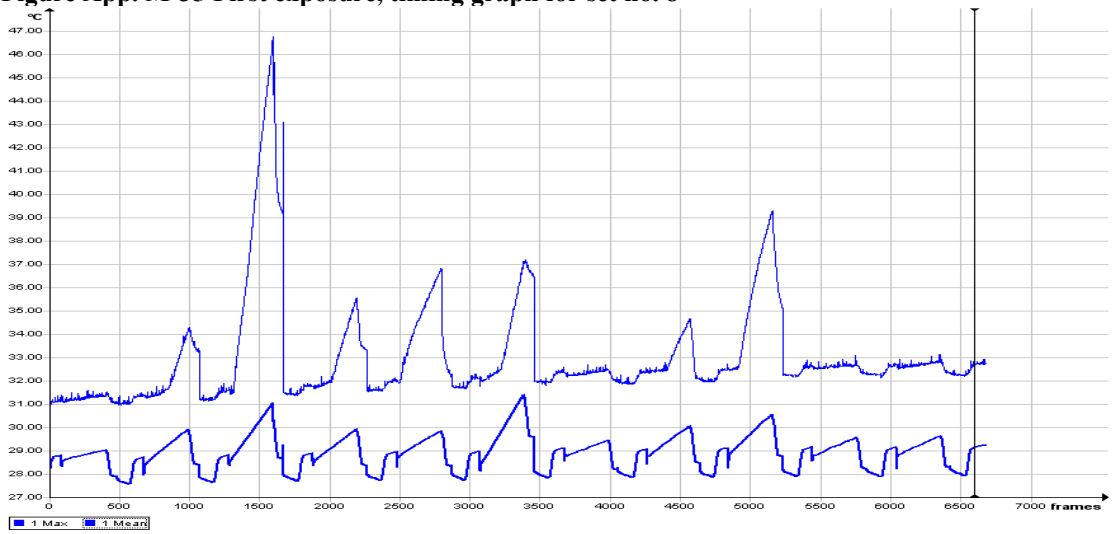

Figure App. M-36 Second exposure, timing graph for set no. 8

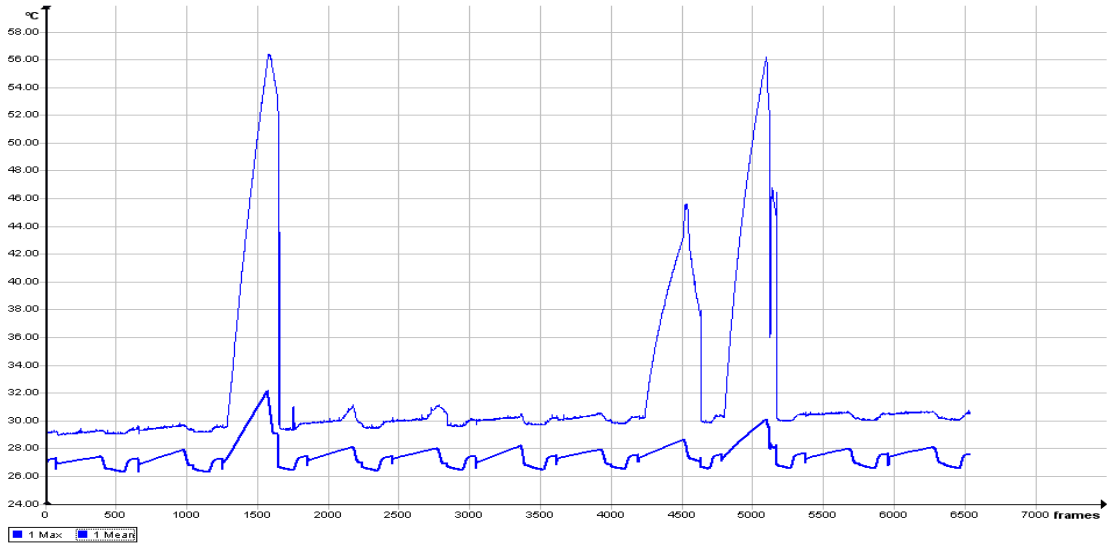

Figure App. M-37 Third exposure, timing graph for set no. 8

Tomography analysis of some of the hot particles:

Particle No. 3 Set No. 8

Position 0 deg **Position 90 deg** **Position 180 deg**

Figure App. M-38 QZ Ohio Ore Particle No. 3 Set No. 8

Tomography analysis of some of the cold particles:

Particle No. 2 Set No. 8

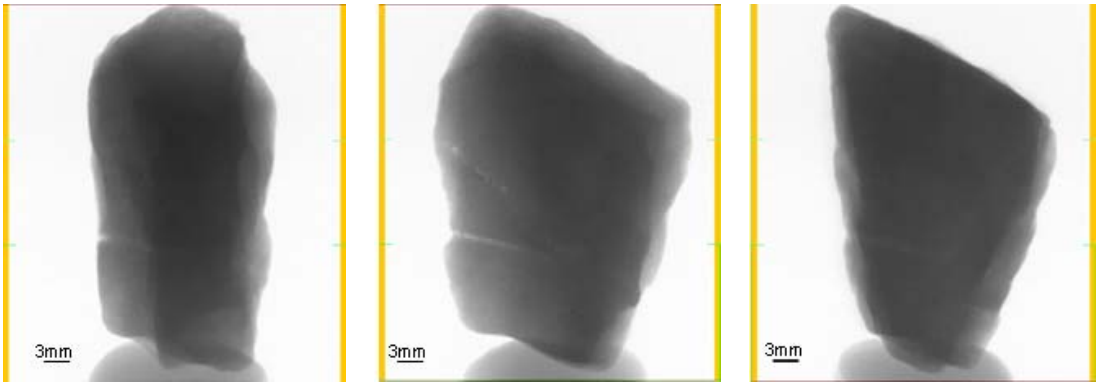

Position 0 deg **Position 45 deg** **Position 60 deg**

Figure App. M-39 QZ Ohio Ore Particle No. 2 Set No. 8

Overlapping particles in both types of cavities

Table App. M-1 Before sorting max ΔT mean for the QZ Ohio Ore:

Multimode Cavity

		particle nur	set	max delta t	mass of pa	Cumulative	Cumulative mass%
1	1	1	8	1.98	12.87	12.87	0.98108
2	2	2	8	2.74	17.44	30.31	2.31053
3	3	3	8	7.26	14.13	44.44	3.38766
4	4	4	8	4.36	13.91	58.35	4.448019
5	5	5	8	3.48	11.86	70.21	5.352106
6	6	6	8	3.12	23.08	93.29	7.111494
7	7	7	8	1.76	10.53	103.82	7.914196
8	8	8	8	3.32	15.24	119.06	9.07594
9	9	9	8	6.66	13.59	132.65	10.11191
10	10	10	8	1.9	17.6	150.25	11.45355
11	11	11	8	1.99	13.66	163.91	12.49485
12	12	1	7	1.86	18.71	182.62	13.92112
13	13	2	7	4.1	16.68	199.3	15.19263
14	14	3	7	2.02	15.83	215.13	16.39935
15	15	4	7	1.67	18.22	233.35	17.78826
16	16	5	7	2.45	18.08	251.43	19.1665
17	17	6	7	1.52	21.77	273.2	20.82603
18	18	7	7	3.02	16.53	289.73	22.08611
19	19	8	7	1.65	18.47	308.2	23.49408
20	20	9	7	2.24	17.1	325.3	24.79761
21	21	10	7	2.29	25.06	350.36	26.70793
22	22	11	7	1.61	16.52	366.88	27.96725
23	23	1	6	2.31	17.69	384.57	29.31576
24	24	2	6	4.48	16.68	401.25	30.58728
25	25	3	6	2.23	12.88	414.13	31.56912
26	26	4	6	1.79	12.19	426.32	32.49836
27	27	5	6	3.34	15.79	442.11	33.70203
28	28	6	6	4.49	13.87	455.98	34.75934
29	29	7	6	2.28	10.75	466.73	35.57881
30	30	8	6	2.72	17.29	484.02	36.89683
31	31	9	6	3.04	20.89	504.91	38.48927
32	32	10	6	8.52	18.31	523.22	39.88505
33	33	11	6	2.19	16.69	539.91	41.15732
34	34	1	5	2.2	24.68	564.59	43.03868
35	35	2	5	1.92	11.43	576.02	43.90999
36	36	3	5	2.05	18.84	594.86	45.34616
37	37	4	5	2.35	15.43	610.29	46.52239
38	38	5	5	14.82	9.49	619.78	47.24581
39	39	6	5	2.21	12.01	631.79	48.16133
40	40	7	5	2.72	14.45	646.24	49.26286
41	41	8	5	5.81	10.64	656.88	50.07394
42	42	9	5	3.53	11.21	668.09	50.92848
43	43	10	5	6.71	15.25	683.34	52.09099
44	44	11	5	1.97	11.52	694.86	52.96916
45	45	1	4	3.6	11.35	706.21	53.83437
46	46	2	4	1.91	16.66	722.87	55.10436
47	47	3	4	2.3	14.75	737.62	56.22875
48	48	4	4	6.76	14.89	752.51	57.36382
49	49	5	4	2.71	13.79	766.3	58.41503
50	50	6	4	2.35	18.04	784.34	59.79022
51	51	7	4	2.06	14.08	798.42	60.86353
52	52	8	4	2.44	14.8	813.22	61.99174
53	53	9	4	2.61	21.73	834.95	63.64821
54	54	10	4	2.5	13.57	848.52	64.68265
55	55	11	4	2.48	12.18	860.7	65.61114
56	56	1	3	2	12.12	872.82	66.53504
57	57	2	3	1.98	15.86	888.68	67.74405
58	58	3	3	2.06	12.66	901.34	68.70912
59	59	4	3	2.6	16.23	917.57	69.94633
60	60	5	3	2.55	15.64	933.21	71.13857
61	61	6	3	2.3	13.6	946.81	72.1753
62	62	7	3	6.07	19.21	966.02	73.63968
63	63	8	3	2.27	12.25	978.27	74.57349
64	64	9	3	2.63	15.31	993.58	75.74057
65	65	10	3	2.31	15.43	1009.01	76.9168
66	66	11	3	2.19	16.21	1025.22	78.15249
67	67	1	2	1.95	9.42	1034.64	78.87058
68	68	2	2	2.67	12.34	1046.98	79.81125
69	69	3	2	6.29	12	1058.98	80.72601
70	70	4	2	2.63	8.89	1067.87	81.4037
71	71	5	2	6.3	16.65	1084.52	82.67293
72	72	6	2	2.41	15.1	1099.62	83.824
73	73	7	2	3.31	15.86	1115.48	85.03301
74	74	8	2	2.08	12.6	1128.08	85.99351
75	75	9	2	2.96	10.92	1139	86.82594
76	76	10	2	2.2	15.11	1154.11	87.97777
77	77	11	2	3.86	13.73	1167.84	89.02441
78	78	1	1	1.8	14.94	1182.78	90.16328
79	79	2	1	2.33	12.75	1195.53	91.13522
80	80	3	1	1.65	12.44	1207.97	92.08352
81	81	4	1	2.29	12.51	1220.48	93.03715
82	82	5	1	10.96	11.43	1231.91	93.90846
83	83	6	1	3.09	12.25	1244.16	94.84228
84	84	7	1	3.97	11.22	1255.38	95.69758
85	85	8	1	2.59	11.89	1267.27	96.60395
86	86	9	1	2.38	12.92	1280.19	97.58885
87	87	10	1	2.24	19.64	1299.83	99.086
88	88	11	1	2.65	11.99	1311.82	100

TWA

	particle nur	set	max delta t	mass of pa	Cumulative	Cumulative
1	1	8	1.82	12.87	12.87	0.98108
2	2	8	4.53	17.44	30.31	2.31053
3	3	8	12.95	14.13	44.44	3.38766
4	4	8	5.96	13.91	58.35	4.448019
5	5	8	4.06	11.86	70.21	5.352106
6	6	8	6.23	23.08	93.29	7.111494
7	7	8	2.84	10.53	103.82	7.914196
8	8	8	5.82	15.24	119.06	9.07594
9	9	8	8.25	13.59	132.65	10.11191
10	10	8	1.62	17.6	150.25	11.45355
11	11	8	2.11	13.66	163.91	12.49485
12	1	7	2.15	18.71	182.62	13.92112
13	2	7	4.97	16.68	199.3	15.19263
14	3	7	2.23	15.83	215.13	16.39935
15	4	7	2	18.22	233.35	17.78826
16	5	7	2.8	18.08	251.43	19.1665
17	6	7	2.18	21.77	273.2	20.82603
18	7	7	4.47	16.53	289.73	22.08611
19	8	7	2.11	18.47	308.2	23.49408
20	9	7	2.69	17.1	325.3	24.79761
21	10	7	4.16	25.06	350.36	26.70793
22	11	7	1.62	16.52	366.88	27.96725
23	1	6	2.61	17.69	384.57	29.31576
24	2	6	5.14	16.68	401.25	30.58728
25	3	6	2.29	12.88	414.13	31.56912
26	4	6	2.23	12.19	426.32	32.49836
27	5	6	2.76	15.79	442.11	33.70203
28	6	6	6.15	13.87	455.98	34.75934
29	7	6	1.37	10.75	466.73	35.57881
30	8	6	4.85	17.29	484.02	36.89683
31	9	6	4.41	20.89	504.91	38.48927
32	10	6	13.86	18.31	523.22	39.88505
33	11	6	2.1	16.69	539.91	41.15732
34	1	5	3.37	24.68	564.59	43.03868
35	2	5	1.59	11.43	576.02	43.90999
36	3	5	2.14	18.84	594.86	45.34616
37	4	5	1.76	15.43	610.29	46.52239
38	5	5	15.04	9.49	619.78	47.24581
39	6	5	2.46	12.01	631.79	48.16133
40	7	5	1.88	14.45	646.24	49.26286
41	8	5	4.53	10.64	656.88	50.07394
42	9	5	2.06	11.21	668.09	50.92848
43	10	5	7.54	15.25	683.34	52.09099
44	11	5	1.44	11.52	694.86	52.96916
45	1	4	4.17	11.35	706.21	53.83437
46	2	4	1.81	16.66	722.87	55.10436
47	3	4	2.36	14.75	737.62	56.22875
48	4	4	7.41	14.89	752.51	57.36382
49	5	4	2.4	13.79	766.3	58.41503
50	6	4	1.37	18.04	784.34	59.79022
51	7	4	1.24	14.08	798.42	60.86353
52	8	4	2.57	14.8	813.22	61.99174
53	9	4	2.35	21.73	834.95	63.64821
54	10	4	1.55	13.57	848.52	64.68265
55	11	4	2.42	12.18	860.7	65.61114
56	1	3	1.77	12.12	872.82	66.53504
57	2	3	1.8	15.86	888.68	67.74405
58	3	3	1.88	12.66	901.34	68.70912
59	4	3	3.51	16.23	917.57	69.94633
60	5	3	1.7	15.64	933.21	71.13857
61	6	3	2.76	13.6	946.81	72.1753
62	7	3	7.72	19.21	966.02	73.63968
63	8	3	1.84	12.25	978.27	74.57349
64	9	3	1.73	15.31	993.58	75.74057
65	10	3	1.67	15.43	1009.01	76.9168
66	11	3	2.09	16.21	1025.22	78.15249
67	1	2	2.58	9.42	1034.64	78.87058
68	2	2	1.85	12.34	1046.98	79.81125
69	3	2	6.32	12	1058.98	80.72601
70	4	2	1.32	8.89	1067.87	81.4037
71	5	2	4.96	16.65	1084.52	82.67293
72	6	2	1.88	15.1	1099.62	83.824
73	7	2	3.13	15.86	1115.48	85.03301
74	8	2	1.75	12.6	1128.08	85.99351
75	9	2	2.24	10.92	1139	86.82594
76	10	2	2.46	15.11	1154.11	87.97777
77	11	2	3.17	13.73	1167.84	89.02441
78	1	1	1.98	14.94	1182.78	90.16328
79	2	1	2.07	12.75	1195.53	91.13522
80	3	1	1.76	12.44	1207.97	92.08352
81	4	1	2.07	12.51	1220.48	93.03715
82	5	1	11.37	11.43	1231.91	93.90846
83	6	1	2.26	12.25	1244.16	94.84228
84	7	1	3.41	11.22	1255.38	95.69758
85	8	1	2.05	11.89	1267.27	96.60395
86	9	1	2.65	12.92	1280.19	97.58885
87	10	1	2.1	19.64	1299.83	99.086
88	11	1	2.51	11.99	1311.82	100

Table App. M-2 After sorting max ΔT mean for QZ Ohio Ore:

Multimode Cavity

		particle nur	set	max delta t	mass of pa	Cumulative	Cumulative mass%	
1	17	6	7	1.52	21.77	21.77	1.659526	
2	22	11	7	1.61	16.52	38.29	2.918846	
3	19	8	7	1.65	18.47	56.76	4.326813	
4	80	3	1	1.65	12.44	69.2	5.275114	
5	15	4	7	1.67	18.22	87.42	6.664024	
6	7	7	8	1.76	10.53	97.95	7.466726	
7	26	4	6	1.79	12.19	110.14	8.395969	
8	78	1	1	1.8	14.94	125.08	9.534845	
9	12	1	7	1.86	18.71	143.79	10.96111	
10	10	10	8	1.9	17.6	161.39	12.30275	
11	46	2	4	1.91	16.66	178.05	13.57275	
12	35	2	5	1.92	11.43	189.48	14.44405	
13	67	1	2	1.95	9.42	198.9	15.16214	
14	44	11	5	1.97	11.52	210.42	16.04031	
15	1	1	8	1.98	12.87	223.29	17.02139	
16	57	2	3	1.98	15.86	239.15	18.2304	
17	11	11	8	1.99	13.66	252.81	19.2717	
18	56	1	3	2	12.12	264.93	20.19561	
19	14	3	7	2.02	15.83	280.76	21.40233	
20	36	3	5	2.05	18.84	299.6	22.8385	
21	51	7	4	2.06	14.08	313.68	23.91182	
22	58	3	3	2.06	12.66	326.34	24.87689	
23	74	8	2	2.08	12.6	338.94	25.83739	
24	33	11	6	2.19	16.69	355.63	27.10966	
25	66	11	3	2.19	16.21	371.84	28.34535	
26	34	1	5	2.2	24.68	396.52	30.22671	
27	76	10	2	2.2	15.11	411.63	31.37854	
28	39	6	5	2.21	12.01	423.64	32.29406	
29	25	3	6	2.23	12.88	436.52	33.27591	
30	20	9	7	2.24	17.1	453.62	34.57944	
31	87	10	1	2.24	19.64	473.26	36.0766	
32	63	8	3	2.27	12.25	485.51	37.01041	
33	29	7	6	2.28	10.75	496.26	37.82989	
34	21	10	7	2.29	25.06	521.32	39.74021	
35	81	4	1	2.29	12.51	533.83	40.69385	
36	47	3	4	2.3	14.75	548.58	41.81824	
37	61	6	3	2.3	13.6	562.18	42.85496	
38	23	1	6	2.31	17.69	579.87	44.20347	
39	65	10	3	2.31	15.43	595.3	45.3797	
40	79	2	1	2.33	12.75	608.05	46.35163	
41	37	4	5	2.35	15.43	623.48	47.52786	
42	50	6	4	2.35	18.04	641.52	48.90305	
43	86	9	1	2.38	12.92	654.44	49.88794	
44	72	6	2	2.41	15.1	669.54	51.03901	
45	52	8	4	2.44	14.8	684.34	52.16722	
46	16	5	7	2.45	18.08	702.42	53.54546	
47	55	11	4	2.48	12.18	714.6	54.47394	
48	54	10	4	2.5	13.57	728.17	55.50838	
49	60	5	3	2.55	15.64	743.81	56.70061	
50	85	8	1	2.59	11.89	755.7	57.60699	
51	59	4	3	2.6	16.23	771.93	58.8442	
52	53	9	4	2.61	21.73	793.66	60.50068	
53	64	9	3	2.63	15.31	808.97	61.66776	
54	70	4	2	2.63	8.89	817.86	62.34544	
55	88	11	1	2.65	11.99	829.85	63.25944	
56	68	2	2	2.67	12.34	842.19	64.20012	
57	49	5	4	2.71	13.79	855.98	65.25133	
58	30	8	6	2.72	17.29	873.27	66.56935	
59	40	7	5	2.72	14.45	887.72	67.67087	
60	2	2	8	2.74	17.44	905.16	69.00032	
61	75	9	2	2.96	10.92	916.08	69.83275	
62	18	7	7	3.02	16.53	932.61	71.09283	
63	31	9	6	3.04	20.89	953.5	72.68528	
64	83	6	1	3.09	12.25	965.75	73.61909	
65	6	6	8	3.12	23.08	988.83	75.37848	
66	73	7	2	3.31	15.86	1004.69	76.58749	
67	8	8	8	3.32	15.24	1019.93	77.74923	
68	27	5	6	3.34	15.79	1035.72	78.95291	
69	5	5	8	3.48	11.86	1047.58	79.85699	
70	42	9	5	3.53	11.21	1058.79	80.71153	
71	45	1	4	3.6	11.35	1070.14	81.57674	
72	77	11	2	3.86	13.73	1083.87	82.62338	
73	84	7	1	3.97	11.22	1095.09	83.47868	
74	13	2	7	4.1	16.68	1111.77	84.75019	2.96 oC
75	4	4	8	4.36	13.91	1125.68	85.81055	
76	24	2	6	4.48	16.68	1142.36	87.08207	
77	28	6	6	4.49	13.87	1156.23	88.13938	
78	41	8	5	5.81	10.64	1166.87	88.95047	
79	62	7	3	6.07	19.21	1186.08	90.41484	
80	69	3	2	6.29	12	1198.08	91.3296	
81	71	5	2	6.3	16.65	1214.73	92.59883	
82	9	9	8	6.66	13.59	1228.32	93.6348	
83	43	10	5	6.71	15.25	1243.57	94.7973	
84	48	4	4	6.76	14.89	1258.46	95.93237	
85	3	3	8	7.26	14.13	1272.59	97.0095	
86	32	10	6	8.52	18.31	1290.9	98.40527	
87	82	5	1	10.96	11.43	1302.33	99.27658	
88	38	5	5	14.82	9.49	1311.82	100	

TWA

	particle nur	set	max delta t	mass of pa	Cumulative	Cumulative mass%	
51	7	4	1.24	14.08	14.08	1.073318	
70	4	2	1.32	8.89	22.97	1.751002	
29	7	6	1.37	10.75	33.72	2.570475	
50	6	4	1.37	18.04	51.76	3.945663	
44	11	5	1.44	11.52	63.28	4.823833	
54	10	4	1.55	13.57	76.85	5.858273	
35	2	5	1.59	11.43	88.28	6.729582	
10	10	8	1.62	17.6	105.88	8.071229	
22	11	7	1.62	16.52	122.4	9.330548	
65	10	3	1.67	15.43	137.83	10.50678	
60	5	3	1.7	15.64	153.47	11.69901	
64	9	3	1.73	15.31	168.78	12.86609	
74	8	2	1.75	12.6	181.38	13.82659	
37	4	5	1.76	15.43	196.81	15.00282	
80	3	1	1.76	12.44	209.25	15.95112	
56	1	3	1.77	12.12	221.37	16.87503	
57	2	3	1.8	15.86	237.23	18.08404	
46	2	4	1.81	16.66	253.89	19.35403	
1	1	8	1.82	12.87	266.76	20.33511	
63	8	3	1.84	12.25	279.01	21.26892	
68	2	2	1.85	12.34	291.35	22.2096	
40	7	5	1.88	14.45	305.8	23.31113	
58	3	3	1.88	12.66	318.46	24.2762	
72	6	2	1.88	15.1	333.56	25.42727	
78	1	1	1.98	14.94	348.5	26.56614	
15	4	7	2	18.22	366.72	27.95505	
85	8	1	2.05	11.89	378.61	28.86143	
42	9	5	2.06	11.21	389.82	29.71597	
79	2	1	2.07	12.75	402.57	30.6879	
81	4	1	2.07	12.51	415.08	31.64154	
66	11	3	2.09	16.21	431.29	32.87722	
33	11	6	2.1	16.69	447.98	34.1495	
87	10	1	2.1	19.64	467.62	35.64666	
11	11	8	2.11	13.66	481.28	36.68796	
19	8	7	2.11	18.47	499.75	38.09593	
36	3	5	2.14	18.84	518.59	39.5321	
12	1	7	2.15	18.71	537.3	40.95836	
17	6	7	2.18	21.77	559.07	42.61789	
14	3	7	2.23	15.83	574.9	43.82461	
26	4	6	2.23	12.19	587.09	44.75385	
75	9	2	2.24	10.92	598.01	45.58628	
83	6	1	2.26	12.25	610.26	46.5201	
25	3	6	2.29	12.88	623.14	47.50194	
53	9	4	2.35	21.73	644.87	49.15842	
47	3	4	2.36	14.75	659.62	50.28281	
49	5	4	2.4	13.79	673.41	51.33402	
55	11	4	2.42	12.18	685.59	52.26251	
39	6	5	2.46	12.01	697.6	53.17803	
76	10	2	2.46	15.11	712.71	54.32986	
88	11	1	2.51	11.99	724.7	55.24386	
52	8	4	2.57	14.8	739.5	56.37206	
67	1	2	2.58	9.42	748.92	57.09015	
23	1	6	2.61	17.69	766.61	58.43866	
86	9	1	2.65	12.92	779.53	59.42355	
20	9	7	2.69	17.1	796.63	60.72708	
27	5	6	2.76	15.79	812.42	61.93075	
61	6	3	2.76	13.6	826.02	62.96748	
16	5	7	2.8	18.08	844.1	64.34572	
7	7	8	2.84	10.53	854.63	65.14842	
73	7	2	3.13	15.86	870.49	66.35743	
77	11	2	3.17	13.73	884.22	67.40406	
34	1	5	3.37	24.68	908.9	69.28542	
84	7	1	3.41	11.22	920.12	70.14072	
59	4	3	3.51	16.23	936.35	71.37793	
5	5	8	4.06	11.86	948.21	72.28202	
21	10	7	4.16	25.06	973.27	74.19234	
45	1	4	4.17	11.35	984.62	75.05755	
31	9	6	4.41	20.89	1005.51	76.65	
18	7	7	4.47	16.53	1022.04	77.91008	
2	2	8	4.53	17.44	1039.48	79.23953	
41	8	5	4.53	10.64	1050.12	80.05062	
30	8	6	4.85	17.29	1067.41	81.36863	
71	5	2	4.96	16.65	1084.06	82.63786	
13	2	7	4.97	16.68	1100.74	83.90938	2.96 oC
24	2	6	5.14	16.68	1117.42	85.18089	
8	8	8	5.82	15.24	1132.66	86.34264	
4	4	8	5.96	13.91	1146.57	87.403	
28	6	6	6.15	13.87	1160.44	88.46031	
6	6	8	6.23	23.08	1183.52	90.21969	
69	3	2	6.32	12	1195.52	91.13445	
48	4	4	7.41	14.89	1210.41	92.26952	
43	10	5	7.54	15.25	1225.66	93.43203	
62	7	3	7.72	19.21	1244.87	94.8964	
9	9	8	8.25	13.59	1258.46	95.93237	
82	5	1	11.37	11.43	1269.89	96.80368	
3	3	8	12.95	14.13	1284.02	97.88081	
32	10	6	13.86	18.31	1302.33	99.27658	
38	5	5	15.04	9.49	1311.82	100	